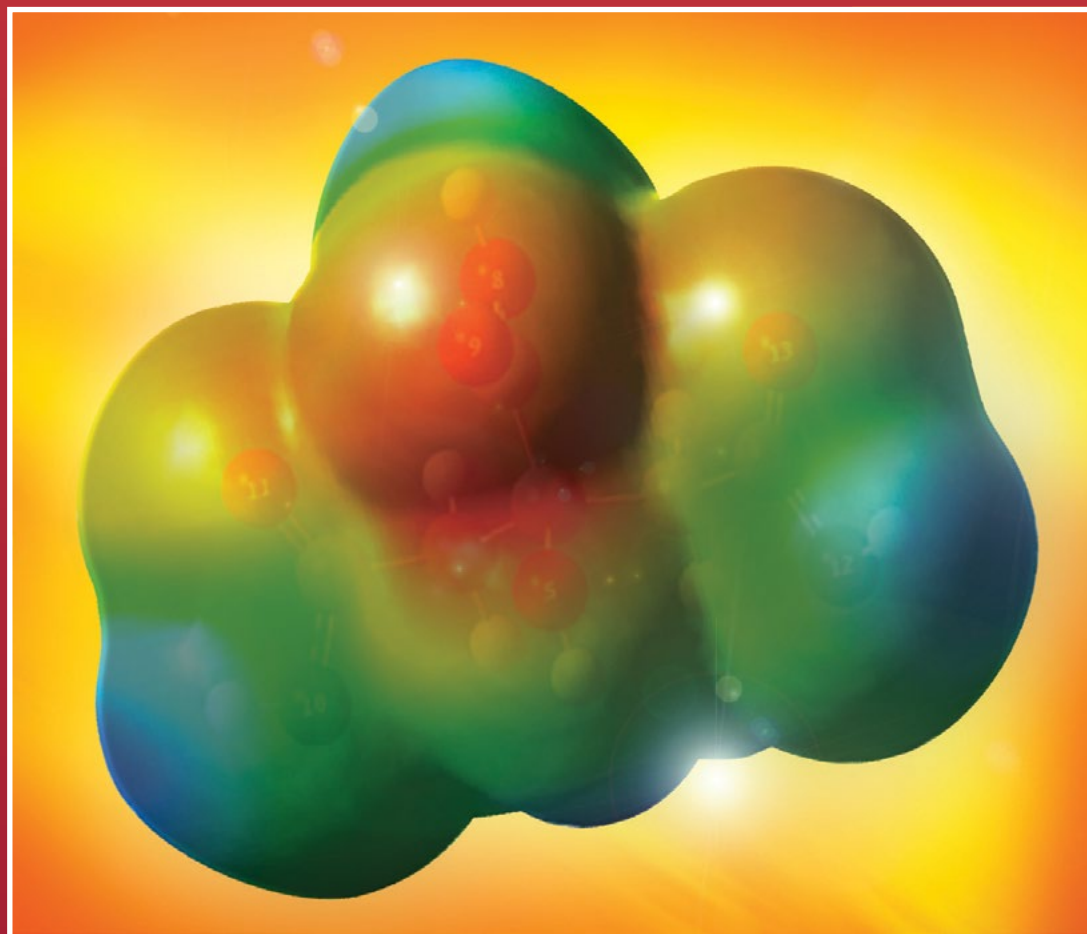




Acta Chimica Slo Acta Chimica Slo Slovenica Acta C

1



65/2018

EDITOR-IN-CHIEF

KSENIJA KOGEJ

Slovenian Chemical Society, Hajdrihova 19, SI-1000 Ljubljana, Slovenija,

E-mail: ACSi@fkt.uni-lj.si, Telephone: (+386)-1-479-8538

ASSOCIATE EDITORS

Janez Cerkovnik, University of Ljubljana, Slovenia

Krištof Kranjc, University of Ljubljana, Slovenia

Ksenija Kogej, University of Ljubljana, Slovenia

Franc Perdih, University of Ljubljana, Slovenia

Aleš Podgornik, University of Ljubljana, Slovenia

Helena Prosen, University of Ljubljana, Slovenia

Damjana Rozman, University of Ljubljana, Slovenia

Melita Tramšek, Jožef Stefan Institute, Slovenia

Irena Vovk, National Institute of Chemistry, Slovenia

ADMINISTRATIVE ASSISTANT

Marjana Gantar Albreht, National Institute of Chemistry, Slovenia

EDITORIAL BOARD

Wolfgang Buchberger, Johannes Kepler University, Austria

Alojz Demšar, University of Ljubljana, Slovenia

Stanislav Gobec, University of Ljubljana, Slovenia

Marko Goličnik, University of Ljubljana, Slovenia

Günter Grampp, Graz University of Technology, Austria

Wojciech Grochala, University of Warsaw, Poland

Danijel Kikelj, Faculty of Pharmacy, Slovenia

Janez Košmrlj, University of Ljubljana, Slovenia

Blaž Likozar, National Institute of Chemistry, Slovenia

Mahesh K. Lakshman, The City College and

The City University of New York, USA

Janez Mavri, National Institute of Chemistry, Slovenia

Friedrich Sreinc, University of Minnesota, USA

Walter Steiner, Graz University of Technology, Austria

Jurij Svete, University of Ljubljana, Slovenia

Ivan Švancara, University of Pardubice, Czech Republic

Jiri Pinkas, Masaryk University Brno, Czech Republic

Gašper Tavčar, Jožef Stefan Institute, Slovenia

Christine Wandrey, EPFL Lausanne, Switzerland

Ennio Zangrando, University of Trieste, Italy

ADVISORY EDITORIAL BOARD

Chairman

Branko Stanovnik, Slovenia

Members

Josef Barthel, Germany

Udo A. Th. Brinkman, The Netherlands

Attilio Cesaro, Italy

Dušan Hadži, Slovenia

Vida Hudnik, Slovenia

Venčeslav Kaučič, Slovenia

Željko Knez, Slovenia

Radovan Komel, Slovenia

Janez Levec, Slovenia

Stane Pejovnik, Slovenia

Anton Perdih, Slovenia

Slavko Pečar, Slovenia

Andrej Petrič, Slovenia

Boris Pihlar, Slovenia

Milan Randić, Des Moines, USA

Jože Škerjanc, Slovenia

Miha Tišler, Slovenia

Durđa Vasić-Rački, Croatia

Marjan Veber, Slovenia

Gorazd Vesnaver, Slovenia

Jure Zupan, Slovenia

Boris Žemva, Slovenia

Majda Žigon, Slovenia

Acta Chimica Slovenica is indexed in: *Chemical Abstracts Plus*, *Current Contents (Physical, Chemical and Earth Sciences)*, *PubMed*, *Science Citation Index Expanded* and *Scopus*. Impact factor for 2016 is IF = 0.983.



Articles in this journal are published under Creative Commons Attribution 3.0 License

<http://creativecommons.org/licenses/by/3.0/>

Izdaja – Published by:

SLOVENSKO KEMIJSKO DRUŠTVO – SLOVENIAN CHEMICAL SOCIETY

Naslov redakcije in uprave – Address of the Editorial Board and Administration

Hajdrihova 19, SI-1000 Ljubljana, Slovenija

Tel.: (+386)-1-476-0252; Fax: (+386)-1-476-0300; E-mail: chem.soc@ki.si

Izdajanje sofinancirajo – Financially supported by:

Slovenian Research Agency, Ljubljana, Slovenia

National Institute of Chemistry, Ljubljana, Slovenia

Jožef Stefan Institute, Ljubljana, Slovenia

Faculty of Chemistry and Chemical Technology at University of Ljubljana, Slovenia

Faculty of Chemistry and Chemical Engineering at University of Maribor, Slovenia

Faculty of Pharmacy at University of Ljubljana, Slovenia

University of Nova Gorica, Nova Gorica, Slovenia



Acta Chimica Slovenica izhaja štirikrat letno v elektronski obliki na spletni strani <http://acta.chem-soc.si>. V primeru posvečenih števil izhaja revija tudi v tiskani obliki v omejenem številu izvodov.

Acta Chimica Slovenica appears quarterly in electronic form on the web site <http://acta.chem-soc.si>. In case of dedicated issues, a limited number of printed copies are issued as well.

Transakcijski račun: 02053-0013322846 Bank Account No.: SI56020530013322846-Nova Ljubljanska banka d. d., Trg republike 2, SI-1520 Ljubljana, Slovenia, SWIFT Code: LJBA SI 2X

Oblikovanje ovitka – Design cover: KULT, oblikovalski studio, Simon KAJTNA, s. p. Grafična priprava za tisk: Majanafin, d. o. o.

Tisk-Printed by: Tiskarna Stušek, Ljubljana

© Copyright by Slovenian Chemical Society

Dear readers of *Acta Chimica Slovenica*



The journal of the Slovenian Chemical Society was first edited in 1953 as *Kemijski zbornik*. In 1993 it was renamed into *Acta Chimica Slovenica* and was initially published as Volume 40. For almost fifty years it was edited only in the printed version, until 1998, when Andrej Petrič

became the editor in chief, the journal obtained an electronic form as a result of his editorial policy. Around that time, I joined the editorial team as a co-editor. So let me briefly describe our work and mention some achievements during the last two decades.

Editorial policy was simple: articles with appropriate scientific value, novelty and interesting to a large number of readers in the international space were published. Some fruitful results were obtained quickly. In 1999, the number of submitted articles exceeded one hundred and only about 40% of these being accepted. In 2002, *ACSi* obtained the impact factor (IF) of 0.12 for the first time. In 2005 and under the editorship of Janez Košmrlj, two-column articles and new technical standards were introduced and *Acta Chimica Slovenica* was given a new and attractive form designed by the academic painter Simon Kajtna. A substantial increase in the number of submitted articles followed. For several years more than 400 articles have been submitted and about one third of these published annually. The preparation of manuscripts for publishing was entrusted to the professional technical editor Stanislav Oražem. In 2007, the impact factor slightly exceeded the magic number one and in the following years, it hovered around this value.

In 2006 I took over the editorship. Here, I would like to express my respect and thanks to those who have contributed to the development and popularity of our journal with their ideas and enthusiastic work from the very beginning.

Due to a large number of submitted manuscripts, new editorial team has been organized with associate editors covering the scientific fields of organic chemistry, inorganic chemistry, analytical chemistry, biochemistry and molecular biology, physical chemistry and materials science, as well as chemical, biochemical and environmental engineering, general chemistry, applied chemistry and biomedical applications. Considering the number of published papers, organic chemistry is the most popular field in the last decade. Since 2006, we have prepared more than twenty issues with invited guest editors on various occasions, dedicated to selected scientific fields. The most cited article has reached almost 100 citations, whereas others on the top ten list have more than 40 citations. In the last decade about 130 papers were published per year, being mainly scientific papers while, reviews and technical papers are rare. The majority of papers have been written by Slovenian authors.

The workload of the editor in chief has been diverse. Taking into account that there has been a little interest for a field editorship, leading a team of voluntary editors was not always easy and required rather complex and diplomatic approach. I was responsible to obtain enough papers per issue to be published. To achieve this I had to establish with my editorial team interesting editorial policy to attract as many readers as possible and consequently authors from all over the world. Appropriate scientific level and novelty of already published papers has worked as advertisement and stimulated scientists to report about their research results.

All submitted manuscripts have first appeared in my mailbox and I had to check if they corresponded to focus and scope of journal as well as if they were prepared according to author guidelines. Those with a positive mark were then assigned to associate editor of the field who started the reviewing process. The editors have been trying to do their best in communication with authors and reviewers next to their teaching and research obligations. Fortunately, there have been more than sixty manuscripts in the reviewing process at every moment, so theoretically there has been enough material for the next issue. Nevertheless, we had to obtain several hundred reviews per year that is two independent reviews per manuscript. It has

been very difficult to find active and quality reviewer who did his job in time. The majority of chosen reviewers have not found time to read the manuscripts or even answer the polite request of the editors. Luckily there has been a large group of communicative reviewers doing the job at various levels of quality and speed. Consequently the reviewing process at ACSi has taken about 3–6 months, strongly depending on reviewer's good will and speed. I had to ask frequently some field editors to finish the reviewing process and accept proper decisions as soon as possible. This has not been a pleasant job, especially because it has been for years repeated on monthly or even weekly basis.

When the reviewing process had finished, the editors sent the documentation with decision to the authors. In the case of positive reviews, authors corrected their manuscript according to the reviewers' comments and returned it to the editor. If everything was well done, the manuscript was accepted and sent to the technical editor.

About a month before release of an issue, communication between editor in chief and technical editor has been intensified to check the proofs, to sort the papers and to prepare the graphical contents. It has always been a special challenge and pleasure for me to prepare together with Simon Kajtna a cover picture from the topics of one paper prepared for publication which tells an interesting story from the wide area of chemistry. After an issue has been edited, we had an editorial meeting, where we discussed the results of our work and made plans for the future issues. I namely believe that a personal contact with a positive energy and in a pleasant atmosphere is intrinsic for fruitful editorial work, apart from the well-established communication by e-mail and phone.

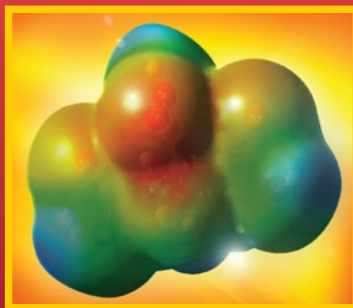
Cost-cutting and financial restrictions also reached *Acta Chimica Slovenica*. The majority of journal costs has been covered by Slovenian Research Agency for decades but have substantially decreased under my editorship. The financial support from Slovenian companies through advertising has been minor. Fortunately, the National Institute of Chemistry and the Jožef Stefan Institute as well as four Slovenian faculties from the broad field of chemistry have helped to cover the publishing expenses. Regrettably, this has allowed mostly the survival of our journal and not its substantial progress. This also caused a reduction of printed copies of an issue from 1200 to 200 for example. Anyhow, we did our best to follow the trends in infor-

mation technology and keep or even increase the value of our journal in the scientific world. ACSi is indexed in the PubMed data base from 2013. After about a six months of preparation we started with a well-known Open Journal System (OJS) in January 2014. Soon after that we started to work on DOI System which was introduced at the beginning of 2015, while later this year we started to check the manuscripts with plagiarism detection program Ithenticate. Making a good use of these systems, we publish electronic versions of manuscripts as soon as they are accepted hoping that this will increase the scientific ranking of our journal. ACSi has been an open access journal for almost two decades, however it is published under *Creative Commons Attribution 3.0 License* from January 2017. Here, I would like to express my gratitude to Alen Orbanic, who is the first to be credited with the implementation of these tools.

Before introduction of OJS system, a large amount of correspondence and data was conducted with diligent and devoted secretaries, regrettably deceased Jana Tepina and already retired Olga Gorše. Now Marjana Gantar continues quality and responsible work at ACSi as an administrative assistant. At this point, I express warm gratitude to my active editorial team, the authors and reviewers, and all the others who have helped to ensure that *Acta Chimica Slovenica* has been published regularly. Special thanks are also to Slavko Kaučič, the former president of the Slovenian Chemical Society and publisher of *Acta Chimica Slovenica*, who has well understood the value and extent of editorial work and has supported us with his constructive attitude. Half a year ago, Albin Pintar took over this role and I am sure that excellent cooperation with editors of *Acta Chimica Slovenica* will continue.

I liked the work for *Acta Chimica Slovenica*. But after a decade being an editor in chief, the time has come to handover the rudder to a new editor with fruitful energy and fresh ideas. I am glad that Ksenija Kogej accepted this challenge. She is communicative, well organized and has valuable scientific and leading references so I am sure that she will be able to complete this role. I wish her and her editorial team to enjoy in editorial work and to increase or at least to keep the interest of readers and the scientific value of *Acta Chimica Slovenica* on the international stage.

Aleksander Pavko

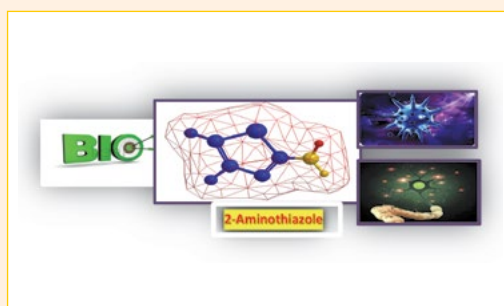


REVIEW

1-22 Organic chemistry

Synthesis of Novel 3D-Rich α -Amino Acid-Derived 3-Pyrazolidinones

Mohamed Ezzat Khalifa

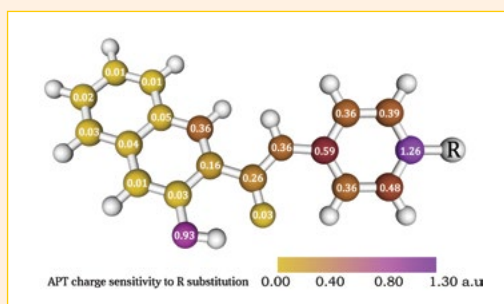


SCIENTIFIC PAPER

23-33 Physical chemistry

B3LYP Study of 3-hydroxynaphthalene-2-carboxanilide *para*-derivatives

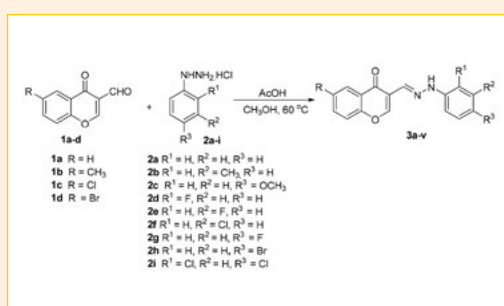
Martin Michalík, Peter Poliak and Vladimír Lukeš



34-49 Organic chemistry

Synthesis and Anti-proliferative Activity of 4*H*-Chromone Based Phenylhydrazones, Pyrazolecarboxylates and Pyrazolylmethanones

Nageswara Rao Rayala, Rajkumar Kommera, Dayakar Cherupally, Ramalinga Murthy Thampunuri, V. Kalivendi Shasi and China Raju Bhimapaka

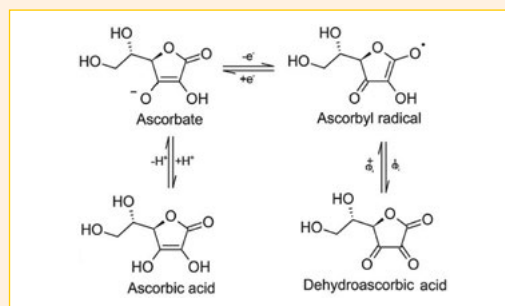


50–58

Analytical chemistry

Cis-dioxo-bis [3-methoxy-2,2-dimethylpropanediamine] Molybdenum/Surfactant-Modified Electrode for Simultaneous Sensing of Ascorbic Acid and Dopamine

Ali Arjmandi, Hamid Reza Zare-Mehrjardi and Hadi Kargar

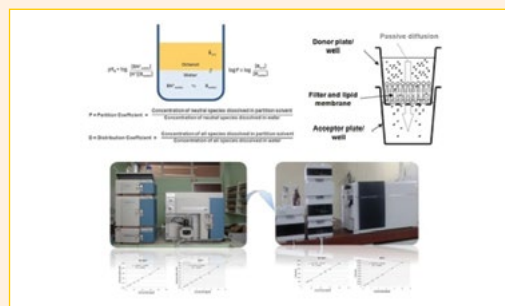


59–64

Biomedical applications

Prediction of *in vivo* Bioavailability by *in vitro* Characterization of Ethylenediamine Dipropanoic Acid Derivatives with Cytotoxic Activity

Biljana K. Tubić, Sandra S. Vladimirov, Bojan D. Marković and Tibor J. Sabo

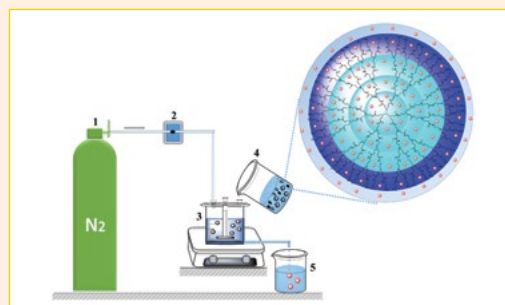


65–74

Analytical chemistry

Evaluation of Jeffamine® Core PAMAM Dendrimers for Simultaneous Removal of Divalent Heavy Metal Ions from Aqueous Solutions by Polymer Assisted Ultrafiltration

Ali Serol Ertürk, Mustafa Ulvi Gürbüz, Metin Tülü and Abdürrezzak Emin Bozdoğan

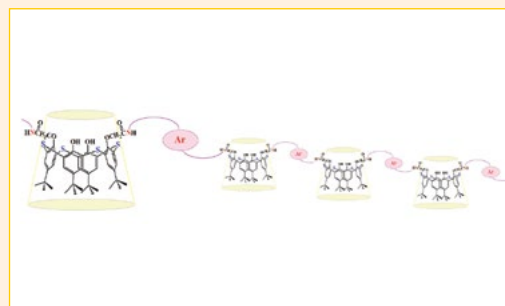


75–85

Organic chemistry

Polythiacalix[4]amides as a Novel Category of Macromolecules; Synthesis, Antibacterial Evaluation and Investigation on their Spectral and Thermophysical Characteristics

Hamed Tashakkorian, Moslem Mansour Lakouraj, Rahimeh Maldar and Zahra Moulana

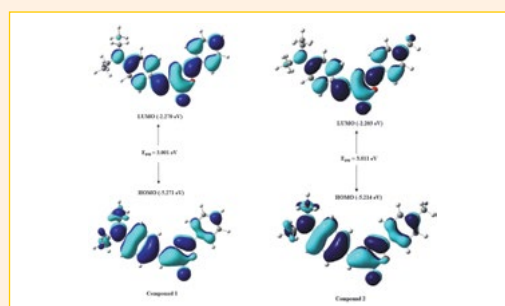


86–96

Organic chemistry

Spectroscopic, Structural and Density Functional Theory (DFT) Studies of Two Oxazol-5-one Derivatives

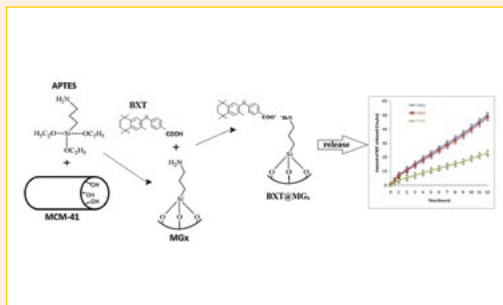
İbrahim Hanif Nazlı, Duygu Barut Celepci, Gül Yakalı, Derya Topkaya, Muhittin Aygün and Serap Alp



97–107 Materials science

Development of New Bexarotene-loaded Mesoporous Silica Systems for Topical Pharmaceutical Formulations

Aurelia Vasile,¹ Maria Ignat, Mirela Fernanda Zaltariov, Liviu Sacarescu, Iulian Stoleriu, Dan Draganescu, Mihai Dumitras and Lacramioara Ochiuz



108–118 Organic chemistry

Synthesis and *in vitro* Bio-activity Evaluation of N4-benzyl Substituted 5-Chloroisatin-3-thiosemicarbazones as Urease and Glycation Inhibitors

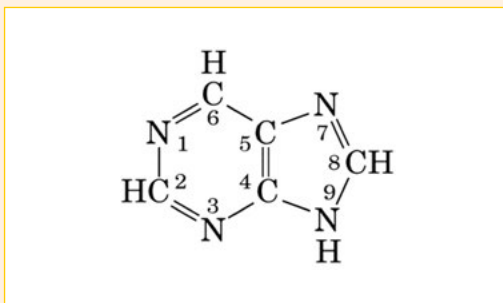
Humayun Pervez, Nazia Khan, Jamshed Iqbal, Sumera Zaib, Muhammad Yaqub¹ and Muhammad Moazzam Naseer



119–126 Physical chemistry

The Effect of Adenine Adsorption on Zn (II) Electroreduction in Acetate Buffer

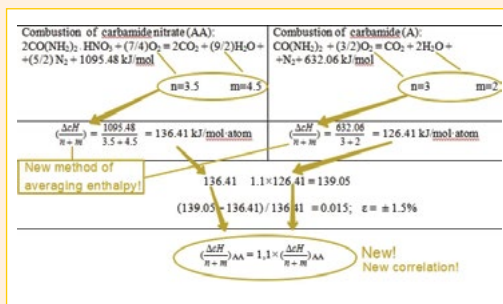
Dorota Gugała-Fekner



127–130 Physical chemistry

Thermochemical Properties and Regularities of Amides, Anilides, and Amidic Acids

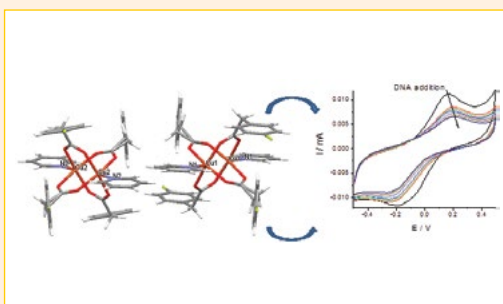
Alma Kairlapovna Ryskaliyeva, Murat Ergalievich Baltabayev and Aigul Moldakhmetovna Zhubatova



131–137 Inorganic chemistry

Effect of Fluorinated Ligand on Structural, Electronic and DNA-binding Properties of Copper Paddlewheel Complex: Synthesis, Structure and Properties

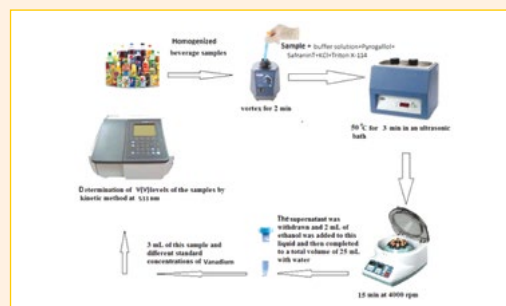
Muhammad Iqbal, Sqib Ali and Muhammad Nawaz Tahir



138–149 Analytical chemistry

Preconcentration and Determination of Trace Vanadium(V) in Beverages by Combination of Ultrasound Assisted-cloud Point Extraction with Spectrophotometry

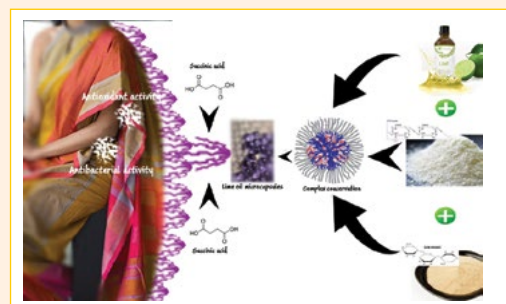
Nuket Kartal Temel and Ramazan Gürkan



150–159 Applied chemistry

Development of a Cotton Smart Textile with Medicinal Properties Using Lime Oil Microcapsules

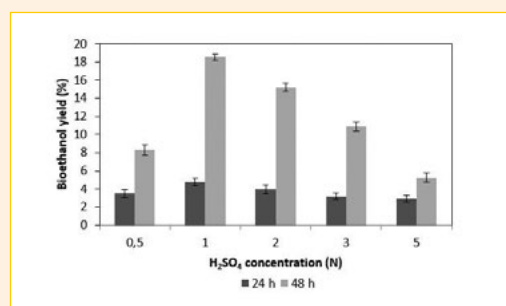
Piyumi B. Wijesirigunawardana and B. Gayani K. Perera



160–165 Chemical, biochemical and environmental engineering

Effect of Chemical Pre-treatments on Bioethanol Production from *Chlorella minutissima*

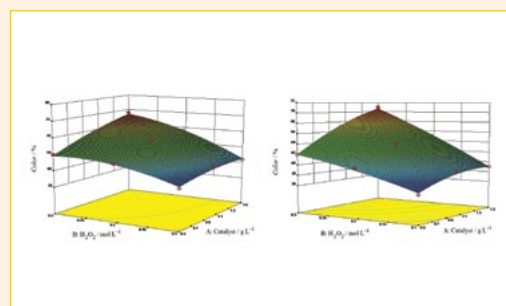
Burcu Şerbetçioglu Sert, Benan İnan and Didem Özçimen



166–171 Chemical, biochemical and environmental engineering

A Comparative Study on a Cationic Dye Removal through Homogeneous and Heterogeneous Fenton Oxidation Systems

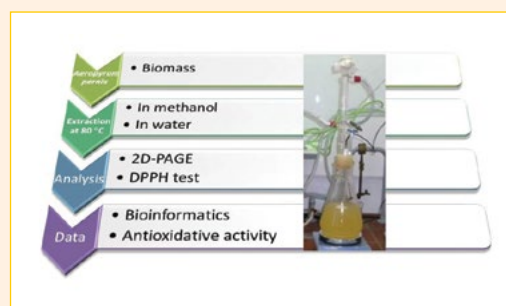
Shima Rahim Pouran, Abolfazl Bayrami, Mohammad Saleh Shafeeyan, Abdul Aziz Abdul Raman and Wan Mohd Ashri Wan Daud



172–182 Biochemistry and molecular biology

Antioxidative Activity of Methanolic and Water Extracts from the Hyperthermophilic Archaeon *Aeropyrum pernix* K1

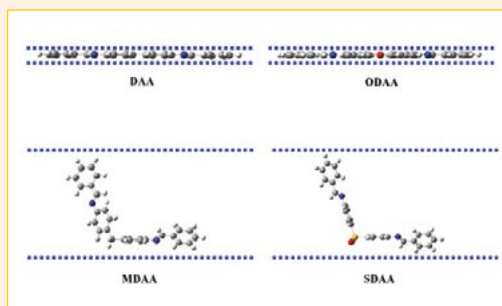
Mihaela Skrt, Polona Jamnik and Nataša Poklar Ulrih



183–190 Materials science

Understanding the Inhibition of Mild Steel Corrosion by Dianiline Schiff Bases: a DFT Investigation

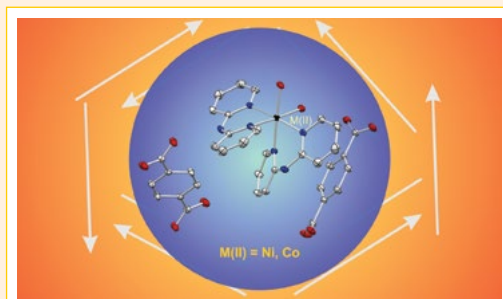
Salah Eddine Hachani, Zelikha Necira, Djamel Eddine Mazouzi and Nadia Nebbache



191–198 Inorganic chemistry

Diaquabis(2,2'-dipyridylamine)M(II) Terephthalate Dihydrates, M(II) = Ni, Co: Synthesis, Crystal Structures, Thermal and Magnetic Properties

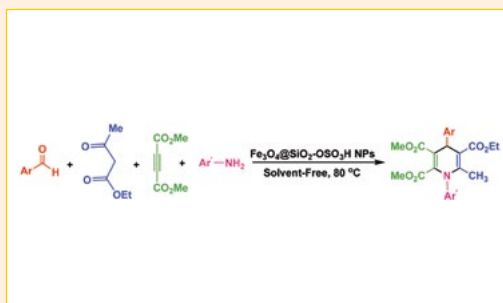
Lidija Radovanović, Jelena Rogan, Dejan Poleti, Marko V. Rodić and Zvonko Jagličić



199–207 Materials science

Synthesis and Antibacterial Evaluation of Some New 1,4-Dihydropyridines in the Presence of Fe₃O₄@Silica Sulfonic Acid Nanocomposite as Catalyst

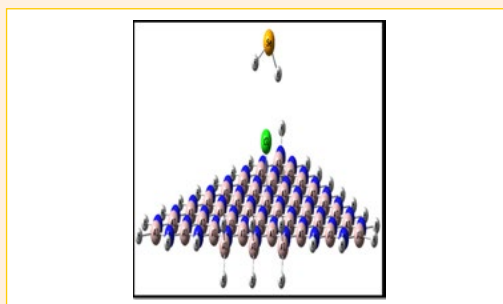
Seyed Mostafa Hasan Nasrollahi, Mohammad Ali Ghasemzadeh1, and Mohammad Reza Zolfaghari



208–212 Physical chemistry

The Cl Functionalized Aluminum Nitride (AlN) and Aluminum Phosphide (AlP) Nanocone Sheets as Hydrogen Selenide (H₂Se) Sensor: a Density Functional Investigation

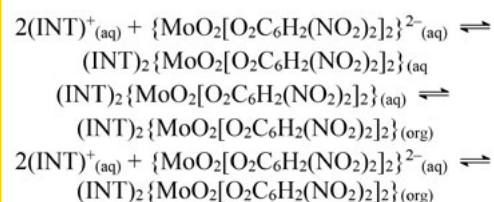
Seyyed Milad Abrishamifar, Negar Heidari, Razieh Razavi, Milad Janghorban Lariche and Meysam Najafi



213–220 Inorganic chemistry

Study on the Chelate Formation and the Ion-association of Anionic Chelate of Molybdenum(VI) with 3,5-Dinitrocatechol and Monotetrazolium Cation

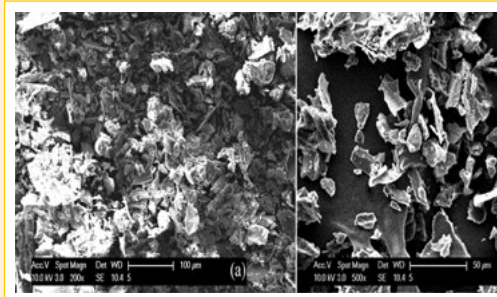
Kirila Stojnova, Vidka Divarova, Petya Racheva, Kristina Bozhinova and Vanya Lekova



221–230 Applied chemistry

Biosorption of 2,4,6-trichlorophenol from Aqueous Medium Using Agro-waste: Pine (*Pinus densiflora* Sieb) Bark Powder

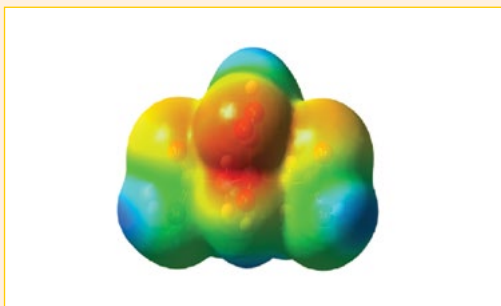
Nadavala Siva Kumar, Mohammad Asif, Mansour I Al-Hazzaa and Ahmed A. Ibrahim



231–238 Physical chemistry

Binding Sites of Deprotonated Citric Acid and Ethylenediaminetetraacetic Acid in the Chelation with Ba^{2+} , Y^{3+} , and Zr^{4+} and Their Electronic Properties: a Density Functional Theory Study

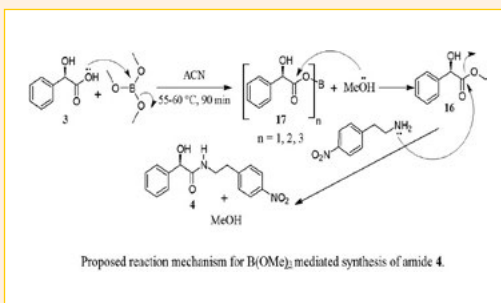
Nor Ain Fathihah Abdullah and Lee Sin Ang



239–245 Organic chemistry

Investigation of Mechanistic Pathway for Trimethyl Borate Mediated Amidation of (*R*)-Mandelic Acid for the Synthesis of Mirabegron, an Antimuscarinic Agent

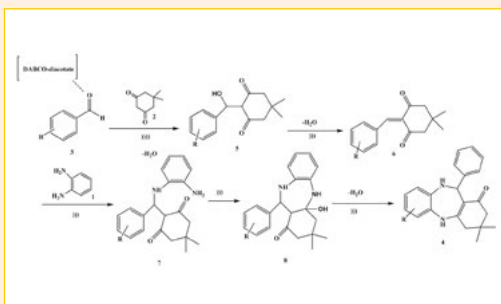
Dattatray G. Deshmukh, Mukund N. Bangal, Mukunda R. Patekar, Vijay J. Medhane and Vijayavithal Thippannachar Mathad



246–252 Organic chemistry

Ultrasound Assisted 1,4-diazabicyclo[2.2.2] Octaniumdiacetate Multicomponent Synthesis of Benzodiazepines: A Novel, Highly Efficient and Green Protocol

Shahriar Sarhandi, Leila Zare Fekri and Esmaeil Vessaly



Review

Recent Developments and Biological Activities of 2-Aminothiazole Derivatives

Mohamed Ezzat Khalifa*

Department of Chemistry, Faculty of Science, Taif University, Taif 21974, Saudi Arabia

* Corresponding author: E-mail: mohamedezzat200@hotmail.com, mohamedezzat@tu.edu.sa

Received: 16-05-2017

Abstract

Aminothiazole nuclei and their various derivatives have been long used as precursors for the synthesis of biologically active molecules. As a typical heterocyclic amine, 2-aminothiazole is a cornerstone for the synthesis of many compounds, including sulfur drugs, biocides, fungicides, various types of dyes for synthetic fibers and chemical reaction accelerators and as intermediates in the synthesis of antibiotics, where a large number of 2-aminothiazoles have been substituted with different groups for various pharmaceutical purposes, besides their activity as corrosion inhibitors for mild steel protection as well. The synthetic utility of 2-amino-4-substituted-thiazoles, their reactions and biological activities have been surveyed and are presented in this review.

Keywords: 2-aminothiazoles, azo compounds, biological activities, corrosion, synthetic fibers, inhibitors.

1. Introduction

The monoazo heterocyclic compounds containing sulphur and/or nitrogen atoms are of widespread use as building blocks in chemistry, where they are known as biologically active compounds with a broad range of activity, and textile dyes as well.^{1–3} As a typical heterocyclic amine, 2-aminothiazole is the starting point for the synthesis of many compounds, including sulfur drugs, biocides, fungicides, dyes and chemical reaction accelerators and as intermediates in the synthesis of antibiotics, where a large number of 2-aminothiazoles have been substituted with different groups for pharmaceutical purposes,^{4–6} and are also used in the syntheses of various types of dyes for synthetic fibers,^{7–15} beside their activity as corrosion inhibitors for mild steel protection,^{16,17} corrosion inhibitors for copper¹⁸ and as an ionophore in the construction of a lutetium(III)-selective membrane sensor.¹⁹ These derivatives continue to attract the attention of biologists because of their widespread use in the treatment of the biological systems. For instance, many papers have been published on the use of these compounds exhibiting antimicrobial,^{20–22} antifungal and anti-inflammatory activity,²³ anesthetic activity,^{4,24} as antiviral drugs,⁶ anti-leukemic agents,²⁵ anti-proliferatives (cytostatic and cytotoxic) with activity against a panel of cell lines (HeLa, L929, HT-29 and T47D),²⁶ as active agents against some enzymes involved in eicosanoid metabolism (5-, 12-, 15-lipoxygenase (LO),

cyclooxygenase-1 and -2 (COX-1 and COX-2)),²⁷ inhibitors anti-TCR antibody induced IL-2 production in mice *in vivo* and reduced lung inflammation in a mouse model of ovalbumin induced allergy/asthma,²⁸ inhibitors for *Mycobacterium tuberculosis* (Mtb, H37Rv and MS, GyrB),^{29,30} as vascular adhesion protein-1 inhibitors (VAP-1),^{31,32} inhibitors of Cdc7 kinase activity in cancer cells,³³ inhibitors of nerve growth factor receptor TrkA,³⁴ inhibitors of p38 α mitogen-activated protein kinase (p38 α MAPK).³⁵ They can also bind to CT-DNA by the intercalative and electrostatic binding mode.³⁶ A clubbed triazolyl thiazole series of cdk5/p25 inhibitors were reported as potentially useful compounds for the possible treatments for Alzheimer's disease.³⁷ Due to its enormous industrial and biological importance, the studies of tautomeric equilibria of 2-aminothiazole and its derivatives have been considered as a hot topic for the scientists.³⁸ The amino-imino tautomeric equilibrium of the isolated, mono-, di- and trihydrate configurations and dimer of 2-aminothiazole and the effects of hydration or self-assistance on the transition state structures corresponding to proton transfer from the amino to imino tautomers, were theoretically and experimentally explored in the gas phase as well as in the solution, which directly affected the orientation of substitution and the product assignments when they reacted with the other compounds.^{39–43} Several spectroscopic investigations, *e.g.* infrared (IR), ultraviolet (UV), density functional theoretical calculations (DFT), Raman spectra (RS),

surface-enhanced Raman spectra (SERS) and nuclear magnetic resonance spectra (NMR), indicated that the 2-aminothiazole derivatives are existing in solution preferentially in the amino tautomer, based on the analysis of their reactivity data.^{44–47} Additionally, the pK_{BH^+} values of 2-aminothiazole and a number of its derivatives showed that these molecules generally exist in the amino aromatic form and are protonated at the aza-nitrogen.⁴⁸

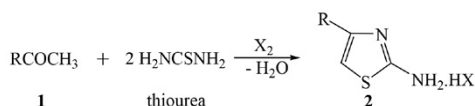
2. Synthesis of 2-Amino-4-substituted-1,3-thiazoles

2.1. From Ketones and Haloketones

Many 2-amino-4-substituted thiazoles are generally synthesized by Hantzsch thiazole synthesis from α -haloketones and thioureas (or thioamides) in polar solvents.⁴⁹

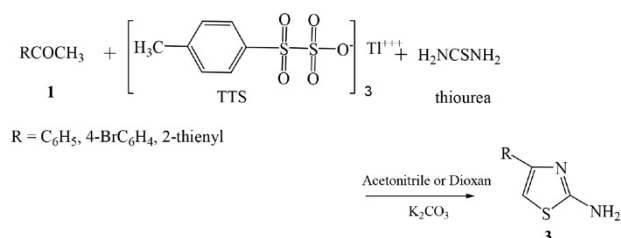
2.1.1. Using Halogen

Ketones of the type **1** react directly with one mol of halogen and two mols of thiourea to give 2-amino halogenated derivatives of the 4-substituted-1,3-thiazole nucleus **2** in excellent yield.^{50,51}

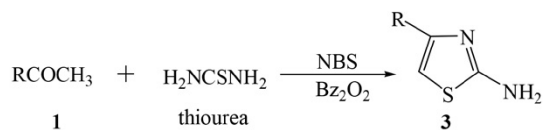


2.1.2. Using Oxidizing Agents

An oxidative process can accomplish the formation of 2-amino-4-substituted-1,3-thiazoles **3** by the reaction of the ketone of the type **1** with thiourea, using a variety of oxidizing agents, namely sulfur chloride, chlorosulfonic acid, thionyl chloride, sulfur monochloride, sulfur trioxide, sulfuric acid, nitric acid and sulfur.⁵² Oxidation of ketones **1** with thallium(III)-*p*-tosylsulphonate (TTS) in refluxing acetonitrile or dioxane followed by the addition of thiourea, yielded the 2-amino-4-substituted-1,3-thiazoles **3** as free bases in good yields upon basification with aqueous potassium carbonate.⁵³

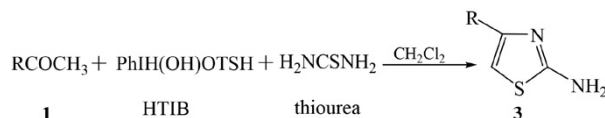


Reaction of the ketones of the type **1** with thiourea in the presence of *N*-bromosuccinimide (NBS) and benzoyl peroxide as radical initiator furnished 2-amino-4-substituted-1,3-thiazoles of the type **3**.⁵³



R = (un)substituted-3-coumarinyl, (un)substituted phenyl

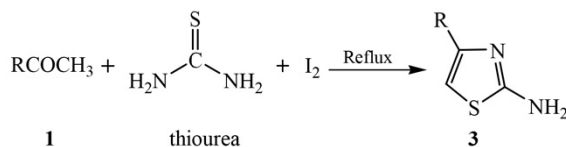
A facile synthesis for the 2-amino-4-substituted-1,3-thiazoles **3** (R = 2-furyl) through a very simple and eco-friendly methodology was reported. Stirring of ketones **1** (R = 2-furyl) with hydroxyl-(tosyloxy)-iodobenzene (HTIB) in dichloromethane at room temperature, provided 2-tosyloxyacetylfuran which underwent smooth transformation with thiourea affording the target compounds **3** in excellent yield.⁵⁴



R = 2-furyl

2.1.3. Using Iodine Catalyst

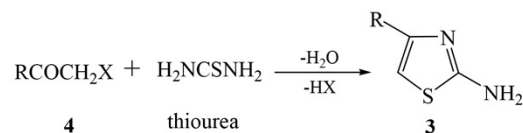
The synthesis of 2-amino-4-substituted-thiazole derivatives **3** has been carried out by treatment of ketones **1** with thiourea and iodine as the catalyst. The synthesized derivatives exhibited promising antiproliferative effect through translational VEGF-A inhibition.^{55–58}



R = C₆H₅, C₆H₄Cl-*p*, C₆H₄OMe-*p*, 4-morpholinophenyl

2.1.4. Using Sodium Fluoride Catalyst

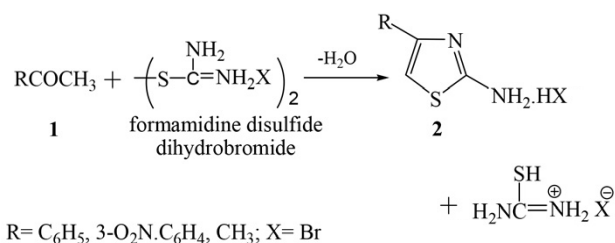
Sodium fluoride was found to be a simple, mild and efficient catalyst in the synthesis of 2,4-disubstituted-1,3-thiazoles **3** obtained by condensation reaction of α -haloketones **4** with thiourea.^{24,59–65}



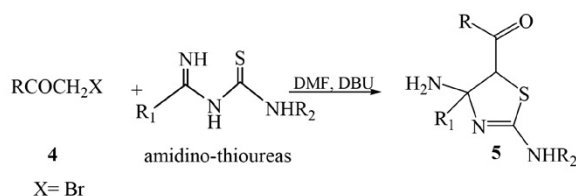
R = 3-coumarinyl, 3-indolyl, 2-thienyl, pyridyl, quinolyl, 2-benzothiazolyl, phenyl, substituted phenyl, methyl, 4-antipyrinyl; X = Br

2.1.5. From Amidine Derivatives

Reaction of ketones **1** with formamidine disulfide dihydrobromide afforded the corresponding hydrobromide salt of 2-amino-4-substituted-1,3-thiazoles **2**.⁶⁶

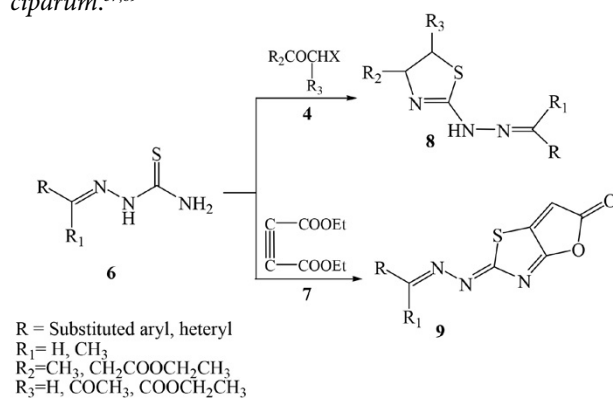


Subsequent treatment of the amidino-thioureas and iodothiureas (R₁ = Aryl; R₂ = ArCH₂S), obtained from the condensation reactions of mixtures of amidines, thiuronium salts and isothiocyanates, with α-haloketone **4** led to the formation of 1,3-thiazoles **5** via base-catalysed ring closure process in the presence of 1,8-diazabicyclo [5.4.0]-7-undecene (DBU).^{67,68}



2. 1. 6. From Thiosemicarbazones

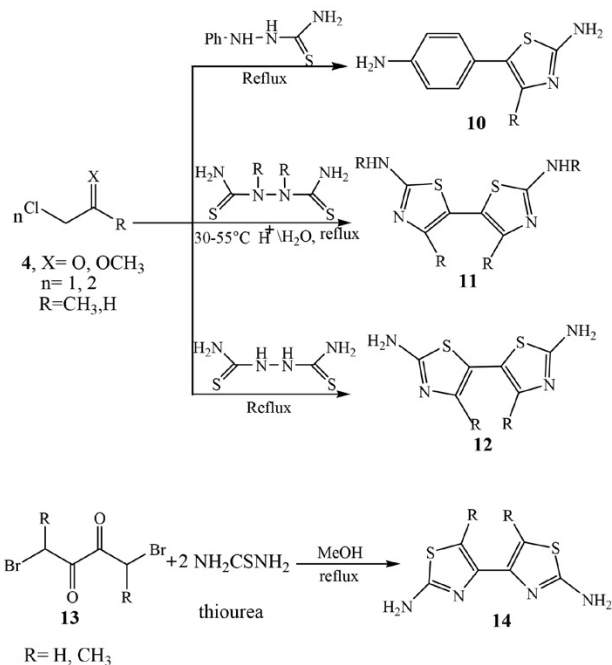
Cyclization reaction between the aryl and heteroarylthiosemicarbazones **6** with aliphatic α-haloketones **4** and/or diethyl acetylenedicarboxylate **7**, afforded the 2-(2-hydrazinyl)thiazole derivatives **8** with a wide range of substitutions at positions 2-, 4- and 5- and furothiazolones **9** respectively. These compounds exhibited antibacterial activity towards two Gram negative (*Proteus mirabilis* and *Serratia marcescens*) and two Gram positive (*Staphylococcus aureus* and *Bacillus cereus*) bacteria, anti-inflammatory activity, inhibition of the carrageenin-induced oedema, and are considered as antimalarial candidates through inhibition of PfENR protein pathway to kill *Plasmodium falciparum*.^{57,69}



2. 1. 7. From Various Thiourea Derivatives

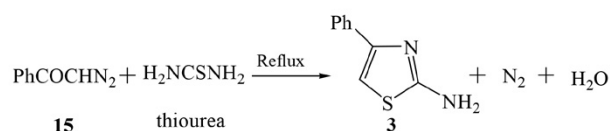
Cyclization reaction of haloketones **4** and/or dihaloketones **13** with various thiourea derivatives afforded the 2-amino-4-substituted-thiazole derivatives **10–12**,

where upon a [5,5]-sigmatropic shift of *N*-phenyl-*N'*-(2-thiazolyl)hydrazines and *N,N'*-bis(2-thiazolyl)hydrazines an acid-catalyzed, benzidine-type rearrangements yielded 2-amino-5-(*p*-aminophenyl)thiazoles **12** and 5,5'-bis(2-aminothiazole)derivatives **14**, respectively.⁷⁰

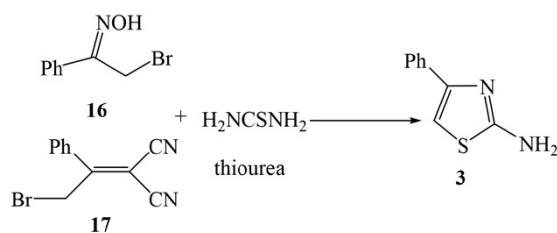


2. 2. From Various Acetophenone Derivatives

Diazoacetophenone **15** was reacted with thiourea to furnish 2-amino-4-phenyl thiazole **3**. The reaction has been affected either by heating an intimate mixture of the reactants on the steam bath, or by refluxing an ethanol solution of the reaction components.⁷¹

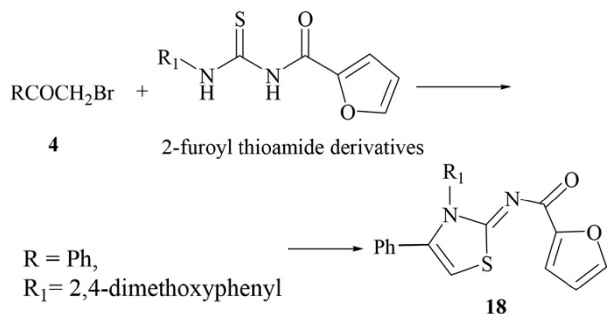


Bromoacetophenoneoxime **16** and 2-bromo-1-phenylethylidenemalononitrile **17** were reacted with thiourea to give 2-amino-4-phenyl thiazole **3**. The ring closure has been accompanied by the elimination of hydroxylamine⁷² or malononitrile,⁷³ respectively.

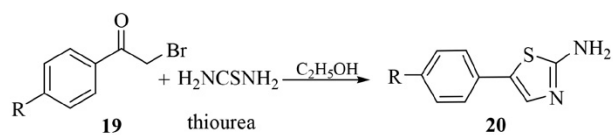


Cyclocondensation of bromoacetophenone with 2-furoyl thioamide derivatives in diluted acetic acid, gave

a series of 2-amino-5-benzoyl-4-(2-furyl)thiazoles **18**. The synthesized derivatives were screened for *in vitro* anti-tubercular activities against *Mycobacterium tuberculosis* H37Rv using the Microplate Alamar Blue Assay (MABA), for antibacterial activities with agar dilution method against clinical *Staphylococcus aureus*, *Escherichia coli*, *Streptococcus pneumoniae* and penicillin-resistant *Streptococcus pneumoniae*,⁷⁴ and exhibited excellent affinity for A_{2A} receptor as well.⁷⁵

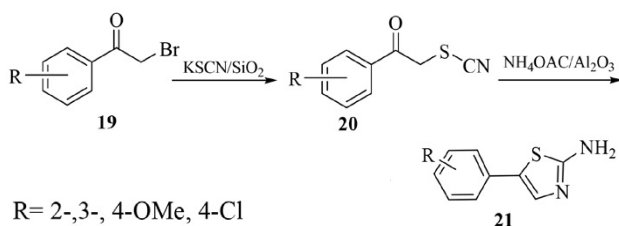


Reaction of haloketophenoxybenzene derivative **19** with thiourea gave the 2-amino-5-[4-(4'-nitrophenoxy)phenyl]thiazole (APPT) **20**. Additionally, a series of novel polyimides were prepared by polycondensation of APPT with various aromatic dianhydrides *via* one-step process and multi heterocyclic Schiff bases were also prepared as anticancer agents against human breast, colon and prostate cell lines. Also, the resulting polyimides have high *T_g* values, excellent thermal and thermo-oxidative stability, as well as good solubility in organic solvents. They had good mechanical properties with low dielectric constants, which are preferred in microelectronics applications.^{58,76–79}



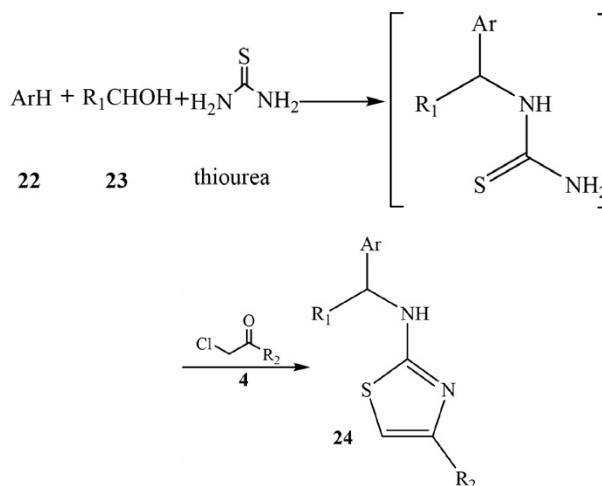
R = 2-,4-nitrophenoxy, imidazolyl

The reaction of bromomethoxyacetophenone derivatives **19** with potassium thiocyanate in dry benzene afforded 2-thiocyanoacetophenones **20**, which underwent cyclization in the presence of alumina-supported ammonium acetate to give 2-aminothiazole analogues **21** as described by Kodomari *et al.* The synthesized compounds exhibited potent and selective human adenosine A3 receptor antagonists.⁸⁰



2. 3. From Aldehydes

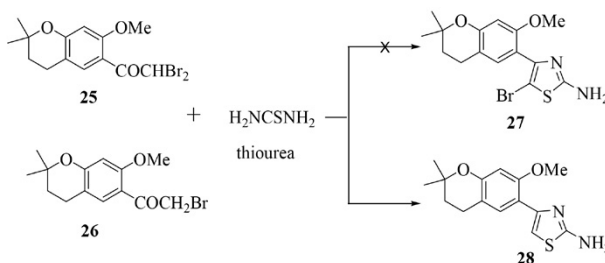
A tandem Aza-Friedel–Crafts reaction/Hantzsch cyclization is described to access various polysubstituted 2-amino-1,3-thiazoles **24** from condensation of thiourea with electron-rich (hetero)aromatic rings **22**, aldehydes **23** and α -chloroketones **4**.⁸¹



Ar = fused aryl and/or heteryl rings
 R₁ = aliphatic and aromatic substrates
 R₂ = aliphatic and aromatic substrates

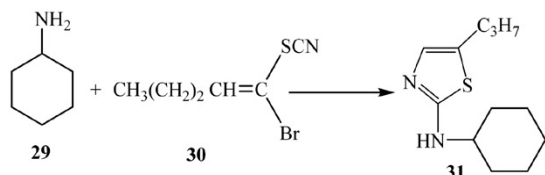
2. 4. From Chroman Derivatives

Instead of the expected product 2-amino-4-(2,2'-dimethyl-7'-methoxychroman-6'-yl)-5-bromothiazole **27**, the product obtained by the condensation of 6-dibromoacetyl-2,2-dimethyl-7-methoxychroman **25** with thiourea was 2-amino-4-(2,2'-dimethyl-7'-methoxychroman-6'-yl)thiazole **28**. This product could be also obtained by the condensation of 6-bromoacetyl-2,2-dimethyl-7-methoxychroman **26** with thiourea. The products obtained were physically applied to a polyurethane varnish as biocide additives. Their anti-microbial activity, against the targeted microorganisms, increases with an increase in the levels of the biocide additive.^{82,83}



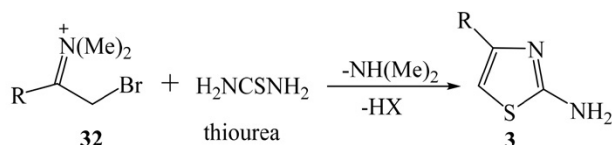
2. 5. From Amines

Action of primary amines on halo-thiocyanato alkenes afforded the 2-amino-1,3-thiazoles, the cyclization taking place with a migration of the sulphur atom on the C=C bond; thus 2-cyclohexylamino-5-propyl-1,3-thiazole **31** was obtained from the condensation of cyclohexylamine **29** and (Z)-bromo-1-thiocyanato-1-pentene **30**.⁸⁴



2. 6. From Imine Derivatives

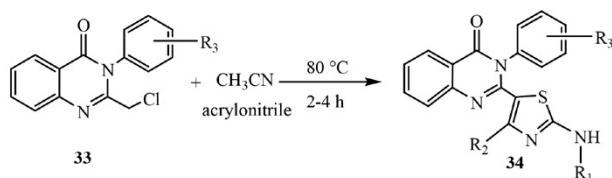
Halo-methyl ketimines **32** (X = Br, Cl) have been condensed with thiourea in methanol to afford 2-amino-4-substituted thiazoles **3**, whereas the *N*-isopropyl moiety had been lost during the condensation of the halo-ketimines.⁸⁵



R = *t*-Bu, Ph, 4-MeC₆H₄

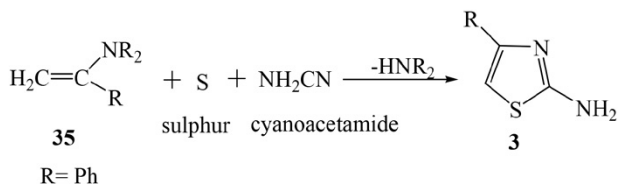
2. 7. From Nitriles

A series of 2-(2,4-disubstituted-thiazole-5-yl)-3-aryl-3*H*-quinazolin-4-one derivatives **34** were designed and synthesized by reaction of active α -halo derivative **33** of substituted quinazolinone with acetonitrile, where the products exhibited selective and dual inhibition against NF-KB, AP-1 mediated transcriptional activation and significant efficiency in the *in vivo* models of inflammation.⁸⁶



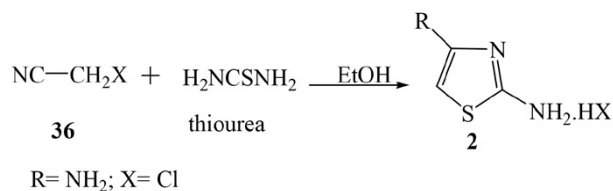
R₁ = methyl, phenyl, *p*-chlorophenyl, *p*-CH₃, phenyl
R₂ = CH₃, Ph, NH₂
R₃ = H, Cl, CH₃, OCH₃, COCH₃

Enamines of the type **35** were reacted with elementary sulphur and cyanamide at room temperature without catalyst to give the corresponding 2-amino-4-substituted thiazoles **3**.⁸⁷



R = Ph

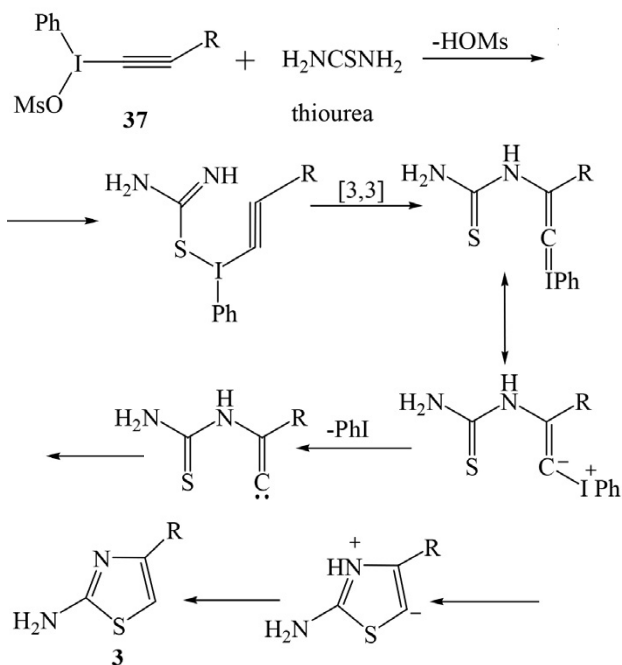
The condensation of thiourea and halogeno-nitriles to form salts of 2,4-diaminothiazole is a general reaction, which is, however, limited by the inactivity of the halogens in some substituted nitriles, *e.g.* chloroacetonitrile **36** reacts with thiourea in cold ethanol to give the halogenated salt of 2-halogenated amino-4-substituted thiazole derivative **2**.⁸⁸



R = NH₂; X = Cl

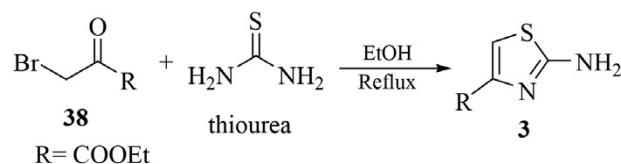
2. 8. From Alkynes

The formation of 2-amino-4-substituted thiazoles **3** (R = C₄H₉, C₆H₅) in a single reaction step from alkynyl(phenyl) iodoniummesylates **37** and thiourea can be rationalized mechanistically by a thiophilic attack of the hypervalent iodine atom on the sulphur atom of the thiocarbonyl group.⁸⁹



2. 9. From Esters

Condensation reaction of bromo ester compound **38** and thiourea in ethanol under reflux afforded the corresponding 2-amino-4-substituted thiazole **3** (R = COOEt), where the prepared compound was a precursor for the synthesis of antiproliferative active compounds in a panel of lung cancer cell lines.⁹⁰



R = COOEt

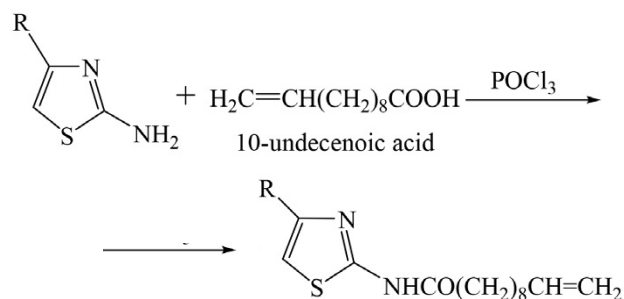
3. Reactions and Chemistry

3. 1. Reactions Involving the Amino Group

3. 1. 1. Acylation by Carboxylic Acids

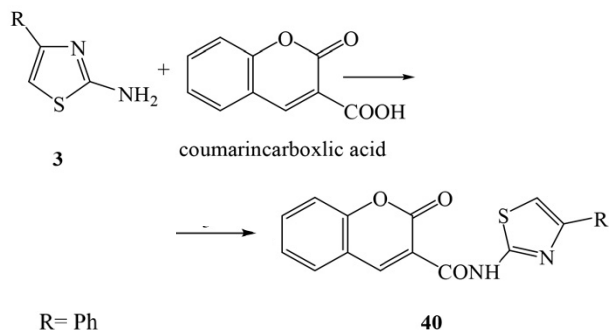
2-Amino-4-substituted thiazoles **3** have been condensed with 10-undecenoic acid in the presence of phos-

phorous oxychloride to afford the corresponding acid amide derivatives **39**.⁵³



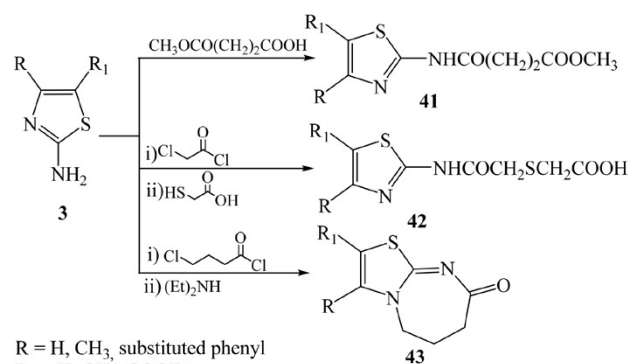
R = Me, Ph, 4-MeOC₆H₄, 4-Cl-C₆H₄

The coumarin carboxamide derivatives **40** have been prepared from the corresponding coumarincarboxylic acid and 2-amino-4-substituted thiazoles **3**. The compounds have been tested for anti-fungal and antibacterial activity.⁹¹



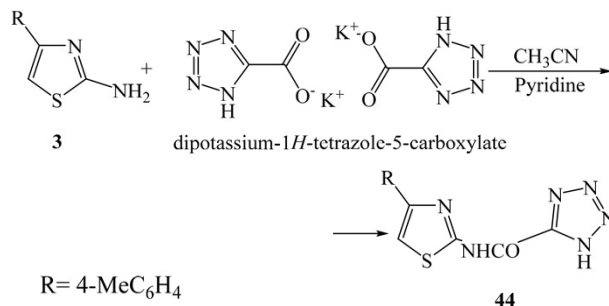
R = Ph

Condensation reaction of 2-aminothiazole derivatives with various types of carbonyl compounds afforded different thiazols, where 2-amino-4,5-disubstituted thiazoles **3** (R = substituted phenyl; R₁ = H, CH₃) condensed with 4-methoxy-4-oxobutanoic acid, 2-chloroacetyl chloride followed by mercaptoacetic acid and/or 4-chlorobutanoyl chloride to form the thiazole based derivatives **41**, **42** and **43**, respectively. The products were considered as lipid carriers having a significant role in the metabolic syndrome in A-FABP/ap2-deficient mice, including type 2 diabetes, atherosclerosis and anticonvulsant gradients.^{92,93}



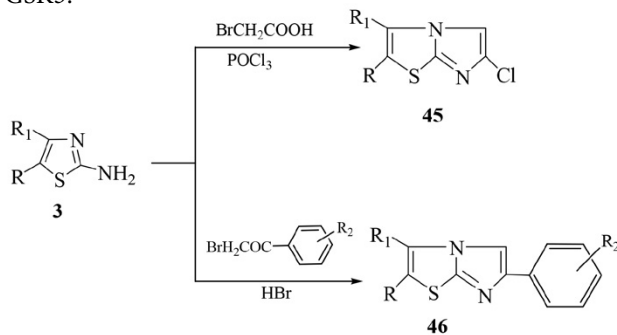
R = H, CH₃, substituted phenyl
R₁ = H, CH₃, COOEt

The 2-amino-4-substituted thiazole tetrazole derivatives **44** have been prepared by the treatment of 2-amino-4-substituted thiazoles **3** with a suspension of dipotassium-1*H*-tetrazole-5-carboxylate in acetonitrile containing pyridine. Compounds **44** exhibited inhibition of anti-passive cutaneous anaphylaxis in rats.⁹⁴



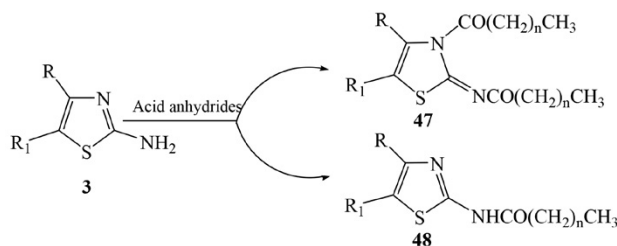
R = 4-MeC₆H₄

Imidazo[2,1-*b*]thiazoles **45** and **46** were synthesized through the reaction of 2-aminothiazoles **3** with different acid derivatives. The study of the synthesized compounds indicated a high degree of selectivity for inhibition of RSK2 compared to a spectrum of other related kinases, resulting in selective inhibition of the MCF-7 breast tumor cell line, as well as selective inhibition of the biomarker GSK3.⁹⁵

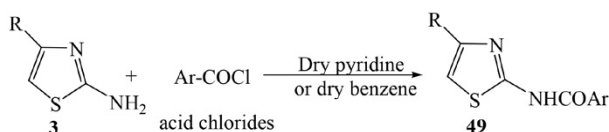


3. 1. 2. Acylation by Acid Anhydrides

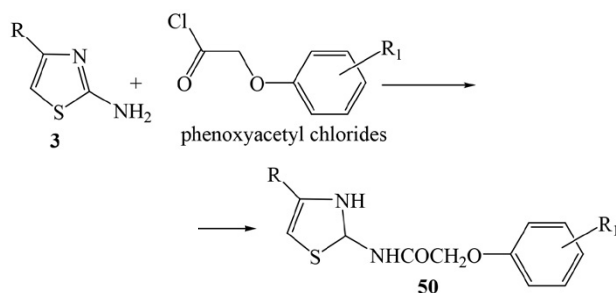
Depending on the reaction conditions, 2-amino-4-substituted thiazoles **3** underwent acylation by acid anhydrides, *e.g.* acetic anhydride, propionic anhydride and butyric anhydride, to give the corresponding 3-acyl-2-acylimino-2,3-dihydrothiazoles **47** (R = Ph; R₁ = 4-NO₂; Ar = 4-(Et₂O)₂POCH₂C₆H₄, n = 1, 2, 3) or *N*-(2-thiazolyl) amides **48** (R = Ph, substituted phenyl, β-naphthyl, 2-thienyl; R₁ = H; n = 1, 2, 3). The target derivatives were found to be useful for the treatment of hyperlipidemia, cataracts, diabetes and as antikinoplastid parasite compounds.^{2,96,97}



pared thiazole-amide skeleton exhibited antibacterial activity.⁹⁸

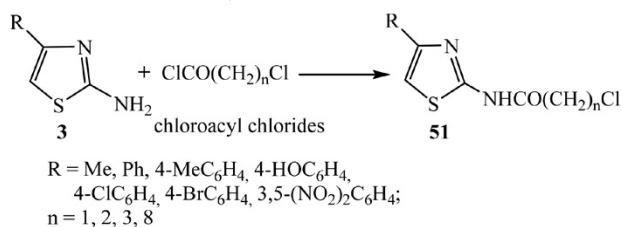


The acylamino derivatives **50** (R = Me, Ph; R₁ = H, Cl, Me, NO₂), had been prepared by the reaction of phenoxyacetyl chloride derivatives with 2-amino-4-substituted thiazoles **3** and tested in the rat passive cutaneous anaphylaxis (PCA) assay by oral administration.^{53,99}



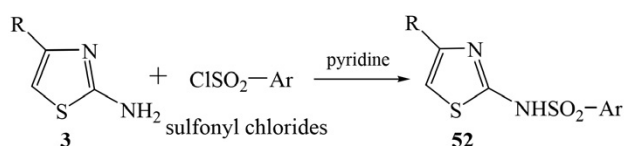
3. 1. 4. Acylation by Chloroacyl Chlorides

2-Amino-4-substituted thiazoles **3** had been reacted with chloroacyl chlorides to give the corresponding 2-(chloroacylamino)-4-substituted-thiazoles **51** showing significant antifungal activity against *Candida albicans*.^{24,100–102} Microwave heating technique was used to prepare optically active thiazole-bearing diamine derivatives **51** (R = 3,5-(NH₂)₂C₆H₄).^{103,104}

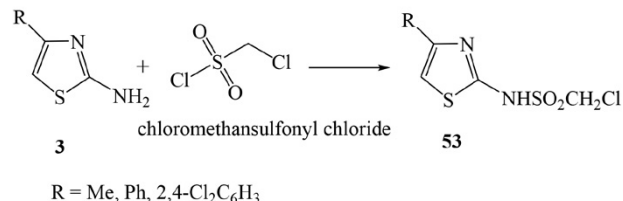


3. 1. 5. Reaction with Aryl Sulfonyl Chlorides

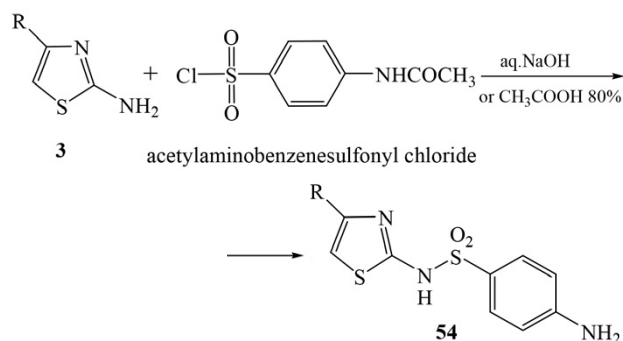
2-Amino-4-substituted thiazoles **3** were reacted with the appropriate sulfonyl chlorides in pyridine to furnish a series of 2-sulfonamido-thiazoles (R = Me, Ph, substituted phenyl; Ar = Ph, substituted phenyl, 4-acetylamino-1-naphthyl, 2-arylnaphth[1,2-*d*]oxazol-5-yl) **52**. The compounds **52** had been evaluated as inhibitors of rat kidney kynurenine 3-hydroxylase using L-[3-³H] kynurenine as the substrate.^{105,106}



2-Amino-4-substituted thiazoles **3** were reacted with chloromethansulfonyl chloride to yield the corresponding C-chloro-N-(2-thiazolyl)methane sulfonamides **53**.¹⁰⁷

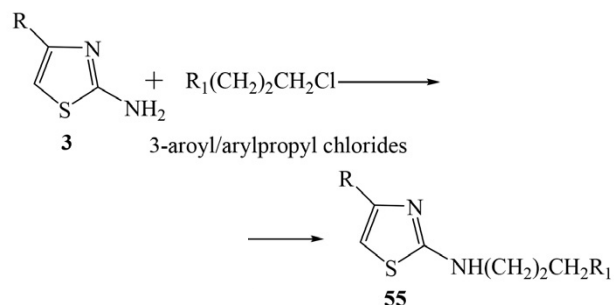


Sulfanilamidothiazoles **54** (R = C₆H₅, 4-BrC₆H₄, 4-MeOC₆H₄, 2,5-(MeO)₂C₆H₃, 2,4-Cl₂-C₆H₃, 2-naphthyl) were synthesized by acylation of 2-amino-4-substituted thiazoles **3** with 4-acetylamino-benzenesulfonyl chloride followed by deacetylation by heating in aqueous NaOH or 80% CH₃COOH.¹⁰⁸



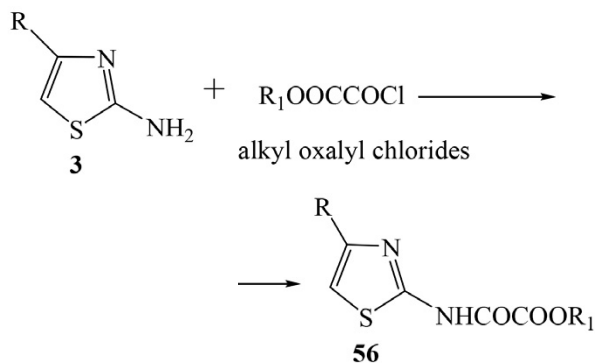
3. 1. 6. Reaction with Alkyl Halides

The 2-(3-aryloxy/arylpropyl)amino-thiazoles **55** (R = Ph; R₁ = 2-thienylcarbonyl, PhCO, 4-PhC₆H₄) had been synthesized from the appropriate 3-aryl/arylpropyl chlorides and 2-amino-4-substituted thiazole **3**.¹⁰⁹



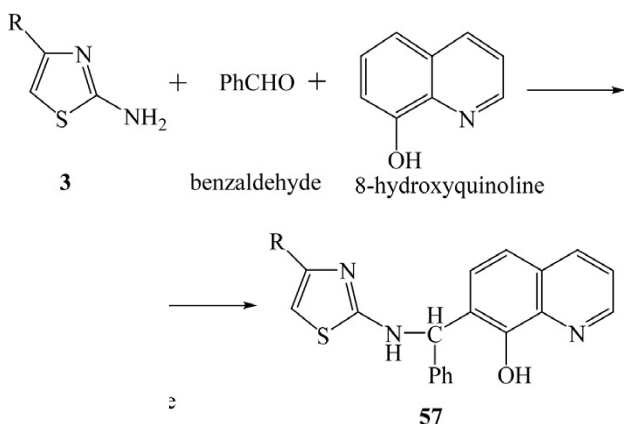
3. 1. 7. Reaction with Chloroxamates

Thiazolyloxamates of the structure **56** (R = Ph, substituted phenyl, biphenyl, cyclohexylphenyl, naphthyl, 2-pyridylmethyl, pentyl; R₁ = lower alkyl, PhCH₂) had been prepared from 2-amino-4-substituted thiazoles **3** by their reaction with alkyl oxalyl chlorides. Compounds **56** were screened for their antiallergic activity in the rat passive cutaneous-anaphylaxis assay.^{53,109–111}

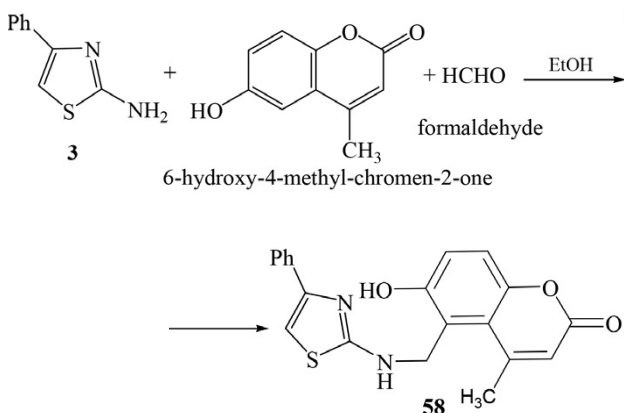


3. 1. 8. Mannich Reaction

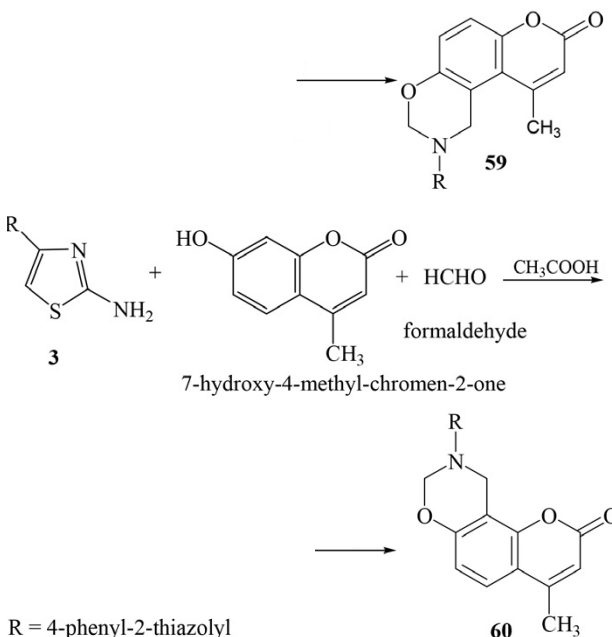
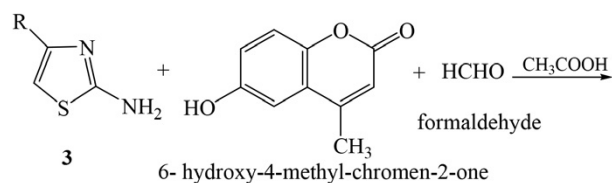
Mannich reaction is known by its occurrence at aromatic amines, aldehydes, and 8-hydroxyquinolines giving the biologically active 7-substituted-8-hydroxyquinoline derivatives. Several researchers have extended this reaction to different heterocyclic amines. Thus, 2-amino-4-substituted thiazoles **3** were condensed with benzaldehyde and 8-hydroxyquinoline to give a series of Mannich bases **57**.⁵³



2-Amino-4-phenylthiazole **3** was reacted with 6-hydroxy-4-methylchromen-2-one and formaldehyde in ethanol affording the expected Mannich product 6-hydroxy-4-methyl-5-[(4-phenyl-2-thiazolylamine)-methyl]-chromen-2-one **58**.¹¹²

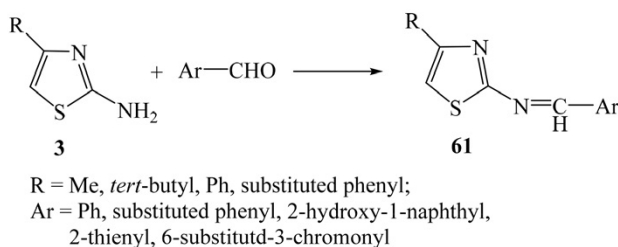


The reaction of 2-amino-4-substituted thiazoles **3** with 6-hydroxy-4-methylchromen-2-one and/or 7-hydroxy-4-methylchromen-2-one and formaldehyde in acetic acid gave the corresponding chromeno-[1,3]oxazinone **59** and/or **60**, respectively.¹¹²



3. 1. 9. Reaction with Aldehydes

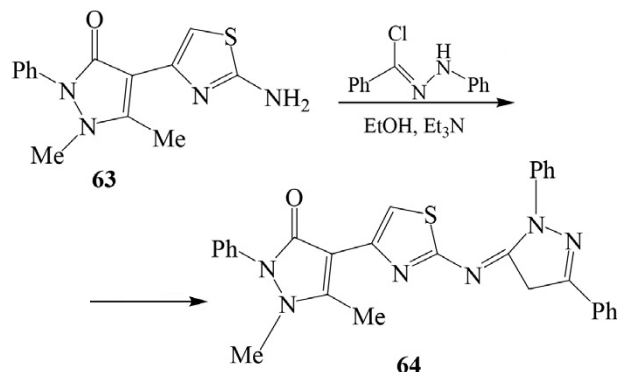
2-Amino-4-substituted thiazoles **3** underwent condensation with different aromatic or heterocyclic aldehydes to give the corresponding Schiff's thiazole bases **61**, which were used to develop **fluorescence chemosensors for detection of Al^{3+}** ions at low concentration range.^{113–118}



3. 1. 10. Reaction with Hydrazonoyl Chlorides

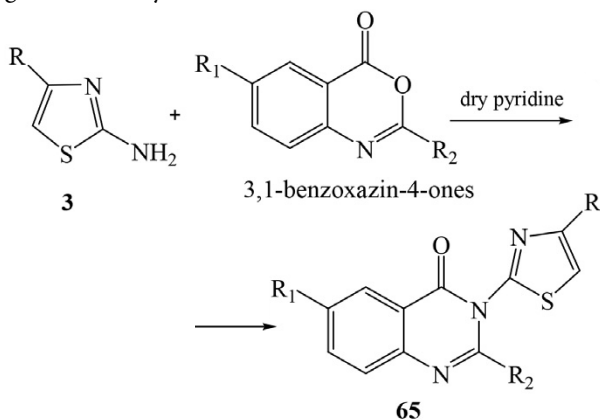
N-(4-(Pyrazol-4-yl)thiazol-2-yl)-*N'*-phenylthiourea derivative **62** was synthesized and then treated with a variety of hydrazonoyl chlorides under basic conditions to afford the corresponding 2-(4-(pyrazol-4-yl)thiazol-2-ylimino)-1,3,4-thiadiazole derivatives **63**. Most of the synthe-

sized compounds were tested for anticancer activity against human hepatocellular carcinoma HepG2, human breast cancer MCF-7 and human lung cancer A549.¹¹⁹



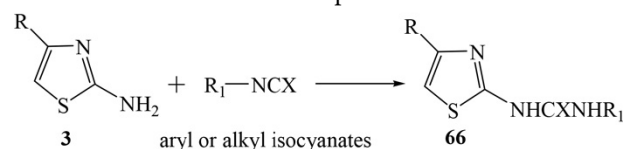
3. 1. 11. Reaction with 3,1-Benzoxazin-4-ones

Condensation of 2-amino-4-substituted thiazoles **3** with substituted 3,1-benzoxazin-4-ones in dry pyridine gave the corresponding thiazolylquinazolones **65** (R = Ph, substituted phenyl, Et, Me₂CHCH₂, thienyl; R₁ = H, Br; R₂ = Me, Ph). The antimicrobial activities of these compounds against a variety of microbes have been determined.¹²⁰



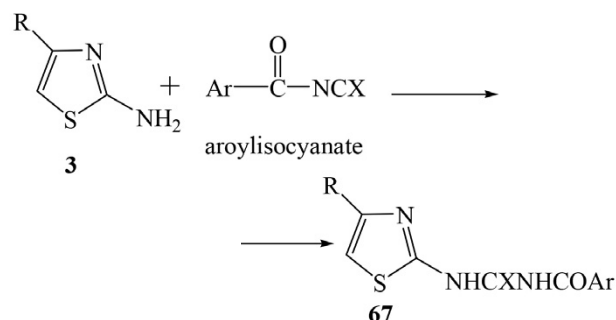
3. 1. 12. Reaction with Nitriles

The 2-amino-4-substituted thiazoles **3** upon reaction with aryl or alkyl isocyanates gave *N*-aryl/alkyl-*N'*-(2-thiazolyl)ureas **66** (R = Ph, 2-pyridyl; R = butyl, cyclohexyl, Ph, 4-ClC₆H₄, 4-MeOC₆H₄, 3,5-(MeO)₂C₆H₃, PhCH=CH; X = O).^{121–123} Also a number of *N*-substituted-*N'*-(4-aryl-2-thiazolyl) thiocarbamides **66** (R = Ph, substituted phenyl; R₁ = Et, PhCH₂, Ph, substituted phenyl, tetra-*O*-acetyl-β-*D*-glucopyranosyl; X = S) had been similarly synthesized as antitubercular compounds.^{124–127}

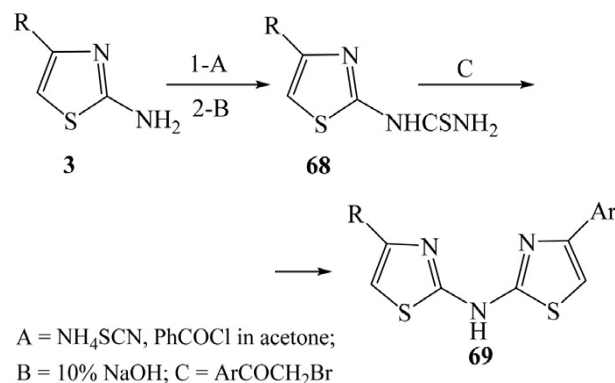


A series of aroylurea and/or thiourea derivatives **67** had been prepared by the reaction of 2-amino-4-substitut-

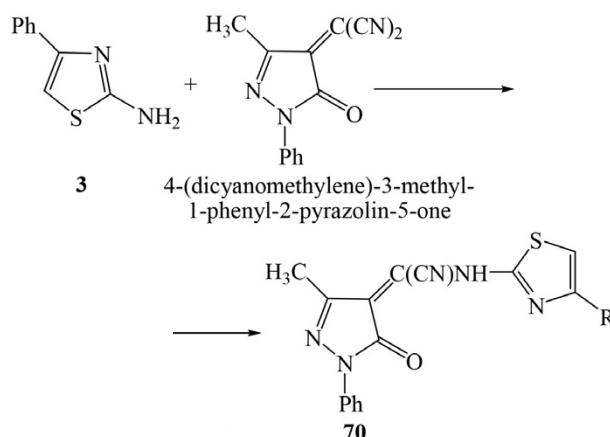
ed thiazoles **3** with aroylisocyanate and/or isothiocyanate, respectively. These products have also been tested for insecticidal, fungicidal and herbicidal activities, where the 2-amino-4-substituted thiazolyl derivatives **67** (R = CF₃, Me, Ph; Ar = 2-BrC₆H₄, Ph) showed the highest insecticidal activity.^{128,129}



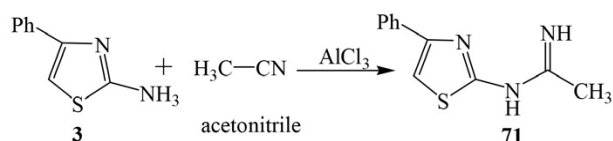
N-(4-Aryl-2-thiazolyl)thioureas **68** (R = C₆H₅, 4-MeOC₆H₄, 4-ClC₆H₄) have been synthesized by the reaction of 2-amino-4-substituted thiazoles **3** with ammonium thiocyanate and benzoyl chloride in dry acetone, followed by alkaline hydrolysis with 10% NaOH. Further condensation of **68** with phenacyl bromides proceeded in ethanol to give the dithiazol-2-ylamines **69** (R = C₆H₅, 4-MeOC₆H₄, 4-ClC₆H₄; Ar = Ph, substituted phenyl). The synthesized compounds exhibited antiinflammatory activity.¹³⁰



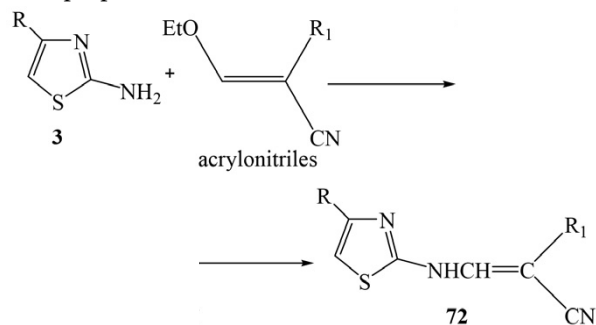
2-Amino-4-phenylthiazole **3** has been condensed with 4-(dicyanomethylene)-3-methyl-1-phenyl-2-pyrazolin-5-one to afford the pyrazolinone derivatives **70**.¹³¹



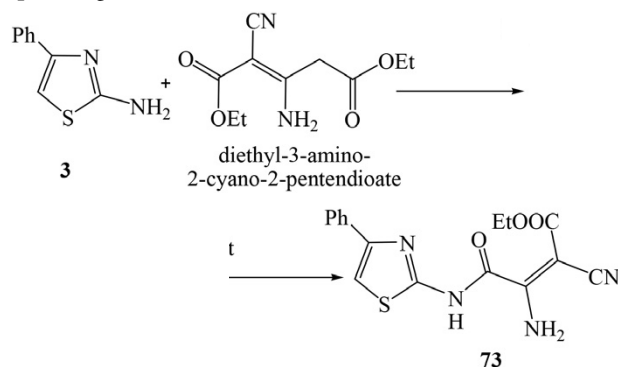
N-(4-Phenyl-2-thiazolyl)acetamide **71** has been obtained from the reaction of 2-amino-4-substituted thiazole **3** with acetonitrile in the presence of anhydrous aluminum chloride.¹³²



2-Amino-4-substituted thiazoles **3** had been reacted with acrylonitrile derivatives (R = alkyl, alkenyl, alkynyl, alkoxy, alkenoxy, alkylsulfonyl, cycloalkyl; R₁ = CN, 1*H*-tetrazol-5-yl)inethoxide-ethanol to give 2-thiazolyl-amino-propenenitriles **72**.⁵³

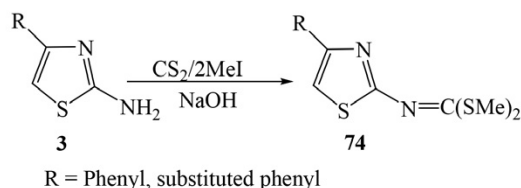


2-Amino-4-phenylthiazole **3** was reacted with diethyl 3-amino-2-cyano-2-pentendioate to yield the corresponding amide derivatives **73**.¹³³



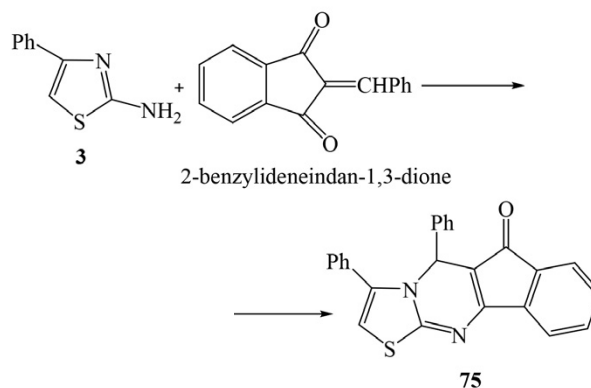
3. 1. 13. Reaction with Carbon Disulphide and Methyl Iodide

The reaction of 2-amino-4-substituted thiazoles **3** with carbon disulphide and methyl iodide in the presence of concentrated aqueous NaOH gave the corresponding dimethyl-*N*-(4-aryl-2-thiazolyl)dithiocarbonimidates **74**.¹³⁴



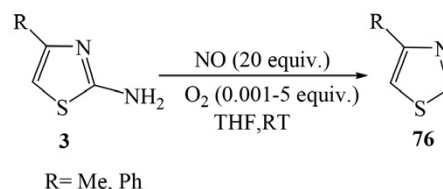
3. 1. 14. Reaction with α,β -Unsaturated Compounds

Thiazoline-pyrimidinyl compound **75** was prepared by the condensation of 2-amino-4-phenylthiazole **3** with 2-benzylideneindan-1,3-dione.¹³⁵

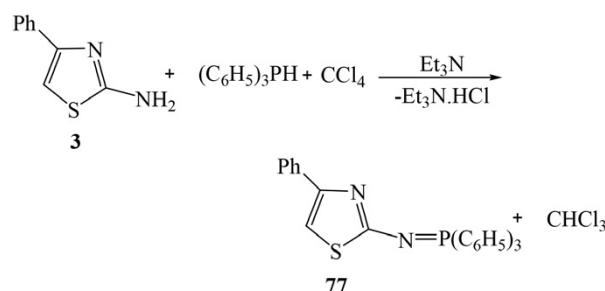


3. 1. 15. Miscellaneous Reactions

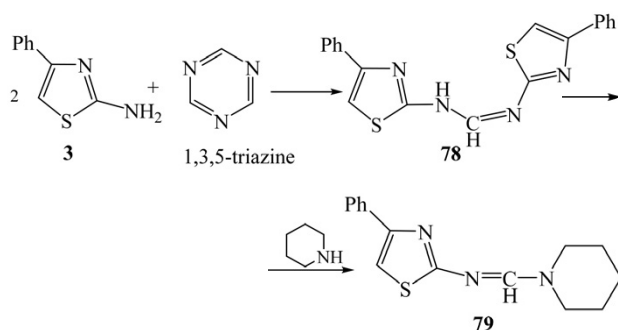
2-Amino-4-substituted-thiazoles **3** had been readily deaminated using nitric oxide (NO) in the presence of catalytic amount of oxygen to afford the corresponding thiazoles **76**.¹³⁶



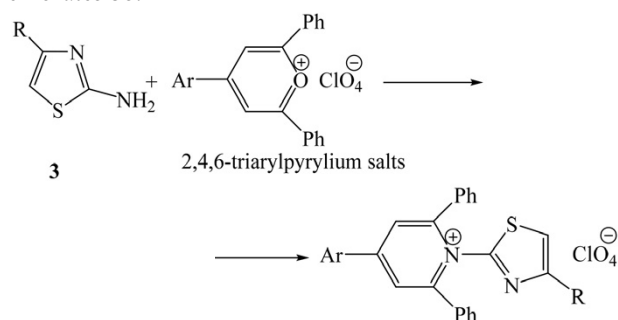
N- α -(4-Phenyl-2-thiazolyl)triphenylphosphinimine **77** was simply prepared by the reaction of 2-amino-4-phenylthiazole **3** with triphenylphosphine (TPP) in the presence of triethylamine (TEA) and carbon tetrachloride (CTC).¹³⁷



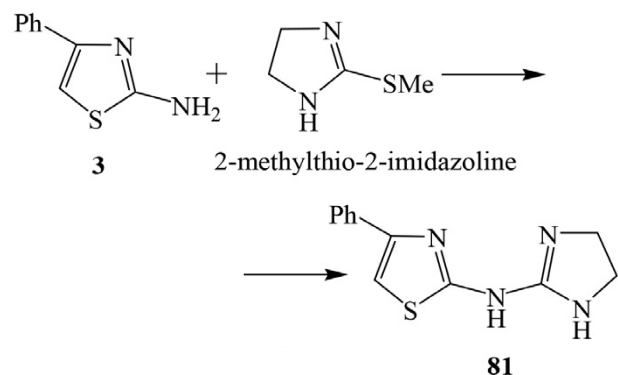
N,N'-Bis-(4-phenyl-2-thiazolyl)formamidine **78** was formed as a result of the reaction between 2-amino-4-phenylthiazole **3** with 1,3,5-triazazine. The intermediate **78** postulated for this reaction type could be identified in an interception reaction by means of secondary amines. As the prototype, the reaction of piperidine with the intermediate product to form 4-phenyl-*N*-((piperidin-1-yl)methylene)thiazol-2-amine **79** (having antibacterial activity) has been reported.¹³⁸



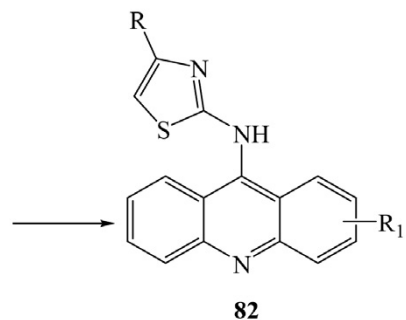
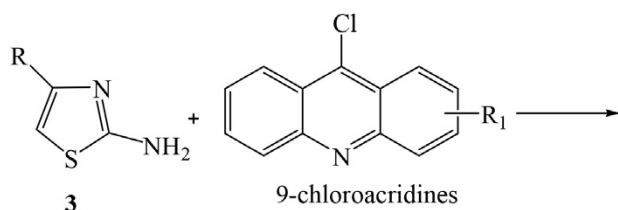
In the presence of an appropriate acid-binding agent (e.g. piperidine acetate or sodium acetate), 2-amino-4-substituted thiazoles **3** had been reacted with 2,4,6-triarylpyrylium salts *via* pyrylium ring transformation yielding 2,4,6-triaryl-1-(4-phenyl-2-thiazolyl)-pyridinium perchlorates **80**.¹³⁹



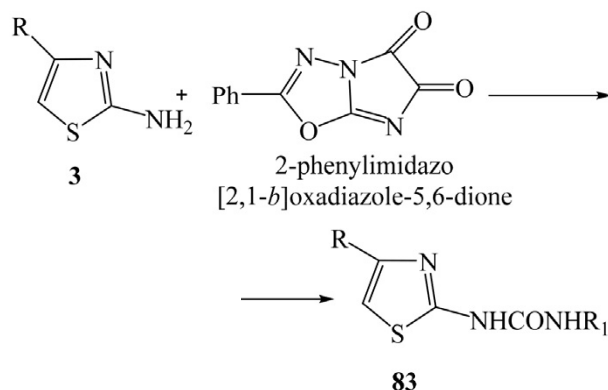
Imidazolines **81** have been prepared by the reaction of 2-methylthio-2-imidazoline with 2-amino-4-phenylthiazole **3** and exhibited bactericidal activity.¹⁴⁰



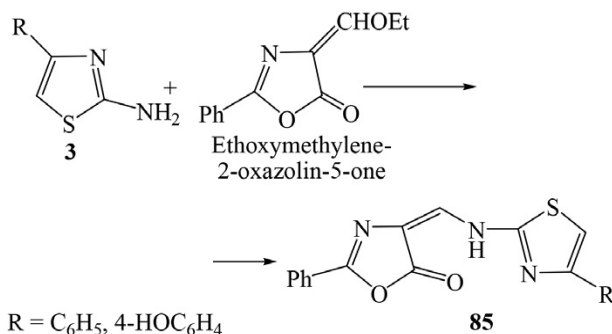
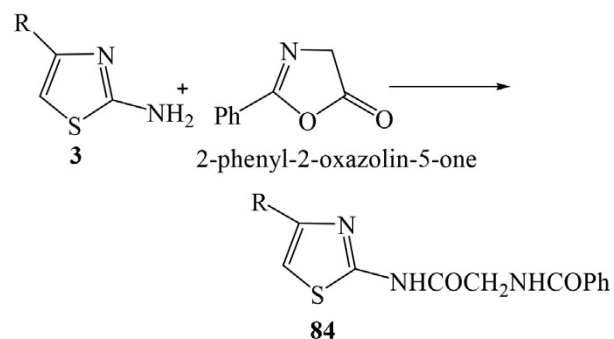
9-(4'-Phenyl-2'-thiazolylamino)acridine derivatives **82** ($R = \text{Ph}$; $R_1 = \text{H}$, 3-Cl, 1-Me, 3-Me) were prepared as fungicides by treatment of 2-amino-4-substituted thiazoles **3** with the corresponding 9-chloroacridines.¹⁴¹



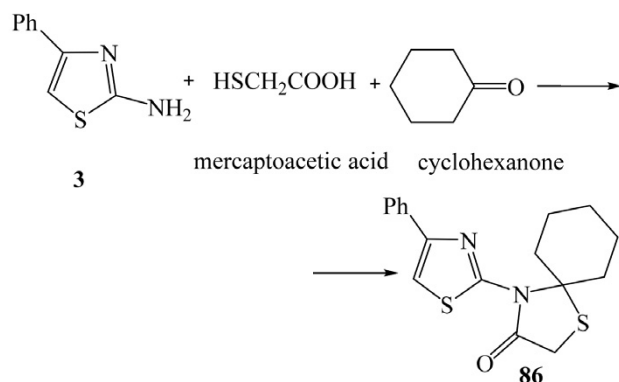
2-Amino-4-substituted thiazoles **3** as nucleophiles have been reacted with 2-phenylimidazo[2,1-*b*]oxadiazole-5,6-dione to give the urea derivatives **83** ($R_1 = 5$ -phenyl-1,3,4-oxadiazol-2-yl).¹⁴²



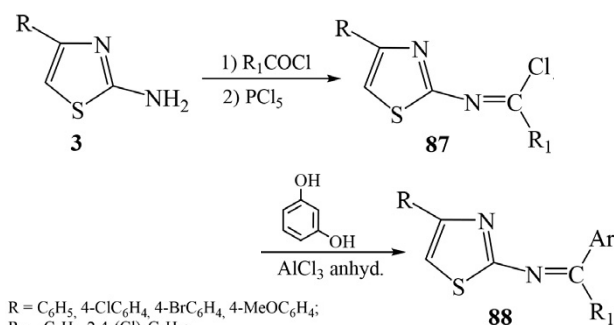
2-Amino-4-substituted thiazoles **3** have been reacted with 2-phenyl-2-oxazolin-5-one to give the corresponding hippurylaminothiazoles **84**. Ethoxymethylene-2-oxazolin-5-one on the other hand have been reacted with 2-amino-4-substituted thiazoles **3** to give the corresponding 4-(2'-thiazolylaminomethylene)-2-oxazolin-5-ones **85**.¹⁴³



4-(4'-Phenyl-2'-thiazolyl)-1-thia-4-azaspiro[4,5]decan-3-one **86** has been prepared by refluxing equivalent quantities of a mixture of cyclohexanone, mercaptoacetic acid and 2-amino-4-phenylthiazole **3** in benzene or toluene.⁵³



Synthesis of *N*-(4'-aryl-2'-thiazolyl)-2,2-diarylmethines **87** was carried out by acylation of 2-amino-4-substituted thiazoles **3** followed by chlorination of the produced amides with phosphorus pentachloride to form the imidochlorides **88**, which have been condensed with resorcinol in the presence of anhydrous aluminum chloride.⁵³



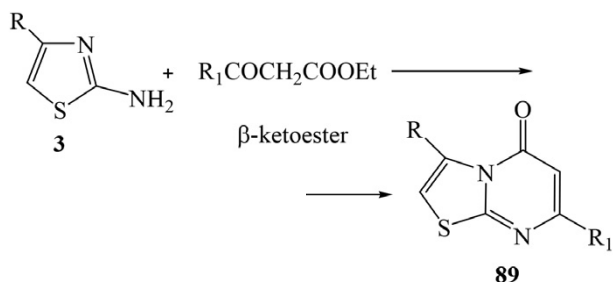
R = C₆H₅, 4-ClC₆H₄, 4-BrC₆H₄, 4-MeOC₆H₄;
 R₁ = C₆H₅, 2,4-(Cl)₂C₆H₃;
 Ar = 2,4-(HO)₂C₆H₃

3. 2. Cyclization Reactions

3. 2. 1. Formation of Thiazolopyrimidin-5-ones

3. 2. 1. 1. Reaction with β-Ketoester

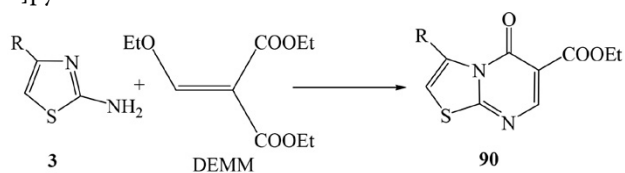
The 3,7-disubstituted-thiazolo[3,2-*a*]pyrimidin-5-ones **89** (R = Me, Ph, *p*-MeC₆H₄, *p*-ClC₆H₄; R₁ = Me, Ph and R = Me, Ph; R₁ = CH=CHR₂; R₂ = substituted and unsubstituted pyridyl) were obtained from the reaction of 2-amino-4-substituted thiazoles **3** with the corresponding β-ketoester.^{144–146}



3. 2. 1. 2. Reaction with Diethyl

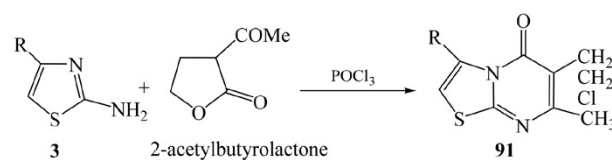
Ethoxymethylenemalonate

2-Amino-4-substituted thiazoles **3** were reacted with diethyl ethoxymethylenemalonate (DEMM) to furnish the corresponding 3-substituted-6-carbethoxy-thiazolo [3,2-*a*]pyrimidin-5-ones **90**.¹⁴⁴



3. 2. 1. 3. Reaction with 2-Acetylbutyrolactone

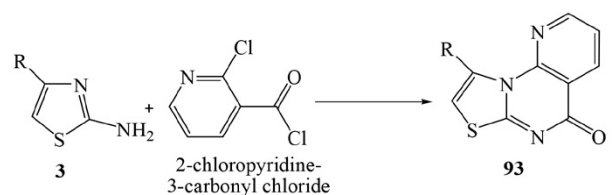
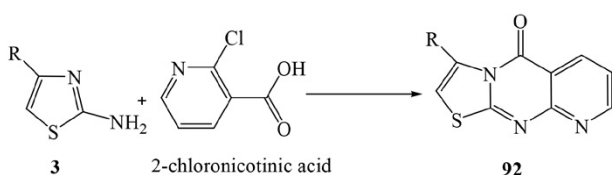
The reaction of 2-amino-4-substituted thiazoles **3** with 2-acetylbutyrolactone and phosphorus oxychloride gave 6-chloroethyl-7-methylthiazolo[3,2-*a*]pyrimidin-5-ones **91**. The synthesized compounds exhibited increased potency towards CNS SNB-75 and renal UO-31 cancer cell lines.¹⁴⁷



R = Ph optionally substituted by 1-2 of halo, C₁₋₄ alkyl, C₁₋₄-alkoxy and CF₃

3. 2. 1. 4. Reaction with Chloronicotinic Acids

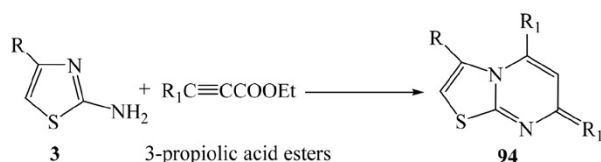
2-Amino-4-substituted thiazoles **3** were reacted with 2-chloronicotinic acid to furnish 3-aryl-5*H*-pyrido[2,3-*d*]thiazolo[3,2-*a*]pyrimidin-5-ones **92** (R = C₆H₅, 4-MeC₆H₄, 4-ClC₆H₄, 4-BrC₆H₄). The reaction of 2-amino-4-substituted thiazoles **3** with 2-chloropyridine-3-carbonyl chloride afforded 9-aryl-5-oxo-5*H*-pyrido[3';2';5,6]pyrimido[2,1-*b*]thiazoles **93** (R = C₆H₅, 4-MeOC₆H₄, 4-ClC₆H₄).¹⁴⁸



3. 2. 2. Formation of Thiazolo[3,2-*a*]pyrimidin-7-ones

3. 2. 2. 1. Reaction with Ethyl Propiolates

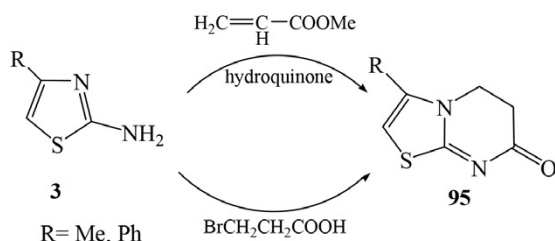
2-Amino-4-substituted thiazoles **3** were reacted with 3-substituted propiolic acid esters to give the corresponding 3,5-disubstitutedthiazolo[3,2-*a*]pyrimidin-7-ones **94**.^{149–151}



R = Me, Ph, 4-Cl-C₆H₄, 4-Br-C₆H₄, 4-MeO-C₆H₄, 4-O₂N-C₆H₄;
R₁ = H, Me, Ph, CH₂Cl, COOEt

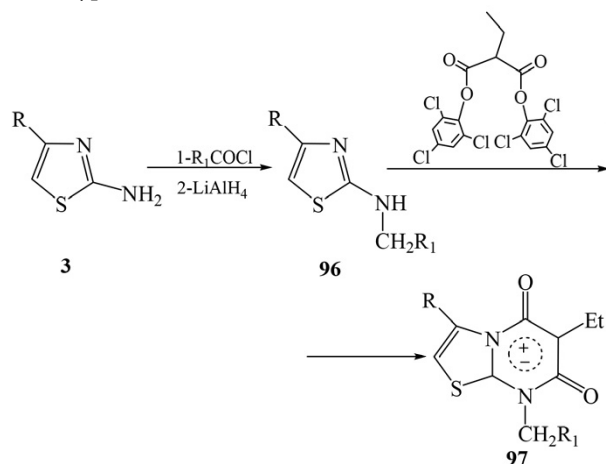
3. 2. 2. Reaction with Methyl Acrylate

2-Amino-4-substituted thiazoles **3** were reacted with methyl acrylate in the presence of hydroquinone or with bromopropionic acid to give 5,6-dihydrothiazolo[3,2-*a*]pyrimidin-7-ones **95**.¹⁵²



3. 2. 3. Formation of Pyrimidin-5,7-diones

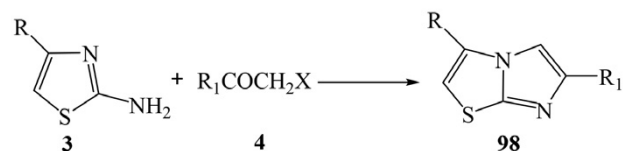
2-Alkylamino-4-phenylthiazoles **96** (R = Me, Ph; R₁ = Me, cyclopropyl) were prepared by acylation reaction of 2-amino-4-substituted thiazole **3**, followed by catalytic reduction. The products were precursor intermediates for the synthesis of the mesoionic thiazolo[3,2-*a*]pyrimidin-5,7-diones **97** obtained by thermal condensation with bis(2,4,6-trichlorophenyl)ethyl malonate and were showed to inhibit cyclic-AMP phosphodiesterase and displayed weak hypotensive effects *in vivo*.¹⁵³



3. 2. 4. Formation of Imidazothiazoles

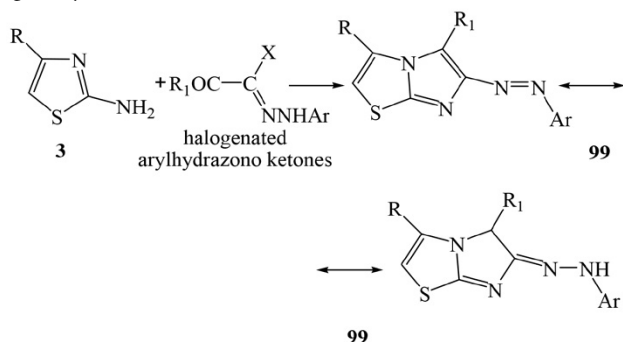
2-Amino-4-substituted thiazoles **3** were reacted with α -halocarbonyl compounds **4**, e.g. (un)substituted phenacyl bromides, *N,N*-disubstituted chloroacetamides, 2-bromoacetylchromones, 3-bromo-2-oxopropionic acid ethyl

ester, to give the corresponding 3,6-disubstituted-imidazo[2,1-*b*]thiazoles **98** with antiinflammatory and analgesic activities.^{90,154–156}

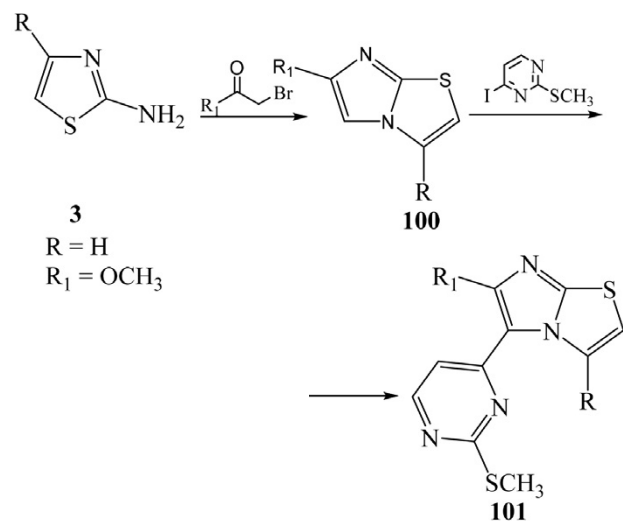


R = phenyl, substituted phenyl, -naphthyl, Me, COOEt;
R₁ = phenyl, substituted phenyl, Et₂NCl, EtHNCl, MeHNCl, C₆H₁₀NCl, substituted-6-chromonyl, COOEt;
X = Br, Cl

Equivalent amounts of 2-amino-4-substituted thiazoles **3** and the halogenated arylhydrazono ketones were refluxed in ethanol in the presence of triethylamine, affording 6-arylazo-3,5-disubstituted-imidazo[2,1-*b*]thiazoles **99** (R = Ph; R₁ = Me, OEt, Ph, substituted phenyl, heteroaryl; Ar = Ph, substituted phenyl; X = Cl, Br) in good yields.^{157,158}

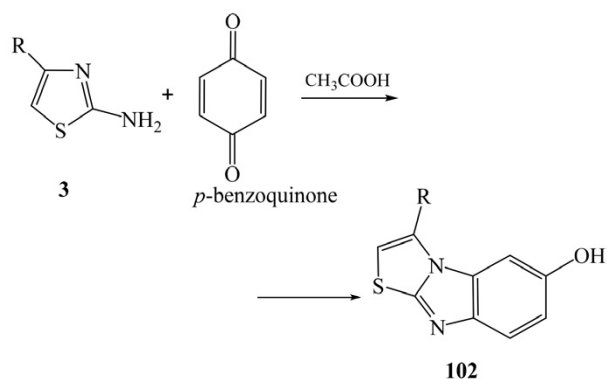


Reaction of 2-amino-4-substituted thiazoles **3** with 4-iodo-2-(methylthio)pyrimidine and oxone afforded a series of imidazo[2,1-*b*]thiazole derivatives **100** and **101**, respectively. The products showed potent activities against melanoma cell lines.¹⁵⁹



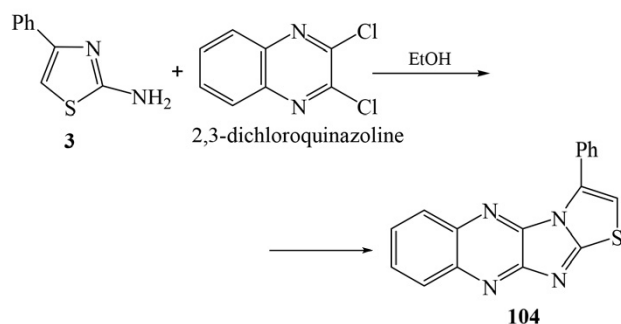
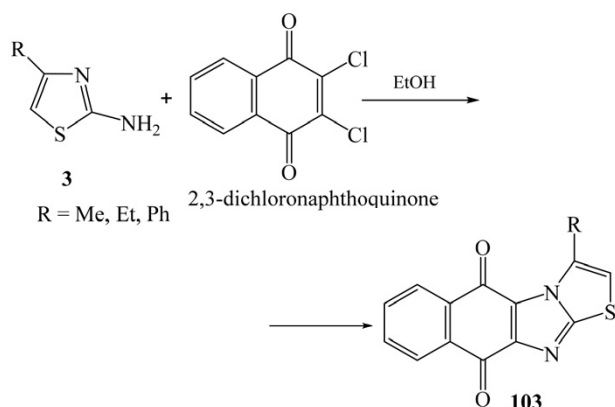
6-Hydroxy-3-substituted thiazolo[3,2-*a*]benzimidazoles **102** were synthesized by condensation of 2-amino

no-4-substituted thiazoles **3** with *p*-benzoquinone in acetic acid.¹⁶⁰

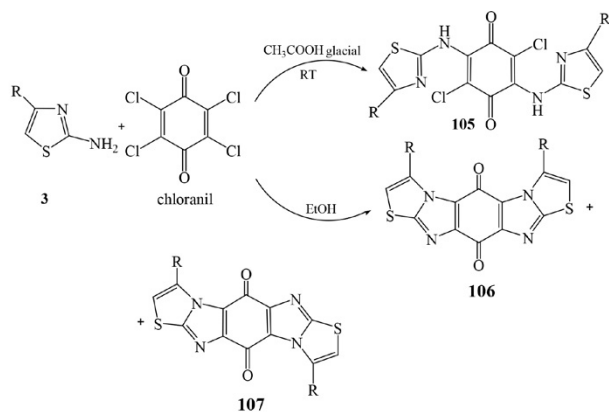


3. 2. 5. Formation of Thiazoloquinones and Quinazoline Derivatives

Thiazoloquinones **103** were obtained in 40–50% yield by refluxing 2-amino-4-substituted thiazoles **3** with 2,3-dichloronaphthoquinone in ethanol.¹⁶¹ Also, 2-amino-4-phenylthiazole was reacted with 2,3-dichloroquinazoline to give the quinazoline derivative **104**.⁵³

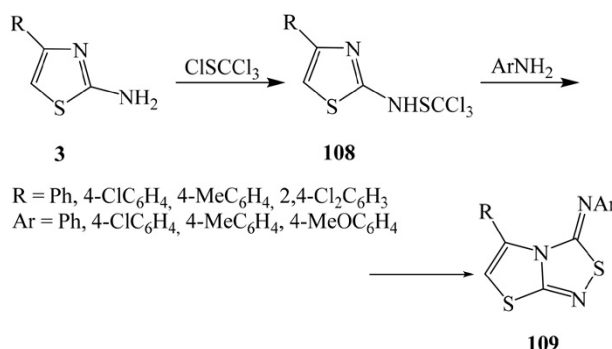


2-Amino-4-substituted thiazoles **3** were reacted with chloranil in glacial acetic acid at room temperature to give the corresponding 2,5-dichloro-3,6-bis(2'-thiazolylamino)-1,4-benzoquinone **105** ($\text{R} = \text{Me, Ph, 4-MeC}_6\text{H}_4, 4-\text{MeOC}_6\text{H}_4, 4-\text{ClC}_6\text{H}_4$).¹⁶² A mixture of **106** (*Z*-form) and **107** (*E*-form) was obtained by heating 2-aminothiazoles with chloranil in ethanolic medium.⁵³



3. 2. 6. Reaction with Aromatic Amines

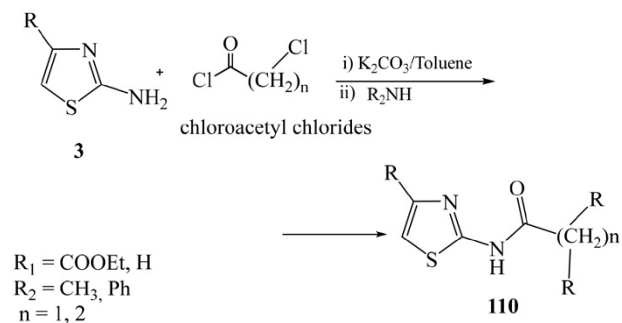
2-Amino-4-substituted thiazoles **3** were reacted at room temperature with perchloromethylmercaptan to give the corresponding 2-thiazolyl trichloromethanesulphenamides **108** which on treatment with aromatic amines afforded the 3,5-disubstituted-3*H*-thiazolo[2,3-*c*][1,2,4]thiadiazoles **109** with antibacterial activity.¹⁶³



3. 3. Nucleophilic Reactions

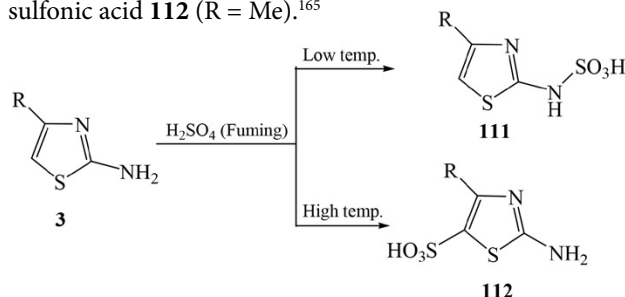
3. 3. 1. Reaction with Aliphatic and Aromatic Amines

A novel series of 2-acetamido and 2-propanamido derivatives of 4-substituted thiazoles **110** was designed and synthesized by the reaction of 2-amino-4-substituted thiazoles **3** with chloroacetyl chloride derivatives, followed by the reaction with secondary aromatic and/or aliphatic amines. The synthesized compounds were subjected to NCI *in vitro* assessment for their antitumor activity and remarkable GI values of 75.5, 69.3, 96.2 and 92.7% to the Leukemia CCRF-CEM cell line were determined.¹⁶⁴



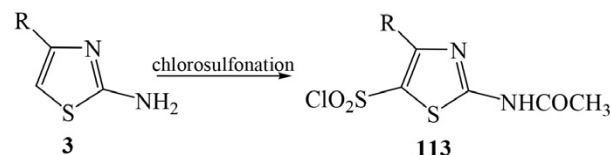
3. 3. 2. Sulphonation

Hurd and Karasch found out that fuming sulfuric acid converted the 2-amino-4-substituted thiazoles **3** to the corresponding 2-thiazolyl-sulfamic acids **111** (R = Me, Ph) at low temperatures, whereas at higher temperatures, the sulfamic acid was converted into an isomeric amino sulfonic acid **112** (R = Me).¹⁶⁵



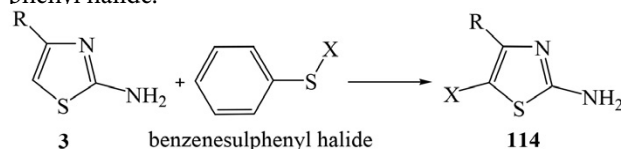
3. 3. 3. Chlorosulphonation

Acetylation of 2-amino-4-substituted thiazoles **3** followed by chlorosulphonation under controlled conditions gave 2-acetyl-amino-4-substituted-thiazole-5-sulfonyl chloride **113**.⁵³



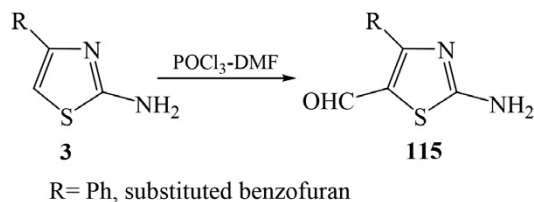
3. 3. 4. Halogenation

2-Amino-4-substituted thiazoles **3** gave the 2-amino-5-halothiazoles **114** (R = Me, Ph; X = Br, Cl) when subjected to the conditions of halogenation using benzenesulphenyl halide.^{166,167}



3. 3. 5. Formylation

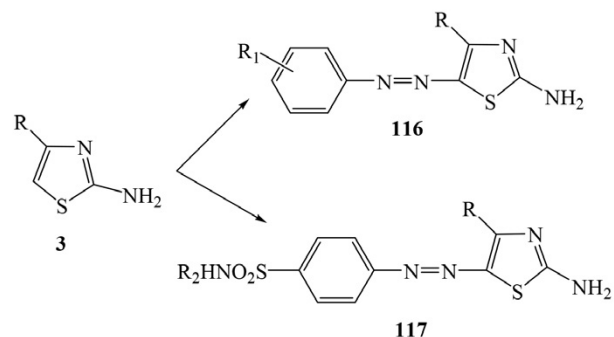
Vilsmeier–Haak formylation of 2-amino-4-substituted thiazoles **3** by POCl₃–DMF yielded the corresponding 5-formylthiazole **115** through electrophilic attack at C-5.¹⁶⁸



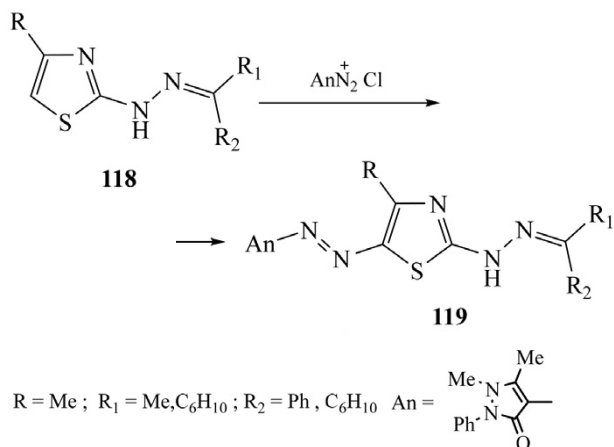
3. 3. 6. Azo Coupling Reactions

2-Amino-4-substituted thiazoles **3** underwent coupling reactions when treated with aromatic diazonium salts or diazotized sulphanilamides to give the corresponding 2-amino-5-arylazothiazoles **116** (R = Me, Ph, 4-ClC₆H₄; R₁ = H, Me, OMe, 4-Cl, 4-phenoxy, 4-(4-chloro-

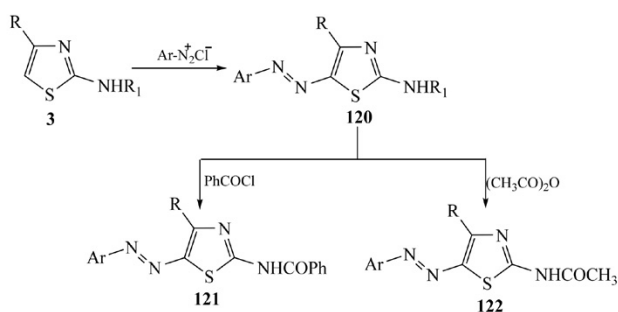
phenoxy) and/or **117** (R = Ph, substituted phenyl; R₂ = H, guanidino, 2-thiazolyl, 2-pyrimidyl and other heterocycles), respectively.^{169–171}



New antipyrynyl azo dyes of the type **119** were prepared by diazo coupling of 4-antipyrynyl diazonium chloride with 2-hydrazono-4-substituted thiazole derivatives **118**. These dyes showed high ability as disperse dyes for dyeing polyester fabrics with acceptable fastness properties.¹⁷²

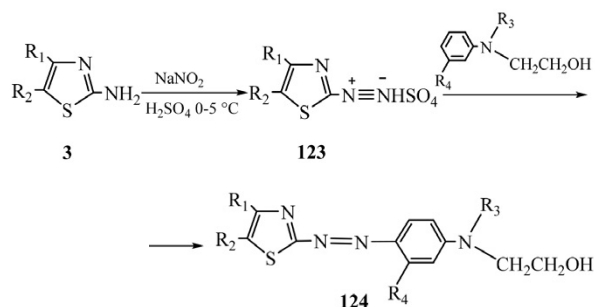


Diazotized aryl amines were coupled with 2-amino-4-substituted-thiazoles **3** to give 5-arylaazo-2-amino-thiazoles **120**, which on reaction with different reagents, such as benzoyl chloride and acetic anhydride yielded the corresponding 2-(N-benzoylamino)-5-arylazothiazole derivatives **121** and 2-(N-acetylamino)-5-arylazothiazole **122**. These mono azo dyes were applied to polyester as disperse dyes and their fastness properties were evaluated.⁷



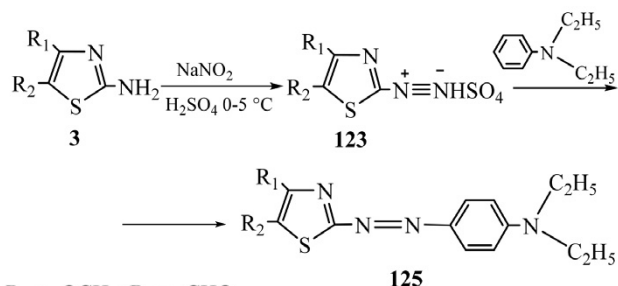
R, R₁ = Ph, H; 4-antipyrynyl, H; Ph, Me; 4-antipyrynyl, Me
Ar = C₆H₅, 4-MeC₆H₄, 4-MeOC₆H₄, 4-O₂NC₆H₄, 4-BrC₆H₄

Coupling of the diazotized 2-amino-2,4-disubstituted-thiazoles **123** ($R = \text{CH}_3$; $R_1 = \text{COCH}_3$) with various *N*-alkyl derivatives of aniline afforded the corresponding 2-azoaryl-2,4-disubstituted-thiazoles **124**. The products were applied as disperse dyes and their dyeing performance has been assessed on cellulose triacetate fabric. The dyed fabrics show good light fastness, very good rubbing, perspiration, washing fastness and excellent sublimation fastness. These dyes have been found to give bright yellow to maroon color shade with very good depth and levelness on fabric,¹⁷³ while **124** ($R_1 = R_2 = \text{Cl}$; $R_3 = \text{C}_2\text{H}_4\text{OH}$; $R_4 = \text{H}$) dyed polyester fiber with superior depth and levelness and fair to very good light fastness, very good to excellent washing and rubbing fastness properties.¹⁷⁴



$R_1, R_2 = \text{CH}_3, \text{COCH}_3, \text{Cl}, \text{Cl}$
 $R_3, R_4 = \text{H}, \text{H}; \text{CH}_3, \text{H}; \text{C}_2\text{H}_5, \text{H}; \text{H}, \text{CH}_3; \text{H}, \text{Cl}; \text{C}_2\text{H}_4\text{OH}, \text{H}$

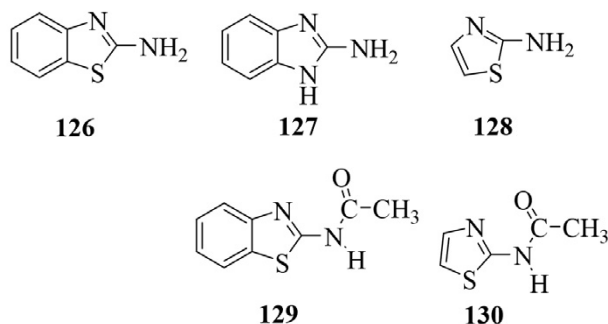
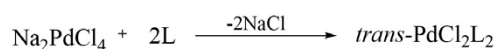
Azo coupling of 5-formylaminothiazole derivative **3** ($R_1 = \text{OCH}_3$; $R_2 = \text{CHO}$) as the diazo component and *N,N*-diethylaniline afforded the formyl aminothiazole dye **125**. The synthesized asymmetrical 2D charge transfer chromophores showed good nonlinear optical response and good thermal stability as well.¹⁷⁵



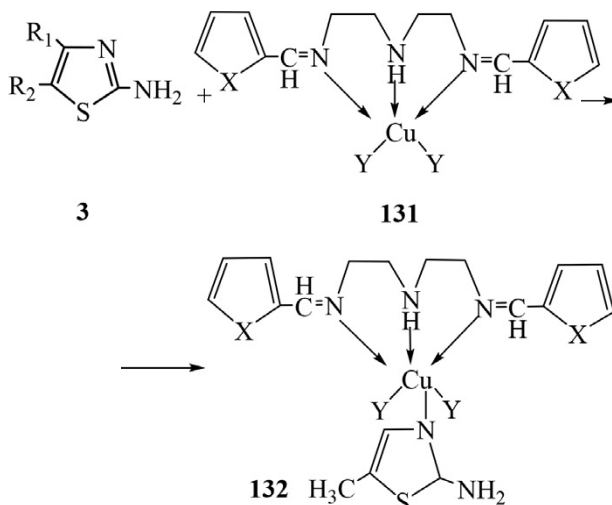
$R_1 = -\text{OCH}_3$; $R_2 = -\text{CHO}$

3. 3. 7. Complexation

Treatment of Na_2PdCl_4 with two equivalents of amino- or acetylamino-thiazoles as ligand (*L*) afforded *trans*- $[\text{PdCl}_2\text{L}_2]$ complexes **126–130** in which the introduced ligands were coordinated to palladium through the endocyclic nitrogen as shown by X-ray crystal structures.¹⁷⁶

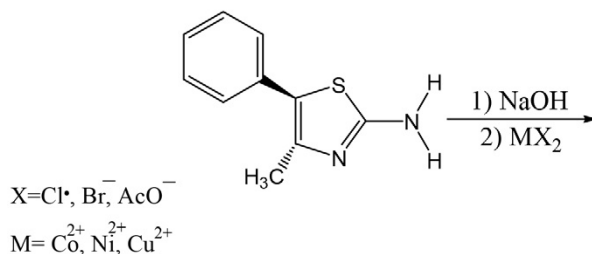


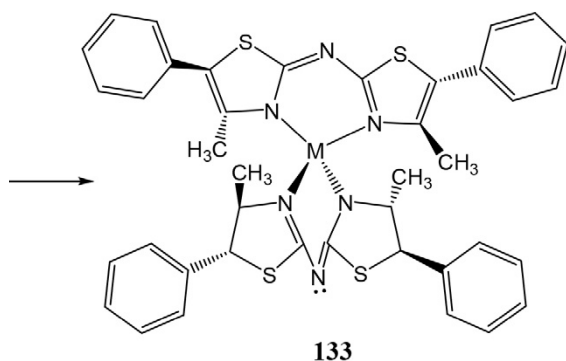
Copper(II) Schiff base coordination compounds of dienes with heterocyclic aldehydes and 2-amino-5-methyl-thiazole **132** were synthesized by stepwise reactions from the starting materials $[\text{Cu}(\text{dienX}_2\text{Y}_2)]$ **131** with 2-amino-4,5-disubstituted-thiazole **3** ($R_1 = \text{H}$, $R_2 = \text{CH}_3$). The isolated compounds are monomers, paramagnetic and electrolytic compounds of the type 1:1.¹⁷⁷



$R_1 = \text{H}$; $R_2 = \text{CH}_3$ $X = \text{O}, \text{S}$; $Y = \text{Cl}, \text{Br}, \text{NO}_3$

Synthesis of three coordination compounds $\text{Co}(\text{L})_2$, $\text{Ni}(\text{L})_2$, and $\text{Cu}(\text{L})_2$ **133** (*L* = bis[(4*R*,5*R*)-4-methyl-5-phenyl-4,5-dihydrothiazol-2-yl]-amine) prepared by template reactions from the optically active ligand (4*R*,5*R*)-4-methyl-5-phenyl-4,5-dihydrothiazol-2-yl-amine **3** and $\text{CoCl}_2 \cdot 6\text{H}_2\text{O}$, $\text{NiBr}_2 \cdot 3\text{H}_2\text{O}$ or $\text{Cu}(\text{OAc})_2 \cdot \text{H}_2\text{O}$. The template reactions involved the condensation of two molecules of thiazol-2-ylamine and elimination of one NH_3 .¹⁷⁸

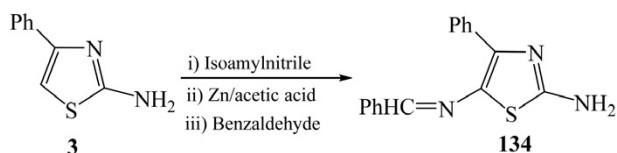




3. 4. Miscellaneous Reactions

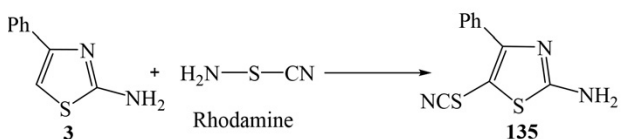
3. 4. 1. Nitrosation Reaction

2-Amino-4-phenylthiazole **3** underwent nitrosation at position 5 when treated with isoamylnitrite to give the corresponding 5-nitroso derivative which can be reduced by zinc in acetic acid followed by condensation with benzaldehyde to produce 2-amino-4-phenyl-5-benzalaminothiazole **134**.¹⁷⁹

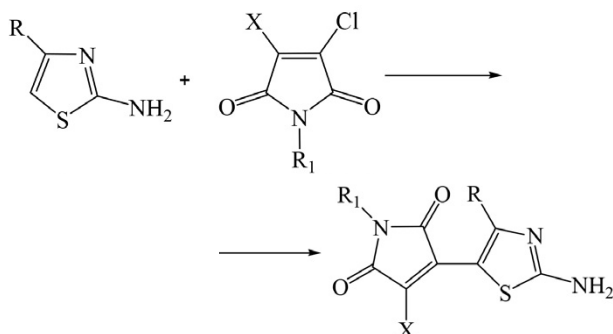


3. 4. 2. Reaction with Rhodamine

2-Amino-4-phenylthiazole **3** reacted with rhodamine (S-cyanothiohydroxylamine) at position 5 to produce the corresponding 2-amino-4-phenyl-5-rhodanthiazole **135**.¹⁸⁰

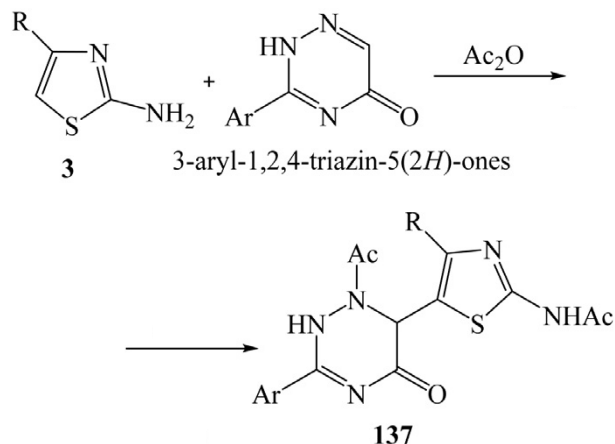


The 2-amino-*N*-substituted maleimidothiazoles **136** (R = halo, C₁₋₄ alkyl, phenyl, substituted phenyl, 2-furyl, 2-thienyl; R₁ = H, aliphatic or aromatic group; X = CN, C₁₋₆ alkylsulfonyl, SO₂-Ph) were prepared by the reaction of 2-amino-4-substituted thiazoles **3** with 2-chloromaleimides.¹⁸¹



3. 4. 4. Reaction with Triazines

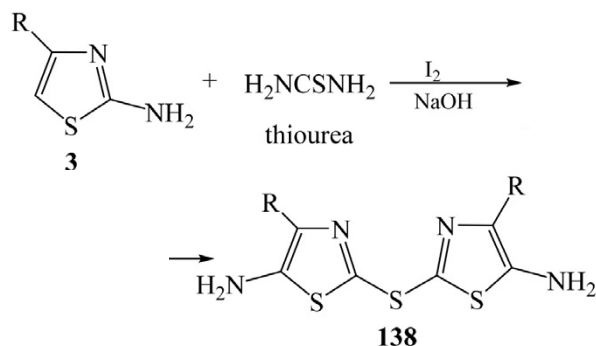
2-Amino-4-substituted thiazoles **3** were reacted in acetic anhydride with 3-aryl-1,2,4-triazin-5(2*H*)-one compounds, yielding 1-acetyl-3-aryl-6-(2-acetyl-amino-5-thiazolyl)-1,6-dihydro-1,2,4-triazin-5-(2*H*)-ones **137**.¹⁸²



R = Ph; Ar = Ph, 4-ClC₆H₄, 4-MeC₆H₄

3. 4. 5. Reaction with Thiourea and Iodine

Synthesis of bis(2-amino-5-thiazolyl)sulphides **138** has been achieved by reacting appropriate 2-amino-4-substituted thiazole **3** with thiourea and elemental iodide at room temperature in the presence of sodium hydroxide.¹⁸³



R = CH₃, CH₃CHCOOEt, C₂H₅, C₂H₅CHCOOEt

4. References

1. D. Das, P. Sikdar, M. Bairagi, *Eur. J. Med. Chem.* **2016**, *109*, 89–98. DOI:10.1016/j.ejmech.2015.12.022
2. U. G. Ibatullin, T. F. Petrushina, L. Y. Leitis, I. Z. Minibaev, B. O. Logvin, *Chem. Heterocycl. Compd.* **1993**, *29*, 612–615. DOI:10.1007/BF00534480
3. K. Singh, S. Singh, J. A. Taylor, *Dyes Pigm.* **2002**, *54*, 189–200. DOI:10.1016/S0143-7208(02)00053-0
4. A. Geronikaki, P. Vicini, N. Dabarakis, A. Lagunin, V. Poroikov, J. Dearden, H. Modarresi, M. Hewitt, G. Theophilidis, *Eur. J. Med. Chem.* **2009**, *44*, 473–481. DOI:10.1016/j.ejmech.2008.04.006

5. C. Papadopoulou, A. Geronikaki, D. Hadjipavlou-Litina, *Farmacology* **2005**, *60*, 969–973.
DOI:10.1016/j.farmac.2005.06.014
6. A. Kreutzberger, A. Tantawy, *Arch. Pharm.* **1981**, *314*, 968–969. DOI:10.1002/ardp.19813141112
7. E. Abdel-Latif, F. A. Amer, M. A. Metwally, M. E. Khalifa, *Pigm. Resin. Technol.* **2009**, *38*, 105–110.
DOI:10.1108/03699420910940608
8. M. E. Khalifa, E. Abdel-Latif, F. A. Amer, M. A. Metwally, *Int. J. Text. Sci.* **2013**, *1*, 62–68.
DOI:10.5923/j.textile.20120106.02
9. M. A. Metwally, H. A. Etman, H. E. Gafer, A. M. Khalil, *Adv. Color Sci. Tech.* **2004**, *7*, 71–78.
10. M. A. Metwally, E. Abdel-Latif, F. A. Amer, *J. Text. Assoc.* **2001**, *62*, 155–159.
11. M. A. Metwally, E. Abdel-Latif, F. A. Amer, *J. Text. Assoc.* **2002**, *63*, 149–154.
12. M. Metwally, M. Khalifa, E. Attia, F. Amer, *Pol. J. Chem. Technol.* **2010**, *12*, 1–6. DOI:10.2478/v10026-010-0001-6
13. M. A. Metwally, E. Abdel-Latif, F. A. Amer, G. Kaupp, *Dyes Pigm.* **2004**, *60*, 249–264.
DOI:10.1016/S0143-7208(03)00153-0
14. M. A. Metwally, E. Abdel-latif, A. M. Khalil, F. A. Amer, G. Kaupp, *Dyes Pigm.* **2004**, *62*, 181–195.
DOI:10.1016/j.dyepig.2003.12.002
15. M. E. Khalifa, E. Abdel-Latif, A. A. Gobouri, *J. Heterocycl. Chem.* **2015**, *52*, 674–680. DOI:10.1002/jhet.2153
16. A. Ongun Yüce, B. Dođru Mert, G. Kardaş, B. Yazıcı, *Corros. Sci.* **2014**, *83*, 310–316. DOI:10.1016/j.corsci.2014.02.029
17. K. Khaled, M. A. Amin, *Corros. Sci.* **2009**, *51*, 1964–1975.
DOI:10.1016/j.corsci.2009.05.023
18. F. Al-Hajjar, F. Al-Kharafi, *Corros. Sci.* **1988**, *28*, 163–171.
DOI:10.1016/0010-938X(88)90093-5
19. M. R. Pourjavid, T. Razavi, *Chin. Chem. Lett.* **2012**, *23*, 343–346. DOI:10.1016/j.ccllet.2011.12.006
20. A. Goblyos, S. N. Santiago, D. Pietra, T. Mulder-Krieger, J. von Frijtag Drabbe Kunzel, J. Brussee, A. P. Ijzerman, *Bioorg. Med. Chem.* **2005**, *13*, 2079–2087.
DOI:10.1016/j.bmc.2005.01.006
21. P. C. Hang, J. F. Honek, *Bioorg. Med. Chem. Lett.* **2005**, *15*, 1471–1474. DOI:10.1016/j.bmc.2004.12.076
22. R. Khunt, N. Datta, A. Parikh, *Indian J. Pharm. Sci.* **2002**, *64*, 170–173.
23. P. Beuchet, M. Varache-Lembège, A. Neveu, J.-M. Léger, J. Vercauteren, S. Larrouture, G. Deffieux, A. Nuhlich, *Eur. J. Med. Chem.* **1999**, *34*, 773–779.
DOI:10.1016/S0223-5234(99)00215-9
24. A. Geronikaki, G. Theophilidis, *Eur. J. Med. Chem.* **1992**, *27*, 709–716. DOI:10.1016/0223-5234(92)90091-E
25. D. S. Prasanna, C. V. Kavitha, K. Vinaya, S. R. Ranganatha, S. C. Raghavan, K. S. Rangappa, *Eur. J. Med. Chem.* **2010**, *45*, 5331–5336. DOI:10.1016/j.ejmech.2010.08.056
26. C. A. Bolos, K. T. Papazisis, A. H. Kortsaris, S. Voyatzi, D. Zambouli, D. A. Kyriakidis, *J. Inorg. Biochem.* **2002**, *88*, 25–36. DOI:10.1016/S0162-0134(01)00344-0
27. C. B. Rödl, D. Vogt, S. B. Kretschmer, K. Ihlefeld, S. Barzen, A. Brüggerhoff, J. Achenbach, E. Proschak, D. Steinhilber, H. Stark, *Eur. J. Med. Chem.* **2014**, *84*, 302–311.
DOI:10.1016/j.ejmech.2014.07.025
28. J. Das, J. A. Furch, C. Liu, R. V. Moquin, J. Lin, S. H. Spergel, K. W. McIntyre, D. J. Shuster, K. D. O'Day, B. Penhallow, C. Y. Hung, A. M. Doweiko, A. Kamath, H. Zhang, P. Marathe, S. B. Kanner, T. A. Lin, J. H. Dodd, J. C. Barrish, J. Wityak, *Bioorg. Med. Chem. Lett.* **2006**, *16*, 3706–3712.
DOI:10.1016/j.bmc.2006.04.060
29. P. Makam, R. Kankanala, A. Prakash, T. Kannan, *Eur. J. Med. Chem.* **2013**, *69*, 564–576. DOI:10.1016/j.ejmech.2013.08.054
30. V. U. Jeankumar, J. Renuka, P. Santosh, V. Soni, J. P. Sridevi, P. Suryadevara, P. Yogeeswari, D. Sriram, *Eur. J. Med. Chem.* **2013**, *70*, 143–153. DOI:10.1016/j.ejmech.2013.09.025
31. T. Inoue, M. Morita, T. Tojo, K. Yoshihara, A. Nagashima, A. Moritomo, M. Ohkubo, H. Miyake, *Bioorg. Med. Chem.* **2013**, *21*, 1219–1233. DOI:10.1016/j.bmc.2012.12.025
32. T. Inoue, M. Morita, T. Tojo, A. Nagashima, A. Moritomo, K. Imai, H. Miyake, *Bioorg. Med. Chem.* **2013**, *21*, 2478–2494.
DOI:10.1016/j.bmc.2013.02.048
33. A. Reichelt, J. M. Bailis, M. D. Bartberger, G. Yao, H. Shu, M. R. Kaller, J. G. Allen, M. F. Weidner, K. S. Keegan, J. H. Dao, *Eur. J. Med. Chem.* **2014**, *80*, 364–382.
DOI:10.1016/j.ejmech.2014.04.013
34. S.-H. Kim, J. S. Tokarski, K. J. Leavitt, B. E. Fink, M. E. Salvati, R. Moquin, M. T. Obermeier, G. L. Trainor, G. G. Vite, L. K. Stadnick, *Bioorg. Med. Chem. Lett.* **2008**, *18*, 634–639.
DOI:10.1016/j.bmc.2007.11.076
35. M. Getlik, C. Grütter, J. R. Simard, H. D. Nguyen, A. Robubi, B. Aust, W. A. van Otterlo, D. Rauh, *Eur. J. Med. Chem.* **2012**, *48*, 1–15. DOI:10.1016/j.ejmech.2011.11.019
36. P. J. Cox, G. Psomas, C. A. Bolos, *Bioorg. Med. Chem.* **2009**, *17*, 6054–6062. DOI:10.1016/j.bmc.2009.06.058
37. M. R. Shiradkar, K. C. Akula, V. Dasari, V. Baru, B. Chiningiri, S. Gandhi, R. Kaur, *Bioorg. Med. Chem.* **2007**, *15*, 2601–2610.
DOI:10.1016/j.bmc.2007.01.043
38. K. Gholivand, S. Farshadian, M. F. Erben, C. O. Della Védova, *J. Mol. Struct.* **2010**, *978*, 67–73.
DOI:10.1016/j.molstruc.2009.12.018
39. A. A. Mohamed, A. W. El-Harby, *J. Mol. Struct.* **2007**, *817*, 125–136. DOI:10.1016/j.theochem.2007.04.024
40. Y. Zeng, Y. Ren, *Int. J. Quantum Chem.* **2007**, *107*, 247–258.
DOI:10.1002/qua.21059
41. D. L. Klayman, J. J. Maul, G. W. Milne, *Tetrahedron Lett.* **1967**, *8*, 281–284. DOI:10.1016/S0040-4039(00)90531-8
42. I. Forfar, C. Jarry, M. Laguerre, J.-M. Léger, I. Pianet, *Tetrahedron* **1999**, *55*, 12819–12828.
DOI:10.1016/S0040-4020(99)00787-5
43. C. Chaimbault, J. Bosc, C. Jarry, J. Leger, N. Marchand-Geneste, A. Carpy, *J. Mol. Struct.* **1999**, *508*, 193–205.
DOI:10.1016/S0022-2860(99)00059-9
44. J. Chouteau, G. Davidovics, J. Metzger, A. Bonzom, *Spectrochim. Acta* **1966**, *22*, 719–735.
DOI:10.1016/0371-1951(66)80102-9
45. C. L. Angyal, R. L. Werner, *J. Chem. Soc.* **1952**, 2911–2915.
DOI:10.1039/jr9520002911

46. W. Wilson, R. Woodger, *J. Chem. Soc.* **1955**, 2943–2948.
DOI:10.1039/JR9550002943
47. X. Chen, Y. Hu, J. Gao, *J. Mol. Struct.* **2013**, 1049, 362–367.
DOI:10.1016/j.molstruc.2013.06.041
48. L. Forlani, P. De Maria, *J. Chem. Soc., Perkin Trans. 2* **1982**, 535–537. DOI:10.1039/p29820000535
49. A. Hantzsch, J. Weber, *Eur. J. Inorg. Chem.* **1887**, 20, 3118–3132.
50. R. M. Dodson, L. C. King, *J. Am. Chem. Soc.* **1945**, 67, 2242–2243. DOI:10.1021/ja01228a059
51. L. C. King, R. J. Hlavacek, *J. Am. Chem. Soc.* **1950**, 72, 3722–3725. DOI:10.1021/ja01164a110
52. R. M. Dodson, L. C. King, *J. Am. Chem. Soc.* **1946**, 68, 871–871. DOI:10.1021/ja01209a049
53. M. A. Metwally, E. Abdel-Latif, F. A. Amer, G. Kaupp, *J. Sulfur Chem.* **2004**, 25, 63–85.
DOI:10.1080/17415990310001632365
54. S. P. Singh, R. Naithani, R. Aggarwal, O. Prakash, *Synth. Commun.* **1998**, 28, 2371–2378. DOI:10.1080/00397919808004289
55. M. Yen, *Dyes Pigm.* **2004**, 63, 1–9.
DOI:10.1016/j.dyepig.2003.12.011
56. T. Prashanth, P. Thirusangu, B. V. Avin, V. L. Ranganatha, B. Prabhakar, S. A. Khanum, *Eur. J. Med. Chem.* **2014**, 87, 274–283. DOI:10.1016/j.ejmech.2014.09.069
57. M. H. Helal, M. A. Salem, M. S. El-Gaby, M. Aljahdali, *Eur. J. Med. Chem.* **2013**, 65, 517–526.
DOI:10.1016/j.ejmech.2013.04.005
58. S. Koppireddi, D. R. Chilaka, S. Avula, J. R. Komsani, S. Kotamraju, R. Yadla, *Bioorg. Med. Chem. Lett.* **2014**, 24, 5428–5431. DOI:10.1016/j.bmcl.2014.10.030
59. P. Czerney, H. Hartmann, *J. Prakt. Chem.* **1983**, 325, 551–560.
DOI:10.1002/prac.19833250405
60. M. Somei, Y. Yamada, K. Kitagawa, K. Sugaya, Y. Tomita, F. Yamada, K. Nakagawa, *Heterocycles* **1997**, 45, 435–438.
DOI:10.3987/COM-97-7734
61. A. M. Farag, H. M. Hassaneen, I. M. Abbas, A. S. Shawali, M. S. Algharib, *Phosphorus Sulfur Silicon Relat. Elem.* **1988**, 40, 243–249. DOI:10.1080/03086648808072921
62. A. Taurins, A. Blaga, *J. Heterocycl. Chem.* **1970**, 7, 1137–1141.
DOI:10.1002/jhet.5570070521
63. R. S. Shadbolt, *J. Chem. Soc. C*, **1971**, 1667–1669.
DOI:10.1039/j39710001667
64. H. Beyer, D. Stehwien, *Arch. Pharm.* **1953**, 286, 13–19.
DOI:10.1002/ardp.19532860104
65. J. Banothu, K. Vaarla, R. Bavantula, P. A. Crooks, *Chin. Chem. Lett.* **2014**, 25, 172–175. DOI:10.1016/j.ccllet.2013.10.001
66. L. C. King, I. Ryden, *J. Am. Chem. Soc.* **1947**, 69, 1813–1814.
DOI:10.1021/ja01199a072
67. T. Masquelin, D. Obrecht, *Tetrahedron* **2001**, 57, 153–156.
DOI:10.1016/S0040-4020(00)01003-6
68. T. M. Potewar, S. A. Ingale, K. V. Srinivasan, *Tetrahedron* **2007**, 63, 11066–11069. DOI:10.1016/j.tet.2007.08.036
69. P. Makam, P. K. Thakur, T. Kannan, *Eur. J. Pharm. Sci.* **2014**, 52, 138–145. DOI:10.1016/j.ejps.2013.11.001
70. B. W. Lee, S. D. Lee, *Tetrahedron Lett.* **2000**, 41, 3883–3886.
DOI:10.1016/S0040-4039(00)00493-7
71. L. C. King, F. Miller, *J. Am. Chem. Soc.* **1949**, 71, 367–368.
DOI:10.1021/ja01169a509
72. M. Masaki, M. Sugiyama, S. Tayama, M. Ohta, *Bull. Chem. Soc. Jpn.* **1966**, 39, 2745–2749. DOI:10.1246/bcsj.39.2745
73. J. Světlík, F. Tureček, *Tetrahedron Lett.* **1984**, 25, 3901–3904.
DOI:10.1016/S0040-4039(01)91199-2
74. X. Lu, X. Liu, B. Wan, S. G. Franzblau, L. Chen, C. Zhou, Q. You, *Eur. J. Med. Chem.* **2012**, 49, 164–171.
DOI:10.1016/j.ejmech.2012.01.007
75. A. G. Cole, T. M. Stauffer, L. L. Rokosz, A. Metzger, L. W. Dillard, W. Zeng, I. Henderson, *Bioorg. Med. Chem. Lett.* **2009**, 19, 378–381. DOI:10.1016/j.bmcl.2008.11.066
76. X. Zhao, Y. F. Li, S. J. Zhang, X. L. Wang, Y. Shao, *Chin. Chem. Lett.* **2007**, 18, 1203–1204.
DOI:10.1016/j.ccllet.2007.08.007
77. X. Zhao, Y.-F. Li, S.-J. Zhang, Y. Shao, X.-L. Wang, *Polymer* **2007**, 48, 5241–5249. DOI:10.1016/j.polymer.2007.07.001
78. N. M. Parekh, B. M. Mistry, M. Pandurangan, S. K. Shinde, R. V. Patel, *Chin. Chem. Lett.* **2017**, 28, 602–606.
DOI:10.1016/j.ccllet.2016.10.021
79. X. Zhao, Q.-F. Geng, T.-H. Zhou, X.-H. Gao, G. Liu, *Chin. Chem. Lett.* **2013**, 24, 31–33. DOI:10.1016/j.ccllet.2012.11.013
80. K. Y. Jung, S. K. Kim, Z. G. Gao, A. S. Gross, N. Melman, K. A. Jacobson, Y. C. Kim, *Bioorg. Med. Chem.* **2004**, 12, 613–623.
DOI:10.1016/j.bmc.2003.10.041
81. G. Chaubet, L. T. Maillard, J. Martinez, N. Masurier, *Tetrahedron* **2011**, 67, 4897–4904. DOI:10.1016/j.tet.2011.04.090
82. V. Ahluwalia, K. Arora, G. Kaur, B. Mehta, *Synth. Commun.* **1987**, 17, 333–340. DOI:10.1080/00397918708077314
83. H. A. El-Wahab, M. A. El-Fattah, N. A. El-Khalik, H. S. Nasar, M. M. Abdelall, *Prog. Org. Coat.* **2014**, 77, 1506–1511.
DOI:10.1016/j.porgcoat.2014.04.026
84. M. Giffard, J. Cousseau, *Tetrahedron Lett.* **1983**, 24, 5085–5088. DOI:10.1016/S0040-4039(00)94047-4
85. N. De Kimpe, W. De Cock, M. Keppens, D. De Smaele, A. Mészáros, *J. Heterocycl. Chem.* **1996**, 33, 1179–1183.
DOI:10.1002/jhet.5570330429
86. R. S. Giri, H. M. Thaker, T. Giordano, J. Williams, D. Rogers, V. Sudersanam, K. K. Vasu, *Eur. J. Med. Chem.* **2009**, 44, 2184–2189. DOI:10.1016/j.ejmech.2008.10.031
87. K. Gewald, H. Spies, R. Mayer, *Adv. Synth. Catal.* **1970**, 312, 776–779.
88. D. Thomae, E. Perspicace, Z. Xu, D. Henryon, S. Schneider, S. Hesse, G. Kirsch, P. Seck, *Tetrahedron* **2009**, 65, 2982–2988.
DOI:10.1016/j.tet.2009.01.104
89. P. Wipf, S. Venkatraman, *J. Org. Chem.* **1996**, 61, 8004–8005.
DOI:10.1021/jo961681c
90. S. P. Shaik, V. L. Nayak, F. Sultana, A. V. Rao, A. B. Shaik, K. S. Babu, A. Kamal, *Eur. J. Med. Chem.* **2017**, 126, 36–51.
DOI:10.1016/j.ejmech.2016.09.060
91. S. Shah, R. H. Mehta, *Indian Chem. Soc.* **1987**, 64, 708–709.
92. Q. Xu, L. Huang, J. Liu, L. Ma, T. Chen, J. Chen, F. Peng, D. Cao, Z. Yang, N. Qiu, *Eur. J. Med. Chem.* **2012**, 52, 70–81.
DOI:10.1016/j.ejmech.2012.03.006
93. S. T. A. Al-Rashood, G. S. Hassan, S. M. El-Messery, K. E. H. El-Taher, M. M. Hefnawy, M. A. Al-Omar, H. I. El-Subbagh,

- Bioorg. Med. Chem. Lett.* **2016**, 26, 445–453.
DOI:10.1016/j.bmcl.2015.11.097
94. J. Yoshinaga, T. Shogaki, T. Kakita, H. Ozeki, Y. Kato, U.S. Patent No. 4,946,855. 7 Aug. 1990.
<https://patents.google.com/patent/US4946855A/en>
95. A. Andreani, M. Rambaldi, A. Locatelli, A. Isetta, *Eur. J. Med. Chem.* **1991**, 26, 335–337.
DOI:10.1016/0223-5234(91)90067-W
96. T. Makino, *Chem. Pharm. Bull. (Tokyo)* **1962**, 10, 576–580.
DOI:10.1248/cpb.10.576
97. C. Nava-Zuazo, F. Chavez-Silva, R. Moo-Puc, M. J. Chan-Bacab, B. O. Ortega-Morales, H. Moreno-Diaz, D. Diaz-Coutino, E. Hernandez-Nunez, G. Navarrete-Vazquez, *Bioorg. Med. Chem.* **2014**, 22, 1626–1633.
DOI:10.1016/j.bmc.2014.01.029
98. J.-R. Li, D.-D. Li, R.-R. Wang, J. Sun, J.-J. Dong, Q.-R. Du, F. Fang, W.-M. Zhang, H.-L. Zhu, *Eur. J. Med. Chem.* **2014**, 75, 438–447. DOI:10.1016/j.ejmech.2013.11.020
99. M. Ban, H. Taguchi, T. Katsushima, M. Takahashi, K. Shinoda, A. Watanabe, T. Tominaga, *Bioorg. Med. Chem.* **1998**, 6, 1069–1076. DOI:10.1016/S0968-0896(98)00065-0
100. H. Paul, U. Richter, G. Huschert, *Arch. Pharm.* **1982**, 315, 17–22. DOI:10.1002/ardp.19823150106
101. M. Selim, O. Tetu, M. Selim, G. Martin, P. Rumpf, *Bull. Soc. Chim. Fr.* **1968**, 2117.
102. G. Turan-Zitouni, Ş. Demirayak, A. Özdemir, Z. A. Kaplancikli, M. T. Yildiz, *Eur. J. Med. Chem.* **2004**, 39, 267–272. DOI:10.1016/j.ejmech.2003.11.001
103. S. Mallakpour, A. Zadehnazari, *J. Adv. Res.* **2014**, 5, 311–318.
DOI:10.1016/j.jare.2013.04.003
104. S. Kamila, K. Mendoza, E. R. Biehl, *Tetrahedron Lett.* **2012**, 53, 4921–4924. DOI:10.1016/j.tetlet.2012.06.116
105. J. M. Sprague, L. Kissinger, *J. Am. Chem. Soc.* **1941**, 63, 578–580. DOI:10.1021/ja01847a063
106. S. Röver, A. M. Cesura, P. Huguenin, R. Kettler, A. Szente, *J. Med. Chem.* **1997**, 40, 4378–4385. DOI:10.1021/jm970467t
107. Z. El-Hewehi, F. Runge, *J. Prakt. Chem.* **1962**, 16, 297–336.
DOI:10.1002/prac.19620160509
108. M. E. Hultquist, R. P. Germann, J. S. Webb, W. B. Wright Jr, B. Roth, J. M. Smith Jr, Y. S. Row, *J. Am. Chem. Soc.* **1951**, 73, 2558–2566. DOI:10.1021/ja01150a042
109. A. Geronikaki, D. Hadjipavlou-Litina, *Arzneimittelforschung* **1998**, 48, 263–265.
110. H. Cousse, G. Mouzin, B. Bonnaud, J. P. Tarayre, J. P. Couzinier, *Arzneimittelforschung* **1986**, 36, 1391–1393.
111. P. Lesimple, D. C. Bigg, *Synthesis* **1991**, 1991, 763–764.
112. N. Mohanty, K. K. Patnaik, M. K. Rout, *J. Indian Chem. Soc.* **1968**, 45, 969.
113. C. K. Bhaskare, P. G. More, *Indian J. Chem.-A* **1986**, 25, 166–169.
114. B. Dash, P. K. Mahapatra, D. Panda, J. M. Pattnaik, *Chem-Inform.* **1985**, 16, DOI:10.1002/chin.198545182
115. C. Hopkinson, G. D. Meakins, R. J. Purcell, *Synthesis* **1991**, 1991, 621–624.
116. C. Bhaskare, P. Hankare, *J. Indian Chem. Soc.* **1995**, 72, 585–587.
117. V. K. Gupta, A. K. Singh, L. K. Kumawat, *Sensors Actuators B: Chem.* **2014**, 195, 98–108.
DOI:10.1016/j.snb.2013.12.092
118. O. Cox, H. Jackson, V. A. Vargas, A. Baez, J. I. Colon, B. C. Gonzalez, M. De Leon, *J. Med. Chem.* **1982**, 25, 1378–1381.
DOI:10.1021/jm00353a020
119. K. M. Dawood, T. M. Eldebss, H. S. El-Zahabi, M. H. Yousef, P. Metz, *Eur. J. Med. Chem.* **2013**, 70, 740–749.
DOI:10.1016/j.ejmech.2013.10.042
120. M. Z. A. Badr, H. A. H. El-Sherief, A. M. Mahmoud, *Bull. Chem. Soc. Jpn.* **1980**, 53, 2389–2392.
DOI:10.1246/bcsj.53.2389
121. J. E. van Muijlwijk-Koezen, H. Timmerman, R. C. Vollaing, J. Frijtag von Drabbe Künzel, M. de Groot, S. Visser, A. P. IJzerman, *J. Med. Chem.* **2001**, 44, 749–762.
DOI:10.1021/jm0003945
122. N. Walchshofer, M. Minjat, B. Tinland, P. Jaussaud, A.-F. Petavy, J. Paris, *Eur. J. Med. Chem.* **1986**, 21, 59–64.
123. G. Romeo, L. Salerno, P. Milla, M. Siracusa, L. Cattel, F. Russo, *Die Pharmazie* **1999**, 54, 19–23.
124. W. Malik, P. Srivastava, S. Merra, *J. Med. Chem.* **1968**, 11, 1268–1269. DOI:10.1021/jm00312a613
125. P. N. Bhargava, S. C. Sharma, *Bull. Chem. Soc. Jpn.* **1965**, 38, 905–909. DOI:10.1246/bcsj.38.905
126. V. Madan, A. Taneja, V. Kudesia, *J. Indian Chem. Soc.* **1991**, 68, 162–163.
127. R. Lakhan, B. P. Sharma, B. N. Shukla, *Il Farmaco* **2000**, 55, 331–337. DOI:10.1016/S0014-827X(00)00032-X
128. G. Yabuta, R. Taguchi, S. Nagato, J. Tokumura, O. Yamada, *J. Agri. Sci. (Tokyo Nogyo Daigaku)* **1990**, 34, 179–185.
129. G. Barnikow, J. Bödeker, *Adv. Synth. Catal.* **1971**, 313, 1148–1154.
130. G. Dhindsa, *Pol. J. Chem.* **1986**, 60, 609–615.
131. S. A. Metwally, G. M. El Naggar, M. I. Younis, T. I. El-Emary, M. H. Elnagdi, *Liebigs Ann. Chem.* **1989**, 1989, 1037–1040.
132. K. T. Potts, S. Husain, *J. Org. Chem.* **1971**, 36, 10–13.
DOI:10.1021/jo00800a004
133. R. M. Mohareb, S. M. Fahmy, *Z. Naturforsch. B Chem. Sci.* **1985**, 40, 664–668.
134. E. S. Darwish, A. M. Abdel Fattah, F. A. Attaby, O. N. Al-Shayea, *Int. J. Mol. Sci.* **2014**, 15, 1237–1254.
DOI:10.3390/ijms15011237
135. F. Z. El-Ablak, M. A. Metwally, *J. Serb. Chem. Soc.* **1992**, 57, 635–635.
136. T. Itoh, Y. Matsuya, K. Nagata, A. Ohsawa, *Chem. Pharm. Bull.* **1997**, 45, 1547–1549. DOI:10.1248/cpb.45.1547
137. J. Bödeker, P. Köckritz, *Adv. Synth. Catal.* **1978**, 320, 1043–1046.
138. A. Kreutzberger, M. Uzbek, *Arch. Pharm.* **1972**, 305, 502–508. DOI:10.1002/ardp.19723050705
139. T. Zimmermann, G. Fischer, J. Teller, H. Dehne, B. Olk, *Adv. Synth. Catal.* **1989**, 331, 843–852.
140. A. Dave, K. Bhatt, N. Undavia, P. Trivedi, *ChemInform.* **1988**, 19, DOI:10.1002/chin.198844164
141. V. K. Mishra, S. C. Bahel, *ChemInform.* **1985**, 16, DOI:10.1002/chin.198539208

142. G. Westphal, P. Henklein, *Z. Chem.* **1969**, *9*, 425–426.
143. A. Tikdari, A. Mukerjee, *ChemInform.* **1987**, *18*.
DOI:10.1002/chin.198545182
144. C. F. H. Allen, H. R. Beilfuss, D. M. Burness, G. A. Reynolds, J. F. Tinker, J. A. VanAllan, *J. Org. Chem.* **1959**, *24*, 779–787.
DOI:10.1021/jo01088a013
145. B. Dash, M. Patra, P. Mahapatra, *J. Inst. Chem.* **1980**, *52*, 92–95.
146. G. Doria, C. Passarotti, R. Sala, R. Magrini, P. Sberze, M. Tibolla, R. Ceserani, G. Arcari, R. Castello, D. Toti, *Il Farmaco* **1985**, *40*, 885–894.
147. A. R. Ali, E. R. El-Bendary, M. A. Ghaly, I. A. Shehata, *Eur. J. Med. Chem.* **2014**, *75*, 492–500.
DOI:10.1016/j.ejmech.2013.12.010
148. M. Sahu, J. Sahu, A. Nayak, *ChemInform.* **1987**, *18*.
DOI:10.1002/chin.198721080
149. D. W. Dunwell, D. Evans, *J. Chem. Soc. C* **1971**, 2094–2097.
DOI:10.1039/j39710002094
150. L. Silpa, J. Petrignet, M. Abarbri, *Synlett.* **2014**, *25*, 1827–1830. DOI:10.1055/s-0034-1378332
151. D. Janietz, B. Goldmann, W. D. Rudorf, *J. Prakt. Chem.* **1988**, *330*, 607–616. DOI:10.1002/prac.19883300414
152. C. D. Hurd, S. Hayao, *J. Am. Chem. Soc.* **1955**, *77*, 117–121.
DOI:10.1021/ja01606a037
153. R. A. Glennon, M. E. Rogers, J. D. Smith, M. El-Said, J. L. Egle, *J. Med. Chem.* **1981**, *24*, 658–661.
DOI:10.1021/jm00138a002
154. F. Palagianio, L. Arenare, E. Luraschi, P. De Caprariis, E. Abignente, M. D'Amico, W. Filippelli, F. Rossi, *Eur. J. Med. Chem.* **1995**, *30*, 901–909.
DOI:10.1016/0223-5234(96)88309-7
155. M. R. Chaurasia, S. K. Sharma, *ChemInform.* **1981**, *12*.
156. G. Trapani, M. Franco, A. Latrofa, A. Carotti, G. Gerichi, M. Serra, G. Biggio, G. Liso, *Eur. J. Med. Chem.* **1996**, *31*, 575–587. DOI:10.1016/0223-5234(96)89553-5
157. A. O. Abdelhamid, H. M. Hassaneen, A. S. Shawali, C. Párkányi, *J. Heterocycl. Chem.* **1983**, *20*, 639–643.
DOI:10.1002/jhet.5570200326
158. F. A. Abdel-Mohdy, A. O. Abdelhamid, *Arch. Pharmacol. Res.* **1992**, *15*, 9–13. DOI:10.1007/BF02973977
159. J. H. Park, M. I. El-Gamal, Y. S. Lee, C. H. Oh, *Eur. J. Med. Chem.* **2011**, *46*, 5769–5777.
DOI:10.1016/j.ejmech.2011.08.024
160. R. Soni, J. Saxena, *Bull. Chem. Soc. Jpn.* **1979**, *52*, 3096–3098.
DOI:10.1246/bcsj.52.3096
161. A. K. El-Shafei, A. Sultan, G. Vernin, *ChemInform.* **1982**, *13*,
DOI:10.1002/chin.198232194
162. A. Hassan, *Pharmazie* **1994**, *49*, 239–242.
163. V. M. Barot, H. B. Naik, *Asian J. Chem.* **1995**, *7*, 669–671.
164. S. M. El-Messery, G. S. Hassan, F. A. Al-Omary, H. I. El-Subbagh, *Eur. J. Med. Chem.* **2012**, *54*, 615–625.
DOI:10.1016/j.ejmech.2012.06.013
165. C. D. Hurd, N. Kharasch, *J. Am. Chem. Soc.* **1946**, *68*, 653–658. DOI:10.1021/ja01208a038
166. E. Hoggarth, *J. Chem. Soc.* **1947**, 114–118.
DOI:10.1039/jr9470000114
167. L. Forlani, A. Medici, *J. Chem. Soc., Perkin Trans. 1* **1978**, 1169–1171. DOI:10.1039/p19780001169
168. M. H. Bahar, B. K. Sabata, *Indian J. Chem. B* **1981**, *20*, 328–329.
169. H. Beyer, G. Wolter, *Eur. J. Inorg. Chem.* **1952**, *85*, 1077–1083.
170. A. S. Shawali, A. O. Abdelhamid, *J. Heterocycl. Chem.* **1976**, *13*, 45–49. DOI:10.1002/jhet.5570130108
171. R. Nigam, V. K. Saxena, B. L. Chowdhury, *Indian Chem. Soc.* **1991**, *68*, 307–309.
172. M. Metwally, E. Abdel-Galil, A. Metwally, F. A. Amer, *Dyes Pigm.* **2012**, *92*, 902–908.
DOI:10.1016/j.dyepig.2011.07.009
173. H. R. Maradiya, *J. Saudi Chem. Soc.* **2010**, *14*, 77–81.
174. D. R. Patel, N. B. Patel, B. M. Patel, K. C. Patel, *J. Saudi Chem. Soc.* **2014**, *18*, 902–913.
175. R. M. El-Shishtawy, F. Borbone, Z. M. Al-Amshany, A. Tuzi, A. Barsella, A. M. Asiri, A. Roviello, *Dyes Pigm.* **2013**, *96*, 45–51. DOI:10.1016/j.dyepig.2012.08.002
176. S. A. Al-Jibori, A. T. Habeeb, G. H. Al-Jibori, N. A. Dayaaf, K. Merzweiler, C. Wagner, H. Schmidt, G. Hogarth, *Polyhedron* **2014**, *67*, 338–343. DOI:10.1016/j.poly.2013.09.007
177. A. T. Chaviara, P. Cox, K. Repana, R. Papi, K. Papazisis, D. Zambouli, A. Kortsaris, D. Kyriakidis, C. Bolos, *J. Inorg. Biochem.* **2004**, *98*, 1271–1283.
DOI:10.1016/j.jinorgbio.2004.05.010
178. R. Ramírez-Trejo, A. Flores-Parra, J. A. Peña-Hueso, E. Mijangos, R. Contreras, N. Barba-Behrens, *Polyhedron* **2010**, *29*, 1007–1014. DOI:10.1016/j.poly.2009.12.003
179. H. Beyer, H. Drews, *Eur. J. Inorg. Chem.* **1954**, *87*, 1500–1505.
180. E. Schmitz, H. Striegler, *Adv. Synth. Catal.* **1971**, *313*, 1125–1130.
181. J. J. Krutak, M. A. Weaver, U.S. Patent No. 5,179,207. 12 Jan. 1993. <https://patents.google.com/patent/US5179207A/en>.
182. V. L. Rusinov, G. V. Zyryanov, T. L. Pilicheva, O. N. Chupakhin, H. Neunhoeffer, *J. Heterocycl. Chem.* **1997**, *34*, 1013–1019. DOI:10.1002/jhet.5570340347
183. R. G. Woodbridge, G. Dougherty, *J. Am. Chem. Soc.* **1949**, *71*, 1744–1745. DOI:10.1021/ja01173a057

Povzetek

Aminotiazolski obroč in njegovi najrazličnejši derivati se že dolgo uporabljajo kot izhodne spojine za sinteze biološko aktivnih molekul. 2-aminotiazol, kot tipični predstavnik heterocikličnih aminov, je osnova za sintezo mnogih spojin, ki vključujejo sulfa zdravila, biocide, fungicide, različne tipe barvil za sintetična vlakna in pospeševalce kemijskih reakcij. Poleg tega nastopajo 2-aminotiazolski derivati kot intermediati pri sintezah antibiotikov, kjer so pogosto substituirani z različnimi skupinami, v odvisnosti od njihove končne farmacevtske namembnosti. Znana je tudi njihova aktivnost v vlogi inhibitorjev korozije pri zaščiti jekla. V tem preglednem članku predstavljam sintezno uporabnost 2-amino-4-substituiranih tiazolov, njihove reakcije in biološke učinke.

Scientific paper

B3LYP Study of 3-hydroxynaphthalene-2-carboxanilide *para*-derivatives

Martin Michalík,* Peter Poliak and Vladimír Lukeš

Department of Chemical Physics, Slovak University of Technology in Bratislava, Radlinského 9, SK-812 37 Bratislava, Slovakia

* Corresponding author: E-mail: martin.michalik@stuba.sk

Received: 17-03-2017

Abstract

A systematic DFT investigation of 3-hydroxy-*N*-phenylnaphthalene-2-carboxamide and its sixteen *para*-derivatives is presented. The structural analysis showed that the energetically preferred conformation of all derivatives is practically planar and it is stabilised *via* intramolecular hydrogen bonds occurring between (C)O...H(3)O atomic pairs. The quantum chemically evaluated partition coefficients logarithms correlate well with Quantitative Structure–Activity Relationship models as well as with experimentally determined isocratic retention factors logarithm. Theoretical gas-phase proton affinities of amido and hydroxyl group together with selected partial atomic charges reflect the terminal phenyl substitution effect. These quantities are linearly dependent on the *in vitro* activity against the *Mycobacterium Kansalii*. Obtained linear correlation functions based on quantum chemically evaluated microscopic properties and selected experimental data may serve as the effective tool in modern drug design for the description of substitution effect.

Keywords: Descriptor of substituent effects, Hammett constants, Retention factor, Biological activity, Acidity

1. Introduction

In the last two decades, much effort has been paid to the development and the synthesis of new antimicrobial chemotherapeutics due to the dramatic increase of drug-resistant bacteria.¹ A large number of biologically active organic compounds consists of an amide (–NH–CO–) moiety with hydrophobic residue in its close vicinity. Due to its electronic properties, the amide functional group is able to interact with a number of enzymes/receptors and affect the biological response.² Therefore the reason for widespread occurrence of amides in pharmaceutical research is obvious. Properties of the amide group can be easily tuned by various chemical modifications. In this context, we can mention salicylanilides.^{3,4} These *N*-substituted hydroxybenzamide derivatives represent compounds with a wide range of pharmacological activities.^{5,6} The exact mechanism of action is still under investigation, but these compounds are known to act as inhibitors of protein kinase epidermal growth factor receptor.⁷ Moreover, the salicylanilides were also found to inhibit bacterial enzymes.^{8–11}

In the drug design and discovery the pharmacokinetic behaviour, *i.e.* solubility, absorption, distribution, metabolism and excretion of a compound play a crucial

role. All these properties strongly depend on the lipophilicity of the compound making it one of the key parameters in the prediction and determination of pharmacological activity of potential drugs.^{12–15} Lipophilicity as defined by IUPAC is the affinity of a molecule or its moiety to lipophilic environment.¹⁶ Generally, it is expressed as octanol-water partition coefficient *P*, which can be determined experimentally and by computational methods. Nowadays, the chromatographic determination of lipophilicity is one of the most popular approaches due to the simple instrumentation and extensive range of measurable lipophilicity values.¹⁷ It can also be expressed by means of lipophilicity indices. The most common one is the retention factor *k*. It is obtained by the reversed phase high performance liquid chromatography (RP-HPLC) with isocratic elution. However, better correlations with log *P* can be reached if the retention factor *k* is extrapolated to the mobile phase with a 0.0% concentration of the organic solvent.¹⁸ On the other hand, popular Molinspiration quantitative structure–activity relationship model (QSAR model) exists as an online partition coefficient calculator and will be denoted as miLog*P*.¹⁹ Based on group contributions, miLog*P* identifies a total of 220 molecular fragments which include charge interactions. Alternatively, the XLog*P*3 values represent a knowledge-based approach

based on additive atom/group model which starts from the known $\log P$ value of a similarly reference compound.²⁰ Finally, the ALogPs is a self-learning method based on the use of associative neural networks to predict the $\log P$ value of a compound from its molecular structure.^{21–23} Despite having certain limitations, these models are used extensively to estimate the $\log P$ values of potential drugs.^{24,25}

Currently, the quantum chemical Density Functional Theory (DFT) method is widely used for the calculation of molecular and electronic structure. It is no surprise that the lipophilicity is tightly related to the molecular electronic structure. Moreover, the effect of various solvents and molecular conformations on the selected properties can be investigated. The DFT can be helpful for evaluation of energy related quantities, geometric parameters, as well as electromagnetic properties of molecules.^{26,27} Structure-activity DFT studies where the authors investigated the dependence of various biological activity descriptors on the lipophilicity and selected parameters have been published.^{28,29} For example, reasonable good correlation was found by studying relationships between $\log P$ and molecular properties for a larger set of polychlorinated biphenyls.³⁰ In the case of aromatic molecules, the substitution effect is often successfully expressed by Hammett or Taft constants.³¹ This approach has some shortcomings. For example, the prediction of *ortho* substitution effect is difficult due to the specific interactions occurring between neighbouring atoms of the added group, e.g. hydrogen bond formation, steric hindrance and steric effects of bulky substituents.³² Next, the correlation of the local microscopic quantities, e.g. isotropic hyperfine coupling constants, nuclear magnetic resonance shifts or partial atomic charges, works very well for the atoms forming the substituted aromatic rings. Nevertheless, identification of next suitable substituent descriptors is still a challenge for theoretical chemists.

The recently published synthesis and biological activity investigations of novel ring substituted hydroxynaphthalene-2-carboxanilides and 2-hydroxynaphthalene-1-carboxanilides represent a follow-up contribution to understanding the structure-activity relationship.^{3,4,9,10} The effect of seven substituents ($-\text{CH}_3$, $-\text{F}$, $-\text{Cl}$, $-\text{Br}$, $-\text{OCH}_3$, $-\text{CF}_3$ and $-\text{NO}_2$) was investigated. The design of these carboxanilides was based on the principle of their ring analogy with salicylanilides. The highest lipophilicity, i.e. retention factor logarithm ($\log k$), as well as a wide range of higher antibacterial and antimycobacterial activities was measured for 3-hydroxynaphthalene-2-carboxanilides. Especially, the well determined biological activity concentration (*MIC*) against *Mycobacterium Kansasii* was found. *In vitro* experiments also showed higher biological toxicity for 3-hydroxy-N-(4-nitrophenyl)naphthalene-2-carboxamide than for its *ortho* and *meta* analogues. Although the substituent effect was studied for seven substituents and the experimental data ($\log k$ and *MIC*) were correlated with electronic Hammett parameters or QSAR $\log P$ values, the

modifications of electronic structure upon the ring substitution were not systematically investigated at the quantum chemical level. It is plausible to suppose that proton affinity (*PA*), bond dissociation enthalpy (*BDE*) and selected partial atomic charges could be promising descriptors for the quantification of substituent contributions to various experimentally relevant quantities used in drug development.

With respect to the above-mentioned facts, we decided to perform the systematic quantum chemical study of 3-hydroxynaphthalene-2-carboxamide *para*-derivatives (Fig. 1). Main goals of this work can be defined as follows: a) theoretical evaluation of DFT- $\log P$ values, partial atomic charges, gas-phase proton affinities of hydroxyl and amide groups for the set of 16 electron donating and electron withdrawing groups; b) correlation of these quantities with Hammett constants and available experimental data ($\log k$ and *MIC*); c) estimation of the influence of terminal phenyl substitution on the energies of frontier orbitals. Finally, the quantum chemically evaluated $\log P$ values will be compared with QSAR models.

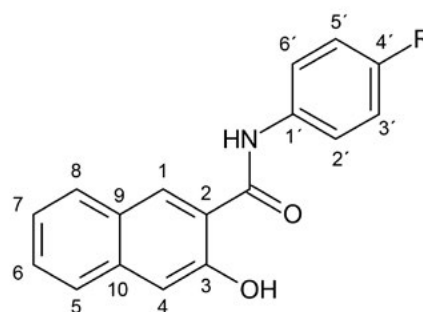


Fig. 1. Schematic structure of studied 3-hydroxynaphthalene-2-carboxamide *para*-derivatives with atom notation.

2. Materials and Methods

In order to get an accurate and precise theoretical description of the electronic and geometric properties of the molecules and of their interactions quantum chemical calculations were performed using Gaussian 09 program package.³³ Optimal geometries of the studied molecules in the neutral and deprotonated forms (see Eq. 2) were calculated in the gas-phase, *n*-octanol and water by the DFT method with B3LYP (Becke's three parameter Lee–Yang–Parr) functional without any constraints (energy cut-off of 10^{-5} kJ mol⁻¹, final RMS energy gradient under 0.01 kJ mol⁻¹ Å⁻¹).^{34,35} In addition, the Grimme's dispersion corrections (GD3BJ) were included for the better description of the intramolecular interactions occurring between the added substituents.³⁶ For all calculations, the triple-zeta 6-311++G(d,p) contracted gaussian basis sets for all atoms were employed.^{37–39} These basis sets can provide reliable molecular geometries and reaction enthalpies at reasonable time expense.^{40–42} The solvent influence was approximated by the continuum Solvation Model based on the

quantum mechanical charge Density (SMD) of a solute molecule interacting with a continuum description of the solvent.⁴³ The optimized structures were confirmed to be real minima by vibrational analysis (no imaginary vibrations). Then, electronic energies of frontier orbitals i.e. the highest occupied molecular orbital (HOMO) describing compounds nucleophilicity and the lowest unoccupied molecular orbital (LUMO) related to compounds electrophilicity was obtained. Partial atomic charges were evaluated using the APT (Atomic Polar Tensors) treatment.⁴⁴ The theoretical partition coefficient logarithm (DFT-log*P*) for the water/*n*-octanol mixture was calculated according to Eq. 1

$$\text{DFT-log } P = \frac{G_{\text{water}} - G_{\text{n-octanol}}}{2.303 RT} \quad (1)$$

where *G* values are the total Gibbs free energies of the solvated molecule, and *R* stands for the gas constant, *R* = 8.3145 J K⁻¹ mol⁻¹.⁴⁵ In the case of studied compounds, two possible anions can be considered. Either hydroxyl group or amide –NH group can be deprotonated. According to the IUPAC notation¹⁶, the gas-phase affinities of the anion were calculated by means of total enthalpies, *H*, from the Eq. 2

$$PA = H(\text{XN}^-/\text{O}^-) + H(\text{H}^+) - H(\text{XNH}/\text{OH}) \quad (2)$$

The symbol *H*(XN⁻/O⁻) stands for the total enthalpy of the formed anion, the *H*(H⁺) is the total enthalpy of the proton and *H*(XNH/OH) represents the total enthalpy of the investigated molecule. The gas-phase proton enthalpy *H*(H⁺) = –6.197 kJ mol⁻¹ was used, i.e. (5/2)*RT*. The Gibbs energies and enthalpies were determined for the room temperature (*T* = 298.15 K). QSAR method tries to find descriptors holding valuable information for designing drugs with maximum biochemical activity, therefore we have used various regression models. The statistical significance of the correlations was tested by examining the correlation coefficient and the standard deviation using Origin software.⁴⁶ Visualization of obtained theoretical results was done by Molekel program package.⁴⁷

3. Results and Discussion

3. 1. Conformational Analysis

From the geometrical point of view, the studied compounds consist of two aromatic moieties which are connected by single bonds to the –NH–CO– bridge. The possible orientations of carbonyl atoms with respect to the hydroxyl group at the naphthyl moiety lead to four conformations. As it is presented for the parental molecule (*R* = H) in Fig. 1S, the energetically preferred conformation **1a** is stabilised *via* the 1.708 Å intramolecular hydrogen bond between (C)O and H(3)O atoms. As it can

be seen in Tab. 1S, the distance increases with the electron-withdrawing character of the substituent. The dimethylamino derivative has the shortest distance of 1.699 Å while the largest value of 1.726 Å is associated with the –NO group. The second possible conformation **2a** can be stabilised by the interaction between H(3)O and H(N) atoms. Interestingly, this intramolecular bond length decreases with the electron-withdrawing character of the substituent. The corresponding distances for the selected derivatives are 1.853 Å for the parental molecule, 1.856 Å for the –N(CH₃)₂ group and 1.839 Å for the –NO group. The calculated Gibbs free energy difference with respect to the most stable conformation of the parental molecule is of 12 kJ mol⁻¹. According to the Boltzmann statistic, the negligible population of the second conformation at 298 K can be predicted. Similar results were obtained also for the substituted *para*-derivatives with the strong electron-donating amino group and the strong electron-withdrawing nitro group. Quantum chemical calculations also predicted practically planar structures of 1-hydroxynaphthalene-2-carboxanilides. The maximal distortion of 8 degrees is between the naphthyl moiety and CO or CN bonds. It seems that the presence of two aromatic moieties connected *via* the alternating single and double bonds ensures the impact on the whole molecular electron structure by phenyl ring substitution. The opposite arrangement of the OH group in conformations **1a** and **2a** leads to the conformations **1b** and **2b** where such intramolecular forces are not present. In the case of the **2b** conformation, the strong steric repulsion between hydrogen atoms of –OH group and –NH– moiety (see Fig. 1S) is responsible for the significant dihedral twist. For example, the dihedral angle C3–C2–C(O)–N(H) is about 38 degrees in all studied derivatives. Next, the mutual subtraction of the relative electronic energies **1a** and **1b** or **2a** and **2b** conformations enables us to estimate the stabilisation effect of these hydrogen bonds. For the (C)O...H(3)O interaction, these energies are approximately two times larger than for the H(3)O...H(N) one. The maximal stabilisation effect is found for the electron-donating –N(CH₃)₂ group (41.6 kJ mol⁻¹). The lowest interaction energy of 35.3 kJ mol⁻¹ exhibits the derivative containing the nitro group. From the energetic point of view, the intramolecular hydrogen bonds in **1a** conformations are moderately strong. The reported literature data for very weak hydrogen bonds between two molecules are of ~4 kJ mol⁻¹ (e.g. C–H...OH₂)⁴⁸ while the extremely strong interaction between ions HF₂⁻ are stabilized with the interaction energy of ~160 kJ mol⁻¹.⁴⁹

3. 2. Substituent Effect on Lipophilicity and Retention Factors

As mentioned in the introduction, the lipophilicity parameter log *P* can be predicted by various QSAR models and also by means of quantum chemical calculations. For

the unsubstituted parental molecule ($R = H$), the quantum chemical DFT- $\log P$ value calculated for n-octanol/water mixture is of 2.23. The empirical models based on the octanol/water measurements give higher values, i.e. 4.48, 4.52 and 3.99 for miLogP, XLogP3 and for ALogPs, respectively. The data collected in Tab. 1 allow a quick comparison of substituent induced changes of the relative lipophilicity values along with the reference lipophilicity of the unsubstituted molecule. The chemical substitution, especially halogenations is able to enlarge the lipophilicity value, which is often used in the drug development.⁵⁰ The maximal QSAR $\log P$ values were found for $-Br$, $-CH=CH_2$ and $-CF_3$ groups while the amino group significantly minimizes this value. The trends obtained by the DFT approach remain the same. As illustrated in Fig. 2S, the quantum chemically evaluated DFT- $\log P$ values can be correlated with the QSAR ones. The best correlation was found with the Mol-Inspiration model (Tab. 2S). The correlation coefficient R after omitting two strong electron donating groups ($-NH_2$ and $-NMe_2$), one electron-withdrawing $-COOH$ group and $CH=CH_2$ reached the value of 0.95. The parameters for linear function are

$$\text{miLogP} = 0.491(51) \times \text{DFT-}\log P + 3.54(12) \quad (3)$$

Experimental retention factors ($\log k$) for six derivatives ($-OCH_3$, $-CH_3$, $-H$, $-F$, $-Br$, $-Cl$, $-CF_3$ and $-NO_2$) were published recently by Kos et al.^{3,4} These experimental values represent the logarithm of the isocratic retention factor determined by means of RP-HPLC with mobile phase containing 60% methanol and 40% water. Except for methoxy group, all substituents cause the increase of $\log k$ with the halogen substituents having the largest impact.

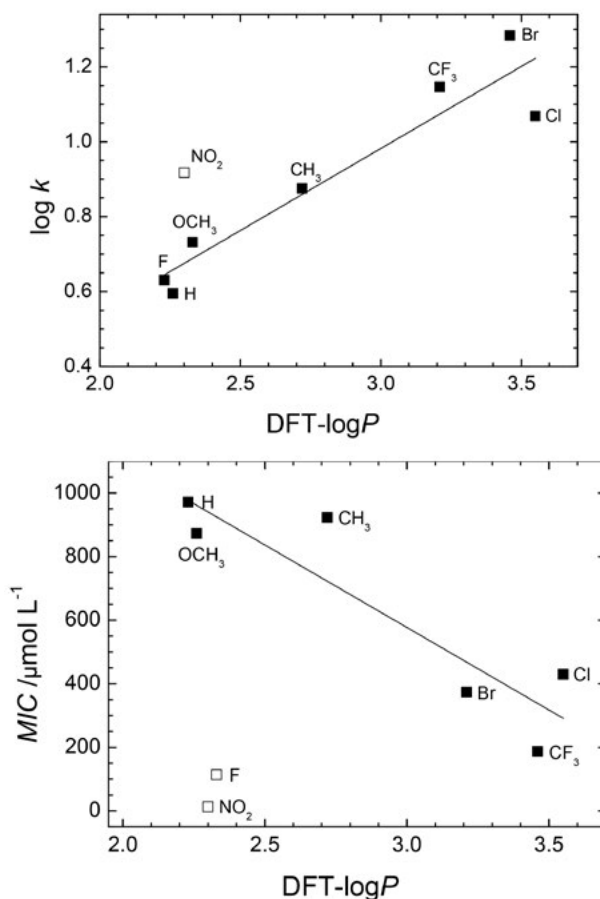


Fig. 2. Dependence of experimental retention factor logarithm ($\log k$) and minimum inhibitory concentration (MIC) against *Mycobacterium Kansasii* on DFT- $\log P$. Open symbols represent the data excluded from the linear regression. DFT- $\log P$ values were calculated for the **1a** conformation in water/n-octanol.

Tab. 1. Hammett constants σ_p , DFT electric dipole moments in Debye, theoretical DFT- $\log P$ values, DFT gas-phase proton affinities (PA) in kJ mol^{-1} , the QSAR predicted $\log P$ and the experimental $\log k$ values^{3,4} for the studied derivatives. B3LYP results are presented for the most stable conformation **1a**.

Substituent	σ_p	D	DFT- $\log P_t$	PA(N-H)	PA(O-H)	miLogP	XLogP3	ALogPs	logk
$-N(CH_3)_2$	-0.83	5.5	2.95	1385	1357	4.58	4.33	3.75	
$-NH_2$	-0.66	5.2	2.25	1381	1352	3.55	3.52	3.02	
$-OH$	-0.37	5.5	1.02	1373	1345	4.00	4.16	3.46	
$-OCH_3$	-0.27	3.3	1.10	1374	1346	4.53	4.17	4.24	0.5951
$-CH_3$	-0.17	4.3	2.72	1373	1344	4.92	4.57	4.49	0.8753
$-CH=CH_2$	-0.02	0.2	2.83	1356	1334	5.33	4.98	4.10	
$-H$	0.00	4.0	2.23	1369	1341	4.48	4.52	3.99	0.6310
$-F$	0.06	4.3	2.33	1359	1334	4.64	4.30	4.63	0.7317
$-SH$	0.15	4.8	2.23	1354	1330	4.71	4.35	3.96	
$-Br$	0.23	4.3	3.21	1349	1326	5.29	4.89	5.26	1.1459
$-Cl$	0.23	4.3	3.55	1354	1330	5.15	4.83	5.19	1.0687
$-CHO$	0.42	0.8	1.10	1329	1312	4.27	3.67	3.40	
$-COOH$	0.45	5.6	0.74	1336	1318	4.39	3.73	3.87	
$-CF_3$	0.54	5.2	3.42	1336	1315	5.37	5.09	4.91	1.2835
$-CN$	0.66	0.3	1.81	1322	1306	4.23	3.92	3.62	
$-NO_2$	0.78	7.1	1.48	1313	1298	4.43	4.03	4.18	0.9175
$-NO$	0.91	6.2	1.91	1312	1300	4.37	3.58	3.53	

The expected trend of increasing lipophilicity with the larger halogen atom can be observed.

After the nitro group exclusion, the data depicted in Fig. 2 show linear relationship between the $\log k$ values and DFT- $\log P$ with the correlation coefficient $R = 0.94$

$$\log k = 0.438(67) \times \text{DFT-}\log P - 0.33(19) \quad (4)$$

In the case of the QSAR $\log P$ values, the obtained slopes with the eliminated nitro group are larger (Fig. 4S), i.e. 0.719 for miLogP, 0.76 for XLogP3 and 0.90 for ALogPs. It seems that the strong electron-withdrawing NO_2 group shows significantly higher experimental $\log k$ value than the evaluated dependences predict. This discrepancy is probably caused by the non-equivalent exhibition of solvent effects in model systems accounted for the $\log P$ determination in comparison with the measurements of retention factors in the solvent mixture. Additionally, the formation of dimer structures is possible⁵¹ which alters the retention factors, and therefore $\log k$.

The dependence of DFT- $\log P$ on the *in vitro* activity against *Mycobacterium Kansasii* (DSM 44162) is also noteworthy (Fig. 2). After exclusion of the data for $-\text{NO}_2$ and $-\text{F}$ substituents, we have obtained the linear function with $R = 0.91$

$$\text{MIC} / \mu\text{mol L}^{-1} = -519(120) \times \text{DFT-}\log P + 2135(354) \quad (5)$$

In general, the antimycobacterial activity of potential drugs is very often affected by the differences in the permeability of the cell walls. Although all investigated compounds have the planar **1a** conformation, their penetration into bacterial cells can be supported by their higher electric dipole moments together with the size of the terminal substituent. The mutual comparison of B3LYP dipole moments collected in Tab. 1 reveals that the most polar molecule is the nitro-derivative with the corresponding value of 7.1 D. For the sake of comparison, we note that the gas-phase B3LYP/6-31++G(d,p) dipole moment of non-substituted nitrobenzene of 4.9 D. This value is slightly higher comparing to the gas-phase experimental value evaluated from the dielectric constants (4.3 D).⁵² On the other hand, fluorine has the highest electronegativity and may have large electronic effect on the neighbouring carbon atoms. Next, fluorine atom can act as a hydrogen bond acceptor, and its three lone pairs even enable to act as a ligand for alkali metals. Therefore, the incorporation of the fluorine atoms in a molecule will make it more lipid soluble. This means it migrates through membranes much more readily, and hence the fluorinated molecule has a higher bioavailability.⁵³

3. 3. Substituent Effect on the Atomic Charge Distribution

The electrostatic field in the vicinity of the molecule determines the macroscopic properties reflected in the ex-

perimental retention factors or $\log k$ values. For the sake of simplicity, this electrostatic field can be approximated as the superposition of partial atomic charges. The magnitudes of these charges are consequently changed with respect to the ring substitution. In other words, the maximal and minimal values were observed for the derivatives containing the strongest electron-withdrawing nitro and the strongest electron-donating dimethylamino groups respectively. The mutual comparison of absolute differences obtained from the atomic partial charges (Q_x) of the above mentioned derivatives help us to determine which part of the molecule is mostly sensitive to the terminal substitution (Fig 3). The individual partial charges of non-hydrogen atoms of 3-hydroxynaphthalene-2-carboxanilide for $-\text{NO}$ and $-\text{N}(\text{CH}_3)_2$ derivatives are available in Tab. 4S

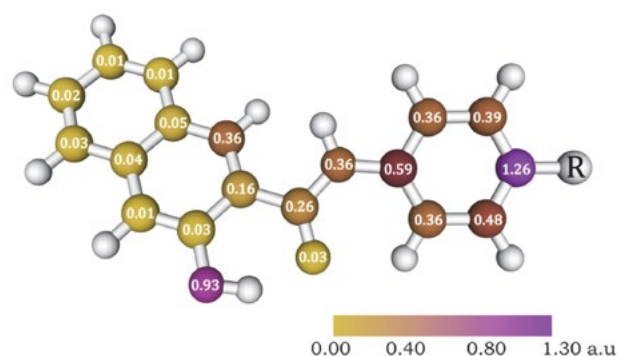


Fig. 3. Absolute differences between the B3LYP APT atomic partial charges in atomic units for non-hydrogen atoms of 3-hydroxynaphthalene-2-carboxanilide moiety of $-\text{NO}$ and $-\text{N}(\text{CH}_3)_2$ derivatives. The calculations were performed for the **1a** conformation.

It seems that the substituent effect expands beyond the amidic bond in the case of the C2 atom and the oxygen atom of the OH group on the naphthyl moiety. However, the negligible charge sensitivity to the substitution can be seen at other naphthyl ring atoms. The linear dependence of the atomic charge on the Hammett constants was found only for C2, N, C1' and C(=O). As shown in Fig. 4S, the positive partial charges on C1' and C(=O) atom increase as the substituent possess a more electron-accepting nature (see Tab. 1). On the other hand, the negative slopes of -0.0940 and -0.215 were observed for the Hammett type dependences for the charges on C2 and N atoms. Based on

Tab 2. Linear dependence parameters and correlation coefficients for the dependence of B3LYP APT partial charges in atomic units of selected carbon and nitrogen atoms on the Hammett constants.

Atom	Slope	Intercept	R
C1'	0.352(28)	0.531(14)	0.956
C2	-0.0940(51)	-0.4127(25)	0.979
C(=O)	0.154(11)	1.4642(58)	0.960
N	-0.215(22)	-1.004(11)	0.929

the comparison of the slope values presented in Tab. 2, we can conclude that C1' and N atoms exhibit the largest changes of partial charges upon the *para*-substitution.

Possible importance of the electrostatic interaction between these atoms and solvent molecules in the chromatographic retention times can be estimated from the direct correlation with the experimental $\log k$ values (Fig. 4). After the exclusion of $\log k$ value for NO_2 substituent and the parental molecule, the following linear regressions with R higher than 0.98 were obtained (partial charges Q_x are in atomic units)

$$\log k = 2.52(30) \times Q_{\text{C1}'} - 0.41(16) \quad (6)$$

$$\log k = -4.53(0.72) \times Q_{\text{N}} - 3.57(71) \quad (7)$$

In the case of the nitro group, relative large atomic partial charges on the substituent atoms were found (Tab. 4S). The charge on the nitrogen atom is positive (1.51 a.u.) and on each of the oxygen atoms is negative (-0.75 a.u.).

Although the relatively high positive atomic charge was also found at the carbon atom of trifluoromethyl, the orientation of fluorine atoms will ensure the electrostatic shielding effect. Therefore the found dependence could be relevant for the prediction of $\log k$ values for the derivatives with terminal substituents containing no unshielded positively charged atom connected directly to the phenyl ring.

From the next dependences illustrated in Fig. 4, it can be concluded that the linearity between the atomic partial charges on C1'/N atoms and the MIC values occurs only for stronger electron-withdrawing and electron-donating groups. Correlation coefficients are better than 0.95 after omitting the parental molecule, methyl and fluoro derivatives. The linear regression equations for partial charges Q_x in atomic units are

$$\text{MIC} / \mu\text{mol L}^{-1} = -1964(198) \times Q_{\text{C1}'} + 1581(125) \quad (8)$$

$$\text{MIC} / \mu\text{mol L}^{-1} = 3071(463) \times Q_{\text{N}} + 3582(485) \quad (9)$$

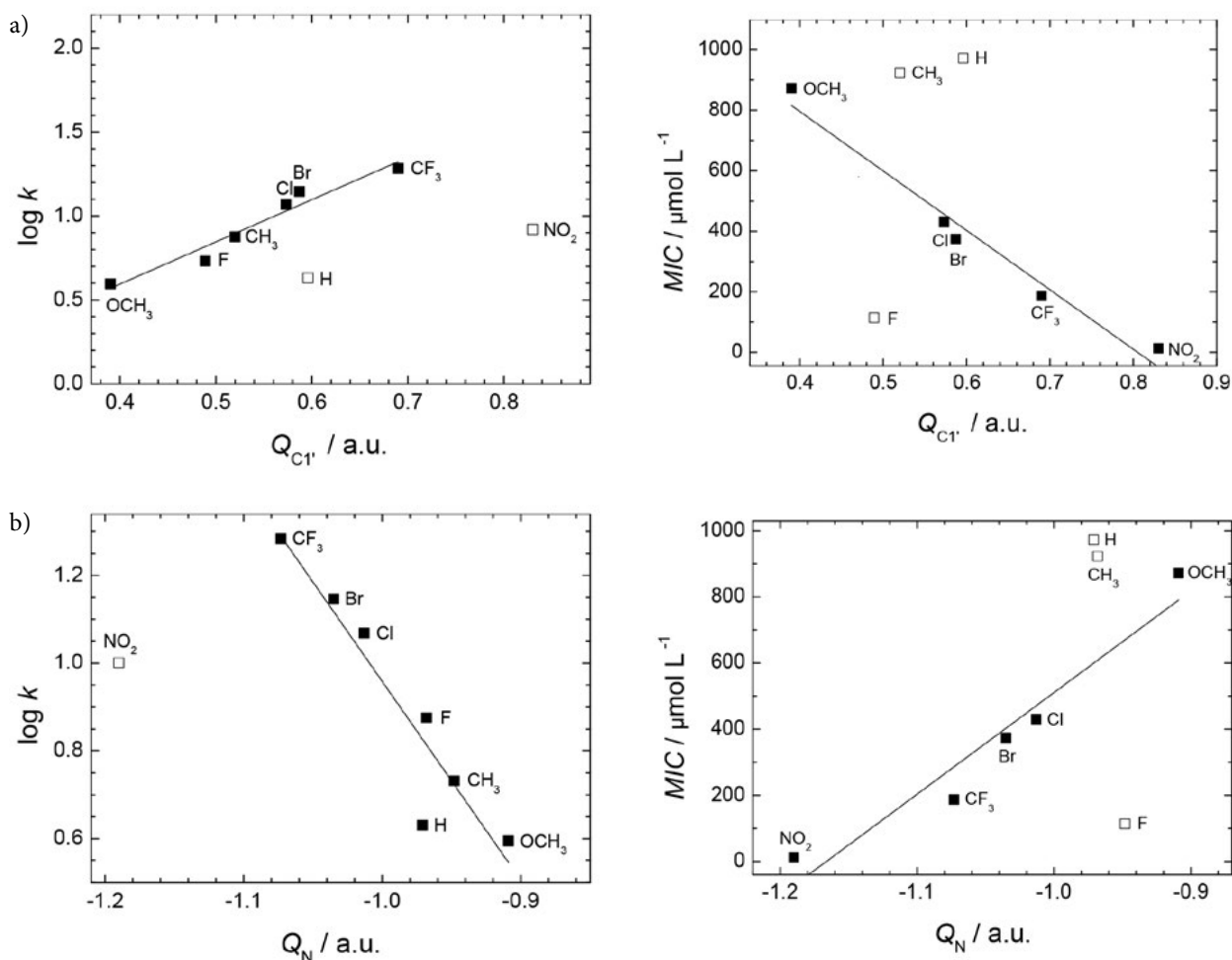


Fig 4. Dependence of the experimental retention factor logarithm ($\log k$) and minimum inhibitory concentration (MIC) against *Mycobacterium Kansasii* on B3LYP APT partial charges at (a) C1' and (b) N atoms. Open symbols represent the data excluded from the linear regression. The calculations were performed for the 1a conformation.

3. 4. Substituent Effect on the Proton Affinities of Amide and Hydroxyl Groups

Despite the fact that the carboxanilide compounds are very weak acids, the energetics of proton abstraction could be affected by the terminal substitution. For the determination of the primary substituent effect, i.e. the influence of the electronic nature of a functional group excluding solvent and other additional effects, the gas-phase calculations of proton affinities (PA) were performed. For the energetically preferred **1a** conformation, amidic group proton affinity of parental molecule is of 1369 kJ mol⁻¹ in gas-phase. The PA for the hydroxyl group connected to the naphthyl moiety is slightly lower, i.e. 1341 kJ mol⁻¹ (see Tab. 1). Chemical accuracy of the used calculation method can be estimated by the comparison with experimental data for well documented simple chemical structures. Experimental gas-phase PA values of phenol and aniline are of 1456 kJ mol⁻¹ ⁵⁴ and 1541 kJ mol⁻¹ ⁵⁵, respectively. Our calculated values are of 1441 kJ mol⁻¹ and 1524 kJ mol⁻¹, respectively.

The addition of a strong electron-donating group to the phenyl ring increases the PA value for amide and hydroxyl groups by about 16 kJ mol⁻¹. On the other hand, the electron-withdrawing substitution is responsible for the almost 60 kJ mol⁻¹ decrease of PA. From the numerical point of view, the reliability of PA value is dependent on the correctly found optimal geometry of the molecule and of its deprotonated form. In the case of these investigated carboxanilide *para*-derivatives in the **1a** conformation, the proton abstraction from the amide group can be responsible for the strong electrostatic interaction between the hydrogen atom of the hydroxyl group and the oxygen atom of the amide group. This interaction can generate two or more energetically different conformations with respect to the hydrogen atom position of the hydroxyl group. On the other hand, the deprotonation of the hydroxyl group in the **1a** conformation leads to strong repulsion between the oxygen atoms while the deprotonated anionic form can occur in various twisted conformations. Despite these complications, the linear dependences with $R = 0.96$ were achieved with respect to the Hammett constants (Fig. 5S). From the linear regression, we obtained the following equations

$$PA(\text{O-H}) / \text{kJ}\cdot\text{mol}^{-1} = -36.1(2.3) \times \sigma_p + 1333.2(1.1) \quad (10)$$

$$PA(\text{N-H}) / \text{kJ}\cdot\text{mol}^{-1} = -46.2(3.5) \times \sigma_p + 1357.2(1.7) \quad (11)$$

Slope values show that the *para* substitution has practically equivalent influence on the proton affinities among investigated groups. It seems that the PA values could be used as the suitable descriptor of the molecular electronic structure which is responsible for the biological activity of investigated 3-hydroxynaphthalene-2-carboxanilides. As illustrated in Fig. 5, both calculated gas-phase proton affinities are linearly dependent on the *in vitro* activity against *Mycobacterium Kansasii* (DSM 44162).

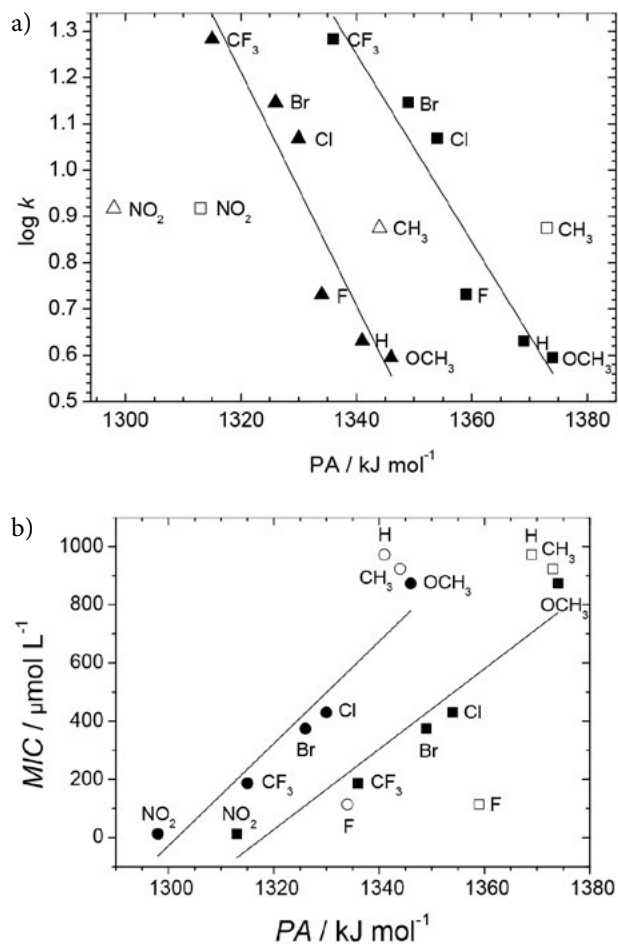


Fig. 5. Dependence of the experimental retention factor logarithm ($\log k$) and minimum inhibitory concentration (MIC) against *Mycobacterium Kansasii* with the gas-phase B3LYP proton affinities (PA). The PAs of amide (squares) and hydroxyl (circles) groups were calculated for the **1a** conformation. Open symbols stand for the data omitted from the linear regression.

The obtained correlation coefficients after exclusion of the parental molecule, methyl and fluorine derivatives are better than 0.97. The fitted parameters for the hydroxyl group are

$$MIC / \mu\text{mol} \cdot \text{L}^{-1} = 17.5(2.5) \times PA - 22800(3300) \quad (12)$$

and for the amide group are

$$MIC / \mu\text{mol} \cdot \text{L}^{-1} = 13.8(2.1) \times PA - 18200(2900) \quad (13)$$

The PAs are in kJ·mol⁻¹. From these dependencies, gas phase PA turns out to be a possible descriptor of MIC values and interestingly the correlation between the microscopic and macroscopic quantity is evident. The contribution of a solvent effect on the proton affinities can be also theoretically evaluated by employing B3LYP/SMD model. Nevertheless, implicit solvent model is fast and robust but still only approximation and has its own limita-

tions. As demonstrated in Tab. 6S, calculated B3LYP/SMD proton affinities are shifted by about 1100 kJ·mol⁻¹ with respect to gas phase. Correlations with experimental quantities are less linear. The obtained correlation coefficients are between 0.89–0.92.

3. 5. Substituent Effect on the Energies of Frontier Molecular Orbitals

The terminal ring substitution should also have the influence on the redox potential. The energies of the Highest Occupied Molecular Orbital (HOMO) and Lowest Unoccupied Molecular Orbital (LUMO) as the next possible descriptors should reflect the differences in the molecular structure of the studied derivatives. As depicted in Fig. 6a, the energy of HOMO (E_{HOMO}) correlates satisfactorily with the Hammett constants. After omitting two strong electron donating groups ($-\text{NH}_2$ and $-\text{NMe}_2$), the correlation coefficient is of 0.96 and the parameters of the fitted dependence are

$$E_{\text{HOMO}} / \text{eV} = -0.282(22) \times \sigma_p - 6.0646(98) \quad (14)$$

The negative slope indicates that the cation formation is supported by the electron-withdrawing substituents. Interestingly, the shapes of HOMO-1 for NH_2 and NMe_2 derivatives are comparable with the HOMO shapes of the remaining species. The HOMO-1 energies for NH_2 and NMe_2 correlate better with the Hammett constants. As can be seen in Fig. 7S, all these molecular orbitals are delocalised over the naphthyl moiety. On the other hand, the lobes of HOMO functions for NH_2 and NMe_2 derivatives are delocalised over the central bridge, phenyl moiety and corresponding lone pair of the added terminal nitrogen atom. In the case of the LUMOs, two distinguished linear dependencies with respect to the Hammett constants were obtained. The parental molecule represents the border group in these dependences (Fig. 6b). For the electron-donating substituents including the parental molecule, the correlation coefficient $R = 0.96$. The linear function parameters based on seven points are

$$E_{\text{LUMO}} / \text{eV} = -0.99(13) \times \sigma_p - 2.091(64) \quad (15)$$

Significantly lower slope was obtained for the derivatives containing the electron-withdrawing substituents

$$E_{\text{LUMO}} / \text{eV} = -0.277(41) \times \sigma_p - 2.191(18) \quad (16)$$

The correlation coefficient evaluated from ten points, where the parental molecule was also included, is of 0.93. Despite the presented linear dependence of HOMO/LUMO energies on the Hammett constants, the dependence of orbital energies on the log k values depicted in Fig. 7S shows no correlation.

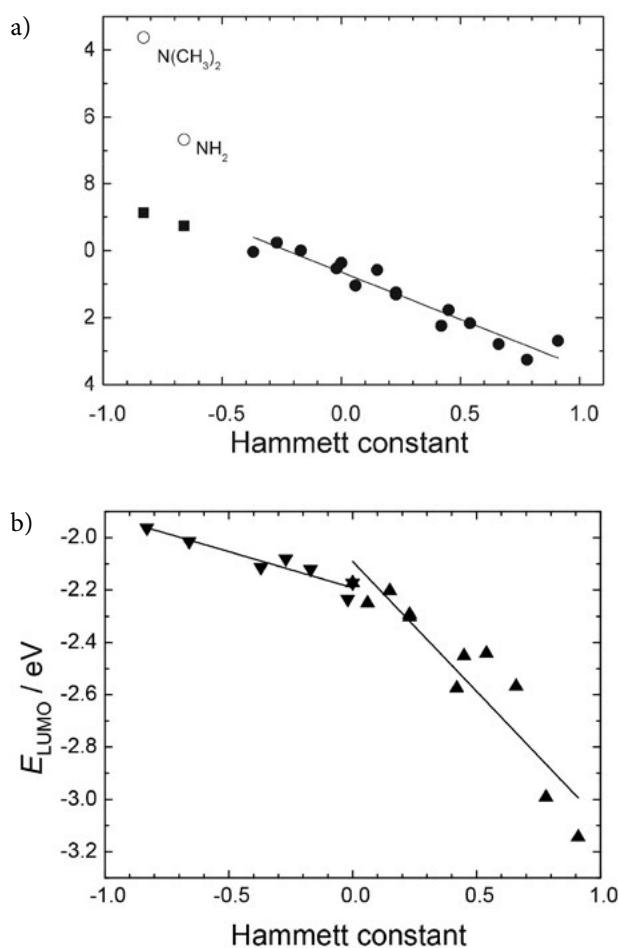


Fig. 6. Dependence of B3LYP energies of frontier orbitals HOMO (a) and LUMO (b) on the Hammett constants. Open symbols represent the data excluded from the linear regression. Squares stand for the HOMO-1 energies. The calculations were performed for the **1a** conformation.

On the other hand, the HOMO energies offer linear dependence on MIC with satisfactory agreement ($R = 0.98$) after rejecting outlying H, F and CH_3 derivatives

$$MIC / \mu\text{mol}\cdot\text{L}^{-1} = 2470(250) \times E_{\text{HOMO}} / \text{eV} + 15600(1500) \quad (17)$$

4. Conclusion

The present work was focused on the systematic quantum chemical investigation of 3-hydroxy-*N*-phenyl-naphthalene-2-carboxamide and its sixteen *para*-derivatives. The structural analysis showed that the **1a** conformations are energetically preferred due to the stabilisation *via* the intramolecular hydrogen bonds occurring between the (C)O...H(3)O atomic pairs. Phenyl ring substitutions affected the whole electronic structure of the molecule as the two aromatic moieties are connected *via*

the alternating single and double bonds with the practically planar arrangement corresponding to the **1a** conformation. The calculations of B3LYP APT atomic charges and proton affinities confirmed indisputable impact on the –NH–CO– bridge atoms and the naphthyl moiety. Next, the substitution effect was estimated from the mutual comparison of the energies of the frontier molecular orbitals. The dependences between the log *P* and the charge variations at specific positions show the linear increase of the lipophilicity with the absolute value of the accumulated charge on a single atom. Based on the comparison with the experimental data obtained for the synthesized derivatives the predicted trends were confirmed. The best correlation between the quantum chemically evaluated log *P* values and the QSAR Molinspiration model was demonstrated. The experimental log *k* values were correlated with the APT charges of the amide nitrogen atom as well. Interestingly, the evaluated partial charges on N and C1' atoms, the gas-phase proton affinities for the dissociation of the amide and hydroxyl group of the naphthyl moiety are linearly dependent on the *in vitro* activity against *Mycobacterium Kansasii* and serve as possible descriptors. Except the parental molecule, fluorine and methyl substituted derivatives, this linearity was demonstrated only for the substituents possessing stronger electron-donating or electron-withdrawing effects. Although the energies of frontier molecular orbitals very well reflects the changes in the electronic structure upon the terminal ring substitution, only HOMO energies can be suggested as the possible descriptor for MIC quantities. Nevertheless, it should be mentioned that experimental data for a larger set of molecules could unambiguously confirm that the found dependences are relevant also for different substituents and the obtained dependences are capable to provide reliable predictions. It could be also stressed out that experimental results were correlated with the gas-phase deprotonation energetics – although the solvent does not change general trends, it usually attenuates the substituent effect. But the theoretical description of the solvent effect is not trivial. Applied implicit solvent model due to the implemented approximations may not improve the quality of predicted trends.

5. Acknowledgments

This work was supported by Slovak Grant Agency VEGA (project no. 1/0594/16) and Slovak Research and Development Agency under the contract No. APVV-15-0053. We are grateful to the HPC centre at the Slovak University of Technology in Bratislava, which is a part of the Slovak Infrastructure of High Performance Computing (SIVVP project, ITMS code 26230120002, funded by the European region development funds, ERDF) for the computational time and resources made available.

Abbreviations

APT	Atomic polar tensor
B3LYP	Becke three-parameter (exchange), Lee-Yang-Parr (correlation)
BDE	Bond dissociation enthalpy
DFT	Density functional theory
HOMO	Highest occupied molecular orbital
LUMO	Lowest unoccupied molecular orbital
MIC	Minimal Inhibitory Concentration
PA	Proton affinity
QSAR	Quantitative structure-activity relationship
RMS	Root mean square
RP-HPLC	Reversed phase high performance liquid chromatography
SMD	Solvation Model based on the quantum mechanical charge Density

Conflicts of Interest

The authors declare that they have no conflicts of interest.

6. References

1. M. A. Toropova, A. M. Veselinović, J. B. Veselinović, D. B. Stojanović and A. A. Toropov, *Comput. Biol. Chem.* **2015**, *59*, 126–130. DOI:10.1016/j.compbiolchem.2015.09.009
2. M. Peško, J. Kos, K. Kráľová and J. Jampilek, *Indian J. Chem., Sect. B: Org. Chem. Incl. Med. Chem.* **2015**, *54B*, 1511–1517.
3. J. Kos, E. Nevin, M. Soral, I. Kushkevych, T. Gonec, P. Bobal, P. Kollar, A. Coffey, J. O'Mahony, T. Liptaj, K. Kralova and J. Jampilek, *Bioorg. Med. Chem.* **2015**, *23*, 2035–2043. DOI:10.1016/j.bmc.2015.03.018
4. J. Kos, I. Zadrazilova, M. Pesko, S. Keltosova, J. Tengler, T. Gonec, P. Bobal, T. Kauerova, M. Oravec, P. Kollar, A. Cizek, K. Kralova and J. Jampilek, *Molecules* **2013**, *18*, 7977–7997. DOI:10.3390/molecules18077977
5. M. Kratky and J. Vinsova, *Mini-Rev. Med. Chem.* **2011**, *11*, 956–967. DOI:10.2174/138955711797068382
6. C. Dank, B. Kirchknopf, M. Mastalir, H. Kählig, S. Felsing, A. Roller, V. Arion and H. Gstach, *Molecules* **2015**, *20*, 1686–1711. DOI:10.3390/molecules20011686
7. C. Liechti, U. Sequin, G. Bold, P. Furet, T. Meyer and P. Traxler, *ChemInform* **2004**, *35*.
8. I. Kushkevych, P. Kollar, A. L. Ferreira, D. Palma, A. Duarte, M. M. Lopes, M. Bartos, K. Pauk, A. Imramovsky and J. Jampilek, *J. Appl. Biomed.* **2016**, *14*, 125–130. DOI:10.1016/j.jab.2016.01.005
9. T. Gonec, J. Kos, I. Zadrazilova, M. Pesko, R. Govender, S. Keltosova, B. Chambel, D. Pereira, P. Kollar, A. Imramovsky, J. O'Mahony, A. Coffey, A. Cizek, K. Kralova and J. Jampilek, *Molecules* **2013**, *18*, 9397–9419. DOI:10.3390/molecules18089397
10. T. Gonec, J. Kos, I. Zadrazilova, M. Pesko, S. Keltosova, J. Tengler, P. Bobal, P. Kollar, A. Cizek, K. Kralova and J. Jampilek, *Bioorg. Med. Chem.* **2013**, *21*, 6531–6541.

- DOI:10.1016/j.bmc.2013.08.030
11. I. Zadrazilova, S. Pospisilova, M. Masarikova, A. Imramovsky, J. M. Ferriz, J. Vinsova, A. Cizek and J. Jampilek, *Eur. J. Pharm. Sci.* **2015**, *77*, 197–207.
DOI:10.1016/j.ejps.2015.06.009
12. P. Duchowicz, E. A. Castro, *Acta Chim. Slov.* **2000**, *47*, 281–292.
13. C. W. Fong, *Comput. Biol. Chem.* **2015**, *58*, 40–54.
DOI:10.1016/j.compbiolchem.2015.05.002
14. A. Guillot, Y. Henchoz, C. Moccand, D. Guillarme, J.-L. Veuthey, P.-A. Carrupt and S. Martel, *Chem. Biodiversity* **2009**, *6*, 1828–1836. DOI:10.1002/cbdv.200900115
15. Ł. Komsta, R. Skibiński, A. Berecka, A. Gumieniczek, B. Radkiewicz and M. Radoń, *J. Pharm. Biomed. Anal.* **2010**, *53*, 911–918. DOI:10.1016/j.jpba.2010.06.024
16. A. Wilkinson and A. McNaught, *IUPAC Compendium of Chemical Terminology (the “Gold Book”)*, Blackwell Science, Oxford, **1997**.
17. C. Liang and H.-z. Lian, *TrAC, Trends Anal. Chem.* **2015**, *68*, 28–36. DOI:10.1016/j.trac.2015.02.009
18. M. H. Abraham, H. S. Chadha and A. J. Leo, *J. Chromatogr. A* **1994**, *685*, 203–211. DOI:10.1016/0021-9673(94)00686-5
19. Molinspiration Cheminformatics **2010**, <http://www.molinspiration.com/services/>, accessed 20.09.2016.
20. R. Wang, Y. Fu and L. Lai, *J. Chem. Inf. Model.* **1997**, *37*, 615–621.
21. R. Estrada-Tejedor, N. Sabaté, F. Broto and S. Nonell, *Afinidad* **2013**, *70*, 250–256.
22. T. Cheng, Y. Zhao, X. Li, F. Lin, Y. Xu, X. Zhang, Y. Li, R. Wang and L. Lai, *J. Chem. Inf. Model.* **2007**, *47*, 2140–2148.
DOI:10.1021/ci700257y
23. I. V. Tetko and G. I. Poda, *J. Med. Chem.* **2004**, *47*, 5601–5604.
DOI:10.1021/jm049509l
24. M. Remko, A. Remková and R. Broer, *Molecules* **2016**, *21*, 185. DOI:10.3390/molecules21020185
25. M. Remko, A. Remková and R. Broer, *Int. J. Mol. Sci.* **2016**, *17*, 388. DOI:10.3390/ijms17030388
26. S. Y. Liao, J. C. Chen, L. Qian, Y. Shen and K. C. Zheng, *Eur. J. Med. Chem.* **2008**, *43*, 2159–2170.
DOI:10.1016/j.ejmech.2007.10.033
27. D. Mikulski, R. Górniak and M. Molski, *Eur. J. Med. Chem.* **2010**, *45*, 1015–1027. DOI:10.1016/j.ejmech.2009.11.044
28. K. Singhal, V. K. Sahu, P. Singh and P. Raj, *Med. Chem. Res.* **2013**, *23*, 1758–1767. DOI:10.1007/s00044-013-0752-8
29. M. Genc, Z. K. Genc, S. Tekin, S. Sandal, M. Sirajuddin, T. B. Hadda, M. Sekerci, *Acta Chim. Slov.* **2016**, *63*, 726–737.
DOI:10.17344/acsi.2016.2428
30. J. Padmanabhan, R. Parthasarathi, V. Subramanian and P. K. Chattaraj, *Bioorg. Med. Chem.* **2006**, *14*, 1021–1028.
DOI:10.1016/j.bmc.2005.09.017
31. C. Hansch, A. Leo and R. W. Taft, *Chem. Rev.* **1991**, *91*, 165–195. DOI:10.1021/cr00002a004
32. M. Charton, *J. Am. Chem. Soc.* **1969**, *91*, 615–618.
DOI:10.1021/ja01031a016
33. M. J. Frisch, G. W. Trucks, H. B. Schlegel, G. E. Scuseria, M. A. Robb, J. R. Cheeseman, G. Scalmani, V. Barone, B. Mennucci, G. A. Petersson, H. Nakatsuji, M. Caricato, X. Li, H. P. Hratchian, A. F. Izmaylov, J. Bloino, G. Zheng, J. L. Sonnenberg, M. Hada, M. Ehara, K. Toyota, R. Fukuda, J. Hasegawa, M. Ishida, T. Nakajima, Y. Honda, O. Kitao, H. Nakai, T. Vreven, J. A. Montgomery, J. E. Peralta, F. Ogliaro, M. Bearpark, J. J. Heyd, E. Brothers, K. N. Kudin, V. N. Staroverov, R. Kobayashi, J. Normand, K. Raghavachari, A. Rendell, J. C. Burant, S. S. Iyengar, J. Tomasi, M. Cossi, N. Rega, J. M. Millam, M. Klene, J. E. Knox, J. B. Cross, V. Bakken, C. Adamo, J. Jaramillo, R. Gomperts, R. E. Stratmann, O. Yazyev, A. J. Austin, R. Cammi, C. Pomelli, J. W. Ochterski, R. L. Martin, K. Morokuma, V. G. Zakrzewski, G. A. Voth, P. Salvador, J. J. Dannenberg, S. Dapprich, A. D. Daniels, Ö. Farkas, J. B. Foresman, J. V. Ortiz, J. Cioslowski and D. J. Fox, *Gaussian Inc. Wallingford, CT* **2009**.
34. C. Lee, W. Yang and R. G. Parr, *Phys. Rev. B* **1988**, *37*, 785–789.
DOI:10.1103/PhysRevB.37.785
35. A. D. Becke, *Phys. Rev. A* **1988**, *38*, 3098–3100.
DOI:10.1103/PhysRevA.38.3098
36. S. Grimme, S. Ehrlich and L. Goerigk, *J. Comput. Chem.* **2011**, *32*, 1456–1465. DOI:10.1002/jcc.21759
37. P. C. Hariharan and J. A. Pople, *Theor. Chim. Acta* **1973**, *28*, 213–222. DOI:10.1007/BF00533485
38. A. D. McLean and G. S. Chandler, *J. Chem. Phys.* **1980**, *72*, 5639–5648. DOI:10.1063/1.438980
39. M. M. Francl, *J. Chem. Phys.* **1982**, *77*, 3654.
DOI:10.1063/1.444267
40. E. Klein, V. Lukeš and M. Ilčin, *Chem. Phys.* **2007**, *336*, 51–57.
DOI:10.1016/j.chemphys.2007.05.007
41. E. Klein and V. Lukeš, *J. Phys. Chem. A* **2006**, *110*, 12312–12320. DOI:10.1021/jp063468i
42. M. Michalik, A. Vagánek and P. Poliak, *Acta Chimica Slovaca* **2014**, *7*, 123–128.
43. A. V. Marenich, C. J. Cramer and D. G. Truhlar, *J. Phys. Chem. B* **2009**, *113*, 6378–6396. DOI:10.1021/jp810292n
44. J. Cioslowski, *J. Am. Chem. Soc.* **1989**, *111*, 8333–8336.
DOI:10.1021/ja00204a001
45. P. W. Atkins, *Physical Chemistry*, 6th ed., Oxford University Press, 1999.
46. Origin, ver. 8.5, OriginLab, Northampton, MA, USA
47. U. Varetto *MOLEKEL Version 5.4* **2009**, Swiss National Supercomputing Centre: Manno.
48. L. Qingzhong, N. Wang and Y. Zhiwu, *J. Mol. Struct.: THEOCHEM* **2007**, *847*, 68–74.
DOI:10.1016/j.theochem.2007.08.035
49. J. W. Larson and T. B. McMahon, *Inorg. Chem.* **1984**, *23*, 2029–2033. DOI:10.1021/ic00182a010
50. C. L. Gentry, R. D. Egleton, T. Gillespie, T. J. Abbruscato, H. B. Bechowski, V. J. Hruby and T. P. Davis, *Peptides* **1999**, *20*, 1229–1238. DOI:10.1016/S0196-9781(99)00127-8
51. S. Tsuzuki, K. Honda, T. Uchimarui and M. Mikami, *J. Chem. Phys.* **2006**, *125*, 124304. DOI:10.1063/1.2354495
52. T. G. Scholte, *Recl. Trav. Chim. Pays-Bas* **2010**, *70*, 50–56.
DOI:10.1002/recl.19510700109
53. M. V. B. Krishna, S. V. Rao, V. S. N. Murthy and D. Karunasagar, *Anal. Methods* **2012**, *4*, 1565.
DOI:10.1039/c2ay05718b

54. L. A. Angel and K. M. Ervin, *J. Phys. Chem. A* **2006**, *110*, 10392–10403.
DOI:10.1021/jp0627426
55. S. W. Wren, K. M. Vogelhuber, T. Ichino, J. F. Stanton and W. C. Lineberger, *J. Phys. Chem. A* **2012**, *116*, 3118–3123.
DOI:10.1021/jp211463r

Povzetek

S teorijo gostonega funkcionala (DFT) smo sistematično raziskali 3-hidroksi-*N*-fenilnaftalen-2-carboksiamid in njegovih šestnajst *para*-derivativov. Strukturna analiza je pokazala, da je energetska ugodnejša konformacija vseh derivatov praktično planarna in stabilizirana preko intramolekularnih vodikovih vezi med (C)O···H(3)O atomskimi pari. Vrednosti logaritmov porazdelitvenih koeficientov, dobljenih s kvantno kemijskimi računi, so v dobri korelaciji tako s kvantitativnimi strukturnimi razmerji kot tudi z eksperimentalno določenimi logaritmi izokratskih retenzijskih faktorjev. Teoretične protonske afinitete amido in hidroksilne skupine v plinski fazi skupaj z izbranimi delnimi atomskimi naboji odražajo terminalni substitucijski učinek fenila in so linearno odvisne od aktivnosti *in vitro* proti *Mycobacterium Kansasii*. Dobljene linearne korelacijske funkcije, ki temeljijo na kvantno kemijsko ovrednotenih mikroskopskih lastnostih in izbranih eksperimentalnih podatkih, lahko služijo kot učinkovito orodje pri načrtovanju zdravilnih učinkovin.

Scientific paper

Synthesis and Anti-proliferative Activity of 4*H*-Chromone Based Phenylhydrazones, Pyrazolecarboxylates and Pyrazolymethanones

Nageswara Rao Rayala,¹ Rajkumar Kommera,¹ Dayakar Cherupally,¹ Ramalinga Murthy Thampunuri,² V. Kalivendi Shasi² and China Raju Bhimapaka^{1,*}

¹ Natural Products Chemistry Division,

² Chemical Biology Division,
CSIR-Indian Institute of Chemical Technology, Hyderabad-500 007, India.

* Corresponding author: E-mail: chinaraju@iict.res.in
Tel: +91-40-27191725; Fax: +91-40-27160512

Received: 18-04-2017

Abstract

Series of 4*H*-chromone-based hydrazones **3a–z**, pyrazolecarboxylates **5a–x** and pyrazolymethanones **6a–u** were prepared and screened for their anti-proliferative activity on A549, HeLa, DU145 and MDAMB 231 cell lines. The hydrazone compound **3s** with a chloro substituent on the chromanone moiety and a methoxy group on the phenyl ring displayed promising activity on A549, HeLa and DU145 cell lines. The compound **5p** with a bromo substituent on the chromanone moiety and a methyl group on the phenyl ring displayed potent activity on DU145. Furopyrazolecarboxylate **5w** having a methyl substituent on the phenyl ring displayed potent activity on HeLa cell line. The pyrazolymethanone **6e** with a fluoro substituent on the phenyl ring and compound **6j** having a methyl substituent on the chromanone moiety and a methoxy group on the phenyl ring have shown promising anti-proliferative activity on HeLa cell line.

Keywords: 3-Formylchromones, pyrazolecarboxylates, pyrazolymethanones, cycloaddition, anti-proliferative activity.

1. Introduction

Hydrazones, pyrazoles and pyrazolymethanones are important heterocyclic compounds.¹ The hydrazone-containing compounds obtained from carboxaldehydes with hydrazines have been shown to exhibit a variety of biological and pharmacological activities,^{2–5} namely antimicrobial, anti-inflammatory, anti-tumor and anti-tubercular. Celebrex and Sildenafil are the pyrazole-based potent drug molecules. Celebrex is a COX-2 selective non-steroidal anti-inflammatory drug used to treat the pain and inflammation.⁶ Sildenafil is a pharmaceutical drug used to treat erectile dysfunction.⁷ Pyrazolymethanones prepared by the reduction of carboxaldehydes were found to be anti-microbial and anti-inflammatory agents.⁸

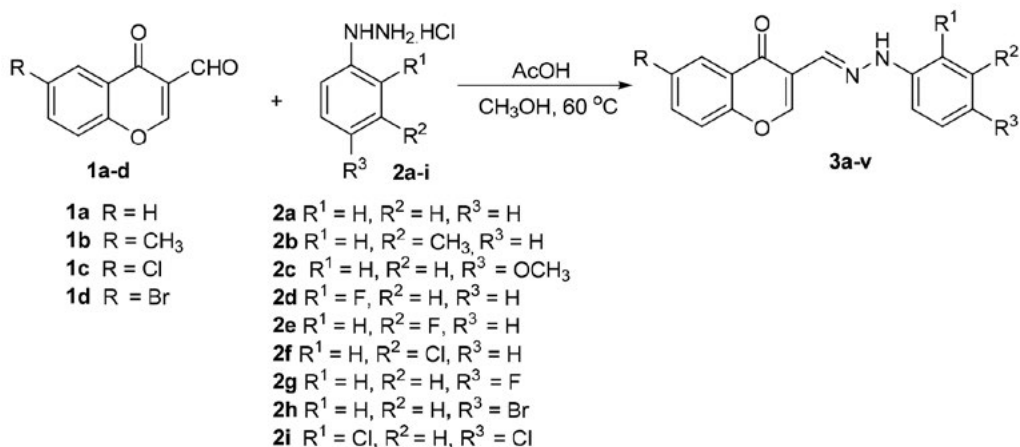
In the course of our efforts in discovery and identification of biologically active compounds,^{9–12} we focused research on 3-formylchromones and prepared series of 4*H*-chromen-1,2,3,4-tetrahydropyrimidine-5-carboxylates.¹³ Further, pyridine, pyridone and benzopyridocarbox-

ylates were reported by three-component, one-pot reaction of 3-formylchromones, benzylamines, 2-aminophenols with 3-oxobutanoates.¹⁴ The present manuscript describes the preparation of 3-formylchromone-based hydrazones, pyrazolecarboxylates, pyrazolymethanones and their anti-proliferative activity.

2. Results and Discussion

2.1. Preparation of (*E*)-3-((2-Phenylhydrazono)methyl)-4*H*-chromen-4-ones **3a–z**

Schemes 1–3 describe the preparation of target compounds **3a–z** starting from 3-formylchromones **1**. The required 3-formylchromones **1a–f** were prepared as per our earlier reported method.¹³ Condensation of 3-formylchromones **1a–d** with phenylhydrazine hydrochlorides **2a–i** in the presence of acetic acid in methanol at 60 °C provided



Scheme 1. Preparation of hydrazones 3a–v

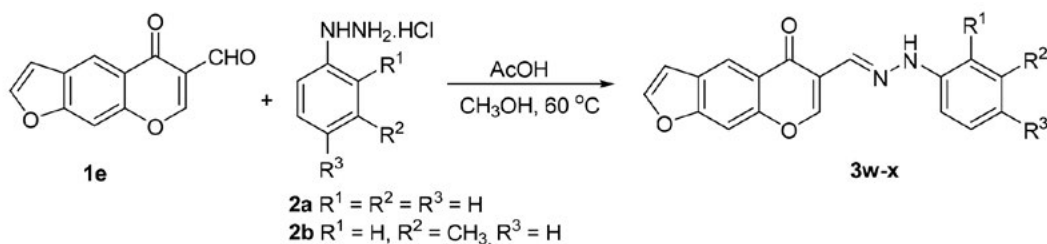
the corresponding hydrazones **3a–v** as yellow color solids (Scheme 1, Table 1). The compounds **3a**, **3j** and **3t** are known and were compared with the literature data.^{15–18} The compounds **3b–i**, **3k–s** and **3u–z** are unknown and were well characterized by spectral data.

Schemes 2 and 3 describe the preparation of linear and angular furo hydrazones **3w–z**. The carboxaldehydes **1e,f** was prepared as per our previous reported method.¹³

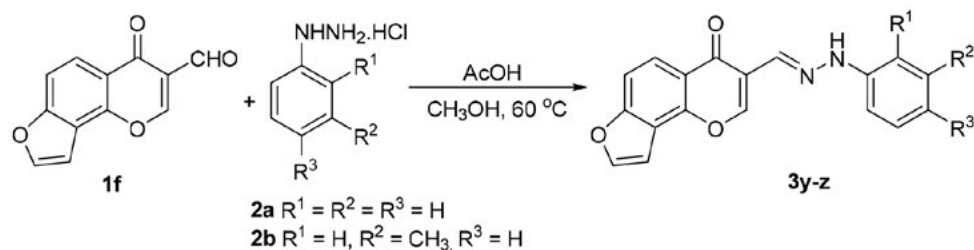
Condensation of carbaldehydes **1e,f** with phenylhydrazine hydrochlorides **2a,b** provided the hydrazones **3w–z** (Table 1).

2. 2. Preparation of Pyrazolecarboxylates 5a–x

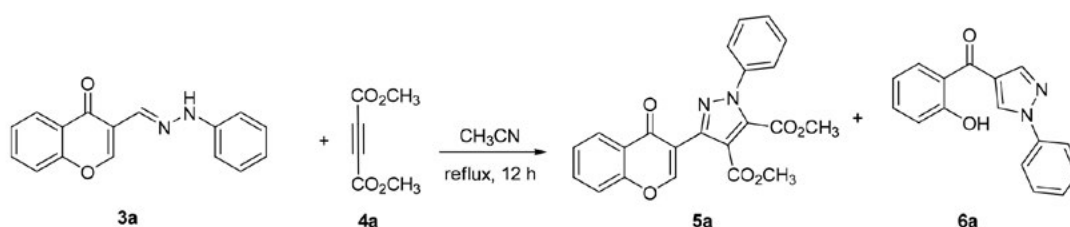
Schemes 4–7 describe the preparation of pyrazolecarboxylates **5a–x** by cycloaddition reaction of hydrazones



Scheme 2. Preparation of hydrazones 3w–x



Scheme 3. Preparation of hydrazones 3y–z



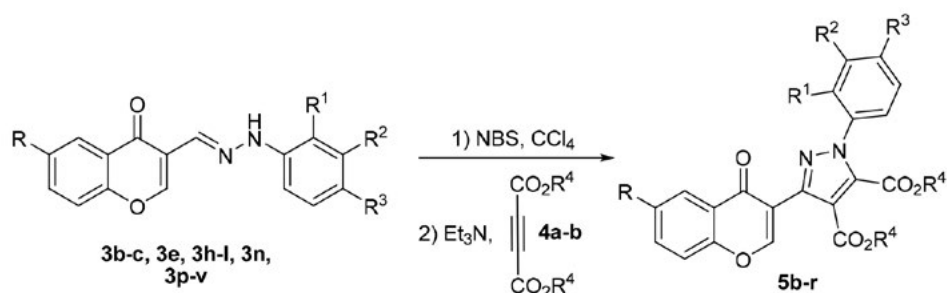
Scheme 4. Preparation of pyrazolecarboxylate 5a

and activated alkynes. Initially, the cycloaddition reaction has been conducted with hydrazone **3a** and acetylenedicarboxylate **4a** in acetonitrile as the solvent under reflux conditions. This reaction provided two compounds, pyrazolecarboxylate **5a** and pyrazolymethanone **6a** (Scheme 4). These two compounds were separated by column chromatography and characterized by spectral data.

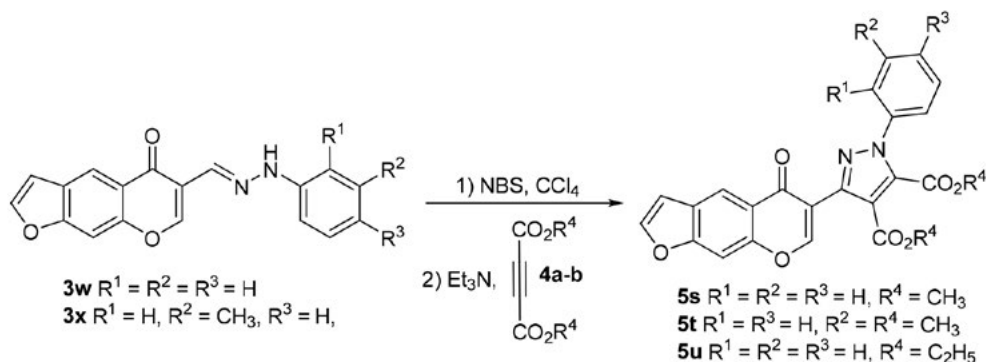
In order to prepare the compound **5a** in an exclusive manner, bromination reaction has been carried out on **3a** with *N*-bromosuccinimide (NBS) in carbon tetrachloride at 55–60 °C. The reaction was monitored by TLC (3–4 h) and the usual workup afforded the corresponding α -bromophenylhydrazonochromone.¹⁹ Next, the [3+2] cycloaddition reaction have been conducted between α -bromophenylhydrazonochromone and acetylenedicarboxylates **4a–b** in the presence of triethylamine. This provided

the corresponding pyrazolecarboxylates **5a** and **5r**. In order to prepare series of pyrazolecarboxylates **5**, the bromination and cycloaddition reactions have been carried out on hydrazones **3b–c**, **3e**, **3h–l**, **3n** and **3p–v** with **4a** to provide a set of pyrazolecarboxylates **5b–q** (Scheme 5, Table 2). The compound **5a** is known and was compared with the literature data.¹⁹ Compounds **5b–r** are new and were well characterized by spectral data.

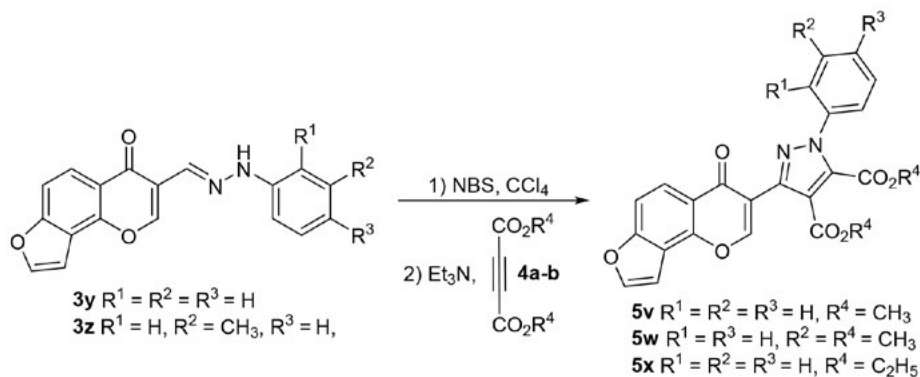
Having achieved the pyrazolecarboxylates, further the preparation of linear and angular pyrazolecarboxylates **5s–x** has been planned. Accordingly, the bromination followed by cycloaddition reaction have been carried out with hydrazones **3w–z** and activated alkynes **4a–b** to provide corresponding pyrazolecarboxylates **5s–x** (Schemes 6 and 7, Table 2). The compounds **5s–x** are unknown and were well characterized by spectral data.



Scheme 5. Preparation of pyrazolecarboxylates **5b–r**



Scheme 6. Preparation of linear furochromenyl pyrazolecarboxylates **5s–u**



Scheme 7. Preparation of angular furochromenyl pyrazolecarboxylates **5v–x**

2. 3. Preparation of pyrazolymethanones

6a–u

The cycloaddition reaction of hydrazone **3a** with acetylenedicarboxylate **4a** provided two compounds, pyrazolecarboxylate **5a** and pyrazolymethanone **6a** Scheme 4. The pyrazolymethanone compound **6a** is known in the literature, however, the development of synthetic procedures for these molecules and their biological properties are not well established, yet. Therefore, a series of pyrazolymethanones **6b–u** have been prepared by the reaction of hydrazones **3a–h**, **3k–s**, **3u–x** with K_2CO_3 in acetonitrile at room temperature (Schemes 8 and 9, Table 3). The known compound **6a** was compared with the literature data²⁰ and the unknown compounds **6b–u** are well characterized by spectral data.

3. Biology

Thus synthesized hydrazones **3a–z**, pyrazolecarboxylates **5a–x** and pyrazolymethanones **6a–u** were screened for their anti-proliferative activity against four cancer cell lines, viz. A549 (lung), HeLa (cervical), DU145 (prostate), MDA MB 231 (breast) by MTT assay.¹³

3. 1. Anti-proliferative Activity of Hydrazones

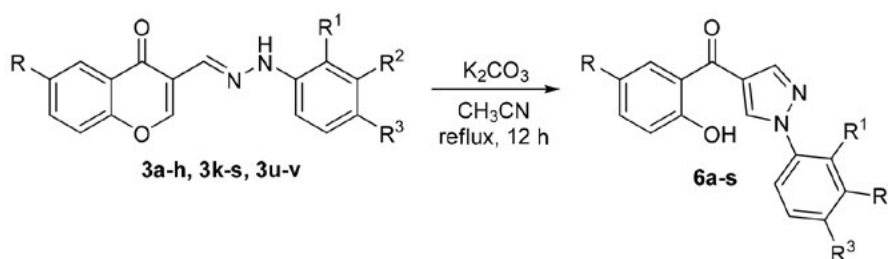
3a–z

The anti-proliferative activity of hydrazones and their IC_{50} values along with standard drug doxorubicin are presented in Table 1. The compounds **3a–i** displayed activity in the range of IC_{50} 46.0–170.1 μM in all the tested cell lines. The presence of a methyl group on the chromanone moiety and a halogen, methyl and methoxy

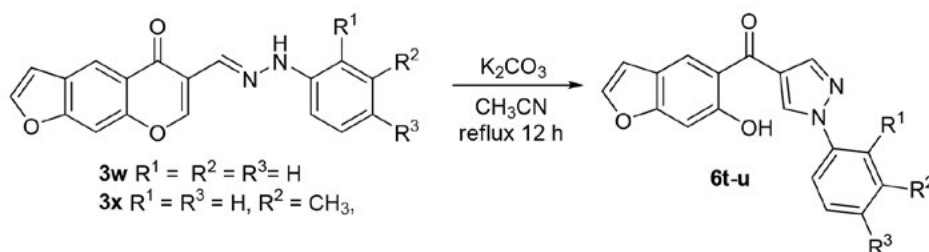
substituents on the phenyl ring in **3j–p** displayed activity in the range of IC_{50} 41.2–494.7 μM in all the tested cell lines. The presence of halogens on chromanones and a methyl or a methoxy group on the phenyl ring in **3q–v** displayed activity in the range of IC_{50} 14.0–355.5 μM in all the tested cell lines. However, compound **3s** (IC_{50} 19.7, 14.0, 17.8 μM) has shown promising activity on A549, HeLa and DU145, respectively. The linear **3w–x** and angular **3y–z** furo chromanones showed activity in the range of IC_{50} 42.1–183.7 μM in all the tested cell lines.

3. 2. Anti-proliferative Activity of Pyrazolecarboxylates 5a–x

The anti-proliferative activity of pyrazolecarboxylates **5a–x** and their IC_{50} values along with the data for the standard drug are presented in Table 2. The compound **5d** (IC_{50} 24.0 μM) having a fluoro substituent on the phenyl ring has shown better activity on A549 when compared to the methyl **5b**, methoxy **5c**, bromo **5e** and chloro **5f** derivatives. The methyl substituted chromanones **5g** (IC_{50} 13.0 μM) and **5h** (IC_{50} 19.0 μM) displayed promising activity on HeLa and DU145, respectively when compared to **5i–k**. The bromo substituted chromanone with a methyl group **5p** (IC_{50} 5.0 μM) or a methoxy group **5q** (IC_{50} 11.0 μM) on the phenyl ring displayed the potent activity. Chloro substituted chromanone **5m** (IC_{50} 24.0 μM) displayed better activity on DU145 when compared to the corresponding methoxy derivative **5n**. The angular furo derivative **5w** (IC_{50} 5.0 μM) has shown potent activity on HeLa and promising activity on DU145 (IC_{50} 15.0 μM) when compared to the corresponding linear furo derivative **5t**.



Scheme 8. Preparation of pyrazolymethanones **6a–s**



Scheme 9. Preparation of linear pyrazolymethanones **6t–u**

Table 1. Anti-proliferative activity of hydrazones*

Compounds	R	R ¹	R ²	R ³	A549	HeLa	DU145	MDA MB 231
3a	H	H	H	H	170.1 ± 8.4	48.5 ± 2.9	91.1 ± 3.8	78.2 ± 3.1
3b	H	H	CH ₃	H	70.6 ± 5.1	151.7 ± 7.8	57.4 ± 2.6	58.3 ± 4.5
3c	H	H	H	OCH ₃	69.7 ± 3.9	63.5 ± 4.5	101.9 ± 5.8	85.4 ± 3.9
3d	H	F	H	H	77 ± 4.8	72.3 ± 6.4	82.8 ± 6.8	69.1 ± 3.9
3e	H	H	F	H	66.2 ± 2.8	77.4 ± 4.9	50.7 ± 2.4	85.6 ± 6.4
3f	H	H	Cl	H	46 ± 2.5	84.5 ± 6.7	59.2 ± 2.9	156.9 ± 11.5
3g	H	H	H	F	49.7 ± 2.1	67.9 ± 3.8	84 ± 3.1	87.3 ± 4.5
3h	H	H	H	Br	46.4 ± 4.6	104.7 ± 8.3	56.8 ± 2.7	154.2 ± 9.7
3i	H	Cl	H	Cl	80.5 ± 6.1	128.2 ± 8.5	80.4 ± 2.5	124.3 ± 9.4
3j	CH ₃	H	H	H	63.3 ± 3.4	164.6 ± 9.8	102.3 ± 8.9	157.2 ± 9.5
3k	CH ₃	H	CH ₃	H	76.6 ± 3.4	77.7 ± 4.8	91.4 ± 3.4	112.5 ± 7.9
3l	CH ₃	H	H	OCH ₃	80.2 ± 3.9	494.7 ± 13.2	103.2 ± 4.9	345.6 ± 16.7
3m	CH ₃	F	H	H	41.2 ± 1.3	101.6 ± 8.7	46.7 ± 3.8	68.3 ± 3.5
3n	CH ₃	H	F	H	92.5 ± 5.4	48 ± 2.1	93.5 ± 2.7	91.5 ± 4.1
3o	CH ₃	H	H	F	63.1 ± 3.4	68.5 ± 6.7	80 ± 3.4	76.5 ± 6.8
3p	CH ₃	H	H	Br	73.7 ± 6.1	58.2 ± 4.4	152.1 ± 10.2	225.3 ± 9.8
3q	Cl	H	H	H	52.2 ± 2.8	75 ± 5.1	355.5 ± 12.1	312.2 ± 18.4
3r	Cl	H	CH ₃	H	45.1 ± 4.8	53.9 ± 4.1	48.1 ± 3.5	78.5 ± 2.7
3s	Cl	H	H	OCH ₃	19.7 ± 2.1	14 ± 1.7	17.8 ± 2.1	74.2 ± 2.8
3t	Br	H	H	H	191.2 ± 12	134.8 ± 9.7	72.1 ± 3.7	69.6 ± 4.1
3u	Br	H	CH ₃	H	76.9 ± 3.7	65.9 ± 4.1	91.2 ± 7.1	227.1 ± 12.1
3v	Br	H	H	OCH ₃	63.4 ± 5.4	66.6 ± 3.4	59.6 ± 3.9	75.4 ± 3.3
3w	–	H	H	H	54.9 ± 3.6	68.9 ± 3.1	92.7 ± 3.8	98.5 ± 6.7
3x	–	H	CH ₃	H	81.2 ± 4.9	64.7 ± 2.4	47.6 ± 1.9	89.3 ± 5.8
3y	–	H	H	H	45.9 ± 2.7	183.7 ± 12.9	62.3 ± 2.5	128.3 ± 8.7
3z	–	H	CH ₃	H	125.6 ± 8.9	95.7 ± 6.4	42.1 ± 2.8	74.2 ± 4.7
Doxorubicin					3.04 ± 1.1	2.51 ± 0.9	3.73 ± 1.3	5.05 ± 1.7

* IC₅₀ (μM) Inhibitory concentration; 3w, 3x are linear and 3y, 3z are the angular compounds.

Table 2. Anti-proliferative activity of pyrazolecarboxylates

Compounds	R	R ¹	R ²	R ³	R ⁴	A549	HeLa	DU-145	MDAMB 231
5a	H	H	H	H	CH ₃	311 ± 6.7	296 ± 5.7	112 ± 5.2	130 ± 3.8
5b	H	H	CH ₃	H	CH ₃	070 ± 3.5	164 ± 4.9	087 ± 4.3	057 ± 4.5
5c	H	H	H	OCH ₃	CH ₃	200>	211 ± 3.9	061 ± 3.7	128 ± 2.5
5d	H	H	F	H	CH ₃	024 ± 3.8	233 ± 4.1	054 ± 2.5	080 ± 3.2
5e	H	H	H	Br	CH ₃	255 ± 5.4	194 ± 3.9	148 ± 3.6	200>
5f	H	Cl	H	Cl	CH ₃	108 ± 4.5	139 ± 4.6	149 ± 3.5	200>
5g	CH ₃	H	H	H	CH ₃	045 ± 4.9	013 ± 2.6	200>	070 ± 4.6
5h	CH ₃	H	CH ₃	H	CH ₃	051 ± 3.4	235 ± 6.9	019 ± 2.1	131 ± 4.9
5i	CH ₃	H	H	OCH ₃	CH ₃	047 ± 3.2	081 ± 5.6	200>	098 ± 4.5
5j	CH ₃	H	F	H	CH ₃	165 ± 5.2	330 ± 6.8	088 ± 2.4	128 ± 4.9
5k	CH ₃	H	H	Br	CH ₃	083 ± 1.5	072 ± 2.9	200>	119 ± 4.6
5l	Cl	H	H	H	CH ₃	056 ± 3.7	282 ± 5.8	123 ± 4.2	113 ± 3.8
5m	Cl	H	CH ₃	H	CH ₃	119 ± 5.7	200>	024 ± 1.4	078 ± 3.4
5n	Cl	H	H	OCH ₃	CH ₃	085 ± 6.4	228 ± 7.7	065 ± 4.2	094 ± 4.1
5o	Br	H	H	H	CH ₃	055 ± 3.4	213 ± 7.6	100>	065 ± 6.1
5p	Br	H	CH ₃	H	CH ₃	111 ± 6.1	194 ± 5.1	005 ± 1.0	019 ± 2.1
5q	Br	H	H	OCH ₃	CH ₃	183 ± 8.7	073 ± .2	200>	011 ± 2.1
5r	H	H	H	H	C ₂ H ₅	066 ± 4.0	161 ± 4.8	084 ± 2.4	200>
5s	–	H	H	H	CH ₃	025 ± 2.5	200>	200>	094 ± 3.9
5t	–	H	CH ₃	H	CH ₃	068 ± 3.7	200>	200>	200>
5u	–	H	H	H	C ₂ H ₅	90 ± 5.10	027 ± 2.2	067 ± 5.1	200>
5v	–	H	H	H	CH ₃	200>	200>	200>	049 ± 2.8
5w	–	H	CH ₃	H	CH ₃	115 ± 4.1	005 ± 1.5	015 ± 2.1	075 ± 4.4
5x	–	H	H	H	C ₂ H ₅	079 ± 4.8	033 ± 2.9	200>	076 ± 4.5
Doxorubicin						3.04 ± 1.1	3.73 ± 1.3	2.51 ± 0.9	5.05 ± 1.7

* IC₅₀ (μM) Inhibitory concentration; 5s–u are the linear and 5v–x are the angular compounds.

3. 3. Anti-proliferative Activity of Pyrazolymethanones 6a–u

The anti-proliferative activity of pyrazolymethanones **6a–u** and their IC_{50} values along with the standard drug are presented in Table 3. The compounds **6a–h** displayed activity in the range of IC_{50} 10.8–164.9 μ M in all the tested cell lines. The fluoro substituted pyrazole **6e** (IC_{50} 10.8 μ M) has shown potent activity on HeLa cell line and promising activity on A549 (IC_{50} 15.6 μ M) when compared to the corresponding methyl **6b**, methoxy **6c**, chloro **6f** and bromo **6h** derivatives. It is interesting to note that the fluoro substituent on the *meta* position **6e** displayed activity when compared to *ortho* **6d** and *para* **6g** analogues. The compound having a methyl substituent on the phenyl ring and a methoxy group on the pyrazole phenyl moiety **6j** (IC_{50} 7.9 μ M) has shown potent activity on HeLa cell line and promising activity on DU145, A549 (IC_{50} 16.1, 19.9 μ M), respectively when compared to methyl **6i** and halogen derivatives **6k–6n**.

Overall in the present series of compounds the hydrazone derivative **3s** displayed promising activity on three cell lines (A549, IC_{50} 19.7; HeLa, IC_{50} 14.0; DU145, IC_{50} 17.8 μ M). Pyrazole carboxylates **5p** and **5w** (IC_{50} 5.0 μ M) displayed potent activity on DU145, HeLa and promising activity on MDAMB 231 (IC_{50} 19.0 μ M) and DU145 (IC_{50} 15.0 μ M). The compound **5q** (IC_{50} 11.0 μ M) displayed potent activity selectively on MDAMB 231. Pyrazolymethanone **6e** (IC_{50} 10.8, 15.6 μ M) displayed potent activity on

HeLa and promising activity on A549. Compound **6j** (IC_{50} 7.9, 16.1, 19.9 μ M) displayed potent activity on HeLa, promising activity on DU145 and A549, respectively.

4. Experimental

4. 1. Chemistry

1H NMR and ^{13}C NMR spectra were recorded on an Avance 300 MHz spectrometer in $CDCl_3$ using TMS as internal standard. FT-IR spectra were recorded on a Nicolet 740 FT-IR spectrometer. Mass spectra were obtained on Agilent ESI-MS instrument. Melting points were determined in open glass capillary tubes on a Mettler FP 51 melting point apparatus and are uncorrected. All the reactions were monitored by thin layer chromatography (TLC) on pre-coated silica gel (60 F₂₅₄ mesh); spots were visualized under UV light. Merck silica gel (60–120; 100–200 mesh) was used for chromatography. All the reactions were carried out using reagent-grade solvents. The reagents were purchased from Sigma-Aldrich and local suppliers (Sd fine & AVRA chemicals Pvt. Ltd, Hyderabad, India).

4. 2. General Procedure for the Preparation of Hydrazones 3a–z

The warmed solution of phenylhydrazine hydrochloride **2a** (0.172 g, 1.2 mmol) and acetic acid (0.5 mL in 1 mL

Table 3. Anti-proliferative activity of pyrazolymethanones

Compounds	R	R ¹	R ²	R ³	A549	HeLa	DU-145	MDAMB 231
6a	H	H	H	H	44.4 ± 2.4	164.9 ± 9.5	45.1 ± 2.7	52.1 ± 3.4
6b	H	H	CH ₃	H	126.7 ± 6.	86.8 ± 2.8	83.3 ± 3.5	93.5 ± 4.8
6c	H	H	H	OCH ₃	143.2 ± 9	85.3 ± 3.1	46.7 ± 6.1	119.3 ± 7.7
6d	H	F	H	H	62.3 ± 2.5	51.1 ± 2.9	87.2 ± 5.8	98.7 ± 3.9
6e	H	H	F	H	15.6 ± 2.7	10.8 ± 1.6	26.1 ± 2.4	45.8 ± 3.1
6f	H	H	Cl	H	98.5 ± 8.1	83.8 ± 4.1	60 ± 3.8	86.6 ± 5.6
6g	H	H	H	F	82.1 ± 4.6	164.9 ± 5.8	51.2 ± 5.2	91.5 ± 4.9
6h	H	H	H	Br	42.5 ± 3.7	56.9 ± 2.7	63.7 ± 4.9	65.2 ± 3.5
6i	CH ₃	H	CH ₃	H	68.5 ± 3.1	45.5 ± 3.5	47.2 ± 2.9	78.6 ± 5.1
6j	CH ₃	H	H	OCH ₃	19.9 ± 1.9	7.9 ± 1.1	16.1 ± 2.5	35.2 ± 2.8
6k	CH ₃	F	H	H	70.8 ± 4.3	73.7 ± 3.1	245.9 ± 9.7	215.1 ± 12.4
6l	CH ₃	H	F	H	82.2 ± 3.5	58.2 ± 3.7	54.4 ± 4.1	119.4 ± 8.9
6m	CH ₃	H	H	F	59.9 ± 2.9	49.3 ± 2.1	66.7 ± 1.9	185.4 ± 9.1
6n	CH ₃	H	H	Br	164.9 ± 7.	67.7 ± 3.9	54.3 ± 2.3	85.2 ± 3.7
6o	Cl	H	H	H	82.7 ± 6.4	50.2 ± 3.1	119.5 ± 6.7	175.2 ± 9.4
6p	Cl	H	CH ₃	H	52.9 ± 2.9	71.3 ± 2.4	55.5 ± 3.1	76.5 ± 1.8
6q	Cl	H	H	OCH ₃	98.3 ± 8.1	51.4 ± 2.9	116.1 ± 5.8	83.5 ± 2.7
6r	Br	H	CH ₃	H	220.2 ± 11	170.3 ± 9.8	64.5 ± 6.4	128.3 ± 6.7
6s	Br	H	H	OCH ₃	61.3 ± 3.8	51.4 ± 1.9	66.1 ± 2.9	75.8 ± 4.1
6t	–	H	H	H	45.6 ± 5.4	164.9 ± 11.2	62.4 ± 4.5	86.5 ± 1.6
6u	–	H	CH ₃	H	125.9 ± 9.	50.9 ± 3.7	82.7 ± 2.3	75.6 ± 2.4
Doxorubicin					3.04 ± 1.1	2.51 ± 0.9	3.73 ± 1.3	5.05 ± 1.7

* IC_{50} (μ M) Inhibitory concentration; **6t–u** are the linear compounds.

H₂O) was added to a stirred solution of 3-formylchromone (0.174 g, 1 mmol) in methanol (2 mL) at room temperature. The reaction mixture was heated to 60 °C for 30 min and then cooled to room temperature. The solid separated was filtered, washed with ice-cold water (5 mL) and then recrystallized from hot methanol providing the corresponding hydrazone **3a**. Similarly, the other hydrazones **3b–z** were prepared from the corresponding 3-formylchromones **1a–f** and phenylhydrazine hydrochlorides **2a–i** under optimized reaction conditions.

(E)-3-((2-Phenylhydrazono)methyl)-4H-chromen-4-one (3a)

Yellow solid. Yield 88%. M.p. 212–213 °C. FT-IR (KBr): ν 3265, 1618, 1526, 1258, 1171 cm⁻¹. ¹H NMR (300 MHz, CDCl₃+DMSO-*d*₆): δ 8.66 (s, 1H, imine), 8.14 (dd, 1H, *J*₁ = 6.2 Hz, *J*₂ = 7.8 Hz), 7.97 (s, 1H, Ar-H), 7.77 (t, 1H, *J* = 6.2 Hz, Ar-H), 7.60 (d, 1H, *J* = 8.5 Hz, Ar-H), 7.47 (t, 1H, *J* = 8.8 Hz, Ar-H), 7.17 (t, 2H, *J* = 7.0 Hz, Ar-H), 7.04 (d, 2H, *J* = 7.0 Hz, Ar-H), 6.72 (t, 1H, *J* = 7.8 Hz, Ar-H). ¹³C NMR (75 MHz, CDCl₃+DMSO-*d*₆): δ 173.6, 154.9, 152.1, 144.5, 142.0, 133.7, 132.1, 128.7, 128.4, 127.1, 123.7, 122.3, 118.9, 118.4, 111.7. ESI-MS: *m/z* [M+H]⁺ 265.

(E)-3-((2-*m*-Tolylhydrazono)methyl)-4H-chromen-4-one (3b)

Yellow solid. Yield 76%. M.p. 231–233 °C. FT-IR (KBr): ν 2977, 1622, 1571, 1491, 1206, 1130, 1094, 872, 748 cm⁻¹. ¹H NMR (300 MHz, CDCl₃+DMSO-*d*₆): δ 8.46 (s, 1H, imine), 7.90 (s, 1H, Ar-H), 7.86 (s, 1H, Ar-H), 7.43 (d, 1H, *J* = 8.8 Hz, Ar-H), 7.34 (d, 1H, *J* = 8.8 Hz, Ar-H), 7.07 (t, 2H, *J* = 8.8, 6.8 Hz, Ar-H), 6.95 (d, 2H, *J* = 7.8 Hz, Ar-H), 6.63 (t, 1H, *J* = 7.8 Hz, Ar-H). ESI-MS: *m/z* [M+H]⁺ 278.

(E)-3-((2-(4-Methoxyphenyl)hydrazono)methyl)-4H-chromen-4-one (3c)

Yellow solid. Yield 89%. M.p. 237–239 °C. FT-IR (KBr): ν 3271, 2901, 1621, 1570, 1464, 1228, 1042, 827, 791 cm⁻¹. ¹H NMR (300 MHz, CDCl₃+DMSO-*d*₆): δ 8.66 (s, 1H, imine), 8.13 (dd, 1H, *J*₁ = 6.8 Hz, *J*₂ = 8.8 Hz, Ar-H), 7.92 (s, 1H, *J* = 7.8 Hz, Ar-H), 7.82–7.76 (m, 1H, Ar-H), 7.66–7.60 (m, 1H, Ar-H), 7.52–7.46 (m, 1H, Ar-H), 7.02–6.98 (m, 2H, Ar-H), 6.82–6.76 (m, 2H, Ar-H), 3.72 (s, 3H, OCH₃). ¹³C NMR (75 MHz, CDCl₃+DMSO-*d*₆): δ 163.5, 150.3, 145.4, 131.9, 131.1, 128.4, 123.9, 119.2, 119.1, 117.2, 115.3, 52.3. ESI-MS: *m/z* 295 [M+H]⁺.

(E)-3-((2-(2-Fluorophenyl)hydrazono)methyl)-4H-chromen-4-one (3d)

Yellow solid. Yield 71%. M.p. 232–234 °C. ¹H NMR (300 MHz, CDCl₃+DMSO-*d*₆): δ 8.60 (s, 1H, imine), 8.23 (s, 1H, Ar-H), 8.16 (d, 1H, *J* = 7.9 Hz, Ar-H), 7.73 (t, 1H, *J* = 6.9 Hz, Ar-H), 7.50–7.42 (m, 2H, Ar-H), 7.04–6.94 (m, 2H, Ar-H), 6.70 (t, 1H, *J* = 6.9 Hz, Ar-H). ¹³C NMR (75 MHz, CDCl₃+DMSO-*d*₆): δ 175.1, 155.9, 153.0, 150.8,

142.5, 134.5, 131.2, 130.6, 125.4, 123.5, 118.8, 114.3. ESI-MS: *m/z* [M+H]⁺ 283.

(E)-3-((2-(3-Fluorophenyl)hydrazono)methyl)-4H-chromen-4-one (3e)

Yellow solid. Yield 73%. M.p. 249–251 °C. FT-IR (KBr): ν 3265, 2793, 1623, 1484, 1171, 816, 779 cm⁻¹. ¹H NMR (300 MHz, CDCl₃+DMSO-*d*₆): δ 8.78 (s, 1H, imine), 8.02 (s, 1H), 7.98 (s, 1H, Ar-H), 7.60 (d, 1H, *J* = 8.8 Hz, Ar-H), 7.54 (d, 1H, *J* = 8.8 Hz, Ar-H), 6.98 (s, 2H, Ar-H), 6.74 (s, 1H, Ar-H).

(E)-3-((2-(3-Chlorophenyl)hydrazono)methyl)-4H-chromen-4-one (3f)

Yellow solid. Yield 69%. M.p. 254–256 °C. ¹H NMR (300 MHz, CDCl₃+DMSO-*d*₆): δ 8.67 (s, 1H, imine), 8.21 (d, 1H, *J* = 7.9 Hz, Ar-H), 8.04 (s, 1H, Ar-H), 7.93 (d, 1H, *J* = 1.2 Hz, Ar-H), 7.76 (d, 1H, *J* = 7.9 Hz, Ar-H), 7.65–7.43 (m, 2H, Ar-H), 7.11 (s, 1H, Ar-H), 6.96 (d, 1H, *J* = 8.6 Hz, Ar-H), 7.70 (d, 1H, *J* = 7.2 Hz, Ar-H). ¹³C NMR (75 MHz, CDCl₃+DMSO-*d*₆): δ 173.4, 161.0, 154.2, 150.3, 144.7, 132.5, 132.2, 128.5, 127.6, 123.6, 121.8, 117.9, 116.6, 109.9, 108.9.

(E)-3-((2-(4-Fluorophenyl)hydrazono)methyl)-4H-chromen-4-one (3g)

Yellow solid. Yield 73%. M.p. 241–243 °C. ¹H NMR (300 MHz, CDCl₃+DMSO-*d*₆): δ 8.80 (s, 1H, imine), 8.12 (dd, 1H, *J*₁ = 7.9 Hz, *J*₂ = 1.5 Hz, Ar-H), 7.96 (s, 1H, Ar-H), 7.82 (dt, 1H, *J*₁ = 8.6 Hz, *J*₂ = 7.6 Hz, *J*₃ = 1.8 Hz, Ar-H), 7.69 (d, 1H, *J* = 8.1 Hz, Ar-H), 7.52 (t, 2H, *J* = 7.1 Hz, Ar-H), 7.06 (d, 3H, *J* = 6.6 Hz, Ar-H). ¹³C NMR (75 MHz, CDCl₃+DMSO-*d*₆): δ 190.3, 175.2, 158.7, 152.5, 142.7, 134.5, 132.1, 130.9, 128.1, 125.4, 123.4, 119.5, 118.8, 117.5, 115.9.

(E)-3-((2-(4-Bromophenyl)hydrazono)methyl)-4H-chromen-4-one (3h)

Pale yellow solid. Yield 77%. M.p. 226–228 °C. FT-IR (KBr): ν 3271, 2901, 1621, 1570, 1464, 1228, 1042, 827, 791 cm⁻¹. ¹H NMR (300 MHz, CDCl₃+DMSO-*d*₆): δ 8.81 (s, 1H, imine), 8.11 (d, 2H, *J* = 7.8 Hz, Ar-H), 7.97 (s, 1H, Ar-H), 7.81 (t, 1H, *J* = 8.4 Hz, Ar-H), 7.68 (d, 1H, *J* = 8.3 Hz, Ar-H), 7.35 (d, 2H, *J* = 8.6 Hz, Ar-H), 7.01 (d, 2H, *J* = 8.6 Hz, Ar-H). ¹³C NMR (75 MHz, CDCl₃+DMSO-*d*₆): δ 173.2, 153.9, 150.2, 142.4, 132.2, 129.7, 127.0, 123.6, 123.4, 121.5, 117.7, 116.6, 112.1, 108.0.

(E)-3-((2-(2,4-Dichlorophenyl)hydrazono)methyl)-4H-chromen-4-one (3i)

Yellow solid. Yield 64%. M.p. 225–227 °C. FT-IR (KBr): ν 3265, 2793, 1623, 1484, 1171 cm⁻¹. ¹H NMR (300 MHz, CDCl₃+DMSO-*d*₆): δ 8.76 (s, 1H, imine), 8.40 (s, 1H), 8.14 (t, 1H, *J*₁ = 6.8 Hz, *J*₂ = 8.8 Hz, Ar-H), 7.80 (dd, 2H, *J*₁ = 7.9 Hz, *J*₂ = 7.1 Hz, Ar-H), 7.66–7.46 (m, 3H, Ar-H), 6.20 (d, 1H, *J* = 7.8 Hz, Ar-H). ESI-MS: *m/z* [M+H]⁺ 333.

(E)-6-Methyl-3-((2-phenylhydrazono)methyl)-4H-chromen-4-one (3j)

Yellow solid. Yield 72%. M.p. 203–205 °C. FT-IR (KBr): ν 3265, 2977, 1622, 1571, 1491, 1206, 1130, 1094, 872, 748 cm^{-1} . ^1H NMR (300 MHz, CDCl_3 + $\text{DMSO}-d_6$): δ 8.55 (s, 1H, imine), 8.03 (d, 1H, $J = 8.8$ Hz), 7.98 (s, 1H, Ar-H), 7.35 (s, 1H, Ar-H), 7.26 (d, 1H, $J = 8.8$ Hz, Ar-H), 7.17 (t, 2H, $J = 8.8$ Hz, Ar-H), 7.04 (d, 2H, $J = 7.8$ Hz, Ar-H), 6.73 (t, 1H, $J = 7.8$ Hz, Ar-H). ^{13}C NMR (75 MHz, CDCl_3 + $\text{DMSO}-d_6$): δ 173.6, 161.6, 150.4, 146.6, 141.3, 138.2, 130.3, 129.7, 128.7, 126.8, 124.4, 122.4, 119.6, 118.7, 117.4, 111.4, 21.0. ESI-MS: m/z $[\text{M}+\text{H}]^+$ 279.

(E)-6-Methyl-3-((2-*m*-tolylhydrazono)methyl)-4H-chromen-4-one (3k)

Yellow solid. Yield 71%. M.p. 222–224 °C. FT-IR (KBr): ν 3276, 1640, 1608 cm^{-1} . ^1H NMR (300 MHz, CDCl_3 + $\text{DMSO}-d_6$): δ 8.55 (s, 1H, imine), 7.96 (s, 1H, Ar-H), 7.92 (s, 1H, Ar-H), 7.52 (d, 1H, $J = 7.0$ Hz, Ar-H), 7.44 (d, 1H, $J = 8.0$ Hz, Ar-H), 7.02 (t, 1H, $J = 8.0$ Hz, Ar-H), 6.85 (s, 1H, Ar-H), 6.81 (d, 1H, $J = 8.0$ Hz, Ar-H), 6.52 (d, 1H, $J = 7.0$ Hz, Ar-H). ^{13}C NMR (75 MHz, CDCl_3 + $\text{DMSO}-d_6$): δ 174.6, 153.7, 151.7, 144.7, 137.9, 135.0, 134.9, 128.6, 127.5, 124.1, 122.6, 119.5, 119.1, 118.1, 112.2, 109.1, 21.0, 20.2. ESI-MS: m/z $[\text{M}+\text{H}]^+$ 293.

(E)-3-((2-(4-Methoxyphenyl)hydrazono)methyl)-6-methyl-4H-chromen-4-one (3l)

Yellow solid. Yield 79%. M.p. 246–248 °C. FT-IR (KBr): ν 3271, 2901, 1621, 1570, 1464, 1228, 1042, 827, 791 cm^{-1} . ^1H NMR (300 MHz, CDCl_3 + $\text{DMSO}-d_6$): δ 8.57 (s, 1H, imine), 7.95 (d, 1H, $J = 7.8$ Hz, Ar-H), 7.54 (s, 1H, Ar-H), 7.37 (s, 1H, Ar-H), 7.20 (s, 1H, Ar-H), 7.01 (d, 2H, $J = 8.6$ Hz, Ar-H), 6.78 (d, 2H, $J = 8.6$ Hz, Ar-H), 3.74 (s, 3H, OCH_3), 2.48 (s, 3H, CH_3). ^{13}C NMR (75 MHz, CDCl_3 + $\text{DMSO}-d_6$): δ 173.0, 152.1, 150.8, 149.4, 137.2, 124.8, 122.5, 121.1, 117.8, 116.3, 112.5, 111.1, 53.3, 18.7. ESI-MS: m/z $[\text{M}+\text{H}]^+$ 309.

(E)-3-((2-(2-Fluorophenyl)hydrazono)methyl)-6-methyl-4H-chromen-4-one (3m)

Yellow solid. Yield 83%. M.p. 230–232 °C. FT-IR (KBr): ν 3283, 1623, 1525, 1462, 1130, 753 cm^{-1} . ^1H NMR (300 MHz, CDCl_3 + $\text{DMSO}-d_6$): δ 8.75 (s, 1H, imine), 8.25 (s, 1H, Ar-H), 7.91 (s, 1H, Ar-H), 7.63 (dd, 1H, $J_1 = 8.4$ Hz, $J_2 = 18$ Hz, Ar-H), 7.57 (s, 1H, Ar-H), 7.55–7.49 (m, 1H, Ar-H), 7.06 (d, 2H, $J = 7.7$ Hz, Ar-H), 6.75 (t, 1H, $J = 6.6$ Hz, Ar-H), 2.46 (s, 3H, CH_3). ^{13}C NMR (75 MHz, CDCl_3 + $\text{DMSO}-d_6$): δ 184.1, 173.0, 169.6, 152.2, 150.4, 133.3, 129.2, 122.8, 122.5, 121.2, 117.5, 116.4, 113.0, 112.1, 18.7. ESI-MS: m/z $[\text{M}+\text{H}]^+$ 297.

(E)-3-((2-(3-Fluorophenyl)hydrazono)methyl)-6-methyl-4H-chromen-4-one (3n)

Yellow solid. Yield 67%. M.p. 261–263 °C. ^1H NMR (300 MHz, CDCl_3 + $\text{DMSO}-d_6$): δ 8.57 (s, 1H, imine), 8.18 (s, 1H, Ar-H), 7.87 (s, 1H, Ar-H), 7.52 (d, 1H, $J = 8.0$ Hz,

Ar-H), 7.43 (d, 1H, $J = 8.0$ Hz, Ar-H), 7.00–6.93 (m, 2H, Ar-H), 6.67 (t, 2H, $J = 6.0$ Hz, Ar-H), 2.43 (s, 3H, CH_3). ^{13}C NMR (75 MHz, CDCl_3 + $\text{DMSO}-d_6$): δ 175.3, 154.5, 153.1, 147.6, 135.8, 131.1, 129.9, 124.8, 123.4, 119.5, 118.9, 108.6, 105.3, 98.9, 20.9. ESI-MS: m/z $[\text{M}+\text{H}]^+$ 297.

(E)-3-((2-(4-Fluorophenyl)hydrazono)methyl)-6-methyl-4H-chromen-4-one (3o)

Yellow solid. Yield 72%. M.p. 264–266 °C. ^1H NMR (300 MHz, CDCl_3 + $\text{DMSO}-d_6$): δ 8.64 (s, 1H, imine), 7.98 (s, 1H, Ar-H), 7.92 (s, 1H, Ar-H), 7.58 (dd, 1H, $J_1 = 8.6$ Hz, $J_2 = 1.8$ Hz, Ar-H), 7.50 (d, 1H, $J = 8.4$ Hz, Ar-H), 7.07–7.01 (m, 2H, Ar-H), 6.95 (t, 2H, $J = 8.4$ Hz, Ar-H), 2.47 (s, 3H, CH_3). ^{13}C NMR (75 MHz, CDCl_3 + $\text{DMSO}-d_6$): δ 189.4, 161.2, 157.9, 157.0, 140.6, 134.4, 133.8, 129.7, 129.2, 126.4, 121.7, 119.8, 115.9, 114.4, 114.7, 18.6. ESI-MS: m/z $[\text{M}+\text{H}]^+$ 297.

(E)-3-((2-(4-Bromophenyl)hydrazono)methyl)-6-methyl-4H-chromen-4-one (3p)

Yellow solid. Yield 78%. M.p. 246–248 °C. FT-IR (KBr): ν 3265, 2977, 1622, 1571, 1491, 1206, 872, 748 cm^{-1} . ^1H NMR (300 MHz, CDCl_3 + $\text{DMSO}-d_6$): δ 8.56 (s, 1H, imine), 7.97 (s, 1H, Ar-H), 7.92 (s, 1H, Ar-H), 7.52 (d, 1H, $J = 7.0$ Hz, Ar-H), 7.44 (d, 1H, $J = 8.0$ Hz, Ar-H), 7.02 (t, 1H, $J = 7.0$ Hz, Ar-H), 6.85 (s, 1H, Ar-H), 6.81 (d, 1H, $J = 8.0$ Hz, Ar-H), 6.53 (d, 1H, $J = 7.0$ Hz, Ar-H). ^{13}C NMR (75 MHz, CDCl_3 + $\text{DMSO}-d_6$): δ 171.3, 154.6, 151.0, 148.5, 144.0, 137.7, 133.3, 106.9, 40.2. ESI-MS: m/z $[\text{M}+\text{H}]^+$ 357.

(E)-6-Chloro-3-((2-phenylhydrazono)methyl)-4H-chromen-4-one (3q)

Yellow solid. Yield 72%. M.p. 229–231 °C. ^1H NMR (300 MHz, CDCl_3 + $\text{DMSO}-d_6$): δ 8.68 (s, 1H, imine), 8.08 (d, 1H, $J = 3.2$ Hz, Ar-H), 7.97 (s, 1H, Ar-H), 7.74 (dd, 1H, $J_1 = 8.8$ Hz, $J_2 = 2.6$ Hz, Ar-H), 7.65 (d, 1H, $J = 8.8$ Hz, Ar-H), 7.19 (t, 2H, $J = 8.4$ Hz, Ar-H), 7.06 (d, 2H, $J = 7.5$ Hz, Ar-H), 6.75 (t, 1H, $J = 7.1$ Hz, Ar-H). ESI-MS: m/z $[\text{M}+\text{H}]^+$ 299.

(E)-6-Chloro-3-((2-*m*-tolylhydrazono)methyl)-4H-chromen-4-one (3r)

Yellow solid. Yield 57%. M.p. 215–217 °C. FT-IR (KBr): ν 3276, 2920, 1640, 1608, 1460, 1297, 1160, 813, 772 cm^{-1} . ^1H NMR (300 MHz, CDCl_3 + $\text{DMSO}-d_6$): δ 8.56 (s, 1H, imine), 8.02 (s, 1H, Ar-H), 7.86 (s, 1H, Ar-H), 7.60 (dd, 2H, $J_1 = 6.8$ Hz, $J_2 = 8.8$ Hz, Ar-H), 6.96 (t, 1H, $J = 7.8$ Hz, Ar-H), 6.79 (s, 1H, Ar-H), 6.75 (d, 1H, $J = 7.8$ Hz, Ar-H), 6.48 (d, 1H, $J = 7.8$ Hz, Ar-H). ^{13}C NMR (75 MHz, CDCl_3 + $\text{DMSO}-d_6$): δ 179.6, 169.4, 161.6, 159.2, 154.7, 153.2, 150.3, 149.5, 148.9, 148.1, 144.4, 143.1, 142.3, 139.9, 139.3, 136.3, 40.8. ESI-MS: m/z $[\text{M}+\text{H}]^+$ 313.

(E)-6-Chloro-3-((2-(4-methoxyphenyl)hydrazono)methyl)-4H-chromen-4-one (3s)

Yellow solid. Yield 61%. M.p. 219–221 °C. FT-IR (KBr): ν 3271, 2901, 1621, 1570, 1464, 1228, 1042 cm^{-1} . ^1H NMR (300 MHz, CDCl_3 + $\text{DMSO}-d_6$): δ 8.56 (s, 1H,

imine), 8.08 (s, 1H, Ar-H), 7.88 (s, 1H, Ar-H), 7.68 (d, 1H, $J = 8.8$ Hz, Ar-H), 7.56 (d, 1H, $J = 8.8$ Hz, Ar-H), 6.96 (d, 2H, $J = 8.4$ Hz, Ar-H), 6.74 (d, 2H, $J = 8.4$ Hz, Ar-H), 3.72 (s, 3H, OCH₃). ¹³C NMR (75 MHz, CDCl₃ + DMSO-*d*₆): δ 173.2, 164.2, 150.4, 146.2, 134.4, 132.2, 129.7, 124.3, 115.9, 117.2, 119.8, 53.2. ESI-MS: m/z [M+H]⁺ 329.

(E)-6-Bromo-3-((2-phenylhydrazono)methyl)-4H-chromen-4-one (3t)

Yellow solid. Yield 72%. M.p. 218–220 °C. FT-IR (KBr): ν 3283, 1623, 1525, 1462, 1258, 1182, 1027, 753 cm⁻¹. ¹H NMR (300 MHz, CDCl₃ + DMSO-*d*₆): δ 8.61 (s, 1H, imine), 8.24 (d, 1H, $J = 1.3$ Hz, Ar-H), 7.94 (s, 1H, Ar-H), 7.82 (dd, 1H, $J_1 = 6.4$ Hz, $J_2 = 8.8$ Hz, Ar-H), 7.53 (d, 1H, $J = 8.8$ Hz, Ar-H), 7.16 (t, 2H, $J = 7.5$ Hz, Ar-H), 7.02 (d, 2H, $J = 7.7$ Hz, Ar-H), 6.72 (t, 1H, $J = 7.1$ Ar-H).

(E)-6-Bromo-3-((2-*m*-tolylhydrazono)methyl)-4H-chromen-4-one (3u)

Yellow solid. Yield 81%. M.p. 240–242 °C. FT-IR (KBr): ν 3276, 2918, 1639, 1602, 1454, 1296, 1159, 813, 773 cm⁻¹. ¹H NMR (300 MHz, CDCl₃ + DMSO-*d*₆): δ 8.70 (s, 1H, imine), 8.23 (d, 1H, $J = 2.5$ Hz, Ar-H), 7.94 (s, 1H, Ar-H), 7.90 (dd, 1H, $J_1 = 8.8$ Hz, $J_2 = 6.8$ Hz, Ar-H), 7.63 (d, 1H, $J = 8.2$ Hz, Ar-H), 7.07 (t, 1H, $J = 7.8$ Hz, Ar-H), 6.89 (s, 1H, Ar-H), 6.84 (d, 1H, $J = 8.3$ Hz, Ar-H), 6.57 (d, 1H, $J = 7.5$ Hz, Ar-H). ESI-MS: m/z [M+H]⁺ 357.

(E)-6-Bromo-3-((2-(4-methoxyphenyl)hydrazono)methyl)-4H-chromen-4-one (3v)

Yellow solid. Yield 66%. M.p. 245–247 °C. FT-IR (KBr): ν 3271, 2901, 1621, 1570, 1464, 1228, 1042, 827, 791 cm⁻¹. ¹H NMR (75 MHz, CDCl₃ + DMSO-*d*₆): δ 8.58 (s, 1H, imine), 8.16 (d, 1H, $J = 8.8$ Hz, Ar-H), 8.02 (d, 1H, $J = 7.8$ Hz, Ar-H), 7.74 (s, 1H, Ar-H), 7.72–7.66 (m, 1H, Ar-H), 7.56–7.40 (m, 2H, Ar-H), 7.23 (d, 2H, $J = 8.4$ Hz, Ar-H), 6.96 (d, 2H, $J = 8.4$ Hz, Ar-H), 3.20 (s, 3H, OCH₃). ¹³C NMR (75 MHz, CDCl₃ + DMSO-*d*₆): δ 172.8, 148.3, 141.1, 137.0, 132.2, 130.0, 124.8, 120.5, 119.7, 119.3, 113.8, 113.7, 54.7.

(E)-6-((2-Phenylhydrazono)methyl)-5H-furo[3,2-*g*]chromen-5-one (3w)

Yellow solid. Yield 72%. M.p. 235–236 °C. FT-IR (KBr): ν 3270, 1631, 1592, 1275, 1173, 1044, 750 cm⁻¹. ¹H NMR (300 MHz, CDCl₃ + DMSO-*d*₆): δ 8.81 (s, 1H, imine), 8.42 (s, 1H, Ar-H), 8.20 (d, 1H, $J = 8.0$ Hz, Ar-H), 8.00 (s, 2H, Ar-H), 7.20 (t, 3H, $J = 8.1$ Hz, Ar-H), 7.06 (d, 2H, $J = 7.7$ Hz, Ar-H), 6.74 (t, 1H, $J = 7.1$ Hz, Ar-H). ¹³C NMR (75 MHz, CDCl₃ + DMSO-*d*₆): δ 190.6, 159.2, 144.5, 141.1, 137.9, 129.7, 128.4, 127.8, 126.4, 123.8, 122.2, 119.1, 118.4, 116.4, 113.8, 105.9, 98.4. ESI-MS: m/z [M+H]⁺ 305.

(E)-6-((2-*m*-Tolylhydrazono)methyl)-5H-furo[3,2-*g*]chromen-5-one (3x)

Yellow solid. Yield 81%. M.p. 238–240 °C. FT-IR (KBr): ν 3265, 2793, 1623, 1484, 1171, 816, 779 cm⁻¹. ¹H

NMR (300 MHz, CDCl₃ + DMSO-*d*₆): δ 9.00 (s, 1H, imine), 8.26 (s, 1H, Ar-H), 8.21 (s, 1H, Ar-H), 7.77 (d, 1H, $J = 1.8$ Hz, Ar-H), 7.22 (d, 1H, $J = 8.0$ Hz, Ar-H), 7.40 (d, 1H, $J = 8.0$ Hz, Ar-H), 7.19 (d, 2H, $J = 7.3$ Hz, Ar-H), 7.10 (s, 1H, Ar-H), 6.91 (s, 1H, Ar-H), 2.45 (s, 1H, CH₃). ¹³C NMR (75 MHz, CDCl₃ + DMSO-*d*₆): δ 189.7, 158.0, 156.8, 144.0, 140.5, 137.6, 129.5, 127.5, 126.4, 123.3, 121.6, 118.3, 116.5, 114.9, 105.5, 97.6, 19.5. ESI-MS: m/z [M+H]⁺ 319.

(E)-3-((2-Phenylhydrazono)methyl)-4H-furo[2,3-*h*]chromen-4-one (3y)

Yellow solid. Yield 85%. M.p. 236–238 °C. FT-IR (KBr): ν 3270, 1631, 1592, 1275, 1173, 1044, 750 cm⁻¹. ¹H NMR (300 MHz, CDCl₃ + DMSO-*d*₆): δ 8.66 (s, 1H, imine), 8.08 (d, 1H, $J = 8.3$ Hz, Ar-H), 7.96–8.00 (m, 3H, Ar-H), 7.62 (d, 1H, $J = 8.8$ Hz, Ar-H), 7.05 (t, 1H, $J = 7.8$ Hz, Ar-H), 6.86 (s, 1H, Ar-H), 6.84 (d, 1H, $J = 7.8$ Hz, Ar-H), 6.54 (d, 1H, $J = 7.8$ Hz, Ar-H). ¹³C NMR (75 MHz, CDCl₃ + DMSO-*d*₆): δ 190.4, 157.4, 143.6, 140.9, 129.5, 128.2, 127.7, 126.6, 126.2, 120.6, 119.8, 118.2, 113.6, 113.1, 103.6, 102.6. ESI-MS: m/z [M+H]⁺ 305

(E)-3-((2-*m*-Tolylhydrazono)methyl)-4H-furo[2,3-*h*]chromen-4-one (3z)

Yellow solid. Yield 42%. M.p. 239–241 °C. FT-IR (KBr): ν 3270, 1631, 1592, 1275, 1173, 1044, 750 cm⁻¹. ¹H NMR (300 MHz, CDCl₃ + DMSO-*d*₆): δ 8.89 (s, 1H, imine), 8.08 (d, 1H, $J = 8.3$ Hz, Ar-H), 7.95 (d, 1H, $J = 8.8$ Hz, Ar-H), 7.77 (s, 1H, Ar-H), 7.72 (s, 1H, Ar-H), 7.68 (d, 1H, $J = 7.8$ Hz, Ar-H), 7.38 (t, 1H, $J = 7.7$ Ar-H), 7.18 (t, 2H, $J = 8.6$ Hz, Ar-H), 7.03 (s, 1H, Ar-H), 2.43 (s, 3H, CH₃). ¹³C NMR (75 MHz, CDCl₃ + DMSO-*d*₆): δ 189.4, 157.1, 155.8, 143.5, 140.3, 137.3, 137.0, 129.2, 127.4, 126.1, 121.1, 117.9, 114.6, 112.6, 102.8, 101.9, 19.0. ESI-MS: m/z [M+H]⁺ 319.

4. 3. General Procedure for the Preparation of Pyrazolecarboxylates 5a–x

The *N*-bromosuccinimide (0.267 g, 1.5 mmol) was added to a stirred solution of (*E*)-3-((2-phenylhydrazono)methyl)-4H-chromen-4-one **3a** (0.264 g, 1 mmol) in benzene at room temperature. The reaction was monitored by TLC, after completion of the reaction, the solvent was removed under reduced pressure and the crude product was used for further reaction without purification. The dimethyl acetylenedicarboxylate (**4a**, 0.168 g, 1.2 mmol) was added to a stirred solution of bromohydrazone derivative in acetonitrile (3 mL) at room temperature under nitrogen atmosphere. The reaction mixture was refluxed for 12 h and after completion of the reaction (TLC), the solvent was removed under reduced pressure, and the resulting residue was purified by column chromatography using silica gel (60–120, hexane–ethylacetate, 9:1) affording **5a** as a colourless solid. Similarly, the compounds **5b–x** were prepared from the corresponding (*E*)-3-((2-phenylhydrazo-

no)methyl)-4*H*-chromen-4-ones **3b–c**, **3e**, **3h–l**, **3n**, **3p–v** with acetylenedicarboxylates **4a–b** under optimized conditions.

Dimethyl 3-(4-Oxo-4*H*-chromen-3-yl)-1-phenyl-1*H*-pyrazole-4,5-dicarboxylate (5a)

Colourless solid. Yield 78%, M.p. 144–145 °C. FT-IR (KBr): ν 2923, 1721, 1656, 1547, 1462, 1245, 1009, 755 cm^{-1} . ^1H NMR (300 MHz, CDCl_3): δ 8.30 (dd, 1H, $J_1 = 7.8$ Hz, $J_2 = 6.4$ Hz, Ar-H), 8.25 (s, 1H, Ar-H), 7.70 (t, 1H, $J = 1.8$ Hz, Ar-H), 7.52–7.41 (m, 7H, Ar-H), 3.85 (s, 3H, OCH_3), 3.79 (s, 3H, OCH_3). ^{13}C NMR (75 MHz, CDCl_3): δ 174.5, 162.2, 160.1, 156.2, 154.1, 144.1, 139.0, 133.5, 129.0, 128.8, 126.5, 125.3, 124.3, 118.1, 52.9, 51.8. ESI-MS: m/z $[\text{M}+\text{H}]^+$ 405.

Dimethyl 3-(4-Oxo-4*H*-chromen-3-yl)-1-*m*-tolyl-1*H*-pyrazole-4,5-dicarboxylate (5b)

Pale yellow solid. Yield 67%. M.p. 156–158 °C. FT-IR (KBr): ν 2925, 1732, 1657, 1463, 1234, 1149, 762 cm^{-1} . ^1H NMR (300 MHz, CDCl_3): δ 8.28 (dd, 1H, $J_1 = 7.4$ Hz, $J_2 = 6.0$ Hz, Ar-H), 8.23 (s, 1H, Ar-H), 7.68 (t, 1H, $J = 1.5$ Hz, Ar-H), 7.60 (d, 2H, $J = 8.6$ Hz, Ar-H), 7.50–7.40 (m, 2H, Ar-H), 7.34 (s, 2H, Ar-H), 7.28–7.21 (m, 3H, Ar-H), 3.86 (s, 3H, OCH_3), 3.78 (s, 3H, OCH_3), 2.45 (s, 3H, CH_3). ^{13}C NMR (75 MHz, CDCl_3): δ 173.0, 166.7, 160.4, 154.5, 154.2, 145.0, 143.3, 139.0, 136.5, 135.3, 134.9, 129.8, 128.9, 125.7, 125.1, 123.9, 121.3, 117.9, 117.6, 53.0, 52.0, 21.0. ESI-MS: m/z $[\text{M}+\text{H}]^+$ 419.

Dimethyl 1-(4-Methoxyphenyl)-3-(4-oxo-4*H*-chromen-3-yl)-1*H*-pyrazole-4,5-dicarboxylate (5c)

Colourless solid. Yield 57%. M.p. 149–151 °C. FT-IR (KBr): ν 2947, 1727, 1603, 1440, 1240, 1103 cm^{-1} . ^1H NMR (300 MHz, CDCl_3): δ 8.28 (dd, 1H, $J_1 = 7.8$ Hz, $J_2 = 6.8$ Hz, Ar-H), 8.23 (s, 1H, Ar-H), 7.68 (t, 1H, $J = 2.2$ Hz, Ar-H), 7.50–7.38 (m, 4H, Ar-H), 6.94 (d, 2H, $J = 8.8$ Hz, Ar-H), 3.86 (s, 3H, OCH_3), 3.84 (s, 3H, OCH_3), 3.74 (s, 3H, OCH_3). ESI-MS: m/z $[\text{M}+\text{H}]^+$ 435.

Dimethyl 1-(2-Fluorophenyl)-3-(4-oxo-4*H*-chromen-3-yl)-1*H*-pyrazole-4,5-dicarboxylate (5d)

Pale yellow solid. Yield 72%. FT-IR (KBr): ν 2950, 2856, 1733, 1655, 1464, 1244, 1125 cm^{-1} . ^1H NMR (300 MHz, CDCl_3): δ 8.30 (s, 1H, imine), 8.26 (d, 1H, $J = 7.5$ Hz, Ar-H), 7.68 (t, 1H, $J = 2.4$ Hz, Ar-H), 7.56 (t, 1H, $J = 1.5$ Hz, Ar-H), 7.50–7.40 (m, 3H, Ar-H), 7.32–7.16 (m, 2H, Ar-H), 3.82 (s, 3H, OCH_3), 3.80 (s, 3H, OCH_3). ^{13}C NMR (75 MHz, CDCl_3): δ 174.8, 162.9, 158.9, 157.6, 154.4, 144.2, 133.8, 130.9, 127.9, 126.1, 125.4, 124.6, 118.0, 116.3, 116.0, 52.7, 52.1. ESI-MS: m/z $[\text{M}+\text{H}]^+$ 423.

Dimethyl 1-(4-Bromophenyl)-3-(4-oxo-4*H*-chromen-3-yl)-1*H*-pyrazole-4,5-dicarboxylate (5e)

Colourless solid. Yield 57%. M.p. 136–138 °C. FT-IR (KBr): ν 2923, 1732, 1655, 1463, 1272, 1157, 769 cm^{-1} . ^1H

NMR (300 MHz, CDCl_3): δ 8.28 (dd, 1H, $J_1 = 7.8$ Hz, $J_2 = 6.6$ Hz, Ar-H), 8.23 (s, 1H, Ar-H), 7.68 (t, 1H, $J = 2.6$ Hz, Ar-H), 7.60 (d, 2H, $J = 8.6$ Hz, Ar-H), 7.50–7.42 (m, 2H, Ar-H), 7.38 (d, 2H, $J = 8.6$ Hz, Ar-H), 3.86 (s, 3H, OCH_3), 3.78 (s, 3H, OCH_3). ^{13}C NMR (75 MHz, CDCl_3): δ 174.4, 162.1, 159.9, 154.1, 144.4, 136.1, 133.6, 132.2, 126.6, 126.0, 125.4, 124.4, 118.1, 117.8, 117.4, 53.0, 52.0.

Dimethyl 1-(2,4-Dichlorophenyl)-3-(4-oxo-4*H*-chromen-3-yl)-1*H*-pyrazole-4,5-dicarboxylate (5f)

Brown solid. Yield 66%. M.p. 129–131 °C. FT-IR (KBr): ν 2793, 1622, 1484, 1301, 1171, 779 cm^{-1} . ^1H NMR (300 MHz, CDCl_3): δ 8.28 (dd, 1H, $J_1 = 7.8$ Hz, $J_2 = 6.8$ Hz, Ar-H), 8.24 (s, 1H, imine), 7.69 (t, 1H, $J = 1.6$ Hz, Ar-H), 7.50 (d, 1H, $J = 7.8$ Hz, Ar-H), 7.46–7.42 (m, 4H, Ar-H), 3.92 (s, 3H, OCH_3), 3.80 (s, 3H, OCH_3). ESI-MS: m/z $[\text{M}+\text{H}]^+$ 473.

Diethyl 3-(6-Methyl-4-oxo-4*H*-chromen-3-yl)-1-phenyl-1*H*-pyrazole-4,5-dicarboxylate (5g)

Colourless solid. Yield 61%. M.p. 131–133 °C. FT-IR (KBr): ν 2923, 2852, 1721, 1656, 1547, 1462, 1245, 1009 cm^{-1} . ^1H NMR (300 MHz, CDCl_3): δ 8.20 (s, 1H, Ar-H), 8.06 (s, 1H, Ar-H), 7.53–7.42 (m, 6H, Ar-H), 7.38 (d, 1H, $J = 8.6$ Hz, Ar-H), 4.29 (q, 2H, $J = 6.8$ Hz, OCH_2), 4.24 (q, 2H, $J = 6.8$ Hz, OCH_2), 1.25 (t, 3H, $J = 6.8$ Hz, CH_3), 1.21 (t, 3H, $J = 6.8$ Hz, CH_3), 2.50 (s, 3H, CH_3). ^{13}C NMR (75 MHz, CDCl_3): δ 175.1, 161.9, 160.0, 154.2, 144.5, 139.0, 137.0, 135.4, 129.1, 125.6, 124.5, 117.8, 62.3, 60.8, 20.9, 14.0, 13.7. ESI-MS: m/z $[\text{M}+\text{H}]^+$ 447.

Dimethyl 3-(6-Methyl-4-oxo-4*H*-chromen-3-yl)-1-*m*-tolyl-1*H*-pyrazole-4,5-dicarboxylate (5h)

Colourless solid. Yield 82%. M.p. 168–170 °C. FT-IR (KBr): ν 2925, 2534, 1735, 1655, 1485, 1233, 1156 cm^{-1} . ^1H NMR (300 MHz, CDCl_3): δ 8.22 (s, 1H, Ar-H), 8.09 (d, 1H, $J = 1.6$ Hz, Ar-H), 7.46 (dd, 1H, $J_1 = 8.3$ Hz, $J_2 = 6.0$ Hz, Ar-H), 7.40–7.30 (m, 3H, Ar-H), 7.28–7.20 (m, 2H, Ar-H), 3.86 (s, 3H, OCH_3), 3.76 (s, 3H, OCH_3), 2.52 (s, 3H, CH_3), 2.46 (s, 3H, CH_3). ^{13}C NMR (75 MHz, CDCl_3): δ 174.3, 160.4, 154.2, 139.4, 135.3, 134.9, 129.8, 128.9, 125.7, 125.1, 123.9, 121.3, 117.9, 53.0, 52.0, 21.3, 21.0. ESI-MS: m/z $[\text{M}+\text{H}]^+$ 433.

Dimethyl 1-(4-Methoxyphenyl)-3-(6-methyl-4-oxo-4*H*-chromen-3-yl)-1*H*-pyrazole-4,5-dicarboxylate (5i)

Colourless solid. Yield 62%. M.p. 179–181 °C. FT-IR (KBr): ν 2923, 1732, 1656, 1222, 1148, 772 cm^{-1} . ^1H NMR (300 MHz, CDCl_3): δ 8.22 (s, 1H, Ar-H), 8.06 (s, 1H, Ar-H), 7.46 (d, 1H, $J = 8.4$, 6.4 Hz, Ar-H), 7.42–7.36 (m, 3H, Ar-H), 6.94 (d, 2H, $J = 8.6$ Hz, Ar-H), 3.86 (s, 3H, OCH_3), 3.84 (s, 3H, OCH_3), 3.76 (s, 3H, OCH_3), 2.50 (s, 3H, CH_3). ESI-MS: m/z $[\text{M}+\text{H}]^+$ 449.

Dimethyl 1-(2-Fluorophenyl)-3-(6-methyl-4-oxo-4*H*-chromen-3-yl)-1*H*-pyrazole-4,5-dicarboxylate (5j)

Colourless solid. Yield 71%. M.p. 170–172 °C. FT-IR (KBr): ν 2924, 2856, 1740, 1648, 1467, 1240, 1190, 1088

cm⁻¹. ¹H NMR (300 MHz, CDCl₃): δ 8.28 (s, 1H, Ar-H), 8.06 (s, 1H, Ar-H), 7.58 (t, 1H, *J* = 1.7 Hz, Ar-H), 7.50–7.17 (m, 5H, Ar-H), 3.84 (s, 3H, OCH₃), 3.82 (s, 3H, OCH₃), 2.50 (s, 3H, CH₃). ¹³C NMR (75 MHz, CDCl₃): δ 175.0, 154.4, 135.1, 130.8, 128.0, 125.5, 124.6, 123.7, 117.9, 116.1, 52.8, 52.3, 29.6. ESI-MS: *m/z* [M+H]⁺ 437, [M+Na]⁺ 459.

Dimethyl 1-(4-Bromophenyl)-3-(6-methyl-4-oxo-4H-chromen-3-yl)-1H-pyrazole-4,5-dicarboxylate (5k)

Brownish solid. Yield 67%. M.p. 145–147 °C. ¹H NMR (300 MHz, CDCl₃): δ 8.20 (s, 1H, imine), 8.06 (s, 1H, Ar-H), 7.61 (d, 2H, *J* = 9.0 Hz, Ar-H), 7.48 (dd, 1H, *J*₁ = 9.0 Hz, *J*₂ = 6.8 Hz, Ar-H), 7.40 (d, 2H, *J* = 2.2 Hz, Ar-H), 7.38–7.36 (m, 1H, Ar-H), 3.86 (s, 3H, OCH₃), 3.78 (s, 3H, OCH₃), 2.50 (s, 3H, CH₃). ESI-MS: *m/z* [M+H]⁺ 497.

Dimethyl 3-(6-Chloro-4-oxo-4H-chromen-3-yl)-1-phenyl-1H-pyrazole-4,5-dicarboxylate (5l)

Colourless solid. Yield 77%. M.p. 152–154 °C. FT-IR (KBr): ν 2924, 2856, 1728, 1659, 1454, 1239, 1036 cm⁻¹. ¹H NMR (300 MHz, CDCl₃): δ 8.23 (s, 1H, Ar-H), 8.09 (s, 1H, Ar-H), 7.53–7.45 (m, 6H, Ar-H), 7.40 (d, 1H, *J* = 8.6 Hz, Ar-H), 3.85 (s, 3H, OCH₃), 3.79 (s, 3H, OCH₃). ¹³C NMR (75 MHz, CDCl₃): δ 175.2, 160.3, 157.3, 154.2, 144.4, 139.0, 136.5, 129.1, 129.0, 126.3, 124.4, 120.7, 119.0, 116.6, 107.0, 100.0, 53.0, 51.9. ESI-MS: *m/z* [M+H]⁺ 439.

Dimethyl 3-(6-Chloro-4-oxo-4H-chromen-3-yl)-1-*m*-tolyl-1H-pyrazole-4,5-dicarboxylate (5m)

Pale brownish solid. Yield 61%. M.p. 154–156 °C. ¹H NMR (300 MHz, CDCl₃): δ 8.24 (d, 1H, *J* = 2.4, Ar-H), 8.22 (s, 1H, imine), 7.63 (dd, 1H, *J*₁ = 9.0 Hz, *J*₂ = 6.8 Hz, Ar-H), 7.46 (d, 1H, *J* = 9.0 Hz, Ar-H), 7.36–7.30 (m, 2H, Ar-H), 7.24–7.18 (m, 2H, Ar-H), 3.84 (s, 3H, OCH₃), 3.80 (s, 3H, OCH₃), 2.45 (s, 3H, CH₃).

Dimethyl 3-(6-Chloro-4-oxo-4H-chromen-3-yl)-1-(4-methoxyphenyl)-1H-pyrazole-4,5-dicarboxylate (5n)

Pale yellow solid. Yield 72%. M.p. 158–160 °C. FT-IR (KBr): ν 2925, 1736, 1653, 1250, 1105, 763 cm⁻¹. ¹H NMR (300 MHz, CDCl₃): δ 8.24 (d, 1H, *J* = 2.4 Hz, Ar-H), 8.20 (s, 1H, Ar-H), 7.60 (dd, 1H, *J*₁ = 9.0 Hz, *J*₂ = 6.8 Hz, Ar-H), 7.44 (d, 1H, *J* = 9.0 Hz, Ar-H), 7.40 (d, 2H, *J* = 9.0 Hz, Ar-H), 6.94 (d, 2H, *J* = 9.0 Hz, Ar-H), 3.86 (s, 3H, OCH₃), 3.84 (s, 3H, OCH₃), 3.78 (s, 3H, OCH₃). ESI-MS: *m/z* [M+H]⁺ 469.

Dimethyl 3-(6-Bromo-4-oxo-4H-chromen-3-yl)-1-phenyl-1H-pyrazole-4,5-dicarboxylate (5o)

Colourless solid. Yield 46%. M.p. 169–171 °C. FT-IR (KBr): ν 2924, 1728, 1659, 1454, 1384, 1239, 1036, 758 cm⁻¹. ¹H NMR (300 MHz, CDCl₃): δ 8.41 (d, 1H, *J* = 2.2 Hz, Ar-H), 8.24 (s, 1H, Ar-H), 7.76 (dd, 1H, *J*₁ = 7.6 Hz, *J*₂ = 6.0 Hz, Ar-H), 7.50–7.44 (m, 5H, Ar-H), 7.39 (d, 1H, *J* = 7.6 Hz, Ar-H), 3.85 (s, 3H, OCH₃), 3.79 (s, 3H, OCH₃). ¹³C NMR (75 MHz, CDCl₃): δ 173.8, 172.4, 159.2, 155.0, 154.5,

138.9, 136.8, 132.3, 129.3, 128.9, 125.8, 124.4, 120.1, 119.0, 111.5, 108.1, 53.2, 52.1. ESI-MS: *m/z* [M+H]⁺ 483.

Dimethyl 3-(6-Bromo-4-oxo-4H-chromen-3-yl)-1-*m*-tolyl-1H-pyrazole-4,5-dicarboxylate (5p)

Colourless solid. Yield 74%. M.p. 151–153 °C. FT-IR (KBr): ν 2925, 1724, 1655, 1493, 1328, 1233, 1155, 1070 cm⁻¹. ¹H NMR (300 MHz, CDCl₃): δ 8.40 (d, 1H, *J* = 2.4 Hz, Ar-H), 8.20 (s, 1H, imine), 7.76 (dd, 1H, *J*₁ = 8.4 Hz, *J*₂ = 6.4 Hz, Ar-H), 7.40–7.30 (m, 3H, Ar-H), 7.23–7.14 (m, 1H, Ar-H), 3.84 (s, 3H, OCH₃), 3.78 (s, 3H, OCH₃), 2.58 (s, 3H, CH₃). ¹³C NMR (75 MHz, CDCl₃): δ 174.5, 162.2, 160.2, 158.1, 150.7, 144.1, 139.2, 136.4, 129.7, 124.9, 121.1, 119.6, 118.3, 117.0, 110.2, 104.1, 52.9, 51.8, 21.2. ESI-MS: *m/z* [M+H]⁺ 497, [M+2]⁺ 499.

Dimethyl 3-(6-Bromo-4-oxo-4H-chromen-3-yl)-1-(4-methoxyphenyl)-1H-pyrazole-4,5-dicarboxylate (5q)

Pale yellow solid. Yield 68%. M.p. 164–166 °C. ¹H NMR (300 MHz, CDCl₃): δ 8.40 (dd, 1H, *J*₁ = 9.0 Hz, *J*₂ = 2.2 Hz, Ar-H), 8.20 (s, 1H, Ar-H), 7.76 (dd, 1H, *J*₁ = 9.0 Hz, *J*₂ = 6.8 Hz, Ar-H), 7.40–7.33 (m, 3H, Ar-H), 6.94 (d, 2H, *J* = 9.0 Hz, Ar-H), 3.86 (s, 3H, OCH₃), 3.84 (s, 3H, OCH₃), 3.78 (s, 3H, OCH₃). ¹³C NMR (75 MHz, CDCl₃): δ 174.4, 162.1, 159.9, 154.1, 144.4, 136.1, 133.6, 132.7, 126.6, 126.0, 125.4, 124.4, 118.1, 117.8, 117.4, 53.0, 52.0.

Diethyl 3-(4-Oxo-4H-chromen-3-yl)-1-phenyl-1H-pyrazole-4,5-dicarboxylate (5r)

Pale yellow solid. Yield 61%. M.p. 119–121 °C. ¹H NMR (300 MHz, CDCl₃): δ 8.30 (dd, 1H, *J*₁ = 7.8 Hz, *J*₂ = 6.4 Hz, Ar-H), 8.22 (s, 1H, Ar-H), 7.68 (t, 1H, *J* = 2.5 Hz, Ar-H), 7.52–7.39 (m, 7H, Ar-H), 4.30 (q, 2H, *J* = 7.1 Hz, OCH₂), 4.24 (q, 2H, *J* = 3.5 Hz, OCH₂), 1.24 (t, 3H, *J* = 4.3 Hz, CH₃), 1.10 (t, 3H, *J* = 3.2 Hz, CH₃). ¹³C NMR (300 MHz, CDCl₃): δ 174.9, 161.8, 159.9, 156.3, 154.2, 144.3, 139.0, 133.6, 126.4, 125.4, 124.4, 118.1, 62.3, 60.7, 13.9, 13.7. ESI-MS: *m/z* [M+H]⁺ 433, [M+Na]⁺ 455.

Dimethyl 3-(5-Oxo-5H-furo[3,2-*g*]chromen-6-yl)-1-phenyl-1H-pyrazole-4,5-dicarboxylate (5s)

Brown solid. Yield 77%. M.p. 176–178 °C. FT-IR (KBr): ν 2953, 1733, 1651, 1457, 1162 cm⁻¹. ¹H NMR (300 MHz, CDCl₃): δ 8.52 (s, 1H, Ar-H), 8.26 (s, 1H, Ar-H), 7.72 (d, 1H, *J* = 1.6 Hz, Ar-H), 7.57 (s, 1H, Ar-H), 7.52–7.41 (m, 5H, Ar-H), 6.90 (d, 1H, *J* = 1.6 Hz, Ar-H), 3.84 (s, 3H, OCH₃), 3.76 (s, 3H, OCH₃). ¹³C NMR (75 MHz, CDCl₃): δ 175.2, 157.3, 154.5, 147.5, 144.4, 139.0, 129.3, 126.3, 124.4, 120.7, 119.0, 116.6, 107.0, 53.0, 51.9. ESI-MS: *m/z* [M+H]⁺ 445.

Dimethyl 3-(5-Oxo-5H-furo[3,2-*g*]chromen-6-yl)-1-*m*-tolyl-1H-pyrazole-4,5-dicarboxylate (5t)

Colourless solid. Yield 68%. M.p. 192–194 °C. FT-IR (KBr): ν 2949, 1721, 1650, 1589, 1460, 1165, 1037 cm⁻¹. ¹H NMR (300 MHz, CDCl₃): δ 8.52 (s, 1H, Ar-H), 8.26 (s, 1H,

Ar-H), 7.72 (s, 1H, Ar-H), 7.58 (s, 1H, Ar-H), 7.36–7.20 (m, 4H, Ar-H), 6.90 (s, 1H, Ar-H), 3.86 (s, 3H, OCH₃), 3.76 (s, 3H, OCH₃), 2.44 (s, 3H, CH₃). ¹³C NMR (75 MHz, CDCl₃): δ 162.6, 160.6, 154.6, 154.2, 147.7, 144.4, 139.6, 138.8, 136.7, 129.9, 128.9, 126.4, 125.0, 121.2, 118.9, 107.0, 53.1, 52.0, 29.3. ESI-MS: *m/z* [M+H]⁺ 459.

Diethyl 3-(5-Oxo-5H-furo[3,2-g]chromen-6-yl)-1-phenyl-1H-pyrazole-4,5-dicarboxylate (5u)

Brown solid. Yield 64%. M.p. 162–164 °C. FT-IR (KBr): ν 2949, 1721, 1650, 1589, 1460, 1165, 1037, 795 cm⁻¹. ¹H NMR (300 MHz, CDCl₃): δ 8.50 (s, 1H, Ar-H), 8.22 (s, 1H, Ar-H), 7.70 (d, 1H, *J* = 2.2 Hz, Ar-H), 7.58–7.39 (m, 5H, Ar-H), 6.90 (s, 1H, Ar-H), 4.29 (q, 2H, *J* = 7.5 Hz, OCH₂), 4.23 (q, 2H, *J* = 4.5 Hz, OCH₂), 1.23 (t, 3H, *J* = 6.7 Hz, CH₃), 1.19 (t, 3H, *J* = 5.2 Hz, CH₃). ¹³C NMR (75 MHz, CDCl₃): δ 174.6, 161.4, 159.5, 153.9, 147.1, 138.9, 128.7, 125.9, 124.1, 120.5, 118.8, 116.7, 106.7, 99.7, 95.8, 61.8, 60.3, 13.8. ESI-MS: *m/z* [M+H]⁺, 473 [M+Na]⁺ 495.

Dimethyl 3-(4-Oxo-4H-furo[2,3-h]chromen-3-yl)-1-phenyl-1H-pyrazole-4,5-dicarboxylate (5v)

Colourless solid. Yield 79%. M.p. 173–175 °C. FT-IR (KBr): ν 2953, 1733, 1651, 1588, 1457, 1269, 1039, 758 cm⁻¹. ¹H NMR (300 MHz, CDCl₃): δ 8.30 (s, 1H, Ar-H), 8.21 (d, 1H, *J* = 8.6 Hz, Ar-H), 7.74 (s, 1H, Ar-H), 7.58–7.42 (m, 6H, Ar-H), 7.12 (s, 1H, Ar-H), 3.86 (s, 3H, OCH₃), 3.78 (s, 3H, OCH₃). ¹³C NMR (75 MHz, CDCl₃): δ 174.6, 162.3, 160.3, 158.2, 153.3, 150.8, 145.7, 144.2, 139.0, 136.4, 129.1, 128.9, 125.7, 124.4, 122.4, 119.6, 118.3, 116.7, 110.4, 104.2, 53.0, 51.9. ESI-MS: *m/z* [M+H]⁺ 445.

Dimethyl 3-(4-Oxo-4H-furo[2,3-h]chromen-3-yl)-1-*m*-tolyl-1H-pyrazole-4,5-dicarboxylate (5w)

Pale yellow solid. Yield 82%. M.p. 189–191 °C. FT-IR (KBr): ν 2952, 1732, 1652, 1588, 1456, 1234, 1039, 763 cm⁻¹. ¹H NMR (300 MHz, CDCl₃): δ 8.28 (s, 1H, Ar-H), 8.18 (dd, 1H, *J*₁ = 8.4 Hz, *J*₂ = 6.4 Hz, Ar-H), 7.72 (s, 1H, Ar-H), 7.52 (d, 1H, *J* = 8.6 Hz, Ar-H), 7.36–7.18 (m, 4H, Ar-H), 7.08 (s, 1H, Ar-H), 3.84 (s, 3H, OCH₃), 3.76 (s, 3H, OCH₃), 2.42 (s, 3H, CH₃). ¹³C NMR (75 MHz, CDCl₃): δ 174.5, 162.2, 160.2, 158.1, 153.2, 150.7, 145.6, 144.1, 139.2, 136.4, 129.7, 128.8, 124.9, 122.3, 121.1, 119.6, 118.3, 117.0, 110.2, 104.1, 52.9, 51.8, 21.2. ESI-MS: *m/z* [M+H]⁺ 459.

Diethyl 3-(4-Oxo-4H-furo[2,3-h]chromen-3-yl)-1-phenyl-1H-pyrazole-4,5-dicarboxylate (5x)

Colourless solid. Yield 78%. M.p. 167–169 °C. FT-IR (KBr): ν 2926, 1731, 1657, 1464, 1221, 762 cm⁻¹. ¹H NMR (300 MHz, CDCl₃): δ 8.26 (s, 1H, Ar-H), 8.20 (d, 1H, *J* = 8.3 Hz, Ar-H), 7.73 (d, 1H, *J* = 2.2 Hz, Ar-H), 7.58–7.42 (m, 6H, Ar-H), 7.10 (s, 1H, Ar-H), 4.29 (q, 2H, *J* = 6.7 Hz, OCH₂), 4.23 (q, 2H, *J* = 4.5 Hz, OCH₂), 1.24 (t, 3H, *J* = 4.5 Hz, CH₃), 1.19 (t, 3H, *J* = 6.5 Hz, CH₃). ¹³C NMR (75 MHz,

CDCl₃): δ 174.8, 161.8, 159.9, 158.1, 153.3, 150.7, 145.7, 144.3, 138.9, 137.1, 129.1, 124.4, 119.6, 118.4, 117.0, 110.3, 104.1, 62.3, 60.7, 13.8, 13.9. ESI-MS: *m/z* [M+H]⁺ 473.

4. 4. General Procedure for the Preparation of Pyrazolymethanones 6a–u

K₂CO₃ (0.276 g, 2 mmol) was added to a stirred solution of (*E*)-3-((2-phenylhydrazono)methyl)-4H-chromen-4-one **3a** (0.264 g, 1 mmol) in acetonitrile (3 mL) at room temperature. The reaction mixture was refluxed for 12 h and after completion of the reaction (TLC), the solvent was removed under reduced pressure. The crude product was purified by column chromatography using silica gel (60–120, hexane–ethyl acetate, 97:3) affording **6a**. Similarly, the compounds **6b–u** were prepared by treating the (*E*)-3-((2-phenylhydrazono)methyl)-4H-chromen-4-ones **3a–h**, **3k–s**, **3u–v** with K₂CO₃.

(2-Hydroxyphenyl)(1-phenyl-1H-pyrazol-4-yl)methanone (6a)

Pale yellow solid. Yield 88%. M.p. 113–114 °C. FT-IR (KBr): ν 3129, 1622, 1589, 1482, 1293 cm⁻¹. ¹H NMR (300 MHz, CDCl₃): δ 12.02 (s, 1H, ArOH), 8.48 (s, 1H, pyrazole H₅), 8.18 (s, 1H, pyrazole H₅), 7.92 (dd, 1H, *J*₁ = 7.9 Hz, *J*₂ = 1.1 Hz, Ar-H), 7.75 (d, 2H, *J* = 7.7 Hz, Ar-H), 7.56–7.48 (m, 3H, Ar-H), 7.39 (t, 1H, *J* = 7.3 Hz, Ar-H), 7.07 (d, 1H, *J* = 8.3 Hz, Ar-H), 6.97 (t, 1H, *J* = 7.9 Hz, Ar-H). ¹³C NMR (75 MHz, CDCl₃): δ 192.0, 162.6, 142.3, 139.1, 135.9, 131.1, 130.4, 129.6, 127.8, 123.3, 120.0, 119.7, 119.0, 118.4. ESI-MS: *m/z* [M+H]⁺ 265.

(2-Hydroxyphenyl)(1-*m*-tolyl-1H-pyrazol-4-yl)methanone (6b)

Yellow thick liquid. Yield 76%. FT-IR (KBr): ν 3447, 1622, 1539, 1483, 1238, 903, 771 cm⁻¹. ¹H NMR (300 MHz, CDCl₃): δ 11.95 (s, 1H, ArOH), 8.39 (s, 1H, pyrazole H₅), 8.09 (s, 1H, pyrazole H₅), 7.84 (dd, *J*₁ = 8.1 Hz, *J*₂ = 1.7 Hz, 1H, Ar-H), 7.52–7.41 (m, 3H), 7.30 (t, 1H, *J* = 7.7 Hz, Ar-H), 7.12 (d, 1H, *J* = 7.5 Hz, Ar-H), 6.99 (d, 1H, *J* = 8.4 Hz, Ar-H), 6.89 (t, 1H, *J* = 7.1 Hz, Ar-H). ¹³C NMR (75 MHz, CDCl₃): δ 192.0, 162.6, 142.2, 139.8, 139.0, 135.9, 131.1, 130.4, 129.4, 128.6, 123.2, 120.4, 120.0, 119.0, 118.4, 116.7, 21.4. ESI-MS: *m/z* [M+H]⁺ 279.

(2-Hydroxyphenyl)(1-(4-methoxyphenyl)-1H-pyrazol-4-yl)methanone (6c)

Yellow thick liquid. Yield 73%. FT-IR (KBr): ν 3422, 2924, 1722, 1590, 1237, 771 cm⁻¹. ¹H NMR (300 MHz, CDCl₃): δ 12.04 (s, 1H, ArOH), 8.39 (s, 1H, pyrazole H₅), 8.15 (s, 1H, pyrazole H₅), 7.91 (dd, 1H, *J*₁ = 7.9 Hz, *J*₂ = 1.3 Hz, Ar-H), 7.64 (d, 2H, *J* = 9.0 Hz, Ar-H), 7.52 (t, 1H, *J* = 6.9 Hz, Ar-H), 7.09–6.93 (m, 4H, Ar-H), 3.86 (s, 3H, OCH₃). ¹³C NMR (75 MHz, CDCl₃): δ 192.0, 162.5, 159.1, 142.0, 135.9, 132.6, 131.1, 130.3, 123.0, 121.3, 120.0, 118.9, 118.4, 114.6, 55.5. ESI-MS: *m/z* [M+H]⁺ 295.

(1-(2-Fluorophenyl)-1H-pyrazol-4-yl)(2-hydroxyphenyl)methanone (6d)

Pale yellow solid. Yield 63%. M.p. 150–152 °C. FT-IR (KBr): ν 3067, 1675, 1501, 1219, 765 cm^{-1} . ^1H NMR (300 MHz, CDCl_3): δ 10.02 (s, 1H, ArOH), 8.32 (s, 1H, pyrazole H_3), 7.89 (d, $J = 8.1$ Hz, 1H, pyrazole H_5), 7.66 (dd, 1H, $J_1 = 7.5$ Hz, $J_2 = 1.5$ Hz, Ar-H), 7.54 (td, 1H, $J_1 = 9.6$ Hz, $J_2 = 1.7$ Hz, Ar-H), 7.44–7.30 (m, 5H). ^{13}C NMR (75 MHz, CDCl_3): δ 184.4, 158.7, 152.2, 143.7, 142.2, 132.7, 132.1, 131.5, 129.5, 126.2, 125.9, 124.9, 124.1, 121.7, 121.6, 120.1. ESI-MS: m/z $[\text{M}+\text{H}]^+$ 283.

(1-(3-Fluorophenyl)-1H-pyrazol-4-yl)(2-hydroxyphenyl)methanone (6e)

Pale yellow solid. Yield 69%. M.p. 104–106 °C. FT-IR (KBr): ν 3127, 1602, 1542, 1245, 757 cm^{-1} . ^1H NMR (300 MHz, CDCl_3): δ 11.98 (s, 1H, ArOH), 8.48 (s, 1H, pyrazole H_3), 8.18 (s, 1H, pyrazole H_5), 7.90 (dd, $J_1 = 8.3$ Hz, $J_2 = 1.5$ Hz, 1H, Ar-H), 7.58–7.46 (m, 4H, Ar-H), 7.14–7.06 (m, 2H, Ar-H), 6.98 (dt, 1H, $J_1 = 8.3$ Hz, $J_2 = 1.5$ Hz, Ar-H). ^{13}C NMR (75 MHz, CDCl_3): δ 191.9, 164.8, 162.7, 161.5, 142.5, 140.3, 136.1, 131.0, 130.4, 123.6, 119.9, 119.0, 118.5, 114.8, 114.5, 107.7, 107.4. ESI-MS: m/z $[\text{M}+\text{H}]^+$ 283.

(1-(3-Chlorophenyl)-1H-pyrazol-4-yl)(2-hydroxyphenyl)methanone (6f)

Yellow solid. Yield 66%. M.p. 94–96 °C. FT-IR (KBr): ν 3127, 1581, 1464, 1215, 752 cm^{-1} . ^1H NMR (300 MHz, CDCl_3): δ 11.97 (s, 1H, ArOH), 8.47 (s, 1H, pyrazole H_3), 8.18 (s, 1H, pyrazole H_5), 7.89 (dd, $J_1 = 7.9$ Hz, $J_2 = 1.5$ Hz, 1H, Ar-H), 7.64 (dd, $J_3 = 3.0$ Hz, 1H, Ar-H), 7.53 (dt, 1H, $J_1 = 8.4$ Hz, $J_2 = 1.5$ Hz, Ar-H), 7.44 (t, 1H, $J = 8.1$ Hz, Ar-H), 7.36 (d, $J = 7.9$ Hz, 1H, Ar-H), 7.07 (d, 1H, $J = 7.5$ Hz, Ar-H), 6.98 (dt, 1H, $J_1 = 8.1$ Hz, $J_2 = 1.0$ Hz, Ar-H). ^{13}C NMR (75 MHz, CDCl_3): δ 191.8, 162.6, 142.5, 140.0, 136.1, 135.5, 131.0, 130.6, 127.8, 123.6, 120.0, 119.1, 118.5, 117.5. ESI-MS: m/z $[\text{M}+\text{H}]^+$ 299.

(1-(4-Fluorophenyl)-1H-pyrazol-4-yl)(2-hydroxyphenyl)methanone (6g)

Pale yellow solid. Yield 74%. M.p. 112–114 °C. FT-IR (KBr): ν 3067, 1675, 1501, 1219, 765 cm^{-1} . ^1H NMR (300 MHz, CDCl_3): δ 12.00 (s, 1H, ArOH), 8.43 (s, 1H, pyrazole H_3), 8.17 (s, 1H, pyrazole H_5), 7.91 (dd, $J_1 = 8.1$ Hz, $J_2 = 1.7$ Hz, 1H, Ar-H), 7.75–7.70 (m, 2H, Ar-H), 7.53 (td, 1H, $J_1 = 7.3$ Hz, $J_2 = 1.7$ Hz, Ar-H), 7.21 (t, 2H, $J = 9.0$ Hz, Ar-H), 7.07 (dd, $J_1 = 8.4$ Hz, $J_2 = 1.2$ Hz, 1H, Ar-H), 6.98 (dt, 1H, $J_1 = 8.1$ Hz, $J_2 = 1.1$ Hz, Ar-H). ^{13}C NMR (75 MHz, CDCl_3): δ 191.9, 162.6, 160.2, 142.3, 136.0, 135.4, 131.1, 130.5, 123.4, 121.7, 121.6, 120.0, 119.0, 118.5, 116.7, 116.4. ESI-MS: m/z $[\text{M}+\text{H}]^+$ 283.

(1-(4-Bromophenyl)-1H-pyrazol-4-yl)(2-hydroxyphenyl)methanone (6h)

Pale yellow solid. Yield 68%. M.p. 115–117 °C. FT-IR (KBr): ν 3112, 2924, 1626, 1542, 1243, 905, 756 cm^{-1} . ^1H

NMR (300 MHz, CDCl_3): δ 11.98 (s, 1H, ArOH), 8.46 (s, 1H, pyrazole H_3), 8.18 (s, 1H, pyrazole H_5), 7.90 (dd, $J_1 = 7.9$ Hz, $J_2 = 1.3$ Hz, 1H, Ar-H), 7.65 (s, 4H, Ar-H), 7.54 (td, 1H, $J_1 = 8.4$ Hz, $J_2 = 1.3$ Hz, Ar-H), 7.08 (d, 1H, $J = 8.3$ Hz, Ar-H), 6.98 (t, 1H, $J = 7.9$ Hz, Ar-H). ^{13}C NMR (75 MHz, CDCl_3): δ 191.9, 162.6, 142.5, 138.0, 136.1, 132.7, 131.0, 130.2, 121.0, 119.0, 118.5.

(2-Hydroxy-5-methylphenyl)(1-*m*-tolyl-1H-pyrazol-4-yl)methanone (6i)

Yellow thick liquid. Yield 73%. FT-IR (KBr): ν 3127, 1629, 1541, 1227, 783 cm^{-1} . ^1H NMR (300 MHz, CDCl_3): δ 11.82 (s, 1H, ArOH), 8.45 (s, 1H, pyrazole H_3), 8.16 (s, 1H, pyrazole H_5), 7.68 (d, $J = 1.3$ Hz, 1H, Ar-H), 7.58 (d, $J = 1.5$ Hz, 1H, Ar-H), 7.51 (d, $J = 7.9$ Hz, 1H, Ar-H), 7.39 (t, $J = 7.7$ Hz, 1H, Ar-H), 7.33 (dd, $J_1 = 8.6$ Hz, $J_2 = 2.2$ Hz, 1H, Ar-H), 7.19 (d, $J = 7.5$ Hz, 1H, Ar-H), 6.97 (d, $J = 8.4$ Hz, 1H, Ar-H), 2.44 (s, 3H, CH_3), 2.34 (s, 3H, CH_3). ^{13}C NMR (75 MHz, CDCl_3): δ 192.0, 160.4, 142.1, 139.8, 139.0, 136.9, 130.9, 130.3, 129.3, 128.5, 128.0, 123.2, 120.4, 119.7, 118.1, 116.7, 21.3, 20.5. ESI-MS: m/z $[\text{M}+\text{H}]^+$ 293.

(2-Hydroxy-5-methylphenyl)(1-(4-methoxyphenyl)-1H-pyrazol-4-yl)methanone (6j)

Yellow solid. Yield 61%. M.p. 128–130 °C. FT-IR (KBr): ν 3131, 1585, 1539, 1225 cm^{-1} . ^1H NMR (300 MHz, CDCl_3): δ 11.83 (s, 1H, ArOH), 8.38 (s, 1H, pyrazole H_3), 8.14 (s, 1H, pyrazole H_5), 7.69 (d, 1H, $J = 1.2$ Hz, Ar-H), 7.64 (d, 2H, $J = 9.0$ Hz, Ar-H), 7.33 (dd, 1H, $J_1 = 8.3$ Hz, $J_2 = 1.5$ Hz, Ar-H), 7.03 (d, 2H, $J = 9.0$ Hz, Ar-H), 6.97 (d, 1H, $J = 8.3$ Hz, Ar-H), 3.86 (s, 3H, OCH_3), 2.34 (s, 1H, CH_3). ^{13}C NMR (75 MHz, CDCl_3): δ 192.0, 160.4, 159.1, 142.0, 136.9, 132.7, 130.9, 130.3, 128.1, 123.1, 121.3, 119.7, 118.2, 114.6, 55.5, 20.5. ESI-MS: m/z $[\text{M}+\text{H}]^+$ 309.

(1-(2-Fluorophenyl)-1H-pyrazol-4-yl)(2-hydroxy-5-methylphenyl)methanone (6k)

Pale yellow solid. Yield 73%. M.p. 115–117 °C. FT-IR (KBr): ν 3063, 1630, 1592, 1230, 757 cm^{-1} . ^1H NMR (300 MHz, CDCl_3): δ 11.80 (s, 1H, ArOH), 8.54 (d, $J = 2.2$ Hz, 1H, pyrazole H_3), 8.20 (s, 1H, pyrazole H_5), 7.94 (dt, 1H, $J_1 = 8.4$ Hz, $J_2 = 2.0$ Hz, Ar-H), 7.68 (d, $J = 1.3$ Hz, 1H, Ar-H), 7.42–7.28 (m, 4H, Ar-H), 6.97 (d, 1H, $J = 8.4$ Hz, Ar-H), 2.34 (s, 3H, CH_3). ^{13}C NMR (75 MHz, CDCl_3): δ 191.9, 160.4, 151.8, 142.0, 137.0, 134.3, 134.1, 130.9, 129.0, 128.1, 125.1, 124.5, 119.6, 118.1, 117.0, 116.8, 20.5. ESI-MS: m/z $[\text{M}+\text{H}]^+$ 297.

(1-(3-Fluorophenyl)-1H-pyrazol-4-yl)(2-hydroxy-5-methylphenyl)methanone (6l)

Yellow solid. Yield 82%. M.p. 136–138 °C. FT-IR (KBr): ν 3141, 1630, 1543, 1228, 759 cm^{-1} . ^1H NMR (300 MHz, CDCl_3): δ 11.77 (s, 1H, ArOH), 8.48 (s, 1H, pyrazole H_3), 8.17 (s, 1H, pyrazole H_5), 7.67 (d, $J = 1.3$ Hz, 1H, Ar-H), 7.58–7.46 (m, 3H, Ar-H), 7.35 (dd, $J_1 = 8.4$ Hz, $J_2 = 2.0$ Hz, 1H, Ar-H), 7.14–7.06 (m, 1H, Ar-H), 6.99 (d, $J = 8.3$

Hz, 1H, Ar-H), 2.35 (s, 3H, CH₃). ¹³C NMR (75 MHz, CDCl₃): δ 191.9, 164.8, 160.5, 142.5, 137.2, 131.1, 130.9, 130.8, 130.3, 128.2, 119.6, 118.3, 114.7, 114.5, 107.7, 107.3, 20.6. ESI-MS: *m/z* [M+H]⁺ 297.

(1-(4-Fluorophenyl)-1H-pyrazol-4-yl)(2-hydroxy-5-methylphenyl)methanone (6m)

Pale yellow solid. Yield 74%. M.p. 125–127 °C. FT-IR (KBr): ν 3120, 1631, 1583, 1222, 836 cm⁻¹. ¹H NMR (300 MHz, CDCl₃): δ 11.79 (s, 1H, ArOH) 8.42 (s, 1H, pyrazole H₃), 8.16 (s, 1H, pyrazole H₅), 7.76–7.70 (m, 2H, Ar-H), 7.67 (d, 1H, *J* = 1.2 Hz, Ar-H), 7.34 (dd, *J*₁ = 8.3 Hz, *J*₂ = 1.9 Hz, 1H, Ar-H), 7.21 (t, 2H, *J* = 8.1 Hz, Ar-H), 6.97 (d, 1H, *J* = 8.4 Hz, Ar-H), 2.34 (s, 3H, CH₃). ¹³C NMR (75 MHz, CDCl₃): δ 191.9, 160.5, 142.3, 137.1, 135.4, 130.8, 130.4, 128.1, 123.5, 121.5, 119.6, 118.2, 116.6, 116.3, 20.5. ESI-MS: *m/z* [M+H]⁺ 297.

(1-(4-Bromophenyl)-1H-pyrazol-4-yl)(2-hydroxy-5-methylphenyl)methanone (6n)

Pale yellow solid. Yield 82%. M.p. 142–144 °C. FT-IR (KBr): ν 3132, 1592, 1539, 1229 cm⁻¹. ¹H NMR (300 MHz, CDCl₃): δ 11.77 (s, 1H, ArOH), 8.46 (s, 1H, pyrazole H₃), 8.17 (s, 1H, pyrazole H₅), 7.65 (brs, 5H, Ar-H), 7.35 (dd, 1H, *J*₁ = 8.4 Hz, *J*₂ = 2.0 Hz, Ar-H), 6.98 (d, 1H, *J* = 8.4 Hz, Ar-H), 2.34 (s, 3H, CH₃). ¹³C NMR (75 MHz, CDCl₃): δ 191.8, 160.5, 142.4, 138.1, 137.1, 132.7, 130.8, 130.1, 128.1, 123.7, 115.0, 119.6, 118.2, 20.5. ESI-MS: *m/z* [M+H]⁺ 357.

(5-Chloro-2-hydroxyphenyl)(1-phenyl-1H-pyrazol-4-yl)methanone (6o)

Pale yellow solid. Yield 67%. M.p. 142–144 °C. FT-IR (KBr): ν 3127, 1581, 1464, 1215, 752 cm⁻¹. ¹H NMR (300 MHz, CDCl₃): δ 11.90 (s, 1H, ArOH), 8.50 (s, 1H, pyrazole H₃), 8.20 (s, 1H, pyrazole H₅), 7.88 (d, 1H, *J* = 2.2 Hz, Ar-H), 7.76 (d, 2H, *J* = 7.5 Hz, Ar-H), 7.57–7.39 (m, 4H, Ar-H), 7.04 (d, 1H, *J* = 9.0 Hz, Ar-H). ¹³C NMR (75 MHz, CDCl₃): δ 190.9, 161.0, 142.2, 139.0, 135.8, 130.4, 130.2, 129.6, 128.0, 123.7, 122.8, 120.6, 120.1, 119.8. ESI-MS: *m/z* [M+H]⁺ 299.

(5-Chloro-2-hydroxyphenyl)(1-*m*-tolyl-1H-pyrazol-4-yl)methanone (6p)

Yellow solid. Yield 81%. M.p. 105–107 °C. FT-IR (KBr): ν 3127, 1624, 1539, 1228 cm⁻¹. ¹H NMR (300 MHz, CDCl₃): δ 11.90 (s, 1H, ArOH), 8.47 (s, 1H, pyrazole H₃), 8.18 (s, 1H, pyrazole H₅), 7.87 (d, 1H, *J* = 2.4 Hz, Ar-H), 7.59 (d, *J* = 1.5 Hz, 1H, Ar-H), 7.53 (d, 1H, *J* = 8.1 Hz, Ar-H), 7.46 (dd, 1H, *J*₁ = 8.8 Hz, *J*₂ = 2.6 Hz, Ar-H), 7.40 (t, 1H, *J* = 7.7 Hz, Ar-H), 7.62–7.51 (m, 3H, Ar-H), 7.40 (t, 1H, *J* = 7.7 Hz, Ar-H), 7.22 (d, 1H, *J* = 7.5 Hz, Ar-H), 7.03 (d, 1H, *J* = 8.8 Hz, Ar-H), 2.46 (s, 1H, CH₃). ¹³C NMR (75 MHz, CDCl₃): δ 190.9, 161.0, 142.1, 139.8, 138.8, 135.7, 130.4, 130.1, 129.4, 128.7, 123.7, 122.6, 120.5, 120.0, 116.8, 21.4. ESI-MS: *m/z* [M+H]⁺ 313.

(5-Chloro-2-hydroxyphenyl)(1-(4-methoxyphenyl)-1H-pyrazol-4-yl)methanone (6q)

Yellow thick liquid. Yield 87%. FT-IR (KBr): ν 3232, 1584, 1517, 1219, 773 cm⁻¹. ¹H NMR (300 MHz, CDCl₃): δ 11.91 (s, 1H, ArOH), 8.39 (s, 1H, pyrazole H₃), 8.16 (s, 1H, pyrazole H₅), 7.87 (d, *J* = 3.0 Hz, 1H, Ar-H), 7.65 (d, 2H, *J* = 9.0 Hz, Ar-H), 7.46 (dd, 1H, *J*₁ = 8.3 Hz, *J*₂ = 2.2 Hz, Ar-H), 7.02 (d, 3H, *J* = 9.0 Hz, Ar-H), 3.87 (s, 3H, OCH₃). ¹³C NMR (75 MHz, CDCl₃): δ 191.0, 161.0, 159.3, 142.0, 135.7, 132.6, 130.4, 130.2, 123.7, 122.6, 121.5, 120.1, 114.7, 55.6. ESI-MS: *m/z* [M+H]⁺ 329.

(5-Bromo-2-hydroxyphenyl)(1-*m*-tolyl-1H-pyrazol-4-yl)methanone (6r)

Pale yellow solid. Yield 68%. M.p. 122–124 °C. FT-IR (KBr): ν 3118, 1630, 1542, 1225, 823 cm⁻¹. ¹H NMR (300 MHz, CDCl₃): δ 11.91 (s, 1H, ArOH), 8.47 (s, 1H, pyrazole H₃), 8.17 (s, 1H, pyrazole H₅), 8.01 (d, 1H, *J* = 2.2 Hz, Ar-H), 7.62–7.51 (m, 3H, Ar-H), 7.40 (t, 1H, *J* = 7.7 Hz, Ar-H), 6.98 (d, 1H, *J* = 8.8 Hz, Ar-H), 2.46 (s, 1H, CH₃). ¹³C NMR (75 MHz, CDCl₃): δ 190.9, 161.4, 142.1, 139.9, 138.9, 138.5, 133.2, 130.5, 129.4, 128.8, 122.6, 121.2, 120.4, 116.8, 110.6, 21.4. ESI-MS: *m/z* [M+H]⁺ 357.

(5-Bromo-2-hydroxyphenyl)(1-(4-methoxyphenyl)-1H-pyrazol-4-yl)methanone (6s)

Pale yellow solid. Yield 87%. M.p. 128–130 °C. FT-IR (KBr): ν 3122, 1615, 1581, 1249, 818 cm⁻¹. ¹H NMR (300 MHz, CDCl₃): δ 11.93 (s, 1H, ArOH), 8.39 (s, 1H, pyrazole H₃), 8.16 (s, 1H, pyrazole H₅), 8.02 (d, *J* = 2.2 Hz, 1H, Ar-H), 7.66 (d, 2H, *J* = 9.0 Hz, Ar-H), 7.60 (dd, 1H, *J*₁ = 9.0 Hz, *J*₂ = 3.0 Hz, Ar-H), 7.03 (d, 2H, *J* = 9.0 Hz, Ar-H), 6.98 (d, 1H, *J* = 9.0 Hz, Ar-H), 3.88 (s, 3H, OCH₃). ¹³C NMR (75 MHz, CDCl₃): δ 190.0, 161.4, 159.3, 142.0, 138.5, 133.2, 132.5, 130.4, 122.5, 121.4, 120.4, 114.7, 110.6, 55.6. ESI-MS: *m/z* [M+H]⁺ 373.

(6-Hydroxybenzofuran-5-yl)(1-*m*-tolyl-1H-pyrazol-4-yl)methanone (6t)

Yellow thick liquid. Yield 83%. FT-IR (KBr): ν 3121, 1634, 1541, 1247, 785 cm⁻¹. ¹H NMR (300 MHz, CDCl₃): δ 12.14 (s, 1H, ArOH), 8.47 (s, 1H, pyrazole H₃), 8.18 (s, 1H, pyrazole H₅), 8.14 (s, 1H, Ar-H), 7.61–7.51 (m, 3H, Ar-H), 7.39 (t, *J* = 7.5 Hz, 1H, Ar-H), 7.20 (d, 1H, *J* = 7.5 Hz, Ar-H), 6.75 (d, 1H, *J* = 1.5 Hz, Ar-H), 2.45 (s, 3H, CH₃). ¹³C NMR (75 MHz, CDCl₃): δ 192.1, 161.1, 159.2, 145.6, 142.2, 139.8, 139.1, 130.4, 129.4, 128.6, 124.6, 123.4, 120.4, 120.2, 117.4, 116.7, 106.7, 100.0, 21.4. ESI-MS: *m/z* [M+H]⁺ 319.

(2-Hydroxy-6-methylphenyl)(1-phenyl-1H-pyrazol-4-yl)methanone (6u)

Yellow solid. Yield 77%. M.p. 111–113 °C. FT-IR (KBr): ν 3447, 1622, 1539, 1483, 1238, 903, 771 cm⁻¹. ¹H NMR (300 MHz, CDCl₃): δ 12.13 (s, 1H, ArOH), 8.47 (s, 1H, pyrazole H₃), 8.17 (s, 1H, pyrazole H₅), 7.80 (d, 1H, *J* = 8.1 Hz, Ar-H), 7.75 (d, *J* = 8.1 Hz, 2H, Ar-H), 7.52 (t, 2H, *J*

= 7.3 Hz, Ar-H), 7.40 (d, $J = 7.5$ Hz, 1H, Ar-H), 6.88 (s, 1H, Ar-H), 6.78 (d, $J = 8.1$ Hz, 1H, Ar-H), 2.39 (s, 3H, CH₃). ¹³C NMR (75 MHz, CDCl₃): δ 191.6, 162.9, 147.7, 142.2, 139.2, 131.1, 130.2, 129.6, 127.8, 125.0, 123.4, 120.3, 119.7, 119.5, 118.6, 117.7, 21.9. ESI-MS: m/z [M+H]⁺ 279.

5. Anti-proliferative Assay

5.1. Cell Proliferation Assay

This assay is a quantitative colorimetric method for determination of cell survival and proliferation. The assessed parameter is the metabolic activity of viable cells.¹³ Metabolically active cells reduce pale yellow tetrazolium salt (MTT) to a dark blue water-insoluble formazan, which can be directly quantified after solubilisation with DMSO. The absorbance of the formazan directly correlates with the number of viable cells. The cells were plated in 96-well plates at a density of 2.0×10^4 in 100 μ L of medium per well of 96-well plate. Cultures were incubated with test compounds (10 μ M) and incubated for 48 h. The medium was replaced with fresh medium containing 100 μ g/mL of 3-(4,5-dimethylthiazol-2-yl)-2,5-diphenyltetrazolium bromide (MTT) for 2–3 h. The supernatant was aspirated and MTT-formazan crystals dissolved in 100 μ L DMSO; OD measured at λ 540 nm (reference wavelength, λ 620 nm) on ELISA reader cell viability % was calculated by comparing the absorbance of treated versus untreated cells.

6. Conclusion

In conclusion, 4H-chromone-based hydrazones, pyrazolecarboxylates and pyrazolylmethanones were synthesized and evaluated for their anti-proliferative activity against four human cancer cell lines. The compounds **5p–q**, **5w**, **6e** and **6j** displayed potent anti-proliferative activity, however, compounds **3s** and **5g–h** have shown promising activity.

7. Acknowledgments

The authors thank Dr. S. Chandrasekhar, Director, CSIR-IICT for constant encouragement. Financial assistance to R. N. R from CSIR, New Delhi is gratefully acknowledged. B. China Raju acknowledges CSIR, New Delhi for financial support through the programme “ORIGIN” (CSC-0108) of XII five year plan.

8. References

- S. Fustero, M. Sanchez-Rosello, P. Barrio, A. Simon-Fuentes, *Chem. Rev.* **2011**, *111*, 6984–7034. DOI:10.1021/cr2000459
- S. Ulloora, R. Shabaraya, R. Ranganathan, A. V. Adhikari, *Eur. J. Med. Chem.* **2013**, *70*, 341–349. DOI:10.1016/j.ejmech.2013.10.010
- M. D. Altintop, A. Ozdemir, G. Turan-Zitouni, *Eur. J. Med. Chem.* **2012**, *58*, 299–307. DOI:10.1016/j.ejmech.2012.10.011
- A. M. Pieczonka, A. Strzelczyk, B. Sadowska, G. Mloston, P. Stączek, *Eur. J. Med. Chem.* **2013**, *64*, 389–395. DOI:10.1016/j.ejmech.2013.04.023
- M. B. Bhalerao, S. T. Dhumal, A. R. Deshmukh, *Bioorg. Med. Chem. Lett.* **2017**, *27*, 288–294. DOI:10.1016/j.bmcl.2016.11.056
- T. Yoshioka, T. Fujita, T. Kanai, Y. Aizawa, T. Kurumada, K. Hasegawa, H. Horikoshi, *J. Med. Chem.* **1989**, *32*, 421–428. DOI:10.1021/jm00122a022
- M. Rinaldi-Carmona, F. Barth, M. Heaulme, D. Shire, B. Calandra, C. Congy, S. Martinez, J. Maruani, G. Neliat, D. Caput, P. Ferrara, P. Soubrie, J. C. Breliere, G. Le Fur, *FEBS Lett.* **1994**, *350*, 240–244. DOI:10.1016/0014-5793(94)00773-X
- Ch. Dayakar, B. S. Kumar, G. Sneha, G. Sagarika, K. Meghana, S. Ramakrishna, R. S. Prakasham, B. C. Raju, *Bioorg. Med. Chem.* **2017**, *25*, 5678–5691. DOI:10.1016/j.bmc.2017.08.042
- B. C. Raju, A. K. Tiwari, J. A. Kumar, A. Z. Ali, Sachin B. Agawane, G. Saidachary, K. Madhusudana, *Bioorg. Med. Chem.* **2010**, *18*, 358–365. DOI:10.1016/j.bmc.2009.10.047
- G. Saidachary, K. Veera Prasad, D. Divya, A. Singh, U. Ramesh, B. Sridhar, B. C. Raju, *Eur. J. Med. Chem.* **2014**, *76*, 460–469. DOI:10.1016/j.ejmech.2014.02.042
- P. Suman, T. R. Murthy, K. Rajkumar, D. Srikanth, Ch. Dayakar, C. Kishor, A. Addlagatta, S. V. Kalivendi, B. C. Raju, *Eur. J. Med. Chem.* **2015**, *90*, 603–619. DOI:10.1016/j.ejmech.2014.11.063
- P. Suman, Ch. Dayakar, K. Rajkumar, B. Yashwanth, P. Yogeeswari, D. Sriram, J. V. Rao, B. C. Raju, *Bioorg. Med. Chem. Lett.* **2015**, *25*, 2390–2394. DOI:10.1016/j.bmcl.2015.04.009
- B. C. Raju, R. N. Rao, P. Suman, P. Yogeeswari, D. Sriram, T. B. Shaik, S. V. Kalivendi, *Bioorg. Med. Chem. Lett.* **2011**, *21*, 2855–2859. <http://doi.org/10.1016/j.bmcl.2011.03.079>
- K. Rajkumar, P. Suman, B. C. Raju, *RSC Adv.* **2015**, *5*, 73850–73858. DOI:10.1039/c5ra10185a
- W. Guangcheng, C. Ming, W. Jing, P. Yaping, L. Luyao, Z. X. Zhen, D. Bing, C. Shan, L. Wenbiao, *Bioorg. Med. Chem. Lett.* **2017**, *27*, 2957–2961. DOI:10.1016/j.bmcl.2017.05.007
- L. Deng, W. Wang, C. Hu, C. Wu, CN103554123, **2016**.
- L. Deng, W. Wang, G. Chen, Q. Yang, X. Gao, Y. Zhou, C. Hu, C. Wu, R. Shen, Y. Wu, CN106083884, **2016**.
- A. Lazarenkow, J. Nawrot-Modranka, E. Brzezinska, U. Krajewska, M. Rozalski, *Med. Chem. Res.* **2012**, *21*, 1861–1868. DOI:10.1007/s00044-011-9703-4
- B. A. Kumar, P. Dipak, S. J. Singh, *Tetrahedron* **1988**, *44*, 1241–1246. DOI:10.1016/S0040-4020(01)85904-4
- M. A. Ibrahim, N. M. El-Gohary, *Heterocycles* **2014**, *89*, 413–425. DOI:10.3987/COM-13-12899

Povzetek

Sintetizirali smo serijo hidrazonov **3a–z**, pirazolkarboksilatov **5a–x** in pirazolilmetanonov **6a–u**, temelječih na ogrodju 4*H*-kromona. Za vse pripravljene spojine smo preučili anti-proliferativne lastnosti proti celičnim linijam A549, HeLa, DU145 in MDAMB 231. Hidrazon **3s** s kloro substituentom na kromanonskem skeletu in z metoksi skupino na fenilnem obroču je izkazoval obetavno aktivnost na celične linije A549, HeLa in DU145. Spojina **5p** z bromo substituentom na kromanonskem skeletu in metilno skupino na fenilnem obroču je izkazala veliko aktivnost proti celični liniji DU145. Furopirazolkarboksilat **5w**, ki vsebuje metilni substituent na fenilnem obroču, je izkazal močno aktivnost proti HeLa celični liniji. Pirazolilmetanon **6e** s fluoro substituentom na fenilnem obroču in spojina **6j** z metilnim substituentom na kromanonskem skeletu ter metoksi skupino na fenilnem obroču sta izkazali obetavne anti-proliferativne lastnosti proti HeLa celični liniji.

Scientific paper

Cis-dioxo-bis [3-methoxy-2,2-dimethylpropanediamine] Molybdenum/Surfactant-Modified Electrode for Simultaneous Sensing of Ascorbic Acid and Dopamine

Ali Arjmandi,¹ Hamid Reza Zare-Mehrjardi^{1,2,*} and Hadi Kargar^{1,2}¹ Department of Chemistry, Payame Noor University, PO BOX 19395-3697 Tehran, Iran² Research Center of Environmental Chemistry, Payame Noor University, Ardakan, Yazd, Iran* Corresponding author: E-mail: hr_zare@pnu.ac.ir, zareanalyst@gmail.com, hr.zaremehr@yahoo.com
Tel.: +98 3532220011; fax: +98 3532228110

Received: 20-04-2017

Abstract

In this work, the carbon paste electrode (CPE) was modified using the *cis*-dioxo-bis[3-methoxy-2,2-dimethylpropanediamine] molybdenum(VI) complex and 1-octanaminium,N,N,N-trioctyl bromide. Using the modified electrode, the best separation of anodic peaks for ascorbic acid and dopamine was obtained in solutions with pH 5.0 and the linear range for ascorbic acid is acquired in the range from 3.0×10^{-6} to 6.0×10^{-3} M and for dopamine from 2.0×10^{-6} to 1.0×10^{-2} M. The limits of detection (S/N = 3) were 4×10^{-7} M and 5×10^{-7} M for dopamine and ascorbic acid, respectively. Surface regeneration and the very easy preparation of the modified CPE together with the very good peak resolution and sub-micromolar detection limits designate the prepared carbon paste electrode appropriate for simultaneous voltammetric determination of dopamine and ascorbic acid.

Keywords: Dopamine; ascorbic acid; modified electrode; Molybdenum Schiff base complex; differential pulse voltammetry

1. Introduction

Recently, the manufacture and design of new voltammetric sensors have been of notable interest.^{1,2} Specialty, detection of secretion neurotransmitters, e.g. ascorbic acid (AA) and dopamine (DA) as a vital nutritional factor, through the improvement of the electrochemical sensors received many interests. DA is a significant transmitter of the nervous system and a hormone and is involved in many biological processes in the human brain and body.^{3,4} In the brain, dopamine primarily controls the reward-motivated behavior, while in the body it is involved in processes such as motor control or the release of other important hormones. Low levels of DA are common in those suffering from Parkinson's disease due to the loss of dopamine-containing neurons in the midbrain. Abnormal dopamine concentrations are also related to schizophrenia, attention deficit hyperactivity disorder (ADHD), and restless legs syndrome (RLS).³ Dopamine does not pass through the brain-blood barrier, and, in the blood vessels, it serves as a local chemical messenger, like a vasodilator, and reduces insulin production or regulates the activity of

lymphocytes. Both – the plant and animal kingdoms contain AA. Among animal organs, anterior pituitary lobe, leukocytes and the liver represent the highest content of AA. Ascorbic acid or vitamin C is not only very popular for its antioxidant properties, but also widely used for the prevention and treatment of the common cold, mental illnesses, infertility, cancers and AIDs. AA is also used in multivitamin preparations and various biological systems.⁵ A serious problem in detection of DA or AA is the overlapping of the anodic peaks of AA and coexisting DA. The anodic oxidation potential of DA is close to that of AA at common solid electrodes and results in the lack of good resolution between their anodic peaks. Several methods have been applied in order to overcome this problem. In recent years, modified carbon paste electrodes have extensively been applied for the determination of DA and AA. For instance, the electrochemical behavior of these biologically important compounds was investigated at the carbon paste electrodes modified with Eriochrome Black T (EBT),⁶ reduced graphene oxide,⁷ N-butylpyridinium hexafluorophosphate,⁸ thionine-nafion ion-paired⁹ and

thionine-nafion supported on multi-walled carbon nanotube.¹⁰ Recently, application of carbon nanotubes in the modification of the carbon paste electrodes has performed for detection of DA.^{11–13} Application of nanoparticles,^{10,11,14–21} complexes of transition metals,^{22–25} surfactants,^{7,15} ionic liquids^{8,12} and polymeric materials,^{23,26} in preparation of modified carbon paste electrodes have attracted most consideration in this regard. Using the electron mediators in modification of the electrodes, causes to decrease the overpotential of the electrochemical process of the interested analyte and of course improve the selectivity and sensitivity of the electrode response.

Previous works showed that Schiff base complexes are efficient electron mediators and the oxidation process of different biological compounds, such as AA can be catalyzed using them.^{27,28} The major drawback in the using of redox mediators in the modification of the electrodes is lack of good resolution for simultaneous determination of different analytes in the mixed samples. On the other hand, the application of an electron mediator together with the ionic surfactant in the preparation of modified electrodes, because of the electrostatic repulsion or attraction between the charged analytes and the surfactant, can separate the voltammetric peaks of different compounds and improve the selectivity for their simultaneous detection. Respect to the charge sign of various analytes and the ionic surfactant, the electrostatic interactions can be exclusive or inclusive that is important for the improvement of the voltammetric resolution between the analytes peak. A nafion/reduced graphene oxide prepared film on the surface of carbon electrode has been applied in electrocatalytic oxidation of ascorbic acid.²⁹ Modification of carbon paste electrode using an ion pair (thionine/nafion) has been reported.¹⁸ This electrode has been effective in simultaneous voltammetric determination of AA and DA by DPV. Triton X-100 (as a neutral surfactant) has been applied in preparation of the modified glassy carbon electrode.³⁰ Results of this work revealed that the hydrophobicity of the surfactant at the surface of the electrode is effective in promoting the electrochemical response of the studied heme proteins.

In the present work, the electrochemical oxidation of AA and DA at the surface of the modified carbon paste electrode containing the *cis*-[Mo(O)₂L]/cationic surfactant is studied. Schiff base complexes are well-known as effective redox mediators and are capable to catalyze the electrochemical oxidation of various organic and biologically important compounds, e.g. ascorbic acid. Of particular interests in this work, are entering of the cationic surfactant into the matrix of the modified electrode and enlargement of the anodic overpotential for DA oxidation. In solutions of pH 5.0, in which all studies are performed, DA exists as the positively charged species. Therefore, the favorable ionic interaction (electrostatic repulsion) between the cationic form of DA and the cationic surfactant (TOA⁺) caused increasing the overvoltage for DA and positive shift

in its anodic peak potential. Modification of the carbon paste electrode using the cationic surfactant results in increasing the anodic overpotential for DA oxidation. In order to obtain a higher sensitivity and selectivity in the voltammetric response of the modified electrode, the effect of the cationic surfactant percent on the separation of the anodic peaks of DA and AA is studied. Noteworthy advantages of the modified-CPE described in this paper such as ease of surface regeneration and fabrication, excellent resolution between the anodic peaks of DA and AA and high stability of the *cis*-[Mo(O)₂L] and cationic surfactant in its matrix designate it very useful for the sensitive and selective simultaneous detection of DA and AA.

2. Experimental

2.1. Materials

For the synthesis of the complex *cis*-dioxo-bis[3-methoxy-2,2-dimethylpropanediamine] molybdenum(VI), a solution of 1 mmol [MoO₂(acac)₂] in 50 mL methanol was added to the solution of 1 mmol 3-methoxy-2,2-dimethylpropanediamine (Schiff base ligand) in 10 mL methanol and the reaction mixture was stirred for 120 min at reflux condition. Then the precipitated orange complexes were filtered and washed with methanol.³¹ For to the preparation of CPEs, spectroscopic mineral oil (Nujol), graphite powder (20 μm), and 1-octanaminium,N,N,N-trioctyl bromide as a cationic surfactant were purchased from Merck. All the other chemicals were analytical reagent grade, purchased from Merck. Using bidistilled deionized water, all aqueous solutions were made up.

Stock solutions of DA and AA were freshly made up in a buffered solution and before voltammetric experiments, purged with pure nitrogen gas (99.999%) for 120 s. The buffered solutions of DA and AA were deoxygenated by purging the pure nitrogen (99.999% from Roham Gas Company) before use for voltammetric studies. Nitrogen gas was passed over the surface of the test solutions during the measurements, in order to avoid the influx of oxygen into the solution.

For the determination of the recovery in spiking of dopamine, the sample of fresh human serum, prepared from Razi Institute of Vaccine and Serum Co. (Tehran, Iran), was filtered and diluted using a 0.1 M acetate buffer solution of pH 5.0. Each tablet was grounded with a mortar and pestle to detect AA in commercial vitamin preparation, then 100 mg of the powdered sample was dissolved in 100 mL of the buffered solution.

2.2. Apparatus

In order to make up the buffered solutions, a digital pH/mV/ion meter (CyberScan model 2500) was used. A common three-electrode system was applied with a platinum wire as a counter electrode, a saturated Calomel ref-

erence electrode, and modified or unmodified carbon paste working electrode. Voltammetric measurements were performed using a computerized potentiostat/galvanostat Autolab model 302 (Eco Chemie Utrecht) controlled with General Purpose Electrochemical System (GPES) software.

2. 3. Preparation of the Carbon Paste Electrodes

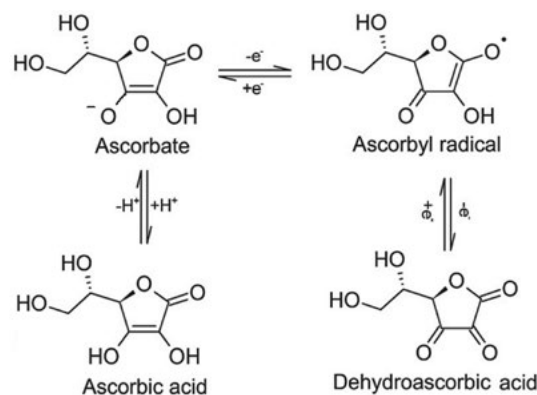
To prepare the unmodified CPE, a suitable amount of mineral oil with powder of graphite (~25:75, w/w) was mixed by hand mixing in a mortar and pestle, then a portion of the resulted mixture was packed into the end of a polyamide tube (ca. 2.5 mm i.d.). A copper pin makes the electrical contact into the back of the composite, in the polyamide tube. The *cis*-[Mo(O)₂L]-modified carbon paste electrode was fabricated by mixing the *cis*-[Mo(O)₂L] (3%, w/w) with powder of graphite and a suitable amount of mineral oil, and then the resulted composite was dissolved in dichloromethane in order to achieve better homogeneity and reproducibility by polishing the electrode surface. For fabrication of the *cis*-[Mo(O)₂L]-modified carbon paste electrode containing surfactant, various percents of cationic surfactant together with 3 wt.% *cis*-[Mo(O)₂L], powder of graphite and a suitable amount of mineral oil were mixed in an appropriate amount of dichloromethane. The solvent of the resulted mixture has been evaporated completely by stirring, and then air dried for one day and packed into the end of a polyamide tube.

3. Results and Discussion

3. 1. Voltammetric Experiments of AA and DA at the Prepared Electrodes

Our previous work revealed that anodic overpotential for ascorbic acid oxidation is reduced and its oxidation process is catalyzed by Schiff base complexes.¹⁷ The electrochemical behavior of 1 mM AA in a buffered solution of pH 5.0 at the surface of the unmodified CPE and the *cis*-[Mo(O)₂L]-modified CPE containing various wt.% of cationic surfactant is studied by cyclic voltammetry. Results of this study are shown in Figure 1A. As can be observed, at the surface of the unmodified carbon paste electrode, a relatively broad wave in 470 mV appeared for the anodic oxidation of AA. But, by introducing the *cis*-[Mo(O)₂L] in the matrix of the carbon paste electrode (*cis*-[Mo(O)₂L]/CPE), the anodic oxidation potential of AA decreased to about 435 mV. At the surface of modified electrodes including *cis*-[Mo(O)₂L] and different wt.% of cationic surfactant, this overpotential is slightly decreased with increasing the amount of surfactant in the matrix of the electrode. A comprehensive explanation of the electrocatalytic oxidation of AA using the *cis*-[Mo(O)₂L]/CPE is

presented in the following. AA, with a pK_a of 4.17, mainly exists as an anionic form (ascorbate, below scheme) under the experimental condition (buffered solution with pH 5.0). Therefore, there is an electrostatic interaction between the anionic form of AA and the cationic surfactant on the surface of the modified-CPE including cationic surfactant (*cis*-[Mo(O)₂L]/CS/CPE). Results of this investigation reveal that the higher percents of cationic surfactant, because of decreasing the electrical conductivity of the electrode and unsuitable mechanical properties, result in worsening the voltammetric response of the modified-CPE, e.g. enlargement of the capacitive background current, broadening the wave shape and lowering the anodic peak. Hence, the percent of cationic surfactant in the matrix of the modified-CPE is optimized to obtain the excellent resolution between the voltammetric responses of DA and AA and also, higher sensitivity in voltammetric peaks (lower background current and greater anodic peak current).



Scheme 1. Ionization of ascorbic acid followed by the oxidation–reduction reactions of ascorbate ions under the experimental condition (buffered solution with pH 5.0).

The electrochemical behavior of 1 mM DA in a buffered solution of pH 5.0 at the surface of the unmodified CPE and the *cis*-[Mo(O)₂L]-modified carbon paste electrode containing various wt.% of cationic surfactant is studied by cyclic voltammetric method. The results of this study are shown in Figure 1B. A pair of redox peaks with anodic and cathodic peak potentials respectively, 608 and 332 mV ($\Delta E_p = 276$ mV) and the ratio of cathodic to anodic peak current (I_{pc}/I_{pa}) nearly 0.88 were acquired for DA at unmodified carbon paste electrode (CPE). As a result, at the surface of CPE, the electrochemical process of DA is quasi-reversible and the oxidation product of DA under the empirical conditions (pH 5.0) is relatively stable.

Previous studies revealed that oxidation product of DA (dopaminequinone) performed an intramolecular 1,4-Michael addition in solutions with higher pHs,³² that in this reaction, a nucleophilic attack of external amine group on dopaminequinone leads to leucodopaminechrome. Thus buffered solution of pH 5.0 was selected for

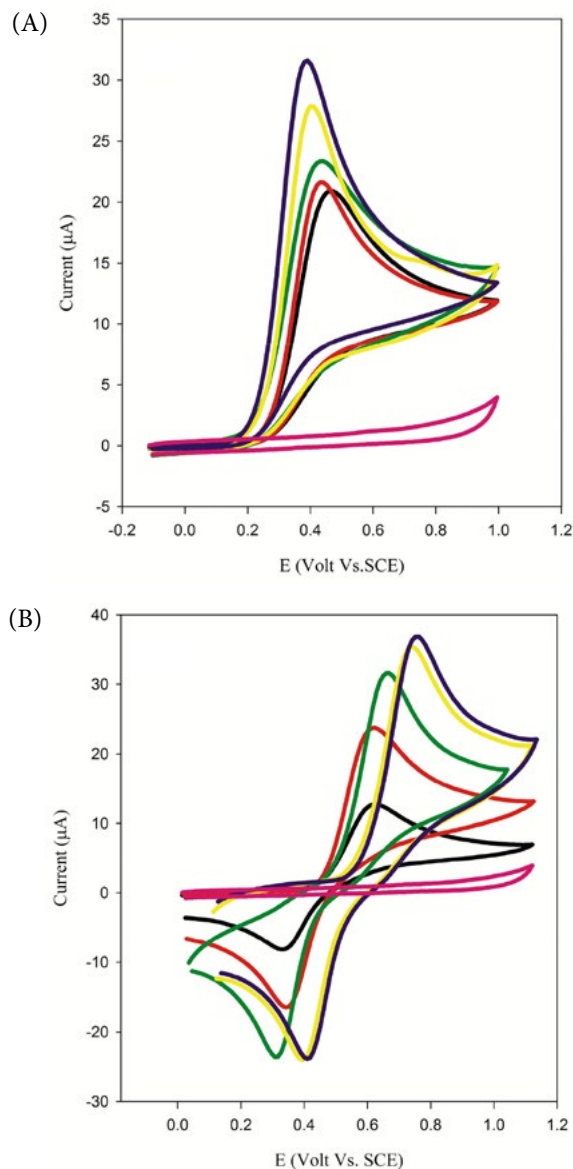


Figure 1. CV responses of blank buffered solution of pH 5.0 using *cis*-[Mo(O)₂L]-modified CPE containing 2% CS (pink) and of 1 mM AA (A) and 1 mM DA (B) in the same buffer at the surface of unmodified CPE (black), CoL/modified CPE containing 0% (red), 1% (green), 2% (yellow) and 3% CS (dark blue). Sweep rate: 100 mVs⁻¹; pulse amplitude: 50 mV.

all experiments of DA in order to obtain a simple electron transfer and prevent the following reactions for DA. In fact, in solutions of pH ≤ 5 , DA contains protonated amine group and mostly exists in cationic form. Hence, the product of anodic oxidation of DA in acidic solutions will be almost stable and can be about 1.0 for ratio of I_{pc}/I_{pa} .

Application of the cationic surfactant in the preparation of the modified-CPE causes an increase in anodic overpotential of DA oxidation, because of the electrostatic interaction at the surface of the modified electrode between the positive charge of cationic surfactant and the cationic form of DA. As a result, the reversibility of the

electrochemical process of DA at the surface of the electrode is decreased (ΔE_p is increases) and its overpotential for oxidation is increased. As can be seen in Figure 1B by increasing the percent of cationic surfactant in the modified carbon paste electrode, this effect is intensified. The result of this effect is excellent resolution between the anodic peaks of AA and DA.

3. 2. Voltammetric Experiments in the Mixed Solutions of DA and AA

Making an approach for separation of anodic peaks and simultaneous detection of AA and DA is very important with respect to mutual quantification. At the traditional solid electrodes, the anodic overpotential for oxidation of AA is the same as that of DA; furthermore, both of AA and DA are present simultaneously in mammalian brain which will cause to overlap the voltammetric responses of these species.³³ Many efforts have been made on the fabrication of the modified electrodes that are capable to separate their anodic peaks and make the feasibility of simultaneous determination of DA and AA.^{21–26}

In this work, *cis*-[Mo(O)₂L]-modified CPE containing cationic surfactant was used for simultaneous voltammetric detection of these compounds. The electrochemical behavior of 1 mM of both DA and AA in a buffered solution of pH 5.0 at the surface of the unmodified CPE and the *cis*-[Mo(O)₂L]-modified carbon paste electrode containing various wt.% of cationic surfactant was studied by cyclic voltammetric method. The results of this study are shown in Figure 2A. Figure 2B shows the differential pulse voltammograms (DPVs) of five prepared electrodes in this solution. These figures revealed that at the surface of the unmodified CPE, only a quasi-reversible wave can be observed for DA and a distinguished wave cannot be obtained for AA, therefore this electrode (unmodified-CPE) isn't suitable for the simultaneous voltammetric detection of DA and AA. By introducing the *cis*-[Mo(O)₂L] in the matrix of carbon paste electrode (*cis*-[Mo(O)₂L]/CPE), a little resolution between anodic peaks of DA and AA is obtained but the detection of each compound in the presence of the other isn't possible because of the overlapping of their anodic peaks. Application of *cis*-[Mo(O)₂L]-modified CPE containing cationic surfactant, results in better resolution of anodic peaks for DA and AA, because of positive shift of DA anodic peak. As can be seen in Figure 2, at the modified-CPE including 2 wt.% of cationic surfactant, the complete resolution between anodic peaks of DA and AA is obtained. The positive shift in anodic peak potentials of DA under the experimental condition (buffered solution of pH 5.0) is a result of the electrostatic repulsion effects between the cationic surfactant and cationic form of dopamine. A better resolution does not obtained by using higher percents of cationic surfactant, whereas the sensitivity of electrode response to DA is decreased because of the resulted anodic overpotential and kinetic limitation for DA. More-

over, this investigation revealed that applied higher percents of cationic surfactant in modification of the electrode caused to limit the voltammetric detection limit for DA and AA (increase the capacitive background current). These efficacies can be obviously seen by comparing of the CVs or DPVs for the different modified CPEs in Figure 2. As a result, the *cis*-[Mo(O)₂L]-modified CPE containing 2 wt.% cationic surfactant was selected for simultaneous detection of DA and AA.

The resulting resolution between the anodic peaks of DA and AA in this investigation (308 mV) is significantly more desirable than other reported voltammetric sensors. The modified electrode with nanocomposite of carbon

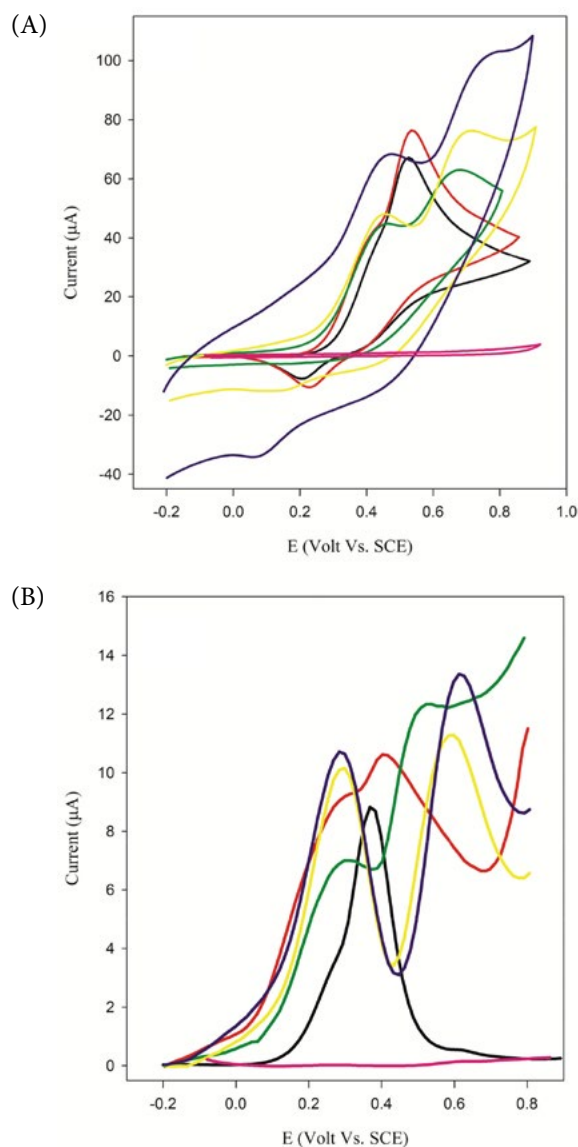


Figure 2. (A) CV and (B) DPV responses of blank buffered solution of pH 5.0 using *cis*-[Mo(O)₂L]/modified CPE containing 2%CS (pink) and of a mixture of 1 mM DA and 1 mM AA in the same buffer at the surface of unmodified CPE (black), CoL/modified CPE containing 0% (red), 1% (green), 2% (yellow) and 3% CS (dark blue). Sweep rate: 100 mVs⁻¹; pulse amplitude: 50 mV.

dots/ferrocene derivative functional Au NPs and graphene obtained a peak resolution for DA and AA about 180 mV using differential pulse voltammetry.³⁴ Application of a nanocomposite containing polypyrrole/Cu_xO–ZnO in modification of the electrode for voltammetric detection of AA and DA resulted in a peak separation of 150 mV.³⁵ The electrode modified with nanoparticles of γ-WO₃ is applied using DPV for simultaneous detection of AA and DA and a peak resolution of 133 mV is obtained.³⁶ In comparison to the previous works, the decay of anodic current between the anodic peaks of DA and AA is taken place close to the capacitive background by using the *cis*-[Mo(O)₂L]-modified CPE containing cationic surfactant. The resulted decay of current significantly causes to decrease the overlapping of the anodic waves of DA and AA, and simultaneous detection of these compounds in mixture samples possesses a more desirable accuracy. Moreover the reproducibility of the detections is improved, due to better stability of DA and AA in slightly acidic condition (pH 5.0).

3. 3. The Effect of pH and Sweep Rate

Voltammetric studies of the buffered solutions with different pHs containing AA and DA were carried out to find out the optimized pH for acquiring the good sensitivity and an excellent resolution between their anodic peaks. In these experiments, 0.1 M phosphate was applied in preparation of buffered solutions of pH 3.0, 6.0 and 7.0, and 0.1 M acetate for pHs 4.0 and 5.0. Table 1 shows the peak potentials and peak currents of cyclic voltammograms obtained at the surface modified CPE in the mixture solutions of DA and AA with different pHs. These results reveal that the best peak separation is resulted in pH 5.0. Therefore, in all voltammetric studies, the buffered solution with pH 5.0 was applied as supporting electrolyte.

In order to investigate the effect of the potential scan rate, cyclic voltammetric experiments were carried out in the buffered solution with pH 5.0. The results revealed that the anodic peak currents (I_{pa}) of DA and AA increase linearly with increasing the square root of the scan rate ($v^{1/2}$) in the range of 25–200 mVs⁻¹. These results corroborate the diffusion-controlled anodic oxidation of DA and AA at

Table 1. Variation of peak potential and peak current of cyclic voltammograms for mixture solutions of DA and AA with different pH using *cis*-[Mo(O)₂L]/modified CPE containing 2 wt.% of cationic surfactant

pH	AA		DA		ΔE_p
	I_{pa} (μA)	E_{pa} (mV)	I_{pa} (μA)	E_{pa} (mV)	
3	24.2	458	23.6	731	273
4	19.9	421	22.5	722	301
5	22.5	395	25.3	710	315
6	18.8	391	23.8	679	288
7	16.5	387	23.3	668	281

the prepared CPE surface. The current function ($I_p/v^{1/2}$) for AA decreased with $v^{1/2}$, which corroborates a catalytic manner for AA at the surface of the modified CPE, whereas for DA this effect can't be seen.

3. 4. Analytical Characterization

The differential pulse voltammetric method using the *cis*-[Mo(O)₂L]-modified CPE containing 2 wt.% of cationic surfactant was applied as a useful approach with low

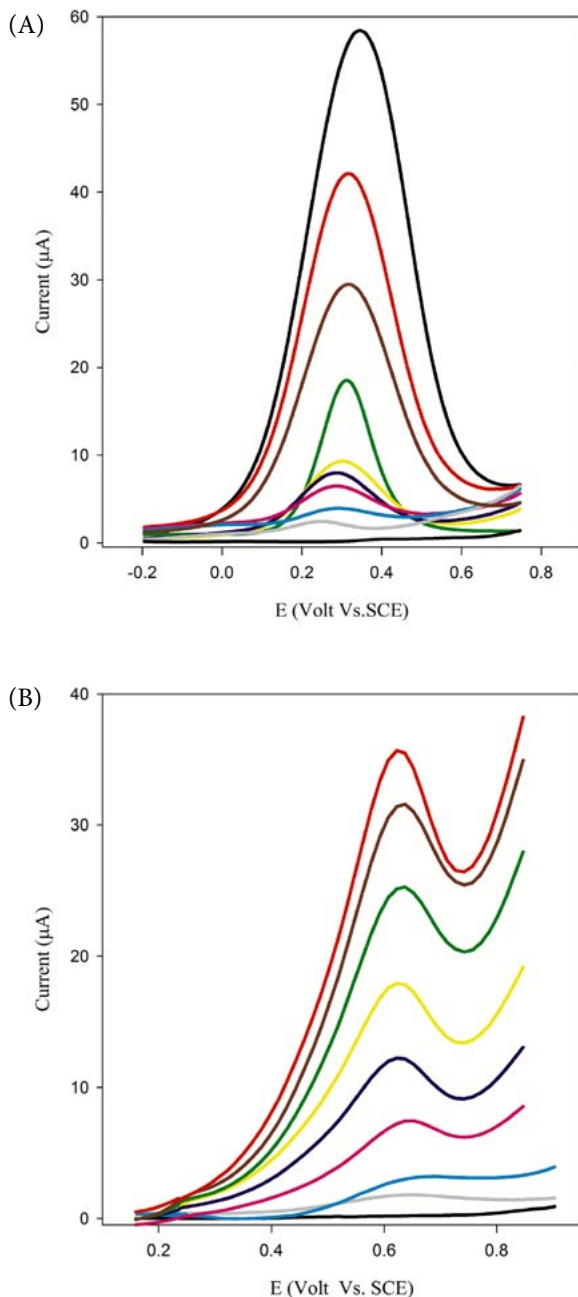


Figure 3. Differential pulse voltammograms of buffered solution of pH 5.0 containing (A) 0.0, 0.1, 0.2, 0.5, 0.8, 1.0, 2.0, 3.0, 4.0, 5.6 and 6.0 mM AA and (B) 0.0, 0.2, 0.3, 0.5, 0.9, 1.0, 1.2, 1.6, 2.2 and 2.5 mM DA (down to up). Pulse amplitude: 50 mV.

limits of detection for detections of DA and AA in a wide range of their concentrations. Supporting electrolyte for these experiments was buffered solutions of pH 5.0. Figure 3 shows some obtained DPV waves in these experiments. By drawing the anodic current signal versus the concentration (the calibration curves), a linear range is obtained that is 2.0×10^{-6} – 1.0×10^{-2} M for DA and 3.0×10^{-6} – 6.0×10^{-3} M for AA (Figure 4). A slope of 9355.75 $\mu\text{A}/\text{M}$ ($R^2 = 0.9985$) is resulted for AA, and a slope of 6534.37 $\mu\text{A}/\text{M}$ ($R^2 = 0.9986$) for DA. The relative standard deviations (R.S.D.) for these slopes on the basis of five replicates were 3.4 and 3.1% for DA and AA, respectively and were less than 3.5% for both DA and AA, based on seven measurements in a period of two months. So the prepared modified CPE in this work revealed to be very stable.

The differential pulse voltammograms obtained in solutions containing 5×10^{-4} M AA and five various amounts of DA from 4×10^{-4} to 2×10^{-3} M are shown in Figure 5A. The waves obtained in solutions including 5×10^{-5} M DA and various amounts of AA in the range of 5×10^{-5} to 9×10^{-4} M is represented in Figure 5B. Using the modified CPE in this work, a linear range for AA in buffered solutions of pH 5.0 is acquired in the range from 4.0×10^{-6} – 7.0×10^{-3} M and for DA from 2.0×10^{-6} – 9.0×10^{-3} M. The respective limits of detection ($S/N = 3$) were 4×10^{-7} M and 5×10^{-7} M for DA and AA, respectively. The resulted limits of detection and linear ranges were very similar to the detections in solutions containing only one of DA or AA. In the presence of 5×10^{-4} M AA, the calibration curve slope for DA was 6403.68 $\mu\text{A}/\text{M}$ ($R^2 = 0.9985$), which was about 98% of the resulted slope value for the separate DA solutions. This slope for AA, in the presence of 5×10^{-5} M DA was 9075.08 $\mu\text{A}/\text{M}$ ($R^2 = 0.9978$).

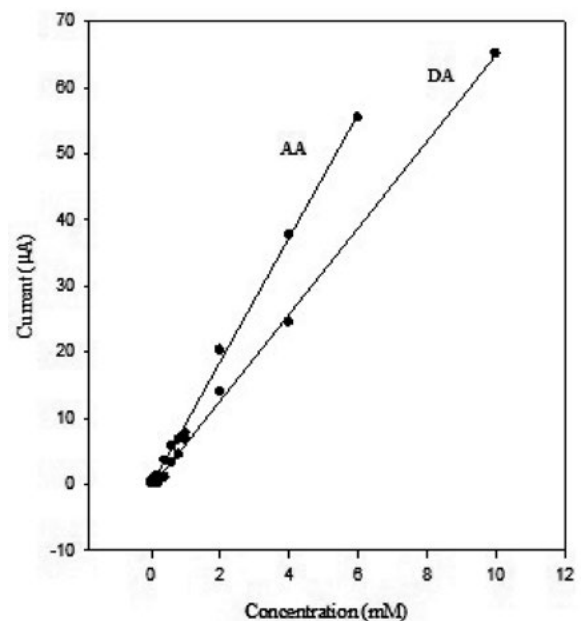


Figure 4. Linear calibration curves of current signals versus DA and AA concentration in the range 10.0 to 1000.0 μM .

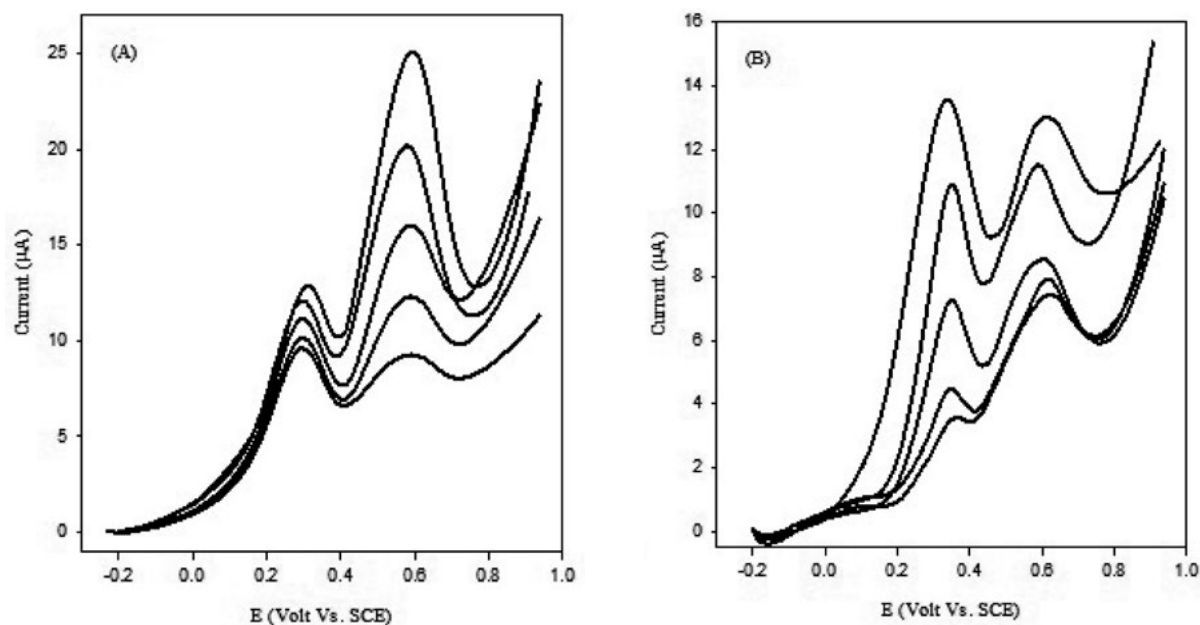


Figure 5. Differential pulse voltammograms for buffered solution of pH 5.0 containing (A) 0.5 mM AA (constant) and various concentrations of DA: 0.4, 0.7, 1.0, 1.6, 2.0 mM. (B) 0.5 mM DA (constant) and various concentrations of AA: 0.05, 0.1, 0.5, 0.7, 0.8 and 0.9 mM. Pulse amplitude: 50 mV.

Table 2. AA analysis results in vitamin preparations using *cis*-[Mo(O)₂L]/modified CPE containing 2 wt.% of cationic surfactant

Sample	Added AA (mg)	AA found (mg/100 mg sample) ^a		
		Present method	Reference method	Recovery (%)
Multivitamin drop ^b		36.3 (± 1.5)	37.0	–
	10.0	45.4 (± 1.8)	–	98.0
	20.0	54.1 (± 1.9)	–	96.1
	30.0	68.1 (± 1.9)	–	102.7
Vitamin C tablet		66.6 (± 1.7)	67.1	–
	10.0	77.5 (± 1.9)	–	101.1
	20.0	85.2 (± 2.0)	–	98.4
	30.0	99.6 (± 2.1)	–	103.1

^aReplicates Number was five. ^bLabeled AA value was 35 mg/mL. Determined values are also in mg/mL.

In order to investigate the selectivity of the modified electrode for simultaneous determination of DA and AA, several potential interfering compounds were selected and checked. It is found that 100-fold K⁺, Na⁺, Ca²⁺, Mg²⁺, Zn²⁺, Cu²⁺, Fe³⁺, NH₄⁺, Cl⁻, NO₃⁻, SO₄²⁻, and HCO₃⁻ did not interfere with determination (signal change < 5%). In the case of coexisting biological compounds such as glucose, fructose, sucrose, lactose, cysteine, epinephrine, acetaminophen, and serotonin, 100-fold of them did not interfere. So, it may be concluded that the method is free from interference by most coexisting substances and shows promising properties for use in real samples with minimal sample preparation. The *cis*-[Mo(O)₂L]-modified CPE containing 2 wt.% of cationic surfactant was successfully used for determination of AA in pharmaceutical preparations through the standard addition method. The analyzed vitamin preparations were effervescent tablets (Osvah Co.), multivitamin drops (Shahre Daro Co.) and vitamin C tablets (Osvah Co.). In addition to vitamin C, the multivita-

min drops contained sodium saccharin and vitamins such as A, D, E, B₁, B₂, B₃, B₆, and B₁₂. As a reference method, the method of U.S. Association of Official Analytical Chemists (AOAC)³⁷ on the basis of using 2,6-dichloro-phenolindophenol was used. Table 2 shows the results of the experiments in different samples of vitamin and the results of

Table 3. Recovery results of the spiked DA to 10.0 mL of the diluted (10-fold) human serum sample

No.	added DA (µM)	Amounts of found ^a DA (µM)	Recovery (%)
1	10.0	9.8	98.0
2	25.0	24.6	98.4
3	50.0	50.7	101.4
4	75.0	76.5	102.0
5	100	98.2	98.2

^a For five replicates in the spiked range of DA concentration, R.S.D. was less than 3.7%.

the spiked samples with AA standard solutions. These results reveal that the prepared electrode could be successfully used for the detection of AA in pharmaceutical samples because of the good enough precision and recovery. This modified electrode was also used for the recovery measurement in dopamine hydrochloride spiking to human serum samples. The results of these experiments are shown in Table 3.

4. Conclusion

The *cis*-[Mo(O)₂L]-modified CPE containing cationic surfactant prepared in the present work can enhance the selectivity and resolution of voltammetric responses of DA and AA. This modified CPE has been revealed to be capable to separate the anodic peaks of DA and AA. Resulted resolution is much better than in the previous reported works. Table 4 shows a comparison of analytical properties for the detection of DA and AA at the prepared electrode in this work and various other electrodes.

Application of the modified CPE in differential pulse voltammetric method in this work, results in a good resolution more than 300 mV for anodic peaks of AA and DA making it very appropriate and efficient for simultaneous detection of these compounds. Surface regeneration and very easy preparation of the modified electrode together with the acceptable selectivity and sensitivity, and good reproducibility of the voltammetric response proved the potential of the electrode. The resulted detection limit was appropriate but higher than some other works in literature. These results represent the prepared modified system is very effective in the fabrication of accessible tools for the simultaneous detection of DA and AA in pharmaceutical and clinical preparations.

5. Acknowledgement

The authors gratefully acknowledge the Payame Noor University providing research facilities for this work.

Table 4. Various modified electrodes: DA and AA analytical properties

Electrode	Experimental condition	Method	ΔE_p (mV)	Linear range (μM)		LOD (μM)		Ref.
				DA	AA	DA	AA	
EBT/CPE	0.1 M KCl	DPV	163	10.0–70.0	-	0.18	0.27	6
SDS/RGO/CPE	pH 7.4 PBS	DPV	178	0.5–5.0	-	0.26	-	7
MWCNT/IL/Pd-NP/CPE	pH 4.5 PBS	DPV	180	0.1–151	0.6–112	0.03	0.2	12
nanoSnO ₂ /MWCNTs/CPE	pH 6.4 PBS	DPV	155	0.3–50	1000–5000	0.03	50	13
PSNSB/CPE	pH 4.6 PBS	DPV	222	0.05–1200	2.5–1003	0.02	0.18	14
AgNPs/CPE	pH 7.5 PBS	DPV	181	1.0–50.0	-	0.08	-	16
Pd-CNF/CPE	pH 7.0 PBS	DPV	244	0.5–160	50–4000	0.2	15	18
SrPdO ₃ /CPE	pH 7.4 PBS	DPV	168	7–70 90–160	-	0.02	-	20
CPE modified with [Fe(II)TSPc] ⁴⁺	pH 7.4 PBS	CV	88	1.0–50	0.9–10.0	0.45	0.75	22
CPE modified with [Cu(bp)(H ₂ O) ₂] _n	pH 5.0 PBS	DPV	200	0.05–30.0	0.05–30.0	0.04	0.02	23
GCE modified with ZnO-Cu _x O-PPy	pH 4.0 BR solution	DPV	150	0.1–130	0.2–1.0	0.04	25.0	38
GCE modified with γ -WO ₃	pH 7.0 PBS	DPV	133	0.1–600	-	0.02	-	39
<i>cis</i> -[Mo(O) ₂ L]-modified CPE containing surfactant	pH 5.0 0.1M acetate buffer	DPV	308	2.0–10000.0	3.0–6000.0	0.4	0.5	This work

Note: EBT, Eriochrome Black T; CPE, carbon paste electrode; SDS, sodium dodecyl sulphate; RGO, reduced graphene oxide; MWCNTs, multiwalled carbon nanotubes; IL, ionic liquid; Pd-NP, Pd nanoparticle; PSNSB, PbS nanoparticles Schiff base; AgNPs, silver nanoparticles; Pd-CNF/CPE, Palladium nanoparticle-loaded carbon nanofibers; [Fe(II)TSPc]⁴⁺, iron(II)tetrasulfophthalocyanine; GCE, glassy carbon electrode; [Cu(bp)(H₂O)₂]_n, polymer of 4,4'-dicyanamidobiphenyl Cu(II) complex; PPy, polypyrrole; γ -WO₃, monoclinic structure of Tungsten trioxide nanoparticles.

6. References

- H. Zhang, J. Zhang, J. Zheng, *Measurement* **2015**, *59*, 177–183. DOI:10.1016/j.measurement.2014.09.044
- D. M. Stankovi, A. Samphao, B. Dojcinovi, K. Kalcher, *Acta Chim. Slov.* **2016**, *63*, 220–226. DOI:10.17344/acsi.2015.1541
- D. W. Martin Jr., P. A. Mayes, V. W. Rodwell (Eds.), Harper's Review of Biochemistry, 19th ed., Lange, Los Altos, CA, **1983**, p. 112.
- R. M. Wightman, C. Amatorh, R. C. Engstrom, P. D. Hale, E. W. Kristensen, W. G. Kuhr, L. J. May, *Neuroscience* **1988**, *25*, 513–523. DOI:10.1016/0306-4522(88)90255-2
- A. J. Downard, A. D. Roddick, A. M. Bond, *Anal. Chim. Acta* **1995**, *317*, 303–310. DOI:10.1016/0003-2670(95)00397-5
- U. Chandra, B. E. K. Swamy, O. Gilbert, B. S. Sherigara, *Int. J. Electrochem. Sci.* **2010**, *5*, 1475–1483.
- H. Vidya, B. E. K. Swamy, *J. Mol. Liq.* **2015**, *211*, 705–711. DOI:10.1016/j.molliq.2015.07.011
- W. Sun, M. Yang, K. Jiao, *Anal. Bioanal. Chem.* **2007**, *389*, 1283–1291. DOI:10.1007/s00216-007-1518-2
- S. Shahrokhian, M. Ghalkhani, *Electrochim. Acta* **2006**, *51*, 2599–2606. DOI:10.1016/j.electacta.2005.08.001
- S. Shahrokhian, H. R. Zare-Mehrjardi, *Electrochim. Acta* **2007**, *52*, 6310–6317. DOI:10.1016/j.electacta.2007.04.023
- A. A. Abdelwahab, Y.-B. Shim, *Sens. Act. B* **2015**, *221*, 659–665. DOI:10.1016/j.snb.2015.07.016
- A. A. Rafati, A. Afraz, A. Hajian, P. Assari, *Microchim. Acta* **2014**, *4*, 1293–1297.
- D. Sun, Q. Zhao, F. Tan, X. Wang, J. Gao, *Anal. Methods* **2012**, *4*, 3283–3289. DOI:10.1039/c2ay25401h
- N. Soltani, N. Tavakkoli, N. Ahmadi, F. Davar, *C. R. Chimie* **2015**, *18(4)*, 438–448. DOI:10.1016/j.crci.2014.07.001
- S. Sharafzadeh, A. Nezamzadeh-Ejhieh, *Electrochim. Acta* **2015**, *184*, 371–380. DOI:10.1016/j.electacta.2015.09.164
- H. Vidya, B. E. K. Swamy, M. Schell, *J. Mol. Liq.* **2016**, *214*, 298–305. DOI:10.1016/j.molliq.2015.12.025
- A. K. Bhakta, R. J. Mascarenhas, O. J. D'Souza, A. K. Satpati, S. Detriche, Z. Mekhalif, J. Dalhalle, *Mater. Sci. Eng., C* **2015**, *57*, 328–337. DOI:10.1016/j.msec.2015.08.003
- J. Huang, Y. Liu, H. Hou, T. You, *Biosens. Bioelectron.* **2008**, *24*, 632–637. DOI:10.1016/j.bios.2008.06.011
- S. Sakthinathan, S. Kubendhiran, Sh. M. Chen, K. Manibalan, M. Govindasamy, P. Tamizhdurai, Sh. T. Huang, *Electroanalysis* **2016**, *28*, 1–11. DOI:10.1002/elan.201600085
- N. F. Atta, S. M. Ali, E. H. El-Ads, A. Galal, *Electrochim. Acta* **2013**, *128*, 16–24. DOI:10.1016/j.electacta.2013.09.101
- J. Yang, W. Li, T. Yang, Sh. Hou, *Int. J. Electrochem. Sci.*, **2016**, *11*, 5691–5701. DOI:10.20964/2016.07.12
- J. Oni, P. Westbroek, T. Nyokong, *Electroanalysis* **2003**, *15*, 847–854. DOI:10.1002/elan.200390104
- E. Ülker, M. Kavanoz, *Acta Chim. Slov.* **2016**, *63*, 47–54.
- M. K. Amini, S. Shahrokhian, S. Tangestaninejad, V. Mirkhani, *Anal. Biochem.* **2001**, *290*, 277–282. DOI:10.1006/abio.2000.4929
- S. Shahrokhian, M. Karimi, *Electrochim. Acta* **2004**, *50*, 77–84. DOI:10.1016/j.electacta.2004.07.015
- Y. V. M. Reddy, V. P. Rao, A. V. B. Reddy, M. Lavanya, M. Venu, M. Lavanya, G. Madhavi, *Mater. Sci. Eng., C* **2015**, *57*, 378–386. DOI:10.1016/j.msec.2015.08.005
- S. Shahrokhian, A. Souri, H. Khajehsharifi, *J. Electroanal. Chem.* **2004**, *565*, 95–101. DOI:10.1016/j.jelechem.2003.09.039
- S. Shahrokhian, H. R. Zare-Mehrjardi, *Electroanalysis* **2007**, *19*, 2234–2242. DOI:10.1002/elan.200703974
- W. Liao, C. Guo, L. Sun, Z. Li, L. Tian, J. He, J. Li, J. Zheng, Z. Ma, Z. Luo, C. Chen, *Int. J. Electrochem. Sci.* **2015**, *10*, 5747–5755.
- K. Chattopadhyay, S. Mazumdar, *Bioelectrochem.* **2000**, *53*, 17–24. DOI:10.1016/S0302-4598(00)00092-1
- H. Kargar, M. N. Tahir, *Acta. Cryst.* **2012**, *E68*, m1297–m1298.
- H. Zhao, Y. Zhang, Z. Yuan, *Anal. Chim. Acta* **2001**, *441*, 117–122. DOI:10.1016/S0003-2670(01)01086-8
- E. W. Kristensen, W. G. Kuhr, R. M. Wightman, *Anal. Chem.* **1987**, *59*, 1752–1757. DOI:10.1021/ac00141a003
- L. Yang, N. Huang, Q. Lu, M. Liu, H. Li, Y. Zhang and S. Yao, *Anal. Chim. Acta* **2016**, *903*, 69–80. DOI:10.1016/j.aca.2015.11.021
- Kh. Ghanbari and N. Hajheidari, *Anal. Biochem.* **2015**, *473*, 53–62. DOI:10.1016/j.ab.2014.12.013
- A. C. Anithaa, N. Lavanya, K. Asokan and C. Sekar, *Electrochim. Acta* **2015**, *167*, 294–302. DOI:10.1016/j.electacta.2015.03.160
- P. Gunriff (Ed.), Official Methods of Analysis of the Association of Official Analytical Chemists (AOAC), vol. 2, 16th ed., Association of Official Analytical Chemists, Arlington, VA, **1995**.
- Kh. Ghanbari, N. Hajheidari, *Anal. Biochem.* **2015**, *473*, 53–62. DOI:10.1016/j.ab.2014.12.013
- A. C. Anithaa, N. Lavanya, K. Asokan, C. Sekar, *Electrochim. Acta* **2015**, *167*, 294–302. DOI:10.1016/j.electacta.2015.03.160

Povzetek

V tem delu opisujemo cis-[Mo(O)₂L]-modificirano elektrodo iz ogljikove paste. Pri optimalnem pH (5,0) raztopin smo dosegli najboljšo ločbo anodnih vrhov askorbinske kisline in dopamina ter linearno zvezo med anodnim tokom in koncentracijo askorbinske kisline v območju od $3,0 \times 10^{-6}$ do $6,0 \times 10^{-3}$ M oziroma koncentracijo dopamina v območju od $2,0 \times 10^{-6}$ do $1,0 \times 10^{-2}$ M. Meja zaznave (S/N=3) za dopamin je bila 4×10^{-7} M, za askorbinsko kislino pa 5×10^{-7} M. Poleg naštetega sta za pripravljeno elektrodo karakteristični še enostavna priprava in regeneracija površine. Opisana elektroda je primerna za sočasno voltametrično določanje dopamina in askorbinske kisline.

Scientific paper

Prediction of *in vivo* Bioavailability by *in vitro* Characterization of Ethylenediamine Dipropanoic Acid Derivatives with Cytotoxic Activity

Biljana K. Tubić,^{1,2,*} Sandra S. Vladimirov,³ Bojan D. Marković³
and Tibor J. Sabo⁴

¹ Agency for Medicines and Medical Devices of Bosnia and Herzegovina

² Faculty of Medicine - Department of Pharmacy, University of Banja Luka

³ Faculty of Pharmacy, University of Belgrade

⁴ Faculty of Chemistry, University of Belgrade

* Corresponding author: E-mail: b.tubic@almbih.gov.ba; biljana.tubic@unibl.rs
Tel.: +38765962309; Fax: +38751450301

Received: 25-04-2017

Abstract

O,O'-diethyl-(*S,S*)-ethylenediamine-*N,N'*-di-2-(3-cyclohexyl)propanoate (DE-EDCP) is novel substance with cytotoxic activity in human leukemic cells. The aim of this study has been to predict *in vivo* bioavailability of the DE-EDCP and its potential metabolite (*S,S*)-ethylenediamine-*N,N'*-di-2-(3-cyclohexyl)propanoic acid (EDCP) by *in vitro* characterization which includes determination of lipophilicity and passive membrane permeability. There has also been evaluated inter-laboratory reproducibility of the bio-analytical method which was previously developed and validated for non-clinical study of the DE-EDCP and EDCP.

Distribution coefficient *n*-octanol/water was 1.68 and 0.03, and apparent permeability coefficient was 4×10^{-4} cm/s and 20×10^{-4} cm/s, for the DE-EDCP and EDCP, respectively.

Observed results have shown that the DE-EDCP is more lipophilic with better membrane retention, but the EDCP has better pass through the membrane. Also, there has been demonstrated a reproducibility and robustness of the proposed bio-analytical method.

Keywords: Transfer of the UHPLC-MS/MS, cross validation, (*S,S*)-ethylenediamine-*N,N'*-di-2-(3-cyclohexyl) propanoic acid esters, membrane permeability, lipophilicity

1. Introduction

Cytotoxic activity of the novel ester derivatives of the (*S,S*)-1,2-ethanediamine-*N,N'*-di-2-(3-cyclohexyl)propanoic acid has been previously proven by the *in vitro* studies on various leukemic cell lines. It was demonstrated that methyl, ethyl, and *n*-propyl esters are toxic to HL-60, REH, MOLT-4, KG-1, JVM-2, and K-562 leukemic cell lines, while the non-esterified compound and the *n*-butyl ester are devoid of cytotoxic action. The *O,O'*-diethyl-(*S,S*)-ethylenediamine-*N,N'*-di-2-(3-cyclohexyl)propanoate dihydrochloride (DE-EDCP), has showed the highest cytotoxic activity on leukemic cell line HL-60 (IC₅₀ in the range of 11 μ M – 45 μ M). Demonstrated data show that the toxicity

is mediated by the caspase-independent apoptosis associated with oxidative stress, mitochondrial dysfunction, and AIF translocation.¹ DE-EDCP has been chosen for further characterization since it had exerted the strongest cytotoxic activity in HL-60 cell line.

In vitro characterization of new pharmaceutical substances includes determination of a lipophilicity and passive membrane permeability. These physicochemical properties of pharmaceutical substances are providing significant information for prediction of the *in vivo* bioavailability by exploring absorption and distribution behaviour of the substance. Lipophilicity is one of many factors involved in biological activity of a drug, and it is often one of

the most influential.² Lipophilicity is usually expressed by the *n*-octanol/water partition coefficient ($\log P$) for neutral molecules and the distribution coefficient ($\log D$) for ionized molecules.³ Method for a determination of the $\log D$ is based on determination of the *n*-octanol/water partition coefficient.² This procedure requires the measurement of the compound concentration in *n*-octanol and water phases after equilibration of both phases according to Eq. (1). Thus, the Eq. (1) can be written as:⁴

$$\log D = \log (c_{\text{octanol}}/c_{\text{water}}) \quad (1)$$

where c_{octanol} and c_{water} are the concentrations of a substance in *n*-octanol and aqueous phase of the partition, respectively.

Method for the *in vitro* prediction of passive membrane permeability that can be used, is the parallel artificial membrane permeability assay (PAMPA). This method is used extensively for the early drug candidate evaluation. PAMPA was first introduced by Kansy et al.^{5–8}

This method has been shown useful in assessing trans-membrane, non-energy dependent, and diffusion of drugs in such a way that a reasonable predictability with *in vivo* (passive) absorption is possible.

The artificial membrane permeability may be expressed either as a percent of transport (%*T*) or as an apparent permeability coefficient P_{app} .

$$\%T = 100 \cdot (A_{\text{R}} \cdot V_{\text{R}}) / (A_{\text{D0}} \cdot V_{\text{D}}) \quad (2)$$

Where A_{D0} and A_{R} are the peak areas of the initial donor solution and the post-incubation receiving solution (from the acceptor wells), V_{R} and V_{D} are the volumes of the receiving and donor solutions.

The %*T* is related to P_{app} based on the following equation:

$$P_{\text{app}} = (V_{\text{D}} \cdot V_{\text{R}}) / ((V_{\text{D}} + V_{\text{R}}) \cdot S \cdot t) \cdot \ln[(100 \cdot V_{\text{D}}) / (100 \cdot V_{\text{D}} - \%T(V_{\text{D}} + V_{\text{R}}))] \quad (3)$$

Where *S* is the surface area of the artificial membrane and *t* is the incubation time.⁵

Generally, compounds that have a $P_{\text{app}} < 10 \times 10^{-6}$ cm/s are classified as low permeability and ones with a $P_{\text{app}} > 10 \times 10^{-6}$ cm/s are classified as high permeability.

In vivo characterization of new pharmaceutical substances includes non-clinical study on animal model. For non-clinical study of cytotoxic activity of the DE-EDCP and its potential metabolite (S,S)-ethylenediamine-*N,N'*-di-2-(3-cyclohexyl)propanoic acid dihydrochloride (EDCP), there has been previously developed and validated the ultra-high performance liquid chromatography tandem mass spectrometry (UHPLC-MS/MS) bio-analytical method.⁹ Bioanalytical methods should be robust.¹⁰ Evaluation of reproducibility (transferability) of bio-analytical method is becoming increasingly important^{11–13} since

the bio-analytical methods are often used in different laboratories during non-clinical and clinical studies. The transfer process requires the procedure to be physically transferred from a laboratory which masters the technique (called sender or originator) to another site (called receiver or recipient).¹⁴ In the context of bio-analysis, method transfer is covered by the Food and Drug Administration (FDA) and European Medicines Agency (EMA) guidance documents on bio-analytical method validation.^{11,13,15} Although the need for method transfer is recognized by both authorities, little is said about the process itself. Several approaches have been described for the method transfers evaluation.^{12,16–24}

New UHPLC-MS/MS bio-analytical method which has been developed and validated for the *in vivo* characterization (non-clinical study) of the DE-EDCP and EDCP⁹ is supposed to be used in different laboratories during the mentioned studies. However, *in vitro* characterization (lipophilicity and membrane permeability) of the DE-EDCP and EDCP has not been investigated until now.

The aim of this study is to predict the *in vivo* bioavailability of the DE-EDCP and its potential metabolite EDCP by the *in vitro* characterization – determination of lipophilicity and passive membrane permeability. In this study, there has also been evaluated the inter-laboratory reproducibility of the previously mentioned bio-analytical method.

2. Experimental

2.1. Chemicals

O,O'-diethyl-(S,S)-ethylenediamine-*N,N'*-di-2-(3-cyclohexyl)propanoate (DE-EDCP), (S,S)-ethylenediamine-*N,N'*-di-2-(3-cyclohexyl)propanoic acid dihydrochloride (EDCP) and the internal standard (S,S)-*O,O'*-dibutyl-1,3-propanediamine-*N,N'*-di-2-(3-cyclohexyl)propanoate dihydrochloride (DB-PDCP), were provided by the Faculty of Chemistry, University of Belgrade, Serbia (Table 1).

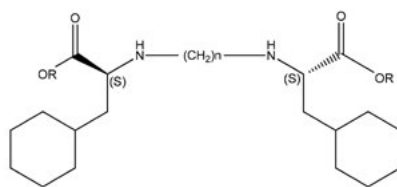
Acetonitrile, methanol, ethyl acetate, diethyl ether, triethanolamine, chloroform and trifluoroacetic acid (HPLC grade), ammonium acetate (CH₃COONH₄), sodium fluoride and KH₂PO₄ (ACS grade) from Fluka (Sigma-Aldrich Co.), *n*-octanol from Fluka AG (Buchs SG, Switzerland) and deionized water (TKA GenPure Ultrapure, Germany), were used. Mouse serum was purchased from Sigma Aldrich (Saint Louis, USA).

2.2. Solutions

Preparation of all standard solutions is described in a previously published study.⁹ Sample preparation is also described previously.⁹ All these solutions were prepared by two different analysts in sending and receiving laboratories.

2.3. Equipment

Solids were weighted by using a 5-digit Mettler analytical balance (Mettler-Toledo International Inc, USA),

Table 1: Structure of EDCP, DE-EDCP, and the internal standard DB-PDCP

Name of compound	Empirical formula	Abbreviation	MW (g/mol)	R	n
(S,S)-ethylenediamine- <i>N,N'</i> -di-2-(3-cyclohexyl)propanoic acid dihydrochloride	C ₂₀ H ₃₈ O ₄ N ₂ Cl ₂	EDCP	441.43	H	2
<i>O,O'</i> -diethyl-(S,S)-ethylenediamine- <i>N,N'</i> -di-2-(3-cyclohexyl)propanoate dihydrochloride	C ₂₄ H ₄₆ O ₄ N ₂ Cl ₂	DE-EDCP	497.54	C ₂ H ₅	2
(S,S)- <i>O,O'</i> -dibutyl-1,3-propanediamine- <i>N,N'</i> -di-2-(3-cyclohexyl)propanoate dihydrochloride	C ₂₉ H ₅₆ O ₄ N ₂ Cl ₂	DB-PDCP	567.67	C ₄ H ₉	3

and less sensitive weighting was performed on the Adventurer Pro analytical balance (OHAUS, USA). Sample preparation was done by using the Eppendorf 5417R micro-centrifuge (Eppendorf, Germany).

2. 4. Sending Laboratory

Development and validation of the method was done in the sending laboratory on the Thermo ACCELA (Thermo Scientific, Waltham, Massachusetts, USA) UHPLC system, coupled to a triple quad Mass Spectrometer Thermo TSQ Quantum Access Max (Thermo Scientific, Waltham, Massachusetts, USA), with a heated electro-spray ionization (HESI) interface.²⁴ A reverse-phase Thermo Scientific Hypersil GOLD aQ column (100 × 2.1 mm 1.9 μm ThermoScientific, and guard cartridge (Thermo Scientific Hypersil GOLD aQ, 10 mm l × 4 mm ID), were used in both laboratories.

2. 5. Receiving Laboratory

In the receiving laboratory, method transfer and validation were carried out on the Agilent 1290 UHPLC system equipped with the Agilent 6420 triple-quad mass detector (Agilent Technologies, Santa Clara, USA) with the electro-spray ionization (ESI) interface.

DE-EDCP, EDCP and IS were eluted by using a mobile phase as previously described.⁹ Quantitation was achieved by the MS–MS detection in the positive ionization mode for the DE-EDCP, EDCP and IS. The MS operating conditions were optimized as following: the capillary voltage was 4500 V, the gas temperature was set to 340 °C and gas flow was 10 l/min and the nebulizer pressure was 35 psi. Nitrogen was used as a collision gas. Fragmented voltage was set to 135 V. Ions detection was performed in the multiple reaction monitoring (MRM) by using the following transitions of *m/z* 425.2 → 197.8 and 226.1 for DE-EDCP, *m/z* 369.3 → 152.1 and 198.1 for EDCP and *m/z*

495.3 → 166.0 and 268.1 for DB-PDCP (IS), respectively, with a scan time of 0.1 s per transition.

Mass Hunter Optimizer software version 6.00 (Agilent Technologies, Santa Clara, USA) was used for automatic optimization of the acquisition parameters. Data Acquisition was performed by using the Mass Hunter Data Acquisition software version 6.00 (Agilent Technologies, Santa Clara, USA).

Qualitative and quantitative data analyses were done by using the Mass Hunter Qualitative software version 6.00 and Mass Hunter Quantitative software version 6.00 (Agilent Technologies, Santa Clara, USA), respectively.

Method transfer was done from the sending laboratory to the receiving laboratory.

The cross-validation samples were analyzed through a fully validated bio-analytical method at the receiving laboratory along with the calibration of the standards and QC samples for the validity of each analytical run. The following validation parameters were evaluated in the receiving laboratory for the UHPLC-MS/MS system: selectivity, linearity, limit of quantification (LLOQ), recovery, accuracy, precision and matrix effects.

Also, cross-validation samples were analyzed by the Passing and Bablok regression analysis. Passing and Bablok regression analysis is a statistical procedure which allows the valuable estimation of the analytical methods agreement and possible systematic bias between them. Results are presented with a scatter diagram and a regression line, as well as a regression equation where an intercept represents a constant and slope proportional measurement error. Confidence intervals of 95% of the intercept and slope, give the explanation whether their value differ from the value zero (intercept) and value one (slope) only by chance, allowing a conclusion of the method agreement and a correction action, if necessary.²⁵

During this study, there have been tested the selectivity, linearity, limit of quantification (LLOQ), recovery (%), matrix effects, accuracy and precision, as described previously.⁹

Cross-validation showed to be successful in terms of the results' traceability between the two instruments (slope and intercept with confidential interval values) and the results of validation parameters (selectivity, linearity, limit of quantification (LLOQ), recovery, accuracy, precision and matrix effects).

2. 6. Determination of the *n*-octanol/water Distribution Coefficient (LogD)

LogD values were determined by using a shake-flask method. In the shake-flask experiment, 5 mg of each substance (DE-EDCP and EDCP) was first mixed with 50 ml of aqueous buffer (pH 7.4). Then, 10 ml of this solution was mixed with 10 ml of the *n*-octanol (water saturated). The sample vial was placed on the shaker and been shaken for 12 h at 250 rpm. After equilibration, it was left to stand for 2 h to phases well separated.

The separated aqueous phase is being centrifuged, the residual drops of the *n*-octanol to be eliminated. The aqueous phase was sampled and assayed by the transferred and cross-validated UHPLC-MS/MS which had been previously validated for the determination of the investigated substances in the aqueous buffer (pH 7.4) in order to determine the logD value. The concentration of the investigated substances in the *n*-octanol phase was obtained as a difference in the concentrations in the aqueous buffer, prior to mixing with the *n*-octanol and after mixing with the *n*-octanol.

2. 7. Prediction of Membrane Permeability (PAMPA test)

The *in vitro* method for the prediction of membrane permeability which was used in these studies, was carried out in a 96-well format. 96-well micro-titer plates (hydrophobic PVDF MultiScreen IPFilter Plate 0.45 μm , from Milipore (Bedford, MA, USA)), were assembled into such a "sandwich" that each composite well was separated by a 125 μm micro filter disc. Filter material in each well of the filtration plate was wetted with 5 μl of the artificial membrane solution, which consisted of 1 % egg lecithin in the *n*-dodecane. Subsequently, the filter plate was placed on the bottom micro-titer plate containing the following donor solution: 300 μl of the compound in the concentration of 0.1 mg/ml dissolved in the buffer KH_2PO_4 0.2M, pH = 7.4. The top acceptor wells of the sandwich, were hydrated with the 300 μl of the buffer KH_2PO_4 0.2M, pH 7.4. To prevent loss by evaporation, the system was first covered with a paraffinic film. The surface area of the artificial membrane was $S = 0.28 \text{ cm}^2$ and the period of incubation was $t = 7200 \text{ s}$ (2 h).

After incubation, the amount of the DE-EDCP and EDCP in the donor and acceptor wells, was determined by the UHPLC-MS/MS method which had been previously transferred and cross-validated.

2. 8. Software

For the determination of lipophilicity ($\text{Log}D_{7.4}$) of the investigated substances by the *in silico* model, there was used the MarvinSketch 4.1.13 (ChemAxon, Budapest, Hungary).

3. Results and Discussion

3. 1. UHPLC-MS/MS Method: Transfer and Cross-validation

Transfer of the ultra-high performance liquid chromatography-electro-spray tandem mass spectrometry (UHPLC-ESI-MS/MS) method for non-clinical studies and the *in vitro* characterization of recently synthesized substances with the cytotoxic activity, DE-EDCP and its potential metabolite EDCP, in biological material, was carried out. The reproducibility and transferability of this bio-analytical method in the mouse serum was evaluated by the validation and cross-validation of the method through using two different UHPLC-MS/MS systems. The parallel displayed values of the observed validation parameters are given in the Table 2.

The method was proven to be highly selective for the analytes, since no interfering peaks from the endogenous compounds were observed at the retention times for the DE-EDCP and EDCP in any of the six independent blank serum extracts evaluated.

Also, cross-validation samples analyzed by the Passing and Bablok regression analysis, showed to be successful in terms of the results' traceability between the two instruments (for DE-EDCP: slope = 0.9821 with lower 95 %-CL = 0.7737 and upper 95 %-CL = 1.1685, and intercept = 0.0547 with lower 95 %-CL = -5.1662 and upper 95 %-CL = 3.4285; for EDCP: slope = 1.0187 with lower 95 %-CL = 0.9522 and upper 95 %-CL = 1.1505, and intercept = -0.0488 with lower 95 %-CL = -0.5347 and upper 95 %-CL = 0.2187).

Overall results of the cross-validation were satisfactory in terms of all the investigated parameters proving that the method can be successfully transferred under the aforementioned conditions. Results of the validation and cross validation demonstrate that the novel UHPLC-MS/MS method for the *in vivo* characterization (non-clinical study) of the novel DE-EDCP and EDCP substances with cytotoxic activity, is appropriately transferred and validated at the receiving laboratory.

3. 2. Validation of the UHPLC-MS/MS in the Aqueous Buffer

The observed UHPLC-MS/MS method was successfully validated for the determination of the investigated substances DE-EDCP and EDCP from an aqueous buffer (pH 7.4). Results of the validation parameters are given in the Table 3.

Table 2: Validation parameters for the DE-EDCP and EDCP on the Thermo ACCELA and the Agilent 1290 UHPLC system

Validation parameter	Sending laboratory (Thermo ACCELA)		Receiving laboratory (Agilent 1290 UHPLC system)	
	DE-EDCP	EDCP	DE-EDCP	EDCP
Linearity of calibration curves	1.3–26.7 ng/ml $y = 0.0461x + 0.0895$, $r = 0.9978$	0.33–6.67 µg/ml $y = 0.1527x + 0.0045$, $r = 0.9987$	3.3–26.7 ng/ml $y = 64.243x + 114.54$, $r = 0.9983$	0.33–6.67 µg/ml $y = 9322.3x - 103.4$, $r = 0.9989$
LLOQ	1.3 ng/ml	0.33 µg/ml	3.3 ng/ml	0.33 µg/ml
Recovery %	90.0–99.3	75.8–100.3	91.0–99.8	77.8–101.5
Matrix effect	95.5–108.2%		96.7–109.4%	
Precision (%CV)	15.99	5.58	3.22	4.00
	13.68	4.43	3.36	2.05
	2.25	5.32	3.97	3.95
	3.49	4.01	1.87	2.00
Accuracy (%RE)	3.01	6.06	17.05	-9.93
	12.61	-2.41	11.50	-14.52
	6.30	-3.20	5.20	-13.13
	1.80	-14.40	1.73	-14.20

y represents the peak area ratio of analyst to IS

Table 3: Validation parameters for the DE-EDCP and EDCP in an aqueous buffer, without a biological matrix (Thermo ACCELA)

Validation parameter	Thermo ACCELA	
	DE-EDCP	EDCP
Linearity of calibration curves	2.0 to 40.0 ng/ml $r = 0.9930$	0.5 to 10.0 µg/ml $r = 0.9997$
LLOQ	2.0 ng/ml	0.50 µg/ml
Precision (%CV)	3.29 to 18.07%	6.09 to 15.50%
Accuracy (%RE)	0.01 to 16.00%	1.48 to 13.50%

3. 3. Determination of the Log $D_{7.4}$ *in vitro/in silico* and the PAMPA Test

Lipophilicity of the observed substances DE-EDCP and EDCP, has been tested by the traditional shake-flask method. Passive membrane permeability has been tested by the PAMPA test. Experimental results that have been obtained in this study are shown in the Table 4. Also, in the Table 4, there can be seen *in silico* results of the lipophilicity of the DE-EDCP and EDCP.

Table 4: Lipophilicity and passive membrane permeability data for the investigated substances DE-EDCP and EDCP

Compound	Log $D_{7.4}$ *	Log $D_{7.4}$	P_{app} (cm/s)	%T	% Membrane retention
EDCP	-1.8	0.03	20×10^{-4}	7.94	6.90
DE-EDCP	4.04	1.68	4×10^{-4}	1.76	97.46

* by MarvinSketch 4.1.13

The results represent obvious difference in the lipophilicity between the DE-EDCP and EDCP. Lipophilicity data obtained through the shake flask method, and membrane permeability data acquired by the PAMPA

test, are correlated with the results gained in the previous *in vitro* activity studies on various leukemic cell lines of the investigated compounds. Compound DE-EDCP with a significant cytotoxic activity,¹ has greater lipophilicity which allows more retention in the cell membrane. This characteristic of the aforementioned compound is particularly important for its activity. On the other hand, the suspected metabolite EDCP is more hydrophilic and passes through the membrane, without retention in the cell membrane.

4. Conclusions

In this study, DE-EDCP and EDCP bioavailability was examined through *in vitro* characterization, by determination of lipophilicity and passive membrane permeability. Observed results are showing that the DE-EDCP is more lipophilic than the EDCP, with better membrane retention.

Additionally, this study proved good reproducibility (transferability) and robustness of the bioanalytical method for *in vivo* characterization of the investigated substances.

5. Acknowledgements

This work was partly supported by the Ministry of Education, Science and Technological Development of the Republic of Serbia, as a part of the Projects No. 172041 and No. 175035. One of the authors (B.T.) is thankful to the Ministry of Science and Technology of the Republic of Srpska for funding the study through the Project 19/6-020/961-169/14.

6. References

1. S. Misirlić Denčić, J. Poljarević, U. Vilimanovich, A. Bogdanović, J. A. Isaković, T. Kravić Stevović, M. Dulović, N. Zogović, M. A. Isaković, S. Grguric-Sipka, V. Bumbasirević, T. Sabo, V. Trajković, I. Marković, *Chem Res Toxicol.* **2012**, *25*, 931–939. DOI:10.1021/tx3000329
2. E. Rutkowska, K. Pajak, K. Jozwiak, *Acta Pol Pharm – Drug Research.* **2013**, *70*, 3–18.
3. X. Xuan, L. Xu, L. Li, C. Gao, N. Li, *Int J Pharm.* **2015**, *490*, 258–264. DOI:10.1016/j.ijpharm.2015.05.019
4. A. Andres, M. Roses, C. Rafols, E. Bosch, S. Espinosa, V. Segarra, J. M. Huerta, *Eur J Pharm Sci.* **2015**, *76*, 181–191. DOI:10.1016/j.ejps.2015.05.008
5. C. Zhu, L. Jiang, M. T. Chen, K. K. Hwang, *Eur J Med Chem.* **2002**, *37*, 399–407. DOI:10.1016/S0223-5234(02)01360-0
6. M. Kansy, F. Senner, K. Gubernator, *J Med Chem.* **1998**, *41*, 1107–1110. DOI:10.1021/jm970530e
7. K. Sugano, H. Hamada, M. Machida, H. Ushio, *J Biomol Screen.* **2001**, *6*, 189–196. DOI:10.1177/108705710100600309
8. F. Wohnsland, B. Faller, *J Med Chem.* **2001**, *44*, 923–930. DOI:10.1021/jm001020e
9. B. Tubić, B. Marković, S. Vladimirov, S. Ristić, B. Ivković, M. Savić, J. Poljarević, T. Sabo, *Acta Chromatogr.* <http://www.akademai.com/doi/pdf/10.1556/1326.2017.29.2.7> (assessed: April 24, 2017)
10. T. Yoneyama, T. Kudo, F. Jinno, R. E. Schmidt, T. Kondo, *The AAPS Journal.* **2014**, *16*, 1226–1236. DOI:10.1208/s12248-014-9653-0
11. M. H. Hill, G. Smith, *Bioanalysis.* **2015**, *7(7)*, 783–787. DOI:10.4155/bio.15.37
12. A. K. Shah, T. H. Karnes, *J Chromatogr B.* **2009**, *877*, 2270–2274. DOI:10.1016/j.jchromb.2009.04.020
13. Food and Drug Administration, Guidance for Industry: Bioanalytical Method Validation U.S. Department of Health and Human Services Food and Drug Administration Center for Drug Evaluation and Research (CDER) Center for Veterinary Medicine (CVM) BP <http://www.fda.gov/downloads/Drugs/.../Guidances/ucm070107.pdf> (assessed: April 24, 2017)
14. E. Rozet, W. Dewe, R. Morello, P. Chaip, F. Lecomte, E. Ziemons, S. K. Boos, B. Boulanger, J. Crommen, Ph. Hubert, *J Chromatogr A.* **2008**, *1189*, 32–41. DOI:10.1016/j.chroma.2007.11.029
15. European Medicines Agency, *Guideline on bioanalytical method validation Doc. Ref: EMEA/CHMP/EWP/192217/2009 Rev. 1 Corr. 2*** http://www.ema.europa.eu/docs/en_GB/document_library/Scientific_guideline/2011/08/WC500109686.pdf (assessed: April 24, 2017)
16. International Society for Pharmaceutical Engineering, *Good Practice Guide: Technology Transfer (Second Edition)* <http://www.ispe.org/ispe-good-practice-guides/technology-transfer> (assessed: April 24, 2017)
17. U. Schepers, H. Watzig, *J Pharmaceut Biomed.* **2005**, *39*, 310–314. DOI:10.1016/j.jpba.2005.03.015
18. W. Dewe, B. Govaerts, B. Boulanger, E. Rozet, P. Chiap, Ph. Hubert, *Chemometr Intell Lab.* **2007**, *85*, 262–268. DOI:10.1016/j.chemolab.2006.07.003
19. C. Hartmann, J. Smayers-Verbeke, W. Penninckx, Y. Vander Heyden, P. Vankeerberghen, L. D. Massart, *Anal Chem.* **1995**, *67*, 4491–4499. DOI:10.1021/ac00120a011
20. D. Chambers, G. Kelly, G. Limentani, A. Lister, R. Lung, E. Warner, *J Pharm Technol.* **2005**, *9*, 64–80.
21. U. Schepers, H. Watzig, *J Pharmaceut Biomed.* **2006**, *41*, 290–292. DOI:10.1016/j.jpba.2005.10.030
22. S. Feng, Q. Liang, D. R. Kinser, K. Newland, R. Guilbaud, *Anal. Bioanal. Chem.* **2006**, *385*, 975–981. DOI:10.1007/s00216-006-0417-2
23. J. Vial, A. Jardy, P. Anger, A. Braun, J. Manet, *J Chromatogr A.* **1998**, *815*, 173–182. DOI:10.1016/S0021-9673(98)00510-X
24. G. de Fontenay, *J Pharmaceut Biomed.* **2008**, *46*, 104–112. DOI:10.1016/j.jpba.2007.09.007
25. L. Bilić-Zulle, *Biochimica Medica.* **2011**, *21(1)*, 49–52. DOI:10.11613/BM.2011.010

Povzetek

(S,S)-O, O-dietil-1,2-etandiamin-*N,N'*-di-2-(3-cikloheksil)propanoat (DE-EDCP) je nova snov s citotoksično aktivnostjo v človeških levkemičnih celicah. Cilj te študije je bil napovedovanje in vivo biološke uporabnosti DE-EDCP in njegovega potencialnega metabolita (S,S)-1,2-etandiamina-*N,N'*-di-2-(3-cikloheksil) propanojske kisline (EDCP) z in vitro karakterizacijo, ki vključuje določanje lipofilnosti in pasivne membranske prepustnosti. Ocenjena je bila medlaboratorijska obnovljivost biološke analitske metode, ki je bila predhodno razvita in potrjena za neklinično študijo DE-EDCP in EDCP.

Porazdelitveni koeficient med *n*-oktanolom in vodo je bil 1,68 in 0,03, navidezni koeficient prepustnosti pa je bil 4×10^{-4} cm/s in 20×10^{-4} cm/s za DE-EDCP in EDCP.

Opaženi rezultati so pokazali, da je DE-EDCP bolj lipofilen z boljšim zadrževanjem v membrani, medtem ko EDCP bolje prehaja skozi membrano. Lahko domnevamo, da je mehanizem citotoksične aktivnosti DE-EDCP na ravni celične membrane. Dokazana je bila ponovljivost in robustnost predlagane bioanalitične metode.

Scientific paper

Evaluation of Jeffamine® Core PAMAM Dendrimers for Simultaneous Removal of Divalent Heavy Metal Ions from Aqueous Solutions by Polymer Assisted Ultrafiltration

Ali Serol Ertürk,^{1,*} Mustafa Ulvi Gürbüz,² Metin Tülü²
and Abdürrezzak Emin Bozdoğan²

¹Department of Basic Pharmaceutical Sciences, Faculty of Pharmacy, Adiyaman University, 02040, Adiyaman, Turkey

²Department of Chemistry, Faculty of Arts and Sciences, Yıldız Technical University, 34210, Esenler, Istanbul, Turkey

* Corresponding author: E-mail: aserturk@gmail.com, aserturk@adiyaman.edu.tr
Tel: +90 (416) 223 38 00 /2760; fax: +90 (416) 223 3809

Received: 27-04-2017

Abstract

Different generations (G3-G4) of amine-terminated Jeffamine® T-403 core poly(amidoamine) PAMAM dendrimers (JCPDs) were used as new macromolecular heavy metal chelating agent templates in polymer assisted ultrafiltration (PAUF) for the investigation of their removal ability for some of the divalent metal ions: Cu, Co, Ni, Cd, and Zn from aqueous solutions under competitive conditions. The effects of pH and generation size of JCPDs were also investigated. Extent of binding (EOB) data can be appropriately expressed by a tetradentate coordination for JCPDs at pH 9 where the maximum removal of metal ions was observed. At pH 9.0, the affinity of both generations towards heavy metal ions was also observed in the decreasing order of Zn(II) > Co(II) > Ni(II) > Cu(II) > Cd(II). Results revealed that the highest total binding capacity was observed for G3-NH₂ (262.79 ± 1.62 mg/g) as a little bit higher than that of G4-NH₂ (257.27 ± 2.57 mg/g). EOB studies also proved the active contribution of amide groups to metal binding ability of PAMAMs. Both generations were selective towards Cu(II) ions at lower pH 5 and pH 7. From these results, it was concluded that studied JCPDs have the desired technical properties to be used for the removal of toxic metals from wastewaters.

Keywords: Poly(amidoamine) PAMAM dendrimers; Jeffamine® T-403; liquid phase retention (LPR); metal complexation; removal of heavy metals

1. Introduction

Toxic, particularly divalent heavy metal ions are the main contaminants of the surface, ground, and coastal water systems that lead to water contamination throughout the world.^{1,2} These pollutants are not only found in wastewaters from various chemical manufacturing, mining, coating, extractive metallurgy but also nuclear and other industries, and greatly threaten the health of human populations and natural ecosystems.

Water free or decontaminated from toxic chemicals and pathogens is fundamental for human health and as raw material for many industries. There are particular cases that endanger the sustenance of this source like a rise in global demand due to population growth, prolonged droughts, and contamination by metals or organic and inorganic compounds.³⁻⁵ Considering the water contami-

nation, most of the available water remediation technologies are useful, but frequently are costly and time-consuming.⁶

The existence of heavy metal ions in water gives rise to numerous risks to human health. In the instance of industries, it leads to a rise in the overall cost of production due to purification processes. Several remedies, one of which is adsorbents such as ion exchange resins and activated charcoal, have been used extensively as an industrial research subject for the removal of heavy metal ions from wastewaters.⁷ These materials have several drawbacks depending on their low selectivity, wide distribution and heterogeneity of pore size and structure for heavy metals. In this point, nanotechnology offers innovative solutions to prevent water contamination. Previous investigations have indicated that the treatment with nanomaterials as chelating agents to remove metal ions from water enhances its

quality and minimizes purification costs.⁸ The potential of this approach to surmount limitations encountered in other removal strategies has been placed as an environmentally friendly method.^{9–12}

Among available chelating agents, dendrimers have been described as the powerful macromolecules to encapsulate metal ions, and further recover and recycle to reuse.¹³ Poly(amido amine) PAMAM dendrimers (PAMAMs) display an outstanding capacity to bind metal ions by forming stable coordination complexes.¹⁴ These nanomaterials are three-dimensional, globular, repetitively branched, and synthetic organic molecules with hyper-branched and uniform structures that allow them numerous advantages as templates for binding of metal ions within their interior.¹⁵ The high density of nitrogen ligands such as amino and amide functional groups that PAMAMs carry, allow them to behave like a container or a template by increasing their binding ability for various toxic and heavy metals.¹⁴ Thus, PAMAMs may serve as potential polyfunctional ligand hosts for metal ions with coordination possibly occurring at the periphery, interior or both. In this sense, it was reported that loading of various metal ions with the implication of useful applications for metal ion sensor coatings on the electrode surface to commercially available amine-terminated PAMAMs are possible.^{16,17}

One of the efficient methods to recover metal ions from contaminant waters is liquid phase polymer-based retention technique (LPR) or polymer assisted ultrafiltration (PAUF).^{2,18–23} Former studies have shown that this method could be successfully used for the selective separation and recovery of heavy metals.^{24–26} Many kinds of water-soluble polymers such as poly(acrylic acid) (PAA) and poly(ethylene imine) (PEI) have been used as templates in LPR for the removal of corresponding various individual metal ions such as Cu(II), Cd(II), Ni(II), Pb(II), Cr(II), Cr(III), Co(II) and many others.²⁷ However, a limited number of studies has been conducted for the competitive or simultaneous removal of metal ion mixtures by polymers, especially for PAMAMs.²⁸ Polymers to be used in LPR studies can be assessed by many parameters but one of the most important parameters is the ligand density of the polymer. Low ligand density of the polymer to be used requires high volume of polymer and this could in-

crease the viscosity of the solution that can lead to deteriorating effect on the permeate reflux.²⁹ Higher generation PAMAMs have a high number of amino groups, and so high ligand density. Furthermore, the chelating properties of PAMAMs can alter due to type of core, repeating branches and surface functional groups.³⁰

Jeffamine[®] T-403 is a polymer, which has large and unsymmetrical chains having propylene oxide repeating units. These large repeating units can retard the steric hindrance but enhance the reactivity and water solubility.³¹ In our former studies, we have demonstrated the microwave-assisted synthesis of Jeffamine[®] core PAMAMs (JCPDs) and their Cu(II) intradendrimer metal complexations.^{31–33} Results of these studies revealed that JCPDs can show interesting chelating abilities towards metal ions as a new type polydentate chelating agent for LPR.

The aim of this study was to investigate the retention properties of different generations JCPDs through the LPR to study the selective and collective removal ability of some of the divalent heavy metal ions: Cu(II), Co(II), Ni(II), Cd(II), Zn(II) from aqueous solutions. Effects of pH and generation size on the complexation and selectivity of these metal ions were also considered.

2. Experimental

2.1. Materials

All chemicals were of analytical grade and obtained from Merck and Fluka. Divalent nitrate salts of Cd, Co, Cu, Ni, Zn were used to prepare standard metal solutions. JCPDs, G3-NH₂ and G4-NH₂, were synthesized according to our recent study,³¹ and detailed experimental procedures including potentiometric titrations are given in the Supplementary Information. The prepared dendrimers were stored in methanolic solution at ± 4 °C. Some selected properties and characterization data of dendrimers are presented in Table 1. The abbreviations G1-NH₂ to G4-NH₂ (first to fourth generation) were suggested for respective JCPDs with molecular weights ranging from 1124 to 10700 g/mol. 18.2 MΩ cm Milli-Q double distilled water was used for the preparation of all standard metal and dendrimer solutions. 0.1 and 0.01 M HNO₃ and NaOH were used to prepare initial pH adjustments. Amicon 8400

Table 1. Selected physico-chemical properties of JCPDs.³¹

Generation	Mw ^a	Mn ^b (SEC)	Mw (SEC)	PDI ^c	Number of tertiary amines (³ N)	Number of primary amines (¹ N)	Number of amides (^a N)	Number of total nitrogen-containing groups (tN)
G1-NH ₂	1124	960	980	1.02	3	6	6	15
G2-NH ₂	2492	2300	2500	1.09	9	12	21	42
G3-NH ₂	5228	4300	4400	1.02	21	24	42	87
G4-NH ₂	10700	9200	9600	1.04	45	48	90	183

^a Theoretical molecular weight (g/mol). ^b Nominal molecular weight (g/mol). ^c Polydispersity Index: PDI = Mw/Mn

stirred ultrafiltration cell with MWCO of 1 kDa regenerated cellulose membranes supplied with Millipore were used in batch-complexation studies.

2. 2. Stock Metal Solutions

Individual stock metal solutions of 1000 mg/L were prepared by the addition of metal nitrate salts ($\text{Cd}(\text{NO}_3)_2 \cdot 4\text{H}_2\text{O}$; $\text{Co}(\text{NO}_3)_2 \cdot 6\text{H}_2\text{O}$; $\text{Cu}(\text{NO}_3)_2 \cdot 3\text{H}_2\text{O}$; $\text{Ni}(\text{NO}_3)_2 \cdot 6\text{H}_2\text{O}$; and $\text{Zn}(\text{NO}_3)_2 \cdot 6\text{H}_2\text{O}$) to a desired volume of 18.2 M Ω cm Milli-Q water.

2. 3. Batch Complexation and PAUF Experiments

A systematic diagram of complexation can be seen in Fig. 1. PAMAMs used in PAUF experiments were JCPDs, G3-NH₂ and G4-NH₂, with the molecular weight of 5228 and 10700 g/mol, respectively. Before PAUF experiments, 250 mL of aqueous multi-metal PAMAM feeding solutions were produced by the addition of the correct amount of individual stock metal solutions of Cd(II), Co(II), Cu(II), Ni(II), and Zn(II). In complexation, the concentrations of G3-NH₂ and G4-NH₂ were 2.84×10^{-5} M and 8.12×10^{-6} M, and the molar ratios of each metal concentration to primary amine groups (1N) of PAMAMs were kept constant at 0.2. The pH of feeding solutions was adjusted to the desired pH by the secure

addition of 0.01 and 0.10 M HNO₃ and NaOH solutions. The feed solutions were stirred well with a magnetic stirrer for 45 min until equilibrium was reached at room temperature 25 ± 2 °C.

After complexation reaction, 150 mL of feed solution was transferred into Amicon 8400 UF cell, capacity of 400 mL. In the UF cell, an ultrafiltration disk membrane (YM-1) made from regenerated cellulose and supplied from Millipore (USA) was used. The commercial membrane had MWCO = 1000 g/mol (1 kDa); diameter of 76 mm and effective membrane area of 41.8 cm². The permeate flux of pure water in Amicon UF cell with regenerated cellulose membrane was equal to 10.95 L m⁻² h⁻¹. The feed solution in UF cell was stirred gently at 250 rpm to reduce the concentration polarization on the membrane surface and provide homogeneity in the solution inside the cell. The filtration cell was pressurized by oxygen-free nitrogen gas. All experiments were conducted by applying a constant operating pressure of 400 kPa. A systematic diagram of PAUF can be seen in Fig.2.

2. 4. Measurement of the Retention and Metal Ion Binding to JCPDs in Aqueous Solutions

Feeding solutions were filtered and permeates were collected in equal time intervals (12 min). After two hours, 10 permeates were collected and the experiments were en-

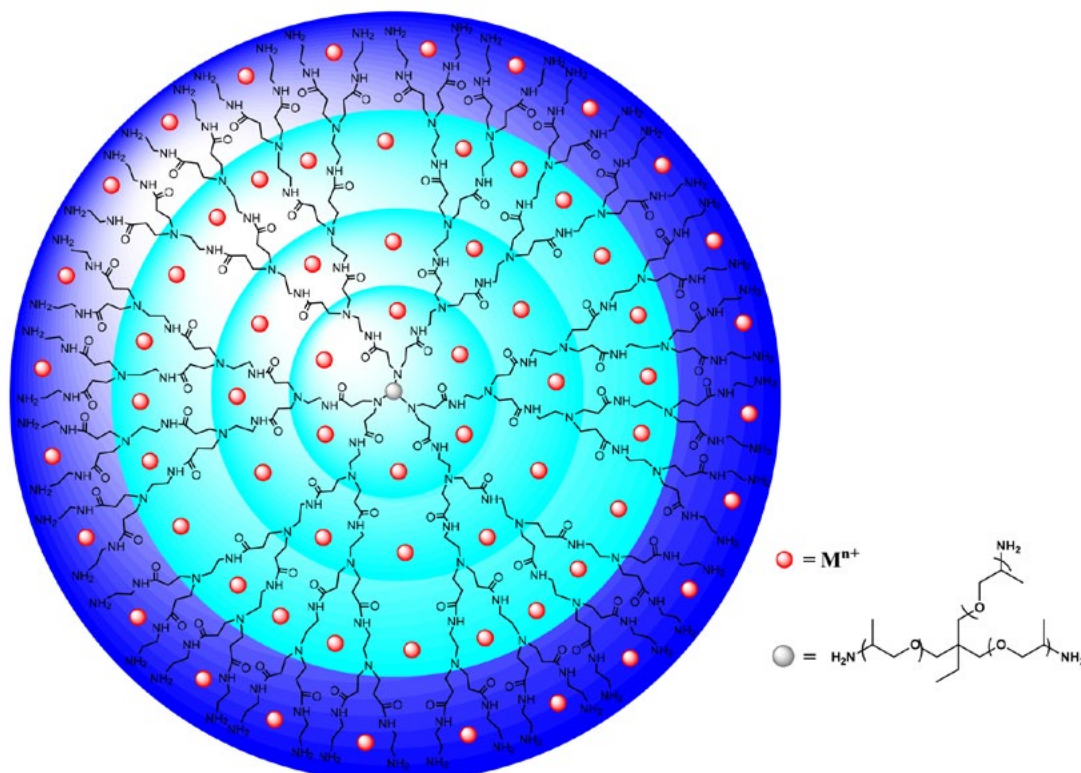


Figure 1. Representative chemical structure of G3-NH₂ Jeffamine[®] and schematic representation of the metal complexation of G3-NH₂

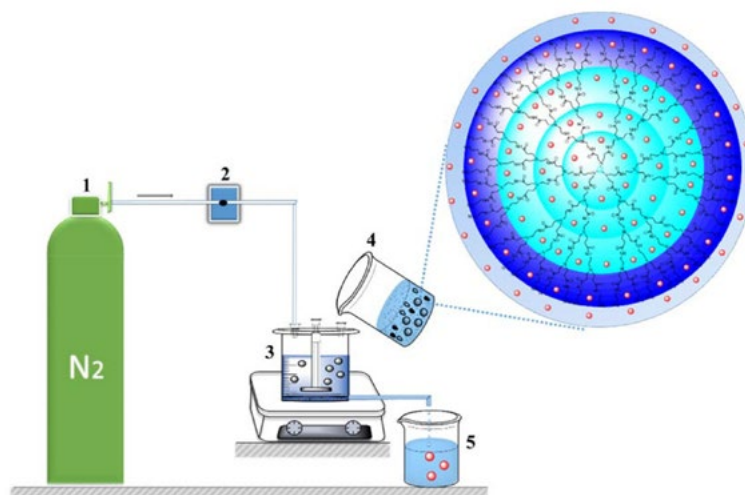


Figure 2. Schematic diagram of batch complexation and polymer assisted ultrafiltration (PAUF) assembly. 1- Cylinder with compressed air (pressure trap); 2- reducer with diaphragm valve and pressure gauge; 3- UF stirred cell; 4- batch stirred tank for complexation reaction (preparation of feed solution) and 5- permeate solution.

ded. Rates of filtrates were determined by continuously weighing the permeates on a digital electronic balance (Precisa), with an accuracy of 0.001 g. This was done to validate the functionality of used UF membrane by observing the initial and in time flux rate ($L\ m^{-2}h^{-1}$) consistency. Metal ion concentrations in each collected permeate were analyzed by atomic absorption spectroscopy (AAS). Percent retention value (R%) or fraction of binding (FB) of each metal ion was calculated by using equation 1.

$$R\% = \left(1 - \frac{C_p}{C_f}\right) \times 100 \quad (1)$$

where, is the concentration of metal ion in initial feed solution (mol/L) and is the concentration of metal ion in permeate flux (mol/L).

The concentration of metal ions bound to dendrimer, C_m (mol/L) is expressed by equation

$$C_m = C_f - C_p \quad (2)$$

The extent of binding (EOB), the number of moles of a metal ion bound per mole of dendrimers was expressed as

$$EOB = \frac{C_m}{C_d} \quad (3)$$

where, is the total concentration of a dendrimer in the aqueous solution in mol/L.

2. 5. Analytical Methods

The concentration of the metal ions in feed and permeate solutions were measured by AAS following the procedure reported in the literature.^{17,19,24} In order to determine Cd(II), Co(II), Cu(II), Ni(II), and Zn(II) concentrations, Shimadzu AA-6800 AAS instrument equipped with hollow cathode lamps (HCLS) was used. All of the chemicals used in experiments were of analytical grade. In all dilutions and standard preparations, 18.2 MΩ cm MilliQ water was used. AAS operating parameters used for the element of interest used throughout in all experiments can be seen in Table 2. Deuterium arc lamp background correction was applied for all the analytes.

3. Results and Discussion

The removal process of heavy metal ions by dendrimer can be affected by a number of parameters such as generation size, pH, formation and type of complexation, accessibility and reactivity of the functional groups available for binding with metal ion at the surface or inner stru-

Table 2. AAS parameters used in the determination of Cd, Co, Cu, Ni and Zn

Parameters	Cd	Co	Cu	Ni	Zn
Wavelength (nm)	228.8	240.7	324.8	232.0	213.9
HCL current (mA)	8.0	12.0	6.0	12.0	8.0
Acetylene flow rate (L/min)	1.8	1.6	1.8	1.6	2.0
Slit width (nm)	1.0	0.2	0.5	0.2	0.5
Background correction	D ₂	D ₂	D ₂	D ₂	D ₂

cture. Tertiary amines, primary amines and amide functional groups are specific metal binding sites for various generations of PAMAMs. Table 1 compares the number of these functional groups for different generation JCPDs. It is clear that higher generations are expected to be more effective than lower generations due to higher number of amino groups (ligands) they possess on an equal equivalent base (Table 1). Thus, the highest two generations of JCPDs, G3-NH₂ and G4-NH₂, were used as the macromolecular templates for the selective and competitive binding of Cd(II), Co(II), Cu(II), Ni(II), and Zn(II) metal ions from aqueous solutions.

3. 1. Analytical Figures of Merit

Detailed calibration and analytical characteristics of the AAS method used for the determination of the feed and permeate Cd(II), Co(II), Cu(II), Ni(II), and Zn(II) can be seen in Table 3. These characteristics are limit of detection (LOD), limit of quantification (LOQ), linear range, regression coefficient and the best line equation. 3 s/m and 10 s/m where s is the standard deviation were used in the calculation of the LOD and LOQ values, respectively. It is clear from Table 3 that R² values for each analyte were found to be at least 0.99. Linear ranges for Cd, Co, Cu, Ni, and Zn elements were in the range of 0.2–2.5, 0.2–4.0, 0.3–4.0, 0.2–5.0, and 0.5–2.0 mg/L, respectively. Four repeated measurements were recorded for the preparation of regression lines and sample measurements, which are correlated with calibration by an appropriate enhancement factor (5–10). The reproducibility of the

concentration measurement was within a maximum deviation of 5% in all cases studied.

3. 2. Effect of Generation Size and pH on the Selective and Competitive Binding of Divalent Heavy Metal Ions Cu(II), Co(II), Ni(II), Cd(II), and Zn(II) by PAUF with JCPDs

Selectivity of different generation JCPDs towards heavy metal ions were investigated at four different pH. In this way, low (pH 3.0, 5.0), neutral (pH 7.0), and high pH (pH 9.0) values were evaluated. Retention (%) profiles of the each metal were calculated by means of eqn. 1.

Table 4 summarizes the heavy metal retention (%) of JCPDs in aqueous solutions as a function of pH. No retention at low pH 3.0 indicates the release of all metal ions by both generations. At neutral pH 7.0 and low pH 5.0, both of the generations were selective towards Cu(II). 65.74 ± 1.18% and 70.96 ± 1.59% Cu(II) were retained at neutral pH 7.0 while 12.33 ± 1.13% and 12.13 ± 0.82% Cu(II) by G3-NH₂ and G4-NH₂ were retained at low pH 5, respectively. Taking into consideration the percent retention results obtained from pH 3.0, 5.0, and 7.0, it can be concluded that G3-NH₂ and G4-NH₂ started to be selective towards metal ions with an increase in pH from pH 3.0 to pH 5.0 and this selectivity was maintained up to pH 7.0.

At pH 7 it is interesting to note that JCPDs presented selectivity for Cu(II) ions with the maximum binding ca-

Table 3. Analytical figures of merit for Cd, Co, Cu, Ni, and Zn

Analytes	LOD (mg/L)	LOQ (mg/L)	Linear range (mg/L)	R ²	Equation (y = mx + n)
Cd	0.0159	0.0530	0.2–2.5	0.9948	0.2452x + 0.0277
Co	0.0228	0.0759	0.2–4.0	0.9960	0.0565x + 0.0041
Cu	0.0259	0.0864	0.3–4.0	0.9980	0.0752x – 0.0105
Ni	0.0205	0.0685	0.2–5.0	0.9966	0.0572x + 0.0224
Zn	0.0128	0.0425	0.5–2.0	0.9969	0.2940x – 0.0618

Table 4. Cd(II), Co(II), Cu(II), Ni(II), and Zn(II) retention% in aqueous solutions of JCPDs as a function of pH.

Generation	pH	Heavy metal ions Retention% ^a				
		Cd (II)	Co (II)	Cu (II)	Ni (II)	Zn (II)
G3-NH ₂	3	–	–	–	–	–
	5	–	–	12.32 ± 1.13	–	–
	7	–	–	65.74 ± 1.18	–	–
	9	23.68 ± 2.13	93.53 ± 1.38	74.23 ± 1.26	85.00 ± 1.36	97.56 ± 1.95
G4-NH ₂	3	–	–	–	–	–
	5	–	–	12.12 ± 0.82	–	–
	7	–	–	70.95 ± 1.59	–	–
	9	22.13 ± 2.89	94.99 ± 2.63	84.38 ± 1.85	86.5 ± 2.36	95.05 ± 3.15

^aRetention% values are presented as mean ± confidence intervals for four repeated measurements

capacity for both generations in the presence of other divalent heavy metal ions. Our results are in good agreement with the previous computational study³⁴ conducted to determine active specific metal binding sites (amino groups) of PAMAMs. Results showed that Cu(II)-PAMAM complex exhibit higher stability due to stronger binding energy, shorter bond distances between the metal center and the ligand, and greater covalent degree because of the higher extent of orbital mixing. This result supports the selectivity towards Cu(II) metal ions at neutral pH but may also have implications for the use of JCPDs as effective ligands in sensing systems in future studies.

When the average metal ion retentions are considered, at higher pH 9.0, the metal binding affinity in generations of JCPDs had the same decreasing order of Zn(II) > Co(II) > Ni(II) > Cu(II) > Cd(II). When the average percent retentions of metal ions by G3-NH₂ in aqueous solutions were considered, it can be concluded that the selectivity follows the order of Zn(II) > Co(II) > Ni(II) > Cu(II) > Cd(II) with more than 74.23% except for Cd(II) 23.68%. In case of the average retention (%) profiles, the affinity of G4-NH₂ toward metal ions was observed in the same decreasing order with more than 84.38% for all metal ions except for Cd(II) 22.13%. However, if the confidence intervals are considered, the decreasing affinity order of G4-NH₂ towards metal ions was in the order of Zn(II) ≈ Co(II) > Ni(II) ≈ Cu(II) > Cd(II). Interestingly, Zn(II) and Co(II) were retained over 90% by both generations in the presence of other metals. This indicated that G3-NH₂ and G4-NH₂ were highly selective towards to Zn(II) and Co(II) at higher pH 9.0 and almost no generation effect can be observable towards metal ions at pH 9. In the case of Cu(II) the retention increased as the generation increased. Indeed, the results could be explained based on extent of protonation (α) of the amino groups of PAMAMs (Fig. S3), and the theory of hard-soft acid-base (HSAB).³⁵ In our experiments, we evaluated the removal of divalent ions of selected heavy transition metals from the first row: Zn, Cu, Ni, Co and second row: Cd by PAUF with JCPDs. According to theory, Cd(II) ion with lower ionic charge and greater ionic size is a kind of soft acid, which may bond to soft base strongly.³⁵ In accordance with the literature,³⁶ JCPDs may be taken as a type of hard base in our case with their good protonation abilities and extent of protonation profiles (Fig. S3). On the other hand, Zn(II), Cu(II), Ni(II), and Co(II) metal ions could be taken as borderline acids and they can bond to both hard and soft bases. When the metal ions and the dendrimers are in the same valence, the polarization of metal ions will take an important role in the interaction with dendrimers. The larger the metal ion radius is, the greater the polarization would be. Therefore, the bonding strength is expected in the decreasing order of Zn(II) (74 pm) > Co(II) (65 pm (low-spin)-74.5 pm (high-spin)) > Cu(II) (73 pm) > Ni(II) (69 pm) for hard acids. Cd(II) (95 pm) is expected to be in the last order as it is a soft acid to the contrary to other metal ions. These expecta-

tions almost validate our observation that the order of retention of metal ions for higher generation G4-NH₂ PAMAM dendrimer was in the order of Zn(II) ≈ Co(II) > Ni(II) ≈ Cu(II) > Cd(II) at pH 9, where almost all of the amino groups are available for binding for metal ions in competition (Fig. S3). Higher or almost equal retention of Ni(II) ions compared to Cu(II) ions could be attributed to Jeffamine® core even if PAMAMs could bind Cu(II) over Ni(II) in waste water.²⁵ It was noteworthy that the position of the metal ions changes dynamically as they interact with the amine-terminated PAMAMs depending on the pH.³⁷ Metal ions proceed to localize to the interior of the dendrimers first contacting the surface amine groups of dendrimers and finally reaching to the core of the dendrimer as the pH increased and dendrimer is fully deprotonated.³⁷ It could be also inferred that metal laden JCPDs could be regenerated by decreasing the pH of the aqueous polymer solutions from pH 9 to pH 3. In other words, it can be possible to remove heavy metals from mixtures at high pH 9.0 and purify or regenerate them at lower pH 3.0 by using both generations of JCPDs as the polymer support for the collective removal of metal ions by PAUF.

3. 3. Selective and Collective Removal of Cu(II), Co(II), Ni(II), Cd(II), and Zn(II)

Fig. 3 shows the EOB and FB of total metal ions in aqueous solutions of JCPDs, G3-NH₂ and G4-NH₂ G3-

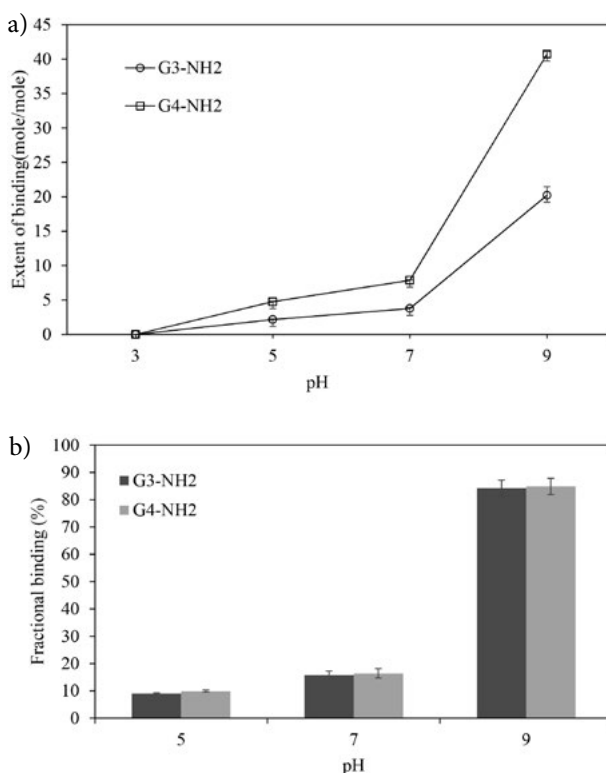


Figure 3. (a) EOB and (b) FB of total metal ions in aqueous solutions of JCPDs at room temperature as a function of pH.

NH₂ has 21 tertiary amine, 42 amide groups and 24 terminal primary amine groups while G4-NH₂ has 45 tertiary amine, 90 amide groups and 48 terminal primary amine groups (Table 1). Both of the G3-NH₂ and G4-NH₂ JCPDs retain selectively Cu(II) ions at pH 5 and neutral pH 7 whereas they bind all metal ions at higher pH 9 (Table 3). Thus, there exist a competition between the metal ions at pH 9. For G3-NH₂ PAMAM dendrimer, EOB of 2.16 ± 0.05 , 3.77 ± 0.06 , 20.22 ± 0.39 ions per dendrimer molecule were observed whilst 4.75 ± 0.08 , 7.87 ± 0.15 , 40.73 ± 1.24 were measured for G4-NH₂ at pH 5, 7 and 9, respectively. It can be concluded that EOB of total metal ions in aqueous solutions of JCPDs goes through a maximum as pH increases. From pH 3 to pH 7, EOB increases linearly for both generations. However, a remarkable increase in EOB for both generations was observed with a pH increase from pH 7 to pH 9. EOB increased from pH 7 to 9 was significantly higher for G4-NH₂ in comparison with G3-NH₂. This could be attributed to the large number of present metal binding sites (amino groups), which increase exponentially with the generation number increase (Table S1). Meanwhile, it could be clearly seen from FB profiles that there is no explicit generation effect on metal binding for JCPDs.

Similar trends in the competition of Cd(II), Co(II), Cu(II), Ni(II), and Zn(II) ions in the presence JCPDs in aqueous solutions with different pH values ranging from pH 3.0 to 9.0 suggest that these metal ions should have the similar binding mechanism for G3-NH₂ and G4-NH₂ or they bind to the similar sites. These sites are in general the internal tertiary amine sites of PAMAMs and they have the limited and alternating number of tertiary amine groups available for binding with metal ions as the generation changed (Table 1). Hence, PAMAMs could have bonded a limited number of metal ions. In the presence of an excess amount of metal ions for binding, there occurs a binding competition between the metal ions towards to JCPDS (Table S1).

To enlighten the mechanism of binding and assess the respective role of amino groups on the uptake of metal ions by different generations of JCPDs at different pH values, the relationship between EOB for metal ions (M(II)) and generation size was illustrated in Fig. 4. The symbols stand for measured EOB values assuming two commonly observed coordination models for M(II) ions: bidentate [i.e., 1M(II)/2N i.e. each M(II) ion coordinates with two amino groups] and tetradentate coordination [i.e., 1M(I-1)/4N]. Fig. 4 suggests that EOB data can be adequately described by a tetradentate coordination model for amine-terminated JCPDS. This result is a promising evidence that at pH 9, all of the available amino groups of dendrimers could take a role in binding by forming tetradentate coordination model. Investigation of the Fig. 4 reveals also that all of the amide groups of JCPDs take an active role in complexation with divalent heavy metal ions only at higher pH 9. In a former study, Ottavani et al.³⁸ characterized that

deprotonation of the amide groups of PAMAMs starts at pH 6 and continues towards the higher pH 12. This result is also consistent with our findings, and with the result reported by Diallo et al.³⁹ that “hard” Lewis acids (metal ions) form strong complexes with “hard” Lewis bases including organic ligands with O and N donors (e.g. amide and amines). In summary, due to high contribution of deprotonated amino groups, maximum bindings were observed at pH 9.

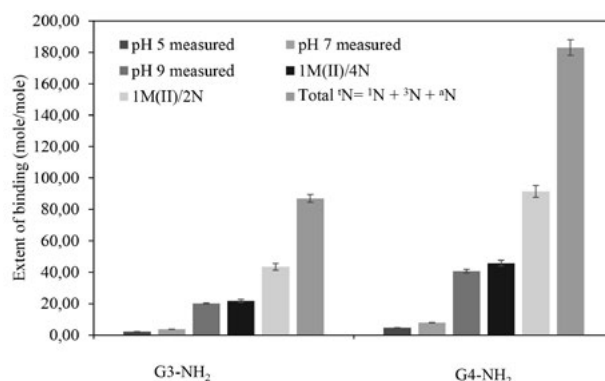


Figure 4. Maximum EOB for M(II) ions in solutions of JCPDs as a function of total number of nitrogen-containing groups (¹N: primary amines; ³N: tertiary amines; ⁴N: amides; total ¹N = ¹N + ³N + ⁴N).

The structure of the amine-terminated PAMAMs is expected to come in densely closed packed-in conformation as the pH increases.⁴⁰ Therefore, the complexation ability of PAMAMs increases with the contribution of compact structure of them with activated amide groups in addition to tertiary and terminal amine groups at the values, especially above pH 7 (Fig. S3). The retention of metal ions inside of PAMAMs can be performed by covalent bonding, hydrogen bonding or entrapping.⁴¹ One of the possible reasons why Cu(II) retention was observed at pH 5, where almost all of the amino groups of PAMAMs are protonated, can be the entrapping of hydrated Cu(II) ion complexes inside the dendrimer due to PAMAMs encapsulation abilities at lower pH.⁴²

Fig. 5 shows the EOB and selectivity features of different generations of amine-terminated JCPDs for metal ion mixture of Cu(II), Co(II), Ni(II), Cd(II), and Zn(II) at higher pH 9, where all of the amino groups of dendrimers are neutral (Fig S3). In Fig. 5, individual EOB values of metal ions while they are in competition with each other in the aqueous solutions of different generations of JCPDs are ranged between 2.51 and 4.73 for G3-NH₂ while 4.76 and 9.29 for G4-NH₂. EOB values for all heavy metals ions increase as the generation number increases due to an increase in the number of specific binding sites with generation size increase. That is, higher binding capacities were observed for G4-NH₂ than those of G3-NH₂. When the average EOB values are considered, it is clear from Fig. 5 that the selectivity follows the order: Zn(II) > Co(II)

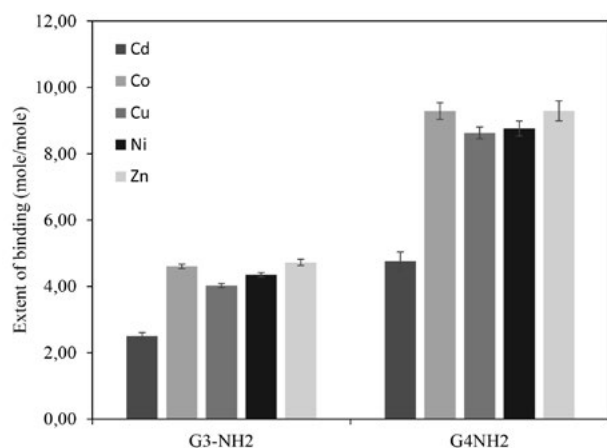


Figure 5. EOB and selectivity properties of different generation JCPDs towards heavy metals Cd(II), Co(II), Cu(II), Ni(II), and Zn(II) at pH 9.

> Ni(II) > Cu(II) for both generations. These results present extra proof that the dendrimer-metal ion interactions depend not only the nature of the media but also the specific binding sites (number of amine groups) of the generation of PAMAMs, electronegativity, and ionic radius of the heavy metals according to Pearson's hard-soft principles.³⁵

3. 4. Effect of Initial Free Metal Ion Concentration on Dendrimer-metal Complexation

Complexation studies of JCPDS, G3-NH₂ and G4-NH₂, with the mixture of heavy metal solutions were evaluated to assess their metal ions removal ability from aqueous solutions. At this point, free metal ion concentration [M²⁺] has a critical importance. If the solubility of metal is not adequate for complexation at the studied pH, then sudden metal hydroxide formation is expected, and this will form a mass deposition on the membrane surface.⁴³ Therefore, it would not be possible to mention a successful membrane dialysis process even if it was reported in a recent study⁴³ that the presence of PAMAM dendrimers in

aqueous solutions does not prevent hydrolysis of metal ions. In dendrimer-multi metal batch complexation process, taking into consideration this factor, we conducted experiments in the pH range of 3.0–9.0, where it was not observed any precipitation of metal hydroxides. A clear precipitation was observed above the pH 9.20. For this reason, batch complexation experiments were conducted between the pH ranges of pH 3.0-9.0 in alignment with the literature.²⁴

3. 5. Metal Ion Uptake

In order to compare the effect of generation on the metal ion uptake of JCPDs, their binding capacities either for Cd(II), Co(II), Cu(II), Ni(II), and Zn(II) ions under competitive conditions (aqueous metal mixture solutions) were determined, and the results were presented in Table 5. As shown in Table 5, the metal ion uptake is ranged between ~48 and ~60 mg metal ion per gram polymer. Binding capacity order of G3-NH₂ is Zn(II) > Cd(II) > Co(II) > Cu(II) > Ni(II) whereas that of G4-NH₂ is Zn(II) > Cu(II) > Co(II) > Cd(II) > Ni(II). It was found that Zn(II), Cd(II), and Co(II) metal ions bonded at over 50 mg/g for both generations at pH 9.

Normally, the total binding capacity of G4-NH₂ is expected to be higher than that of G3-NH₂ when the number of metal binding sites of JCPDs are considered (Table 1). However, we observed the total binding capacity of G3-NH₂ (262.79 ± 1.62 mg/g) as a little bit higher than that of G4-NH₂ (257.27 ± 2.57 mg/g). This result reveals an important point that the binding capacities of dendrimers not only depend on the pH of the media, EOP and type of the dendrimer but also on the structural conformation that the generation has.

It was reported that a portion of metal hydrates resides in the water pools in the open structure of the earlier generation dendrimers (G<4). This finding reveals that generation-3 PAMAM, with more open structure, can entrap more water molecules that can complex the metal ions in comparison with generation-4 PAMAMs.³⁷ Our finding is in good agreement with these results and could be used to explain why G3-NH₂ has a binding capacity higher than G4-NH₂.

Table 5. Metal ion uptake and binding properties of different generation (G3-G4) JCPDS under competitive conditions at pH 9.

Metal ion (M(II))	G3-NH ₂ (mg/g) ^a	G4-NH ₂ (mg/g) ^a
Cd	53.98 ± 0.21	50.02 ± 0.29
Co	51.92 ± 0.20	51.16 ± 0.32
Cu	48.95 ± 0.14	51.25 ± 0.24
Ni	48.83 ± 0.14	48.06 ± 0.26
Zn	59.11 ± 0.13	56.78 ± 0.18
Total	262.79 ± 1.62	257.27 ± 2.57

^aAverage binding capacity (mg/g) for four repeated measurements.

4. Conclusions

The performance of different generations of JCPDs in removing some of the divalent heavy metal ions from aqueous solutions was investigated in this paper. The highest heavy metal ion removal or binding capacity was observed for G3-NH₂. JCPDs were detected to be selective at pH 5.0 and at neutral pH 7.0 under competitive conditions with other heavy metals. At high pH 9.0, both generations could remove all of the metal ions present in the media. The affinity of both generations towards metal ions was also observed in the same decreasing order of Zn(II) > Co(II) > Ni(II) > Cu(II) > Cd(II) when the average retention percentages were considered. Only the Cu(II) retention increased with increasing generation and pH. Zn(II) and Co(II) were retained over 90% retention for both generations at pH 9.0. Regeneration of metal laden PAMAMs could be achieved by decreasing the pH of aqueous solution to lower than 5. These results indicate that amine-terminated JCPDs are expected to be new promising macromolecular chelating agent templates for the removal of toxic heavy metals from wastewaters. Results also imply that generation-3 and 4 amine-terminated JCPDs effectively interact with metal ions, and thus might provide a convenient competitor in nanosensing for future studies.

5. Acknowledgements

This research has been supported by Yıldız Technical University Scientific Research Projects Coordination Department (Project Number: 2012-01-02-DOP05). Authors claim that there is no conflict of interest. We are grateful to Assist. Prof. Dr. Müzeyyen Ertürk for many helpful discussions.

6. References

- W. Stumm and J. J. Morgan, Book Aquatic chemistry: chemical equilibria and rates in natural waters, Wiley, 1996.
- M. Barakat, *Arabian J. Chem.* **2011**, *4*, 361–377. DOI: 10.1016/j.arabjc.2010.07.019.
- C. Lin, D. Yang, C. Li, Q. Li, G. Shi, Y. Wang, Y. Zhou and M. Liu, *Beijing Daxue Xuebao (Ziran Kexue Ban)/Acta Scientiarum Naturalium Universitatis Pekinensis* **2013**, *49*, 426–434.
- T. A. Kurniawan, M. E. T. Sillanpää and M. Sillanpää, *Crit. Rev. Environ. Sci. Technol.* **2012**, *42*, 1233–1295. DOI:10.1080/10643389.2011.556553.
- W. J. Weber Jr: Water Science and Technology, 2002, pp. 241–246.
- A. Fakhru'l-Razi, A. Pendashteh, L. C. Abdullah, D. R. A. Biak, S. S. Madaeni and Z. Z. Abidin, *J. Hazard. Mater.* **2009**, *170*, 530–551. DOI:10.1016/j.jhazmat.2009.05.044.
- A. Zolotov Yu, O. M. Petrukhin, G. I. Malofeeva, E. V. Marcheva, O. A. Shiryaeva, V. A. Shestokov, V. G. Miskar'yants, V. I. Nefedov, I. Murinov Yu and E. Nikitin Yu, *Anal. Chim. Acta* **1983**, *148*, 135–157. DOI:10.1016/S0003-2670(00)85160-0.
- N. Savage and M. S. Diallo, *J. Nanopart. Res.* **2005**, *7*, 331–342. DOI:10.1007/s11051-005-7523-5.
- A. Benhamou, M. Baudu, Z. Derriche and J. P. Basly, *J. Hazard. Mater.* **2009**, *171*, 1001–1008. DOI:10.1016/j.jhazmat.2009.06.106.
- C. Barrera-Díaz, M. Palomar-Pardavé, M. Romero-Romo and F. Ureña-Núñez, *J. Polym. Res.* **2005**, *12*, 421–428. DOI:10.1007/s10965-005-3323-y.
- D. Mohan and C. U. Pittman Jr, *J. Hazard. Mater.* **2006**, *137*, 762–811. DOI:10.1016/j.jhazmat.2006.06.060.
- N. Sankaramakrishnan, P. Kumar and V. Singh Chauhan, *Sep. Purif. Technol.* **2008**, *63*, 213–219. DOI:10.1016/j.seppur.2008.05.002.
- Y. Niu and R. M. Crooks, *C. R. Chim.* **2003**, *6*, 1049–1059. DOI:10.1016/j.crci.2003.08.001.
- A. Rether and M. Schuster, *React. Funct. Polym.* **2003**, *57*, 13–21. DOI:10.1016/j.reactfunctpolym.2003.06.002.
- F. Zeng and S. C. Zimmerman, *Chemical reviews* **1997**, *97*, 1681–1712.
- L. Balogh and D. A. Tomalia, *J. Am. Chem. Soc.* **1998**, *120*, 7355–7356. DOI:10.1021/ja980861w.
- M. S. Diallo, L. Balogh, A. Shafagati, J. H. Johnson, W. A. Goddard and D. A. Tomalia, *Environ. Sci. Technol.* **1999**, *33*, 820–824. DOI:10.1021/es980521a.
- K. E. Geckeler and K. Volchek, *Environ. Sci. Technol.* **1996**, *30*, 725–734. DOI:10.1021/es950326l.
- B. Y. Spivakov, K. Geckeler and E. Bayer, *Nature* **1985**, *315*, 313–315.
- R.-S. Juang and M.-N. Chen, *Ind. Eng. Chem. Res.* **1997**, *36*, 179–186. DOI: 10.1021/IE960311B.
- O. Sanli and G. Asman, *J. Appl. Polym. Sci.* **2000**, *77*, 1096–1101. DOI:10.1002/1097-4628(20000801)77:5<1096::AID-APP17>3.0.CO;2-F.
- P. Canizares, A. Perez and R. Camarillo, *Desalination* **2002**, *144*, 279–285. DOI:10.1016/S0011-9164(02)00328-4.
- J. Muslehiddinoglu, Y. Uludag, H. O. Ozelge and L. Yilmaz, *J. Membr. Sci.* **1998**, *140*, 251–266. DOI:10.1016/S0376-7388(97)00280-9.
- M. S. Diallo, S. Christie, P. Swaminathan, L. Balogh, X. Shi, W. Um, C. Papelis, W. A. Goddard, III and J. H. Johnson, Jr., *Langmuir* **2004**, *20*, 2640–2651. DOI:10.1021/la036108k.
- M. S. Diallo, S. Christie, P. Swaminathan, J. H. Johnson and W. A. Goddard, *Environ. Sci. Technol.* **2005**, *39*, 1366–1377. DOI:10.1021/es048961r.
- M. Tulu and K. E. Geckeler, *Polym. Int.* **1999**, *48*, 909–914. DOI:10.1002/(SICI)1097-0126(199909)48:9<909::AID-PI244>3.0.CO;2-E.
- B. L. Rivas, E. D. Pereira and I. Moreno-Villoslada, *Prog. Polym. Sci.* **2003**, *28*, 173–208. DOI:10.1016/S0079-6700(02)00028-X.
- J. N. Asaad, N. E. Ikladious, F. Awad and T. Müller, *The Canadian Journal of Chemical Engineering* **2013**, *91*, 257–263. DOI:10.1002/cjce.21634.
- L. Dambies, A. Jaworska, G. Zakrzewska-Trznadel and B. Sar-

- towska, *J. Hazard. Mater.* **2010**, *178*, 988–993. DOI:10.1016/j.jhazmat.2010.02.035.
30. B. Klajnert and M. Bryszewska, *Acta Biochim. Pol.* **2000**, *48*, 199–208.
31. A. S. Ertürk, M. Tülü, A. E. Bozdoğan and T. Parali, *Eur. Polym. J.* **2014**, *52*, 218–226. DOI:10.1016/j.eurpolymj.2013.12.018.
32. M. Tülü and M. Şenel, *J. Appl. Polym. Sci.* **2008**, *109*, 2808–2814. DOI:10.1002/app.28353.
33. A. S. Ertürk, M. U. Gurbuz, M. Tulu and A. E. Bozdoğan, *RSC Adv.* **2015**, *5*, 60581–60595. DOI:10.1039/C5RA11157A.
34. M. B. Camarada, M. Zúñiga, J. Alzate-Morales and L. S. Santos, *Chem. Phys. Lett.* **2014**, *616–617*, 171–177. DOI:10.1016/j.cplett.2014.10.022.
35. R. G. Pearson, *J. Am. Chem. Soc.* **1963**, *85*, 3533–9. DOI:10.1021/ja00905a001.
36. Y. Niu, L. Sun and R. M. Crooks, *Macromolecules* **2003**, *36*, 5725–5731. DOI:10.1021/ma034276d.
37. M. L. Tran, L. R. Gahan and I. R. Gentle, *J. Phys. Chem. B* **2004**, *108*, 20130–20136. DOI:10.1021/jp037569h.
38. M. F. Ottaviani, F. Montalti, N. J. Turro and D. A. Tomalia, *J. Phys. Chem. B* **1997**, *101*, 158–166.
39. M. S. Diallo, W. Arasho, J. H. Johnson and W. A. Goddard Iii, *Environ. Sci. Technol.* **2008**, *42*, 1572–1579. DOI:10.1021/es0715905.
40. I. Lee, B. D. Athey, A. W. Wetzel, W. Meixner and J. R. Baker, *Macromolecules* **2002**, *35*, 4510–4520. DOI:10.1021/ma010354q.
41. A. E. Beezer, A. S. H. King, I. K. Martin, J. C. Mitchell, L. J. Twyman and C. F. Wain, *Tetrahedron* **2003**, *59*, 3873–3880. DOI:10.1016/S0040-4020(03)00437-X.
42. M. F. Ottaviani, F. Montalti, N. J. Turro and D. A. Tomalia, *The Journal of Physical Chemistry B* **1997**, *101*, 158–166. DOI:10.1021/jp962857h.
43. P. Ilaiyaraja, A. Deb and D. Ponraju, *J Radioanal Nucl Chem* **2015**, *303*, 441–450. DOI:10.1007/s10967-014-3462-x.

Povzetek

Različni generaciji (G3-G4) Jeffamine® T-403 dendrimerov (JCPD) z osnovno strukturo poli(amidoamin) PAMAM dendrimerov in s terminalnimi aaminskimi skupinami smo uporabili kot novo makromolekularno osnovo za kompleksiranje težkih kovin v procesu ultrafiltracije s pomočjo polimerov (PAUF). Raziskali smo njihovo zmožnost za odstranjevanje nekaterih divalentnih kovinskih ionov: Cu, Co, Ni, Cd in Zn iz vodnih raztopin pod kompetitivnimi pogoji. Raziskali smo tudi učinek pH in generacije JCPD. Rezultate za obseg vezave (EOB) lahko ustrezno razložimo s tetradentatno koordinacijo z JCPD pri pH 9, pri katerem smo opazili največji delež odstranjenih kovinskih ionov. Pri pH 9,0 smo za obe generaciji opazili naslednjo selektivnost nasproti ionom težkih kovin: Zn(II) > Co(II) > Ni(II) > Cu(II) > Cd(II). Največjo skupno vezavno kapaciteto smo opazili za G3-NH₂ (262,79 ± 1,62 mg/g) in je bila nekoliko višja kot za G4-NH₂ (257,27 ± 2,57 mg/g). EOB študija je tudi dokazala aktiven prispevek amidnih skupin na PAMAM k zmožnosti vezave kovin. Obe generaciji sta bili selektivni za Cu(II) ione pri nižjem pH 5 in pH 7. Iz teh rezultatov lahko sklepamo, da imajo obravnavani JCPD zelene tehnične lastnosti za uporabo pri odstranjevanju strupenih kovin iz odpadnih vod.

Scientific paper

Polythiacalix[4]amides as a Novel Category of Macromolecules; Synthesis, Antibacterial Evaluation and Investigation on their Spectral and Thermophysical Characteristics

Hamed Tashakkorian,¹ Moslem Mansour Lakouraj,^{2,*} Rahimeh Maldar² and Zahra Moulana³

¹ Cellular and Molecular Biology Research Center (CMBRC), Health Research Institute, Babol University of Medical Sciences, Babol, 4717641367, Iran

² Department of Polymer Chemistry, Faculty of Chemistry, University of Mazanadaran, Babolsar, 47416 95447, Iran

³ Infectious Diseases & Tropical Medicine Research Center, Babol University of Medical Sciences, Babol, 47176 41367, Iran

* Corresponding author: E-mail: lakouraj@umz.ac.ir
TelFax: (+) 98-1135302350

Received: 04-06-2017

Abstract

Polythiacalix[4]amides as a novel category of polyamides, with high sorption capability towards some environmentally hazardous metal cations, especially Hg^{2+} , have been synthesized via direct polycondensation protocol using a thiacalix[4] arene dicarboxylic acid and commercial diamines. The polyamides were obtained in high yields and possess inherent viscosities in the range of 0.55–0.75 dl/g. The photophysical characteristic was studied by looking for the maximum absorption wavelength of each polymer using UV absorption spectroscopy. Thermogravimetric analysis displayed high thermal stability for these polyamides in range of 337 to 346 °C at the point of 10% weight loss, and their char yields were about 32.9–58.5% at 600 °C. Also, glass transition temperatures were between 157 and 178 °C. To survey on possible sorption capability of these polythiacalixamides, solid–liquid extraction of some toxic transition metal cations, such as Cu^{2+} , Co^{2+} , Cd^{2+} , Pb^{2+} and Hg^{2+} from wastewater was performed. Antibacterial evaluation was conducted using Gram positive and Gram negative bacteria strains and some reliable results have been obtained. The results showed some promising features of their ability for being employed as possible ingredients of industrial antibacterial membranes.

Keywords: Supramolecular chemistry; Thiacalixarene; Antibacterial evaluation; Sorption capability; Thermal Stability; Polyamide

1. Introduction

In the last decade, scientists in the field of supramolecular chemistry have designed novel architectures of host molecules with which area of receptor chemistry has been developed.^{1–4} Supramolecules, such as cyclodextrins and crown ethers, calixarene and their derivatives including polycalixarenes have been employed widely in catalysis,^{5–8} molecular recognition or ion separation^{9,10} and as sensors^{11–13} during recent years. Calixarenes structures provide interesting platforms for improving the reception capability of chemical structures by special modifications. Smart functionalization at the both upper and/or lower

rim with specific complexing groups as well as replacement of CH_2 bridge by oxygen or sulfur, can improve the ionic and molecular binding properties. Functionalization will increase the chance for recognition and separation of the target rare or toxic guests which is essential from economic and environmental point of view. For instance, sieving specific ions, such as H^+ and Li^+ or also attaching to the Au(111) single crystal surface are important strategies in energy conversion and storage systems and also in electrochemical applications, respectively.¹⁴ During the last decade, novel bioactive compounds with significant antibacterial and antifungal characteristics have emerged.

Moreover, binding these bioactive compounds with platforms, such as calixarenes, has created the unique category of bioactive supramolecular compounds. These structures have noteworthy activities against cancerous cells and have demonstrated antibacterial and antifungal characteristics.¹⁵ One of the particular compounds of this family is called thiacalixarene, which has sulfur atoms instead of common methylene bridges and shows some surprising features of these macrocycles. Thiacalixarene and its derivatives display some unique properties which led them to be introduced in different applications from host–guest to supramolecular chemistry and also as molecular receptors.^{16–24} Based on the reported findings, these sulfur-containing structures have attracted much attention in calixarene chemistry because of their usage in selective extraction of more polarizable transition metal ions instead of hard metal ions, such as alkali and alkaline earth cations.^{25–30}

In macromolecular science, it has been proved that calixarene based ionophores have a great acceptability in modern chemistry because of their extreme capability in functionalization from bridge position up to both sides of the rims. As well, polymer scientists took advantage of these structures for preparation of ions-selective polymers or in producing efficient metal cations absorbent membranes. Furthermore, researchers who are studying the field of polymers focused their attention on the growing demands for novel antimicrobial compounds as major concerns for improving the standards of public health. Numerous strategies have been established to overcome the existence of medical device related infections. Therefore, preparations of polymeric materials containing antimicrobial moieties attracted much interest in recent years^{31,32} and are commercially available in the forms of sutures, tubing, containers, films, dental implants, and catheters. As a part of our continuing study on the synthesis and physical properties of calixarene based polymers,^{33–36} the main goal of this research is to combine the extraction abilities towards heavy metal ions with antimicrobial properties by using thiacalixarene to introduce a novel type of polythiacalixamides. These high performance polyamides possess moieties with unique cavity size, thermal stability and also having acceptable antibacterial activities. We wish these polymers can be applied in polymeric antibacterial membranes which are being incorporated in environmental applications and also in medical devices.

2. Experimental

2.1. Apparatus and Materials

Melting points were determined on an Electro Thermal 9100 apparatus in a sealed capillary and are uncorrected. ¹H NMR spectra were recorded on a Bruker Avance III 400 MHz spectrometer in CDCl₃ and DMSO-*d*₆ with TMS

as internal standard. IR spectra were recorded on a Bruker FTIR spectrometer as KBr pellets. For ultraviolet-visible (UV-Vis) measurements, Cecil UV-Visible spectrophotometer was applied. Inherent viscosities of polymers were determined by using an Ostwald viscometer. Elemental analyses were performed by a CHN-O-Rapid Heraeus elemental analyzer (Wellesley, MA). Differential scanning calorimetry (DSC) and thermogravimetric analysis (TGA) were recorded on a Perkin-Elmer Pyris Diamond and Pyris 6 TGA Consumables, respectively. Thermo Fisher Scientific ICE 3300 Atomic Absorption Spectrometer (AAS) was employed for determination of the metal ions. All materials and reagents were of standard analytical grade, purchased from Fluka or Merck companies, and used without further purification. Commercial grade solvents such as acetone, acetonitrile, methanol, toluene and *n*-hexane were dried and stored over 4 Å molecular sieves.³⁷

2.2. Synthesis

The thiacalixarene dicarboxylic acid **3** and its precursors, compounds **1** and **2** were synthesized according to the literature procedures (Scheme 1).^{38–40} The FT-IR, ¹H NMR, and ¹³C NMR spectral data and melting points of the prepared compounds were compared with the original data given in the corresponding articles. As illustrated in Scheme 2, the thiacalixarene-based polyamides **A–D** employed in this study were synthesized from condensation polymerization of thiacalixarene dicarboxylic acid with commercial diamines.

General Procedure for Polymerization of 5,11,17,23-Tetra-*tert*-butyl-25,27-bis-[carboxymethoxy]-26,28-dihydroxy-2,8,14,20-tetrathiacalix[4]arene (**3**) with Commercial Diamines

A 25 mL two-necked, round-bottomed flask equipped with a reflux condenser, magnetic stirrer and gas inlet was charged with 1.2 mmol of triphenylphosphite, 1 mmol pyridine and 5 mL of dry NMP. The solution was agitated at room temperature for 15 min under nitrogen atmosphere. Then, 1 mmol of thiacalix[4]arene dicarboxylic acid **3** was added to the solution. After a few minutes, 1 mmol of commercial diamine was dissolved in the reaction mixture. The temperature was raised to 110 °C and the solution stirred for 14 h. Polythiacalixamide was produced during direct phosphorylation polymerization and precipitated by pouring the flask content into the cold methanol. After stirring for half an hour, it was filtered using Büchner funnel and washed with hot water and methanol, respectively. All of the polythiacalixamides mentioned in this work were prepared using the same procedure. The synthesized polymers were then dried overnight under vacuum at 120 °C to afford corresponding polymers in 70–85% yields. The characteristic physical and spectral data of polythiacalixamides **A–D** are given in Tables 1–3.

2. 3. Survey on Transition Metal Removal using pTCAs

Investigation on sorption behavior of polythiacalixamides (pTCAs) was carried out based on the following batch-wise procedure. pTCA ($25 \cdot 10^{-3}$ g) were added to 10 mL aliquot solution of the corresponding metal nitrate ($10 \cdot 10^{-3}$ mol L⁻¹). Then to have a precise comparison with our previously reported polycalixarenes (PCA), they were immersed in the test solutions and stirred at 25 °C for 3 h. After the specified time, pTCAs were filtered off and the concentrations of the remaining metal ions in the aqueous phase (C_e) were determined using atomic absorption spectroscopy. The percent sorption of ions (S%) and distribution coefficient (K_d) were calculated as:

$$S\% = C_i - \frac{C_e}{C_i} \times 100 \quad (1)$$

C_i : Initial metal ion concentration

$$K_d = \frac{a/\text{g of dry resin}}{B/\text{mL of solution}} \quad (2)$$

A: Amount of ion absorbed by resin

B: Amount of metal remaining in solution

2. 4. Experimental Section: Determination of Antibacterial Activity

Synthesized polymers and monomers containing 1,2,4-triazole units were evaluated for their anti-bacterial activity against microorganisms including the two Gram positive bacteria *Staphylococcus aureus* (ATCC 259230) and *Bacillus subtilis* (PTCC 1156) and three Gram negative bacteria: *Escherichia coli* (PTCC 1533), *Pseudomonas aeruginosa* (PTCC 1707) and *Klebsiella pneumoniae* (ATCC 11296). These common Gram positives and Gram negatives bacteria were investigated at different concentrations of the tested compounds using broth microdilution procedure. The compounds sensitivity of the strains was assayed for positive or negative growth after 24–48 h. The MIC test was repeated at least three times for each antimicrobial agent. Then antibacterial activities of the compounds were compared with known and effective antibiotics penicillin, ciprofloxacin, and gentamicin at the same concentration.

2. 4. 1. Minimum Inhibitory Concentration (MIC)

MIC is the lowest concentration which can cause complete growth inhibition. The broth microdilution method was applied to evaluate the MIC⁴¹ 100 µL of Muller-Hilton broth, containing 10⁵ CFU mL⁻¹ of each bacterium, was added to each well. 100 µL of polythiacalixamide solutions with the maximum starting concentra-

tions 500 µg/mL were poured in the first well of 96 sterilized well micro plates and then diluted to half concentrations in the next wells, respectively. After dilution micro plates were incubated at 37 °C for 24 h. The first well which was completely transparent and had no bacterial growth, was considered for MIC. Each concentration was tested three times and the results were averaged.

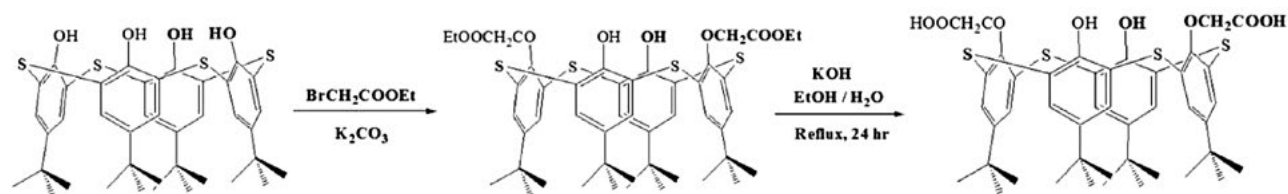
2. 4. 2. Minimum Bactericidal Concentration (MBC)

The minimum bactericidal concentration (MBC) is the lowest concentration at which an antimicrobial agent will kill a particular microorganism. The MBC is determined from broth dilution MIC tests by sub-culturing to agar plates that do not contain the test agent. The MBC is identified by determining the lowest concentration of antibacterial agent that reduces the viability of the initial bacterial inoculum by $\geq 99.9\%$. 10 µL of the content without turbidity wells was cultivated on the Muller-Hilton plate. The number of colonies was counted after 24 h at 37 °C. The first well which had equal or less than 3 colonies, was regarded as MBC. Antibacterial agents are usually regarded as bactericidal if the MBC is no more than three times of the MIC concentration.

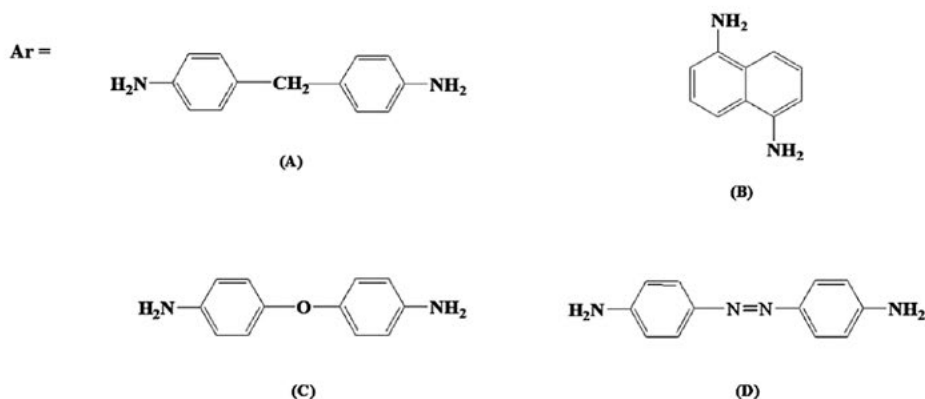
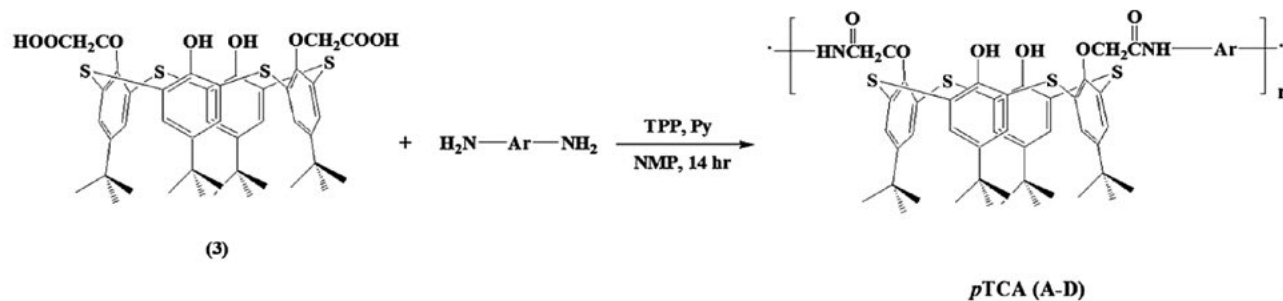
3. Results and Discussion

3. 1. Characterization and Discussion

In developing countries water pollution, especially industrial and agricultural effluents with high levels of toxicity, have been of serious concern. The progressive increase in environmental pollutants emerged the global search for novel, efficient and applicable compounds with high sorption capability. In the last decade macrocyclic supramolecules especially calixarene family, were introduced as a potential sensor for recognition and separation of toxic elements, including Pb²⁺, Cd²⁺ and Hg²⁺.^{42–44} Among them, thiacalixarene and its derivatives having sulfur as an excellent auxiliary chelating agent in their structure have an effective interaction with transition metal cations. Incorporation of thiacalixarene in the backbone of the polymeric materials could help us to prepare such an interesting membrane with great applicability. Therefore, preparation of novel thermally stable polythiacalixamides (pTCAs) having flexible chelating cavity in their backbone and studying their potential capability in the extraction of transition metal ions particularly Hg²⁺ as hazardous cation is disclosed in this research. To have some reliable polymers with excellent cation extraction ability and high thermal stability, we decided to prepare polyamide with promising properties using *para-tert*-butylthiacalixarene dicarboxylic acid and commercial diamines. To achieve this goal, at first parent thiacalixarene was synthesized as revealed in the material section, using *para-tert*-butylphenol



Scheme 1. Synthesis of thiacalix[4]arene dicarboxylic acid 3



Scheme 2. Synthesis of polythiacalixamides pTCA A–D

and sulfur. Then it was functionalized with bromoethyl acetate to obtain the corresponding diester derivative and consequently the product was hydrolyzed using potassium hydroxide to give thiacalix[4]arene dicarboxylic acid as a functionalized monomer (Scheme 1). Then polythiacalixamides, pTCA A–D were obtained via direct polycondensation reaction of thiacalix[4]arene dicarboxylic acid 3 with various commercially available aromatic diamines using triphenylphosphite (TPP) and pyridine as condensation

agents (Scheme 2). All the polymerization reactions afforded clear solutions which were cooled down and poured into the cold methanol while being stirred.

The structure and composition of the synthesized polyamides were characterized by a number of physico-chemical methods, *i.e.* ^1H NMR, IR, UV spectroscopy and elemental analysis. Also thermal stability and sorption capability of the pTCA A–D were determined and detailed completely in this article. ^1H NMR spectra of all the pre-

Table 1. FTIR and ^1H NMR spectral data for the synthesized polythiacalixamides

Polymer	FTIR (Absorption peaks) cm^{-1}			^1H NMR (chemical shift) ppm		
	C=O	N-H	important peaks	N-H (amide proton)	CH_2 (aliphatic)	Ar-H (aromatic Proton)
pTCA A	1685	3360	–	12.75	4.58	6.90–7.88
pTCA B	1695	3355	–	12.10	4.97	7.05–7.95
pTCA C	1686	3368	1597 (N=N)	12.47	4.56	7.08–7.95
pTCA D	1682	3351	–	12.31	4.63	7.11–7.86

Table 2. Elemental analysis (CHN) of polythiacalixamides

Polymer	Calculated (%)			Found (%)		
	C	H	N	C	H	N
pTCA A	70.35	6.19	4.68	70.02	6.01	4.72
pTCA B	68.94	5.92	5.02	68.61	5.72	4.98
pTCA C	66.77	5.72	9.16	66.21	5.54	8.90
pTCA D	68.11	5.84	4.67	67.86	5.57	4.43

pared compounds clearly corresponded to the ascribed structures including monomer and polyamides by the number of signals and their multiplicities. Characteristic physical data of synthesized polymers are shown in Tables 1–3 and explained here in detail. Specified peaks in IR spectra of the polyamides at 1685, 1695, 1682 and 1686 cm^{-1} , respectively, indicate the characteristic stretching vibration of amidic carbonyl bonds of pTCA A–D. Amide proton (N–H) was also observed in ^1H NMR spectra of polyamides A–D around $\delta = 12.4$ ppm. The IR and ^1H NMR spectral data of the polythiacalixamides are summarized in Table 1.

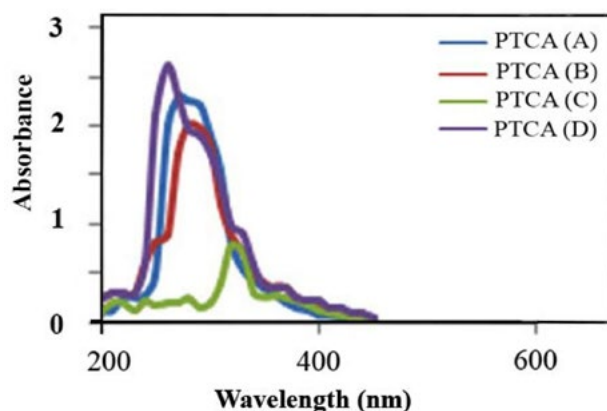


Fig. 1. UV Spectra of polythiacalixamides pTCA A–D

The study on photophysical characteristic of polythiacalixamides A–D was performed by UV-absorption spectroscopy and results are displayed as curves in Figure 1. The maximum of absorption wavelengths (λ_{max}) were observed at 270, 281, 323 and 262 nm for pTCA A–D, re-

spectively. pTCA C has a noticeable 53 nm red shift compared to the other polymers due to the conjugation of N=N group with phenyl rings in polymer chain.

To study on their applicability as a membrane in industry, considering the solubility in industrial solvent is essential. So, the solubilities of the pTCA A–D were investigated in variety of solvents and the results are represented in Table 3. The synthesized polyamides were soluble in aprotic polar solvents, such as NMP, DMF, DMSO, DMAc and in dioxane on heating. Existence of bulky thiacalixarene macrocycle in the backbone and creating free space between polymeric chains improved the solubility parameter relative to traditional polyamides. These polyamides were synthesized in high yields, with inherent viscosities in the range of 0.55–0.75 dL/g at 25 °C in NMP, which are summarized in Table 3.

3. 2. Sorption of Heavy Metal Cations

Functionalization of thiacalix[4]arenes especially at the lower rim makes them more effective as extractant.^{45–47,40} Hence, we investigated the preparation of a thiacalixarene derivative which has been functionalized at the lower rim and employed it in the backbone of the polymeric chain. Then we evaluated the transition metal ions sorption capability of these polymers by solid-liquid extraction procedure. Therefore, some metal cations with great importance from environmental view, such as Cu^{2+} , Co^{2+} , Cd^{2+} , Pb^{2+} and Hg^{2+} were chosen and their aqueous solutions were treated with pTCAs A–D. The results including sorption percentage (S%) and distribution coefficients (K_d) are illustrated in Tables 4–5. From the results given in Tables 4 and 5, it has been observed that pTCAs A–D have excellent extraction ability for Hg^{2+} , Pb^{2+} , Cd^{2+} and Co^{2+} from aqueous solution while exhibit some less promising capability toward Cu^{2+} . In comparison with our recent studies on polycalixarenes (PCA),^{33–35} it is clear that the presence of four sulfur atoms at the bridge position enhances the complexation of thiacalixarene moieties with the larger size metal cations and results in reasonably higher sorption ability. Exact cavity size and tight complexation of thiacalixarene macrocycle with metal cations are the key factors for the observed higher efficiency (Scheme 3). The above mentioned parameters can also

Table 3. Solubility behavior and inherent viscosity of polythiacalixamides

Polymer	DMF	DMAc	NMP	DMSO	Dioxane	Tetralin	η (dL/g) ^a
pTCA A	+h	+	+	+	+h	–	0.57
pTCA B	+h	+	+	+	+	–	0.75
pTCA C	+h	+	+	+	+h	–	0.55
pTCA D	+h	+	+	+h	+h	–	0.61

+, soluble at room temperature, +h, soluble on heating; –, insoluble; DMF: *N,N*-dimethylformamide; DMAc: *N,N*-dimethylacetamide; NMP: *N*-methyl-2-pyrrolidone; DMSO: dimethyl sulfoxide; Tetralin: 1,2,3,4-tetrahydronaphthalene. ^a Inherent viscosity was measured at a concentration of 0.5 dL/g in NMP at 30 °C.



Scheme 3. Polythiacalixamide complexation with large cations

play an important role in the lower sorption capabilities of unfunctionalized monomeric calix and thiacalixarene as well as previously prepared polycalixarenes, relative to pTCAs A–D.

Table 4. Sorption percentage (S %) of heavy metal cations by pTCAs

Polymer	Hg ²⁺	Pb ²⁺	Cd ²⁺	Co ²⁺	Cu ²⁺
pTCA A	93.2	92.2	91.2	85.8	30.4
pCA (CH ₂)	–	–	41.8	40.9	53.7
pTCA B	90.0	89.5	93.2	80.0	57.3
pCA (Naph.)	–	–	38.7	36.3	36.7
pTCA C	93.3	92.3	90.0	83.1	59.3
pCA (Azo)	–	–	36.4	44.2	48.0
pTCA D	91.1	89.2	91.1	84.6	55.1
pCA (Oxy)	–	–	39.4	38.3	51.8

Table 5. Distribution coefficients (K_d) of heavy metal cations by pTCAs

Polymer	Hg ²⁺	Pb ²⁺	Cd ²⁺	Co ²⁺	Cu ²⁺
pTCA A	5314.4	4728.2	4044.4	2416.9	174.6
pTCA B	3600.0	3409.5	5314.4	1600.0	536.7
pTCA C	5314.4	4600.1	3600.0	1966.8	582.8
pTCA D	4044.4	3303.7	4094.3	2197.4	488.9

3. 2. 1. Sorption of Transition Metal Cations at Different pH

To evaluate the effect of pH on the sorption efficiency of pTCAs toward transition metal cations, some experiments have been performed in the pH range of 1.0 to 11. It was found that at lower pH (up to pH 4.0), cations, especially Hg(II), were in the free ionic form,⁴⁶ and the existing hydrogen cations (H⁺) will strongly compete with the transition metal ions for binding with unoccupied sites of pTCAs. Since, the active sites of pTCA, which consists of sulfur, hydroxyl and amide groups, are protonated in the presence of hydrogen cations. The strong electrical repul-

sion prevents the metal cations to reach the complexation sites and will cause lower adsorption values. So, the lower adsorption efficiencies of pTCAs in strongly acidic media were expected. Surprisingly the removal efficiency increased at pH about 5 to 7 and decreased slightly at pH greater than 9. Maximum sorption efficiency in the pH range 5–7 for pTCA can be attributed to the more polarizable characteristics of chelating groups of pTCAs. In this regard, the larger flexible thiacalixamide macrocyclic units can form more effective complexes with metal cations, particularly the larger ones, such as Hg(II) and Pb(II). It is worthy to mention that metal cations may precipitate with hydroxide ions at higher pH (≥ 9) and therefore slightly decreases in the adsorption results were normal. Therefore, neutral conditions were preferred for heavy metal removal experiments.

3. 3. Thermal Stability

To explore the thermal stability of polythiacalixamides, thermal analyses including DSC and TGA were performed. The results, especially initial decomposition temperatures (IDTs) of pTCA A–D show that these polymers have considerable thermal stability. IDT data and other thermal properties such as T_g , T_{max} , char yields of the pTCAs A–D are also summarized in Table 6. The pTCAs showed glass transition temperatures (T_g), in the range of 157–178 °C by DSC, which are meaningful owing to such bulky pendant groups. The increasing order of T_g corresponds to the increase in the order of rigidity and polarity of the polymer backbones. The relatively higher T_g value (178 °C) of pTCA B may be a result of structural stiffness caused by interchain forces between naphthalene units which solidify the polymer backbone and help polymer packing. The more solidity and better packing means the larger rotation barrier and less flexibility. The thermal stability of polyamides was evaluated by TGA in nitrogen atmosphere. The Figure 2 inset depicts a typical set of TGA curves for polyamide pTCA A–D in nitrogen. The decomposition temperatures (T_d) at 10% weight loss in nitrogen atmosphere were taken from the original TGA thermograms and are summarized in Table 6. All the polythiacalixamides exhibited good thermal stability. As evident in Table 6, the 10% weight loss of pTCAs A–D was in the range of 337–346 °C. The amounts of carbonized residues, char yields, were in the range of 39.1–58.5 wt% at 700 °C in nitrogen. The high char yields of these polyamides can be attributed to their high aromatic content. To survey more on the thermal characteristics of these polymers and to see the effect of sulfur atom on the thermal stability, comparison with the previously prepared PCA³³ was performed. By considering the results mentioned in Table 6, the thermal stability parameters (e.g. IDTs) of the synthesized polythiacalixamides relative to that of reference polyamides show negligible differences between these two series of polyamides. Polythiacalix-

Table 6. Thermophysical properties of polythiacalixamides

Polymer	T_g^a	T_{ini}^b	$T_{10\%}^b$	T_{max}^c	char yield (wt %) ^d
pTCA A	160	276	337	385	58.5
pCA (CH ₂)	155	285	340	363	46
pTCA B	178	317	341	358	39.1
pCA (Naph.)	162	302	323	356	56.2
pTCA C	157	310	340	356	46.3
pCA (Azo)	157	312	353	369	49.9
pTCA D	161	324	346	354	32.9
pCA (Oxy)	152	328	352	368	47.8

degradability and having very low permissible limit (0.001 ppm) in drinking water, even trace amounts of Hg ions must be removed from aquatic systems. During last decades different methods have been developed to eliminate mercury in all forms involving elemental, inorganic and organic compounds. Different kinds of sorbents have been applied to meet this need and some of the recent and important sorbents are presented in Table 7. Most of them have some limitations, including temperature dependence, working pH range, time of contact etc. Herein, we introduce polythiacalix[4]amides as novel functionalized polyamides which have shown some promising applicability

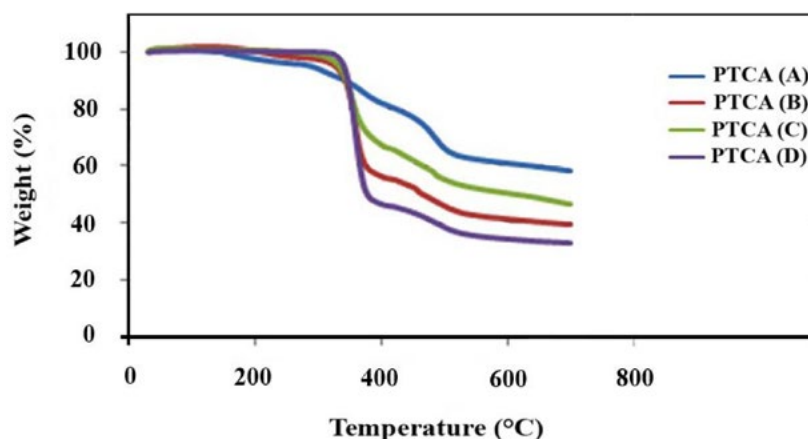


Fig. 2. TGA curves for polythiacalixamides pTCA A–D

amides showed slightly higher T_g values owing to unique features of sulfur atoms. Phenolic structures can rotate through the low energy barrier sulfur atoms to create different conformers prior to polymerization. So, as a result of low bulkiness of thiacalixarene, polythiacalixamides relative to polycalixamides with fixed methylene bridge groups and fixed cylindrical calixarene structures create lesser interchain cavity sizes and therefore more interchain forces will form. Thus, it is noteworthy to emphasize that polythiacalixamides due to the existence of polar coordinating sulfur atoms and adjustable conformers, represented high sorption capability, good solubility in industrial solvents and together with their significant thermal properties offer processability and applicability as a membrane.

3. 4. Overview on Mercury Removal

Contamination of the environment with mercury which is naturally occurring in the earth's crust and released with volcanic activity as well as industrial activities, such as the burning of fossil fuels, ore processing, medical and municipal waste incineration, and the use of dental amalgams is a serious concern. Because of the hazardous characteristic of mercury, such as its high toxicity, non-bio-

toward removal of some hazardous heavy metals, especially Hg(II) ions. As a result of acceptable thermal property and solubility as well as excellent sorption capability, pTCA can be employed in membrane technologies which focus on the reduction of mercury via recycling of Hg²⁺ from aqueous wastes and also reducing emissions from industrial activities.

3. 5. Antibacterial Evaluation

The *in vitro* antibacterial activity of the synthesized polythiacalixamides against clinical isolates of Gram positive and Gram negative pathogens, such as *Escherichia coli* (ATCC 25922), *Staphylococcus aureus* (ATCC 25923), *Klebsiella pneumoniae* (NCTC 5056), *Pseudomonas aeruginosa* (1561) and *Bacillus subtilis* 1715 (PY79) bacterial strains was tested and compared with penicillin, ciprofloxacin and gentamicin as reference antibacterials. In these experiments, minimum inhibitory concentrations (MICs) and minimum bactericidal concentration (MBCs) were determined and their activities were interrelated by the known antibiotics penicillin, ciprofloxacin and gentamicin applied as known standards. The evaluation of the antibacterial properties demonstrated that the polymers showed acceptable inhibition capabilities at different levels which

Table 7. Comparison of sorption efficiency of pTCA A with some of those reported in removal of mercury ions (Hg²⁺)

Entry	Absorbents	Quantity of sorbent	Concentration of Hg ²⁺	Time	Sorption capability (%)	Ref
1	FeS ₂ (Pyrite), N ₂ atmosphere	2 g/L	2 mg L ⁻¹	(pH:4.1) 7 d (pH:6.4) 2 d (pH:10.4) 2 h	95	[48]
2	Aluminum electrode (electrocoagulation method)	4 cm × 1 cm	2 × 10 ⁻⁵ M	(pH 7) 15 min	99.85	[49]
3	Iron electrode (electrocoagulation method)	4 cm × 0.8 cm	2 × 10 ⁻⁵ M	(pH 7) 15 min	99.95	[50]
4	Thiacrown polymer	20 mg/5 mL	4–200 mg L ⁻¹	(pH 1.5 to 6.2) 30 min	>95	[51]
5	Bamboo leaf powder	4 g L ⁻¹	100 mg L ⁻¹	(pH ≈7) 60 min	80	[52]
6	Activated carbon prepared from <i>C. pentandra</i> hulls	200 mg/50 mL	40 mg L ⁻¹	(pH 6.0) 90 min	99.7	[48]
7	Activated carbon prepared from <i>P. aureus</i> hulls	225 mg/50 mL	40 mg L ⁻¹	(pH 7.0) 100 min	98	[48]
8	Activated carbon prepared from <i>C. arietinum</i> waste	300 mg/50 mL	40 mg L ⁻¹	(pH 7.0) 110 min	96.29	[48]
9	Thio chelating resin (GMA–DVB)	100 mg/100 mL	5 × 10 ⁻³ M	(pH 5.8) 80 min	≈100	[53]
10	Thiol chelating resin (polystyrene)	100 mg/20 mL	400 mg L ⁻¹	(pH 1.5) 8 h	≈100	[54]
11	Bayberry tannin-immobilized collagen fiber	100 mg/100 mL	200.0 mg L ⁻¹	(pH 7.0) 24 h	98.34	[55]
12	Hydrous manganese oxide	100 mg/10 mL	1.0 × 10 ⁻⁸ mol L ⁻¹	(pH 2.2) 30 min	96.1	[56]
13	Hydrous tin oxide	100 mg/10 mL	1.0 × 10 ⁻⁸ mol L ⁻¹	(pH 2.2) 60 min	93.1	[56]
14	Hydrous ferric oxide	100 mg/10 mL	1.0 × 10 ⁻⁵ mol L ⁻¹	(pH 8.68) 65 min	62	[57]
15	Hydrous tungsten oxide	100 mg/10 mL	1.0 × 10 ⁻⁵ mol L ⁻¹	(pH 4.42) 95 min	93.5	[58]
16	Carbonaceous sorbent from rice husk	75 mg/100 mL	200 mg L ⁻¹	(pH 6) 120 h	>90	[59]
17	Chitosan-coated cotton fibers	100 mg/25 mL	0.008 mol L ⁻¹	(pH 5) 20 h	≈99	[60]
18	Manganese dioxide nano-whiskers	10 mg/100 mL	10 mg L ⁻¹	(pH 5.5) 1 h	≈99	[60]
19	Poly(acrylic acid) modified seed gum	100 mg/20 mL	100 mg L ⁻¹	(pH 6) 4 h	92.36	[61]
20	<i>Polythiacalix[4]amides</i>	25 mg/10 mL	10 × 10⁻³ M	(pH 7) 3h	93.2	-

was necessary for being incorporated in food and medical industries. The MIC was the lowest concentration with no visible growth. The growth of bacteria was observed in the cells with lower concentrations than MIC. The solutions with no visible growth were then spread on agar plates and incubated at 37 °C for 24 h to obtain MBC values.

The good activity can be attributed to the presence of pharmacologically active thiacalixarenes which are constituent part of the polymeric backbone. Also this result can probably be ascribed to the high-value nucleophilic characteristics of sulfur atoms which could modify the electronic density in the polymeric chains and thereby in-

fluence the absorption, distribution and metabolism of the bioactive molecules.

The mentioned antibiotics were evaluated for their antibacterial activity against standard bacteria strains according to table CLSI (2011). Results are presented in Table 8. As can be seen, all of the standard samples were very sensitive against ciprofloxacin antibiotic. The lowest MIC was recorded for *E. coli* which was about 0.015 µg/mL. However, *B. subtilis* and *S. aureus* were sensitive toward gentamicine and penicillin antibiotics according to antimicrobial measurements data given in Table 8. The MBC results show that examined antibiotics were so much effective toward the

Table 8. Comparison of *in vitro* antibacterial activities of the synthesized polymers, monomers and known antibiotics after 24–48 h, conc. µg/mL

Bacteria Polymer	Gram negative				Gram positive					
	<i>Escherichia coli</i>		<i>Pseudomonas aeruginosa</i>		<i>Klebsiella pneumoniae</i>		<i>Bacillus subtilis</i>		<i>Staphylococcus aureus</i>	
	MIC	MBC	MIC	MBC	MIC	MBC	MIC	MBC	MIC	MBC
pTCA A	125	250	250	>250	250	>250	31.2	125	62.5	125
pTCA B	187.5	375	>375	–	187.5	>375	375	>375	375	>375
pTCA C	>250	–	>250	–	>250	–	>250	–	250	>250
Penicillin	8	>8	>8	–	>8	–	0.125	0.5	0.062	0.125
Ciprofloxacin	0.015	0.062	0.062	0.125	0.031	0.062	0.031	0.125	0.031	0.062
Gentamicin	4	8	>128	–	>128	–	4	8	0.5	1

mentioned microorganisms. Antibacterial experiments indicated that these polymers have displayed some reliable bactericidal efficiency in high concentrations. On the other hand, *in vitro* antibacterial assay of the synthesized poly-calixamides A–C exhibited acceptable activities against all Gram positive and Gram negative strains tested. pTCA D was removed from these experiments due to its low solubility which was necessary for micro dilution procedure. Even though the synthesized pTCA A–D were not in the range of the known commercial antibiotics mentioned above, we can still achieve some antibacterial applicability with using these polymers in the next generation of industrial food and medical appliances or in coating equipments which need high thermal stability, acceptable solubility for processing, and reliable antimicrobial characteristic at the same time.

4. Conclusions

In macromolecular science it has been proved that calixarene-based ionophores have great acceptability in modern chemistry because of their extreme capability in functionalization from bridge position up to the rims. Therefore, we have taken the advantage of these structures for preparation of ion-selective as well as antibacterial polymers to suggest novel formulations for producing antibacterial membranes. Hence, the main goal of this work is to achieve polyamides with potential great sorption capability which could be applied in polymeric sorbents and membranes. Moreover, preparation of antibacterial polyamides which have both antibacterial characteristics and also high temperature bearing capacity was the other goal of this study. So, these ambitions were accomplished by incorporation of thiacalixarene moiety into the polyamide chains via polycondensation of thiacalixarene dicarboxylic acid with commercial diamines. The performed experiments demonstrated the characteristic features, such as solubility in organic solvents, photophysical behavior, thermal stability and sorption capabilities of polythiacalixamides, besides their reliable and valuable antibacterial properties. Among them, high extraction efficiencies toward Hg^{2+} , Pb^{2+} , Cd^{2+} and Co^{2+} was exceptional and they seem to be good choices for additional sorption studies in

the future. These polyamides bearing unique structure of thiacalixarene with precisely oriented amide functionality and sulfur atoms, provide excellent complexation site for the cations and of course for interaction with cell walls of Gram positive and negative pathogens. Moreover, their intrinsic thermal stability and favorable solubility makes them potentially applicable for advanced industrial purposes and in fabricating medical appliances.

5. Acknowledgments

The financial supports by Babol University of medical sciences as well as Research Council of Mazandaran University are gratefully acknowledged. Also we should appreciate Fariba Asgharpour (M.Sc.) for helping us in the evaluation of antibacterial characteristics.

6. References

- J. Luo, Y. S. Zheng, *Curr. Org. Chem.* **2017**, *16*, 483–506. DOI:10.2174/138527212799499813
- K. Gloe, *Macrocyclic chemistry (Current trends and future perspectives)*, Kluwer Academic Publishers, Dordrecht, **2005**.
- W. Walkowiak, C.A. Kozłowski, *Desalination* **2009**, *240*, 186–197. DOI:10.1016/j.desal.2007.12.041
- J. W. Steed, J. L. Atwood, *Supramolecular Chemistry*, second ed. Wiley, New York, **2009**. DOI:10.1002/9780470740880
- O. H. Rubio, R. Taouil, F. M. Muñiz, L. M. Monleón, L. Simón, F. Sanz, J. R. Morán, *Org. Biomol. Chem.* **2017**, *15*, 477–485. DOI:10.1039/C6OB02237E
- S.B. Maamar, N. Jadambaa, F. Vocanson, F. Meganem, C. Felix, I. Dumazet-Bonnamour, *J. Supramol. Chem.* **2009**, *21*, 450–454. DOI:10.1080/10610270802195586
- S. Sayin, F. Ozcan, M. Yilmaz, *Desalination* **2010**, *262*, 99–105. DOI:10.1016/j.desal.2010.05.053
- R. Ebdelli, A. Rouis, J. Davenas, I. Bonnamour, H. Ben Ouada, *Sensor Lett.* **2011**, *9*, 2241–2244. DOI:10.1166/sl.2011.1779
- S. Sayin, M. Yilmaz, *Desalination* **2011**, *276*, 328–335. DOI:10.1016/j.desal.2011.03.073
- I. Akin, S. Erdemir, M. Yilmaz, M. Ersoz, *J. Hazard. Mat.* **2012**, *223–224*, 24–30. DOI:10.1016/j.jhazmat.2012.03.043

11. J. W. Steed, P.A. Gale, *Supramolecular chemistry: from molecules to nanomaterials*, John Wiley & Sons, Ltd. New York, **2012**.
12. S. M. Baghbanian, Y. Babajani, H. Tashakkorian, S. Khaksar, M. Farhang, *C. R. Chim.* **2013**, *16*, 129–134.
DOI:10.1016/j.crci.2012.10.014
13. M. M. Lakouraj, H. Tashakkorian, M. Rouhi, *Chem. Sci. Trans.* **2013**, *2*, 739–748.
14. B. Genorio, *Acta Chim. Slov.* **2016**, *63*, 496–508.
DOI:10.17344/acsi.2016.2289
15. Z. D. Ghezelbash, K. A. Dilmaghani, *Acta Chim. Slov.* **2016**, *63*, 790–797.
16. M. D. Shah, Y. K. Agrawal. Calixarene: A new architecture in the pharmaceuticals, *J. Sci. Indust. Res.* **2012**, *71*, 21–26.
17. D. Reinhoudt, *Supramol. Chem.* **2016**, *28*, 342–350.
DOI:10.1080/10610278.2015.1109326
18. S. L. Debbert, B. D. Hohand, D. J. Dulak, *J. Chem. Educ.* **2016**, *93*, 372–375. DOI:10.1021/acs.jchemed.5b00641
19. F. Zhang, Y. Sun, D. Tian, W. S. Shin, J. S. Kim, H. Li, *Chem. Commun.* **2016**, *52*, 12685–12693.
DOI:10.1039/C6CC05876K
20. R. Lamartine, C. Bavoux, F. Vocanson, A. Martin, G. Senlis, M. Perrin, *Tetrahedron Lett.* **2001**, *42*, 1021–1024.
DOI:10.1016/S0040-4039(00)02131-6
21. S. Bouhroum, F. Arnaud-Neu, Z. Asfari, J. Vicens, *J. Supramol. Chem.* **2005**, *17*, 629–635.
DOI:10.1080/10610270500211693
22. Y. K. Agrawal, J. P. Pancholi, *Ind. J. Chem.* **2007**, *46A*, 1373–1382.
23. A. Zaghbani, R. Tayeb, M. Dhahbi, M. Hidalgo, F. Vocanson, I. Bonnamour, P. Seta, C. Fontàs, *Sep. Purif. Technol.* **2007**, *57*, 374–379. DOI:10.1016/j.seppur.2007.03.025
24. Y. Li, X. Hu, X. Song, T. Sun, *Environ. Poll.* **2012**, *167*, 93–100.
DOI:10.1016/j.envpol.2012.03.042
25. A. Akdoğan, M. Deniz, S. Cebecioglu, A. Sen, H. Deligöz, *Sep. Sci. Technol.* **2002**, *37*, 973–980. DOI:10.1081/SS-120002226
26. E. A. Shokova, V. V. Kovalev, *Russ. J. Org. Chem.* **2002**, *39*, 1–28. DOI:10.1023/A:1023416409935
27. H. Deligöz, *J. Incl. Phenom.* **2006**, *55*, 197.
DOI:10.1007/s10847-006-9096-z
28. M. H. Patel, V. B. Patel, P. S. Shrivastav, *Tetrahedron* **2008**, *64*, 2057–2062. DOI:10.1016/j.tet.2007.12.048
29. M. Tabakci, M. Yilmaz, *Bioresour. Technol.* **2008**, *99*, 6642–6655. DOI:10.1016/j.biortech.2007.11.066
30. H. Deligöz, S. Memon, *Pak. J. Anal. Environ. Chem.* **2011**, *12*, 1–24.
31. B. Dizman, M. O. Elasri, L. J. Mathias, *J. Appl. Polym. Sci.* **2004**, *94*, 635–642. DOI:10.1002/app.20872
32. G. Thenmozhi, D. Jaya Kumar, M. Gopalswamy, R. Jaya Santhi, *Pharma. Chem.* **2011**, *3(6)*, 325–333.
33. M. M. Lakouraj, H. Tashakkorian, *J. Macromol. Sci. Part A*, **2012**, *49*, 806–813. DOI:10.1080/10601325.2012.714318
34. M. M. Lakouraj, H. Tashakkorian, *J. Macromol. Sci. Part A*, **2013**, *50*, 310–320. DOI:10.1080/10601325.2013.755859
35. M. M. Lakouraj, H. Tashakkorian, *J. Supramol. Chem.* **2013**, *25*, 221–232. DOI:10.1080/10610278.2012.758366
36. V. Hasantabar, M. M. Lakouraj, H. Tashakkorian, M. Rouhi, *Des. Monomers Polym.* **2016**, *19*, 607–618.
DOI:10.1080/15685551.2016.1187440
37. D. D. Perrin, W. L. F. Armarego, *Purification of laboratory chemicals*, Pergamon Press, Oxford, UK, **1988**.
38. H. Kumagai, M. Hasegawa, S. Miyanari, Y. Sugawa, Y. Sato, T. Hori, S. Ueda, H. Kamiyama, S. Miyano, *Tetrahedron Lett.* **1997**, *38*, 3971–3972. DOI:10.1016/S0040-4039(97)00792-2
39. T. Sone, Y. Ohba, K. Moriya, H. Kumada, K. Ito, *Tetrahedron* **1997**, *53*, 10689–10698.
DOI:10.1016/S0040-4020(97)00700-X
40. B. Masci, Z. Asfari, V. Böhmer, J. Harrowfield, J. Vicens, *Calixarenes 2001*, Kluwer Academic Publishers, Dordrecht, Netherlands, **2001**, 235–249.
41. C. R. Mahon, D. C. Lehman, G. Jr. Manuselis, *Textbook of diagnostic microbiology*, Elsevier Health Sciences, London, **2014**.
42. A. F. Danil De Namor, W.B. Aparicio-Aragon, M. T. Goitia, A. R. Casal, *J. Supramol. Chem.* **2004**, *16*, 423–433.
DOI:10.1080/10610270410001721944
43. V. Arora, H. M. Chawla, S. P. Singh, *Arkivoc* **2007**, (ii), 172–200.
44. I. I. Abbas, J. K. Chaaban, *J. Supramol. Chem.* **2012**, *24*, 213–219. DOI:10.1080/10610278.2011.643795
45. C. Wieser, C. B. Dieleman, D. Matt, *Coord. Chem. Rev.* **1997**, *165*, 93–161. DOI:10.1016/S0010-8545(97)90153-3
46. C. D. Gutsche, *Calixarenes revisited*, Royal Society of Chemistry, Cambridge, **1998**.
47. D. M. Roundhill, H. F. Koch, *Chem. Soc. Rev.* **2002**, *31*, 60–67.
DOI:10.1039/b003141k
48. M. M. Rao, Reddy D. H. K. Kumar, P. Venkateswarlu, K. Seshaiah, *J. Environ. Manage.* **2009**, *90*, 634–643.
DOI:10.1016/j.jenvman.2007.12.019
49. J. Bower, K. S. Savage, B. Weinman, M. O. Barnett, W. P. Hamilton, W. F. Harper, *Environ. Pollut.* **2008**, *156*, 504–514.
DOI:10.1016/j.envpol.2008.01.011
50. C. P. Nansu-Njiki, S. R. Tchamango, P. C. Ngom, A. Darchen, E. Ngameni, electrodes, *J. Hazard. Mat.* **2009**, *168*, 1430–1436. DOI:10.1016/j.jhazmat.2009.03.042
51. T. F. Baumann, J. G. Reynolds, G. A. Fox, *React. Funct. Polym.* **2000**, *44*, 111–120.
DOI:10.1016/S1381-5148(99)00085-1
52. D. K. Mondal, B. K. Nandi, M. K. Purkait, *J. Environ. Chem. Eng.* **2013**, *1*, 891–898. DOI:10.1016/j.jece.2013.07.034
53. A. A. Atia, A. M. Donia, A. M. Yousif, *React. Funct. Polym.* **2003**, *56*, 75–82. DOI:10.1016/S1381-5148(03)00046-4
54. L. Joseph, V. N. S. Pillai, *Environ. Pollut.* **1987**, *48*, 213–222.
DOI:10.1016/0269-7491(87)90035-2
55. X. Huang, X. Liao, B. Shi, *J. Hazard. Mat.* **2009**, *170*, 1141–1148. DOI:10.1016/j.jhazmat.2009.05.086
56. S. P. Mishra, S. S. Dubey, D. Tiwari, *J. Colloid Interface Sci.* **2004**, *279*, 61–67.
57. S. P. Mishra, (Miss) Vijaya, *J. Colloid Interface Sci.* **2006**, *296*, 383–388. DOI:10.1016/j.jcis.2005.11.040
58. E. I. El-Shafey, *J. Hazard. Mat.* **2010**, *175*, 319–327.
DOI:10.1016/j.jhazmat.2009.10.006
59. R. Qu, C. Sun, F. Ma, Y. Zhang, C. Ji, Q. Xu, C. Wang, H. Chen,

J. Hazard. Mat. **2009**, 167, 717–727.

DOI:10.1016/j.jhazmat.2009.01.043

60. K. P. Lisha, S. M. Maliyekkal, T. Pradeep, *Chem. Eng. J.* **2010**,

160, 432–439. DOI:10.1016/j.cej.2010.03.031

61. V. Singh, S. K. Singh, S. Maurya, *Chem. Eng. J.* **2010**, 160, 129–137. DOI:10.1016/j.cej.2010.03.020

Povzetek

Politiakaliks[4]amidi so nova kategorija poliamidov z velikimi sorpcijskimi sposobnostmi za nekatere okoljsko nevarne kovinske ione, zlasti Hg^{2+} . Pripravili smo jih s pomočjo direktne sinteze s polikondenzacijskim protokolom z uporabo tiakaliks[4]aren dikarboksilne kisline in komercialnih diaminov. Poliamide, ki so nastali na ta način, smo izolirali z visokimi izkoristki; njihove viskoznosti so bile v območju 0.55–0.75 dl/g. Fotofizične lastnosti smo določili z merjenjem valovne dolžine z maksimalno absorpcijo za vsak polimer s pomočjo UV absorpcijske spektroskopije. Termogravimetrične analize so pokazale visoko termično stabilnost teh poliamidov v območju od 337 do 346 °C, kjer je prišlo do 10 % izgube mase; izkoristki oglja na koncu so bili pri 600 °C 32.9–58.5 %. Temperature steklastega prehoda so bile med 157 in 178 °C. Da bi raziskali možne sorpcijske lastnosti teh politiakaliksamidov, smo iz odpadnih voda izvedli ekstrakcijo trdno–tekoče nekaterih strupenih ionov kovin prehoda, kot so Cu^{2+} , Co^{2+} , Cd^{2+} , Pb^{2+} in Hg^{2+} . Antibakterijske študije smo izvedli z Gram pozitivnimi in Gram negativnimi bakterijami ter dobili nekatere obetajoče rezultate, ki kažejo na možnost uporabe teh politiakaliksamidov kot sestavin za industrijske antibakterijske membrane.

Spectroscopic, Structural and Density Functional Theory (DFT) Studies of Two Oxazol-5-one Derivatives

İbrahim Hanif Nazlı,¹ Duygu Barut Celepci,^{2,*} Gül Yakalı,³
Derya Topkaya,⁴ Muhittin Aygün² and Serap Alp⁴

¹ Dokuz Eylül University, Graduate School of Natural and Applied Science, Izmir, TURKEY

² Dokuz Eylül University, Faculty of Science, Department of Physics, Izmir, TURKEY

³ Akdeniz University, Serik Gülsün-Süleyman Süral Vocational School of Higher Education,
Department of Opticianry Program, Antalya, TURKEY

⁴ Dokuz Eylül University, Faculty of Science, Department of Chemistry, Izmir, TURKEY

* Corresponding author: E-mail: duygu.barut@deu.edu.tr

Received: 06-06-2017

Abstract

In this study, two oxazol-5-one derivatives, C₂₀H₂₀N₂O₂ (1) and C₂₁H₂₂N₂O₂ (2), were synthesized by getting condensed *p*-*N,N*-diethylaminobenzaldehyde with two presented hippuric acid derivatives and in further studies they were analysed spectrochemically. Molecular and crystal structures of the compounds were determined by single-crystal X-ray diffraction and the results revealed that the molecular packing of the crystal structures were stabilized by weak intra- and intermolecular interactions also with C–O⋯π, C–H⋯π and π⋯π stacking interactions. Computational studies were also performed using DFT method at B3LYP/6-311G(d,p) level of theory. Vibrational modes and chemical shifts were calculated and compared with the experimental data. In addition, frontier molecular orbitals and molecular electrostatic potential surfaces were simulated. The calculated results show that the optimized geometries can well reproduce the crystal structure. Purpose of this study was to survey the effects of the reactants, which were condensed with each other to produce oxazol-5-one, upon the characteristic properties and crystal forms of the final oxazol-5-one.

Keywords: Oxazol-5-one, Crystal structure, DFT, Frontier molecular orbitals

1. Introduction

Variety of amino acids and of course peptides can be synthetically obtained from glycine with the classical Erlenmeyer–Plöchl azlactone synthesis.^{1–5} Due to the five-membered heterocyclic core, oxazol-5-ones are biologically active molecules and widely used in biomedical applications.^{6–9} Oxazol-5-ones have found important roles as drugs, enzyme inhibitors and fluorescent sensors.^{7–10} Oxazol-5-ones are also used in dye industry owing to the fact that oxazol-5-ones are easily obtainable in crystalline states and they possess promising photochemical/photophysical properties due to their chromophore group.^{10,11} Herein, we report on the synthesis, spectral characterization and theoretical studies of two oxazol-5-one derivatives. The experimental FT-IR, ¹H NMR, ¹³C NMR studies were performed. Structures of the compounds were confirmed by single-crystal X-ray diffraction studies. Theoretical cal-

culations were also carried out in order to corroborate the experimental results.

1. 1. Synthesis of Oxazol-5-one

Generally oxazol-5-ones are synthesized by Erlenmeyer–Plöchl azlactone reaction. Hippuric acid (*N*-benzoylglycine) derivatives turn into 2-aryloxazol-5-ones in the presence of acetic anhydride as the reaction media, besides the addition of sodium acetate, acetic anhydride and aromatic aldehydes they condense into 2-aryl-4-arylmethylene-oxazol-5-ones which are known as unsaturated azlactones.

2. Materials and Methods

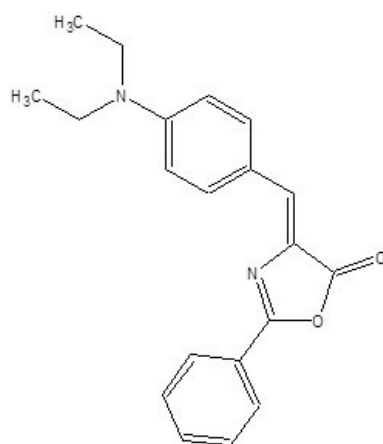
Some reagents (toluene, ethanol, ethyl acetate, sodium acetate, *p*-*N,N*-diethylaminobenzaldehyde) were obtained

from commercial sources and used without further purification, acetic anhydride was purified by distillation, hippuric acid derivatives were synthesised and used after purification.

2. 1. Analytical Instruments and Spectroscopy Techniques

Melting points were determined by Barnstead Electrothermal 9,100 instrument. FT-IR spectra were recorded by Perkin-Elmer Spectrum BX FTIR spectrometer using KBr pellets. NMR data were measured by Varian 3.2 400 MHz spectrometer in CDCl₃ solutions and chemical shifts were expressed in ppm downfield from tetramethylsilane.

2. 2. Synthesis

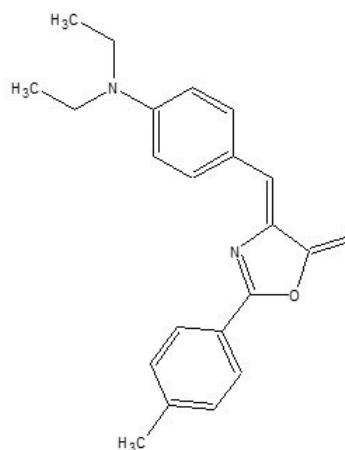


Scheme 1. Chemical diagrams of the compounds 1 and 2.

rs at 100 °C and stirred at room temperature overnight. 3 mL of ethanol was added to cooled oily-solid like mixture and was put into fridge for 2–3 hours. Precipitate was filtered, washed with ethanol, and recrystallized from toluene. Determined melting point of 2 is 153.9 °C.

2. 3. X-Ray Crystallography

Single crystal X-ray diffraction data of (4Z)-4-(*p*-*N,N*-diethylaminophenylmethylene)-2-phenyloxazol-5-one (1) and (4Z)-4-(*p*-*N,N*-diethylaminophenylmethylene)-2-(*p*-tolyl)oxazol-5-one (2) were collected at room temperature on an Rigaku-Oxford Xcalibur diffractometer with an Eos-CCD detector using graphite-monochromated Mo-K α radiation ($\lambda = 0.71073 \text{ \AA}$). Data col-



2. 2. 1. Synthesis of 4-(*p*-*N,N*-Diethylaminophenylmethylene)-2-phenyloxazol-5-one (1)

2.82 mmol *p*-*N,N*-diethylaminobenzaldehyde, 2.82 mmol *N*-benzoylglycine (hippuric acid) and 2.82 mmol sodium acetate was added to 3 mL of redistilled acetic anhydride. Reaction mixture was stirred under dry conditions for 4–5 hours at 100 °C, thereafter stirred at room temperature overnight. 3 mL of ethanol was added to cooled oily-solid like mixture and left in refrigerator for 2–3 hours. Precipitation occurred so that mixture was filtered, solid obtained washed with ethanol and recrystallized from hexane–ethyl acetate solution. Determined melting point of 1 is 134.5 °C.

2. 2. 2. Synthesis of 4-(*p*-*N,N*-Diethylaminophenylmethylene)-2-(*p*-tolyl)oxazol-5-one (2)

p-*N,N*-Diethylaminobenzaldehyde (5.18 mmol), *p*-toluoylglycine (5.18 mmol) and sodium acetate (5.18 mmol) was added to 4 mL of redistilled acetic anhydride. Reaction mixture was stirred under desiccant for 4–5 hou-

lections and reductions along with absorption corrections were performed using CrysAlis^{Pro} software package.¹² Structure solutions were performed using SHELXT embedded in the Olex2.^{13,14} Refinement of coordinates and anisotropic thermal parameters of non-hydrogen atoms were carried out by the full-matrix least-squares method in SHELXL.¹⁵ All hydrogen atoms of both compounds were placed in geometrically idealized positions (C–H = 0.93–0.96–0.97 Å). The details of the crystal data, data collection and structure refinement of the compounds are summarized in Table 1.

2. 4. Computational Details

The synthesized compounds 1 and 2 have been optimized at DFT/B3LYP method, using 6-311G(d,p) basis set. Also, the harmonic vibrational frequencies and NMR spectra were calculated at the same levels of theory for the optimized structures. The calculated frequencies were scaled down by using single scaling factor 0.9669 for DFT/B3LYP/6-311G(d,p) level, in order to improve the agreement with the experimental values.¹⁶ The ¹H and ¹³C iso-

Table 1. Crystal data and structure refinement parameters for the compounds **1** and **2**.

	1	2
Empirical formula	C ₂₀ H ₂₀ N ₂ O ₂	C ₂₁ H ₂₂ N ₂ O ₂
Formula weight	320.38	334.41
Temperature (K)	294 (2)	294 (2)
Crystal system / space group	Triclinic / <i>P</i> -1	Triclinic / <i>P</i> -1
<i>Unit cell dimensions</i>		
<i>a</i> (Å)	7.5779(7)	7.8711(6)
<i>b</i> (Å)	10.6860(11)	11.0322(9)
<i>c</i> (Å)	11.1813(9)	11.1509(8)
α (°)	108.647(9)	108.341(7)
β (°)	96.641(7)	99.513(6)
γ (°)	93.094(8)	90.893(7)
Volume (Å ³)	848.16(14)	904.10(13)
<i>Z</i> / <i>D</i> _{calc} (mg m ⁻³)	2 / 1.254	2 / 1.228
Absorption coefficient (mm ⁻¹)	0.082	0.080
<i>F</i> (000)	340	356
Reflections collected / unique	4592 / 3197 [R _{int} = 0.0187]	4692 / 3420 [R _{int} = 0.0196]
Data / restraints / parameters	3197 / 0 / 219	3420 / 0 / 229
Goodness of fit on <i>F</i> ²	1.022	1.028
Final <i>R</i> indices [<i>I</i> > 2σ(<i>I</i>)]	R ₁ = 0.0495, wR ₂ = 0.1030	R ₁ = 0.0486, wR ₂ = 0.1092
<i>R</i> indices (all data)	R ₁ = 0.0782, wR ₂ = 0.1193	R ₁ = 0.0733, wR ₂ = 0.1238
Largest difference peak and hole (eÅ ⁻³)	0.145 / -0.172	0.164 / -0.179

tropic shielding tensors referenced to the TMS calculations were performed by using gauge invariant atomic orbital (GIAO) method in chloroform solvent.¹⁷ Highest occupied molecular orbital (HOMO), lowest unoccupied molecular orbital (LUMO) and MEP have been calculated from optimized geometry of the molecules. All calculations were carried out with the Gaussian 09W and Gauss View molecular visualization program.^{18,19}

3. Results and Discussions

3.1. Crystal Structure

The atomic numbering scheme of the crystal structures and the optimized geometries which has the most favourable conformation of the compound **1** and **2** are shown in Figures 1a and b. Molecules crystallize in triclinic system with *P*-1 space group. Selected bond distances, bond angles and torsion angles together with corresponding values obtained by means of X-ray crystallographic analysis and DFT calculations are compared and listed in Table 2.

The structures of the title compounds comprise of a *p*-*N,N*-diethylaminophenylmethylene fragment bridged by the methine C4 atom and an oxazol-5-one ring, linked to the phenyl ring in compound **1**, whereas the *p*-tolyl moiety in **2**. The oxazol-5-one rings are almost planar for both compounds, with a r.m.s. deviation of -0.006(2) Å for **1** and 0.004(1) Å for **2**. Phenyl rings are twisted slightly out of these planes, with the dihedral angles between two rings being 12.80(2)^o and 6.41(2)^o, respectively. Similarly, there is a twist between the *p*-*N,N*-diethylaminophenyl moiety

and oxazol-5-one ring [dihedral angles are 18.89(2)^o and 17.71(2)^o; C4/C5/C10/C9 torsion angles are -175.68(1)^o and 173.58(1)^o, respectively], that are linked through the C3=C4 double bonds. The olefinic C3=C4 double bond lengths [1.347(1) Å for **1** and 1.354(1) Å for **2**] are slightly longer than the formal C=C bond, but mostly consistent with double bonds in similar studies.^{20–23} The molecules adopt a *Z* conformation about these olefinic bonds with C5 *cis* to N1. C2=O2 bond distances are also shown to have a typical double bond character with lengths of 1.196(1) Å and 1.201(1) Å, respectively.²⁴ The C3–C4–C5 angles are 129.90(1)^o and 129.62(1)^o, respectively, being quite large. These angle values and the exocyclic angles of C3 and C5 (Table 2) are in accordance with the repulsive intramolecular interactions between the N1 and H10 atoms, similar to the oxazol-5-one derivatives reported previously.^{25–27} Bond lengths, angles and torsion angles of **1** and **2** are comparable with the similar compounds, especially for the oxazol-5-one rings, O1–C2–O2 exocyclic bond angles and N1/C3/C4/C5 torsion angles. Except the torsion angles, the bond parameters are comparable with the other oxazol-5-one derivatives.^{28–32} N1/C3/C4/C5 torsion angles [-7.78(1) Å for **1** and 8.39(1) Å for **2**] are slightly different. Also, as can be seen from the results, there is a good correlation between the experimental and theoretical data. The observed differences can be attributed to the fact that while the theoretical calculations are made for an isolated molecule in the gas phase, the experimental results obtained are those of the molecules in the solid state.

In the compound **1**, there are only weak C–H...O intermolecular interactions and C–H...N intramolecular interactions. In addition, there are strong C–O...π interacti-

ons [Cg3: C15-C20; O...Cg3: 3.786(4) Å; symmetry code (ii): $-x, 2-y, 1-z$], two strong $\pi\cdots\pi$ interactions with 3.34(2) Å distance between the centroids Cg1...Cg1 and 3.85(2) Å distance between the centroids Cg1...Cg3 [Cg1:O1/C1/N1/C3/C2; Cg1...Cg1 symmetry code (iii): $1-x, 2-y, 1-z$; Cg1...Cg3 symmetry code (iv): $-x, 2-y, 1-z$]. The compound **1** consists of a dimeric arrangement of molecules around an inversion centre formed via a C-H...O intermolecular hydrogen bond linking the molecules along the *a* axis

(Figure 2). This centrosymmetric hydrogen-bonded dimers are formed with an (22) ring motif.³³

Molecular packing in the crystal structure of the compound **2** was determined by the weak intramolecular C-H...N and C-H...O interactions, C-H... π stacking interactions and van der Waals forces. Molecules are linked to each other through the C-H... π interaction between the methyl H21C atom and *p*-*N,N*-diethylaminophenyl moiety of the adjacent molecule with C21-H21C...Cg2^v

Table 2. Selected interatomic distances (Å), angles and torsion angles (°) for the compounds **1** and **2** as observed experimentally and as calculated using DFT/ B3LYP/6-311G(d,p) method.

Compound	1		2	
	Experimental	Calculated	Experimental	Calculated
Bond Lengths				
C1–O1	1.374(1)	1.372	1.382(1)	1.374
C2–O1	1.394(1)	1.413	1.396(1)	1.412
C2–O2	1.196(1)	1.197	1.201(1)	1.197
C1–N1	1.280(1)	1.291	1.287(1)	1.292
C3–N1	1.398(1)	1.396	1.400(1)	1.396
N2–C8	1.357(1)	1.376	1.364(1)	1.377
N2–C11	1.452(1)	1.463	1.459(1)	1.462
N2–C13	1.453(1)	1.462	1.456(1)	1.462
C3–C4	1.347(1)	1.362	1.354(1)	1.361
C4–C5	1.430(1)	1.436	1.437(1)	1.437
Bond Angles				
C1–N1–C3	105.55(1)	105.80	105.63(1)	105.811
N1–C3–C2	108.31(1)	108.66	108.31(1)	108.658
N1–C3–C4	128.16(1)	129.20	128.50(1)	129.238
N1–C1–O1	115.85(1)	115.79	115.73(1)	115.757
N1–C1–C15	127.22(1)	127.14	127.26(1)	127.192
C1–O1–C2	105.46(1)	105.92	105.44(1)	105.940
O1–C2–O2	121.31(1)	122.10	121.44(1)	122.107
O1–C2–C3	104.80(1)	103.80	104.87(1)	103.834
O2–C2–C3	133.88(1)	134.1	133.67(1)	134.059
O1–C1–C15	116.88(2)	117.07	117.00(1)	117.051
C8–N2–C11	121.38(1)	121.87	121.44(1)	121.853
C8–N2–C13	122.41(1)	121.95	121.71(1)	121.971
C11–N2–C13	116.15(1)	116.17	116.78(1)	116.174
N2–C8–C7	121.74(1)	121.66	121.67(1)	121.667
N2–C8–C9	122.00(1)	121.62	121.93(1)	121.634
N2–C11–C12	113.15(1)	113.97	113.39(1)	113.942
N2–C13–C14	112.40(1)	121.87	112.55(1)	113.968
C3–C4–C5	129.90(1)	130.33	129.62(1)	130.302
C4–C5–C10	123.78(1)	124.22	124.01(1)	124.257
Torsion Angles				
O1–C1–C15–C16	-11.87(1)	-0.56(2)	6.57(1)	0.460
N1–C1–C15–C16	170.39(1)	179.46	-174.42(1)	-179.530
N1–C1–C15–C20	-10.81(1)	-0.55	5.57(1)	0.566
N1–C3–C4–C5	-7.78(1)	-0.18	8.39(1)	0.167
C3–C4–C5–C6	170.69(1)	179.70	-174.73(1)	-179.798
C4–C5–C10–C9	-175.68(1)	-179.90	173.58(1)	179.919
O2–C2–C3–C4	-0.94(1)	0.015	0.83(1)	-0.053
C7–C8–N2–C11	7.01(1)	-5.70	-6.36(1)	5.335
C9–C8–N2–C13	4.42(1)	-5.64	-3.62(1)	5.812

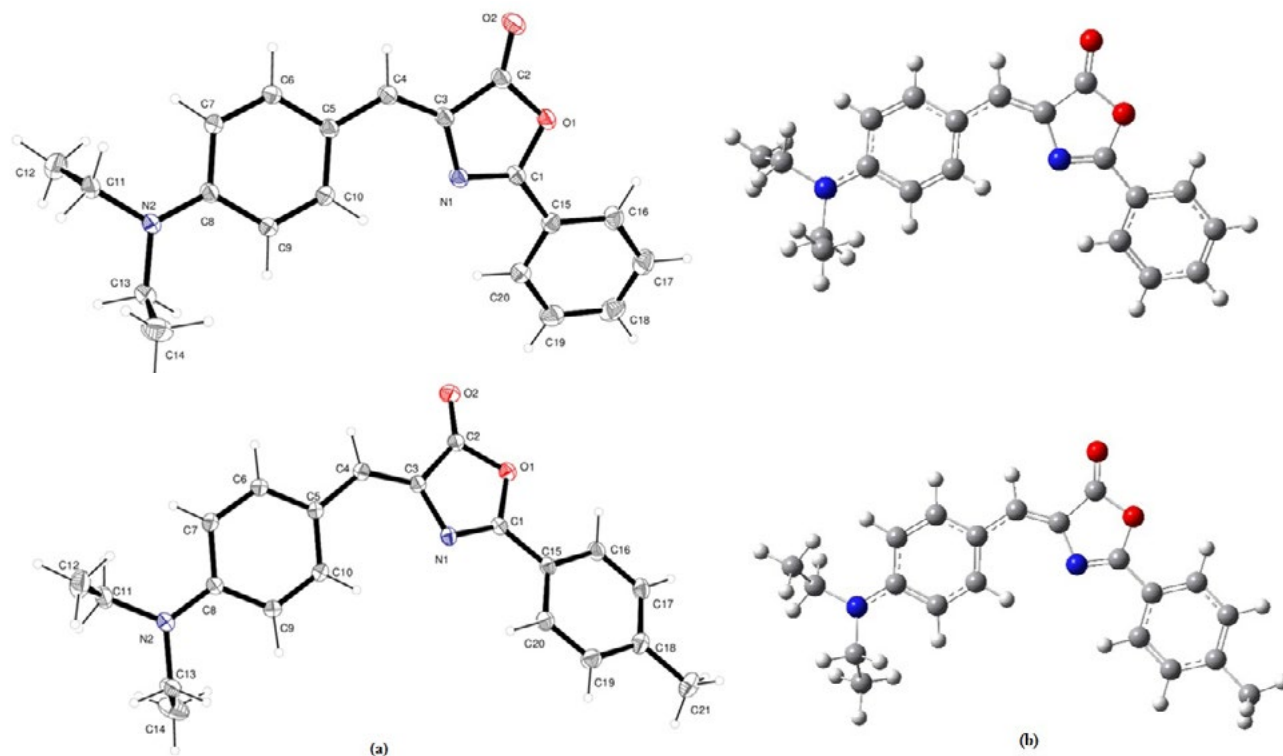


Figure 1. (a) The molecular structure of the compounds 1 and 2 with atom numbering scheme and 30% probability displacement ellipsoids and (b) optimized structures for DFT/ B3LYP/6-311G(d,p) level.

Table 3. Hydrogen bonds (Å, °).

Molecule	D–H...A	D–H	H...A	D...A	D–H...A
1	C10–H10...N1	0.93	2.46	3.088(3)	125
	C16–H16...O1	0.93	2.49	2.8001(3)	100
	C11–H11A...O2 ⁱ	0.97	2.56	3.4428(4)	151
2	C10–H10...N1	0.93	2.45	3.0930(3)	126
	C16–H16...O1	0.93	2.48	2.8030(2)	101
	C21–H21C...Cg2 ^v	0.96	2.97	3.8267(3)	149

Symmetry codes: (i) 1–x, 1–y, 1–z; (v) x, y, 1+z.

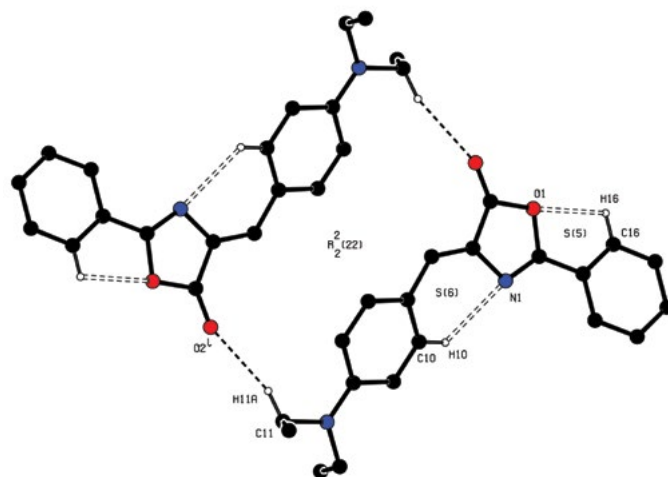


Figure 2. The formation of the hydrogen bond motif through C11–H11A...O2ⁱ hydrogen bonds for the compound 1 [$1+x, 1+y, +z$]. For the sake of clarity, H atoms not involved in the motif have been omitted, and only the interacting atoms are labeled.

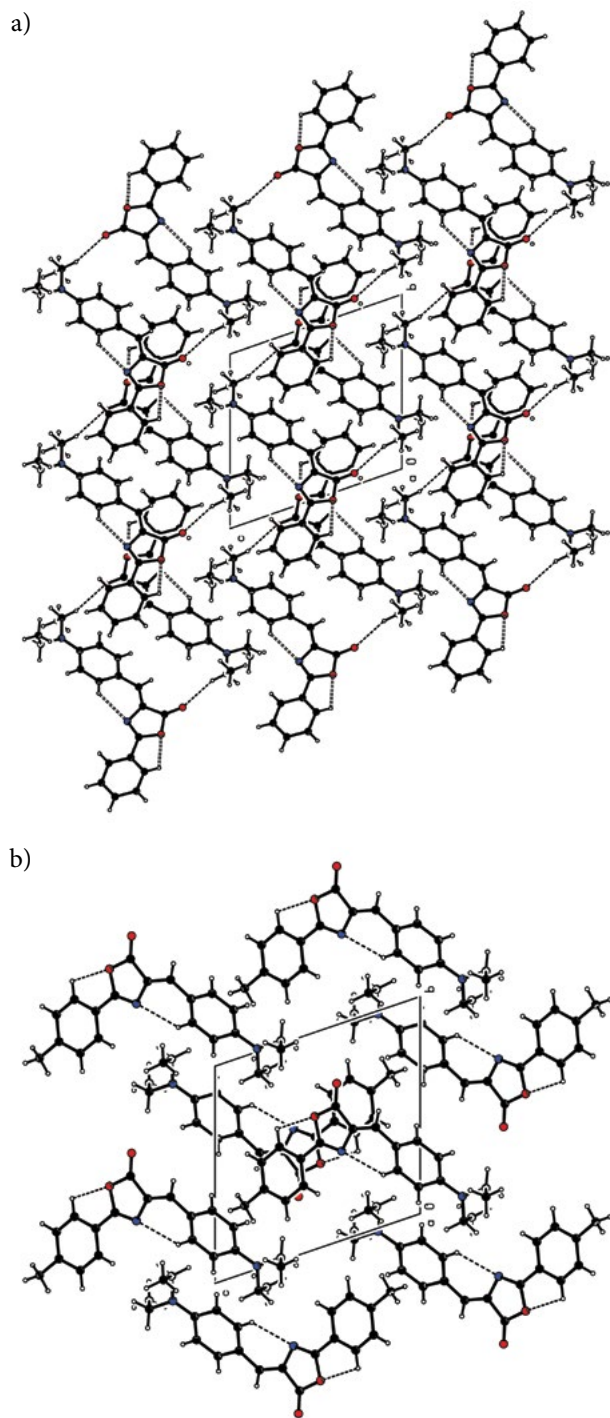


Figure 3. (a) A view along the *a* axis of unit cell showing the intermolecular hydrogen bonding interactions and formation of (22) ring motif belongs to the compound **1**. (b) A view along the *a* axis of the crystal packing of the compound **2**.

separation of 2.97 Å [Cg(2): C5-C10]. For both compounds, intermolecular and intramolecular interactions and C–H... π interactions with their symmetry codes are listed in Table 3 and crystal packing diagrams are given in Figures 3a and b.

3. 2. Frontier Molecular Orbitals

The highest occupied molecular orbital (HOMO) and lowest unoccupied molecular orbital (LUMO) are the basic orbitals that play an important role in chemical stability. The HOMO shows the ability to donate an electron, whereas the LUMO as an electron acceptor shows the ability to obtain an electron. This also predicts the nature of electrophiles and nucleophiles at the atom where the HOMO and LUMO are stronger.³⁴ The energy gaps of the compounds **1** and **2** were calculated using B3LYP/6-311G(d,p) level (Figure 4). For both compounds, highest electron density lies mainly on the oxazol-5-one ring and on (diethylamino)benzylidene moiety. The HOMO energy levels are calculated at $-5.271(2)$ and -5.214 eV, respectively. On the other hand, the electrons are more distributed over the phenyl for the LUMO with the energy of -2.27 and -2.203 eV, respectively. The energy gaps of HOMO and LUMO could be determined to be about 3.001 eV for the compound **1** and 3.011 eV for **2**, which indicate the molecules become less stable and more reactive.

3. 3. Molecular Electrostatic Potential

The molecular electrostatic potential (MEP) is a reactivity map displaying probable region for the electrophilic and nucleophilic attacks and hydrogen bonding interactions of the molecules.³⁵ In order to predict the reactive part of the electrophilic and nucleophilic attack, the MEP of the title compounds were also calculated from B3LYP/6-311G(d,p) optimized geometry. In the compounds **1** and **2**, the negative regions (red) of the MEP which are around the O2 and O1 atoms bounded to oxazol-5-one ring, were related to electrophilic reactivity that is responsible for intermolecular hydrogen bonding for compound **1**, intramolecular hydrogen bonds for compound **2** and positive regions (blue) which are around the hydrogen atoms correspond to nucleophilic reactivity (Figure 5).

3. 4. Analysis of the Vibrational Spectra

The infrared spectra of the title compounds were recorded in the 4000–600 cm^{-1} region using FT-IR spectrophotometer and are presented in Figure 6. The vibrational band assignments were determined at B3LYP/6-311G(d,p) theory level. It is well-known that the vibrational wavenumbers obtained by DFT computations usually overestimate their experimental counterparts. These discrepancies can be corrected either by computing anharmonic corrections or by introducing a scaled field.³⁶ The visual check for the vibrational band assignments were also performed by using GaussView molecular visualization program. There are no negative frequencies in the calculated IR spectra, which indicates a stable optimized geometry. The selected harmonic vibrational IR frequencies and the corresponding experimental values are listed in Table 4. The infrared spectra of the compounds have some

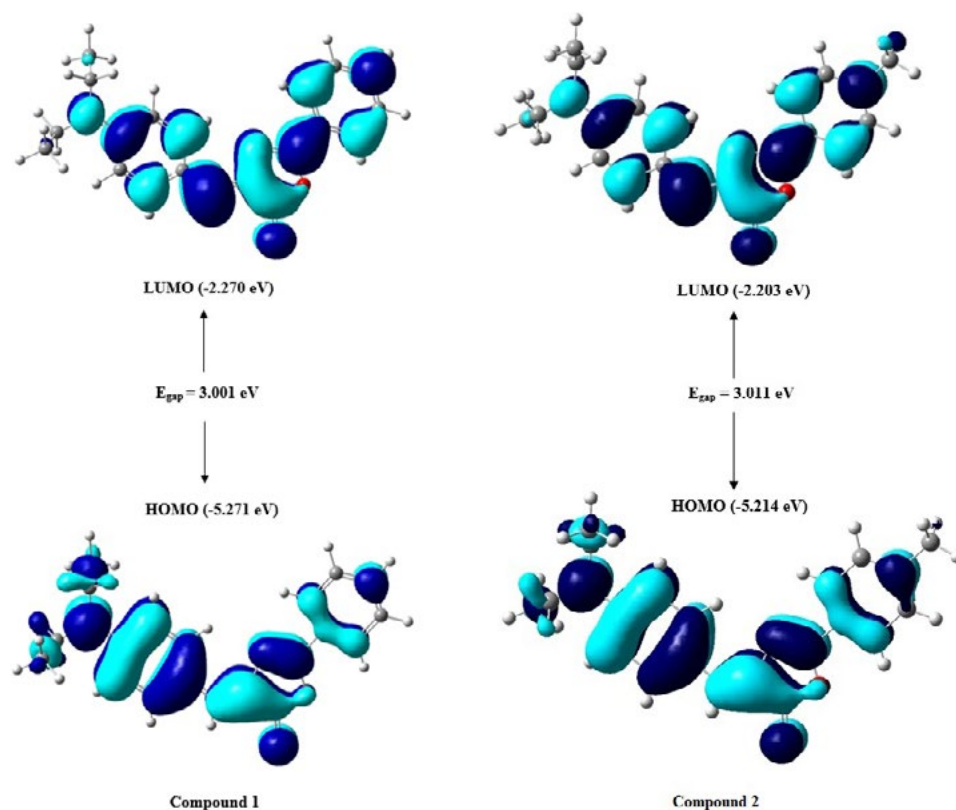


Figure 4. Frontier molecular orbital surfaces and energy levels for the HOMO and LUMO of the compounds 1 and 2 computed at B3LYP/6-311G(d,p) level.

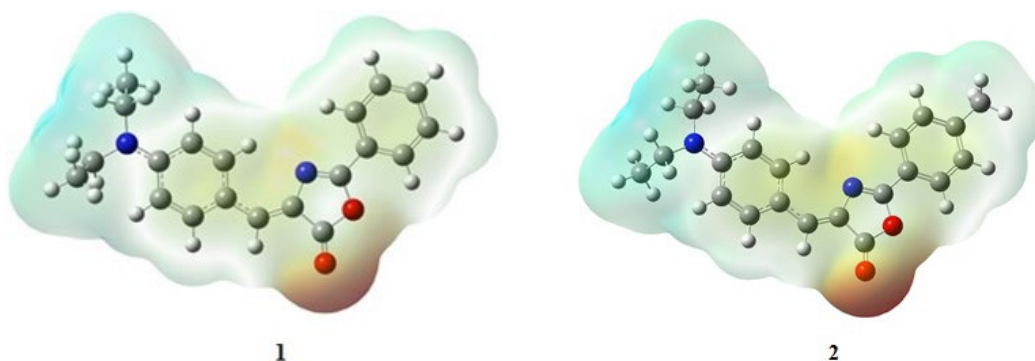


Figure 5. Molecular electrostatic potential surface (MEP) of the compounds 1 and 2.

characteristic bands of the stretching vibrations of the =C–H, –C–H, C=O, C=C–O etc. groups, in plane bending vibrations of C–H, C–H₂, C–H₃ groups and out of plane bending vibrations for =C–H, C–H₃ groups. In addition to these vibrations, some wagging, scissoring, twisting and rocking vibrations are obtained by theoretical study. There are some discrepancies between the observed and calculated data. This is because the experimental data were taken as KBr pellets, whereas the theoretical calculations were performed for isolated molecule in the gaseous phase.

The most characteristic bands of aliphatic –CH₂– and –CH₃ groups are those arising from C–H stretching

vibrations which experimentally occur in general region of 3000–2840 cm⁻¹. The asymmetrical/symmetrical stretching for –CH₂– groups is observed near 2926/2853 cm⁻¹ and for –CH₃ groups near 2962/2872 cm⁻¹, respectively. These standard values can be slightly changed depending on the surrounding of the alkyl moiety. Besides the aromatic C–H stretching bands which occurred at 3100–3000 cm⁻¹, all obtained experimental C–H bending vibrational data are compatible with expected values as well as stretching vibrational data.

C–H stretching vibrations were calculated at 3106/3104 cm⁻¹ for symmetric and 3081/3063 cm⁻¹ for

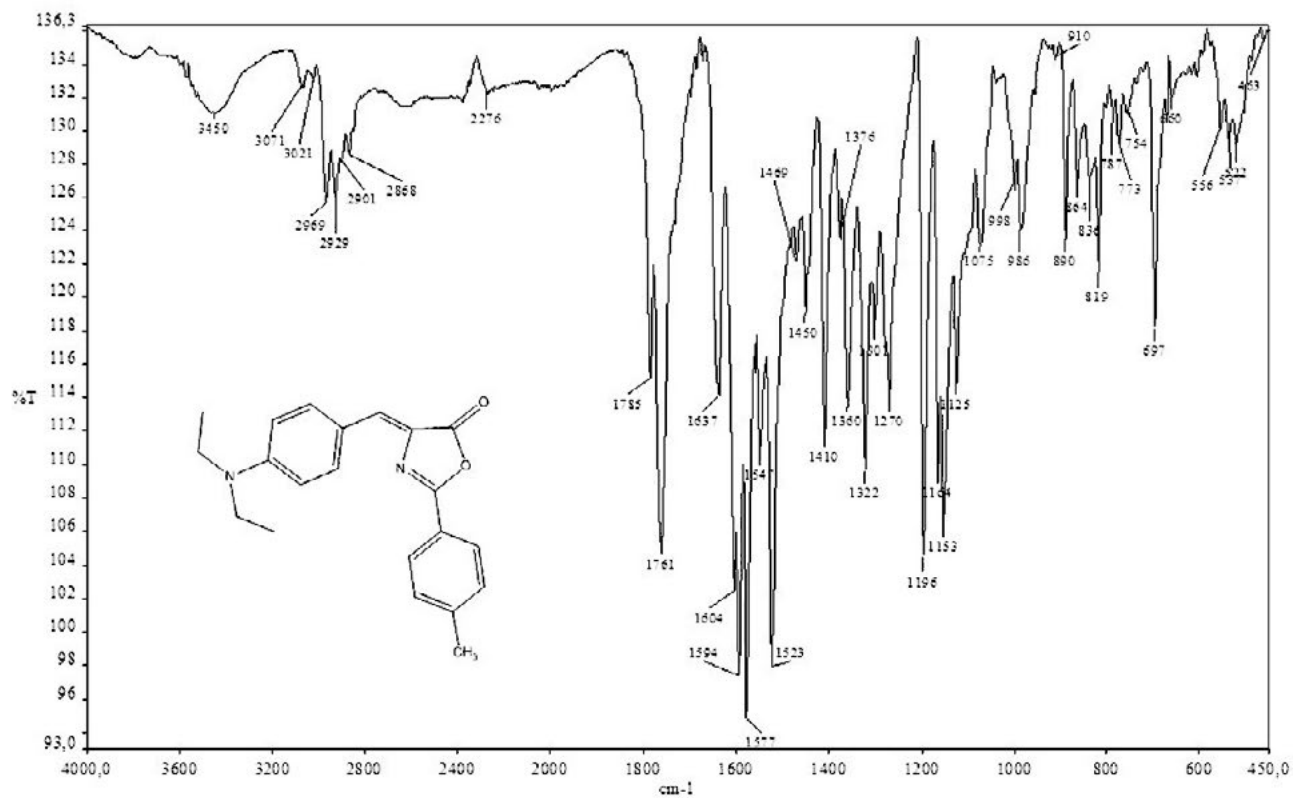
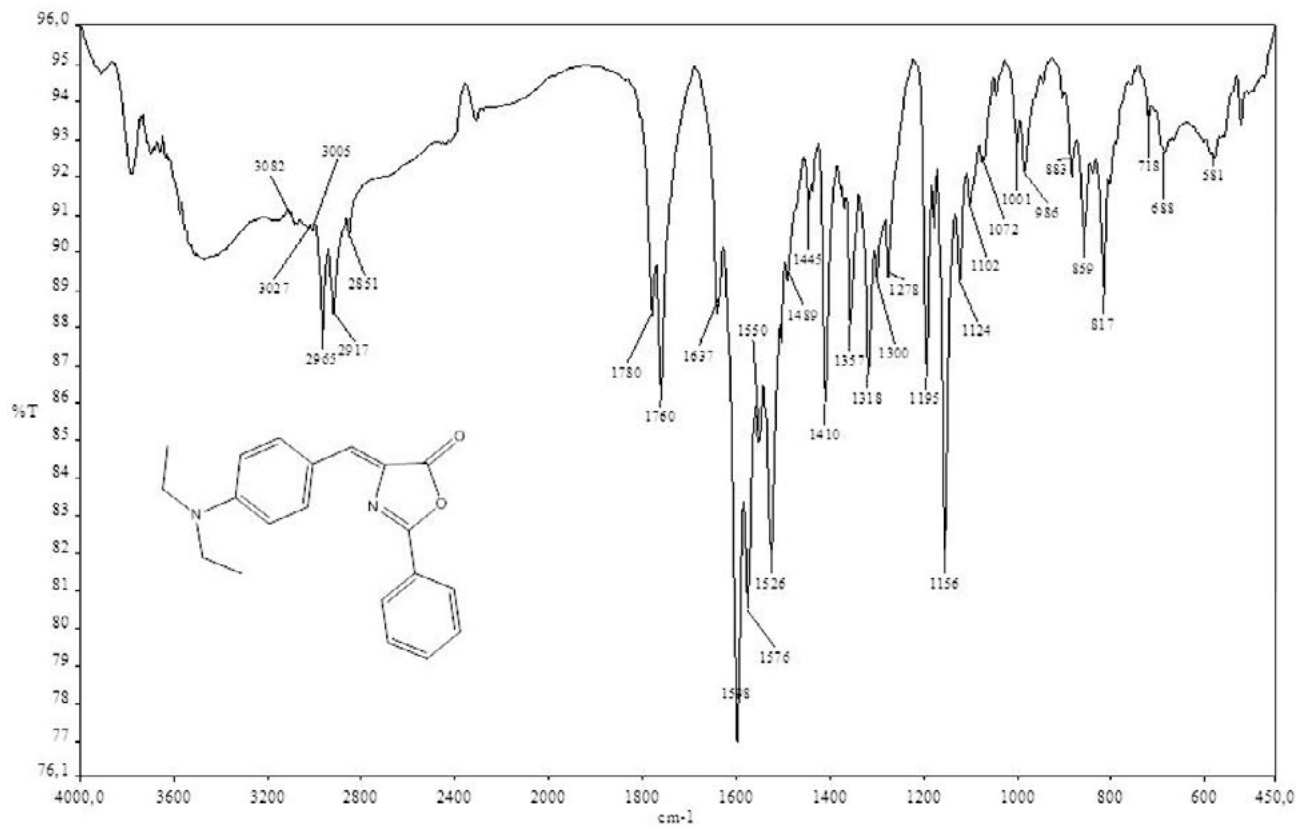


Figure 6. IR spectra of the title compounds 1 (above) and 2 (below).

Table 4. Comparison of the observed and calculated vibrational spectrum of the compounds.

Bond assignment ^a	IR, cm ⁻¹ (experimental)		Scaled frequency, cm ⁻¹ (calculated B3LYP/6-311G(d,p))	
	1	2	1	2
ν_{sym} (C-H) _{aromatic}	3021	3027	3106	3104
ν_{asym} (C-H ₂)	2929	2917	3092	3102
ν_{asym} (C-H ₃)	2969	2965	3100	3099
ν_{asym} (C-H) _{aromatic}	3071	3082	3081	3063
ν (C-H)	–	–	3047	3046
ν_{sym} (C-H ₂)	2886	2851	3043	3043
ν_{sym} (C-H ₃)	2901	2901	3038	3028
ν (C=O)	1785	1780	1857	1795
ν (C=C)	1637	1637	1646	1632
α (C-H) _{aromatic}	1594	1598	1599	1592
α (C-H ₂)	1469	1489	1457	1496
γ (C-H) _{aromatic}	–	–	1459	1457
Γ (C-H ₃)	1450	1445	1449	1451
β (C-H ₃)	1360	1357	1352	1351
ω (C-H ₂)	1322	1318	1349	1349
τ (C-H ₂)	1270	1278	1275	1278
ν (C-C-H ₃)	1196	1195	1179	1191
γ (C-H)	1124	1125	1131	1133
τ (C-H) _{aromatic}	890	883	930	928
Γ (C-H)	–	–	925	926
ω (C-H) _{aromatic}	819	817	800	811
γ (C-H ₂)	754	718	769	766

^a Abbreviations: ν -stretching; β -in plane bending; α -scissoring; γ -rocking; Γ -out of plane bending; τ -twisting, ω -wagging. Subscripts: *asym*, asymmetric; *sym*, symmetric.

asymmetric bands which are in the characteristic region for the identification of C–H stretching vibrations in the compounds **1** and **2**, respectively. The symmetric stretching vibrations of C–H₂ are determined at 2886/2851 cm⁻¹ and asymmetric stretching vibrations are determined at 2929/2917 cm⁻¹. Similarly, C–H₃ symmetric vibrational modes are observed at 2901 cm⁻¹ for both compounds, whereas the asymmetric modes are identified at 2969/2965 cm⁻¹.³⁷ These results are considerably compatible with the experimental data.

Other characteristic bands C=O, C=C, etc. were also detected. As usually, carbonyl stretching band at five-membered heterocyclic core shows around 1780 cm⁻¹, C=C stretching bands at *exo* positions shows around 1640 cm⁻¹, experimentally. These two values are also overlapping with our experimental results. In contrast to experimental value, calculated ν (C=O) vibration band was detected quite high for compound **1** (1857 cm⁻¹). This can be attributed to the strong intermolecular hydrogen bond (C11–H11B...O2).

3. 5. ¹H and ¹³C NMR Analysis

Experimental ¹H and ¹³C NMR of the title compounds were recorded in CDCl₃. Theoretical calculations carried out in the chloroform solvent (with respect to TMS) at the B3LYP/6-311G(d,p) method by adopting GIAO method and compared to the experimental chemical shift values,

Table 5. Comparison of the experimental and calculated ¹H NMR values in chloroform.

Atom	Experimental		Theoretical (B3LYP/6-311G(d,p))	
	1	2	1	2
H4	7.19	7.17	4.66	6.56
H6	8.14	8.03	5.22	6.96
H7	6.72	6.72	3.44	6.17
H9	6.72	6.72	4.41	6.33
H10	8.14	8.03	6.24	8.81
H11A	3.45	3.45	0.71	2.99
H11B	3.45	3.45	0.48	2.66
H12A	1.23	1.23	2.62	0.64
H12B	1.23	1.23	3.04	0.35
H12C	1.23	1.23	4.25	0.82
H13A	3.45	3.45	0.69	3.03
H13B	3.45	3.45	0.51	2.67
H14A	1.23	1.23	4.22	0.85
H14B	1.23	1.23	1.00	0.39
H14C	1.23	1.23	2.71	0.66
H16	8.13	8.03	5.91	7.49
H17	7.50	7.29	5.26	6.91
H18	7.50	–	5.13	–
H19	7.50	7.29	5.73	7.04
H20	8.13	8.11	5.84	7.96
H21A	–	2.44	–	1.56
H21B	–	2.44	–	1.99
H21C	–	2.44	–	2.08

Table 6. Comparison of the experimental and calculated ^{13}C NMR values in chloroform.

Atom	Experimental		Theoretical (B3LYP/6-311G(d,p))	
	1	2	1	2
C1	160.20	160.44	160.79	161.74
C2	168.68	168.78	165.90	167.68
C3	132.15	132.79	125.28	127.82
C4	135.21	135.05	127.41	133.55
C5	121.07	121.14	119.11	123.47
C6	128.74	129.51	129.30	138.67
C7	111.36	111.34	101.28	110.11
C8	150.11	149.97	150.99	152.29
C9	111.36	111.34	104.00	111.48
C10	128.74	129.51	128.17	136.11
C11	44.68	44.66	28.08	42.93
C12	12.64	12.64	14.29	7.69
C13	44.68	44.66	30.76	42.99
C14	12.64	12.64	9.85	7.97
C15	126.40	123.61	125.70	125.27
C16	127.74	127.95	121.54	129.34
C17	127.67	127.70	120.31	130.12
C18	133.44	142.92	121.42	146.57
C19	127.67	127.70	121.90	130.30
C20	127.74	127.95	122.30	128.43
C21	–	21.79	–	19.20

are presented in Tables 5 and 6. For the B3LYP/6-311G(d,p) method, the chemical shift value of tetramethylsilane (TMS) $\sigma_0(^{13}\text{C}) = 179.7024$ ppm and $\sigma_0(^1\text{H}) = 31.3919$ ppm was obtained.³⁸ For the compound **1**, NMR spectral data show that the C2 atom has the highest chemical shift value (168.68 ppm), whereas the methyl C12 and C14 atoms have the least one (12.64 ppm). Similarly in **2**, the highest chemical shift is for C2 with the value of 168.78 ppm and the least for C12 and C14 atoms at the range of 12.64 ppm. In the experimental spectrum, the signal of the C18 atom of the phenyl moiety was observed at 133.44 ppm in the compound **1**. But this value is higher in the **2** (142.92 ppm), because of the presence of a methyl group. ^1H NMR chemical shift values are calculated at 0.48–6.24 and 0.35–7.96 ppm for **1** and **2**, respectively. They are experimentally observed at 1.23–8.14 and 1.23–8.11 ppm, respectively.

4. Conclusions

Compounds **1** and **2** have been synthesized and characterized by FT-IR, ^1H NMR, ^{13}C NMR and X-ray single-crystal diffraction. In addition, density functional modeling studies of the oxazol-5-one derivatives have been reported in this study. The calculated geometric parameters by using the DFT with the 6-311G(d,p) basis set are mostly compatible with the X-ray structure. The vibrational band assignments and NMR shift values were performed at the same theory level to compare the experimental

and calculated values of the compounds. These calculated and experimental results are in good agreement with the explanatory differences.

5. Acknowledgment

The authors acknowledge Dokuz Eylül University for the use of the Oxford Rigaku Xcalibur Eos Diffractometer (purchased under University Research Grant No: 2010.KB.FEN.13).

6. Supplementary Material

Crystallographic data as .cif files for the structures reported in this paper have been deposited at the Cambridge Crystallographic Data Center with CCDC 1547713 for compound **1** and 1547714 for **2**. Copies of the data can be obtained free of charge at <http://www.ccdc.cam.ac.uk/conts/retrieving.html> or from the Cambridge Crystallographic Data Center, 12, Union Road, Cambridge CB2 1EZ, UK. fax: (+44) 1223-336-033, email: deposit@ccdc.cam.ac.uk.

7. References

- S. Chandrasekhar, P. Karri, *Tetrahedron Lett.* **2006**, *47*, 5763–5766. DOI:10.1016/j.tetlet.2006.06.006
- T. Rosen, B. M. Trost, I. Fleming, C. H. Heathcock Eds., In *comprehensive organic synthesis*, Oxford: Peragmon 2, **1991**, 402–407.
- G. P. Aguado, A. G. Monglioni, R. M. Ortuño, *Tetrahedron: Asymmetry* **2003**, *14*, 217–223. DOI:10.1016/S0957-4166(02)00749-8
- (a) J. Plöchl, *Chem. Ber.* **1883**, *16*, 2815; DOI:10.1002/cber.188301602235
(b) J. Plöchl, *Chem. Ber.* **1884**, *17*, 1616. DOI:10.1002/cber.18840170215
- F. Erlenmeyer, *Ann. Chem.* **1893**, 275.
- G. Ozturk, S. Alp, S. Timur, *Dyes Pigm.* **2008**, *76*, 792–798. DOI:10.1016/j.dyepig.2007.02.005
- K. M. Khan, U. R. Mughal, M. A. Lodhi, M. I. Choudhary, *Lett. Drug Des. Discovery*, **2008**, *5*, 52–56. DOI:10.2174/157018008783406624
- K. M. Khan, U. R. Mughal, M. T. H. Khan, Zia-Ullah, S. Perveen, M. I. Choudhary, *Bioorg. Med. Chem.* **2006**, *14*, 6027–6033. DOI:10.1016/j.bmc.2006.05.014
- M. A. Mesaik, S. Rahat, K. M. Khan, M. I. Choudhary, M. Shahnaz, Z. Ismaeil, Atta-ur-Rahman, A. Ahmad, Zia-Ullah, *Bioorg. Med. Chem.* **2004**, *12*, 2049–2057. DOI:10.1016/j.bmc.2004.02.034
- S. İçli, A. O. Doroshenko, S. Alp, N. A. Abnamova, S. I. Egorova, A. S. Astley, *Spectrosc. Lett.* **1999**, *32*, 553–569. DOI:10.1080/00387019909350006

11. K. Ertekin, C. Karapire, S. Alp, B. Yenigül, S. İçli, *Dyes Pigm.* **2003**, *56*, 125–133. DOI:10.1016/S0143-7208(02)00125-0
12. Rigaku, CrysAlisPro Software System, Version 1.171.38.43. Rigaku Oxford Diffraction, **2015**.
13. G. M. Sheldrick, *Acta Crystallogr. Sect. A* **2015**, *71*, 3–8. DOI:10.1107/S2053273314026370
14. O. V. Dolomanov, L. J. Bourhis, R. J. Gildea, J. A. K. Howard, H. Puschmann, *J. Appl. Cryst.* **2009**, *42*, 339–341. DOI:10.1107/S0021889808042726
15. G. M. Sheldrick, *Acta Crystallogr. Sect. C* **2015**, *71*, 3–8. DOI:10.1107/S2053229614024218
16. K. K. Irikura, R. D. Johnson, III, R. N. Kacker, *J. Phys. Chem. A* **2005**, *109*, 8430–8437. DOI:10.1021/jp052793n
17. A. R. Katritzky, N. G. Akhmedov, A. Guven, J. Doskocz, R. G. Akhmedova, S. Majumder, C. D. Hall, *J. Mol. Struct.* **2006**, *787*, 131. DOI:10.1016/j.molstruc.2005.10.041
18. M. J. Frisch, G. W. Trucks, H. B. Schlegel, G. E. Scuseria, M. A. Robb, J. R. Cheeseman, G. Scalmani, V. Barone, B. Men- nucci, G. A. Petersson, H. Nakatsuji, M. Caricato, X. Li, H. P. Hratchian, A. F. Izmaylov, J. Bloino, G. Zheng, J. L. Sonnen- berg, M. Hada, M. Ehara, K. Toyota, R. Fukuda, J. Hasega- wa, M. Ishida, T. Nakajima, Y. Honda, O. Kitao, H. Nakai, T. Vreven, J. A. Montgomery Jr., J. E. Peralta, F. Ogliaro, M. Bear- park, J. J. Heyd, E. Brothers, K. N. Kudin, V. N. Staroverov, T. Keith, R. Kobayashi, J. Normand, K. Raghavachari, A. Ren- dell, J. C. Burant, S. S. Iyengar, J. Tomasi, M. Cossi, N. Rega, J. M. Millam, M. Klene, J. E. Knox, J. B. Cross, V. Bakken, C. Adamo, J. Jaramillo, R. Gomperts, R. E. Stratmann, O. Yazyev, A. J. Austin, R. Cammi, C. Pomelli, J. W. Ochterski, R. L. Mar- tin, K. Morokuma, V. G. Zakrzewski, G. A. Voth, P. Salvador, J. J. Dannenberg, S. Dapprich, A. D. Daniels, O. Farkas, J. B. Foresman, J. V. Ortiz, J. Cioslowski, D. J. Fox, Gaussian 09, Revision B.01, Gaussian, Inc., Wallingford CT, **2010**.
19. R. Dennington, T. Keith, J. Millam, GaussView, Version 5, Semichem Inc., Shawnee Mission, KS, **2009**.
20. Y. F. Sun, Y. P. Cui, *Acta Crystallogr. Sect. E* **2008**, *64*, o678. DOI:10.1107/S1600536808005746
21. A. M. Asiri, H. M. Faidallah, T. R. Sobahi, S. W. Ng, E. R. T. Tiekink, *Acta Crystallogr. Sect. E* **2012**, *68*, o1154. DOI:10.1107/S1600536812011579
22. M. Cygler, C. P. Huber, *Can. J. Chem.* **1986**, *64*, 2064–2067. DOI:10.1139/v86-341
23. R. Sevinçek, G. Öztürk, M. Aygün, S. Alp, O. Büyükgüngör, *J. Struct. Chem.* **2011**, *52*, 405–411. DOI:10.1134/S0022476611020247
24. N. Khelloul, K. Toubal, N. Benhalima, R. Rahmani, A. Chouaih, A. Djafri, F. Hamzaoui, *Acta Chim. Slov.* **2016**, *63*, 619–626. DOI:10.17344/acsi.2016.2362
25. R. Sevinçek, M. Aygün, S. Alp, C. Kazak, *J. Chem. Crystallogr.* **2011**, *41*, 1140–1144. DOI:10.1007/s10870-011-0059-x
26. S. Karmakar, A. N. Talukdar, *Indian J. Phys. A* **2004**, *78*, 923–925.
27. Y. F. Sun, X. L. Wang, J. K. Li, Z. B. Zheng, R. T. Wu, *Acta Crystallogr. Sect. E* **2007**, *63*, o4426. DOI:10.1107/S1600536807051458
28. M. Parveen, F. Ahmad, A. M. Malla, S. Azaz, M. R. Silva, P. S. P. Silva, *RSC Adv.* **2015**, *5*, 52330–52346.
29. R. Sevinçek, G. Öztürk, M. Aygün, M. Y. Ergün, S. Alp, O. Büyükgüngör, *Spectrosc. Lett.* **2009**, *42*, 1–6. DOI:10.1080/00387010802428708
30. K. N. Subbulakshmi, B. Narayana, H. S. Yathirajan, M. Ak- kurt, O. Çelik, C. C. Ersanlı, C. Glidewell, *Acta Crystallogr. Sect. C* **2015**, *71*, 742–751. DOI:10.1107/S2053229615013637
31. A. M. Asiri, S. W. Ng, *Acta Crystallogr. Sect. E* **2009**, *65*, o1746. DOI:10.1107/S1600536809024593
32. V. G. Kasradze, E. V. Salimova, F. Z. Galin, O. S. Kukovinets, Z. A. Starikova, M. Yu. Antipin, *J. Struct. Chem.* **2010**, *51*, 599–602. DOI:10.1007/s10947-010-0089-9
33. J. Bernstein, R. E. Davis, L. Shimon, N. L. Chang, *Angew. Chem. Int. Ed. Engl.* **1995**, *34*, 1555–1573. DOI:10.1002/anie.199515551
34. M. Govindarajan, S. Periandy, K. Carthigayen, *Spectrochim. Acta A* **2012**, *97*, 411–422. DOI:10.1016/j.saa.2012.06.028
35. E. Scrocco, J. Tomasi, *Adv. Quantum. Chem.* **1978**, *103*, 115–193. DOI:10.1016/S0065-3276(08)60236-1
36. İ. E. Kibriz, Y. Sert, M. Sacmacı, E. Sahin, İ. Yıldırım, F. Uçun, *Spectrochim. Acta A* **2013**, *114*, 491–501. DOI:10.1016/j.saa.2013.05.022
37. R. M. Silverstein, G. C. Bassler, T. C. Morrill, *Spectrometric identification of organic compounds*, Fifth Ed., John Wiley and Sons Inc., Singapore, **1991**.
38. B. Kirste, *Chem. Sci. J.* **2016**, *7*, 127–131. DOI:10.4172/2150-3494.1000127

Povzetek

V okviru predstavljene raziskave smo s kondenzacijo *p*-*N,N*-dietilaminobenzaldehida z dvema derivatoma hipurne kisline sintetizirali dva oksazol-5-onska derivata, C₂₀H₂₀N₂O₂ (**1**) in C₂₁H₂₂N₂O₂ (**2**); oba smo v nadaljevanju študije tudi spektrokemijsko analizirali. Molekulski in kristalni strukturi smo določili z rentgensko difrakcijo monokristalov; izkazalo se je, da sta strukturi obeh kristalov stabilizirani s šibkimi intra- in intermolekularnimi interakcijami, kot tudi s C–O…π, C–H…π and π…π interakcijami. Računske študije smo izvedli z DFT metodo na nivoju B3LYP/6-311G(d,p). Izračunali smo vibracijske konstante in kemijske premike ter jih primerjali z eksperimentalnimi podatki. Simulirali smo tudi mejne molekulske orbitale in molekulske elektrostatske potencialne površine. Izračunani rezultati so pokazali, da se računsko optimizirani geometriji zelo dobro skladata z eksperimentalnima rezultatoma, dobljenima iz kristalne strukture. Namen je bil tudi ugotoviti učinek različnih reaktantov na kondenzacijo do oksazol-5-onov, na njihove značilne lastnosti in kristalne oblike končnih produktov.

Scientific paper

Development of New Bexarotene-loaded Mesoporous Silica Systems for Topical Pharmaceutical Formulations

Aurelia Vasile,¹ Maria Ignat,^{1,2,*} Mirela Fernanda Zaltariov,²
Liviu Sacarescu,² Iulian Stoleriu,⁴ Dan Draganescu,⁵ Mihai Dumitras¹
and Lacramioara Ochiuz³

¹ Department of Chemistry, "Alexandru Ioan Cuza" University from Iasi, 11 Carol I Blvd., 700506, Iasi, Romania

² Institute of Macromolecular Chemistry "Petru Poni" Iasi, Aleea Grigore Ghica Voda, nr. 41A 700487 Iasi, Romania

³ Faculty of Pharmacy, "Gr.T. Popa" University of Medicine and Pharmacy from Iasi, 16 Universitatii Street, 700115, Iasi, Romania

⁴ Faculty of Mathematics, "Alexandru I. Cuza" University, 11 Bvd. Carol I, Iași, 700506, România

⁵ APIS Laboratories LTD, street Prof. Petru Olteanu 2F, Iasi

* Corresponding author: E-mail: maria.ignat@uaic.ro, ignat.maria@icmpp.ro

Received: 18-06-2017

Abstract

The present study reports the first time use of MCM-41 mesoporous silica as highly efficient carrier for bexarotene – an antineoplastic agent specific for cutaneous T-cell lymphoma treatment. Bexarotene is highly toxic and poor-water soluble, having low bioavailability in the conventional pharmaceutical forms. Comparative uptake of bexarotene on amino-functionalized silica host at various functionalization degrees is discussed in details taking into account all structural features, of matrix as well as properties of the drug molecules. The obtained results proved a successful bexarotene loading on amino-functionalized MCM-41 silica. The bexarotene molecules are adsorbed on the active centers in non-crystalline state proving the major role of the silica amino-functionalization for the drug solubility and bioavailability enhancing. *In vitro* dissolution tests showed a prolonged release of bexarotene during 12 h, reaching 50% release of loaded active molecules. The prolonged release has been demonstrated to be a result of the presence of aminopropyl groups on the silica pore walls.

Keywords: Aminofunctionalized mesoporous silica, carrier bexarotene, release

1. Introduction

Generally, if a drug provides high therapeutic efficacy, diminished side effects and does not induce unacceptable toxicity levels, it is used in disease treatment. These requirements can be accomplished, in the case of the existing medication, by using new administration possibility as transport and controlled delivery systems. Nowadays, due to their advantages as the ability to incorporate lipophilic and hydrophilic substances, low toxicity, extended persistence into the blood stream, the gradual and controlled drug release and safe administration (produces no local inflammatory reaction), as well as the allowance to be used in adequate doses and to target the drug, controlled Drug

Delivery Systems (DDS) are increasingly preferred compare to conventional administration methods.¹⁻⁴

Since 2001, when M. Vallet-Regi et al.⁵ made known the first results, due to their biocompatibility and relative easily adjustable physicochemical properties, the use of mesoporous silica materials for the development of such controlled drug delivery systems, caught the attention of many researchers. Among them, MCM-41 type mesoporous silica, has found to have remarkable applications in DDS preparation (to be used for treatment of various diseases: inflammatory, cancer, diabetes, neurological disorders, even as carriers in gene therapy or biosensors for diagnosis), as well to have a huge potential for diversification of such systems. The key properties of this versatile mate-

rial are due to the ordered structure at meso-scale level (ordered pores ranging in size from 2 to 10 nm), and surface chemistry that allows the insertion in a controlled manner of new functionalities and thus potential applications. The high specific surface area ($>1000 \text{ m}^2/\text{g}$), large pore volume ($\sim 1.0\text{--}2.0 \text{ cm}^3/\text{g}$), and consequently the high sorption/hosting capacity for bioactive molecules, the relative simple, inexpensive, environmentally friendly and controllable synthesis procedure, the biocompatibility and lack of toxicity, explain the particular interest reflected in a large number of publications worldwide. Thus, pure or modified MCM-41 mesoporous silica was used as carrier for various types of drugs, such as ibuprofen,⁶ aspirin,^{7,8} naproxen,⁹ doxorubicin,¹⁰ captopril,¹¹ erythromycin,¹² celecoxib,¹³ econazole nitrate,¹⁴ famotidine,¹⁵ mesalazine,¹⁶ tetracycline,¹⁷ alendronate,^{18,19} curcumin,^{20,21} folic acid,²² etc. More information can be found in exhaustive investigation on drug release from silica-based ordered mesoporous materials, reported by Maria Vallet-Regi et. al. in 2015.²³

Also, are known core-shell nanoparticles consisting of magnetic iron oxide cores and MCM-41 mesoporous silica shells with controllable magnetization for nanoconfinement of antineoplastic agents.^{24,25} Such systems may be used to transport drugs to the diseased organ of a patient, when an external magnetic field is applied.

The controlled functionalization of the MCM-41 silica pore surface (internal surface) results in fine tuning of the host-guest chemistry, an essential factor for modified drug delivery systems (MDDSs) preparation. Only for particles smaller than 100 nm with a high specific surface area, the selective functionalization of the external and internal surface is relevant. Both adsorption of the bioactive agent (physisorption) and its release (diffusion) are influenced by the hydrothermal stability, pore size and structure, functionalization (the density of the organic fragments attached to the surface), surface polarity, the properties of the bioactive agent, and the loading method. Physical interaction forces between bioactive molecules and the pore walls and the diffusion through the pores are fully controllable through internal surface functionalization.

Generally, the surface modification of MCM-41 silica by functionalization can be accomplished through: (i) the co-condensation process during synthesis procedure, (ii) by post-synthesis grafting process, and (iii) surfactant displacement. Although, by involving the co-condensation process, the distribution of the functional groups is uniform, the removal of the structuring agent is difficult, laborious and there is a risk to leave in the structure undesirable fragments of the surfactant/co-surfactant molecules for the biomedical applications. For this reason, most often, the grafting of the organic fragments on the calcined MCM-41 silica surface by post-synthesis treatments is preferred.

Bexarotene (4-(1-(5,6,7,8-tetrahydro-3,5,5,8,8-pentamethyl-2-naphthalenyl) ethenyl) benzoic acid) (BXT) is

an antineoplastic specific agent for treatment of cutaneous T-cell lymphoma (CTCL). However, poor water solubility and low dissolution rate significantly limit the bioavailability of BXT. In topical applications, bexarotene usually induces irritant dermatitis, requiring a careful monitoring and a gradual dose increase to provide a correct therapeutic ratio.²⁶

In the present study, is proposed a way to overcome these disadvantages, namely the preparation of BXT-based modified drug delivery systems characterized by and enhanced solubility, therefore and bioavailability, and a prolonged release in order to develop new dosage forms for treatment of cutaneous T-cell lymphoma.

Mesoporous silica, MCM-41 type, used for the preparation of such systems have been synthesized by an innovative method (sonochemical), modified through amino-functionalization and loaded with the specific drug. The obtained MDDSs systems were subjected to *in vitro* testing in order to establish the release profile of the drug.

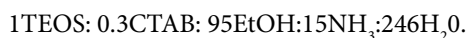
2. Experimental Section

2.1. Materials

Test experiment was performed using the following reagents: tetraethyl orthosilicate (TEOS, 98%, Merck) as the silicon source; cetyltrimethylammonium bromide (CTAB, 99%, Merck) as the cationic surfactant structuring agent; 3-aminopropyltriethoxysilane (APTES, 99%, Sigma-Aldrich) as a functionalizing agent; bexarotene (BXT, 98% Zhejiang Sanmen Hengkang China Pharmaceutical Co. Ltd.) as an antineoplastic agent, absolute ethanol (99.3% Chemical Company, RO); aqueous ammonia (NH_3 , min.25% Chemical Company, RO), hydrochloric acid (35–38%, Chemical Company, RO), toluene (98%, P. A. Chemical Company, RO). All reagents have been used without further purification. Deionized water was obtained with water purification Elga PureLab system. Reagents as trifluoroacetic acid (TFA, Merck, Germany); acetonitrile (chromatographic purity, Merck, Germany); glacial acetic acid (Merck, Germany); potassium phosphate (Sigma Aldrich, Germany), ethyl alcohol (pro analysis, Sigma Aldrich, Germany) double distilled water: Millipore, conductivity – $0.01 \mu\text{S} / \text{cm}$ were used for HPLC analysis.

2.2. Synthesis Procedure

The synthesis of MCM-41 mesoporous silica was carried out in alkaline conditions by ultrasonication process using an ultrasonic generator SONICS VIBRA Cell TM Model CV 33 operating in a pulse mode (3/1 s on/off cycle) for 2 hours, and a constant temperature of 25°C . The reaction mixture had the following molar composition:



Initially, the well-known amount of CTAB was dissolved in a corresponding calculated volume of distilled water, until a clear solution was obtained. Then, to the CTAB solution ethanol is added and the obtained mixture was subjected to an ultrasound irradiation for 5 min. Further, the ultrasonication is continued for another 15 min, when aqueous ammonia was added to the reaction mixture. Finally, during ultrasonication, in the first 20 min of working time the TEOS was added drop wise to the reaction mixture, and left for maturation for 2 h.

The obtained product was centrifuged, washed several times with distilled water until a negative test for the presence of bromine have been reached, and then dried in air at room temperature. To create porosity, the structure directing agent was removed by calcination at 550 °C for 6h with a rate of temperature increase of 1°/min. The resulted product was denoted as M.

2. 3. Amino-functionalization of Mesoporous Silica

Although at the start point of preliminary tests for the immobilization of BXT bioactive agent on the M sample have shown retention of large amounts, BXT molecules diffuse outward due to the weak electrostatic and steric influences of the silicate framework.

The obtained results justify the necessity of the controlled modification of MCM-41 mesoporous silica surface through bonding some functional groups that increase physical interaction with BXT molecules. For this purpose, modification of M sample with 3-aminopropyltriethoxysilane was performed. Three different samples were obtained with different functionalization degree expressed in weight percentage of aminopropyl groups. In grafting process, the isolated and vicinal silanol groups act as efficient anchoring points for further functionalization by elimination reactions. The grafting process occurred in anhydrous conditions which are essential for prevention organosilane reaction with water. Before functionalization, samples were dried at 150 °C for 5 h, to remove the physically adsorbed water.

The typical grafting experiment has been carried out by contacting 1 g of M sample with 30 mL of anhydrous toluene, followed by magnetic stirring (during 30 min), drop wise adding of a specified quantity of APTES (the APTES amount was varied between 2.25 and 4.33 mmol), afterward the mixture was refluxed at 110 °C, for 8h.

The final products were separated by centrifugation, washed with ethanol, and let to dry at room temperature. The obtained samples were labeled as MG_x (x – functionalization degree: 1; 2; 3).

2. 4. Preparation of Modified Drug Delivery Systems (MDDS)

The loading process of guest molecules on the mesoporous silica is based on the physical adsorption from

solution. Because BXT in almost water insoluble, anhydrous ethanol have been chosen as solvent. In order to determine the required time for reaching equilibrium, the kinetics of the adsorption process have been studied. The kinetic study was carried out using a 1 mg/mL BXT solution, at native pH of 4.5 under magnetic stirring at room temperature (20 ± 0.5 °C) under light-sealed conditions and dark. In order to avoid the experimental errors induced by withdrawing aliquots of solution, each point of the study was evaluated in separate solutions. This way, at all times we ensured 100 mg of MG_x matrix in contact with 50 ml of drug solution. The adsorbed amount was determined indirectly by measuring the solution concentration before and after adsorption. The prepared MDDSs were noted as BXT@MG₁, BXT@MG₂ and BXT@MG₃.

2. 5. Study of the *in vitro* Dissolution of BXT from Prepared MDDSs

Taking into account the poor solubility of BXT in water or phosphate buffer solution,^{27,28} the *in vitro* dissolution tests of the three systems (BXT@MG₁, BXT@MG₂, BXT@MG₃) were carried out using ethyl alcohol:phosphate buffer solution (ratio of 3:1) as dissolution media. The test was performed on a SR8 Plus Series (AB & L JASCO, Chatsworth, CA, USA) apparatus 2 (paddles) equipped with a Dissoette autosampler (Hanson Research Corporation, Chatsworth, CA, USA) according to the following protocol: a specific amount of MDDS containing 50 mg of BXT was placed in different flasks filled with 100 mL of dissolution medium. The mixtures were magnetically stirred (with a rotation speed of 50 rpm), at 37 ± 0.5 °C; the sampling interval was set at 30 min during the first hour of the test, and at 60 min for the next 12 h, respectively. Aliquots (3 mL) were withdrawn and subjected to HPLC analysis in order to determine the amount of the released BXT. After every sampling, the aliquots were replaced with equal volumes of dissolution medium at 37 °C. The amount of released BXT in the dissolution medium was assessed by the HPLC-DAD method described below.

The chromatographic method applied for the *in vitro* release tests was developed and validated in-house. The determinations were made on a HPLC Dionex Ultimate™ 3000 (Thermo Fisher Scientific Inc., USA), equipped with UV-VIS Diode Array Detector and Hypersil GOLD column (Thermo Fisher Scientific Inc., USA), 4.6 × 150 mm, 5 μm, and a universal pre-column (Thermo Fisher Scientific Inc., USA). The dosing method was validated for as follows: the mobile phase consisted of 0.1% trifluoroacetic acid / acetonitrile aqueous solution in a ratio of 20/80 at a flow rate of 1.6 mL/min; temperature in the column compartment is kept constant at 40 °C; the volume of injected solution is 20 μL. Chromatograms have been registered at λ = 262 nm; linearity is in the range of 0.1 to 1 mg / mL; calibration curve equation, y = 934.49x + 0,986; the detec-

tion limit is 0.00822 mg/mL and the limit of quantification is 0.02491 mg/mL.

2. 6. Characterization

The degree of ordering for the pure and functionalized MCM-41 samples was determined by Small-Angle X-ray Scattering (SAXS) technique using a Bruker-Nanosar U instrument equipped with a 3-pinhole collimation optics which provides a precisely parallel X-ray beam with virtually no background and high intensity. The scattering intensity was measured as a function of scattering angle in the range $2\theta = 0.5\text{--}3.5^\circ$.

Textural properties were determined from nitrogen sorption isotherms, registered on a Quantachrome Nova 2200e Surface Area & Pore Analyzed. Prior to the measurements, all samples have been outgassed in vacuum for 12 h, at room temperature. The specific surface area (S_{BET} m²/g) was calculated from the linear part of the isotherm applying multipoint BJH (Brunauer-Emmett-Teller) method. The mean pore diameter (D_p , nm) was taken from the PSD (pore size distribution), calculated using BJH (Barrett-Joyner-Halenda) method applied to the adsorption branch of isotherm, as the peak centre. The total pore volume (TPV, cm³/g) was estimated from the nitrogen adsorbed amount at $P/P_0 = 0.95$.

Transmission Electron Microscopy (TEM) investigations were performed using a HT7700 HITACHI microscope operated in high contrast mode at 100 kV accelerating voltage. The samples were prepared by direct deposition of solid gels particles on 300 mesh formvar-coated carbon grids (Ted Pella).

The study on BXT immobilization was followed using an HPLC Dionex Ultimate™ 3000 (Thermo Fisher Scientific Inc., USA).

FTIR spectra were recorded on a Bruker Vertex 70 type FTIR spectrometer. Registered spectra were obtained on KBr pellets containing prepared samples, in the range of 400–4000 cm⁻¹ with a resolution of 2 cm⁻¹ at room temperature.

TG analysis was performed using a Diamond Pyris TG-DTA thermobalance (Perkin-Elmer) apparatus under N₂ flow. Thermograms were recorded at a heating rate of 10 K/min, sample mass of about 10 mg, temperature interval 40–700 °C.

3. Results and Discussions

3. 1. Structural and Morphological Characterization

Although X-ray diffraction (XRD) is an ideal method to identify the material structure, the nanoparticles are of particular case exhibiting drawbacks as shifting of the diffraction peaks resulting in network parameters modification (compare to the bulk) and peak widening as a result of

occasional presence of disordered crystallographic phase. For the structural analysis of the studied samples we considered SAXS (Small Angle X-ray Scattering) technique which is sensitive to the inhomogeneous electronic density. In addition, SAXS results were correlated with those obtained by TEM (Transmission Electron Microscopy). As observed, the Fig. 1 shows SAXS profiles of pure (M) and amino-functionalized (MG_x) mesoporous silica samples.

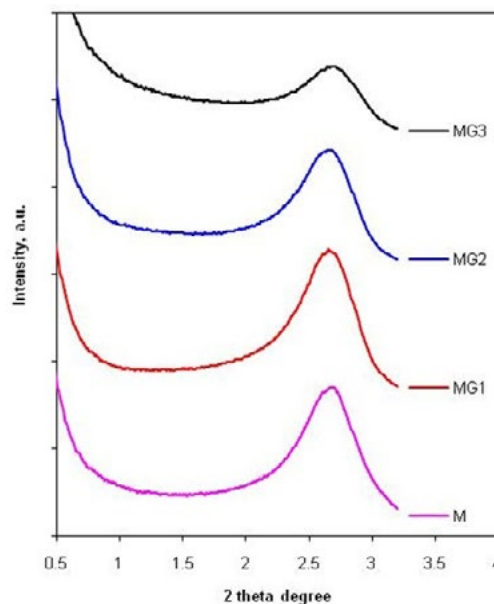


Figure 1. SAXS profiles of the pure (M) and amino-functionalized mesoporous silica MG_x samples.

As it is observed, the control sample (M) exhibit a clear peak centered at $2\theta = 2.69^\circ$, that is characteristic to the typical hexagonal arrangement of the cylindrical channels of mesoporous MCM-41 type silica. When the silica material has been grafted with amino-functionalized groups, we found that the peak intensity decrease with the increase of functionalization degree as a result of organic fragment attachment to the pore walls (Fig.1). The Scherrer equation allowed calculating the interplanar distances as 3.29 nm for M, 3.31 nm for MG₁, 3.32 for MG₂, and 3.28 nm for MG₃ samples, respectively.

For the morphology development of the synthesized samples, TEM technique has been involved. Thus, the TEM images obtained are presented in Fig.2 showing a clear parallelism of the pores arranged concentric in a spherical particle. The medium measured size of the silica particles is about 250 nm. The particle size distribution show the mean particle diameter in the range of 150–300 nm (Fig.2c); there are only few particles 2% that have diameter smaller than 100 nm and 8% of particles have diameters in the range of 300–400 nm, thus the mesoporous silica nanoparticles being suitable for biomedical applications.

It is found that after the amino-grafting (in the case of MG₁ sample, Fig.2b) and BXT-loading (in the case of

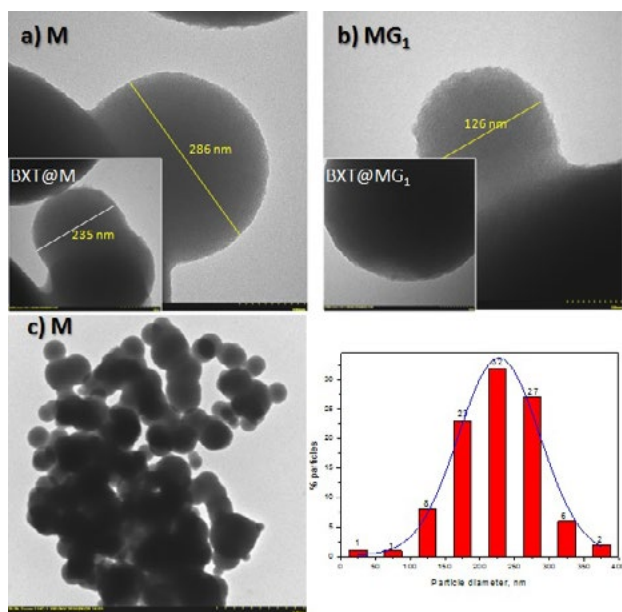


Figure 2. TEM images of: (a) M sample; (b) MG_1 sample; BXT@M sample (a inset); BXT@ MG_1 sample (b inset); (c) particle size distribution of M sample.

BXT@M and BXT@ MG_1 samples, Fig.2a inset and 2b inset, respectively) the silica material retains the ordered porous structure, providing its stability during considered processes. Therefore, both SAXS and TEM results show an evident hexagonal ordered pore structure of MCM-41 type silica which is maintained even it has been functionalized and/or loaded with antineoplastic agent.

3. 2. Textural Characterization

The specific surface area and porosity have a decisive influence on the silica material performance applied in ad-

sorption processes, catalysis and not least in preparation of drug delivery systems. In this study it is used the usual nitrogen sorption method for determining the specific surface area and porosity features. The obtained values for the specific surface area, pore volume and diameter are listed in Table 1. According to IUPAC classification,²⁹ the starting MCM-41 sample (M), as well as amino-functionalized silica samples (MG_x) reveals type IV nitrogen adsorption isotherms (Fig. 3 left). These isotherms exhibit the capillary condensation in the range of $P/P_0 = 0.2-0.3$ and a very narrow hysteresis loop of type H1, both features being characteristic to mesoporous materials. The inflection is due to the capillary condensation, and the hysteresis appears in the range of multilayer physisorption being associated with the capillary condensation process in the mesoporous structure. The H1 hysteresis proves the presence of uniform pores exhibiting a very narrow pore size distribution. The obtained textural characteristics of M sample ($S_{BET} = 1060 \text{ m}^2/\text{g}$; $V_p = 0.790 \text{ cm}^3/\text{g}$; $D_p = 2.32 \text{ nm}$) are in good agreement with the literature. The Fig.3 right (inset) shows the narrow pore size distribution with a single sharp peak of M silica sample.

The narrow pore size distribution (Fig.3 right), is maintained even after amino-functionalization process mentioning that the pore diameter decreases with increase of functionalization degree (Table I). For amino-functionalized samples, there is a noticeable decrease in the value of all texture parameters (S_{BET} , V_p , D_p), explained by bonding a number of organic fragments on the inner surface of the pores. Textural parameters diminishing is a function of functionalization degree (expressed by a percentage content of aminopropyl groups, Table I), being inversely proportional to it (once increased the functionalization degree, the textural parameters are diminished).

In the case of BXT@ MG_x systems (the isotherms are not shown here) a different behavior was observed dependent on the functionalization degree. Thus nitrogen sorp-

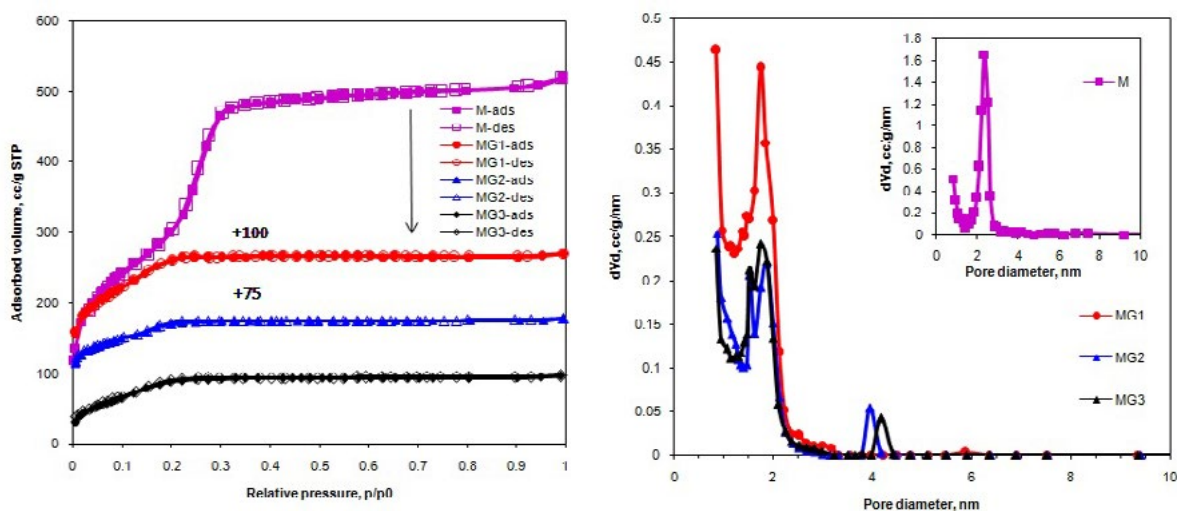


Figure 3. Nitrogen adsorption isotherms for pure and amino-functionalized silica samples MG_x (left); corresponding pore size distributions (right).

tion isotherm for BXT@MG₁ system kept the same type I, which at high relative pressures exhibit a small H1 type hysteresis loop associated with the capillary condensation process in the secondary porosity (interparticle pores). Simultaneously have been observed a drastically decrease of the specific surface area which is due to the occupation of an important volume fraction of the pores with BXT molecules, and the pore sizes are in the range of micropores (<2 nm) (Table 1). At the same time, the nitrogen adsorption isotherms for BXT@MG₂ and BXT@MG₃ systems show the absence of porosity (the isotherms being of type II which are characteristic to non-porous materials) suggesting the pore filling or blocking.

3.3. Drug Loading

Kinetic curves describing the adsorption process of BXT molecules on MG_x series samples, expressed by a decrease of the drug concentration in the solution are shown in Fig. 4.

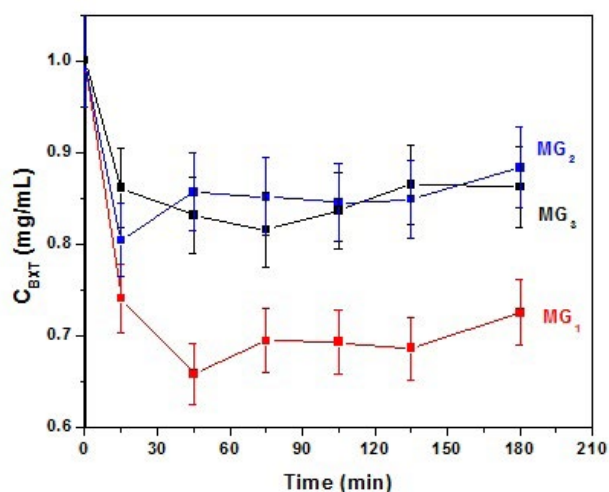
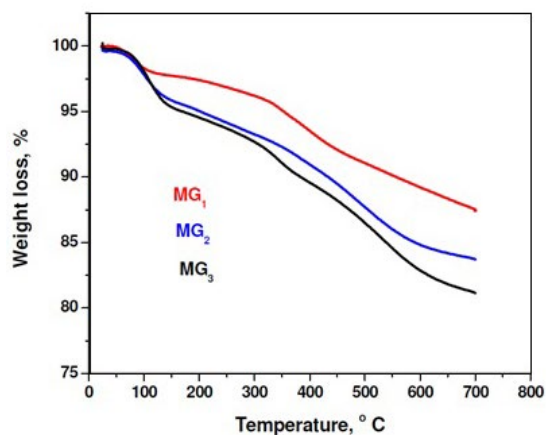


Figure 4. Adsorption kinetics of BXT molecules on MG_x matrices.



It is found that the diffusion process of BXT molecules through mesoporous silica structure and their adsorption on the active centers is relative fast, reaching the equilibrium in only 3 h.

The amount of aminopropyl groups calculated from thermogravimetric analysis (TG) on amino-functionalized mesoporous silica samples have the following values: 10.26 wt% for MG₁ sample, 12.14 wt% for MG₂ sample, and 14.18 wt% for MG₃ sample (Table I).

The Figure 4 reveals a maximum BXT loading for MG₁ sample which has a minimum functionalization degree compare to the other MG_x samples. The BXT loading varies inversely with the functionalization degree according to the following series: MG₁ > MG₂ > MG₃.

This result shows that the optimum of the functionalization degree in the study conditions is of 10.26 wt% owned to MG₁ sample. At 12.14 wt%, and 14.18 wt%, respectively of functionalization degree, the low loading level is due to the large number of organic fraction (aminopropyl groups) grafted on the pore walls which produce the filling of a large fraction of the pore volume and thus diffusion hindrances, either by pore blocking at the entrance or by the formation of pillars inside pores. The retained BXT quantity (228.6 mg/g for MG₁ sample; 180.5 mg/g for MG₂ sample; and 165.4 mg/g for MG₃ sample) varies inversely to the functionalization degree, the best loading being exhibited by MG₁ sample.

Because BXT molecules are retained involving electrostatic forces, the crystallization on the active centers is blocked, leading to enhanced drug solubility, bioavailability respectively. Thus, due to the unique structure of the amino-functionalized mesoporous silica, the textural properties and internal surface chemistry could be considered as highly efficient carrier for BXT molecules.

3.4. Thermogravimetric Analysis

The amount of amino-groups attached to the mesoporous silica MG_x surface was determined by thermograv-

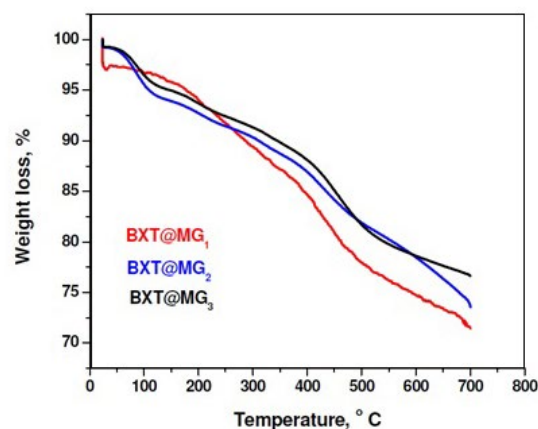


Figure 5. Thermogravimetric curves for functionalized silica samples (MG₁, MG₂, MG₃) and bexarotene loaded samples (BXT@MG₁, BXT@MG₂, BXT@MG₃).

imetric analysis. This method is sensitive to the total amount of the organic functions present on the mesoporous silica surface. The obtained thermogravimetric curves are presented in Figure 5a.

As observed, all samples show a mass loss at low temperatures (around 150 °C) which is due to the water molecules desorption. The mass loss at higher temperatures than 150 °C is due to the decomposition of aminopropyl groups anchored on the mesoporous silica surface, showing a successful surface functionalization (Table 1). The functionalization degree varies in the series $MG_1 < MG_2 < MG_3$.

At temperatures above 150 °C, the BXT@MG_x systems show higher mass loss compare to only aminofunctionalized samples due to decomposition of aminopropyl groups anchored on the silica surface, as well as bexarotene molecules desorption. Thus, the BXT@MG₁ system shows a BXT loading of 14.04 wt%, 8.208 wt% for BXT@MG₂ system, and 4.117 wt% for BXT@MG₃ system (Table 1). These results indicate that the BXT loading is in good agreement with the functionalization degree. The functionalization degree of 10.26 wt% which is characteristic to BXT@MG₁ system can be considered to be an optimum in the present study conditions, suggesting the induction of a sufficient powerful electrostatic field for retention of BXT molecules. As well, the fraction of the pore volume occupied by the aminopropyl groups is small enough not to hinder BXT molecules hosting. The increase of the functionalization degree (the case of BXT@MG₂ and BXT@MG₃ systems) lead to a decrease of bexarotene loaded as a result of diminishing the available pore volume for BXT molecules. The loading level with BXT in the case of all MG_x samples show that the silica pores have not been blocked by the aminopropyl groups, functionalization being beneficial.

3. 5. FTIR Analysis

Mesoporous silica sample M, amino-functionalized (MG_x), as well modified drug delivery systems, (BXT@M

and BXT@MG_x), were analyzed by FTIR spectroscopy with the aim to highlight the presence of amino groups and the anticancer agent on the silica surface.

It is well known that an IR spectrum is composed of two distinct regions: the fingerprint region in the range of 1450–500 cm⁻¹ and the functional groups range of 4000–1450 cm⁻¹. The fingerprint region contains, usually a series of absorption bands due to all vibration modes that occur inside molecule. It is difficult to assign individual absorption in this region but their apparition is very important because is unique for each compound being used to identify a compound. In the region of functional groups are less absorption bands being relatively easy to identify their nature.

The corresponding spectra for the functionalized silica hosts (MG_x), compare to pure silica matrix (M), are presented in Fig. 6a.

Both, in the fingerprint region and amino-functional groups are observed modifications as the result of the functionalization process. In the fingerprint region the spectra are similar, the absorption bands being localized at 1060 cm⁻¹ and 806 cm⁻¹ are assigned to symmetric and asymmetric stretching vibrations of Si-O-Si which are dominant with an increase intensity and a small shift toward low frequency, characterizing the spectra of MG_x samples, as a result of the influences of vibrations that occur in APTES molecule.

The main differences between spectra of M sample and amino-functionalized silica samples (MG_x) are found in the range of functional groups and consist of: (i) the presence of absorption bands centered at 2924 cm⁻¹ and 2855 cm⁻¹ assigned to the stretching vibrations of (C-H) (typical bands for alkyl C-H stretching frequencies); (ii) the band at about 1643 cm⁻¹ might be attributed to asymmetric deformation of protonated amine groups -NH₃⁺;³⁰ (iii) the absorption band at 1551 cm⁻¹ is assigned to symmetric bending vibration of NH₂ or NH₃⁺ groups. All these supplementary absorptions present in the FTIR spectra of MG_x samples show a success functionalization process.

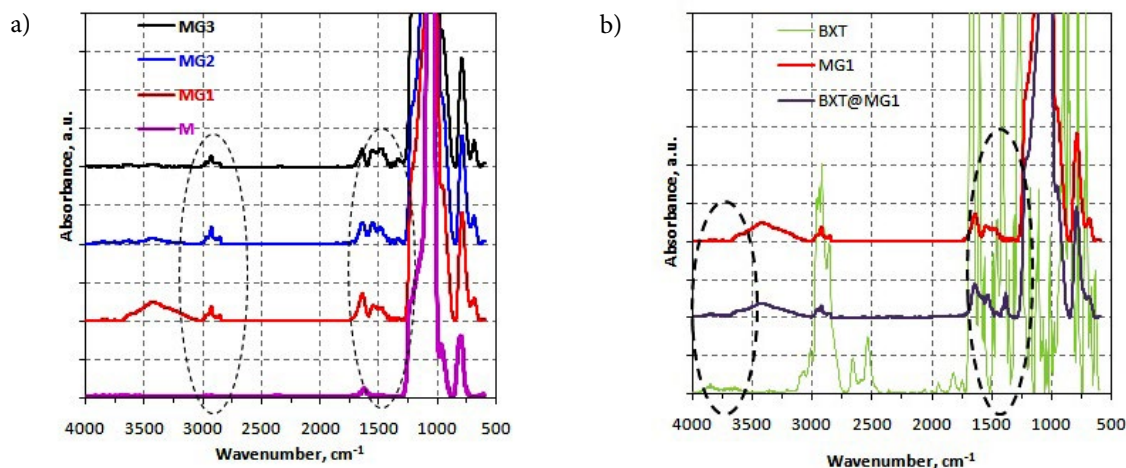


Figure 6. a) FTIR spectra for amino-functionalized MG_x samples compare to pure silica M sample; b) FTIR spectra for BXT@MG₁ system compare to MG₁ and BXT samples.

Table 1. Textural and thermogravimetric parameters of the aminofunctionalized MG_x samples and BXT@MG_x systems.

Sample	S _{BET} , m ² /g	V _p , m ³ /g	D _p , nm	Water content, wt%	Aminopropyl group content, wt%	BXT loading, wt%
M	1060	0.790	2.32	–	–	–
MG ₁	608	0.256	1.73	2.26	10.26	–
MG ₂	303	0.148	1.62	4.14	12.14	–
MG ₃	288	0.147	1.52	4.67	14.18	–
BXT@M	802	0.443	2.21	–	–	–
BXT@MG ₁	53	0.039	1.33	4.23	10.26	14.04
BXT@MG ₂	22	0.027	–	6.09	12.14	8.208
BXT@MG ₃	–	–	–	5.05	14.18	4.117

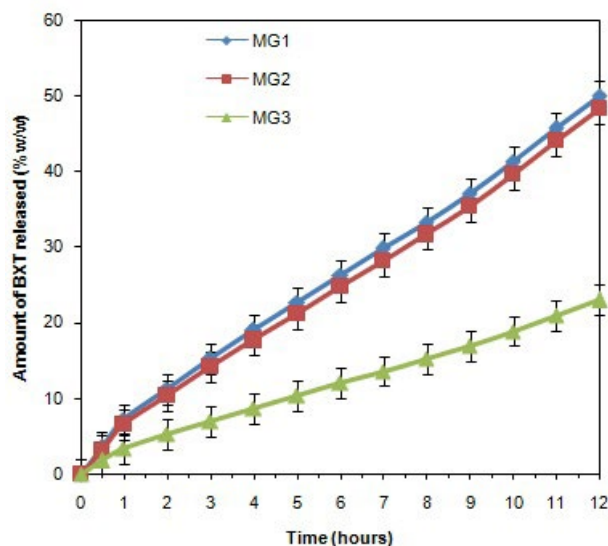
In the case of BXT, because the literature does not report so many and incomplete data, the comparative study with the data obtained in this work was almost impossible. Were used informations reported by the International Agency for Research on Cancer (World Health Organization),³¹ where are indicated the following band to be characteristic to BXT compound: 2959 cm⁻¹; 1677 cm⁻¹; 1278 cm⁻¹.

The characteristic FTIR spectra of the BXT@MG₁ system are presented in Fig.6b compare to MG₁ and BXT samples. It was found that each spectrum characterizing MDDS systems exhibit modifications in the region of 3900-3600 cm⁻¹, and 1600-1300 cm⁻¹ respectively (Fig. 6b) which are due to the presence of BXT molecules.

The obtained thermogravimetric and FTIR results show the amino-modification of the silica surface and BXT loading have been reach successful.

3. 6. Analysis of *in vitro* Drug Release Kinetics

In order to predict and correlate the behavior of the *in vitro* BXT release from the MDDSs studied, a suitable

**Figure 7.** *In vitro* dissolution release of BXT from BXT@MG_x systems.

mathematical model was used. Thus, the experimental data obtained from the *in vitro* dissolution tests of BXT from MDDSs were investigated using four predictable models: zero-order and first-order kinetics, Higuchi, and Korsmeyer-Peppas models.^{32,33} The simulation analysis, plotting and data fitting have been performed using Matlab 7.1 software. The Akaike Information Criterion (AIC) and the correlation coefficient R² were the criteria for selecting the model that most dependably describes the release profile of each formula. In a reliable prediction model, the value of R² is as close to 1 as possible, and AIC has the lowest values possible.³⁴

In vitro dissolution tests gave the results that highlight a prolonged release of BXT from the studied systems during 12 h. BXT@MG₁ and BXT@MG₂ systems were conducted to a 50% release of loaded BXT, while BXT@MG₃ system releases only 22.97% (Fig. 7).

$$\begin{aligned} \text{(Cumulative release (\%))} &= \\ &= \frac{\text{Amount of BXT released to solution}}{\text{Amount of BXT placed in MDDS}} * 100 \end{aligned} \quad (1)$$

These values are due to the presence of aminopropyl groups on the pore walls which reduce the liquid medium influx and delay the drug release because of the steric hindrance.

The obtained kinetics results for BXT release were fitted to mathematic models and are listed in Table 2. Correlating the quantity of released BXT with functionalization degree and porosity features of the amino-functionalized hosts and MDDSs systems we can conclude that in the case of BXT@MG₃ system the physical interaction between BXT molecules and grafted aminopropyl groups on the silica pore walls are stronger and diffusion restrictions are more important due to the large number of aminopropyl groups.

Kinetics analysis of BXT release by fitting selected mathematical models conducted to results presented in Table 2.

The data presented in Table 2 show a very good description of *in vitro* release rate of bexarotene from BXT@MG₁ and BXT@MG₂ systems by the first order kinetic model given by the following equation:

$$\text{Log } C = \text{Log } C_0 - \frac{K_t}{2.303} \quad (2)$$

Where, C_0 – initial concentration of drug; K = first order constant; t = time.³⁵

The R^2 values obtained for BXT@MG₁ and BXT@MG₂ systems were close to 0.990 (namely: 0.9816 for BXT@MG₁ and 0.9821 for BXT@MG₂, respectively). This result shows that BXT release from such systems occurs through a Fickian diffusion mechanism (Fick's first law) which is associated with concentration gradient, diffusion distance.

Table 2. Results of curve fitting of the *in vitro* BXT release profile from DDS silica based.

Kinetic model	Model Coefficients	MDDS System		
		MG ₁	MG ₂	MG ₃
Zero-order	K_0	3.8194	3.6649	1.7505
	R^2	0.9136	0.9237	0.9113
	AIC	49.4720	46.7538	26.3153
First-order	K_1	0.0503	0.0477	0.0195
	R^2	0.9816	0.9821	0.9489
	AIC	26.2972	25.0074	18.0581
Higuchi	K_H	12.1607	11.6362	5.5762
	R^2	0.9277	0.9187	0.9292
	AIC	46.7955	47.7164	22.9385
Korsmeyer-Peppas	n	0.8	0.8	0.7
	K_p	6.2042	5.9472	2.8438
	R^2	0.9723	0.9740	0.9783
	AIC	34.4399	32.6389	7.1675

In the case of BXT@MG₃ system, the release rate of BXT is best described by Korsmeyer-Peppas model given by the following equation:

$$\frac{M_t}{M_\infty} = K_t^n \quad (3)$$

Where: M_t and M_∞ denote the cumulative mass of drug released at time t and at infinite time, respectively;

K – is a kinetic constant characteristic of the drug-carrier system;

n – is an exponent (release index), which gives the information about the release mechanism of drug.

To find out the mechanism of drug release (exponent n – release index), first 60% of the drug release data were fitted in Korsmeyer-Peppas model.³⁶

The index release value, $n = 0.7$, for BXT@MG₃ system is in the range $0.45 < n < 0.89$ indicating a BXT release through an anomalous transport by diffusion processes (a non Fickian or anomalous diffusion is present).³⁷

This result highlights the fact that the amino-functionalization degree of mesoporous silica MCM-41 plays a very important role in the loading and release processes of guest drug molecules. Therefore, the differences in physicochemical properties such as the surface area and porosity determine the drug release mechanism via influence of the accessibility and mobility of drug molecules inside the pores of silica material and then their release behavior.

4. Conclusions

Mesoporous silica MCM-41 type have been synthesized and modified by post-synthetic grafting method with various level of amino-functionalization, loaded with specific antineoplastic drug specific for treatment of cutaneous T-cell lymphoma and investigated as carrier in MDDS systems. To the best of our knowledge, it is the first time studied such MDDS systems, BXT@MCM-41 mesoporous pure or amino-functionalized silica type.

The structural, textural and morphological characteristics evidenced the highly ordered structure degree of MCM-41, hexagonal arrangement of pores, spherical morphology of nanoparticles, specific surface area, pore size distribution in good agreement with the data reported elsewhere. Amino-functionalization by post-synthetic grafting diminished textural characteristics (specific surface area, pore diameter and volume) closely related to the functionalization degree. While occupying a certain fraction of the pore volume by aminopropyl groups, was modified the nitrogen adsorption isotherm type from type IV to type I, characterizing microporous materials.

TG and FTIR results showed the amino-modification of the silica surface and BXT loading have been reaching successful. Loading of amino-functionalized mesoporous silica with antineoplastic agent specific for cutaneous T-cell lymphoma, as *in vitro* release it was shown to be dependent of amino-functionalization degree thus illustrating truth fullness of the aim of the present study.

The control of the drug release process through amino-functionalization was demonstrated by release rate fitting (kinetics curves) using four mathematical models considered to be the most appropriate. It has been demonstrated the prolonged release of the drug from the studied modified drug delivery systems is due to the unique structural properties of mesoporous silica MCM-41 and to the controlled modification of the surface chemistry and textural features through amino-functionalization.

In the BXT@MG_x type systems, the bexarotene molecules are adsorbed on the active centers (aminopropyl groups) in non-crystalline state proving the major role of amino-functionalized MCM-41 silica for the solubility enhancing of BXT in water (enhancing dissolution of poorly-water soluble bexarotene) and by this of the drug bio-availability.

The results of the present study show that due to the unique structure, textural properties and internal surface chemistry of the amino-functionalized mesoporous silica, MCM-41, this is high efficiently carrier for the studied antineoplastic agent, and the obtained MDDSs systems are promising in biomedical applications, especially in controlled DDSs for obtaining topical formulations.

5. Acknowledgments

This work was performed through the Partnerships in priority areas program - PN II, developed with support of MEN - UEFISCDI, project PNII-PT-PCCA-2013-4-2024 (TOP-CTCL).

6. References

- Z. Lin, W. Gao, H. Hu, K. Ma, B. He, W. Dai, X. Wang, J. Wang, X. Zhang, Q. Zhang, *J Control Release*. **2014**, *174*, 161–70. DOI:10.1016/j.jconrel.2013.10.026
- C. Loira-Pastoriza, K. Todoroff, R. Vanbever, *Adv. Drug Deliv. Rev.* **2014**, *75*, 81–91. DOI:10.1016/j.addr.2014.05.017
- M. D. Chavanpatil, P. Jain, S. Chaudhari, R. Shear, P. R. Vavia, *Int. J. Pharm.* **2006**, *316*, 86–92. DOI:10.1016/j.ijpharm.2006.02.038
- C. W. Vendruscolo, I. F. Andreatza, M. S. Ganter, C. Ferrero, T. M. B. Bresolin, *Int. J. Pharm.* **2005**, *296*, 1–11. DOI:10.1016/j.ijpharm.2005.02.007
- M. Vallet-Regi, A. Rámila, R. P. del Real, J. Pérez-Pariente, *Chem. Mater.* **2001**, *13*, 308–311. DOI:10.1021/cm0011559
- J. Andersson, J. Rosenholm, S. Areva, M. Linden, *Chem Mater.* **2004**, *16*, 4160–4167. DOI:10.1021/cm0401490
- W. Zeng, X. F. Qian, Y. B. Zhang, J. Yin, Z. K. Zhu, *Mat. Res. Bull.* **2005**, *40/5*, 766–772. DOI:10.1016/j.materresbull.2005.02.011
- A. Datt, I. El-Maazawi, S. C. Larsen, *J. Phys. Chem. C*. **2012**, *116(34)*, 18358–18366. DOI:10.1021/jp3063959
- D. Halamova, V. Zelenak, *J. Incl. Phenom. Macrocycl. Chem.* **2012**, *72*, 15–23. DOI:10.1007/s10847-011-9990-x
- G. Q. Silveira, R. S. da Silva, L. P. Franco, M. D. Vargas, C. M. Ronconi, *Micropor. Mesopor. Mat.* **2015**, *206*, 226–233. DOI:10.1016/j.micromeso.2014.12.026
- F. Qu, G. Zhu, S. Huang, S. Li, S. Qiu, *Chemphyschem.* **2006**, *7(2)*, 400–406. DOI:10.1002/cphc.200500294
- S. Wang, *Micropor. Mesopor. Mat.* **2009**, *117 /1-2*, 1-9. DOI:10.1016/j.micromeso.2008.07.002
- Ş. Gunaydin, A. Yilmaz, *Turk. J. Chem.* **2015**, *39*, 317–333. DOI:10.3906/kim-1409-56
- V. Ambrogi, L. Perioli, C. Pagano, F. Marmottini, M. Moretti, F. Mizzi, C. Rossi, *J. Pharm. Sciences.* **2010**, *99*, 4738–4745. DOI:10.1002/jps.22183
- Q. Tanga, Y. Xu, D. Wu, Y. Sun, *J. Solid State Chemistry.* **2006**, *179*, 1513–1520. DOI:10.1016/j.jssc.2006.02.004
- M. Popova, A. Szegedi, K. Yoncheva, S. Konstantinov, G. P. Petrova, H. A. Aleksandrov, G. N. Vayssilov, P. Shestakova, *Micropor. Mesopor. Mat.* **2014**, *198*, 247–255. DOI:10.1016/j.micromeso.2014.07.044
- B. Koneru, Y. Shi, Y.-C. Wang, S. H. Chavala, M. L. Miller, B. Holbert, M. Conson, A. Ni, A. J. Di Pasqua, *Molecules* **2015**, *20*, 19690–19698. DOI:10.3390/molecules201119650
- M. Vallet-Regi, F. Balasa, M. Colilla, M. Manzano, *Solid State Sci.* **2007**, *9*, 768–776. DOI:10.1016/j.solidstatesciences.2007.03.026
- L. Ochiuz, M. C. Luca, I. Stoleriu, M. Moscalu, D. Timofte, G. Tantar, A. Stefanache, *Farmacia*, **2016**, *64*, 131–134.
- A. Bolouki, L. Rashidi, E. Vasheghani-Farahani, Z. Piravi-Vanak, *Int. J. Nanosci. Nanotechnol.* **2015**, *11(3)*, 139–146.
- R. Kotcherlakota, A. K. Barui, S. Prashar, M. Fajardo, D. Briones, A. Rodríguez-Diéguez, C. R. Patra, S. Gómez-Ruiz, *Biomater Sci.* **2016**, *4(3)*, 448–459. DOI:10.1039/C5BM00552C
- F. Porta, G. E. Lamers, J. Morhayim, A. Chatzopoulou, M. Schaaf, H. den Dulk, C. Bachendorf, J. I. Zink, *Adv. Healthcare Mater.* **2013**, *2*, 281–286. DOI:10.1002/adhm.201200176
- A. L. Doadrio, A. J. Salinas, J. M. Sánchez-Montero, M. Vallet-Regi, *Curr Pharm Des.* **2015**, *21*, 6189–6213. DOI:10.2174/1381612822666151106121419
- A. M. Tomoiaga, B. I. Cioroiu, V. Nica, A. Vasile, *Colloids Surf B: Biointerfaces.* **2013**, *111*, 52–59. DOI:10.1016/j.colsurfb.2013.05.019
- A. M. Tomoiaga, L. Ochiuz, A. Vasile, *J. Nanotech. Diagn. Treat.* **2013**, *1*, 26–35. DOI:10.12974/2311-8792.2013.01.01.4
- B. D. Smith, L. D. Wilson, *Curr. Probl. Cancer.* **2008**, *32*, 43–87. DOI:10.1016/j.currprobcancer.2007.12.002
- L. Chen, Y. Wang, J. Zhang, L. Hao, H. Guo, H. Lou, D. Zhang, *Eur J Pharm Biopharm.* **2014**, *87*, 160–169. DOI:10.1016/j.ejpb.2013.12.005
- R. P. Gogineni, Rapid liquid chromatography UV detection method development and validation of multiclass drugs in active pharmaceutical ingredients and pharmaceutical dosage forms and applicability to biological matrices. PhD thesis (2014), Acharya Nagarjuna University. Available at: <http://hdl.handle.net/10603/31065>, Accessed: 11 August 2016.
- M. Thommes, K. Kaneko, A. V. Neimark, J. P. Olivier, F. Rodriguez-Reinoso, J. Rouquerol, K.S.W. Sing, *Pure Appl. Chem.* **2015**, *19* pages.
- J. Kim, P. Seidler, C. Fill, L.S. Wan, *Surf Sci.* **2008**, *602*, 3323–3330. DOI:10.1016/j.susc.2008.09.001
- IARC Handbooks of Cancer Prevention, p 317 – 324.
- N. Ahuja, P. K. Om, B. Singh, *Eur. J. Pharm. and biopharm.* **2007**, *65*, 26–38. DOI:10.1016/j.ejpb.2006.07.007
- L. Ochiuz, C. Grigoras, M. Popa, I. Stoleriu, C. Munteanu, D. Timofte, L. Profire, A.G. Grigoras, *Molecules.* **2016**, *21(7)*, 858–874. DOI:10.3390/molecules21070858
- M. C. Gohel, K. G. Sarvaiya, A. R. Shah, B. K. Brahmabhatt, *Indian J. Pharm. Sci.* **2009**, *71*, 142–144. DOI:10.4103/0250-474X.54281
- K. H. Ramteke, *Sch. Acad. J. Pharm.* **2014**, *3(5)*, 388–396.

36. R. W. Korsmeyer, R. Gurny, E. Doelker, P. Buri, N. A. Peppas, *Int. J. Pharm.* **1983**, 15, 25–35.
DOI:10.1016/0378-5173(83)90064-9
37. N. A. Peppas, *Pharm Acta Helv.* **1985**, 60, 110–111.

Povzetek

V pispevku poročamo o prvi uporabi MCM-41 mezoporoznega silicijevega dioksida kot zelo učinkovitega nosilca za beksaroten, antineoplastičnega zdravila namenjenega zdravljenju bolnikov s kožnim T-celičnim limfomom (CTCL). Beksaroten je zelo strupen in slabo topen v vodi, z nizko biološko uporabnostjo v običajnih farmacevtskih oblikah. Podani so rezultati o absorpciji beksarotena na amino-funkcionalizirane nosilce silicijevega dioksida z različnimi stopnjami funkcionalizacije ob upoštevanju vseh strukturnih značilnosti tako nosilca kot tudi lastnosti molekul zdravilne učinkovine. Dobljeni rezultati so pokazali uspešno vezavo beksarotena na amino-funkcionaliziran silicijev dioksid MCM-41. Molekule beksarotena se adsorbirajo na aktivnih centrih v nekrystalnični fazi, kar nakazuje na pomembno vlogo amino kislinskega funkcionaliziranja nosilca na topnost zdravilne učinkovine in izboljšanje biološke uporabnosti. *In vitro* testi raztapljanja so pokazali podaljšano sproščanje beksarotena v 12 urah in 50 % sproščanje vezanih aktivnih molekul. V raziskavi smo dokazali, da je podaljšano sproščanje učinkovine posledica prisotnosti aminopropilnih skupin na stenah silicijevih por.

Scientific paper

Synthesis and *in vitro* Bio-activity Evaluation of N^4 -benzyl Substituted 5-Chloroisatin-3-thiosemicarbazones as Urease and Glycation Inhibitors

Humayun Pervez,^{1,*} Nazia Khan,¹ Jamshed Iqbal,² Sumera Zaib,^{2,3} Muhammad Yaqub¹ and Muhammad Moazzam Naseer^{4,*}

¹ Institute of Chemical Sciences, Organic Chemistry Division, Bahauddin Zakariya University, Multan 60800, Pakistan

² Centre for Advanced Drug Research, COMSATS Institute of Information Technology, Abbottabad 22060, Pakistan

³ Department of Bioinformatics & Biotechnology, International Islamic University, Islamabad 44000, Islamabad, Pakistan

⁴ Department of Chemistry, Quaid-i-Azam University, Islamabad 45320, Pakistan

* Corresponding author: E-mail: pdhpervez@hotmail.com; moazzam@qau.edu.pk

Received: 19-06-2017

Abstract

A series of fifteen N^4 -benzyl substituted 5-chloroisatin-3-thiosemicarbazones **5a–o** were synthesized and screened mainly for their antiurease and antiglycation effects. *Lemna aquinocalis* growth and *Artemia salina* assays were carried out to determine their phytotoxicity and cytotoxicity potential. All the compounds proved to be extremely effective urease inhibitors, demonstrating enzyme inhibition much better than the reference inhibitor, thiourea (IC_{50} values 1.31 ± 0.06 to 3.24 ± 0.15 vs. 22.3 ± 1.12 μ M). On the other hand, eight out of fifteen compounds tested, *i.e.* **5b**, **5c**, **5h–k**, **5m** and **5n** were found to be potent glycation inhibitors. Of these, five *viz.* **5c**, **5h–j** and **5n** proved to be exceedingly efficient, displaying glycation inhibition greater than the reference inhibitor, rutin (IC_{50} values 114.51 ± 1.08 to 229.94 ± 3.40 vs. 294.5 ± 1.5 μ M).

Keywords: 5-Chloroisatin, Glycation inhibition, Heterocyclics, Schiff bases, Thiosemicarbazones, Urease inhibition

1. Introduction

Isatin and its derivatives are known to have a diversity of chemotherapeutic activities.^{1–35} Of the isatin derivatives, isatin-thiosemicarbazones have been found to exhibit a range of biological properties, including antiulcer,¹ anticancer,^{1,4,7,12,21–23} antimicrobial,^{1–3,5,7,22,24,25} antituberculosis,^{26–28} antiviral^{1,2,5,7,12,28} and enzyme inhibitory activities.^{1,4,11,17} Incited by these findings and as a part of our synthetic work on bioactive isatin derivatives, we have recently reported the synthesis of numerous N^4 -aryl substituted isatin-3-thiosemicarbazones (thiourea derivatives) as antimicrobial,^{36–39} cytotoxic,^{38–42} phytotoxic,^{38–41,43} antileishmanial⁴⁴ and more importantly antiurease^{36–40,43,45} compounds. SAR studies in the synthesized thiosemicarbazones disclosed that in some cases the nature and location of the substituent on the phenyl ring attached to thiosemicarbazone N^4 and/or the existence of lipophilic/inductively electron-withdrawing functions (Cl, F, F_3CO , NO_2) at po-

sition 5 of the isatin moiety played a significant role in inducing and/or increasing certain activities, including urease inhibition. In view of this and as an extension of our earlier studies^{36–47} aiming to the synthesis of novel isatin derivatives with enhanced or diverse biological activities, we very recently reported the synthesis of a series of N^4 -benzyl substituted 5-nitroisatin-3-thiosemicarbazones (derivatives of thiourea, a substrate-like urease inhibitor) as highly effective urease inhibitors.⁴⁸ Interestingly, all these compounds demonstrated either induced or increased urease inhibitory activity in comparison to the respective N^4 -phenyl substituted derivatives tested in our earlier assays.^{38,45} Furthermore, a number of other derivatives of thiourea are reported to show promising glycation inhibitory activity.^{49–53} Also, some isatin-derived imines (Schiff bases) have been recognized as potent inhibitors of glycation.^{54,55} Prompted by these observations and as a continuation of our previous studies on bioactive isatin

derivatives, we have synthesized a series of fifteen title thiosemicarbazones (a class of Schiff bases) and tested them principally for their antiurease and antiglycation influences. *L. aequinocitalis* growth and *A. salina* assays were carried out to determine their phytotoxic and cytotoxic effects, respectively.

This paper is one of the first to report on N^4 -benzyl substituted isatin-thiosemicarbazones possessing urease and glycation inhibitory potential. In it we limit our discussion to those compounds which have concurrently attached lipophilic/inductively electron-withdrawing chloro substituent at position 5 of the isatin scaffold and the benzyl functions (modified by placing one inductively electron-donating and one or two electron-attracting groups around the phenyl ring) to thiosemicarbazone N^4 .

2. Results and Discussion

This study describes the preparation and *in vitro* testing of antiurease, antiglycation, phytotoxic and cytotoxic potentiality of fourteen presently and one formerly reported²² N^4 -benzyl substituted 5-chloroisatin-thiosemicarbazones **5b–o** and **5a**, respectively.

2. 1. Chemistry of Compounds 5a–o

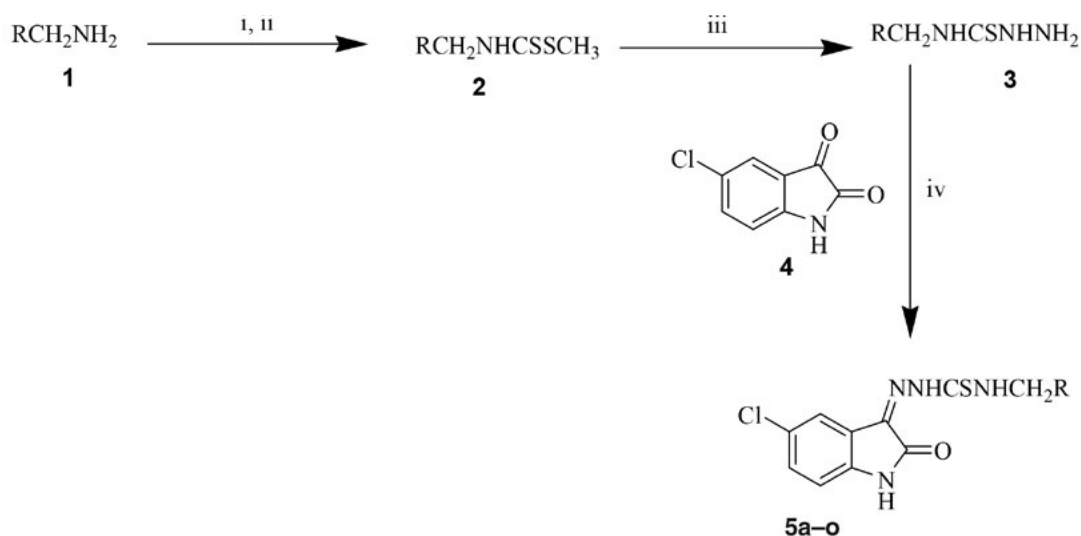
Appropriate N -substituted thiosemicarbazides **3** were reacted with 5-chloroisatin **4** in 50% ethanol (aq.) to furnish the respective thiosemicarbazones **5a–o** (Scheme 1). The structures of **5a–o** were established by elemental

and spectral analyses. Acceptable elemental data were obtained in all the cases. The infrared (IR) spectra of **5a–o** showed absorption bands in the 3375–3051, 1737–1684, 1620–1599 and 1193–1149 cm^{-1} regions attributed to NH, C=O, C=N and C=S functions, respectively.^{22,56,57} The proton nuclear magnetic resonance (^1H NMR) spectra displayed two separate singlets at δ 7.50–11.36 and 10.84–12.75 for indole NH and thiosemicarbazone N^2 -H. The thiosemicarbazone N^4 -H appeared as a triplet at δ 8.03–10.91 in all the cases,^{22,27} except **5e**, **5g** and **5h**, wherein it resonated as a singlet at δ 8.26, 10.91 and 10.85, respectively. Similarly, the benzyl CH_2 protons were observed as a doublet at δ 4.40–5.02 in all the cases,^{22,27} except **5b**, **5g** and **5h**; in the case of **5h** they appeared as a singlet at δ 3.79, whilst in **5b** and **5g** they resonated together with the DMSO and DMSO, CH_3 group protons, respectively. The carbon nuclear magnetic resonance (^{13}C NMR) spectra of compounds **5a–o** upheld the IR and ^1H NMR conclusions. Also, the EI (electron impact) mass spectra of all the compounds displayed molecular ions with mixed intensity and the fragments characteristic of isatin and thiosemicarbazone moieties. The main fragmentation path engaged the split of endocyclic NH–CO and exocyclic NH–CS, N–N bonds.⁵⁷ The proposed fragmentation pattern of **5i** is depicted in Figure S1.

2. 2. Biology of Compounds 5a–o

2. 2. 1. Urease Inhibition (*in vitro*)

The synthesized N^4 -benzyl substituted 5-chloroisatin-3-thiosemicarbazones **5a–o** were tested for their urease



Scheme 1. Reagents and conditions: (i) Et_3N , MeOH, CS_2 , stir, 30 °C (internal), 75 min., r.t., 1 h; (ii) CH_3I , MeOH, stir, –10 °C, 20 min., r.t., 2 h; (iii) $\text{NH}_2\text{NH}_2 \cdot \text{H}_2\text{O}$, EtOH, reflux, 2 h; (iv) 50% EtOH (aq.), reflux, 2 h.

inhibitory effects and found to be extremely effective inhibitors of the enzyme, displaying superb inhibition ($IC_{50} = 1.31 \pm 0.06$ to $4.07 \pm 0.11 \mu\text{M}$) in contrast to the reference inhibitor, thiourea, which showed inhibitory activity with IC_{50} value $22.3 \pm 1.12 \mu\text{M}$ in this assay (Table 1).

SAR studies in the N^4 -benzyl substituted isatin-thiosemicarbazones **5a–o** divulged that in comparison to compound **5a** having no functional group on the phenyl ring of the benzyl group attached to thiosemicarbazone N^4 , all the rest compounds except **5d** and **5k**, regardless of the number, type and place of the functionalities present on the phenyl ring, displayed enhanced enzymatic inhibition (IC_{50} values 1.31 ± 0.06 to 3.05 ± 0.15 vs. $3.24 \pm 0.15 \mu\text{M}$). Compound **5l** bearing chloro substituent at position 3 of the phenyl ring was the most effective urease inhibitor of the series in the present assay, demonstrating two and half, and seventeen times larger activity than compound **5a** and the reference inhibitor, thiourea, respectively ($IC_{50} = 1.31 \pm 0.06$ vs. 3.24 ± 0.15 and $22.3 \pm 1.12 \mu\text{M}$). The next most effective enzyme inhibitor was **5e** possessing methoxy group at position 2 of the phenyl ring. This compound showed a somewhat lesser inhibitory activity than **5l** but is still about two and fifteen times more active than compound **5a** and thiourea (IC_{50} value 1.45 ± 0.23 vs. 1.31 ± 0.06 , 3.24 ± 0.15 and $22.3 \pm 1.12 \mu\text{M}$, respectively). The third most effective inhibitor of the enzyme was compound **5j** having fluoro group at position 4 of the phenyl ring. This compound like **5e** appeared to be a bit less active than **5l** (IC_{50} value 1.77 ± 0.24 vs. $1.31 \pm 0.06 \mu\text{M}$) but about two and twelve times more active than compound **5a** and thiourea (IC_{50} value 1.77 ± 0.24 vs. 3.24 ± 0.15 and $22.3 \pm 1.12 \mu\text{M}$, respectively). The isomeric compounds **5h** and **5i** possessing fluoro functionalities at positions 2 and 3 of the phenyl ring, however, demonstrated comparatively inferior but comparable enzymatic inhibition ($IC_{50} = 2.03 \pm 0.14$ and $2.07 \pm 0.09 \mu\text{M}$, respectively). The remaining relatively more effective inhibitors of the enzyme were the dichloro-substituted derivatives **5n** and **5o**. Among these, **5n** with the substituents at positions 2 and 4 of the phenyl ring displayed about two fold larger enzymatic inhibition in comparison to the monochloro-substituted compound **5k** having the substituent at position 2 of the phenyl ring (IC_{50} value 2.36 ± 0.16 vs. $4.07 \pm 0.11 \mu\text{M}$). On the other hand, **5o** possessing the substituents at positions 3 and 4 of the phenyl ring exhibited distinctly decreased inhibitory activity in contrast to monochloro-substituted compound **5l** (the most potent inhibitor of the series) with the substituent at position 3 of the phenyl ring (IC_{50} value 1.97 ± 0.16 vs. $1.31 \pm 0.06 \mu\text{M}$).

Interestingly, out of fifteen N^4 -benzyl substituted 5-chloroisatin-thiosemicarbazones **5a–o** tested in the present assay, five *viz.* **5e**, **5f**, **5k**, **5l** and **5o** were found to display enhanced urease inhibitory activity when compared with the corresponding N^4 -phenyl substituted 5-chloroisatin-thiosemicarbazones tested in our earlier assay.⁴³ For instance, compounds **5e**, **5k** and **5l** with 2-me-

thoxy-, 2-chloro- and 3-chloro-benzyl functions attached to N^4 of the thiosemicarbazone moiety demonstrated enzyme inhibitory activity with IC_{50} values 1.45 ± 0.23 , 4.07 ± 0.11 and 1.31 ± 0.06 , whereas the corresponding N^4 -phenyl substituted thiosemicarbazones displayed enzymatic inhibition with IC_{50} values 54.76, 54.35 and $38.91 \mu\text{M}$, respectively. Similarly, compounds **5f** and **5n** possessing 3-methoxy- and 2,4-dichloro-benzyl groups at N^4 of the thiosemicarbazone moiety showed inhibitory activity with IC_{50} values 2.63 ± 0.15 and $2.36 \pm 0.16 \mu\text{M}$, while the respective N^4 -phenyl substituted thiosemicarbazones displayed only 22.35 and 26.06% inhibition of the enzyme at $100 \mu\text{M}$ concentration. This indicated that the N^4 -benzyl substituted 5-chloroisatin-thiosemicarbazones **5e**, **5k**, **5l** and more importantly **5f**, **5n** compared with the related N^4 -phenyl substituted 5-chloroisatin-thiosemicarbazones interfered with the enzyme quite efficiently, causing much pronounced enhancement in their enzyme inhibitory potential.

The above results revealed that the attachment of varied benzyl groups (possessing one inductively electron-donating and one or two electron-withdrawing functional groups on the phenyl ring) to N^4 of the thiosemicarbazone moiety caused the molecules to intermingle with the enzyme differently and in some cases more competently. Moreover, exhibition of enhanced enzymatic inhibition by N^4 -benzyl substituted isatin-thiosemicarbazones in contrast to the parallel N^4 -aryl substituted ones may be explained on the basis of their better hydrophobic character, which may play a role in their indiscriminate walk process to the active site, and in the hydrophobic binding near the active site of the enzyme.

Table 1. Inhibition of Jack bean urease by compounds **5a–o**

Compound	R	$IC_{50} \pm \text{SEM} (\mu\text{M})^a$
5a	C_6H_5	3.24 ± 0.15
5b	2- $\text{CH}_3\text{C}_6\text{H}_4$	2.47 ± 0.21
5c	3- $\text{CH}_3\text{C}_6\text{H}_4$	2.55 ± 0.22
5d	4- $\text{CH}_3\text{C}_6\text{H}_4$	3.69 ± 0.15
5e	2- $\text{CH}_3\text{OC}_6\text{H}_4$	1.45 ± 0.23
5f	3- $\text{CH}_3\text{OC}_6\text{H}_4$	2.63 ± 0.15
5g	4- $\text{CH}_3\text{OC}_6\text{H}_4$	2.96 ± 0.19
5h	2- FC_6H_4	2.03 ± 0.14
5i	3- FC_6H_4	2.07 ± 0.09
5j	4- FC_6H_4	1.77 ± 0.24
5k	2- ClC_6H_4	4.07 ± 0.11
5l	3- ClC_6H_4	1.31 ± 0.06
5m	4- ClC_6H_4	3.05 ± 0.15
5n	2,4-(Cl) $_2\text{C}_6\text{H}_3$	2.36 ± 0.16
5o	3,4-(Cl) $_2\text{C}_6\text{H}_3$	1.97 ± 0.16
Thiourea ^b		22.3 ± 1.06

^a Standard error of the mean; ^b Standard inhibitor for urease.

2. 2. 2. Antiglycation Activity (*in vitro*)

The synthesized *N*⁴-benzyl substituted 5-chloroisatin-3-thiosemicarbazones **5a–o** were further tested for their antiglycation potentiality, using rutin as the reference inhibitor of glycation. Out of fifteen compounds tested, eight *i.e.* **5b**, **5c**, **5h–k**, **5m** and **5n** proved to be potent antiglycating agents, showing varied antiglycation activity ($IC_{50} = 114.51 \pm 1.08$ to $433.88 \pm 2.66 \mu\text{M}$). Compounds **5c**, **5h–j** and **5n** displayed superb inhibitory activity even better than the reference inhibitor, rutin (IC_{50} values 114.51 ± 1.08 to 229.94 ± 3.40 vs. $294.5 \pm 1.5 \mu\text{M}$) (Table 2) and may thus act as convincing leads for further studies.

The limited structure-activity relationship (SAR) studies in the synthetic thiosemicarbazones **5a–o** indicated that compound **5c** possessing methyl substituent at position 3 of the phenyl ring attached to *N*⁴ of the thiosemicarbazone moiety was the most potent antiglycating agent of the series in the present assay, exhibiting antiglycation activity with IC_{50} value $114.51 \pm 1.08 \mu\text{M}$. The next most potent antiglycating derivative was **5j** bearing the fluoro substituent at position 4 of the phenyl ring. This compound displayed a bit lesser inhibition of glycation than the most potent derivative **5c** but much larger than the reference inhibitor, rutin (IC_{50} value 168.71 ± 8.58 vs. 114.51 ± 1.08 and $294.5 \pm 1.50 \mu\text{M}$, respectively). The third most active antiglycating agent was found to be compound **5i** bearing the fluoro substituent at position 3 of the phenyl ring, demonstrating a somewhat lower activity than **5j** but still considerably higher than the reference inhibitor, rutin ($IC_{50} = 202.21 \pm 0.55$ vs. 168.71 ± 8.58 and $294.5 \pm 1.5 \mu\text{M}$, respectively). The remaining relatively more potent glyca-

tion inhibitors **5h** and **5n** possessing fluoro and chloro substituents at positions 2 and 2,4 (*ortho* and *para*) of the phenyl ring, respectively, showed inhibitory activity with IC_{50} values 229.94 ± 3.40 and $217.71 \pm 1.65 \mu\text{M}$. The other potent compounds *viz.* **5b** and **5k**, **5m** having methyl and chloro substituents at positions 2 and 2,4 of the phenyl ring, respectively, demonstrated moderate antiglycation activity with IC_{50} values 333.06 ± 9.80 and 343.75 ± 2.76 , $433.88 \pm 2.66 \mu\text{M}$. The rest of the compounds *viz.* **5d–g** and **5l** displayed less than 50% inhibition of glycation and were, therefore, not assessed further for their IC_{50} values. Compound **5a** showed an anomalous behaviour, displaying enhancement in glycation.

The above results showed that the CH_3 , F and Cl groups worked as active moieties in causing effective inhibition of glycation. Further, the location and/or the number of the substituents on the phenyl ring played a key role in improving the glycation inhibitory potency of the compounds.

2. 2. 3. Phytotoxicity (*in vitro*)

The synthetic thiosemicarbazones **5a–o** were also tested for their phytotoxic influences at 1000, 100, 10 or 500, 50, 5 $\mu\text{g}/\text{mL}$ concentrations. Out of fifteen compounds tested, nine *viz.* **5c**, **5d**, **5h–5m** and **5o** were found to be active, demonstrating weak or non-significant (5–93%) phytotoxic activity at 1000 or 500 $\mu\text{g}/\text{mL}$ concentrations in comparison to paraquat (the standard herbicide) which showed 100% plant growth inhibition at 0.015 $\mu\text{g}/\text{mL}$ concentration (Table 3).

Table 2. Antiglycation activity of compounds **5a–o**

Compound	R	Concentration (μM)	Inhibition (%)	$IC_{50} \pm \text{SEM}^a$ (μM)
5a	C_6H_5	250	–	
5b	2- $\text{CH}_3\text{C}_6\text{H}_4$	500	57.96	333.06 ± 9.80
5c	3- $\text{CH}_3\text{C}_6\text{H}_4$	250	65.32	114.51 ± 1.08
5d	4- $\text{CH}_3\text{C}_6\text{H}_4$	250	37.42	
5e	2- $\text{CH}_3\text{OC}_6\text{H}_4$	250	31.34	
5f	3- $\text{CH}_3\text{OC}_6\text{H}_4$	1000	45.00	
5g	4- $\text{CH}_3\text{OC}_6\text{H}_4$	500	21.96	
5h	2- FC_6H_4	500	59.27	229.94 ± 3.40
5i	3- FC_6H_4	500	68.08	202.21 ± 0.55
5j	4- FC_6H_4	250	66.15	168.71 ± 8.58
5k	2- ClC_6H_4	1000	70.77	343.75 ± 2.76
5l	3- ClC_6H_4	1000	33.22	
5m	4- ClC_6H_4	1000	54.60	433.88 ± 2.66
5n	2,4-(Cl) $_2\text{C}_6\text{H}_3$	500	78.17	217.71 ± 1.65
5o	3,4-(Cl) $_2\text{C}_6\text{H}_3$	62.5	19.29	
Rutin ^b		1000	86.00	294.50 ± 1.50

^a Standard error of the mean; – Enhancement in glycation; ^b Standard inhibitor of glycation.

Table 3. Growth inhibition of *Lemna aequinoctialis* by compounds **5a–o** at different concentrations

Compound	R	1000	100	10	500	50	5
		$\mu\text{g/mL}$ G.I. (%)	$\mu\text{g/mL}$ G.I. (%)	$\mu\text{g/mL}$ G.I. (%)	$\mu\text{g/mL}$ G.I. (%)	$\mu\text{g/mL}$ G.I. (%)	$\mu\text{g/mL}$ G.I. (%)
5a	C ₆ H ₅	–	–	–	00	00	00
5b	2-CH ₃ C ₆ H ₄	00	00	00	–	–	–
5c	3-CH ₃ C ₆ H ₄	06	00	00	–	–	–
5d	4-CH ₃ C ₆ H ₄	25	10	00	–	–	–
5e	2-CH ₃ OC ₆ H ₄	00	00	00	–	–	–
5f	3-CH ₃ OC ₆ H ₄	00	00	00	–	–	–
5g	4-CH ₃ OC ₆ H ₄	00	00	00	–	–	–
5h	2-FC ₆ H ₄	10	05	00	–	–	–
5i	3-FC ₆ H ₄	14	00	00	–	–	–
5j	4-FC ₆ H ₄	93	00	00	–	–	–
5k	2-ClC ₆ H ₄	05	05	00	–	–	–
5l	3-ClC ₆ H ₄	20	00	00	–	–	–
5m	4-ClC ₆ H ₄	25	00	00	–	–	–
5n	2,4-(Cl) ₂ C ₆ H ₃	–	–	–	00	00	00
5o	3,4-(Cl) ₂ C ₆ H ₃	–	–	–	15	00	00

2. 2. 4. Cytotoxicity (*in vitro*)

The synthesized thiosemicarbazones **5a–o** were further screened for their cytotoxicity potential by a brine shrimp (*Artemia salina*) bioassay. All the compounds gave LD₅₀ values larger than 2.43×10^{-4} M to 2.91×10^{-4} M in this assay and were thus considered to be almost inactive.

2. 2. 5. Molecular Docking Studies of Compounds **5a–o**

All the compounds showed interactions with His409, Ala436, His492, Asp494, Arg609, His519, Arg639, His593, Ala636 and His594. Figure 1 represents the putative bind-

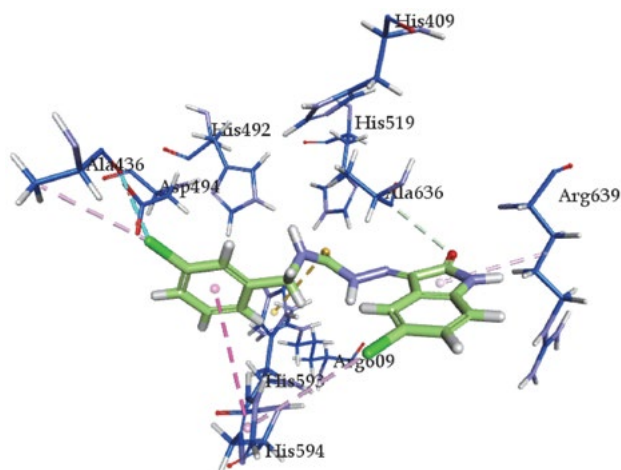


Figure 1. The putative binding mode of **5l** (the most active inhibitor; light green colored) in the active site pocket of Jack bean urease.

ing mode of **5l**, the most potent inhibitor of the enzyme Jack bean urease. Hydrogen-bonding interactions were observed between the oxygen and hydrogen atoms of the inhibitors and the amino acid residues Ala436, Ala636, Arg639, Arg609 and His593. The 3-chlorobenzyl group was directed towards amino acids Ala436, Asp494 and His492, whereas the remaining part of the compound was directed towards Arg639 and Ala636.

All the synthetic derivatives **5a–o** were docked inside the active site of the enzyme. No specific interactions were noticed with Ni atoms by any compound; however, aromatic interactions were observed in the active pocket of the enzyme, as shown in Figure 2. This suggests that all the compounds exhibit inhibitory activity by blocking the entrance of the catalytic domain in the enzyme. The docking scores were obtained in the range of -19.57 to -16.27 and are given in Table 4.



Figure 2. Common binding modes of all the inhibitors inside the active site pocket of the urease enzyme.

2. 2. 5. 1. ADME Profile of *N*⁴-Benzyl Substituted 5-Chloroisatin-3-thiosemicarbazones 5a–o

Drug-likeness is a qualitative property of chemicals evaluated with respect to factors like bioavailability. In order to evaluate drug-likeness of the synthetic derivatives 5a–o, ADME (Absorption, Distribution, Metabolism and Excretion) properties were taken into account. The parameters selected for the purpose were octanol-water distribution coefficients (Slog *P* and log *P*), the log solubility in water (log *S*), the number of hydrogen bond acceptors (HBAH), the number of hydrogen bond donors (HBDH) and the topological polar surface area (TPSA). Along with *in silico* evaluation of ADME profile, free binding energies were also calculated for all the derivatives. The TPSA values indicated that all the compounds 5a–o can be easily penetrable in the form of drugs, as they showed polar surface area in the range of 95–107 Å². Typically, for molecules to penetrate the blood–brain barrier and, therefore, to act as receptors, an area less than 120 Å² is usually needed and molecules with a polar surface area of greater than 120–140 Å² tend to be poor in permeating cell membranes.⁵⁸ In general, compounds with molecular weight less than 500, HBAH less than 10, HBDH less than 5 and a log*P* value of less than 5 are treated as orally bioavailable with favorable ADME profile.^{59,60} The determined ADME properties of compounds 5a–o are given in Table 4. All the trial compounds exhibited favorable ADME properties and no violation of Lipinski's rule was observed. According to Lipinski's rule of 5, only two violations are allowed in the molecular docking studies.^{61–63}

3. Experimental

3. 1. General

Melting points (uncorrected) were measured on a Fisher–Johns melting point apparatus. Elemental analyses

were carried out using a Leco CHNS-9320 (USA) instrument. IR (KBr discs) spectra were recorded with a Shimadzu Prestige-21 or Shimadzu 8400 spectrophotometer. ¹H NMR spectra were obtained in CDCl₃/DMSO-*d*₆ with Bruker Avance/Spectrospin 300 and Bruker Avance 400 spectrometers, using tetramethylsilane (TMS) as the internal standard. ¹³C NMR spectra were determined in DMSO-*d*₆ with a Bruker Avance 300 spectrometer, operating at 75 MHz. EI (electron impact) mass spectra were obtained on MAT-312 and JEOL MSRoute mass spectrometers. All the chemicals and reagents used in the present study were purchased from Merck-Schuchardt, Fluka and Sigma-Aldrich.

3. 2. Synthesis of *N*-Substituted Thiosemicarbazides 3

The *N*-substituted thiosemicarbazides used in this study were synthesized according to the synthetic route reported in the literature.⁶³

3. 3. Synthesis of Isatin-thiosemicarbazones 5a–o

Appropriate thiosemicarbazides 3 (5 mmol) were treated with 5-chloroisatin 4 (5 mmol) in 50% aqueous ethanol (25 mL) under reflux for 2 h. The solid formed during heating in each case was filtered and washed thoroughly with hot aqueous ethanol, affording the required compounds 5a–o in pure form.

N-Benzyl-2-(5-chloro-2-oxo-2,3-dihydro-1*H*-indol-3-ylidene)-1-hydrazinecarbothioamide (5a)

Yellow crystals; Yield: 81%; m.p. 270–272 °C (lit.²² m.p. 245 °C); IR (KBr, cm⁻¹): 3375, 3159 (NH), 1691 (C=O), 1618 (C=N), 1164 (C=S); ¹H NMR (DMSO-*d*₆, 400 MHz): δ 4.87 (d, *J* = 6.4 Hz, 2H, benzyl CH₂), 6.93 (d, *J* = 8.4 Hz, 1H, indole C₇-H), 7.24–7.28 (m, 1H, benzyl C₄-H),

Table 4. Free binding energy and ADME profile of compounds 5a–o

Compound	Free binding energy	log <i>P</i>	log <i>S</i>	Slog <i>P</i>	M. Wt.	HBAH	HBDH	TPSA
5a	-17.8283	4.987	-5.7985	2.9269	344.826	6	3	97.61
5b	-19.3512	5.283	-6.2724	3.2353	358.853	6	3	97.61
5c	-19.5795	5.322	-6.2724	3.2353	358.853	6	3	97.61
5d	-16.5393	5.285	-6.2724	3.2353	358.853	6	3	97.61
5e	-16.9345	4.941	-5.8488	2.9355	374.852	7	4	106.84
5f	-17.4872	4.980	-5.8488	2.9355	374.852	7	4	106.84
5g	-18.5219	4.943	-5.8488	2.9355	374.852	7	4	106.84
5h	-16.7386	5.138	-6.0934	3.066	362.816	6	3	97.61
5i	-17.3204	5.177	-6.0934	3.066	362.816	6	3	97.61
5j	-16.9446	5.140	-6.0934	3.066	362.816	6	3	97.61
5k	-19.2379	5.577	-6.5328	3.5803	379.271	6	3	97.61
5l	-17.1999	5.616	-6.5328	3.5803	379.271	6	3	97.61
5m	-16.3547	5.579	-6.5328	3.5803	379.271	6	3	97.61
5n	-16.2771	6.206	-7.267	4.2337	413.716	6	3	97.61
5o	-17.3941	6.206	-7.267	4.2337	413.716	6	3	97.61

7.31–7.36 (m, 4H, benzyl C₂-H, C₃-H, C₅-H, C₆-H), 7.37 (dd, $J_1 = 7.4$ Hz, $J_2 = 2.4$ Hz, 1H, indole C₆-H), 7.71 (d, $J = 7.7$ Hz, 1H, indole C₄-H), 9.90 (t, $J = 6.4$ Hz, 1H, CSNH), 11.29 (s, 1H, indole NH), 12.48 (s, 1H, NNH); ¹³C NMR (DMSO-*d*₆, 75 MHz): δ 47.18 (CH₂), 112.53 (CH), 120.46 (CH), 121.86, 126.46, 127.03 (CH), 127.26 (CH), 128.29 (CH), 130.41 (CH), 130.80, 138.22, 140.96, 162.38, 177.71; EI-MS (70 eV) *m/z* (%): 346/344 (M⁺, 13/36), 318/316 (8/20), 270/268 (9/25), 195 (19), 181 (20), 164 (13), 152 (33), 131 (17), 106 (57), 91 (100), 77 (16), 65 (35). Anal. Calcd. for C₁₆H₁₃ClN₄OS (344): C, 55.81; H, 3.78; N, 16.28. Found: C, 55.68; H, 3.75; N, 16.21.

***N*-(2-Methylbenzyl)-2-[5-chloro-2-oxo-2,3-dihydro-*H*-indol-3-ylidene]-1-hydrazinecarbothioamide (5b)**

Yellow crystals; Yield 81%; m.p. 230–232 °C; IR (KBr, cm⁻¹): 3363, 3173 (NH), 1697 (C=O), 1605 (C=N), 1159 (C=S); ¹H NMR (DMSO-*d*₆, 400 MHz): δ 2.50 (DMSO, CH₃), 3.30 (DMSO, benzyl CH₂), 6.90 (d, $J = 8.3$ Hz, 1H, indole C₇-H), 7.30 (td, $J_1 = 6.8$ Hz, $J_2 = 2.5$ Hz, 1H, benzyl C₅-H), 7.45–7.55 (m, 3H, benzyl C₃-H, C₄-H, C₆-H), 7.76 (d, $J = 8.0$ Hz, 1H, indole C₆-H), 7.94 (d, $J = 1.8$ Hz, 1H, indole C₄-H), 10.91 (t, $J = 7.5$ Hz, 1H, CSNH), 11.36 (s, 1H, indole NH), 12.62 (s, 1H, NNH); ¹³C NMR (DMSO-*d*₆, 75 MHz): δ 113.03 (CH), 114.15, 122.16, 122.35, 123.65 (CH), 128.21 (CH), 129.25 (CH), 130.68 (CH), 131.12, 132.71 (CH), 133.40 (CH), 137.45, 141.57, 162.23, 177.55; EI-MS (70 eV) *m/z* (%): 360/358 (M⁺, 2/7), 330 (2), 282 (5), 209 (3), 195 (3), 181 (42), 178 (35), 152 (31), 145 (18), 120 (62), 105 (100), 91 (32), 77 (61), 65 (18), 51 (28). Anal. Calcd. for C₁₇H₁₅ClN₄OS (358): C, 56.98; H, 4.19; N, 15.64. Found: C, 56.75; H, 4.15; N, 15.59.

***N*-(3-Methylbenzyl)-2-[5-chloro-2-oxo-2,3-dihydro-*H*-indol-3-ylidene]-1-hydrazinecarbothioamide (5c)**

Yellow fluffy crystals; Yield 80%; m.p. 202–204 °C; IR (KBr, cm⁻¹): 3361, 3192 (NH), 1697 (C=O), 1600 (C=N), 1153 (C=S); ¹H NMR (DMSO-*d*₆, 300 MHz): δ 2.30 (s, 3H, CH₃), 4.85 (d, $J = 8.4$ Hz, benzyl CH₂), 6.94 (d, $J = 8.4$ Hz, 1H, indole C₇-H), 7.07–7.26 (m, 4H, benzyl C₂-H, C₄-H, C₅-H, C₆-H), 7.38 (dd, $J_1 = 8.4$ Hz, $J_2 = 2.1$ Hz, 1H, indole C₆-H), 7.73 (d, $J = 2.1$ Hz, 1H, indole C₄-H), 9.90 (t, $J = 6.0$ Hz, 1H, CSNH), 11.31 (s, 1H, indole NH), 12.49 (s, 1H, NNH); ¹³C NMR (DMSO-*d*₆, 75 MHz): δ 111.86 (CH), 112.17 (CH), 112.65 (CH), 115.79, 120.81 (CH), 121.69, 126.53, 129.76 (CH), 130.83 (CH), 132.08, 141.41, 156.89, 160.14, 162.33, 178.62; EI-MS (70 eV) *m/z* (%): 360/358 (M⁺, 2/5), 330 (3), 282 (6), 209 (5), 181 (58), 152 (37), 138 (16), 120 (81), 105 (100), 91 (34), 77 (59), 65 (21), 51 (22). Anal. Calcd. for C₁₇H₁₅ClN₄OS (358): C, 56.98; H, 4.19; N, 15.64. Found: C, 56.88; H, 4.14; N, 15.58.

***N*-(4-Methylbenzyl)-2-[5-chloro-2-oxo-2,3-dihydro-*H*-indol-3-ylidene]-1-hydrazinecarbothioamide (5d)**

Yellow crystals; Yield 87%; m.p. 210–212 °C; IR (KBr, cm⁻¹): 3300, 3194 (NH), 1684 (C=O), 1599 (C=N), 1157

(C=S); ¹H NMR (DMSO-*d*₆, 400 MHz): δ 2.29 (s, 3H, CH₃), 4.65 (d, $J = 5.0$ Hz, 2H, benzyl CH₂), 6.94 (d, $J = 7.5$ Hz, 1H, indole C₇-H), 7.07–7.33 (m, 4H, benzyl C₂-H, C₃-H, C₅-H, C₆-H), 7.38 (dd, $J_1 = 7.5$ Hz, $J_2 = 2.0$ Hz, 1H, indole C₆-H), 7.73 (d, $J = 2.0$ Hz, 1H, indole C₄-H), 9.89 (t, $J = 7.5$ Hz, 1H, CSNH), 11.31 (s, 1H, indole NH), 12.48 (s, 1H, NNH); ¹³C NMR (DMSO-*d*₆, 75 MHz): δ 20.67 (CH₃), 46.95 (CH₂), 112.52 (CH), 113.69 (CH), 120.46 (CH), 121.85, 126.46, 126.95 (CH), 127.28 (CH), 128.82, 135.16, 136.14, 140.93, 162.38, 177.68; EI-MS (70 eV) *m/z* (%): 360/358 (M⁺, 2/7), 331 (2), 281 (5), 205 (3), 191 (3), 181/179 (13/19), 151 (29), 137 (40), 125 (55), 111 (81), 97 (96), 83 (77), 71 (86), 57 (100). Anal. Calcd. for C₁₇H₁₅ClN₄OS (358): C, 56.98; H, 4.19; N, 15.64. Found: C, 56.74; H, 4.13; N, 15.56.

***N*-(2-Methoxybenzyl)-2-[5-chloro-2-oxo-2,3-dihydro-*H*-indol-3-ylidene]-1-hydrazinecarbothioamide (5e)**

Yellow crystals; Yield 86%; m.p. 275–277 °C; IR (KBr, cm⁻¹): 3356, 3093 (NH), 1737 (C=O), 1606 (C=N), 1182 (C=S); ¹H NMR (DMSO-*d*₆, 400 MHz): δ 3.85 (s, 3H, CH₃), 4.40 (d, $J = 5.0$ Hz, 2H, benzyl CH₂), 6.88–7.03 (m, 3H, benzyl C₃-H, C₆-H, indole C₇-H), 7.23–7.30 (m, 2H, benzyl C₄-H, C₅-H), 7.39 (dd, $J_1 = 7.5$ Hz, $J_2 = 2.0$ Hz, 1H, indole C₆-H), 7.61 (s, 1H, indole C₄-H), 8.26 (s, 1H, CSNH), 10.60 (s, 1H, indole NH), 10.84 (s, 1H, NNH); ¹³C NMR (DMSO-*d*₆, 75 MHz): δ 55.82 (CH₃), 111.04 (CH), 112.01 (CH), 117.25 (CH), 120.66, 125.24 (CH), 126.15 (CH), 127.22 (CH), 128.29 (CH), 128.76, 131.39, 132.45, 142.06, 155.17, 157.20, 165.03; EI-MS (70 eV) *m/z* (%): 358 (3), 221 (3), 206 (2), 195 (100), 179 (69), 163 (45), 136 (42), 121 (79), 104 (10), 91 (73), 77 (12), 65 (10), 51 (6). Anal. Calcd. for C₁₇H₁₅ClN₄O₂S (374): C, 54.55; H, 4.01; N, 14.97. Found: C, 54.42; H, 3.95; N, 14.89.

***N*-(3-Methoxybenzyl)-2-[5-chloro-2-oxo-2,3-dihydro-*H*-indol-3-ylidene]-1-hydrazinecarbothioamide (5f)**

Yellow crystals; Yield 85%; m.p. 212–214 °C; IR (KBr, cm⁻¹): 3371, 3180 (NH), 1699 (C=O), 1605 (C=N), 1157 (C=S); ¹H NMR (DMSO-*d*₆, 300 MHz): δ 3.74 (s, 3H, CH₃), 4.87 (d, $J = 6.3$ Hz, 2H, benzyl CH₂), 6.84 (dd, $J_1 = 8.1$ Hz, $J_2 = 2.4$ Hz, 1H, benzyl C₄-H), 6.92–6.95 (m, 3H, indole C₇-H, benzyl C₂-H, C₆-H), 7.27 (t, $J = 8.1$ Hz, 1H, benzyl C₅-H), 7.38 (dd, $J_1 = 9.0$ Hz, $J_2 = 2.4$ Hz, 1H, indole C₆-H), 7.73 (d, $J = 2.1$ Hz, 1H, indole C₄-H), 9.90 (t, $J = 6.3$ Hz, 1H, CSNH), 11.32 (s, 1H, indole NH), 12.49 (s, 1H, NNH); ¹³C NMR (DMSO-*d*₆, 75 MHz): δ 113.04 (CH), 114.14, 115.88 (CH), 122.17, 123.63 (CH), 124.43 (CH), 126.31, 126.52, 129.30 (CH), 130.86 (CH), 131.30, 133.44 (CH), 141.61, 162.21, 177.97; EI-MS (70 eV) *m/z* (%): 376/374 (M⁺, 3/9), 298 (3), 209 (17), 194 (42), 181 (69), 178 (11), 152 (64), 138 (40), 136 (98), 121 (100), 109 (44), 106 (22), 91 (87), 77 (77), 65 (64), 51 (43). Anal. Calcd. for C₁₇H₁₅ClN₄O₂S (374): C, 54.55; H, 4.01; N, 14.97. Found: C, 54.45; H, 3.96; N, 14.92.

***N*-(4-Methoxybenzyl)-2-[5-chloro-2-oxo-2,3-dihydro-1*H*-indol-3-ylidene]-1-hydrazinecarbothioamide (5g)**

Yellow fluffy crystals; Yield 89%; m.p. 190–192 °C; IR (KBr, cm^{-1}): 3369, 3267 (NH), 1687 (C=O), 1620 (C=N), 1164 (C=S); ^1H NMR (DMSO- d_6 , 400 MHz): δ 2.50 (DMSO, CH_3 , benzyl CH_2), 3.45 (DMSO, benzyl CH_2), 6.91 (d, $J = 8.3$ Hz, 1H, indole C_7 -H), 7.14 (td, $J_1 = 7.6$ Hz, $J_2 = 1.8$ Hz, 1H, benzyl C_5 -H), 7.42–7.55 (m, 3H, benzyl C_2 -H, C_3 -H, C_6 -H), 7.95–7.99 (m, 2H, indole C_4 -H, C_6 -H), 10.91 (s, 1H, CSNH), 11.36 (s, 1H, indole NH), 12.60 (s, 1H, NNH); ^{13}C NMR (DMSO- d_6 , 75 MHz): δ 20.66 (CH_3), 40.34 (CH_2), 100.00, 113.02 (CH), 114.16, 122.20, 123.66 (CH), 128.88 (CH), 129.23 (CH), 129.86 (CH), 130.97, 133.36 (CH), 138.83 (CH), 140.76, 141.54, 162.23, 177.33; EI-MS (70 eV) m/z (%): 374 (M^+ , 3), 298 (2), 209 (4), 194 (55), 181 (33), 178 (10), 161 (59), 152 (30), 136 (64), 134 (38), 121 (100), 109 (26), 106 (22), 91(38), 77 (77), 65 (28), 51 (44). Anal. Calcd. for $\text{C}_{17}\text{H}_{15}\text{ClN}_4\text{O}_2\text{S}$ (374): C, 54.55; H, 4.01; N, 14.97. Found: C 54.42; H, 3.96; N, 14.90.

***N*-(2-Fluorobenzyl)-2-[5-chloro-2-oxo-2,3-dihydro-1*H*-indol-3-ylidene]-1-hydrazinecarbothioamide (5h)**

Orange fluffy crystals; Yield 87%; m.p. 260–262 °C; IR (KBr, cm^{-1}): 3375, 3116 (NH), 1697 (C=O), 1605 (C=N), 1161 (C=S); ^1H NMR (DMSO- d_6 , 400 MHz): δ 3.79 (s, 2H, benzyl CH_2), 6.85–6.92 (m, 2H, benzyl C_6 -H, indole C_7 -H), 7.20–7.37 (m, 3H, benzyl C_3 -H, C_4 -H, C_5 -H), 7.51 (d, $J = 7.8$ Hz, 1H, indole C_6 -H), 8.02 (s, 1H, indole C_4 -H), 10.85 (s, 1H, CSNH), 11.36 (s, 1H, indole NH), 12.62 (s, 1H, NNH); ^{13}C NMR (DMSO- d_6 , 75 MHz): δ 55.23 (CH_2), 111.16 (CH), 111.68 (CH), 112.98 (CH), 114.15, 117.61 (CH), 122.15, 123.77 (CH), 129.13 (CH), 130.87, 133.36 (CH), 139.32, 141.47, 159.17, 162.28, 175.99; EI-MS (70 eV) m/z (%): 364/362 (M^+ , 2/4), 336/334 (2/4), 288/286 (1/3), 195 (4), 181 (25), 167 (20), 152 (27), 138 (16), 124 (73), 109 (100), 83 (52), 75 (25), 61 (27), 57 (20). Anal. Calcd. for $\text{C}_{16}\text{H}_{12}\text{FClN}_4\text{OS}$ (362): C, 53.04; H, 3.31; N, 15.47. Found: C, 52.91; H, 3.28; N, 15.39.

***N*-(3-Fluorobenzyl)-2-[5-chloro-2-oxo-2,3-dihydro-1*H*-indol-3-ylidene]-1-hydrazinecarbothioamide (5i)**

Yellow crystals; Yield 77%; m.p. 242–244 °C; IR (KBr, cm^{-1}): 3242, 3205 (NH), 1692 (C=O), 1605 (C=N), 1157 (C=S); ^1H NMR (DMSO- d_6 , 400 MHz): δ 4.90 (d, $J = 7.5$ Hz, 2H, benzyl CH_2), 6.95 (d, $J = 8.4$ Hz, 1H, indole C_7 -H), 7.07–7.23 (m, 3H, benzyl C_2 -H, C_5 -H, C_6 -H), 7.37–7.46 (m, 2H, benzyl C_4 -H, indole C_6 -H), 7.72 (d, $J = 2.5$ Hz, 1H, indole C_4 -H), 9.94 (t, $J = 7.5$ Hz, 1H, CSNH), 11.32 (s, 1H, indole NH), 12.52 (s, 1H, NNH); ^{13}C NMR (DMSO- d_6 , 75 MHz): δ 46.64 (CH_2), 112.56 (CH), 113.63 (CH), 113.74 (CH), 113.96 (CH), 114.08 (CH), 119.34 (CH), 120.45, 123.23 (CH), 126.47, 130.22 (CH), 130.35 (CH), 130.47, 141.06, 141.15, 141.26, 162.38, 164.07, 177.88; EI-MS (70 eV) m/z (%): 364/362 (M^+ , 19/49), 336/334 (12/33), 288/286 (7/23), 197/195 (5/17), 183/181 (52/81), 154/152 (13/37), 140/138 (5/12), 124 (76), 109 (100), 83 (12), 75

(7), 61 (7), 57 (3). Anal. Calcd. for $\text{C}_{16}\text{H}_{12}\text{FClN}_4\text{OS}$ (362): C, 53.04; H, 3.31; N, 15.47. Found: C, 52.90; H, 3.27; N, 15.39.

***N*-(4-Fluorobenzyl)-2-[5-chloro-2-oxo-2,3-dihydro-1*H*-indol-3-ylidene]-1-hydrazinecarbothioamide (5j)**

Orange crystals; Yield 86%; m.p. 252–254 °C; IR (KBr, cm^{-1}): 3350, 3059 (NH), 1703 (C=O), 1600 (C=N), 1149 (C=S); ^1H NMR (DMSO- d_6 , 300 MHz): δ 4.86 (d, $J = 7.5$ Hz, 2H, benzyl CH_2), 6.93 (d, $J = 8.4$ Hz, 1H, indole C_7 -H), 7.15–7.22 (m, 2H, benzyl C_2 -H, C_6 -H), 7.36–7.44 (m, 3H, benzyl C_3 -H, C_5 -H, indole C_6 -H), 7.71 (d, $J = 2.4$ Hz, 1H, indole C_4 -H), 9.92 (t, $J = 6.0$ Hz, 1H, CSNH), 11.31 (s, 1H, indole NH), 12.49 (s, 1H, NNH); ^{13}C NMR (DMSO- d_6 , 75 MHz): δ 113.05 (CH), 114.16, 122.06, 123.76 (CH), 124.06 (CH), 125.08 (CH), 125.94 (CH), 129.98 (CH), 132.46, 133.52 (CH), 139.70, 141.59, 162.29, 164.87, 176.23; EI-MS (70 eV) m/z (%): 364/362 (M^+ , 1/3), 288/286 (1/3), 197/195 (1/3), 183/181 (20/135), 154/152 (12/36), 124/122 (69/19), 109 (100), 97 (21), 83 (32), 75 (29), 61 (39), 57 (25). Anal. Calcd. for $\text{C}_{16}\text{H}_{12}\text{FClN}_4\text{OS}$ (362): C, 53.04; H, 3.31; N, 15.47. Found: C, 52.88; H, 3.28; N, 15.42.

***N*-(2-Chlorobenzyl)-2-[5-chloro-2-oxo-2,3-dihydro-1*H*-indol-3-ylidene]-1-hydrazinecarbothioamide (5k)**

Yellow fluffy crystals; Yield 89%; m.p. 230–232 °C; IR (KBr, cm^{-1}): 3358, 3174 (NH), 1693 (C=O), 1610 (C=N), 1193 (C=S); ^1H NMR (DMSO- d_6 , 400 MHz): δ 4.94 (d, $J = 9.0$ Hz, 2H, benzyl CH_2), 6.96 (d, $J = 8.5$ Hz, 1H, indole C_7 -H), 7.29–7.41 (m, 4H, benzyl C_3 -H, C_4 -H, C_5 -H, C_6 -H), 7.41 (d, $J = 8.5$ Hz, 1H, indole C_6 -H), 7.73 (s, 1H, indole C_4 -H), 9.92 (t, $J = 7.5$ Hz, 1H, CSNH), 11.34 (s, 1H, indole NH), 12.57 (s, 1H, NNH); ^{13}C NMR (DMSO- d_6 , 75 MHz): δ 44.97 (CH_2), 112.58 (CH), 120.50 (CH), 126.49, 126.91 (CH), 127.12 (CH), 127.64 (CH), 128.13 (CH), 129.16 (CH), 130.26, 130.75, 135.08, 141.05, 162.40, 178.20; EI-MS (70 eV) m/z (%): 352/350 (10/10), 345/343 (36/89), 199/197 (10/20), 183/181 (19/33), 167/165 (14/16), 154/152 (11/28), 140/138 (41/22), 125 (100), 106 (9), 89 (13), 75 (10), 63 (8), 51 (5). Anal. Calcd. for $\text{C}_{16}\text{H}_{12}\text{Cl}_2\text{N}_4\text{OS}$ (378): C, 50.79; H, 3.17; N, 14.81. Found: C, 50.65; H, 3.13; N, 14.72.

***N*-(3-Chlorobenzyl)-2-[5-chloro-2-oxo-2,3-dihydro-1*H*-indol-3-ylidene]-1-hydrazinecarbothioamide (5l)**

Yellow crystals; Yield 80%; m.p. 228–230 °C; IR (KBr, cm^{-1}): 3333, 3065 (NH), 1705 (C=O), 1605 (C=N), 1174 (C=S); ^1H NMR (DMSO- d_6 , 300 MHz): δ 4.88 (d, $J = 6.3$ Hz, 2H, benzyl CH_2), 6.95 (d, $J = 8.4$ Hz, 1H, indole C_7 -H), 7.32–7.43 (m, 5H, benzyl C_2 -H, C_4 -H, C_5 -H, C_6 -H, indole C_6 -H), 7.72 (d, $J = 8.5$ Hz, 1H, indole C_4 -H), 9.95 (t, $J = 6.3$ Hz, 1H, CSNH), 11.33 (s, 1H, indole NH), 12.51 (s, 1H, NNH); ^{13}C NMR (DMSO- d_6 , 75 MHz): δ 47.07 (CH_2), 113.08 (CH), 120.95 (CH), 122.33, 126.49 (CH), 126.94 (CH), 127.50 (CH), 130.74 (CH), 131.00, 131.58, 133.41, 141.33, 141.55, 162.90, 178.77; EI-MS (70 eV) m/z (%):

380/378 (M⁺, 2/3), 304/302 (2/3) 198 (16), 181 (52), 152 (50), 140 (76), 138 (40), 125 (100), 113 (17), 106 (13), 89 (80), 75 (58), 63 (58), 51 (43). Anal. Calcd. for C₁₆H₁₂Cl₂N₄OS (378): C, 50.79; H, 3.17; N, 14.81. Found: C, 50.68; H, 3.12; N, 14.72.

N-(4-Chlorobenzyl)-2-[5-chloro-2-oxo-2,3-dihydro-1H-indol-3-ylidene]-1-hydrazinecarbothioamide (5m)

Orange crystals; Yield 84%; m.p. 280–282 °C; IR (KBr, cm⁻¹): 3290, 3053 (NH), 1688 (C=O), 1611 (C=N), 1180 (C=S); ¹H NMR (DMSO-*d*₆, 400 MHz): δ 4.87 (d, *J* = 7.5 Hz, 2H, benzyl CH₂), 6.95 (d, *J* = 7.5 Hz, 1H, indole C₇-H), 7.37–7.41 (m, 5H, benzyl C₂-H, C₃-H, C₅-H, C₆-H, indole C₆-H), 7.72 (s, 1H, indole C₄-H), 9.95 (t, *J* = 7.5 Hz, 1H, CSNH), 11.32 (s, 1H, indole NH), 12.50 (s, 1H, NNH); ¹³C NMR (DMSO-*d*₆, 75 MHz): δ 46.49 (CH₂), 112.56 (CH), 120.44 (CH), 121.82, 126.46, 128.25 (CH), 129.15 (CH), 130.46 (CH), 130.94, 131.58, 137.26, 141.00, 162.38, 177.77; EI-MS (70 eV) *m/z* (%): 380/378 (M⁺, 22/32), 352/350 (13/20), 211/209 (5/13), 200/198 (29/58), 195 (25), 181 (92), 165 (19), 152 (46), 140 (46), 125 (100), 106 (9), 89 (15), 77 (10), 61 (12). Anal. Calcd. for C₁₆H₁₂Cl₂N₄OS (378): C, 50.79; H, 3.17; N, 14.81. Found: C, 50.64; H, 3.13; N, 14.75.

N-(2,4-Dichlorobenzyl)-2-[5-chloro-2-oxo-2,3-dihydro-1H-indol-3idene]-1-hydrazinecarbothioamide (5n)

Yellow crystals; Yield 75%; m.p. 248–250 °C; IR (KBr, cm⁻¹): 3300, 3051 (NH), 1687 (C=O), 1606 (C=N), 1159 (C=S); ¹H NMR (CDCl₃, 400 MHz): δ 5.02 (d, *J* = 6.0 Hz, 2H, benzyl CH₂), 6.83 (d, *J* = 8.4 Hz, 1H, indole C₇-H), 7.24–7.26 (m, 1H, benzyl C₅-H), 7.29 (dd, *J*₁ = 8.4 Hz, *J*₂ = 2.0 Hz, 1H, indole C₆-H), 7.43 (d, *J* = 2.0 Hz, 1H, benzyl C₃-H), 7.45 (d, *J* = 8.4 Hz, 1H, benzyl C₆-H), 7.53 (d, *J* = 2.0 Hz, 2H, indole C₄-H, CSNH), 8.03 (brs, 1H, indole NH), 12.69 (s, 1H, NNH); ¹³C NMR (DMSO-*d*₆, 75 MHz): δ 45.11 (CH₂), 113.05, 120.98 (CH), 122.23 (CH), 127.00 (CH), 127.79 (CH), 129.09, 129.90 (CH), 131.01 (CH), 131.62, 132.76, 132.98, 134.86, 141.54, 162.86, 178.70; EI-MS (70 eV) *m/z* (%): 379/377 (17/22), 199/197 (12/18), 181 (52), 176/174 (30/52), 166 (11), 159 (100), 124 (34), 111 (29), 102 (26), 89 (42), 75 (54), 63 (42), 51 (28). Anal. Calcd. for C₁₆H₁₁Cl₃N₄OS (412): C, 46.60; H, 2.67; N, 13.59. Found: C, 46.44; H, 2.63; N, 13.54.

N-(3,4-Dichlorobenzyl)-2-[5-chloro-2-oxo-2,3-dihydro-1H-indol-3-ylidene]-1-hydrazinecarbothioamide (5o)

Orange fluffy crystals; Yield 74%; m.p. 272–274 °C; IR (KBr, cm⁻¹): 3300, 3192 (NH), 1689 (C=O), 1608 (C=N), 1157 (C=S); ¹H NMR (CDCl₃, 400 MHz): δ 4.94 (d, *J* = 6.0 Hz, 2H, benzyl CH₂), 6.82 (d, *J* = 8.4 Hz, 1H, indole C₇-H), 7.24 (m, CDCl₃, benzyl C₆-H), 7.29 (dd, *J*₁ = 8.4 Hz, *J*₂ = 2.0 Hz, 1H, indole C₆-H), 7.43 (d, *J* = 8.0 Hz, 1H, benzyl C₅-H), 7.47 (d, *J* = 1.6 Hz, 1H, benzyl C₂-H), 7.50 (brs, 1H, CSNH), 7.54 (d, *J* = 2.0 Hz, indole C₄-H), 8.03 (brs, 1H, indole NH), 12.75 (s, 1H, NNH); ¹³C NMR

(DMSO-*d*₆, 75 MHz): δ 46.56 (CH₂), 113.06, 120.93 (CH), 122.25 (CH), 126.97 (CH), 128.18 (CH), 129.71 (CH), 130.05 (CH), 131.00, 131.34, 131.63, 139.98, 141.53, 162.87, 178.37; EI-MS (70 eV) *m/z* (%): 414/412 (M⁺, 2/2), 384/382 (2/2), 234/232 (9/8), 195 (9), 161 (58), 159 (100), 138(31), 111 (26), 102 (22), 89 (43), 75 (48), 63 (47), 51(27). Anal. Calcd. for C₁₆H₁₁Cl₃N₄OS (412): C, 46.60; H, 2.67; N, 13.59. Found: C, 46.50; H, 2.63; N, 13.52.

3. 4. Biological Assays

In vitro antiurease, antiglycation, phytotoxicity and cytotoxicity potential of the synthesized thiosemicarbazones was determined according to the literature protocols.^{64,55,43,42}

3. 5. Molecular Docking Studies

Molecular docking studies were performed in accordance with the protocol used in our recently published article.⁶⁵

4. Conclusions

In this study, a series of fifteen N⁴-benzyl substituted 5-chloroisatin-3-thiosemicarbazones **5a–o** were synthesized and screened primarily for urease and glycation inhibitory potential. All the synthetic thiosemicarbazones emerged as highly effective urease inhibitors, demonstrating enzymatic inhibition even better than the reference inhibitor, thiourea, used in the assay. These compounds, by displaying non-significant phytotoxic influences, draw a great deal of consideration towards their effectiveness as important inhibitors of soil ureases because they might be combined with fertilizers in minute amounts to greatly improve the usefulness of nitrogen consumption. Also, being non-toxic, they could prove to be promising candidates for orally effective remedial agents used for the treatment of certain clinical conditions induced by microbial ureases. In antiglycation assay, five out of fifteen compounds tested, *i.e.* **5c**, **5h–j** and **5n** were recognized as extremely effective inhibitors of glycation, showing inhibitory activity much larger than the reference inhibitor, rutin, and may thus act as credible leads for further studies.

This study presents the first example of exhibiting glycation inhibition by N⁴-benzyl substituted isatin-thiosemicarbazones and offers a firm base for additional studies on such compounds to build up more persuasive and safer glycation inhibitors of pharmaceutical interest.

5. Acknowledgements

H. Pervez acknowledges the Higher Education Commission (HEC), Pakistan for funding under National Re-

search Support Program for Universities (Project No. 20-873/R&D/07/452).

6. References

1. J. F. M. da Silva, S. J. Garden, A. C. Pinto, *J. Braz. Chem. Soc.* **2001**, *12*, 273–324. DOI:10.1590/S0103-50532001000300002
2. S. N. Pandeya, S. Smitha, M. Jyoti, S. K. Sridhar, *Acta Pharm.* **2005**, *55*, 27–46.
3. G. Cerchiaro, A. M. C. Ferreira, *J. Braz. Chem. Soc.* **2006**, *17*, 1473–1485. DOI:10.1590/S0103-50532006000800003
4. K. L. Vine, L. Matesic, J. M. Locke, M. Ranson, D. Skropeta, *Anti-Cancer Agents Med. Chem.* **2009**, *9*, 397–414. DOI:10.2174/1871520610909040397
5. B. Bhriagu, D. Pathak, N. Siddiqui, M. S. Alam, W. Ahsan, *Int. J. Pharm. Drug Res.* **2010**, *2*, 229–235.
6. T. Aboul-Fadl, F. A. S. Bin-Jubair, *Int. J. Res. Pharm. Sci.* **2010**, *1*, 113–126.
7. M. Pal, N. K. Sharma, J. K. Priyanka, K. K. Jha, *J. Adv. Sci. Res.* **2011**, *2*, 35–44. DOI:10.1016/j.jare.2010.08.005
8. V. Raj, *Int. J. Curr. Pharm. Res.* **2012**, *4*, 1–9.
9. P. Pakravan, S. Kashanian, M. M. Khodaei, F. J. Harding, *Pharmacol. Rep.* **2013**, *65*, 313–335. DOI:10.1016/S1734-1140(13)71007-7
10. K. M. Khan, M. Khan, M. Ali, M. I. Qadir, S. Perveen, A. Karim, M. I. Choudhary, *J. Chem. Soc. Pak.* **2013**, *35*, 987–993.
11. K. L. Vine, L. Matesic, J. M. Locke, D. Scropeta, Recent Highlights in the Development of Isatin-based Anticancer Agents, in: M. Prudhomme (Ed.), *Advances in Anticancer Agents in Medicinal Chemistry*, Bentham Science Publishers, Sharjah (UAE), **2013**, pp. 254–312. DOI:10.2174/9781608054961113020008
12. A. S. Grewal, *Int. J. Pharm. Res.* **2014**, *6*, 1–7.
13. G. Mathur, S. Nain, *Med. Chem.* **2014**, *4*, 417–427.
14. S. Adhikari, S. B. Bari, A. Samanta, *J. Appl. Chem. Res.* **2014**, *8*, 31–40.
15. P. Phogat, P. Singh, *Cent. Nerv. Syst. Agents Med. Chem.* **2015**, *15*, 28–31. DOI:10.2174/1871524915666150213122246
16. A. Z. Hussain, M. N. Meeran, *Res. J. Pharm. Biol. Chem. Sci.* **2015**, *6*, 1598–1601.
17. F. Rahim, F. Malik, H. Ullah, A. Wadood, F. Khan, M. T. Javid, M. Taha, W. Rehman, A. U. Rehman, K. M. Khan, *Bioorg. Chem.* **2015**, *60*, 42–48. DOI:10.1016/j.bioorg.2015.03.005
18. M. Khan, K. M. Khan, F. Rahim, Samreen, S. Perveen, A. Karim, Imtiazuddin, M. I. Choudhary, *J. Chem. Soc. Pak.* **2015**, *37*, 520–526.
19. A. Corona, R. Meleddu, F. Esposito, S. Distinto, G. Bianco, T. Masaoka, E. Maccioni, L. Menéndez-Arias, S. Alcaro, S. F. J. Le Grice, E. Tramontano, *PLoS One* **2016**, *11*, 1–18.
20. G. M. Ziarani, R. Moradi, N. Lashgari, *Arxivoc* **2016**, (*i*), 1–81.
21. N. Karali, N. Terzioğlu, A. Gürsoy, *Arch. Pharm. (Weinheim)* **2002**, *335*, 374–380. DOI:10.1002/1521-4184(200211)335:8<374::AID-ARDP374>3.0.CO;2-K
22. G. Ermut, N. Karali, I. Cetin, M. Topcul, S. Birteksoz, *Marmara Pharm. J.* **2013**, *17*, 147–154.
23. M. T. Gabr, N. S. El-Gohary, E. R. El-Bendary, M. M. El-Kerdawy, N. Ni, *Eur. J. Med. Chem.* **2017**, *128*, 36–44. DOI:10.1016/j.ejmech.2017.01.030
24. X. M. Zhang, H. Guo, Z. S. Li, F. H. Song, W. M. Wang, H. Q. Dai, L. X. Zhang, J. G. Wang, *Eur. J. Med. Chem.* **2015**, *101*, 419–430. DOI:10.1016/j.ejmech.2015.06.047
25. N. D. Thanh, N. T. K. Giang, T. H. Quyen, D. T. Huong, V. N. Toan, *Eur. J. Med. Chem.* **2016**, *123*, 532–543. DOI:10.1016/j.ejmech.2016.07.074
26. N. Karali, A. Gürsoy, F. Kandemirli, N. Shvets, F. B. Kaynak, S. Özbey, V. Kovalishyn, A. Dimoglo, *Bioorg. Med. Chem.* **2007**, *15*, 5888–5904. DOI:10.1016/j.bmc.2007.05.063
27. O. Guzel, N. Karali, A. Salman, *Bioorg. Med. Chem.* **2008**, *16*, 8976–8987. DOI:10.1016/j.bmc.2008.08.050
28. D. Banerjee, P. Yogeewari, P. Bhat, A. Thomas, M. Srividya, D. Sriram, *Eur. J. Med. Chem.* **2011**, *46*, 106–112. DOI:10.1016/j.ejmech.2010.10.020
29. P. Davidovich, V. Aksenova, V. Petrova, D. Tentler, D. Orlova, S. Smirnov, V. Gurzhiy, A. L. Okorokov, A. Garabadzhiu, G. Melino, N. Barlev, V. Tribulovich, *ACS Med. Chem. Lett.* **2015**, *6*, 856–860. DOI:10.1021/acsmchemlett.5b00011
30. J. Haribabu, G. R. Subhashree, S. Saranya, K. Gomathi, R. Karvembu, D. Gayathri, *J. Mol. Struct.* **2016**, *1110*, 185–195. DOI:10.1016/j.molstruc.2016.01.044
31. S. Gao, J. Zang, Q. Gao, X. Liang, Q. Ding, X. Li, W. Xu, C. J. Chou, Y. Zhang, *Bioorg. Med. Chem.* **2017**, *25*, 2981–2994. DOI:10.1016/j.bmc.2017.03.036
32. Z. Xie, G. Wang, J. Wang, M. Chen, Y. Peng, L. Li, B. Deng, S. Chen, W. Li, *Molecules* **2017**, *22*, 659. DOI:10.3390/molecules22040659
33. C. Melis, R. Meleddu, A. Angeli, S. Distinto, G. Binaco, C. Capasso, F. Cottiglia, R. Angius, C. T. Supuran, E. Maccioni, *J. Enzyme Inhib. Med. Chem.* **2017**, *32*, 68–73.
34. R. Meleddu, S. Distinto, A. Corona, E. Tramontano, G. Bianco, C. Melis, F. Cottiglia, E. Maccioni, *J. Enzyme Inhib. Med. Chem.* **2017**, *130*, 130–136.
35. G. Wang, J. Wang, D. He, X. Li, J. Li, Z. Peng, *Chem. Biol. Drug Des.* **2017**, *89*, 456–463. DOI:10.1111/cbdd.12867
36. H. Pervez, M. S. Iqbal, M. Y. Tahir, M. I. Choudhary, K. M. Khan, *Nat. Prod. Res.* **2007**, *21*, 1178–1186. DOI:10.1080/14786410601129770
37. H. Pervez, M. S. Iqbal, M. Y. Tahir, F. H. Nasim, M. I. Choudhary, K. M. Khan, *J. Enzyme Inhib. Med. Chem.* **2008**, *23*, 848–854. DOI:10.1080/14756360701746179
38. H. Pervez, N. Manzoor, M. Yaqub, F. H. Nasim, K. M. Khan, *Med. Chem. Res.* **2012**, *21*, 2251–2262. DOI:10.1007/s00044-011-9745-7
39. H. Pervez, N. Saira, M. S. Iqbal, M. Yaqub, K. M. Khan, *Med. Chem. Res.* **2013**, *22*, 5878–5889. DOI:10.1007/s00044-013-0575-7
40. H. Pervez, Z. H. Chohan, M. Ramzan, F. H. Nasim, K. M. Khan, *J. Enzyme Inhib. Med. Chem.* **2009**, *24*, 437–446. DOI:10.1080/14756360802188420

41. H. Pervez, M. Ramzan, M. Yaqub, K. M. Khan, *Lett. Drug Des. Discov.* **2011**, *8*, 452–458.
DOI:10.2174/157018011795514159
42. H. Pervez, N. Saira, M. S. Iqbal, M. Yaqub, K. M. Khan, *Molecules* **2011**, *16*, 6408–6421. DOI:10.3390/molecules16086408
43. H. Pervez, M. Ramzan, M. Yaqub, F. H. Nasim, K. M. Khan, *Med. Chem.* **2012**, *8*, 505–514.
DOI:10.2174/1573406411208030505
44. H. Pervez, N. Manzoor, M. Yaqub, K. M. Khan, *J. Enzyme Inhib. Med. Chem.* **2014**, *29*, 628–632.
DOI:10.3109/14756366.2013.836641
45. H. Pervez, N. Manzoor, M. Yaqub, A. Khan, K. M. Khan, F. H. Nasim, M. I. Choudhary, *Lett. Drug Des. Discov.* **2010**, *7*, 102–108. DOI:10.2174/157018010790225840
46. H. Pervez, M. Ahmad, S. Zaib, M. Yaqub, M. M. Naseer, J. Iqbal, *Med. Chem. Commun.* **2016**, *7*, 914–923.
DOI:10.1039/C5MD00529A
47. M. Ahmad, H. Pervez, S. Zaib, M. Yaqub, M. M. Naseer, S. U. Khan, J. Iqbal, *RSC Adv.* **2016**, *6*, 60826–60844.
48. H. Pervez, N. Khan, S. Zaib, M. Yaqub, M. M. Naseer, M. N. Tahir, J. Iqbal, *Bioorg. Med. Chem.* **2017**, *25*, 1022–1029.
DOI:10.1016/j.bmc.2016.12.012
49. H. M. Faidullah, K. A. Khan, A. M. Asiri, *J. Fluorine Chem.* **2011**, *132*, 131–137. DOI:10.1016/j.jfluchem.2010.12.009
50. C. S. Shantharam, D. M. Suyoga Vardhan, R. Suhas, M. B. Sridhara, D. C. Gowda, *Eur. J. Med. Chem.* **2013**, *60*, 325–332.
DOI:10.1016/j.ejmech.2012.12.029
51. C. S. Shantharam, D. M. Suyoga Vardhan, R. Suhas, D. C. Gowda, *Bioorg. Khim.* **2014**, *40*, 479–490.
DOI:10.7868/S0132342314040125
52. C. S. N. Shantharama, M. S. Raghu, *Eur. J. Pharm. Med. Res.* **2015**, *2*, 220–228.
53. D. M. Suyoga Vardhan, C. S. Shantharam, R. Suhas, D. Channe Gowda, *J. Saudi Chem. Soc.* **2017**, *21*, S248–S257.
54. K. M. Khan, U. R. Mughal, N. Ambreen, A. Khan, S. Perveen, M. I. Choudhary, *Lett. Drug Des. Discov.* **2009**, *6*, 358–362.
DOI:10.2174/1570180810906050358
55. K. M. Khan, M. Khan, M. Ali, M. Taha, S. Rasheed, S. Perveen, M. I. Choudhary, *Bioorg. Med. Chem.* **2009**, *17*, 7795–7801.
DOI:10.1016/j.bmc.2009.09.028
56. A.-M. M. E. Omar, N. H. Eshba, H. M. Salama, *Arch. Pharm.* **1984**, *317*, 701–709.
57. N. Karali, *Eur. J. Med. Chem.* **2002**, *37*, 909–918.
DOI:10.1016/S0223-5234(02)01416-2
58. K. Asokkumar, L. T. Prathyusha, M. Umamaheshwari, T. Sivashanmugam, V. Subhadradevi, P. Jagannath, A. Madeswaran, F. Salesheir, *J. Chil. Chem. Soc.* **2012**, *57*, 1442–1446.
DOI:10.4067/S0717-97072012000400022
59. D. E. Clark, S. D. Pickett, *Drug Discov. Today* **2000**, *5*, 49–58.
60. S. Ekins, Y. Nikolsky, T. Nikolskaya, *Trends Pharmacol. Sci.* **2005**, *26*, 202–209.
61. W. J. Egan, G. Zlokarnik, P. D. J. Grootenhuys, *Drug Discov. Today Technol.* **2004**, *1*, 381–387.
DOI:10.1016/j.ddtec.2004.11.002
62. C. A. Lipinski, F. Lombardo, B. W. Dominy, P. J. Feeney, *Adv. Drug Deliv. Rev.* **2001**, *46*, 3–26.
DOI:10.1016/S0169-409X(00)00129-0
63. W. T. Ashton, C. L. Cantone, L. L. Chang, S. M. Hutchins, R. A. Strelitz, M. MacCoss, R. S. L. Chang, V. J. Lotti, K. A. Faust, T.-B. Chen, P. Bunting, T. W. Schom, S. D. Kivlighn, P. K. S. Siegl, *J. Med. Chem.* **1993**, *36*, 591–609.
DOI:10.1021/jm00057a009
64. M. K. Rauf, A. Talib, A. Badshah, S. Zaib, K. Shoaib, M. Shahid, U. Flörke, I. U. Din, J. Iqbal, *Eur. J. Med. Chem.* **2013**, *70*, 487–496.
65. M. K. Rauf, S. Zaib, A. Talib, M. Ebihara, A. Badshah, M. Bolte, J. Iqbal, *Bioorg. Med. Chem.* **2016**, *24*, 4452–4463.
DOI:10.1016/j.bmc.2016.07.042

Povzetek

Sintetizirali smo serijo petnajstih N^4 -benzil substituiranih 5-kloroizatin 3-tiosemikarbazonov **5a–o** in preverili njihove antiureazne in antiglikacijske učinke. Da bi ugotovili fitotoksični in citotoksični potencial pripravljenih spojin, smo izvedli teste rasti organizmov *Lemma aequinocitalis* in *Artemia salina*. Za vse spojine smo ugotovili, da so izjemno učinkoviti inhibitorji ureaz, saj so testirani encim inhibirale mnogo bolje kot referenčni inhibitor tiosečnina (IC_{50} vrednosti 1.31 ± 0.06 do 3.24 ± 0.15 proti $22.3 \pm 1.12 \mu\text{M}$ za tiosečnino). Po drugi strani pa smo za osem testiranih spojin (t.j. **5b**, **5c**, **5h–k**, **5m** in **5n**) izmed petnajstih ugotovili, da so zelo močni inhibitorji glikacije. Od teh se jih je pet (t.j. **5c**, **5h–j** in **5n**) izkazalo za izjemno učinkovite, saj so glikacijo inhibirali celo bolj kot referenčni inhibitor rutin (IC_{50} vrednosti 114.51 ± 1.08 do 229.94 ± 3.40 proti $294.5 \pm 1.5 \mu\text{M}$ za rutin).

Scientific paper

The Effect of Adenine Adsorption on Zn (II) Electroreduction in Acetate Buffer

Dorota Gugala-Fekner

Faculty of Chemistry, Maria Curie-Skłodowska University, Lublin, Poland.

* Corresponding author: E-mail: gugala@poczta.umcs.lublin.pl

Received: 20-06-2017

Abstract

The paper presents the thermodynamic analysis of adenine adsorption on a mercury electrode in an acetate buffer at pH 3 and pH 4. Adsorption energy and constants were determined using the Frumkin isotherm and the virial isotherm. Stronger adsorption in the buffer at pH 3 was observed in comparison to the buffer at pH 4. Using cyclic voltammetry and Faraday impedance measurement, an inhibitory effect of adenine on the kinetics of Zn (II) ion electro-reduction was observed.

Keywords: Adsorption, isotherm electrosorption, differential capacity, adenine

1. Introduction

A fundamental issue of electro-chemistry, both applied and theoretical, is the adsorption of organic compounds on the interface of electrode – aqueous electrolyte solution.

The results of adsorption studies facilitate the description of the structure and properties of the double electric layer and may facilitate interpretation of the effect of the double layer on the kinetics of electrode processes.^{1–4}

Among other things, the information can be used to improve the function of corrosion inhibitors,^{5–7} controllers of metal electro-precipitation, organic electro-synthesis⁸ or electro-analytical techniques.^{9–11}

Adenine and guanine are two most important purine nucleobases that are present in all nucleic acids.¹² Purines consist of a pyrimidine ring fused with the imidazole ring. In the five-membered heterocyclic imidazole ring there are two nitrogen atoms. One of them is situated in position 7 (N7) and it is basic due to the fact that its lone electron

pair does not participate in the aromatic π electron sextet. This nitrogen atom can be in unprotonated form. The other nitrogen atom of the imidazole ring (N9) is not basic because its lone electron pair participates in the π electron sextet, analogically as in the case of the nitrogen atom in the pyrrole ring (Figure 1).

Problem behavior of adenine in acetate buffer was already taken by Xin Zao and all.^{13–15} There is no literature data concerning the behaviour of adenine in solutions at pH 3 and 4, which encourages the studying of the adsorption of this compound. The selection of these pH values results from the fact that information concerning adenine adsorption will be used to study the kinetics of specific non-organic depolarisers, e. g. Zn(II), Cd(II) or Pb(II) ions in the presence of this organic compound. The basic electrolyte has to be a buffer solution because adenine used in the studies displays alkaline properties. The selected buffer is an acetate buffer which is poorly adsorbed on mercury.

The results presented in the work constitute part of the complex studies of the adsorptive properties of adenine, and its effect on the kinetics and mechanism of selected electrode processes.

Because of the wish to create a system extremely similar to the standard one, which is influenced by various thermodynamic dependencies, a dropping mercury electrode.

The mercury electrode is very close to the ideally polarizable electrode. That is because it has an almost ideally

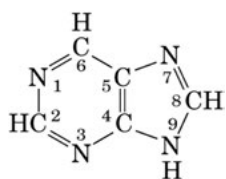


Figure 1. Structural formula of adenine.

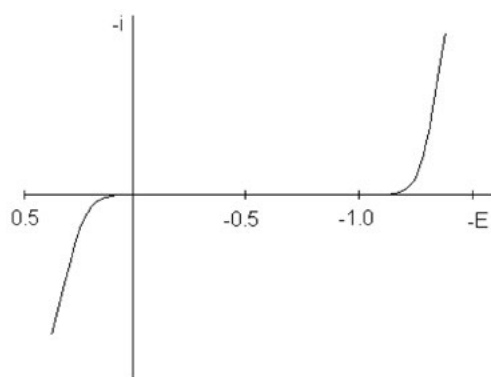


Figure 2. Polarization curve of the mercury electrode in 0,1 mol L⁻¹ HNO₃.¹⁶

smooth and pure surface of mercury which is a liquid at room temperature. Figure 2 presents the polarization range of mercury electrode in an inert solvent.

The polarization range of the electrode is limited on the negative potentials side by decomposition of the main electrolyte (hydrogen is released) and on positive potentials side by electrochemical dissolution of the electrode material. The range of polarization depends on the composition and acidity of the main electrolyte and on average it ranges from +0.2 to -1.5 V. Because of the relatively narrow range of anodic polarization the mercury electrode is most frequently used over a wide cathodic range, thus reducing the depolarizers that are present in the solution.

The rapid development of genetics and bio-technology in recent years has induced intensive and detailed studies of properties of the basic components of nucleic acids: pyrimidine and purine derivatives and respective nucleosides.^{17,18} The use of a charged interface on an electrode facilitates the obtaining of systems similar to those which can be found in living organisms close to an interface: charged cellular membrane/systemic fluid. The selection of a mercury electrode featuring perfect polarisability facilitates the use of various thermo-dynamic dependencies, which in turn facilitate a thorough description of properties of the studied organic substance on the interface electrode/electrolyte solution.

The aim of the work was to describe the adsorptive properties of adenine by means of the parameters of the virial isotherm and the Frumkin isotherm and to study the effect of adenine on Zn(II)ion electro-reduction on a mercury electrode.

The use of Zn(II)ions as a depolarizer results from their quasi-reversible reduction on the mercury electrode. One can observe the change in kinetics of the reaction, both as concerns its inhibition and acceleration. The fact that zinc obtained as a result of reduction readily forms an amalgam with mercury is another advantage.

The attractiveness of Zn(II)ions as a depolarizer is also related to the fact that the determined kinetic param-

eters of its electroreduction make it possible in selected systems to examine indirectly the structure of the adsorption layer on the mercury electrode.

The bases for the calculation of these isotherms are values determined experimentally: differential capacity of the double layer, potential of zero charge and surface tension at this potential.

By means of cyclic voltammetry and Faraday impedance, different effects of adenine in acetate buffers at pH 3 and pH 4 on the kinetics of Zn(II)ion electro-reduction were demonstrated.

2. Experimental

Studies of adsorptive properties of adenine on a mercury electrode were performed in buffers at pH 3, 4, 5 and 6 and the presented work concerns the studies of the adsorptive properties of adenine in acetate buffers at pH 3 and 4. The adsorption of adenine on a mercury electrode in acetic buffers at pH 3 and 4 is described by means of the adsorption isotherms constants calculated from the surface pressure as a function of electrode potential and adsorbate bulk concentration. The adsorption parameters from the double-layer were calculated based on the data from the differential capacity-potential curves.

Analytical grade C₅H₅N₅ and CH₃COOH and CH₃COONa (Fluka) were used without further purification. Water and mercury were double distilled before use. The adenine solutions of concentrations, ranging from 5 × 10⁻⁵ mol L⁻¹ to 2 × 10⁻³ mol L⁻¹, were prepared immediately before every measurement. The chosen surfactant concentrations were lower than the surfactant critical micelle concentration. The solutions were deaerated by passing high purity nitrogen over the solution during the measurements, at 298 ± 0.1 K. The three-electrode system was used, with a dropping mercury electrode as a working electrode, and an Ag/AgCl as a reference electrode, to which all potentials in this paper are referred, and a platinum electrode as the auxiliary electrode. A controlled growth mercury drop electrode (area 0.0090928 cm²) (CGMDE), manufactured by MTM (Poland), was used. The differential capacity, C, of the double layer was measured with an Autolab frequency response analyser, (Eco Chemie, The Netherlands), using the AC impedance technique. The repeatability of the capacitance measurements was ± 5%. The measurements were carried out at several frequencies in the range from 400 to 2000Hz, with an amplitude of 0.05 V. The equilibrium capacities were obtained by the extrapolation of the dependence of the measured capacity versus the square root of the frequency to zero frequency.

The potential of zero charge, E_z, was measured using a streaming electrode. The interfacial tension, γ_z, at E_z was measured by the maximum bubble pressure method according to Schiffrin. The accuracy of determination of γ_z

was $\pm 0.2 \text{ mN m}^{-1}$. The charge density and surface tension were obtained by the back integration of the differential capacity-potential dependences. No corrections were made for the effect of the medium on the activity of the supporting electrolyte^{19,20} and the activity coefficient of the adsorbate.

The Zn(II) ions electro-reduction studies were performed by means of the cyclic voltammetry and measurement of Faraday impedance using the Autolab frequency response analyser.

3. Results and Discussion

3.1. Analysis of Experimental Data

The experimental data and calculated thermo-dynamic parameters presented herein are related to the adsorption of adenine from an acetate buffer, each with a different pH, allowing supplementing the information about the mechanism of adsorption of this compound on a mercury electrode.

The differential capacity of the double layer was the main source of experimental data that were used to determine adsorption parameters for the examined systems. Measurements of differential capacity were made at various AC frequencies. Differential capacity values for the double layer obtained in direct measurements were extrapolated to zero frequency. This ensures obtaining capacity values corresponding to the equilibrium of the adsorption-desorption process. Figure 3 present the correlations between the extrapolated differential capacity of the double layer and the electrode potential at various adenine concentrations in the applied acetate buffers.

The analysis of the curves of differential capacity indicates a totally different change in differential capacity in an acetate buffer at pH 3 in comparison to a buffer at pH 4 in the absence of adenine. The minimum differential capacity is observed in the buffer at pH 3 with $E = -0.5 \text{ V}$, whereas in the buffer at pH 4 the capacity decreases. In both buffers without adenine at $E > -0.8 \text{ V}$, the values of differential capacity are practically constant. A different shape of the curves of differential capacity without adenine for pH 3 in comparison to pH 4 may result from stronger adsorption of acetic acid molecules in the buffer at pH 3.

In the case of the acetate buffer at pH 3, the addition of adenine in the solution causes various changes in the differential capacity in the function of its concentration and electrode potential. The nature of the changes in the shape of the curves $C = f(E)$ for adenine solutions in comparison to the curve for the basic electrolyte indicates different effects in two areas of potential $E > -0.65 \text{ V}$ and $E < -0.65 \text{ V}$. With less negative potentials, an increase in the value of the differential capacity of adenine is observed, whereas for the area of potentials $E < -0.65 \text{ V}$ a lowering of the curve $C = f(E)$ for adenine solutions is observed and is

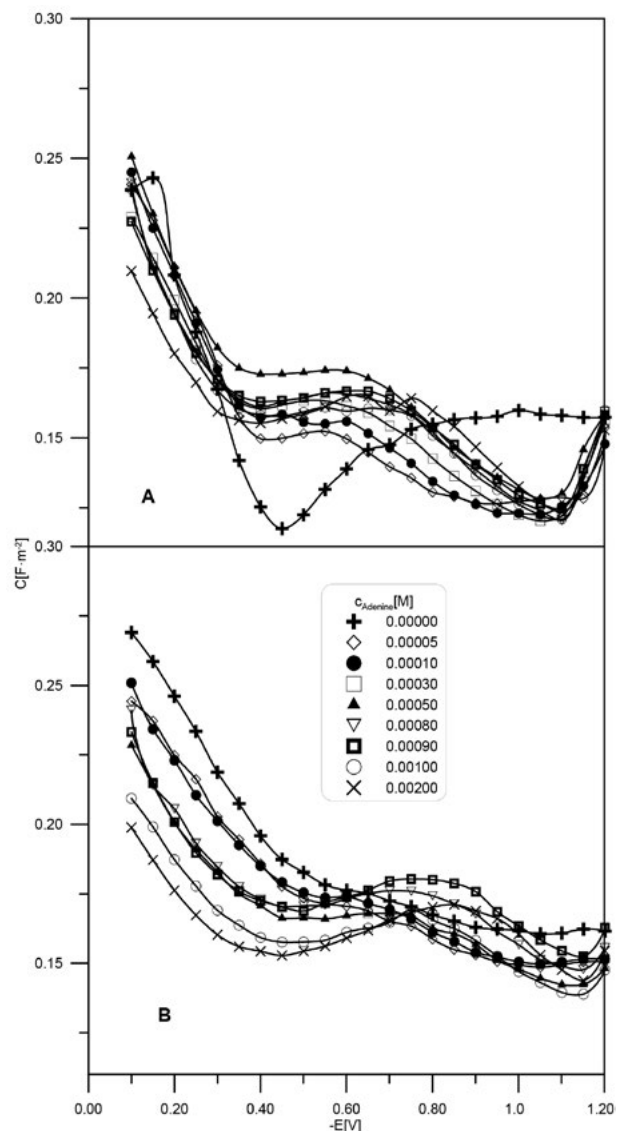


Figure 3. The differential capacity-potential curves at Hg/acetate buffer pH 3 (A) pH 4 (B) for various adenine concentrations as in figure legend.

the greatest with the lowest of all the applied concentrations. The values of potential for which the curve of differential capacity of the buffer at pH 3 crosses the respective curves for adenine and turn to values which are more negative with an increase in adenine concentration. An increase in adenine concentration causes an increase in the value of the differential capacity practically in the whole range of potentials.

Three areas of potential can be distinguished in the shape of the curves for the differential capacity for buffers at pH 4: $-0.2 \text{ V} < E < -0.65 \text{ V}$ and $-0.65 \text{ V} < E < -1.0 \text{ V}$ and $-1.0 \text{ V} < E < -1.2 \text{ V}$. The first area features a gradual decrease in the differential capacity with an increase in adenine concentration. With a potential of approx. -0.65 V , curves for the differential capacity cross. In the second area of potentials, the differential capacity in the presence

of higher adenine concentrations is generally higher than the values obtained for the stock solution. For lower adenine concentrations, the differential capacity is lower. With a potential more negative than -1.0 V, a decrease in the differential capacity is observed for all adenine concentrations as opposed to the standard electrolyte. This may be a consequence of changes in mutual interactions, mainly electrostatic, between adsorbed molecules. Increasing the differential capacity by adenine may be a result of chemical interaction of the aromatic ring of adenine with the surface of the mercury electrode.

As Table 1 indicates, E_z values in buffer solutions with increasing pH without adenine shift toward negative potentials, which is associated with an increased concentration of acetate anions. The addition of adenine to the standard electrolyte at pH 3 causes a shift of E_z toward less negative potentials, whereas in an acetate buffer at pH 4 causes a shift toward more negative potentials. Such changes in the potential of zero charge E_z , with an increase in adenine concentration in an acetate buffer at pH 4 indicate that a dipole molecule of adenine adsorbs on the surface of mercury with the negative pole, i. e. with the aromatic ring.

In the buffer at pH 3, the adenine molecule is more strongly protonated and adsorbs on the mercury electrode with the positive pole.

In the absence of any organic substance, γ_z values increase with an increase in pH of the basic electrolyte. In each of the considered systems, the introduction of lower adenine concentrations causes an increase in γ_z values, whereas higher adenine concentrations lower γ_z values. Changes in E_z and γ_z in the function of adenine concentration are similar in both of the used buffers.

The results of measurements of the potential of zero charge and the surface tension with this potential served as the constant of integration for differential capacity curves. On the basis of dependence 1, charge density on the surface of the electrode is obtained.

$$\sigma = \int_{E_z}^E CdE \quad (1)$$

Table 1. The values of the zero charge potentials E_z vs Ag/AgCl electrode and surface tension γ_z at E_z for the studied systems.

c / mol/L	pH 3		pH 4	
	$-E_z$ / V	γ_z / mN m ⁻¹	$-E_z$ / V	γ_z / mN m ⁻¹
0	0.38	453	0.41	417
$5.0 \cdot 10^{-5}$	0.39	465	0.40	469
$1.0 \cdot 10^{-4}$	0.39	465	0.40	465
$3.0 \cdot 10^{-4}$	0.39	455	0.40	458
$5.0 \cdot 10^{-4}$	0.38	456	0.40	458
$8.0 \cdot 10^{-4}$	0.38	451	0.40	453
$9.0 \cdot 10^{-4}$	0.38	449	0.40	452
$1.0 \cdot 10^{-3}$	0.38	448	0.40	449
$2.0 \cdot 10^{-3}$	0.37	445	0.41	446

Twofold integration of differential capacity curves serves to calculate the value of surface tension in accordance with equation 2.

$$\gamma = \gamma_z - \int_{E_z}^E \int C dE \quad (2)$$

The obtained values of surface charge were used to determine parameters characterising the maximum adsorption: potential of the maximum adsorption E_{\max} and charge of the maximum adsorption σ_{\max} (Figure 4).

Respectively, for pH 3, $E_{\max} = 0.34$ V, $\sigma_{\max} = +0.43 \times 10^{-2}$ C m⁻² and for pH 4, $E_{\max} = 0.33$ V, $\sigma_{\max} = +1.12 \times 10^{-2}$ C m⁻². The possibility of accurate determination of E_{\max} and σ_{\max} indicates a physical nature of adenine adsorption (physisorption).

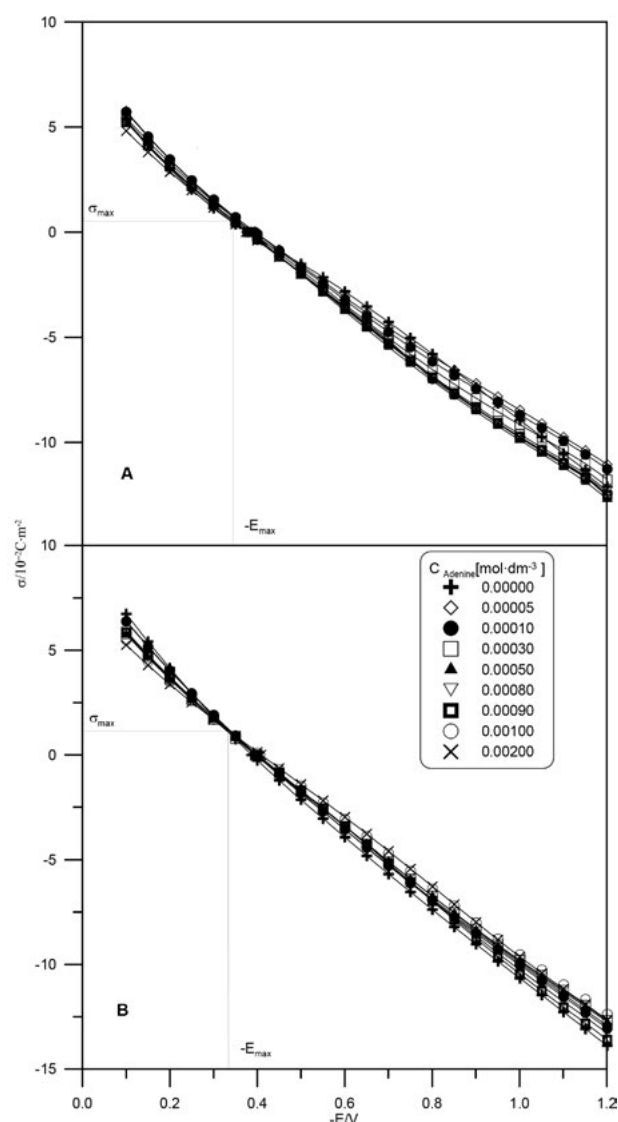


Figure 4. Correlation between the surface charge density on mercury and the potential of the electrode for an acetate buffer at pH 3 (A) and pH 4 (B) in the function of adenine concentration.

3. 2. Adsorption Isotherms

The adsorption of adenine was described using the relative surface excess, Γ' , which, according to the Gibbs adsorption isotherm, is given by:

$$\Gamma' = \frac{1}{RT} \left(\frac{\partial \Phi}{\partial \ln c} \right)_E \quad (3)$$

where c is the bulk concentration of adenine and Φ is the surface tension, as in $\Phi = \gamma_0 - \gamma$, where γ_0 is the surface tension of the basic electrolyte, and γ is the surface tension for the solution containing adenine.

Values of adenine surface concentrations expressed as relative surface excess were analysed in order to obtain

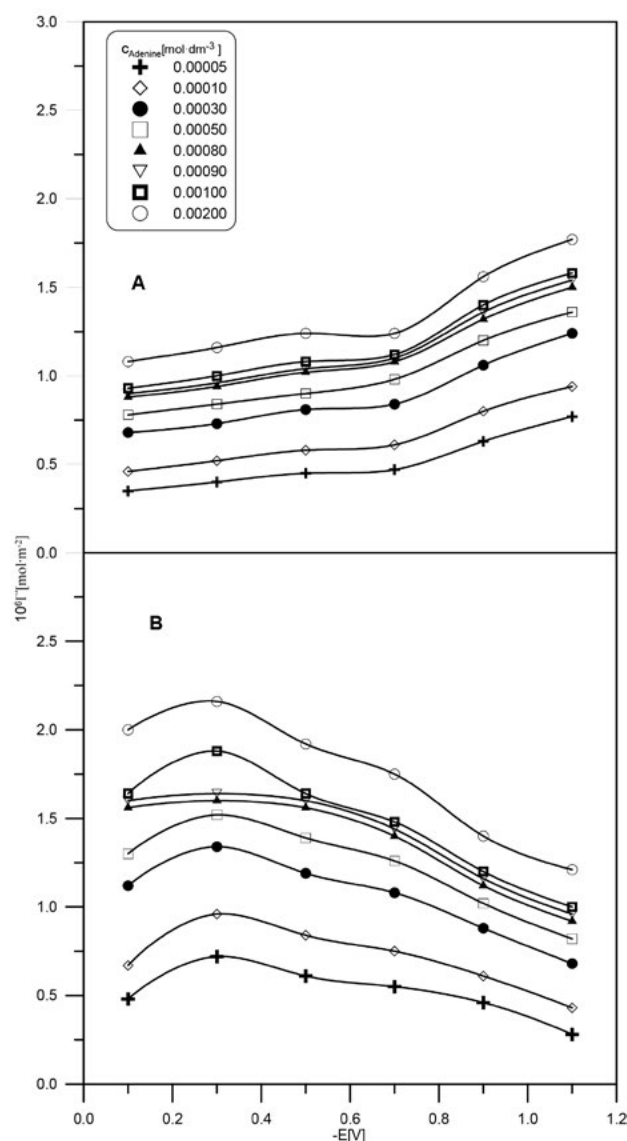


Figure 5. Relative surface excess of adenine as a function of the potential and adenine concentration in the bulk, in the acetic buffers pH 3 (A) and pH 4 (B).

a more complete picture of the adsorption of the tested substance (Figure 5).

The course of changes in the values of relative surface excess Γ' for each of the studied systems is different. Presumably, it is caused by the fact that in the acetate buffer at pH 3, a molecule of adenine adsorbs on the surface of a mercury electrode with the positive pole. An increase in surface excess for adenine toward less negative potentials indicates electro-static interaction between a protonated molecule of adenine with an increasingly negatively charged surface of a mercury electrode. In the acetate buffer at pH 4, a dipole molecule of adenine adsorbs on the surface of mercury with the negative pole. Slightly bell-shaped dependence $\Gamma' = f(E)$ in the buffer solution at pH 4 indicates a physical nature of adenine adsorption on a mercury electrode.

The adsorption of adenine was further analysed on the basis of constants obtained from the Frumkin isotherm.^{21–26} The Frumkin isotherm (Figure 6) constants were determined from the equation:

$$\beta x = \left[\frac{\Theta}{1-\Theta} \right] \exp(-2A\Theta) \quad (4)$$

where x is the mole fraction of adenine in the solution, β is the adsorption coefficient: $\beta = \exp(-\Delta G^0/RT)$, ΔG^0 is the standard Gibbs energy of adsorption, A is the interaction parameter, and Θ is the coverage value $\left(\Theta = \frac{\Gamma'}{\Gamma_s} \right)$. The surface excess at saturation, Γ_s , was estimated by extrapolating the $1/\Gamma'$ vs. $1/c_{C_5H_5N_5}$ lines at different electrode potentials to $1/c_{C_5H_5N_5} = 0$. The Γ_s value obtained this way was:

$3.23 \times 10^{-6} \text{ mol m}^{-2}$ for pH 3 of the basic electrolyte and $3.45 \times 10^{-6} \text{ mol m}^{-2}$ for pH 4. The surface occupied by one adenine, S ($S \equiv 1/\Gamma_s$), is 0.514 nm^2 and 0.481 nm^2 respectively for the buffer with a pH of 3 and a pH of 4.

The obtained values are comparable and indicate a flat orientation of adsorbed adenine molecules in both systems.

The values of free energy ΔG_F^0 and adsorption factor $-A_F$ obtained in linear tests of the Frumkin isotherm are presented in Table 2.

The values of parameter $-A_F$ in both buffers indicate a repulsive interaction between adsorbed adenine molecules, but in the buffer at pH 3 this interaction is increasingly weaker toward less negative potentials, whereas in the buffer at pH 4 the repulsive interaction clearly intensifies toward more negative potentials. Changes in the repulsive interaction between adsorbed molecules of adenine insignificantly affect a change in adsorption energy.

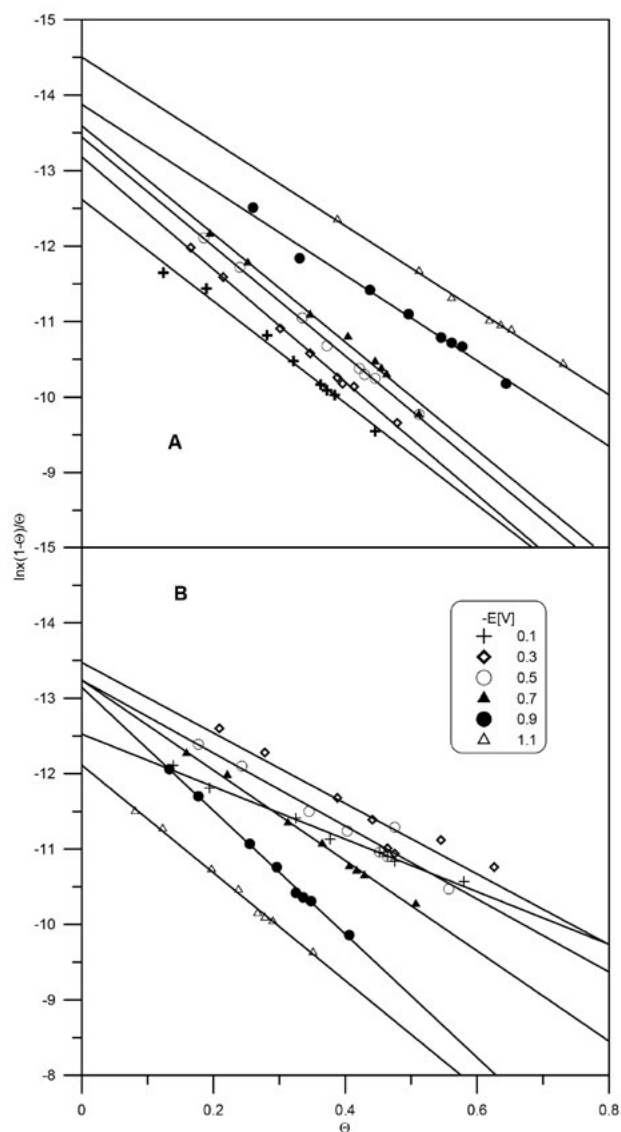


Figure 6. Linear test of the Frumkin isotherm in the system acetic buffer pH 3 (A) and pH 4 (B) + adenine for different electrode potentials.

Values of adsorption energy in both buffers are comparable except that in the buffer at pH 3 they increase (in an absolute sense) toward more negative potentials, which

indicates electro-static interaction between a protonated molecule of adenine and the surface of an electrode. In the acetate buffer at pH 4, these values display slight dependence on potential.

The previously presented Frumkin isotherms are encumbered with errors resulting from discrepancies between theoretical and experimental values Γ_s . Therefore, virial isotherms in which the parameter does not occur were used to check adsorption parameters.

By means of the linear test of the virial isotherm, values of the second virial factor B were determined from the slopes of the lines whereas values of adsorption energy ΔG_v^0 were obtained by extrapolating these lines to value $\Gamma = 0$ using the standard state 1 mol dm^3 in the solution and $1 \text{ molecule cm}^{-2}$ on the surface of the electrode.

The obtained values of adsorption energy and the second virial factor B in the function of electrode potential are presented in Table 2. The trends in changes in adsorption parameters obtained from the virial isotherm have a similar shape to those obtained from the Frumkin isotherm.

3. 3. Electroreduction Kinetics of Zn(II)ion in the Presence of Adenine in an Acetate Buffer at pH 3 and pH 4.

Studies of the effect of adenine on kinetics of Zn^{2+} ion reduction were performed using various measurement techniques, e. g. cyclic voltammetry and measurement of Faraday impedance.²²

Potentials of anode peak E_a and cathode peak E_k for Zn(II)ion reduction were determined from the shape of cyclic voltammetric curves, and the difference of potentials for anode and cathode peaks was calculated from dependence 5.

$$\Delta E = E_a - E_k \quad (5)$$

The differences of potentials for anode and cathode peaks are a good qualitative criterion of the assessment of reversibility of the electrode process. They are presented in Table 3.

On the basis of the obtained ΔE values, it can be stipulated that Zn(II) reduction reactions are irreversible in

Table 2. The constants of Frumkin (F) and virial (V) isotherms for the system: the acetic buffer pH 3 and pH 4 + adenine; E, - ΔG^0 , B.

-E / V	pH 3				pH 4			
	$\Delta G_F^0 / \text{kJ mol}^{-1}$	$-A_F$	$\Delta G_V^0 / \text{kJ mol}^{-1}$	B / $\text{nm}^2/\text{molecula}$	$\Delta G_F^0 / \text{kJ mol}^{-1}$	$-A_F$	$\Delta G_V^0 / \text{kJ mol}^{-1}$	B / $\text{nm}^2/\text{molecula}$
0.10	31.56	4.70	109.20	2.52	31.04	1.75	108.60	1.08
0.30	32.45	4.80	110.20	2.52	33.04	2.10	111.10	1.30
0.50	33.49	4.90	110.70	2.52	32.80	2.47	110.60	1.43
0.70	33.56	4.60	111.00	2.38	32.80	3.00	110.20	1.55
0.90	34.21	3.70	112.30	2.12	32.65	4.13	109.40	1.91
1.10	35.42	3.50	113.70	2.06	30.37	4.13	107.40	1.77

Table 3. Values of potentials anodic and cathodic peaks and their difference for the system: 5×10^{-3} mol L⁻¹ Zn(II) in the buffer solutions at pH 3 and pH 4 without adenine and for various adenine concentrations.

$C_{\text{adenine}} / \text{mol/L}$	pH 3			pH 4		
	$-E_a / \text{V}$	$-E_k / \text{V}$	$\Delta E / \text{V}$	$-E_a / \text{V}$	$-E_k / \text{V}$	$\Delta E / \text{V}$
0	0.90	1.05	150	0.92	1.02	98
$5.0 \cdot 10^{-5}$	0.82	1.05	228	0.92	1.02	105
$1.0 \cdot 10^{-4}$	0.81	1.05	236	0.92	1.02	105
$3.0 \cdot 10^{-4}$	0.81	1.05	244	0.92	1.03	108
$5.0 \cdot 10^{-4}$	0.81	1.06	247	0.92	1.03	113
$8.0 \cdot 10^{-4}$	0.81	1.06	252	0.92	1.03	109
$9.0 \cdot 10^{-4}$	0.80	1.06	262	0.92	1.03	111
$1.0 \cdot 10^{-3}$	0.80	1.07	262	0.92	1.03	112
$2.0 \cdot 10^{-3}$	0.80	1.06	264	0.92	1.03	114
$3.0 \cdot 10^{-3}$	0.78	1.07	274	0.92	1.03	114
$4.0 \cdot 10^{-3}$	0.84	1.10	257	0.92	1.03	113
$5.0 \cdot 10^{-3}$	0.80	1.07	268	0.92	1.03	114

both buffer solutions and that adenine added to solutions has an irreversibility effect by decelerating the reduction reaction of zinc ions. In the buffer solution at pH 3 without adenine, inhibition of Zn(II) reduction is stronger due to stronger adsorption of molecules of acetic acid. The addition of adenine to the buffer more significantly inhibits Zn(II) electro-reduction in comparison to the buffer at pH 4. This is a consequence of stronger adenine adsorption in the buffer at pH 3 (Table 2).

Measurement of Faraday impedance was used to verify the results obtained from cyclic voltammetry. Values of activation resistance R_a were determined at potentials corresponding to minimal R_a values. In both studied buffer solutions, an increase in R_a is observed with an increase in adenine concentration (Table 4). The inhibiting effect is much more weaker in solutions at pH 4. The determined R_a values (pH 4) slightly increase in comparison to the values obtained at pH 3. Such behavior can be the result of larger protonation level in acetate buffer at pH 3 in

Table 4. Minimal values of activation resistance at given potentials in the system: 5×10^{-3} mol L⁻¹ Zn(II) in buffer solutions at pH 3 and pH 4 in the presence of increasing adenine concentrations.

$C_{\text{adenine}} / \text{mol dm}^{-3}$	pH 3		pH 4	
	$-E / \text{V}$	$R_a / \Omega \text{ cm}^2$	$-E / \text{V}$	$R_a / \Omega \text{ cm}^2$
0	0.98	3.88	0.97	0.85
$5.0 \cdot 10^{-5}$	0.98	2.19	0.97	1.17
$1.0 \cdot 10^{-4}$	0.98	2.59	0.97	1.33
$3.0 \cdot 10^{-4}$	0.97	4.55	0.98	1.58
$5.0 \cdot 10^{-4}$	0.98	6.38	0.98	1.79
$8.0 \cdot 10^{-4}$	0.98	7.87	0.98	1.84
$9.0 \cdot 10^{-4}$	0.98	8.47	0.98	1.95
$1.0 \cdot 10^{-3}$	0.98	9.00	0.98	1.93
$2.0 \cdot 10^{-3}$	0.98	11.90	0.98	2.02
$3.0 \cdot 10^{-3}$	0.99	12.72	0.98	2.26
$4.0 \cdot 10^{-3}$	1.00	13.51	0.98	2.15
$5.0 \cdot 10^{-3}$	0.99	13.41	0.99	2.39

comparison to the one in the solution at pH 4. It causes stronger repulsive interactions between protonated molecules of adenine and Zn(II) ions. As a result, the access of depolarizer ions to the electrode surface is more difficult thus inhibiting effect of adenine is larger in pH 3

4. Conclusions

Experimental data and the results of thermodynamic analysis concerning adenine adsorption on a mercury electrode in an acetate buffer at two pH values (pH 3 and pH 4) presented in the work helped to observe certain regularities.

The comparison of the shape of the differential capacity curves obtained in the function of adenine concentration indicates differences in the adsorptive properties of adenine between the acetate buffer at pH 3 and the acetate buffer at pH 4.

The shape of dependences of relative surface excess in the function of potential indicates a physical nature of adenine adsorption in the buffer at pH 4, whereas electrostatic interaction between adsorbed molecules of adenine and the surface of the electrode occurs in the buffer at pH 3.

The shift of the value of potential of zero charge E_z with an increase in adenine concentration in the buffer at pH 4 toward more negative potentials indicates the absence of interaction between π electrons of the aromatic ring of adenine with the surface of the mercury electrode. In the case of the buffer at pH 3, the direction of changes in E_z depends on the adenine concentration.

Studies of the kinetics of Zn (II) ion electro-reduction using cyclic voltammetry and Faraday impedance measurement led to a conclusion that in the buffer at pH 3, Zn(II) ion electro-reduction is more irreversible than in the buffer at pH 4. The addition of adenine has a slightly greater effect on the inhibition of the electrode process in

a solution of pH 3, in which the adenine molecule is more protonated than in a solution of pH 4. The inhibitory effect of adenine most probably results from blocking the surface of the mercury adsorbing with organic molecules. It grows with increasing its concentration and decrease in the pH of the buffer solution.

5. References

1. S. A. Kuznetsov, M. Gaune-Escard, *J. Electroanal. Chem.* **2006**, 595, 11–22. DOI:10.1016/j.jelechem.2006.02.036
2. L. Massot, P. Chamelot, L. Cassayre, P. Taxil, *Electrochimica Acta.* **2009**, 54, 6361–6366. DOI:10.1016/j.electacta.2009.06.016
3. J. Nieszporek, D. Gugała, D. Sieńko, J. Szaran, J. Saba, *Electrochimica Acta.* **2006**, 51, 2278–2281. DOI:10.1016/j.electacta.2005.03.079
4. B. Timmer, M. Sluyters-Renbach, J. H. Sluyters, *Surface Science.* **1969**, 18, 44–61. DOI:10.1016/0039-6028(69)90266-0
5. M. Sciendo, *Corrosion Science.* **2008**, 50, 2070–2077. DOI:10.1016/j.corsci.2008.04.007
6. A.-R. El-Sayed, A. M. Shaker, H. M. A. El-Lateef, *Corrosion Science.* **2010**, 52, 72–81. DOI:10.1016/j.corsci.2009.08.047
7. J. Zwierzykowska, *Ochrona przed korozją*, **1962**, 101, 15–20.
8. F. Beck, *Elektroorganische Chemie*, Velag Chemie, Weinheim, **1974**.
9. B. Wyrwas, A. Szymanski, Z. Lukaszewski, *Anal Chim Acta.* **1995**, 305, 31.
10. Z. Lukaszewski, A. Szymanski, B. Wyrwas. *Trac Trends Anal Chem.* **1996**, 15(10), 525. DOI:10.1016/S0165-9936(96)00064-7
11. J. Lenik, *Mater Sci Eng C.* **2014**, 45, 109–116. DOI:10.1016/j.msec.2014.08.072
12. A. Avranas, U. Retter, K. Lunkenheimer, *Journal of Colloid and Interface.* **2000**, 227, 398–407. DOI:10.1006/jcis.2000.6870
13. X. Zhao, W. Jin, J. Chen, Z. Gao, F. Wang, *Analytica Chimica Acta.* **1994**, 289, 163–169. DOI:10.1016/0003-2670(94)80099-5
14. X. Zhao, W. Jin, J. Tang, *Electroanalysis.* **1996**, 8, 370–374. DOI:10.1002/elan.1140080413
15. K.-J. Huang, D.-J. Niu, J.-Y. Sun, C. -H. Han, Z. -W. Wu, Y. -L. Li, X. -Q. Xiong, *Colloids and Surfaces B: Biointerfaces.* **2011**, 82, 543–549. DOI:10.1016/j.colsurfb.2010.10.014
16. J. R. De Wille, *Introduction to Electrophysiological Methods and Instrumentation Franklin Bretschneider*, Academic Press is an Imprint of Elsevier **2006**.
17. C. Prado, F. Prieto, M. Rueda, J. Feliu, A. Aldaz, *Electrochimica Acta.* **2007**, 52, 3168–3171. DOI:10.1016/j.electacta.2006.09.062
18. A. De Batisti, S. Trasatti, *J. Electroanal. Chem.* **1974**, 54, 1–17. DOI:10.1016/S0022-0728(74)80375-X
19. D. M. Mohilner, H. Nakadomari, *J Phys Chem.* **1973**, 77, 1594–1596. DOI:10.1021/j100631a024
20. D. M. Mohilner, L. M. Bowman, S. J. Freeland, H. Nakadomari, *J. Electrochem. Soc.* **1973**, 120, 1658–1670. DOI:10.1149/1.2403324
21. A. Nosal – Wiercińska, *Electroanalysis.* **2014**, 26, 1013–1023. DOI:10.1002/elan.201400010
22. D. M. Bastidas, P. P. Gomez, E. Cano, *Rev. Metal. Madrid.* **2005**, 41, 98–106. DOI:10.3989/revmetalm.2005.v41.i2.192
23. M. A. Quiroz, F. Cordova, L. Salgado, M. Viniegra, Y. Meas, G. Diaz. *Revista Mexicana de Fisica.* **1995**, 41, 386–395.
24. D. Gugała-Fekner, J. Nieszporek, D. Sieńko, *Monatsh. fur Chemie.* **2015**, 146, 541–545. DOI:10.1007/s00706-014-1382-7
25. V. L. Kolev, K. D. Danov, P. A. Kralchevsky, G. Broze, A. Mehreteab. *Langmuir*, **2002**, 18, 9106–9109. DOI:10.1021/la0259858
26. H. J. El-Aila, K. M. Elsousy, K. A. Hartany, *Arabian Journal of Chemistry*, **2016**, 9, S198–S203. DOI:10.1016/j.arabjc.2011.03.002

Povzetek

V prispevku je predstavljena termodinamična analiza adsorpcije adenina na živosebrni elektrodi v acetatnem pufru pri pH 3 in pH 4. Z uporabo Frumkinove in virialne izoterme smo določili energijo in konstante adsorpcije. Izkazalo se je, da je adsorpcija v pufru pri pH 3 močnejša kot v pufru pri pH 4. Pri izvedbi ciklične voltometrije in meritvah Faradayeve impedance smo opazili inhibitorski učinek adenina na kinetiko elektro redukcije ionov Zn (II).

Scientific paper

Thermochemical Properties and Regularities of Amides, Anilides, and Amidic Acids

Alma Kairlapovna Ryskaliyeva,* Murat Ergalievich Baltabayev and Aigul Moldakhmetovna Zhubatova

Kazakh National Agrarian University, 8 Abay Av., 050000 Almaty, Kazakhstan

* Corresponding author: E-mail: aryskaliyeva@mail.ru

Received: 08-07-2017

Abstract

The thermodynamic properties of carbamide and its alkyl substituted were studied insufficiently. In this article, the enthalpies of combustion of $\Delta_c H$ of some amides, anilides and amidic acids have been determined experimentally; their standard enthalpies of formation have been calculated. Linear dependences between the average atomic enthalpy of combustion of $\Delta_c H$ amides and their basicity constants in acidic aqueous solutions of pK_{BH}^+ have been established; a correlation that relates the enthalpies of combustion of amides and the corresponding amidic acids has been found.

Keywords: Enthalpy of combustion, thermochemistry, amides, correlation analysis

1. Introduction

Amides, anilides and their derivatives play an important role in various biochemical processes and are therefore widely used as analytical and organic reagents in plant growing, animal husbandry, and pharmacology. Despite the broad practical application, thermochemical properties of carbamide and its alkyl substituted were studied insufficiently.^{1–3} Recently, along with experimental methods of studying thermochemical properties, the methods of establishing empirical correlations based on the application of regression and correlation analyses of thermochemical data are rapidly developing.

In this paper, the results of the experiments carried out by the method of bomb calorimetry to determine the enthalpies of combustion of 11 amides, 5 anilides, and 8 amidic acids and calculate their standard enthalpies of formation are presented. The original methods for calculating the intensive values of enthalpies of combustion as well as empirical correlations linking the intensive values of the enthalpies of combustion of amides and amidic acids are found.

2. Experimental

An industrial calorimeter B-08-MA (manufacturer: JSC “Almatinskiy zavod Etalon”, the Republic of Kazakhstan, Almaty) with an isothermal jacket and a stationary

self-packing calorimetric bomb ($V_{int.} = 325 \text{ cm}^3$), equipped with two valves (for input and output of gases), was used to determine the enthalpies of combustion of the studied compounds. The measurement error of the calorimeter was $\pm 0.1\%$, which was absolutely insufficient to make precise measurements. Therefore, in order to improve the accuracy of the determination of the energy of combustion of substances, we, in collaboration with the scientists of the Scientific Research Institute of Physico-Chemical Problems of the Belarusian State University, Minsk, have refined the following parts: the jacket thermostating system, the oxygen purification system, the samples ignition system, the calorimetric vessel, and the calorimetric bomb. As a result, the implemented improvement of the calorimeter made it possible to increase the accuracy of obtained thermochemical values to $\pm 0.01\%$.

Benzoic acid, which is used in calorimetry as an energy reference, must have a very high purity. We used reference benzoic acid K-1, produced by D. I. Mendeleev Institute for Metrology (VNIIM), St. Petersburg, which had a purity of 99.997 mol%.⁴ Also, benzoic acid produced by the National Institute of Standards and Technology of the United States was used as a calorimetric standard; according to the certificate, its purity was 99.997 mol%, and moisture content – about 0.002%.⁵

The test samples of amides, anilides, and amidic acids were burned as tablets without or with a special polyethylene film which served as an auxiliary substance. In

the experiment, industrial amides and anilides of “pure” quality were used. They were initially purified with help of several recrystallization stages from a water-ethanol mixture and absolute alcohol. After that, they were purified by sublimation in a vacuum and then stored in a desiccator over phosphorus pentoxide until a constant mass. Amides, synthesized at the Department of Inorganic Chemistry of Al-Farabi Kazakh National University, were purified by recrystallization from water and ethyl alcohol. The content of the main component in the combustion objects was ~99.80%. This was established by the results of elemental and gravimetric (Rossini’s method)⁶ analyses.

The masses of combustible samples and polyethylene were determined on microbalances with an accuracy of $\pm 2 \cdot 10^{-5}$ g. Moreover, the amount of substance was chosen in such a way so that the temperature rise in the experiment corresponded to the temperature rise when the reference substance was burned.⁷

After the completion of the experiment, the combustion gases were analyzed for CO₂ content by the Rossini method (accuracy $\pm 0.05\%$). The analysis for CO content was carried out with help of indicator tubes (sensitivity $6 \cdot 10^{-6}$ kg l⁻¹).

The software for processing calorimetric experiments on combustion of the studied substances and determination of the value of enthalpy of combustion was provided by V. V. Simirsky,⁸ the scientist of Belarusian State University.

The enthalpies of combustion ($\Delta_c H^0$) and the calculated values of the formation enthalpies ($\Delta_f H^0$) for all the amides, anilides and amide acids studied by us are presented in Table 1.

3. Results and Discussion

Empirical correlations are widespread in all sections of chemistry; they allow us to quantitatively describe chemical processes, to systematize facts and to carry out calculations. One efficient way of establishing quantitative empirical correlations is to transform extensive values into intensive ones, since the latter describe the properties of chemicals more adequately.

The thermodynamic characteristics of a solid matter referred to one mole of structural units and expressed in a stoichiometric gross formula are given in reference books. However, reference thermodynamic values do not allow comparing even the same solid matters which participate in the same chemical processes. Therefore, Kh. K. Ospanov⁹ used average atomic thermodynamic characteristics to describe the differences in the reactivity of solids of the same type such as natural oxides, sulphides, and silicates in homogeneous chemical processes. The simplicity of Ospanov’s method of transforming extensive values into intensive ones is striking. For instance, the average atomic enthalpy of combustion of carbamide,

Table 1. Standard enthalpies of combustion and formation of amides and their derivatives

Compound	$-\Delta_c H^0$, kJ mol ⁻¹	$-\Delta_f H^0$, kJ mol ⁻¹
N, N-methylacetylcarbamide	2154.32 ± 2.28	563.10 ± 2.28
Oxamide	851.70 ± 2.27	507.01 ± 2.27
α-cyanoacetamide	1565.43 ± 2.52	186.80 ± 2.52
N, N-dimethylacetamide	2598.04 ± 37.41	282.30 ± 37.41
α-phenylacetamide	4210.40 ± 3.79	224.02 ± 3.79
Propionamide	3550.10 ± 0.82	291.37 ± 0.82
Valeramide	3140.62 ± 0.84	329.04 ± 0.84
Isovaleramide	3149.68 ± 1.73	390.02 ± 1.73
Salicylamide	3352.32 ± 2.21	402.68 ± 2.21
Nicotinamide	3083.78 ± 1.69	131.85 ± 1.69
N, N-dimethylbenzamide	4959.91 ± 1.02	153.87 ± 1.02
Formanilide	3591.40 ± 1.72	177.23 ± 1.72
2,4-dimethylacetanilide	5501.93 ± 0.83	291.20 ± 0.83
P-aminoacetanilide	4341.30 ± 2.28	267.10 ± 2.28
Benzanilide	6576.05 ± 4.68	111.80 ± 4.68
Salicylicanilide	6379.64 ± 3.01	308.21 ± 3.01
Carbamide nitrate (2: 1)	1095.48 ± 1.88	977.82 ± 1.88
Biuret Nitrate (1: 1)	881.73 ± 4.74	762.83 ± 4.74
Nitrate oxamide (1: 1)	1315.24 ± 2.09	186.39 ± 2.09
α-cyanoacetamide nitrate (1: 1)	2304.01 ± 2.86	408.86 ± 2.86
Nitrate propionamide (6: 1)	12309.66 ± 4.83	908.06 ± 4.83
Valeramide nitrate (6: 1)	19586.59 ± 15.07	1784.51 ± 15.07
Nitrate isovaleramide (6: 1)	20287.65 ± 18.96	1093.45 ± 18.96
Nicotinamide nitrate (1: 1)	2949.05 ± 4.78	412.49 ± 4.78

which equals to 79.01 kJ/(g-atom), is the molar enthalpy of combustion of carbamide 632.08 kJ mol⁻¹ divided by 8 atoms (since the gross formula of carbamide CH₄N₂O contains one carbon atom, four hydrogen atoms, two nitrogen atoms and one oxygen atom – total 8 atoms). This is a thermodynamic characteristic of a solid matter recalculated by one mole of atoms, in which there are one fraction of carbon, four of hydrogen, two of nitrogen and one of oxygen.

It is known that amides can be considered as bases. According to the Brønsted-Lowry theories, the base strength can be quantitatively described by the exponent of the basicity constant pK_{BH}⁺.

We have established almost a linear relationship between the exponent of basicity constant and the average atomic enthalpy of combustion of the studied amides (Table 2). The high correlation coefficient r = 0.992 between the values considered also allowed us to calculate the linear regression coefficients by the method of least squares and to find the following empirical correlation:

$$\Delta_c H = 83.72 (pK_{BH}^+ - 1) \text{ kJ/(g-atom)} \quad (1)$$

Table 2. The correlation dependence between the average atomic enthalpy of combustion $\Delta_c H$ (kJ(g-atom)⁻¹) of amides and their basicity constants in acidic aqueous solutions of pK_{BH}⁺ (r = 0.992)

Amide	$-\Delta_c H, \text{ kJ (g-atom)}^{-1}$	pK _{BH} ⁺
Carbamide	79.01	0.05
Acetamide	131.78	-0.62
α -phenylacetamide	204.39	-1.30
Phenylcarbamide	203.69	-1.30
Benzamide	221.88	-1.74

Based on this correlation (1), the following series of changes of the basicity of the amides can be proposed: carbamide > acetamide > α -cyanoacetamide > valeramide > isovaleramide > nicotinamide > salicylamide > α -phenylacetamide > N, N-dimethylbenzamide.

Thus, correlation (1) can become one of the ways of estimation the enthalpies of combustion $\Delta_c H$ of unexplored amides.

The next method of transformation of combustion enthalpies is based on the stoichiometric balance of the combustion reaction equation. For example, the more carbon and hydrogen in the compound formula, the more carbon dioxide and water will be generated as a result of combustion, the more oxygen is required for combustion and the greater the numerical value of the combustion enthalpies. This proposition underlies A. A Ravdel's equation:¹⁰

$$-\Delta_c H = 204.2 n + 44.4 m + \Sigma x_i$$

where,

n – the number of oxygen atoms required for the combustion of one mole of the substance;

m – the number of water molecules formed;

Σx_i – additive correction (thermal characteristic of the same type of substances).

The parameters of Ravdel's equation (n and m) reflect the balance of oxygen and water in the combustion reaction equation. These are parameters of the extensiveness of the combustion process. Therefore, the value of the enthalpy of combustion divided by the sum of the parameters of Ravdel's equation (n + m) should serve as an intensive value that can have a correlation with the physico-chemical properties of the substance being burnt. For example, complete combustion of one mole of carbamide requires three moles of oxygen and, as a result, two moles of water are formed; therefore n + m = 5. Consequently, the enthalpy of combustion of carbamide normalized by the oxygen-water balance will have the following quantitative value:

$$\left(\frac{\Delta_c H}{n+m}\right) = \frac{632.06}{3+2} = 126.41 \text{ kJ}$$

A comparison of the normalized values (Table 3) of the standard combustion enthalpies of the amides (A) and the corresponding amidic acids (AA) allowed us to establish a linear regression equation with a high correlation coefficient R = 0.997:

$$\left(\frac{\Delta_c H}{n+m}\right)_{AA} = 1.1 \times \left(\frac{\Delta_c H}{n+m}\right)_A \quad (2)$$

Table 3. The relationship between the normalized values of the enthalpies of combustion of amides and their corresponding amidic acids (nitrates)

Amide (A)	$\frac{\Delta_c H}{n+m}$	Amidic acids (AA)	$\frac{\Delta_c H}{n+m}$	$\epsilon, \%$
carbamide	126.4	carbamide nitrate 1:1	136.9	1.6
valeramide	157.3	valeramide nitrate 6:1	166.0	4.2
α -cyanoacetamide	173.9	cyanoacetamide nitrate 1:1	200.4	0.7
nicotinamide	181.4	nicotinamide nitrate	196.6	-4.5
oxamide	276.8	oxamide nitrate	328.8	7.4

The relative deviation of the experimental values of

$\left(\frac{\Delta_c H}{n+m}\right)_{AA}$ from correlation (2) does not exceed 7.4%, which

is the generally accepted accuracy (~10%) for Lauthier-Karapet'yants correlations.¹¹ Thus, correlation (2) can be used for computational determination of enthalpies of combustion of amidic acids, which have been not yet studied in thermochemistry, applying the thermochemical characteristics of the corresponding amides.

4. Conclusion

By the method of bomb calorimetry, the enthalpies of combustion $\Delta_c H$ of 11 amides, 5 anilides, and 8 amidic acids were experimentally determined. Their standard enthalpies of formation were calculated. A linear dependence between the average atomic values of the enthalpy of combustion of amides $\Delta_c H$ and their basicity constants in acidic aqueous solutions pK_{BH}^+ was found:

$$\Delta_c H = 83.72 \times pK_{BH}^+ - 83.72$$

A correlation that relates the normalized values of the enthalpies of combustion of amides and their nitrates was found:

$$\left(\frac{\Delta_c H}{n+m}\right)_{AA} = 1.1 \left(\frac{\Delta_c H}{n+m}\right)_A$$

Povzetek

Z meritvami v bombnem kalorimetru smo določili sežigne entalpije, $\Delta_c H$, nekaterih amidov, anilidov in amidnih kislin (nitrato) ter izračunali njihove standardne tvorbene entalpije. Ugotovili smo linearno odvisnost med povprečno $\Delta_c H$ in konstantno bazičnosti v kislih vodnih raztopinah, pK_{BH}^+ ter postavili zvezo med $\Delta_c H$ amidov in ustreznih amidinskih kislin (nitrato).

5. References

1. A. K. Ryskalieva, G. V. Abramova, N. N. Nurakhmetov, R. Sh. Erkasov, *Russ. J. Phys. Chem. A.*, **1991**, *4*, 1068–1070.
2. A. K. Ryskalieva, P. Sh. Erkasov, G. V. Abramova, N. N. Nurakhmetov, *Izv. Vyssh. Uchebn. Zaved., Khim. Khim. Tekhnol.*, **1991**, *9*, 25–27.
3. A. K. Ryskalieva, G. V. Abramova, R. Sh. Erkasov, N. N. Nurakhmetov, *Russ. J. Phys. Chem. A.*, **1992**, *3*, 797–799.
4. Yu. I. Aleksandrov, T. R. Osipova, V. F. Yushkevich, in: B. N. Oleinik (Ed): *Methods and Means of Calorimetry of Thermophysical Measurements (Metody I Sredstva Kalometrii Teplofizicheskikh Izmereniy)* D. I. Mendeleev Institute for Metrology (VNIIM), St. Petersburg, Russia, **1984**, 250 p.
5. Nat. Bur. Stand. Certificate of Analysis, Standard Reference Material 39-I Benzoic Acid, Calorimetric Standard, Washington: D. C., **1968**, №20234. -pp. 44–59
6. F. D. Rossini *Experimental thermochemistry*, Interscience Publishers Inc., New York, USA, **1956**, 326p.
7. V. P. Kolesov *Fundamentals of thermochemistry*, SSU, Moscow, Russia, **1996**, 204 p.
8. V. V. Simirsky, Ph. D. Thesis, Belarusian State University, Minsk, **1986**.
9. Kh. K. Ospanov, *General principles of prediction of differences in reactivity of minerals and solvents in the conditions of processing of mineral raw materials*, Kazakh University, Almaty, Kazakhstan, **2015**, 409 p.
10. *Quick Reference of Physico-Chemical Variables*, (Ed): A. A. Ravdel and A. M. Ponomareva, Chemistry, St. Petersburg, Russia, **1983**, 232p.
11. A. K. Ryskalieva, Ph. D. Thesis, Al Farabi Kazakh National University, Almaty, **1998**.

Scientific paper

Effect of Fluorinated Ligand on Structural, Electronic and DNA-binding Properties of Copper Paddlewheel Complex: Synthesis, Structure and Properties

Muhammad Iqbal,^{1,*} Sqib Ali^{2,*} and Muhammad Nawaz Tahir³¹Department of Chemistry, Bacha Khan University, Charsadda 24420, KPK, Pakistan²Department of Chemistry, Quaid-i-Azam University, Islamabad 45320, Pakistan³Department of Physics, University of Sargodha, Sargodha, Pakistan

* Corresponding author: E-mail: iqbalmo@yahoo.com, iqbalmo@bkuc.edu.pk (M. Iqbal)

Tel.: +92 91 6002934; fax: +92 91 6540060.

drsa54@hotmail.com, saqibali@qau.edu.pk (S. Ali).

Tel.: +92 51 90642130; fax: +92 51 90642241.

Received: 17-07-2017

Abstract

This paper presents synthesis, structural description and properties of a binuclear paddlewheel copper(II) carboxylate complex with formula [(py)Cu(μ-L)₄Cu(py)], where py = pyridine and L = 4-fluorophenylacetate. Structural characteristics, electronic absorption and DNA-binding properties of the synthesized complex have been compared to those of the non-fluorinated analogues (where F is replaced by H, -CH₃ and -OCH₃) already reported and the modifications successfully ascribed to fluorine. The complex exhibits typical paddlewheel structure and there are two crystallographically independent molecules in the unit cell. The electronic absorption spectrum of complex is also different and the mode and extent of DNA-binding ability of complex are significantly altered owing to the presence of suitably substituted fluorine. The effect of fluorine is clearly manifested in the modified properties of synthesized complex.

Keywords: *p*-fluorophenylacetate, copper complex, crystal structure, DNA-binding

1. Introduction

The design and synthesis of new functional complexes is the most widely explored area of research in coordination chemistry. Properties of metal complexes arise from metal ion as well as attached ligands. The metal based properties are a function of the type and number of metal ions per molecule. Thus, binuclear complexes have been found to possess enhanced biological, catalytic and magnetic properties compared to the mononuclear analogues.^{1–3} Similarly, type and oxidation state of metal ion drastically alter the properties of resulting complex.⁴

The other most important part of a complex are the attached ligands that have a crucial role in steering a complex to its desired properties.^{5,6} Ligand not only stabilizes a metal ion in a given oxidation state but also the geometry around it in a coordination complex.⁴ Ligands can carry metal ion to its biological target in chemically variable medium of biological systems.⁷ The beauty and diversity of synthetic coordina-

tion chemistry stems from the variable bonding strength and modes of the ligands having suitable donating sites.^{8–10} Moreover, the properties of a complex can be modified *via* changing substituents on the attached ligands.^{11,12}

In continuation of our previous work^{13–15} we experienced a substantial change in properties of a complex having fluorine substituent instead of hydrogen, methyl and methoxy groups. Modification in structure, absorption spectrum and DNA-binding ability of the fluorinated complex were observed compared to other analogues and such alterations have been presented here as a function of fluorine substituent.

2. Experimental

2.1. Materials and Methods

Anhydrous CuSO₄, 4-fluorophenylacetic acid, pyridine, NaHCO₃, KCl and sodium salt of salmon sperm

DNA were obtained from Fluka, Switzerland. Solvents like methanol, chloroform and dimethyl sulfoxide were obtained from Merck, Germany, and used as such without drying. Water used was singly distilled. Melting point was obtained in a capillary tube using a Gallenkamp, serial number C040281, U. K, electro-thermal melting point apparatus. FT-IR spectrum was recorded on a Nicolet-6700 FT-IR spectrophotometer, Thermo Scientific, USA, in the range from 4000 to 400 cm^{-1} using attenuated total reflectance (ATR) technique.

2. 2. Single crystal X-ray Crystallographic Study

X-ray single crystal analysis of the complex was performed at 296 K on a Bruker Kappa APEX-II CCD diffractometer using graphite-monochromated Mo-K α radiation ($\lambda = 0.71073 \text{ \AA}$). Crystal structure was solved by direct method followed by final refinement carried on F^2 with full-matrix least-squares using the program SHELXL-97.¹⁶ The H-atoms were included in calculated positions and treated as riding atoms: C-H = 0.93, 0.96 and 0.97 \AA for CH, CH₃ and CH₂ H-atoms, respectively, with $U_{\text{iso}}(\text{H}) = kU_{\text{eq}}(\text{C})$, where $k = 1.5$ for CH₃ and 1.2 for all other H-atoms. One of the ligands in each crystallographically independent molecules is disordered with occupancy ratio of 0.501(10):0.499(10). Benzene rings were treated as regular hexagons with C-atoms having equal anisotropic thermal parameters. Similarly, the substituted fluoro atoms on the phenyl rings were also treated as having equal anisotropic thermal parameters with one another.

2. 3. DNA interaction Study by Cyclic Voltammetry

Voltammetric experiments were performed using an SP-300 potentiostat, serial number 0134, BioLogic Scientific Instruments, France. Measurements were carried out in aqueous DMSO (1:4) solution containing 0.01 M KCl, under an N₂ saturated environment in a conventional three-electrode cell with saturated silver/silver chloride electrode (Ag/AgCl) as reference, a platinum wire as counter and a bare glassy carbon electrode (GCE) with a surface area of 0.196 cm^2 as the working electrode. Prior to experiment, GCE was polished with alumina (Al₂O₃) on a nylon buffing pad followed by washing with acetone and finally with distilled water. Electrochemical measurements were carried out at room temperature ($25 \pm 0.5 \text{ }^\circ\text{C}$).

An appropriate amount of sodium salt of salmon sperm DNA (SSDNA) was dissolved in distilled water and stirred overnight. Nucleotide to protein (N/P) ratio of ~1.9 was obtained from the ratio of absorbance at 260 and 280 nm ($A_{260}/A_{280} = 1.9$), indicating that SSDNA is sufficiently free from protein.¹⁷ SSDNA concentration was determined *via* absorption spectroscopy using molar absorption coef-

ficient of 6600 $\text{M}^{-1} \text{ cm}^{-1}$ (260 nm) for SSDNA.¹⁸ Voltammograms of 3 mM solution of the complex prepared in aqueous DMSO (1:4) were taken in absence and presence of 10, 20, 30, 40, 50, 60, 70 and 80 μM DNA. Moreover, in order to calculate various redox parameters, cyclic voltammograms were also recorded on 50, 75, 100, 125, 150, 175, 200, 400, 600, 900, 1200 and 1400 mV s^{-1} , before and after adding DNA to solutions of the complex.

2. 4. DNA Interaction Study by Absorption Spectroscopy

Solutions of the complex for UV-Visible spectrophotometric analysis were prepared in aqueous DMSO (1:4) at a concentration of 6 mM. UV absorption titrations were performed by keeping concentration of the complex fixed while varying SSDNA concentration. Equivalent solutions of SSDNA were added to each of complex and reference solutions to eliminate the absorbance of SSDNA itself. Spectra of complex-SSDNA solutions were recorded at room temperature ($25 \pm 1 \text{ }^\circ\text{C}$) using cuvettes of 1 cm path length.

2. 5. Procedure for the Synthesis of Complex

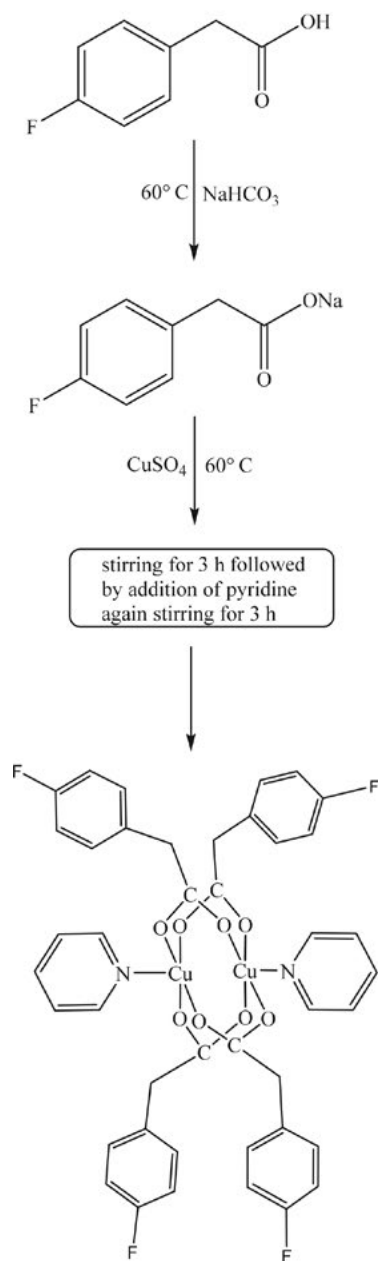
Sodium bicarbonate (0.504 g, 6.00 mmol) was reacted with an equimolar quantity (0.925 g, 6.00 mmol) of 4-fluorophenyl acetic acid at 60 $^\circ\text{C}$ in distilled water. After complete neutralization of acid with base, aqueous solution of copper sulphate (0.478 g, 3.00 mmol) was added drop wise. The reaction mixture was stirred for 3 h at 60 $^\circ\text{C}$ as depicted in Scheme 1. This was followed by the addition of methanolic solution of pyridine (0.24 mL, 3.0 mmol) with continued stirring for further 3 h under same reaction conditions. The final product was filtered, washed thoroughly with distilled water and air dried. The dried solid was recrystallized from a mixture of chloroform and methanol (1:1).

Light blue crystals; m.p. 182–183 $^\circ\text{C}$; Yield (70%). FT-IR (cm^{-1}): $\nu(\text{OCO})_{\text{asym}} = 1650$, $\nu(\text{OCO})_{\text{sym}} = 1442$ ($\Delta\nu = 208$), $\nu\text{CH}_2 = 2920$, $\nu(\text{Ar-H}) = 3031$, $\nu(\text{Ar-F}) = 1162$, $\nu\text{Ar}(\text{C}=\text{C}) = 1586$ and 1438, $\nu(\text{Cu-O}) = 422$, $\nu(\text{Cu-N}) = 475$.

3. Results and Discussion

3. 1. FT-IR Data

FT-IR spectrum of the complex contained all characteristic bands. The bonding mode of carboxylate moiety was indicated by its characteristic intense bands at 1650 and 1442 cm^{-1} corresponding to asymmetric and symmetric OCO stretching vibrations, respectively. This was supported by the appearance of a Cu-O absorption band at 422 cm^{-1} which indicated coordination of the carboxylate ligand through oxygen. Value of $\Delta\nu = \{\nu_{\text{asym}}(\text{OCO}) -$



Scheme 1. Synthetic procedure for complex

$\nu_{\text{sym}}(\text{OCO})$ calculated for complex was 208 cm^{-1} showing bonding modes of carboxylate moiety to copper(II) ion typical of bridging bidentate fashion.¹⁹ In addition, the appearance of C=N stretching band of complex at a frequency of 1592 cm^{-1} instead of its normally observed characteristic region ($1610\text{--}1625\text{ cm}^{-1}$)^{20,21} indicated the involvement of nitrogen atom of pyridine in bonding with copper(II) ion.²² This was further supported by the appearance of a new medium intensity band at 475 cm^{-1} attributable to a Cu–N vibration.²³ Aromatic C=C and C–H stretching vibrations were observed at 1586 and 1438 and 3031 cm^{-1} , respectively. Methylene C–H stretching frequency of complex was observed at 2920 cm^{-1} , supported by the presence

of bands at 692 and 1398 cm^{-1} corresponding to its rocking and bending deformations, respectively.

3. 2. Crystal Structure Description

Ortep diagram of complex with atom numbering scheme is shown in Fig. 1 and crystal refinement parameters and important bond lengths and angles are given in Tables 1 and 2. Complex crystallizes in triclinic system with space group $P\bar{1}$ having two crystallographically independent molecules in the unit cell as shown in Fig. 2. Complex displays the classical paddlewheel structure having four carboxylate ligands bonded in a syn–syn configuration, bridging the two copper(II) ions. The coordination environment around each copper ion is $\{\text{CuNO}_4\}$ where four oxygen atoms of carboxylate ligands occupy the square base while a pyridine molecule occupies the axial coordination site resulting in square pyramidal coordination geometry for each Cu(II) ion. The Cu...Cu and average Cu–O distances are $2.6411(8)$ and $1.9585(4)\text{ \AA}$, respectively, which are close to those observed for structurally related dimer of Cu(II) ions with trifluoroacetate and phenylacetate ligands already reported $[\text{Cu}_2(\text{CF}_3\text{CO}_2)_4(\text{CH}_3\text{CN})_2]$ (where Cu...Cu = $2.766(1)$ and Cu–O = $1.969(5)\text{ \AA}$).^{24–26} Cu–N distance ($2.174(4)\text{ \AA}$) is comparable to those found for apical N-donor acetonitrile ligand ($2.114(2)\text{ \AA}$)²⁵ but longer than those found for imidazole N-donor ligand ($1.9815(15)\text{ \AA}$) in mononuclear octahedral carboxylate complex.²⁷ This is attributed to the elongation of apical Cu–ligand bond distance as a consequence of repulsion exerted by the doubly occupied d_{z^2} -orbital along this axis.²⁸ However, the basic strength of the N-donor ligand also determines the Cu–N bond length.²⁹ The trans angles

Table 1. Structure refinement parameters of the complex

Chemical formula	$\text{C}_{42}\text{H}_{34}\text{F}_4\text{Cu}_2\text{N}_2\text{O}_8$
FW (g mol^{-1})	897.79
Temperature (K)	296(2)
Crystal system	Triclinic
Space group	$P\bar{1}$
a (\AA)	12.0582(3)
b (\AA)	12.9571(4)
c (\AA)	14.6191(4)
α ($^\circ$)	78.873(2)
β ($^\circ$)	74.229(3)
γ ($^\circ$)	69.542(2)
V (\AA^3)	2047.26(11)
Z	2
ρ_{calc} (g cm^{-3})	1.456
Absorption coeff. (mm^{-1})	1.111
$F(000)$	916
Reflections collected	30120
Independent reflections	7330
Data/restraints/parameters	7330 / 8 / 530
Goodness-of-fit on F^2	0.988
$R[F^2 > 2\sigma(F^2)]$, $wR(F^2)$	0.0482, 0.110

(O–Cu–O) of the square base, consisting of four O atoms in complex are 167.76(15) and 168.15(12)°. Moreover, all

Table 2. Selected Bond lengths and angles of complex

Distances, Å	
Cu1–O1	1.958(4)
Cu1–O2	1.952(4)
Cu1–O3	1.961(4)
Cu1–O4	1.953(4)
Cu1–N1	2.174(4)
Cu1–Cu1	2.6411(8)
Angles, °	
O4–Cu1–O1	87.90(16)
O2–Cu1–O3	89.48(16)
O1–Cu1–O2	97.04(16)
O4–Cu1–O3	90.92(16)
O1–Cu1–O3	167.76(15)
O4–Cu1–O2	168.15(12)
O4–Cu1–N1	100.03(16)
O1–Cu1–N1	92.15(13)
O2–Cu1–N1	89.19(16)
O3–Cu1–N1	94.78(16)
O4–Cu1–Cu1	82.5(1)
O1–Cu1–Cu1	84.7(1)
O2–Cu1–Cu1	83.5(1)
O3–Cu1–Cu1	85.4(1)
N1–Cu1–Cu1	174.4(1)

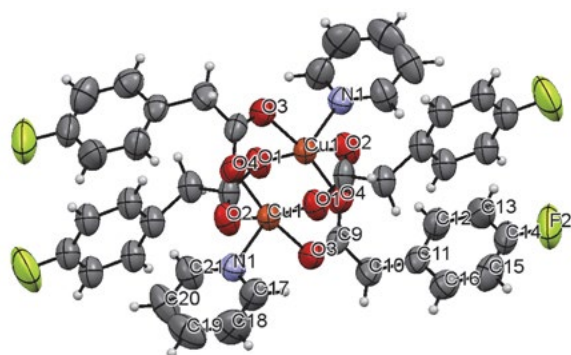


Fig. 1. Structure of the complex tetrakis(4-fluorophenylacetato- μ -O,O')bis(pyridine-N)dicopper(II) with numbering scheme.

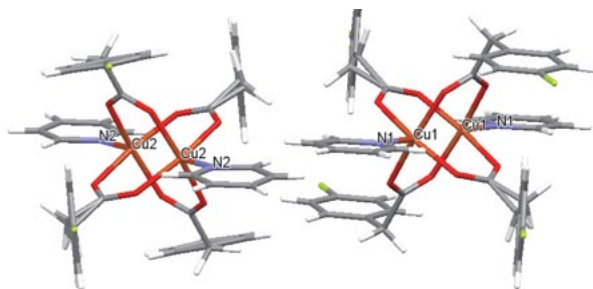


Fig. 2. Two crystallographically independent molecules in the unit cell.

the O–Cu...Cu bond angles in complex range from 82.5(1) to 85.4(1)° while the O–Cu–N bond angles are in the range 89.19(16)–100.03(16)°. All these angle ranges are typical of paddlewheel type complexes. The molecule is centrosymmetric with center of inversion at midpoint between two copper ions.

Supramolecular structure: Crystal packing of complex is shown in Fig. 3, which is quite different from that of 4-chlorophenylacetate complex with copper,¹⁵ although one might think that there is mere replacement of F for Cl. It may be due to the presence of two crystallographically independent molecules in the unit cell of the former complex. Similarly, C–H...O type interactions are found between hydrogen atoms of C10–H10B and O8 and C31–H31B and O3.

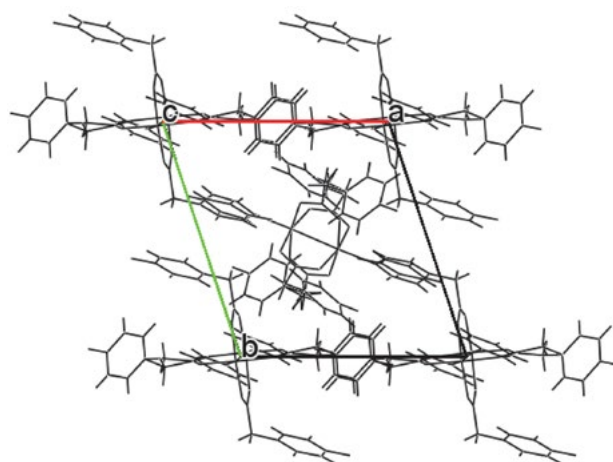


Fig. 3. Packing diagram of the complex along *c*-axis.

3. 3. Cyclic Voltammetry

Electrochemical study of the complex shows an anodic peak at 0.175 V corresponding to Cu(I)/Cu(II) process and a cathodic peak at –0.20 V corresponding to Cu(II)/Cu(I) reduction.^{2,30} The higher value of peak separation precludes the possibility of reversibility of two redox processes as shown in Fig. 4A.

DNA binding study through cyclic voltammetry

Cyclic voltammetry was employed to explore DNA binding ability of complex at various scan rates. The shift in peak potential was used to decide about the mode of DNA binding activity of complex. A negative shift in peak potential i.e., to less positive region (or to more negative region in case of reduction signal) on addition of DNA indicates electrostatic mode of interaction with complex,^{31,32} while a positive shift in potential i.e., to more positive region (or to less negative region in case of reduction signal) exhibits an intercalative mode. However, pure electrostatic or intercalative modes of interaction are seldom encountered and more often a mixed behavior is usually observed.

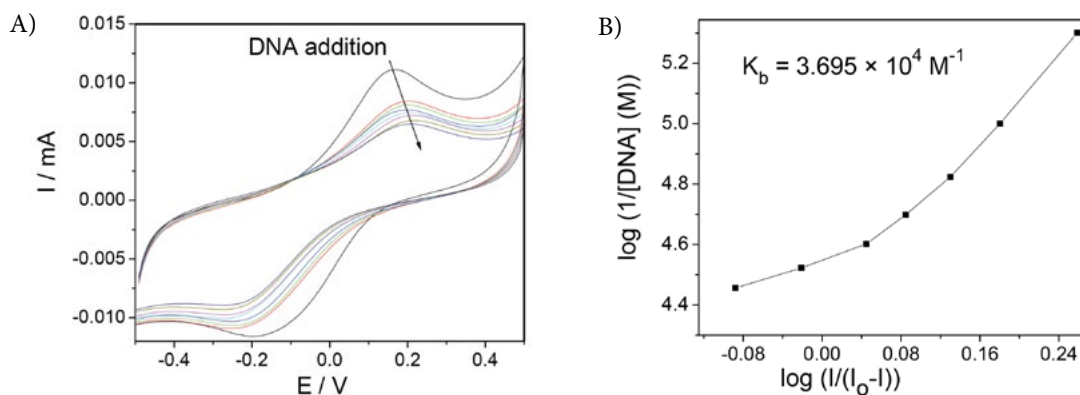


Fig. 4. A: voltammograms of complex at scan rate 100 mV/s in absence and presence of DNA showing a shift in peak potential towards more positive values. B: plot for calculation of binding constant K_b .

Anodic peak of synthesized complex experienced shift to more positive region (or to less negative region in the case of reduction peaks) with addition of DNA. On successive DNA addition there is further shifting of peak potential to more positive potential region as shown in Fig. 4A. This type of binding with DNA is termed as intercalative mode. The predominant intercalative ability of the complex is ascribed to the presence of planar aromatic rings. However, since fluoro groups are more efficient electrostatic binders, there must be a significant contribution of electrostatic interaction to the binding of complex along with intercalation between DNA base pairs.

In addition to peak shift, peak current experienced a diminution on the addition of DNA to complex solution. On the basis of decrease in peak current of the unbound complex by addition of different concentrations (10 to 80 μM) of SSDNA, the binding constant was calculated. The plot of $\log 1/[\text{DNA}]$ vs. $\log I/(I_0 - I)$ gave rise to a straight line (Fig. 4B), whose intercept was used to calculate the binding constant using an already reported procedure.³³ The value of K_b calculated for complex was $3.695 \times 10^4 \text{ M}^{-1}$ which is higher than those of the non-fluorinated structural analogues where F is substituted by H, $-\text{CH}_3$ and $-\text{OCH}_3$,^{13–15} having K_b values 0.033×10^4 , 1.44×10^4 and $1.007 \times 10^4 \text{ M}^{-1}$, respectively. Since the rest of structural parameters are the same, the higher value of K_b must be due to the presence of *para*-fluoro groups, enhancing interaction of complex with DNA. It can be inferred that there is electrostatic interaction of complex owing to the electronegative F atom along with intercalation of aromatic rings. This leads to facile formation of complex-DNA adduct leading to relatively higher K_b value.

The DNA binding ability of the complex was also confirmed by calculating the diffusion coefficient of complex before and after DNA addition. This was accomplished by measuring voltammograms at different scan rates before and after DNA addition and putting the relevant parameters in the Randles-Sevcik equation.³⁴

The slope values for D_0 calculation were obtained making use of the respective i_p vs. $v^{1/2}$ plots for oxidation process employing Bard and Faulkner relation.³⁵

Values of D_0 thus calculated for complex before and after DNA addition were 7.912×10^{-8} and $0.305 \times 10^{-8} \text{ cm}^2\text{s}^{-1}$. The lower value of diffusion coefficient of DNA-bound complex compared to that of the unbound complex shows a reduction in the mobility of the former.^{36,37} The reduction in mobility of complex with DNA addition shows adduct formation between the two having hampered mobility in solution.

3. 4. Absorption Spectroscopy

The complex exhibited a broad absorption band (shown in Fig. 5A) with $\lambda_{\text{max}} = 737 \text{ nm}$ corresponding to *d-d* transition of Cu^{2+} and has been found typical of square pyramidal copper(II) geometry in solution.^{38–40} This shows the relative stability of paddlewheel structure and that square pyramidal structure is retained in solution. The band in *d-d* region is expected to be sensitive to the nature (basicity and bond length) of attached apical and basal ligands. As the bond length of attached ligands increases, the band is shifted to shorter wavelength (higher energy) region.⁴¹ The same has been observed here where the non-fluoro analogues (where F is replaced by H,¹³ CH_3 ,¹⁴ OCH_3 ¹⁵) give rise to bands at 720 nm with $\text{Cu}-\text{N}_{\text{av}}$ distance of 2.158(2) Å compared to 2.174(4) Å of the synthesized fluoro-complex. Using Beer-Lambert's Law, ϵ value has been calculated to be $141 \text{ (L mol}^{-1} \text{ cm}^{-1})$ for complex.

DNA study through absorption spectroscopy

The variation in λ_{max} of complex on addition of DNA can be used to measure the ability of complex to bind with DNA. A blue shift in λ_{max} indicates electrostatic while red shift indicates intercalative mode of interaction with DNA.^{42,43} Shift in λ_{max} is usually accompanied with a pronounced decrease in absorbance which can be used to calculate the extent of interaction i.e., binding constant K_b . On successive addition of 10–70 μM DNA to complex

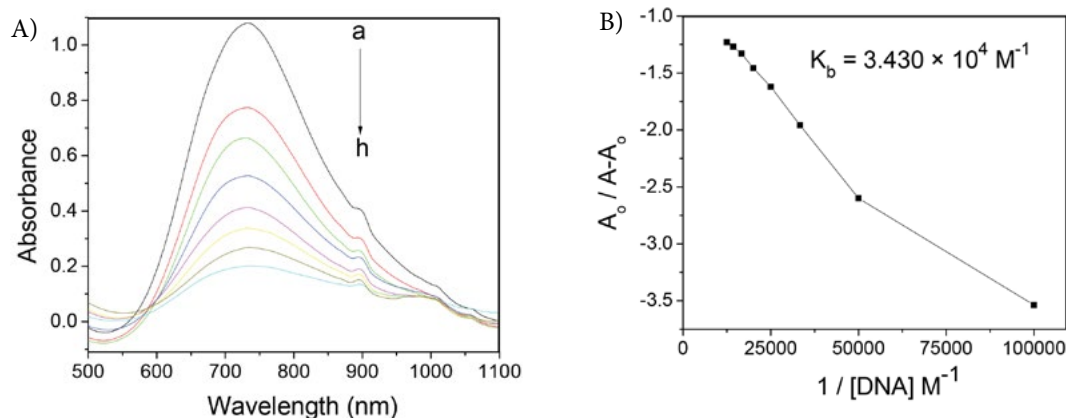


Fig. 5. A, reduction in absorbance of pure complex with addition of DNA. B, plot for calculation of binding constant K_b .

solution, there was extensive reduction in absorbance of complex along with a small red shift as shown in Fig. 5A. Using the famous Benesi-Hildebrand equation,⁴⁴ the binding constant was calculated from slope to intercept ratio of the plot of $A_0/A - A_0$ vs. $1/[DNA]$ as shown in Fig. 5B. Value of K_b was found out to be $3.430 \times 10^4 \text{ M}^{-1}$ which is in good agreement with K_b value obtained through cyclic voltammetry. The binding mode of complex has been found to be mixed type where intercalation is accompanied by electrostatic groove binding mode as well. The later binding mode may be due to the presence of polar fluoro group which enhances electrostatic interaction with DNA. Thus, the properties of complex have been modified substantially on changing the substituent on attached ligand.

4. Conclusion

A new copper(II) complex has been synthesized which represents new addition to the existing database on paddlewheel type complexes. Its structural, electronic absorption and DNA-binding properties have been compared to those of the non-fluorinated analogues. The peak position in absorption spectrum of complex is shifted in accordance to the altered basic strength of fluorophenylacetate ligand. Electrostatic contribution is included in DNA-binding mode of complex and the extent of DNA-binding is enhanced three times owing to the presence of fluorine in complex. The effect of fluorine is clearly manifested in the modified properties of synthesized complex.

Supplementary data: Crystallographic data for the structure reported in this paper has been deposited with the Cambridge Crystallographic Data Centre, CCDC # 934064. Copies of this may be obtained free of charge from The Director, CCDC, 12, Union Road Cambridge CB2 1EZ [Fax: +44 (1223)336 033] or e.mail: deposit@ccdc.cam.ac.uk.

5. References

- C. Lipinski, A. Hopkins, *Nature* **2004**, 432, 855–861. DOI:10.1038/nature03193
- N. V. Kulkarni, A. Kamath, S. Budagumpi, V. K. Revankar, *J. Mol. Struct.* **2011**, 1006 580–588. DOI:10.1016/j.molstruc.2011.10.008
- A. Prisecaru, M. Devereux, N. Barron, M. McCann, J. Collier, A. Casey, V. McKee, A. Kellett, *Chem. Commun.* **2012**, 48, 6906–6908. DOI:10.1039/c2cc31023f
- T. Storr, P. Verma, R. C. Pratt, E. C. Wasinger, Y. Shimazaki, T. D. P. Stack, *J. Am. Chem. Soc.* **2008**, 130, 15448–15459. DOI:10.1021/ja804339m
- E. V. Nosova, T. N. Moshkina, G. N. Lipunova, I. V. Baklanova, P. A. Slepukhin, V. N. Charushin, *J. Fluorine Chem.* **2015**, 175, 145–151. DOI:10.1016/j.jfluchem.2015.04.010
- J. Zhu, C. Ni, B. Gao, J. Hu, *J. Fluorine Chem.* **2015**, 171, 139–147. DOI:10.1016/j.jfluchem.2014.08.011
- P. Ruiz-Sanchez, C. Konig, S. Ferrari, R. Alberto, *J. Biol. Inorg. Chem.* **2011**, 16, 33–44. DOI:10.1007/s00775-010-0697-z
- D. Barut, N. Korkmaz, S. T. Astley, M. Aygün, *Acta Chim. Slov.* **2015**, 62, 88–94. DOI:10.17344/acsi.2014.734
- X.-Z. Zhang, Y. Gu, Y. Li, A. Liu, F. Liu, Z. You, H.-L. Zhu, *Acta Chim. Slov.* **2016**, 63, 721–725. DOI:10.17344/acsi.2016.2421
- A. Mushtaq, S. Ali, M. N. Tahir, H. Ismail, B. Mirza, M. Saadiq, M. A. Haleem, M. Iqbal, *Acta Chim. Slov.* **2017**, 64, 397–408. DOI:10.17344/acsi.2017.3250
- V. T. Kasumov, F. Suzergoz, E. Sahin, O. Celik, M. Aslanoglu, *J. Fluorine Chem.* **2014**, 162, 78–89. DOI:10.1016/j.jfluchem.2014.03.011
- T. M. Jeitner, E. Kristoferson, J. A. Azcona, J. T. Pinto, C. Stalneck, J. W. Erickson, H. F. Kung, J. Li, K. Ploessl, A. J. L. Cooper, *J. Fluorine Chem.* **2016**, 192, 58–67. DOI:10.1016/j.jfluchem.2016.10.008
- M. Iqbal, S. Ali, Z.-U. Rehman, N. Muhammad, M. Sohail, V. Pandarinathan, *J. Coord. Chem.* **2014**, 67, 1731–1745. DOI:10.1080/00958972.2014.926337
- M. Iqbal, S. Ali, N. Muhammad, M. Sohail, *Polyhedron* **2013**, 57, 83–93. DOI:10.1016/j.poly.2013.04.020
- M. Iqbal, I. Ahmad, S. Ali, N. Muhammad, S. Ahmed, M.

- Sohail, *Polyhedron* **2013**, *50*, 524–531.
DOI:10.1016/j.poly.2012.11.037
16. G. M. Sheldrick, *Acta Cryst.* **2008**, *A 64*, 112–122.
17. S. Dey, S. Sarkar, H. Paul, E. Zangrando, P. Chattopadhyay, *Polyhedron* **2010**, *29*, 1583–1587.
DOI:10.1016/j.poly.2010.01.022
18. C. V. Sastri, D. Eswaramoorthy, L. Giribabu, B. G. Maiya, *J. Inorg. Biochem.* **2003**, *94*, 138–145.
DOI:10.1016/S0162-0134(02)00622-0
19. S. Leconte, R. Ruzziconi, *J. Fluorine Chem.* **2002**, *117*, 167–172. DOI:10.1016/S0022-1139(02)00161-6
20. K. V. Shuvaev, S. Sproules, J. M. Rautiainen, E. J. L. McInnes, D. Collison, C. E. Anson, A. K. Powell, *Dalton Trans.* **2013**, *42*, 2371–2381. DOI:10.1039/C2DT31946B
21. C. Jayabalakrishnan, K. Natarajan, *Transit. Met. Chem.* **2002**, *27*, 75–79. DOI:10.1023/A:1013437203247
22. Z. H. Abd El-Wahab, M. M. Mashaly, A. A. Salman, B. A. El-Shetary, A. A. Faheim, *Spectrochim. Acta A* **2004**, *60*, 2861–2873. DOI:10.1016/j.saa.2004.01.021
23. M. Shakir, N. Begum, S. Parveen, P. Chingsubam, S. Tabasum, *Synth. React. Inorg. Met. Org. Chem.* **2004**, *34*, 1135–1148. DOI:10.1081/SIM-120039262
24. A. Motreff, R. C. da Costa, H. Allouchi, M. Duttine, C. Mathoniere, C. Duboc, J. M. Vincent, *J. Fluorine Chem.* **2012**, *134*, 49–55. DOI:10.1016/j.jfluchem.2011.03.002
25. M. Iqbal, M. Sirajuddin, S. Ali, M. Sohail, M. N. Tahir, *Inorg. Chim. Acta* **2016**, *440*, 129–138.
DOI:10.1016/j.ica.2015.10.042
26. B. Shen, P.-F. Shi, Y.-L. Hou, F.-F. Wan, D.-L. Gao, B. Zhao, *Dalton Trans.* **2013**, *42*, 3455–3463.
DOI:10.1039/C2DT32515B
27. M. A. Agotegaray, M. Dennehy, M. A. Boeris, M. A. Grela, R. A. Burrow, O. V. Quinzani, *Polyhedron* **2012**, *34*, 74–83.
DOI:10.1016/j.poly.2011.12.005
28. M. A. Halcrow, *Chem. Soc. Rev.* **2013**, *42*, 1784–1795.
DOI:10.1039/C2CS35253B
29. A. S. Potapov, G. A. Domina, T. V. Petrenko, A. I. Khlebnikov, *Polyhedron* **2012**, *33*, 150–157.
DOI:10.1016/j.poly.2011.11.039
30. C. Di Nicola, F. Garau, Y. Y. Karabach, L. M. D. R. S. Martins, M. Monari, L. Pandolfo, C. Pettinari, A. J. L. Pombeiro, *Eur. J. Inorg. Chem.* **2009**, 666–676. DOI:10.1002/ejic.200800842
31. M. T. Carter, M. Rodriguez, A. J. Bard, *J. Am. Chem. Soc.* **1989**, *111*, 8901–8911. DOI:10.1021/ja00206a020
32. M. S. Mohamed, A. A. Shoukry, A. G. Ali, *Spectrochim. Acta Part A* **2012**, *86*, 562–570. DOI:10.1016/j.saa.2011.11.015
33. Q. Feng, N. Q. Li, Y. Y. Jiang, *Anal. Chim. Acta* **1997**, *344*, 97–104. DOI:10.1016/S0003-2670(97)00008-1
34. J. Wang, *Analytical Electrochemistry*, 1st ed., VCH Publishers, 1994, pp. 165–166.
35. A. J. Bard and L. R. Faulkner, *Electrochemical Methods, Fundamentals and Applications*, 2nd ed., Wiley, New York, 2004, p-236.
36. M. Chauhan, K. Banerjee, F. Arjmand, *Inorg. Chem.* **2007**, *46*, 3072–3082. DOI:10.1021/ic061753a
37. G.-Y. Li, K.-J. Du, J.-Q. Wang, J.-W. Liang, J.-F. Kou, X.-J. Hou, L.-N. Ji, H. Chao, *J. Inorg. Biochem.* **2013**, *119*, 43–53.
DOI:10.1016/j.jinorgbio.2012.09.019
38. S. Majumder, M. Fleck, C. R. Lucas, S. Mohanta, *J. Mol. Struct.* **2012**, *1020*, 127–133. DOI:10.1016/j.molstruc.2012.04.003
39. S. S. Massoud, F. R. Louka, Y. K. Obaid, R. Vicente, J. Ribas, R. C. Fischer, F. A. Mautner, *Dalton Trans.* **2013**, *42*, 3968–3978.
DOI:10.1039/c2dt32540c
40. A. Domínguez-Martín, D. Choquesillo-Lazarte, J. A. Dobado, I. Vidal, L. Lezama, J. M. González-Pérez, A. Castiñeiras, J. Niclós-Gutiérrez, *Dalton Trans.* **2013**, *42*, 6119–6130.
DOI:10.1039/c2dt32191b
41. A. Theodorou, M. A. Demertzis, D. Kovala-Demertzi, E. E. Lioliou, A. A. Pantazaki, D. A. Kyriakidis, *BioMetals* **1999**, *12*, 167–172. DOI:10.1023/A:1009246122577
42. L. Jia, J. Shi, Z.-H. Sun, F.-F. Li, Y. Wang, W.-N. Wu, Q. Wang, *Inorg. Chim. Acta* **2012**, *391*, 121–129.
DOI:10.1016/j.ica.2012.05.014
43. X. Li, Y.-T. Li, Z.-Y. Wu, Y.-J. Zheng, C.-W. Yan, *Inorg. Chim. Acta* **2012**, *385*, 150–157. DOI:10.1016/j.ica.2012.01.047
44. M. Y. Ni, Y. Wang, H. L. Li, *Pol. J. Chem.* **1997**, *71*, 816–822.

Povzetek

V prispevku predstavljamo sintezo, strukturo in lastnosti dvojedrnega bakrovega(II) karboksilato kompleksa s formulo [(py)Cu(μ-L)₄Cu(py)], kjer je py = piridin in L = 4-fluorofenilacetat. Strukturne značilnosti in elektronsko absorpcijo sintetiziranega kompleksa ter vezavo na DNA smo primerjali z že objavljenimi nefluoriranimi analogi (kjer so na mestu F atoma vezane H, –CH₃ in –OCH₃ skupine) ter modifikacije pripisali prisotnemu fluorovemu atomu. Kompleks ima tipično strukturo vodnega kolesa. V asimetrični enoti sta prisotni dve kristalografsko neodvisni molekuli. Elektronski absorpcijski spekter kompleksa se razlikuje od nefluoriranih analogov, opazna je tudi razlika v načinu in jakosti vezave na DNA zaradi prisotnega fluoro substituenta. Vpliv fluorovega atoma je razviden na podlagi spremenjenih lastnosti sintetiziranega kompleksa.

Scientific paper

Preconcentration and Determination of Trace Vanadium(V) in Beverages by Combination of Ultrasound Assisted-cloud Point Extraction with Spectrophotometry

Nuket Kartal Temel^{1,*} and Ramazan Gürkan¹¹ Department of Chemistry, Faculty of Science, University of Cumhuriyet, TR-58140, Sivas, Turkey

* Corresponding author: E-mail: nkartaltemel@cumhuriyet.edu.tr

Received: 30-07-2017

Abstract

A novel ultrasound assisted-cloud point extraction method was developed for preconcentration and determination of V(V) in beverage samples. After complexation by pyrogallol in presence of safranin T at pH 6.0, V(V) ions as ternary complex are extracted into the micellar phase of Triton X-114. The complex was monitored at 533 nm by spectrophotometry. The matrix effect on the recovery of V(V) from the spiked samples at 50 $\mu\text{g L}^{-1}$ was evaluated. In optimized conditions, the limits of detection and quantification of the method, respectively, was 0.58 and 1.93 $\mu\text{g L}^{-1}$ in linear range of 2–500 $\mu\text{g L}^{-1}$ with sensitivity enhancement and preconcentration factors of 47.7 and 40 for preconcentration from 15 mL of sample solution. The recoveries from spiked samples were in range of 93.8–103.2% with a relative standard deviation ranging from 2.6% to 4.1% (25, 100 and 250 $\mu\text{g L}^{-1}$, n: 5). The accuracy was verified by analysis of two certified samples, and the results were in a good agreement with the certified values. The intra-day and inter-day precision were tested by reproducibility (as 3.3–3.4%) and repeatability (as 3.4–4.1%) analysis for five replicate measurements of V(V) in quality control samples spiked with 5, 10 and 15 $\mu\text{g L}^{-1}$. Trace V(V) contents of the selected beverage samples by the developed method were successfully determined.

Keywords: Ultrasound assisted-cloud point extraction, V(V), Pyrogallol, Safranin T, Beverages, Spectrophotometry

1. Introduction

Vanadium generally exists as two species as V(V) and V(IV), and V(V) is more toxic than V(IV) for living organisms because it can damage the respiratory, nervous and digestive systems.^{1,2} While low levels of vanadium are necessary for humans, high concentrations can cause damage by creating a toxic effect. V(V) is also known to be a stronger inhibitor of the enzyme Na- and K-ATPase than V(IV).³

Vanadium is more likely to be present in food.^{4,5} In fact, it generally exists at levels ranging from 1 to 5 $\mu\text{g kg}^{-1}$ in drinks and fruit juices,⁶ from 4 to 41 $\mu\text{g L}^{-1}$ in tea infusions,⁷ up to 90 $\mu\text{g L}^{-1}$ in wines⁸ and Environmental Protection Agency (EPA) has reported that the allowed limit of vanadium is 50 mg L^{-1} .⁹ Because of the low levels of vanadium in foodstuffs, development of simple, easy to use, safe, fast and sensitive analytical methods is of great importance for environmental risk assessment. A number of analytical detection techniques are used for vanadium determination. In general, the most commonly used analyti-

cal techniques are flame atomic absorption spectrometry (FAAS),^{10,11,12} electrothermal atomic absorption spectrometry (ET-AAS), which is also known as graphite furnace AAS (GF-AAS),¹³ inductively coupled plasma mass spectrometry (ICP-MS),^{14,15} neutron activation analysis (NAA),¹⁶ inductively coupled plasma-optical emission spectrometry (ICP-OES),¹⁷ fluorometry,^{18,19} requiring sample pretreatment steps such as ion-exchange,²⁰ solid phase extraction (SPE),^{21,22} liquid phase microextraction (LPME),²³ and cloud point extraction (CPE).^{24–28}

CPE is superior to traditional solvent extraction because of its high extraction yield and preconcentration factor, and has several advantages such as simplicity, inexpensiveness, operational safety and use of non-toxic reagents.^{29,30} Before detection, CPE is used as a separation and preconcentration method using a surfactant to cause the generation of micellar surroundings and phase separation when a nonionic surfactant solution (or its mixture with cationic or anionic surfactant) as extractant is heated above the critical temperature. At the determined tempera-

ture, the surfactant-rich phase is separated from the diluted aqueous phase by adding a small volume of hydrophobic substance.³¹ The CPE process has successfully been used for the separation and preconcentration of trace levels of V(V) or V(IV) from different sample matrices^{6,29,32–36} using different chelating agents. In this sense, there are some publications dealing with CPE-spectrophotometric determination of vanadium in different sample matrices with their own advantages and disadvantages.^{24–28} Moreover, solidified floating organic drop microextraction (SFODME)³⁷ and on-line temperature-assisted ionic liquid based dispersive liquid liquid microextraction (on line TA-IL-DLLME)³⁸ in combination with spectrophotometry as further preconcentration tools prior to analysis were also used for sensitive determination of vanadium in environmental samples.

The objective of the present study is to develop a simple, sensitive and selective ultrasound assisted-CPE (UA-CPE) method coupled to spectrophotometry for determining vanadium levels present in beverages. Ultrasound energy was used to increase the extraction rate at micellar interface and to improve the extraction efficiency. The proposed method is based on the complexation reaction of V(V) by pyrogallol in the presence of cationic phenazine group dye, safranin T as ion-pairing agent at pH 6.0, and extraction of the formed ternary complex into the micellar rich phase of Triton X-114. In order to attain high recovery, selectivity, and precision for the determination of V(V) in beverage matrices by spectrophotometry after preconcentration by UA-CPE, the various analytical parameters affecting the complex formation and the extraction efficiency with minor sample treatment were investigated and optimized. The UA-CPE procedure can be an alternative to other separation/preconcentration procedures for the trace analysis of vanadium in other sample matrices of nutritional and toxicological importance like foodstuffs.

2. Experimental

2. 1. Instrumentation

The absorbance measurements were performed using a double-beam UV-Visible Spectrophotometer (Shimadzu UV-1800 PC, Kyoto, Japan) equipped with the 1.0-cm quartz cells. The pH measurements were made using Jenway 3010 pH meter (Staffordshire, UK). A centrifuge apparatus (Hettich Universal, Universal-320, Hettich Centrifuges, UK) was used for the phase-separation procedure. An ultrasonic bath operating with a frequency of 40 kHz at power of 300 Watt (UCS-10 model, Seoul, Korea) was used efficiently to control and to keep constant the determined temperature for the UA-CPE.

2. 2. Reagents and Solutions

The analytically pure reagents were used, and all solutions were prepared from doubly distilled water

during the analysis. Stock solution of V(V) (1000 mg L⁻¹) was prepared from ammonium metavanadate. All standard solutions were prepared daily. A 0.1 mmol L⁻¹ safranin T and 0.081 mmol L⁻¹ pyrogallol solution were prepared from standard solutions. To protect its stability against oxidation, it was prepared by dissolving in methanol containing 1.0 mol L⁻¹ HCl and diluting with water, and kept in dark. The solutions (1.0%, w/v) of Triton X-114 and Triton X-45 (Sigma) as extractants were prepared by thoroughly mixing with vortex in 100 mL of water, and were used without further purification. The electrolyte solutions of 0.01 mol L⁻¹ were prepared by using suitable amounts of KCl and KNO₃ in deionized water. The universal Britton-Robinson buffer solutions at pHs ranging from 3.0 to 8.0 were prepared by mixing H₃BO₃, H₃PO₄ and CH₃COOH at equal molar concentrations (0.04 mol L⁻¹) with 0.2 mol L⁻¹ NaOH and adjusting to a suitable pH value by a pH meter.

2. 3. Procedure for UA-CPE

In the UA-CPE, an adequate amount (approx. 3.0 mL) of sample solution or a standard V(V) solution in a linear range of 2–500 µg L⁻¹, 1.6 mmol L⁻¹ of B-R buffer solution at pH 6.0, 1.6 µmol L⁻¹ of pyrogallol, 2.0 µmol L⁻¹ of safranin T, 6.0 mmol L⁻¹ of KCl solution, and 0.05% (w/v) Triton X-114, respectively, were sequentially transferred to a conical tube. Then, the solution was diluted to 50 mL with water. Afterwards, the resultant solution was placed in an ultrasonic bath (300 W, 40 kHz) and sonicated at 50 °C for 3 min. The final solution was centrifuged at 4000 rpm for 15 min for separation of the aqueous and surfactant-rich phases. After centrifugation it was cooled down in an ice bath for 10 min to facilitate phase separation. After cooling in an ice bath, the supernatant aqueous phase was separated from the aqueous bulk phase. The surfactant rich phase in the tube was diluted by adding 1.5 mL of ethanol to reduce its viscosity. The above mentioned procedures were also repeated for blank solution. At last, the total V contents as V(V) of all the pretreated and extracted samples and SRMs were spectrophotometrically monitored at 533 nm.

2. 4. Sample Preparation

All beverage samples used in this study were purchased from a supermarket in Sivas, Turkey. Firstly, 25 mL of beverage samples were pretreated by trichloroacetic acid (3.0% (w/v), 5 mL) for destruction of organic matrix due to being rich in protein and fat. Subsequently, the mixture was mixed with vortex, precipitated at 4000 rpm for 15 min and filtered by the membrane filter. Before analysis, in order to test the accuracy and precision of the proposed method, all samples including the pretreated milk samples were subjected to two digestion process in parallel, until obtaining completely clear, colorless, homogenous digests.

The steps of the experimental procedure: 20 mL of beverage samples in plastic type boxes, 6 mL of 65% (w/w) HNO₃ and 4 mL of 30% (w/w) H₂O₂ (3:2, v/v) were transferred in a 100 mL conical flask. The obtained mixture was heated at 120 °C nearly to dryness. The mixture was diluted to 50 mL with water after cooling to room temperature and centrifuged. The pH of the mixtures was adjusted to the desired values (7.0) using 0.1 mol L⁻¹ NaOH solution. The process was then repeated to determine total V levels as a measure of V(V) concentration by taking approximately 3 mL of the beverage samples at the optimal conditions.

The steps of the second sample digestion treatment using ultrasound: 20 mL of the samples, a mixture of 4 mol L⁻¹ HNO₃, 4 mol L⁻¹ HCl and 0.5 mol L⁻¹ H₂O₂ (1:1:1, v/v) were sequentially transferred to the 100 mL conical flask. Then, the resultant solution was diluted to 100 mL with water and kept in the ultrasonic bath for 20 min at 60 °C (300 W, 40 kHz). The phases were separated by centrifugation for 15 min at 4000 rpm. The separated solution was completed to 50 mL with water, and its pH was adjusted to 7.0 by NaOH solution. The process was applied to determine total V levels as a measure of V(V) amount by taking approximately 3 mL of the sample under the optimal conditions.

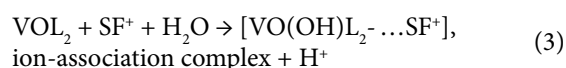
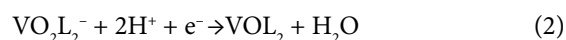
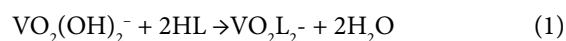
3. Results and Discussion

In order to determine the optimum conditions, the analytical variables involved in complex formation such as pH, buffer concentration, concentrations of pyrogallol as chelating agent, safranin T as ion pairing reagent and surfactants, including operational factors affecting extraction efficiency such as centrifugation rate and time, temperature and time for the determination of V(V) at 50 µg L⁻¹ were investigated in detail.

3.1. Effect of pH

CPE procedures used in the separation and extraction of metal ions need the formation of a hydrophobic metal-chelate complex to be extracted in the surfactant-rich phase. The pH plays a significant role in metal-chelate complex formation. It affects the charge of the analyte, therefore it affects the generation of the extractable hydrophobic complex between the metal and primary/secondary ligands with the hydrophilic and hydrophobic centers of surfactant.³⁹ Thus, extraction efficiency is highly dependent on the pH at which complex formation is investigated. A set of similar experiments were carried out in the pH range of 3.0–8.0 in Britton Robinson buffer. The effects of pH on the extraction of V(V) complex are given in Figure 1(a). In the pH range of 5.5–6.0, extraction was quantitative. When the pH values are below or above 6.0, extraction efficiency decreases due to uncomplete

complex formation and probable degradation of the complex (for fast oxidation of VO(OH)⁺ species with dissolved oxygen) at increased pHs, respectively.³³ The V(V) ion is often present in forms of VO₂⁺ (pH < 3.5), H₂VO₄⁻ or VO₂(OH)₂⁻ (pH 3.5–7.5) and HVO₄²⁻ or VO₃(OH)₂⁻ (pH 7.513.0).^{40,41} However, V(IV) starts to hydrolyze and dimerize at pH 4.0; the pK_a value of the [VO(H₂O)₅]²⁺ ion has been noticed to be in the range 5.3–6.0. At pH 5.0, insoluble VO(OH)₂ starts to form, which turns into water-soluble [(VO)₂(OH)₅]⁻ and [VO(OH)₃]⁻ complexes in strongly alkaline aqueous solution. As a result of reduction of V(V) to V(IV) in the presence of a reducing, chelating agent such as pyrogallol (HL) and redox sensitive ion-pairing reagent, safranin T, it can be expected that V(IV), proportional to V(V) concentration, forms a pH dependent anionic chelate complex in presence of safranin T as follows:



Therefore, pH 6.0 was selected as the optimal value. When considering complex formation with V(V) or V(IV), it is implied that V(V) can be reduced to V(IV) easily owing to the sufficient redox potential (VO₂⁺/VO²⁺: 1.00 V in a strongly acidic solution) given in the literature.⁴² Also, it was assumed that V(V) was reduced to V(IV), and this fact was confirmed by ESR analysis of vanadium adsorption on a persimmon tannin gel from the NH₄VO₃ solution at pH 6.0, due to the formation of a stable complex of V(IV) with catechol and pyrogallol groups in the gel. With a complex formation constant of pK_f: 16.67, this state is attributed to the fact that vanadyl cation, VO²⁺, a strong acid, forms stable complexes with both strong bases, catechol and pyrogallol, as a result of the tannin gel adsorbs VO²⁺ ions with high efficiency.⁴³ In a similar way, it was confirmed that in the interaction with 2,6-dithiolphenol at pH 4.0, V(V) initially reduced to V(IV), and the produced V(IV) gave anionic chelate complex, VOL₂²⁻, and then formed ion-pairing complexes with hydrophobic amines, *o*-, *m*- and *p*-toluidine derivatives (as R-NH₃⁺) detected by both spectrophotometry and ESR spectrometry.⁴⁴ Moreover, so as to support the mechanism of complex formation, from potentiometric titration data obtained in two separate studies,^{45,46} including other studies based on ion-association,^{47,48} it has been observed that pK_a value of chelate complex formed between vanadyl ion, VO²⁺ and pyrogallol at pHs near to neutral is 5.40 where it spontaneously forms a highly stable complex with a logK_f ranging from 22.97 to 21.68 at pHs near to neutral, gradually decreasing with increasing temperature in range of 25–45 °C. Also, under optimal conditions, it has been ob-

served that after pre-reduction and hydrolysis in absence and presence of safranin T as ion pair, vanadium is complexed with pyrogallol in form of anionic $\text{VO}(\text{OH})\text{L}_2^-$ with a $\log K_f$ of 20.9 with relative error of -3.6% at pH 6.0, and then extracted as the hydrophobic ternary complex in form of $\text{VO}(\text{OH})\text{L}_2\text{SF}$ into the micellar phase with stoichiometric ratios 1:2 and 1:2:1, as determined using the molar ratio and Job's continuous variation methods. In light of all these findings, the influence of buffer concentration in range of $0.15\text{--}2.0\text{ mmol L}^{-1}$ at pH 6.0 in Figure 1(b) was also investigated, and the maximal and stable signal was provided at a buffer concentration of 1.6 mmol L^{-1} .

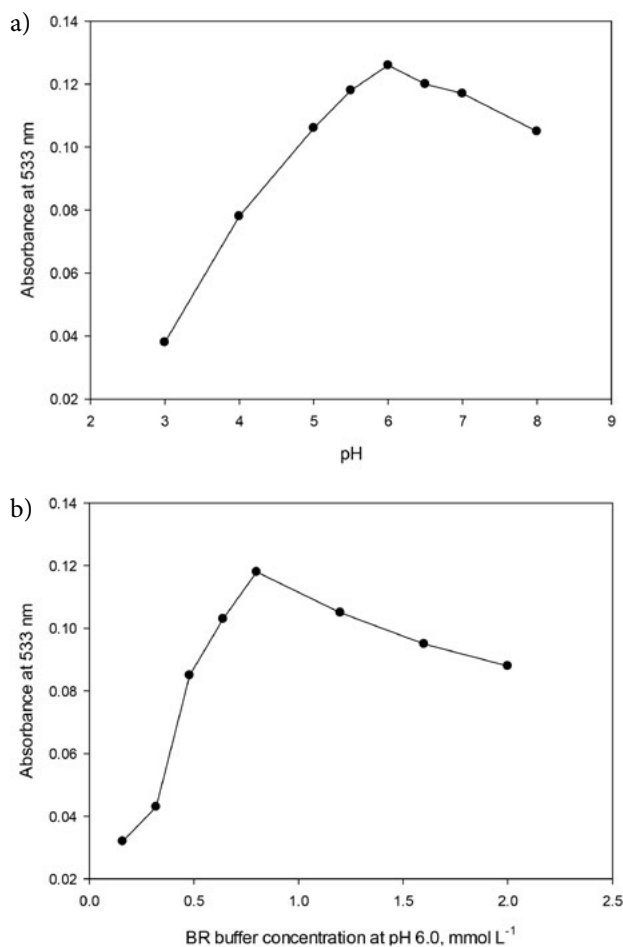


Figure 1. The influence of (a) pH and (b) B-R buffer concentration at pH 6.0 on the analytical signal. Conditions: $50\text{ }\mu\text{g L}^{-1}$ V(V), $1.6\text{ }\mu\text{mol L}^{-1}$ pyrogallol, $2.0\text{ }\mu\text{mol L}^{-1}$ safranin T, 6.0 mmol L^{-1} KCl solution, and 0.05% (w/v) Triton X-114 at $50\text{ }^\circ\text{C}$ and incubation for 3 min.

3. 2. Effect of Pyrogallol and Safranin T Concentrations

At the optimal pH, the influence of the pyrogallol amount as the main chelating agent in the range of $0.3\text{--}4\text{ }\mu\text{mol L}^{-1}$ was studied, and the results are demonstrated in Figure 2(a). It can be seen that the analytical signal value for V(V) initially increases with increasing slope and

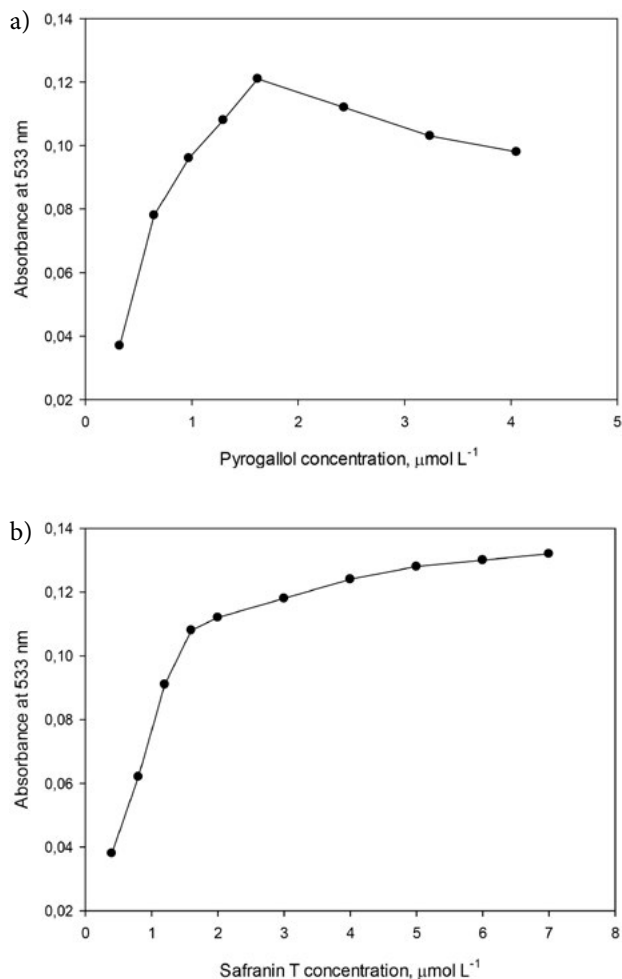


Figure 2. The influence of (a) pyrogallol concentration and (b) safranin T concentration at pH 6.0 on the analytical signal. Conditions: $50\text{ }\mu\text{g L}^{-1}$ V(V), 0.8 mmol L^{-1} B-R buffer at pH 6.0, 6.0 mmol L^{-1} KCl solution, and 0.05% (w/v) Triton X-114 at $50\text{ }^\circ\text{C}$ and incubation for 3 min.

reaches the maximum value while pyrogallol concentration linearly increases up to a concentration of $1.6\text{ }\mu\text{mol L}^{-1}$. At higher concentrations than $1.6\text{ }\mu\text{mol L}^{-1}$, the analytical signal gradually decreases, due to the charge transfer complex formation between pyrogallol and safranin T in absence of V(V) by donor-acceptor mechanism.⁴⁹ Therefore, pyrogallol concentration of $1.6\text{ }\mu\text{mol L}^{-1}$ was chosen as the optimal concentration for the subsequent experiments.

The influence of safranin T amount as ion-pairing reagent on the extraction yield of V(V) was studied in the range of $0.4\text{--}7\text{ }\mu\text{mol L}^{-1}$; the obtained results are represented in Figure 2(b). The absorbance value increased with increasing ion-pairing concentration for V(V), so as to show a linear relationship with two different slopes. However, the absorbance sharply increases with a sensitivity increase of 9-fold in low concentration region of $0.4\text{--}2\text{ }\mu\text{mol L}^{-1}$. After the concentration of $2\text{ }\mu\text{mol L}^{-1}$, in a similar way, the absorbance shows a linear increase in range of $2\text{--}7\text{ }\mu\text{mol L}^{-1}$.

L^{-1} , but this increase in signal slows down with a lower slope, so as thermodynamically to reach a plateau at a saturation point. Perhaps, the aggregation of safranin T at higher concentrations may cause a decrease in the absorbance value. The literature findings show that safranin T, which is a redox-sensitive dye, has a dimerization constant of K_D : 4.73 at high concentrations.⁵⁰ Thus, $2 \mu\text{mol L}^{-1}$ of safranin T was determined as the optimal value for further studies.

3. 3. Effect of Triton X-114 Concentration

The nonionic surfactant concentration as extractant is one of the most important factors affecting the CPE of metal ions. Usually, non-ionic surfactants such as Triton X-114, Triton X-45, PONPE 7.5 were extensively used in CPE of V(V). The non-ionic surfactants are used to create micelle aggregates, these very efficiently capture the complexes, so as to get simple phase separation. The surfactants

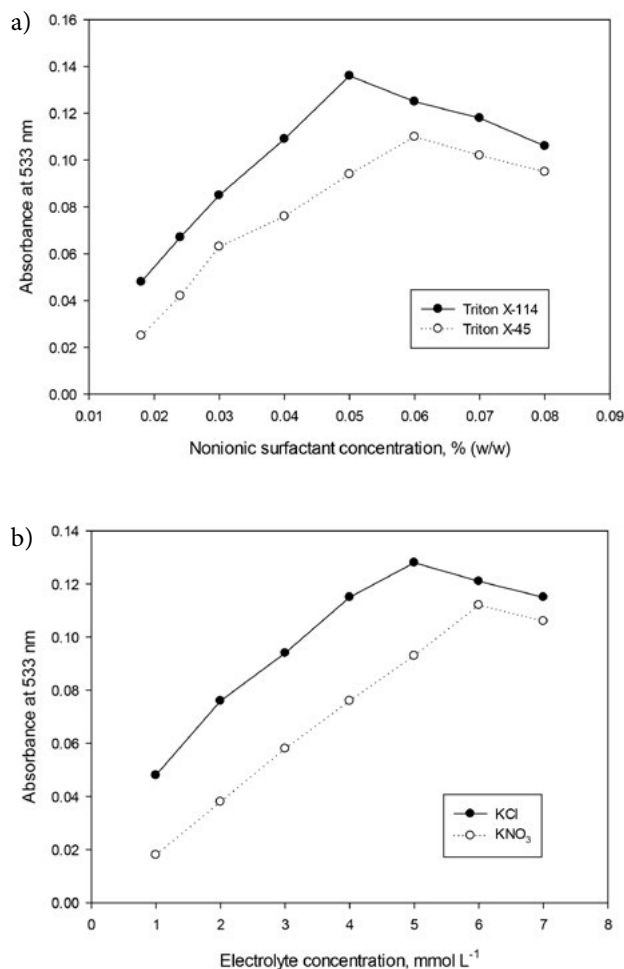


Figure 3. The influence of (a) nonionic surfactant concentration and (b) electrolyte concentration at pH 6.0 on the analytical signal. Conditions: $50 \mu\text{g L}^{-1}$ V(V), 0.8 mmol L^{-1} B-R buffer at pH 6.0, $1.6 \mu\text{mol L}^{-1}$ pyrogallol, $2.0 \mu\text{mol L}^{-1}$ safranin T at $50 \text{ }^\circ\text{C}$ and incubation for 3 min.

have relatively low cloud point temperature, high extraction yield, are commercially available, of high purity, nonvolatile and of low toxicity.^{51,52} However, surfactant concentrations in range of 0.006–0.06% (w/w) were used. Figure 3(a) shows the effect of non-ionic surfactant concentration, the maximal extraction efficiency and higher signal was obtained by using 0.05% (w/w) Triton X-114 while a concentration of 0.06% (w/w) for Triton X-45 was needed. Thus, Triton X-114 with a significant sensitivity difference was chosen as adequate non-ionic surfactant. Its concentration of 0.05% (w/w) was fixed for subsequent studies. At values above this concentration, the extraction efficiency was slightly lower due to the increase in the volume and the viscosity of the surfactant-rich phase.⁵³ Below this value, the decrease in the absorbance as a measure of extraction efficiency is due to deficiency of the surfactant assemblies to extract the hydrophobic complex quantitatively.⁵⁴

3. 4. Effect of Ionic Strength

The ionic strength of the solution can influence the extraction process and yield of extraction owing to altered density of the aqueous phase and remarkably simplify phase separation. Therefore, the effect of ionic strength on the CPE was also studied by observing the extraction efficiency for several electrolyte solutions such as KCl and KNO_3 concentration in the range $1\text{--}7 \text{ mmol L}^{-1}$. The values in Figure 3(b) show that the presence of increased concentration of electrolyte can increase the micelle size and aggregation amount and a decrease in the equilibrium temperature is observed, but the critical micelle concentration (CMC) remains stable. Besides, inorganic salts enhance the hydrophobic interactions among surfactant aggregates and analytes. The obtained results indicate that both electrolyte solutions can affect the UA-CPE. However, the best analytical signal was provided at a KCl concentration of 5.0 mmol L^{-1} with a significant sensitivity difference. Therefore, 5.0 mmol L^{-1} KCl was chosen as optimal value.

3. 5. Effects of Equilibrium Temperature and Incubation Time

In this study, equilibrium temperature and incubation time were also optimized. In order to obtain the maximal preconcentration factor from sample volume of 15 mL, the UA-CPE should be performed at temperatures higher than the determined temperature for cloud-point. The effect of equilibrium temperature for Triton X-114 was studied in range of $30\text{--}60 \text{ }^\circ\text{C}$ under ultrasonic power (300 W, 40 kHz). The matrix became blurry when the solutions were placed in the ultrasonic bath with temperature equal to and higher than $30 \text{ }^\circ\text{C}$ due to its low cloud point temperature ($23 \text{ }^\circ\text{C}$), and the temperature had a notable effect on the extraction yield and the analytical signal was maximal in temperature range of $45\text{--}50 \text{ }^\circ\text{C}$. Figure 4(a) shows that the absorbance of the analyte reaches maxi-

mum in 50 °C. The decrease in absorbance at temperature higher than 50 °C is likely due to the dissociation of the metal-chelate complex. Therefore, 50 °C was selected as the optimal temperature. The effect of incubation time on UA-CPE at 50 °C was studied within the range of 1–20 min in order to attain the equilibrium between two phases. From results in Figure 4(b), it is clear that an incubation time of 10 min is enough for quantitative extraction of analyte by UA-CPE.

The effect of centrifugation time at 4000 rpm was studied for time interval 5–20 min. It was found that a centrifugation time of 15 min was sufficient for efficient phase separation.

3. 6. Effect of Viscosity

Since the surfactant-rich phase provided by UA-CPE is quite viscous, in order to facilitate the detectability of samples by spectrophotometer, the viscosity must be re-

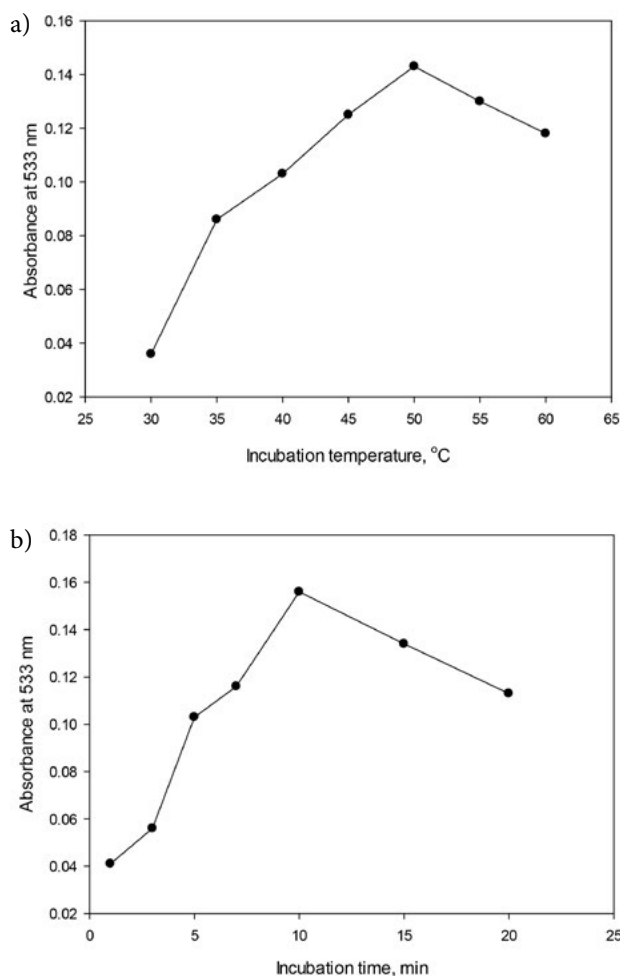


Figure 4. The influence of (a) incubation temperature and (b) incubation time at pH 6.0 on the analytical signal. Conditions: 50 $\mu\text{g L}^{-1}$ V(V), 0.8 mmol L^{-1} B-R buffer at pH 6.0, 1.6 $\mu\text{mol L}^{-1}$ pyrogallol, 2.0 $\mu\text{mol L}^{-1}$ safranin T, 6.0 mmol L^{-1} KCl solution, and 0.05% (w/v) Triton X-114.

duced by addition of a diluent into the surfactant-rich phase. To establish the most suitable diluent, several organic solvents such as THF, acetone, acetonitrile, ethanol and methanol was investigated. From calibration curves constructed between absorbance and vanadium concentrations of 10, 20, and 40 $\mu\text{g L}^{-1}$ with a wavelength difference ranging from 3 to 15 nm, ethanol gave the best analytical sensitivity (m/s, where m and s, respectively, are the slope of calibration curve and standard deviation of measurement) and was found to be suitable for dilution of surfactant-rich phase. Therefore, the surfactant-rich phase was diluted to 1.5 mL using ethanol. At these conditions, the analytical signals were maximal and reproducible.

3. 7. Effect of Sample Volume

A significant amount of sample solution is necessary to provide the maximal enrichment factor in terms of a new method development. The compatibility with Beer's law was studied by monitoring the absorbance of serial solutions of V(V) in different concentrations. For this purpose, 3, 5, 10, 15, 20, 25, 30 and 35 mL of solutions containing 600 ng of V(V) were pretreated and extracted by UA-CPE under the optimal conditions. For this purpose, the sample volume was sequentially varied from 3 to 35 mL, the extraction was performed, the extract was diluted to 1.5 mL with ethanol, and the absorbance of each sample was measured against a sample blank. The results showed that by increasing the sample volume up to 15 mL, the extraction efficiency was gradually increased and became constant at higher volumes. Therefore, a sample volume of 15 mL was selected as optimal for maximal enrichment factor.

3. 8. Analytical Figures of Merit

Under the optimized conditions, as can be seen in Table 1, the limits of detection and quantification (LOD: $3s_{\text{blank}}/m$ and LOQ: $10s_{\text{blank}}/m$, in which the s_{blank} and m , respectively, are the standard deviation of ten replicate measurements of sample blank and slope of the calibration curve) of the method for V(V) were 0.58 and 1.93 $\mu\text{g L}^{-1}$, the recovery rates were in range of 93.8–103.2% (25, 100 and 250 $\mu\text{g L}^{-1}$, n: 5), the precision (as RSD%) was in range of 2.6–4.1% (25, 100 and 250 $\mu\text{g L}^{-1}$, n: 5), the linear working range was 2–500 $\mu\text{g L}^{-1}$, and the sensitivity enhancement factor was 47.7 for enrichment or preconcentration of 15 mL sample by UA-CPE. The sensitivity enhancement factor was calculated from the slopes of the calibration curves established after and before preconcentration, in which the linear working range without preconcentration is 40–1200 $\mu\text{g L}^{-1}$ with limits of detection and quantification of 9.1 and 30.3 $\mu\text{g L}^{-1}$. The corresponding linear regression equations after and before preconcentration are as follows:

$$\text{Abs} = (2.29 \pm 0.20) \times 10^{-3} \text{C}[\text{V(V)}, \mu\text{g L}^{-1}] + (7.1 \pm 0.44) \times 10^{-3} \text{ with } r^2: 0.9943 \text{ after preconcentration by UA-CPE,}$$

Table 1. The analytical features of the proposed preconcentration method

Analytical parameters	After preconcentration with UA-CPE	Before preconcentration with UA-CPE
Linear working range, $\mu\text{g L}^{-1}$ (n: 10)	2–500	40–1200
Intercept, b	$(7.1 \pm 0.44) \times 10^{-3}$	0.0135
Slope, m	$(2.29 \pm 0.20) \times 10^{-3}$	4.8×10^{-5}
Regression coefficient, r^2	0.9943	0.9965
Limit of detection, LOD $\mu\text{g L}^{-1}$	0.58	9.1
Limit of quantification, LOQ, $\mu\text{g L}^{-1}$	1.93	30.3
RSD % (25, 100 and 250 $\mu\text{g L}^{-1}$, n: 5)	2.6–4.1	2.35–3.80
Recovery % (25, 100 and 250 $\mu\text{g L}^{-1}$, n: 5)	93.8–103.2	96.5–101.5
Sample volume, mL	15	–
Consumptive index, mL	0.375	–
Enrichment or preconcentration factor*	40	–
Sensitivity enhancement factor**	47.7	–

*The factor, described as ratio of sample volume to consumptive index, in which the extraction and preconcentration of V(V) is quantitative for sample volume of 15 mL. **The ratio of slopes of the calibration curves with and without preconcentration with UA-CPE.

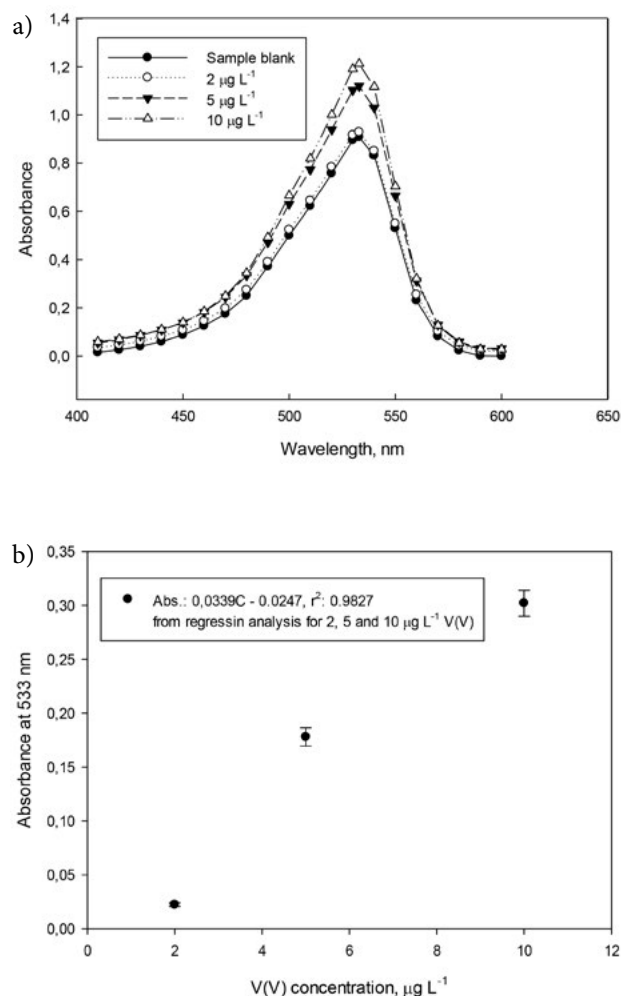


Figure 5. (a) The absorption spectra of the micellar system with increasing V(V) concentration at 2, 5 and 10 $\mu\text{g L}^{-1}$ plus sample blank as a function of measurement wavelength (nm), λ_{max} . (b) The linearity fit of the micellar system between V(V) concentration in range of 2–10 $\mu\text{g L}^{-1}$ and absorbance corrected against sample blank at 533 nm.

$\text{Abs} = 4.8 \times 10^{-5} C [V(V), \mu\text{g L}^{-1}] + 0.0135$ with r^2 : 0.9965 before preconcentration.

Another variable that describes the preconcentration process, such as consumptive index (CI),⁵⁵ was determined. The consumptive index is described as the sample volume (mL), consumed to reach a unit of enrichment factor (EF): $\text{CI} = V_{\text{sample}} (\text{mL}) / \text{EF}$, where V_{sample} is the sample volume.

Under the optimal conditions, the absorption spectra of the micellar system, which has a maximum absorption at 533 nm, for three concentration levels of V(V) (2, 5 and 10 $\mu\text{g L}^{-1}$) including a sample blank is presented in Figure 5(a). Also, linearity fit with a sensitivity increase of 9-fold in slope of calibration for linear working range of 2–10 $\mu\text{g L}^{-1}$ is given in Figure 5(b).

3.9. The Matrix Effect

In this study, in order to show the selectivity of the method, the effect of possible interference of some metal ions on the quantitative analysis of V(V) (50 $\mu\text{g L}^{-1}$) was tested. The results obtained in this investigation are summarized in Table 2. A relative error of less than 5% was considered to be within the range of acceptable error. It is clear that interfering ions, which can potentially be found in environmental samples with tolerance ratio ranging from 25 to 1500, did not exhibit a matrix effect in determination of 50 $\mu\text{g L}^{-1}$ of V(V) by this procedure. Therefore, it can be concluded that the developed method is fairly selective.

3.10. The Analytical Applications of the Method

The analytical applicability of the developed UA-CPE method was checked by the quantitation of V(V) in

Table 2. The interfering effect of the possible matrix components on three replicate measurements of 50 µg L⁻¹ of V(V) (n: 3)

Coexisting ions	[Interferent] / [V ⁵⁺] ratio	Mean recovery ± SD* (%)
Na ⁺ , K ⁺ , NH ₄ ⁺ , Ca ²⁺ , Mg ²⁺	1500:1	98.0 ± 2.5
Zn ²⁺	1250:1	101.0 ± 3.5
F ⁻ , NO ₃ ⁻ , Cl ⁻ , Br ⁻ , Mn ²⁺ , Fe ²⁺	1000:1	97.2 ± 3.5
SO ₄ ²⁻ , HPO ₄ ²⁻ , HCO ₃ ⁻	750:1	98.0 ± 2.5
Cd ²⁺ , Ag ⁺	600:1	97.5 ± 2.5
As ³⁺ , Sb ³⁺ , Mn ²⁺	500:1	96.0 ± 2.5
Ni ²⁺	500:1	101.5 ± 2.5
Pb ²⁺	400:1	97.5 ± 3.0
Formaldehyde, phenol	350:1	97.4 ± 2.0
Sn ²⁺ , Al ³⁺	250:1	98.5 ± 2.5
Co ²⁺ , Cr ³⁺	200:1	97.5 ± 2.5
NO ₂ ⁻ , C ₂ O ₄ ²⁻	150:1	96.5 ± 3.0
HSO ₃ ⁻ , Ascorbic acid	100:1	94.5 ± 2.5
V ⁴⁺ , Sn ⁴⁺	75:1	101.0 ± 2.5
Fe ³⁺ , Cu ²⁺	50:1	98.1 ± 3.0
Mo ⁶⁺	25:1	95.5 ± 2.5

* The percent recoveries plus standard deviations obtained from three replicate measurements of binary mixtures

Table 3. (a) The verification of the method accuracy by the replicate measurements of total V levels in the selected CRMs without and with spiking at levels of 5 and 15 µg L⁻¹ after pretreatment and dilution (n: 5)

The CRMs	Certified value, µg L ⁻¹ or µg kg ⁻¹	After wet digestion with mixture of conc. HNO ₃ -H ₂ O ₂ (3:2, v/v) at 130°C				After ultrasonic-assisted extraction with HCl-0.5 mol L ⁻¹ H ₂ O ₂ (1:1:1, v/v) at 60°C				**The one- paired t-test
		Added	*Found	RSD %	Recovery %	Added	*Found	RSD %	Recovery %	
SRM 1643e	37.86 ± 0.59 µg L ⁻¹	–	38.5 ± 0.7	1.8	–	–	37.6 ± 0.6	1.6	–	2.04, 0.97
Trace elements in water		5	43.2 ± 0.8	1.9	94.0	5	42.3 ± 0.8	1.9	98.0	–
		15	53.1 ± 1.0	1.9	97.3	15	52.4 ± 1.0	1.9	99.3	
SRM 1515	***52 ± 3 µg kg ⁻¹	–	50.8 ± 2.1	4.1	–	–	51.5 ± 2.0	3.9	–	1.28, 0.56
Apple leaves	after dilution at	5	55.4 ± 2.2	4.0	92.0	5	56.2 ± 2.1	3.7	94.0	–
	1:5 ratio	15	65.3 ± 2.3	3.5	97.0	15	66.2 ± 2.2	3.3	98.0	–

* The mean values plus their standard deviations of five replicate measurements ** The tabulated t-value is 2.78 for degree of freedom of 4 at 95% confidence interval for the statistical comparison of the mean values obtained by two analytical methods with certified value *** Where the certified value is 260 ± 30 µg kg⁻¹ (k: 2.0 for 95% confidence interval)

Table 3. (b) The reproducibility and repeatability for the replicate measurements of total V in quality control samples spiked with 5, 10 and 15 µg L⁻¹ (n: 5)

Samples	Spiked concentration, µg L ⁻¹	Intra-day precision			Inter-day precision		
		*Found	Recovery%	RSD%	*Found	Recovery%	RSD%
Semi-skimmed milk	–	14.8 ± 0.5	–	3.4	14.5 ± 0.6	–	4.1
	5	19.5 ± 0.6	94.0	3.1	19.1 ± 0.6	92.0	3.1
	10	24.6 ± 0.7	98.0	2.8	24.0 ± 0.7	95.0	2.9
	15	29.6 ± 0.8	99.0	2.7	29.1 ± 0.8	97.0	2.7
Apple vinegar	–	55.8 ± 2.0	–	3.6	55.5 ± 2.2	–	4.0
	5	60.5 ± 2.1	94.0	3.5	60.0 ± 2.2	90.0	3.7
	10	65.4 ± 2.2	96.0	3.4	65.0 ± 2.3	95.0	3.5
	15	70.5 ± 2.3	98.0	3.3	70.1 ± 2.4	97.0	3.4

*The mean values plus their standard deviations of five replicate measurements

beverages in contact with plastic products. The standard calibration curve was used in sample analysis. The accuracy and the validity of the extraction process was checked and verified by analysis of two standard reference materials, SRM 1515 Apple leaves and SRM 1643e Trace elements in water, representing the sample matrix. These data are summarized in Table 3(a). The obtained results were statistically in good agreement with the certified values with and without dilution. Also, the intra-day and inter-day precision studies for reliability of the results were conducted for the five replicate measurements of vanadium in quality control samples spiked with 5, 10 and 15 $\mu\text{g L}^{-1}$, shown in Table 3(b). The intra-day and inter-day precision (as RSD%) have been in range of 2.7–4.1% and 2.7–3.6% for the selected sample matrices, apple vinegar and semi-skimmed milk, respectively, while the recovery rates from spiked samples are in range of 94.0–99.0% and 92.0–97.0%.

Finally, the method after preconcentration with UA-CPE was applied to the determination of trace V(V) in some beverage samples after pretreatment with two different di-

gestion procedures. The obtained results and the recoveries for the spiked samples are presented in Table 4. These results demonstrate that the recoveries for the spiked samples are in range of 95–98% with a lower RSD than 4.6%. When the mean values obtained by two analytical digestion approaches are compared, it can be seen that the experimental t-values (0.16–1.15) are statistically lower than the tabulated t-value of 2.31 for degree of freedom of 8 at 95% confidence interval, so as not to show a significant difference between the results. These results clearly indicate that the developed method can be reliably applied to the analysis of the selected beverage samples without any matrix effect.

3. 11. Comparison to Other Reported Preconcentration Methods

A comparison of the method performance with those of other preconcentration methods in literature for vanadium determination in beverage samples is given in Table 5. Apparently, the presented method has low LOD

Table 4. The results of total V analysis in beverages in contact with plastic products (n: 5)

Samples	After wet digestion with mixture of conc. $\text{HNO}_3\text{-H}_2\text{O}_2$ (3:2, v/v) at 130°C				After ultrasonic-assisted extraction with mixture of 4.0 mol L ⁻¹ $\text{HNO}_3\text{-4.0 mol L}^{-1}$ $\text{HCl-0.5 mol L}^{-1}$ H_2O_2 at 60°C				**The two-paired t-test
	Added, $\mu\text{g L}^{-1}$	*Found, $\mu\text{g L}^{-1}$	RSD%	Recovery%	Added, $\mu\text{g L}^{-1}$	*Found, $\mu\text{g L}^{-1}$	RSD%	Recovery%	
Semi-skimmed milk	–	15.1 ± 0.6	4.0	–	–	14.8 ± 0.5	3.4	–	0.23
	10	24.7 ± 0.8	3.2	96.0	10	24.5 ± 0.7	2.9	97.0	–
Buttermilk	–	14.3 ± 0.5	3.5	–	–	14.1 ± 0.5	3.5	–	0.22
	10	23.8 ± 0.8	3.4	95.0	10	23.8 ± 0.7	2.9	97.0	–
Grape vinegar1	–	56.4 ± 2.0	3.5	–	–	56.1 ± 2.0	3.6	–	0.16
	10	66.1 ± 2.2	3.3	97.0	10	65.8 ± 2.1	3.2	97.0	–
Apple vinegar1	–	75.5 ± 2.5	3.3	–	–	75.2 ± 2.4	3.2	–	0.20
	10	85.2 ± 2.6	3.1	97.0	10	84.8 ± 2.5	2.9	96.0	–
Grape vinegar2	–	36.7 ± 1.2	3.3	–	–	36.4 ± 1.2	3.3	–	0.40
	10	46.3 ± 1.4	3.0	96.0	10	46.1 ± 1.3	2.8	97.0	–
Apple vinegar2	–	42.3 ± 1.5	3.5	–	–	39.8 ± 1.4	3.5	–	0.48
	10	51.8 ± 1.6	3.1	95.0	10	49.5 ± 1.5	3.0	97.0	–
Pomegranate	–	13.8 ± 0.6	4.3	–	–	13.5 ± 0.5	3.7	–	0.36
	10	23.5 ± 0.8	3.4	97.0	10	23.1 ± 0.7	3.0	96.0	–
Orange juice	–	39.3 ± 1.3	3.3	–	–	38.8 ± 1.3	3.4	–	0.48
	10	48.8 ± 1.5	3.1	95.0	10	48.6 ± 1.5	3.1	98.0	–
Apricot juice	–	35.5 ± 1.2	3.4	–	–	35.2 ± 1.2	3.4	–	0.39
	10	45.2 ± 1.5	3.3	97.0	10	44.8 ± 1.4	3.1	96.0	–
Cherry juice	–	14.3 ± 0.5	3.5	–	–	14.0 ± 0.5	3.6	–	0.41
	10	24.0 ± 0.8	3.3	97.0	10	23.7 ± 0.8	3.4	97.0	–
Apple soda	–	15.7 ± 0.6	3.8	–	–	15.5 ± 0.6	3.9	–	0.79
	10	25.5 ± 0.8	3.1	98.0	10	25.2 ± 0.8	3.2	97.0	–
Lemonate soda	–	10.6 ± 0.4	3.8	–	–	10.3 ± 0.4	3.0	–	0.70
	10	20.2 ± 0.7	3.5	96.0	10	20.0 ± 0.6	3.0	97.0	–
Banana flavored milk	–	8.6 ± 0.4	4.6	–	–	8.3 ± 0.3	3.6	–	1.15
	10	18.3 ± 0.6	3.3	97.0	10	18.0 ± 0.5	2.8	97.0	–
Cherry flavored milk	–	9.5 ± 0.4	4.2	–	–	9.6 ± 0.4	4.2	–	0.71
	10	19.2 ± 0.7	3.6	97.0	10	19.3 ± 0.6	3.1	97.0	–

* The mean values plus their standard deviations of five replicate measurements ** Based on statistical comparison of the mean values obtained by two analytical digestion approaches, in which the tabulated t-value is 2.31 for degree of freedom of 8 at 95% confidence interval.

(0.58 $\mu\text{g L}^{-1}$), wide linear range (2–500 $\mu\text{g L}^{-1}$), minimal solvent consumption, quantitative recovery (93.8–103.2%), good accuracy (2.6–4.1%) and precision (2.4–4.1%), short analysis time (13 min), high sensitivity enhancement factor (47.7) and reasonable enrichment factor (40) from pre-concentration of 15 mL of sample, and these analytical features are comparable or even better than those of most of the other pre-concentration methods in Table 5. The combination of the UA-CPE with spectrophotometry as an alternative to the other previously reported detection techniques such as FAAS, ET-AAS, GF-AAS and ICP-OES offers several advantages including simplicity, easy to use, inexpensiveness, high recoveries, high pre-concentration factor, and great extraction yield. The proposed method provides advantages such as wider linear working range, lower limit of determination, and precision with a reasonable sensitivity enhancement factor.

4. Conclusions

In this study, a new, accurate, precise, sensitive and selective UA-CPE procedure for extraction and pre-concentration of trace vanadium present in the selected beverages using safranin T and pyrogallol at pH 6.0 has been reported before its determination by spectrophotometry at 533 nm. The UA-CPE procedure is simple, easy to use, safe, rapid, eco-friendly and inexpensive pre-concentration

tool. After separation and pre-concentration of analyte from sample matrix, spectrophotometry at 533 nm as detection tool, which does not require expert user in his/her area and that can be readily accessible in almost every analytical research laboratory, was reliably used to monitor the vanadium levels in sample matrix. The method allows detection of vanadium at levels of 0.58 $\mu\text{g L}^{-1}$ with sensitivity enhancement of 47.7, thus it can be used as an alternative to other analytical methods in the monitoring of free vanadium in the complex samples. The method was successfully applied to the extraction, pre-concentration and determination of total V (as V(V) selected as analyte) in beverage samples after pretreatment with acid mixture, and satisfactory results were obtained.

5. Acknowledgements

Authors are also grateful to Prof. Dr. Mehmet Akçay for allowing the conduction of experimental studies in analytical research laboratories and fruitful discussions regarding this research paper.

6. References

1. T. S. Anirudhan, P. G. Radhakrishnan, *Chem. Eng. J* **2010**, *165*, 142–150. DOI:10.1016/j.cej.2010.09.005

Table 5. The analytical performance data obtained by using UA-CPE coupled to spectrophotometry and other reported techniques in determination of vanadium in the selected beverage samples

Detection	Preconcentration procedure	Linear working range, $\mu\text{g L}^{-1}$	LOD, $\mu\text{g L}^{-1}$	Preconcentration factor or enhancement factor	RSD %	Sample consumption, mL	Analysis time, min	References
Spectrophotometry	SPE	110–3000	0.07	90	2.1	450	–	[22]
GF-AAS	CPE	2–50	0.05	100	5.8–7.5	50	75	[24]
Spectrophotometry	CPE	10–100 for V(IV), 1–70 for V(V)	0.12, 0.037	159, 99	0.67	10	55	[25]
Spectrophotometry	CPE	0.5–10 mg L^{-1}	0.113 mg L^{-1}	50	3.40	10	50	[26]
Spectrophotometry	CPE	0.05–0.6 mg L^{-1}	5.51	20, 15	2.43	5	12	[27]
Spectrophotometry	CPE	up to 510	0.7	90	2.1	40	≥ 120	[28]
GF-AAS	CPE	1.0–60	0.05	20	3.9	10	10	[6]
FIA/Catalytic fluorimetry	CPE	0.02–10	0.007	50	1.8	10	25	[32]
ET-AAS	Ion-exchange	0–2	0.02	–	3.2	50	17	[20]
FAAS	UA-CPE	5–250	1.55	115	3.5	50	25	[34]
HR-CS-GFAAS	CPE	1–50	0.13	13.3	2.5	–	35	[29]
Spectrophotometry	SFDOME	3–100	0.94	38	3.90	50	20	[37]
Spectrophotometry	UA-CPE	2–500	0.58	47.7 ^a , 40 ^b	2.6–4.1	15	13	The present method

Notes: (a) The sensitivity enhancement factor is the slope ratio of calibration curves after and before extraction; (b) ratio of the aqueous phase to final volume of eluent phase; FAAS: flame atomic absorption spectrometry; SPE: solid phase extraction; CPE: cloud point extraction; GFAAS: graphite furnace atomic absorption spectrometry; ET-AAS: electrothermal atomic absorption spectrometry; UA-CPE: ultrasound assisted-cloud point extraction; ICP-OES: inductive coupled plasma optical emission spectrometry; FIA/Catalytic fluorimetry: flow injection analysis- catalytic fluorimetry; HR-CS-GFAAS: high resolution continuous source graphite furnace atomic absorption spectrometry; SFDOME: solidified floating organic drop microextraction

2. A. Padilla-Rodríguez, J. A. Hernández-Viezcas, J. R. Peralta-Videa, J. L. Gardea-Torresdey, O. Perales-Pérez, F. R. Román-Velázquez, *Microchem. J.* **2015**, *118*, 1–11. DOI:10.1016/j.microc.2014.07.011
3. B. Patel, G. E. Henderson, S. J. Haswell, R. Grzeskowiak, *Analyst* **1990**, *115*, 1063–1066. DOI:10.1039/an9901501063
4. D. G. Barceloux, *J. Toxicol. Clin. Toxicol.* **1999**, *37*, 265–278. DOI:10.1081/CLT-100102425
5. ATSDR, Draft toxicological profile for vanadium, Atlanta, 2009, 378 <http://www.atsdr.cdc.gov/toxprofiles/tp58.pdf>
6. H. Filik, D. Aksu, *Food Anal. Methods* **2012**, *5*, 359–365. DOI:10.1007/s12161-011-9254-9
7. M. S. Dundar, H.B. Saglam, *Trace Elem. Electroly.* **2004**, *21*, 60–63. DOI:10.5414/TEP21060
8. P. L. Teissedre, M. Krosniak, K. Portett, F. Gasct, A. L. Waterhouse, J. J. Serranot, J. C. Cabanist, G. Crosto, *Food Addit. Contam.* **1998**, *15*, 585–591. DOI:10.1080/02652039809374685
9. Naeemullah, T. G. Kazi, M. Tuzen, *Food Chem.* **2015**, *172*, 161–165. DOI:10.1016/j.foodchem.2014.09.053
10. M. J. C. Taylor, J. F. van Staden, Review. *Analyst* **1994**, *119*, 1263–1276. DOI:10.1039/an9941901263
11. A. Adachi, K. Ogawa, Y. Tsushi, N. Nagao, T. Kobayashi, *Water Res.* **1997**, *31*, 1247–1250. DOI:10.1016/S0043-1354(96)00379-X
12. A. Gaspar, J. Posta, *Fresenius J. Anal. Chem.* **1998**, *360*, 179–183. DOI:10.1007/s002160050671
13. K. Fujiwara, T. Morikawa, K. Fuwa, *Bunseki Kagaku* **1986**, *35*, 361–367. DOI:10.2116/bunsekikagaku.35.4_361
14. C. C. Chery, K. De Crèmer, R. Cornelis, F. Vanhaecke, L. Moens, *J. Anal. At. Spectrom.* **2003**, *18*, 1113–1118. DOI:10.1039/B301682J
15. H. Liu, S. J. Jiang, *J. Anal. At. Spectrom.* **2002**, *17*, 556–559. DOI:10.1039/b111577b
16. R. S. S. Murthy, D. E. Ryan, *Anal. Chem.* **1983**, *55*, 682–684. DOI:10.1021/ac00255a023
17. P. P. Coetzee, J. L. Fischer, M. Hu, *Water SA* **2002**, *28*, 37–44. DOI:10.4314/wsa.v28i1.4865
18. S. Kawakubo, K. Ogihara, M. Iwatsuki, *Analyst* **1995**, *120*, 2719–2723. DOI:10.1039/an9952002719
19. F. Garcia-Sanchez, A. Navas, M. Santiago, F. Grases, *Talanta* **1981**, *28*, 833–837. DOI:10.1016/0039-9140(81)80025-2
20. I. López-García, P. Vinas, R. Romero-Romero, M. Hernández-Córdoba, *Talanta* **2009**, *78*, 1458–1463. DOI:10.1016/j.talanta.2009.02.045
21. F. Z. Xie, X. C. Lin, X. P. Wu, Z. H. Xie, *Talanta* **2008**, *74*, 836–843. DOI:10.1016/j.talanta.2007.07.018
22. L. Rostampour, M. A. Taher, *Talanta* **2008**, *75*, 1279–1283. DOI:10.1016/j.talanta.2008.01.045
23. A. N. Anthemidis, K. I. G. Ioannou, *Talanta* **2009**, *79*, 86–91. DOI:10.1016/j.talanta.2009.03.005
24. S. Khan, T. G. Kazi, J. A. Baig, N. F. Kolachi, H. I. Afridi, S. Kumar, A. Q. Shah and G. A. Kandhro *J. Iran. Chem. Soc.* **2011**, *8*(4), 897–907. DOI:10.1007/BF03246545
25. Z. A. A. Khammas, Z. T. Ibrahim, K. J. Al-adilee *Int. Res. J. Pure & Appl. Chem.* **2015**, *8*(1), 33–48. DOI:10.9734/IRJPAC/2015/16431
26. Z. A-A. Khammas, R. A. Rashid *Sci. J. Anal. Chem.* **2015**; *3*(5), 61–70. DOI:10.11648/j.sjac.20150305.14
27. E. Ghasemi, M. Kaykhan *Anal. Mets.* **2015**, *31*, 407–411.
28. T. S. Stefanova, K. K. Simitchiev, K. B. Gavazov *Chem. Pap.* **2015**, *69*(4), 495–503.
29. G. M. Wuilloud, J. C. A. de Wuilloud, R. G. Wuillou, M. F. Silva, R. A. Olsina, L. D. Martinez, *Talanta* **2002**, *58*, 619–627. DOI:10.1016/S0039-9140(02)00366-1
30. V. S. Souza, L. S. G. Teixeira, M. A. Bezerra, *Microchemical Journal* **2016**, *129*, 318–324. DOI:10.1016/j.microc.2016.06.029
31. C. B. Ojeda, F. S. Rojas, *Anal. Bioanal. Chem.* **2009**, *394*, 759–782. DOI:10.1007/s00216-009-2660-9
32. E. K. Paleologos, M. A. Koupparis, M. I. Karayannis, P. G. Veltsistas, *Anal. Chem.* **2001**, *73*, 4428–4433. DOI:10.1021/ac010395k
33. Y. Liu, J. Xu, Y. Xue, J. Wang, Y. Chang, C. Xue, *J. Environ. Anal. Chem.* **2015**, *95*, 258–270. DOI:10.1080/03067319.2014.1002494
34. R. Gürkan, S. Korkmaz, N. Altunay, *Talanta* **2016**, *155*, 38–46. DOI:10.1016/j.talanta.2016.04.012
35. X. Zhu, Z. Zhu, S. Wu, *Microchim. Acta* **2008**, *161*, 143–148. DOI:10.1007/s00604-007-0762-7
36. T. Madrakian, A. Afkhami, R. Siri, M. Mohammadnejad, *Food Chem.* **2011**, *127*, 769–773. DOI:10.1016/j.foodchem.2010.12.144
37. S. Dadfarnia, A. M. H. Shabani, A. Mirshamsi *Turk. J. Chem.* **2011**, *35*, 625–636.
38. P. Berton, E. M. Martinis, R. G. Wuilloud, *J. Hazard. Mater.* **2010**, *176*, 721–728. DOI:10.1016/j.jhazmat.2009.11.094
39. M. F. Silva, E. S. Cerutti, L. D. Martinez, *Microchim Acta* **2006**, *155*, 349–364. DOI:10.1007/s00604-006-0511-3
40. K. Zih-Perenyi, A. Lasztity, Z. Horvath, A. Levai, *Talanta* **1998**, *47*, 673–679. DOI:10.1016/S0039-9140(98)00106-4
41. J. Krakowiak, D. Lundberg, I. Persson, *Inorg. Chem.* **2012**, *51*, 9598–9609. DOI:10.1021/ic300202f
42. M. K. Islam, C. Tsuboya, H. Kusaka, S. Aizawa, T. Ueki, H. Michibata, K. Kanamori, *Biochim. et Biophys. Acta* **2007**, *1770*, 1212–1218.
43. A. Nakajima, *Talanta* **2002**, *57*, 537–544. DOI:10.1016/S0039-9140(02)00068-1
44. K. A. Kuliyevev, N. A. Verdizade, *American J. Chem.* **2015**, *5*, 10–18.
45. R. C. Skevington A study of the organic complexes of oxovanadium (IV). Bachelor of Science Thesis, Wollongong University College, The University of New South Wales, Australia, 1968.
46. Gao Zhu-Qing, Cai Xiao-Dong, Cheng Lei-Lei, Ling Kai-Cheng *Adv. Mat. Res.* 2011, 396–398, 2225–2229. DOI:10.4028/www.scientific.net/AMR.396-398.2225
47. G. B. Gavazov, Zh. Simeonova, A. Alexandrov *Russian J. Inorg. Chem.* 2001, 46(3), 427–431.
48. K. B. Gavazov, T. S. Stefanova *Croat. Chem. Acta* 2014, 87(3), 233–240. DOI:10.5562/cca2436
49. A. K. Jana, S. Rajavenii *Spectrochim. Acta A* 60 (2004) 2093–2097. DOI:10.1016/j.saa.2003.10.041

50. A. Niazi, A. Yazdanipour, J. Ghasemi, M. Kubista, *Spectrochim. Acta A* **2006**, 65, 73–78. DOI:10.1016/j.saa.2005.09.030
51. R. P. Frankewich, W. L. Hinze, *Anal. Chem.* **1994**, 66, 944–954. DOI:10.1021/ac00079a005
52. M. E. F. Laespada, J. L. P. Pavón, B. M. Cardero, *Analyst* **1993**, 118, 209–212. DOI:10.1039/AN9931800209
53. F. Shemirani, M. Baghdadi, M. Ramezani, *Talanta* **2005**, 65, 882–887. DOI:10.1016/j.talanta.2004.08.009
54. N. Baghban, A. M. H. Shabani, S. Dadfarnia, A. A. Jafari, *Croat. Chem. Acta* **2012**, 85, 85–90. DOI:10.5562/cca1803
55. Z. L. Fang, VCH, New York, **1993**, 85–128.

Povzetek

Razvili smo novo ekstrakcijsko metodo s surfaktantom in s pomočjo ultrazvoka za predkoncentracijo in določitev V(V) v vzorcih pijač. Po tvorbi kompleksa s pirogalolom v prisotnosti safranina T pri pH 6,0 smo V(V) ione ekstrahirali kot ternarni kompleks v micelarno fazo Tritona X-114. Kompleks smo spremljali pri 533 nm s spektrofotometrijo. Ocenili smo učinek matrice na izkoristek ekstrakcije V(V) iz obogatenih vzorcev (koncentracija $50 \mu\text{g L}^{-1}$). Pri optimalnih pogojih je bila meja zaznave $0,58 \mu\text{g L}^{-1}$, meja določitve $1,93 \mu\text{g L}^{-1}$ pri linearnem območju $2\text{--}500 \mu\text{g L}^{-1}$ in s povečanjem občutljivosti 47,7 ter s predkoncentracijskim faktorjem 40 za predkoncentracijo iz 15 mL raztopine vzorca. Izkoristki iz obogatenih vzorcev so bili v območju 93,8–103,2% z relativnim standardnim odklonom od 2,6% do 4,1% (25, 100 in $250 \mu\text{g L}^{-1}$, n: 5). Točnost smo preverili z analizo dveh certificiranih vzorcev in rezultati so se dobro skladali s certificiranimi vrednostmi. Natančnost znotraj dneva in med dnevi smo preverili z določitvijo ponovljivosti (3,3–3,4%) in obnovljivosti (3,4–4,1%) na petih ponovitvah analize V(V) v vzorcih za kontrolo kvalitete z dodanimi 5, 10 in $15 \mu\text{g L}^{-1}$ vanadija. Z razvito metodo smo uspešno določili koncentracije V(V) v sledovih v izbranih vzorcih pijač.

Scientific paper

Development of a Cotton Smart Textile with Medicinal Properties Using Lime Oil Microcapsules

Piyumi B. Wijesirigunawardana and B. Gayani K. Perera*

Department of Chemistry, University of Colombo, Colombo 03, Sri Lanka

* Corresponding author: E-mail: gayani@sci.cmb.ac.lk

Received: 01-08-2017

Abstract

The present study focused on using microencapsulation technique to develop an antioxidant and antibacterial active smart cotton fabric using encapsulated lime oil (LO). LO microcapsules were prepared *via* the complex coacervation method using chitosan and gum arabic wall materials. UV-Visible and FTIR spectrometry verified the successful encapsulation of LO. The synthesized LO microcapsules were irregular in shape and differed in size between 15–160 μm according to the optical and SEM images. The loading of the microcapsules was found to be $2943 \pm 128 \mu\text{L/g}$ with a loading efficiency of $82 \pm 4\%$. The antioxidant activity of the LO microcapsules was $1336 \pm 17 \mu\text{g PGE/g}$ (Folin-Ciocalteu assay). Brine shrimp lethality assay indicated that the cytotoxicity of LO was minimized upon microencapsulation. Succinic acid was used as the binder to incorporate the LO microcapsules on to the cotton fabric. The SEM images confirmed the steady attachment of LO microcapsules to the cotton fibres. The cotton fabric containing LO microcapsules displayed significant antibacterial activity against four bacterial species prior to and after subjecting the fabric to wash conditions.

Keywords: Smart textiles, Microencapsulation, Lime oil, Antioxidant, Antibacterial

1. Introduction

The enhancement of the quality and standards of life styles of people expands with the gradual improvement of the medicinal and technological knowledge. This in turn leads to the emergence of innovative and value-added products related to health and beauty.¹ The textile industry has nowadays become more competitive due to the production of active, multifunctional and interactive smart textiles.² Smart textiles are also known as intelligent textiles and these are produced by introducing various useful properties to the fibres of the fabric.² A textile becomes more attentive to consumers when it starts to exhibit useful properties, especially when it is in contact with the human body. Thus, smart technology has contributed towards solving numerous problems in the textile industry that cannot be addressed by traditional textile processing.^{1,3,4}

Microencapsulation has been a useful technique since 1990s to produce smart textile materials.⁵ Microencapsulation is a micro packaging technique which produces microcapsules containing a desired encapsulated active material. The size of the microcapsule vary between 1 to 1000 μm .^{1,6,7} Therefore, microencapsulation can be defined as the process of coating of small solid particles or liquid

droplets or dispersions of solid particles with a continuous film.^{1,8} The method of microencapsulation can be chosen according to the properties of its core and coating materials and the user requirements of the final product.^{1,5,6,8} The core material is also called the internal phase, encapsulate, payload or the fill.^{1,5} The core content of the microcapsules may be released to the exterior in a controlled manner by friction, pressure, change of temperature, diffusion through the polymer wall, dissolution of the polymer wall coating or by biodegradation.⁵ The polymer coating surrounding the active ingredient or the encapsulated material in microcapsules is also called the wall, shell, external phase, membrane or matrix. The nature of the wall material can be natural, semi-synthetic or synthetic and it must be capable of forming a non-reactive cohesive film around the core material.^{1,6,9} The wall material helps to determine the strength, flexibility, permeability, optical properties and stability of the microcapsules.^{1,5}

Microencapsulation provides a range of advantages to the encapsulated core material. These include protection of active ingredients against heat, light, acidity, alkalinity, moisture and oxidation as well as the controlled release of the encapsulated material. Furthermore, microencapsulation enables to disguise the unpleasant flavors or odors of the core materials and also allows the easy han-

dling of core materials due to the powder-like nature of the final microcapsulated product.^{1,5,9}

Among the wide range of microencapsulation methods in use, the most often used ones in the textile industry are the coacervation and interfacial polymerization methods.⁷ During this research, complex coacervation method was selected to synthesize lime oil microcapsules, using gum arabic and chitosan as the wall materials. During complex coacervation method, a polymer rich wall material is deposited around the core material.^{5,10} A wide variety of natural materials such as gelatin, agar, gum, sodium alginate, calcium alginate, dextran, fat and fatty acid starch, chitosan, caseinate, sucrose, and wax can be used as the wall material during complex coacervation.¹

Nowadays, more commercial applications of microencapsulation can be found in the textile industry because of its capability of being adjusted for different tasks.⁵ The microencapsulation technique is used to develop and modify textiles with new enhanced properties such as polychromic and thermochromic textiles, fire proofing textiles, fragrance releasing textiles, cosmetic textiles, therapeutic textiles and medical textiles.^{5,7}

The cooperation between the medical profession and the textile industry has successfully resulted in the development of bio-medical smart textiles that fulfill a specific market niche and thereby providing bioactive body care to understand and satisfy the consumer needs and physiological conditions of the human skin.⁵ For an example, microencapsulation technique has led the textile industry to produce medicinal fabrics with durable fragrances that are useful in aromatherapy.^{11,12} Microcapsules are synthesized in aromatherapy using essential oils such as lavender, almond, jasmine, saffras, myrrh, rosemary, lime and pine.^{2,8} Such microcapsules are often used to treat health conditions such as insomnia, headache, and to prevent bad odor.¹² However, the direct application of fragrances to fibers failed to survive for a significant time period or few wash cycles due to the volatility of all fragrances.^{12,13} The present study was mainly focused on the microencapsulation of lime essential oil and development of a medicinal smart textile using the synthesized lime oil microcapsules that provides medicinal properties upon releasing of the active core ingredients to the exterior under controlled conditions. Lime essential oil is one of the most reasonably priced and best therapeutic essential oils. Pure lime oil is a mixture of volatile compounds obtained by mechanically rupturing or cold pressing the peel of the fruit of lime tree (*Citrus aurantifolia*).^{14,15,16} Citric essential oils are commonly composed of terpenes such as α -thujene, α -pinene, camphene, sabinene, β -pinene, myrcene, α -terpinene, *p*-cymene, linalool, and d-limonene.¹⁸ Lime oil is a powerful healing agent of acne, asthma, colds, dull skin, flu and sore throats. It also displays other beneficial properties such as antiseptic, antioxidant, antiviral, antiinflammatory, antinitrosaminic, astringent, aperitif, bactericide, antitumor and disinfectant

activities. Furthermore, lime oil is also known for its hypocholesterinemic, cardiotoxic, sedative and stomachic activities^{15,16,18}

In order to characterize the synthesized lime oil microcapsules, optical and scanning electron microscopic images, UV-Visible and FT-IR spectra, anti-oxidant assays, anti-bacterial assays and cytotoxicity assay were carried out. After the characterization of synthesized lime oil microcapsules, the main focus of this research was to successfully apply the lime oil microcapsules on to a cotton fabric using succinic acid as the binder.¹⁹

2. Experimental

2. 1. Preparation of Lime Oil Microcapsules by Complex Coacervation Method

A portion of 2.5 g of gum arabic was mixed with 50 mL of distilled water and the mixture was stirred at 50 °C for about 20 minutes until all the gum arabic was completely dissolved. The mixture was kept at room temperature. A mixture of 1.0 g of chitosan, 50 mL of distilled water and 4.0 mL of pure lime oil was stirred at 600 rpm for about 10 minutes at room temperature until an emulsion was obtained. While stirring, the prepared emulsion was added dropwise into the gum arabic solution kept in an ice bath. The mixture was stirred continuously for another hour. Prepared lime oil microcapsules were well washed with a 70% ethanol solution to remove any remaining unencapsulated oil. The removal of the unencapsulated oil was monitored by using the UV-Visible spectra of each wash. The washed capsules were gravity filtered and dried inside a desiccator. The microcapsules were kept in refrigerator until further use.²⁰

2. 2. Verification of Lime Oil Microencapsulation

A portion of 0.08 g of washed microcapsules was transferred into a falcon tube containing 2.0 mL of 70% ethanol. Another 0.08 g of washed microcapsules was transferred into another falcon tube containing 2.0 mL of 70% ethanol and it was well crushed using a glass rod, followed by sonication for 15 minutes. Both samples were centrifuged at 4000 rpm for 10 minutes. The supernatants were collected separately. UV-Visible spectra of the supernatants and pure lime oil were obtained and the spectra were compared. The absorbance values of both intact (un-crushed) and crushed microcapsule samples at 243 nm were recorded (the wavelength at which the maximum absorbance for pure lime oil was observed) and compared. A mixture of gum arabic, chitosan and 70% ethanol was used as the blank for the UV-Visible spectroscopic experiments. FT-IR spectra were also obtained to verify the encapsulation of lime oil in microcapsules.

2. 3. Investigation of the Morphology of Microcapsules

The prepared lime oil microcapsules were observed under the optical and scanning electron microscopes.

2. 4. Determination of the Loading and Loading Efficiency of Lime Oil Microcapsules

A concentration series was prepared by dissolving pure lime oil in 70% ethanol. The absorbance of the standard series was measured at 243 nm and a standard curve was developed. A portion of 0.05 g washed microcapsules was transferred into an eppendorf tube. The microcapsules were well crushed mechanically and 1 mL of 70% ethanol was added. The sample was sonicated for about 15 minutes. The crushed sample was centrifuged 4000 rpm for 10 minutes. The absorbance of the supernatant was measured at 243 nm. Loading of lime oil microcapsules was calculated by using the standard curve. Loading efficiency of the microcapsules was calculated using the following equation (1). The experiment was carried out in triplicate.^{21,22}

$$\text{Loading efficiency (\%)} = \frac{\text{Volume of encapsulated lime oil in microcapsules}}{\text{Volume of total lime oil used}} \times 100 \quad (1)$$

2. 5. Folin Ciocalteu Assay

2. 5. 1. Preparation of the Folin Ciocalteu Reagent

A portion of 10.0 g of sodium tungstate and 2.5 g of sodium molybdate were dissolved in 70.0 mL of distilled water in a round bottom flask. A volume of 5.0 mL of 85% of H_3PO_4 acid and 10.0 mL of concentrated HCl were added into the round bottom flask. The mixture was refluxed for 10 hours inside a fume hood. Portion of 15.0 g of lithium sulphate, a volume of 5.0 mL of distilled water and one drop of liquid bromine were added. The mixture was refluxed for another 15 minutes. The mixture was allowed to cool at room temperature and finally the volume was adjusted to 100.0 mL with distilled water.²⁴

2. 5. 2. Folin-Ciocalteu Assay Procedure

A standard series was prepared using pyrogallol in methanol. A volume of 2.0 mL of 2% (w/v) sodium bicarbonate was mixed with 100 μL of each standard solution. The samples were incubated for 2 minutes. A volume of 100 μL of Folin Ciocalteu reagent was added to each sample. The samples were incubated for 30 minutes in the dark. The absorbance of each sample was measured at 750 nm using the UV-Visible spectrophotometer. The standard curve was developed. The same procedure was carried out with 0.04 g/mL methanolic solutions of crushed and uncrushed microcapsules and pure lime oil (an equivalent amount to that encapsulated in microcap-

sules). The antioxidant activity of the test samples was determined using the standard curve. The experiment was carried out in triplicate.^{23,24}

2. 6. Brine Shrimp Lethality Assay to Test the Cytotoxic Activity of Lime Oil Microcapsules

Brine shrimp eggs were hatched using 3.8% NaCl solution inside a glass container. Ten nauplii were transferred into a 5 mL solution of 3.8% NaCl. An aliquot of 50 μL of an ethanolic solution containing crushed or uncrushed microcapsules (prepared by mixing 0.08 g of crushed or uncrushed microcapsules in 1.0 mL of 70% ethanol) or pure lime oil (an equivalent amount to the encapsulated amount in microcapsules) was added. A 50 μL aliquot of 70% of ethanol was used as the negative control. Each sample was observed for a period of 8 hours and the numbers of live and dead nauplii were recorded after each hour. The experiment was carried out in triplicate and the percentage mortality was calculated for each experiment using the following equation (2).²³

$$\text{Percentage mortality (\%)} = \frac{\text{no. of dead brine shrimp nauplii}}{\text{Total no. of brine shrimp nauplii}} \times 100 \quad (2)$$

2. 7. Antibacterial Activity of Lime Oil Microcapsules

Antibacterial activity of crushed, uncrushed and unencapsulated lime oil (a similar equivalent to the amount encapsulated in the crushed microcapsule sample) was tested against *Escherichia coli* (ATCC 35218), *Bacillus cereus* (ATCC 11778), *Salmonella typhimurium* (ATCC 14028), and *Staphylococcus aureus* (ATCC 25923) using the disk diffusion assay according to previously published protocols.^{15, 23}

2. 8. Incorporation of Lime Oil Microcapsules Into Cotton Fabric

A portion of 0.3 g of microcapsules was mixed with 3.0 mL saturated succinic acid. The sample was stirred overnight. Microcapsules were filtered and resuspended in 1 mL of distilled water. A piece of 5 \times 5 cm^2 cotton cloth was dipped in the aqueous solution of microcapsules. The cloth was air dried and ironed. Antibacterial activity of the microcapsule incorporated cotton fabric was investigated and the SEM images of the same fabric were taken.

To investigate the wash fastness of the microcapsules incorporated fabric, a piece of 5 \times 5 cm^2 microcapsule incorporated cotton fabric was stirred at 500 rpm for 30 min. Cloth disks were cut from the washed cloth and the disks were mechanically crushed to break the attached microcapsules. Antibacterial activity of the microcapsule incor-

porated washed cotton fabric was investigated and the SEM images were also taken of the same cloth.

3. Results and Discussion

3.1. Verification of Lime Oil Microencapsulation

UV-Visible spectra of crushed and uncrushed lime oil microcapsules were used to verify the lime oil encapsulation in microcapsules.

Table 1. UV absorbance of uncrushed and crushed lime oil microcapsules at 243 nm wave length

Test sample	UV absorbance at 243 nm
Uncrushed lime oil microcapsules	No absorbance
Crushed lime oil microcapsules	3.267 ± 0.1

According to the results shown in Table 1, it was observed that the mechanically crushed microcapsules recorded a significantly higher UV absorbance value at 243 nm wavelength compared to the uncrushed microcapsules. Therefore, it can be concluded that lime oil was successfully encapsulated in the prepared microcapsules and the encapsulated oil can be released upon mechanical crushing of the microcapsule wall.

FT-IR spectra were also obtained for unencapsulated lime oil, the crushed microcapsules (Figures 1 & 2), chitosan and gum arabic (Figures 3 & 4) to verify the encapsulation of lime oil.

Similar absorption peaks at characteristic wavelength number were the indication of similar functional groups in crushed microcapsules, unencapsulated lime oil, gum arabic and chitosan spectra. A broad characteristic peak can be observed at 3400 approximately in four spectra. That was an indication of the presence of –OH functional group in all four samples. This functionality can be seen in linalool present in lime oil as well as in gum arabic

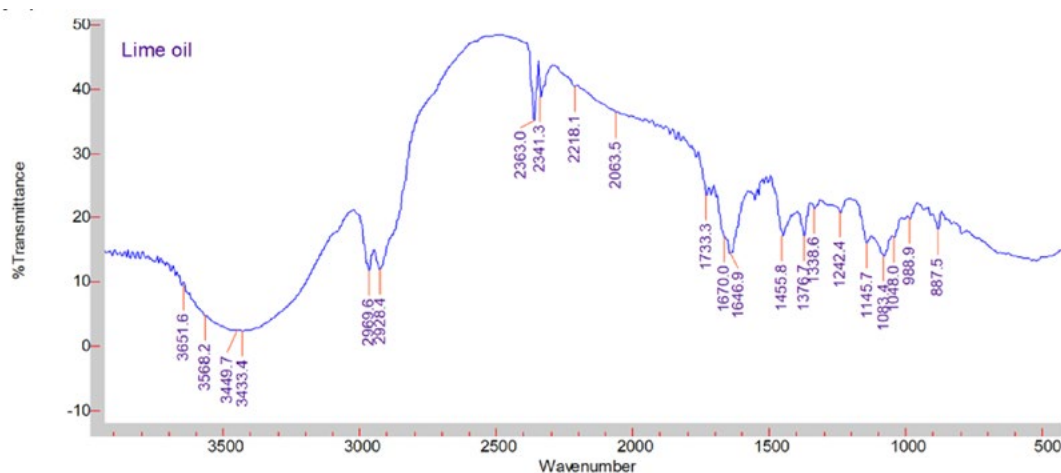


Figure 1. FT-IR spectrum of unencapsulated lime oil

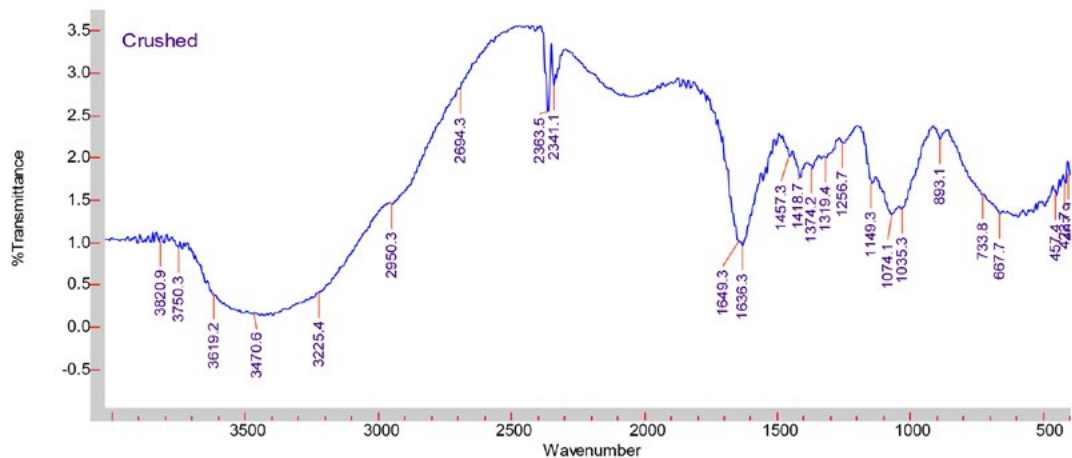


Figure 2. FT-IR spectrum of crushed microcapsules

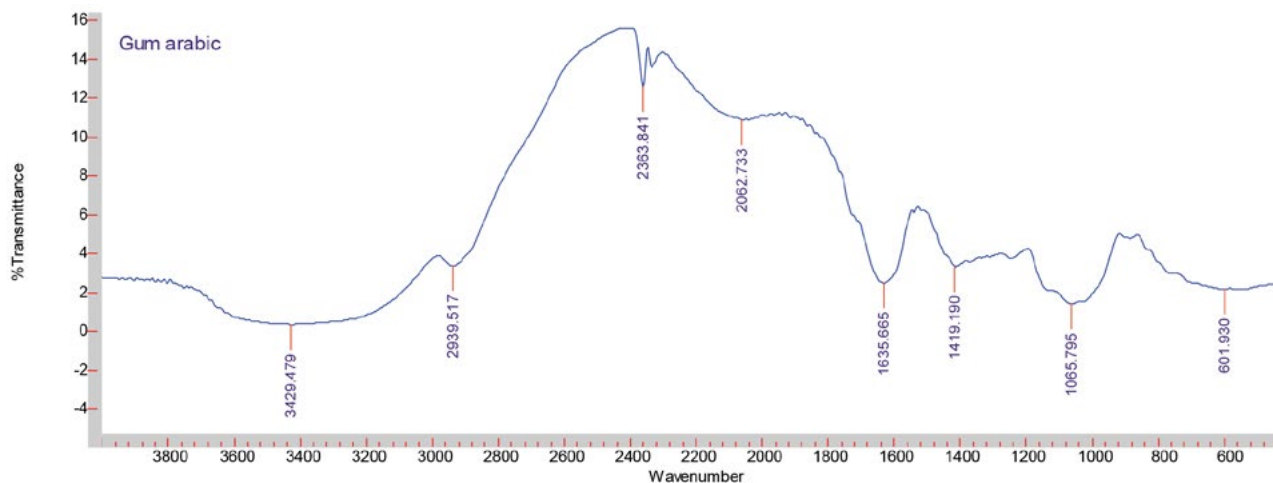


Figure 3. FT-IR spectrum of gum arabic

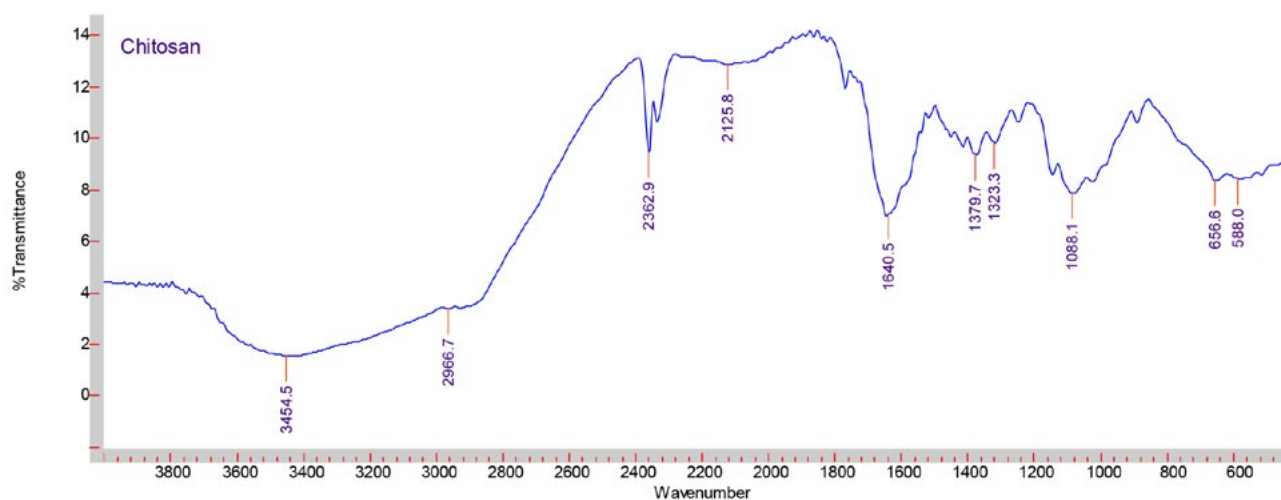


Figure 4. FT-IR spectrum of chitosan

and chitosan. There was an absorption W shaped peak around at 2950 in the unencapsulated lime oil spectrum. It was an indication of the presence of alkyl $-CH$ bonds. This functionality can be seen in limonene which is one of the major constituents of lime oil. The peak that was observed in unencapsulated lime oil and crushed microcapsule spectra around 1650 may be an indication of the presence of a conjugated carbonyl group. This functionality can be seen in citral present in lime oil. Thus, according to the IR data, it can be suggested that lime oil has been successfully encapsulated.

3. 2. Investigation of the Morphology of Lime Microcapsules

The morphological characterization of the resultant lime oil microcapsules was carried out using the optical microscope (Figure 5) and the scanning electron microscope (Figure 6).

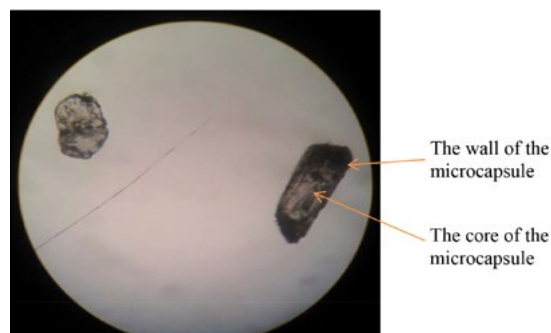


Figure 5. An optical microscopic image of lime oil microcapsules ($\times 100$ magnification)

According to microscopic images, it can be suggested that the resultant lime oil microcapsules were irregular in shape and their sizes ranged between 15–300 μm . The SEM images indicated that the synthesized microcapsules were composed of rough walls.

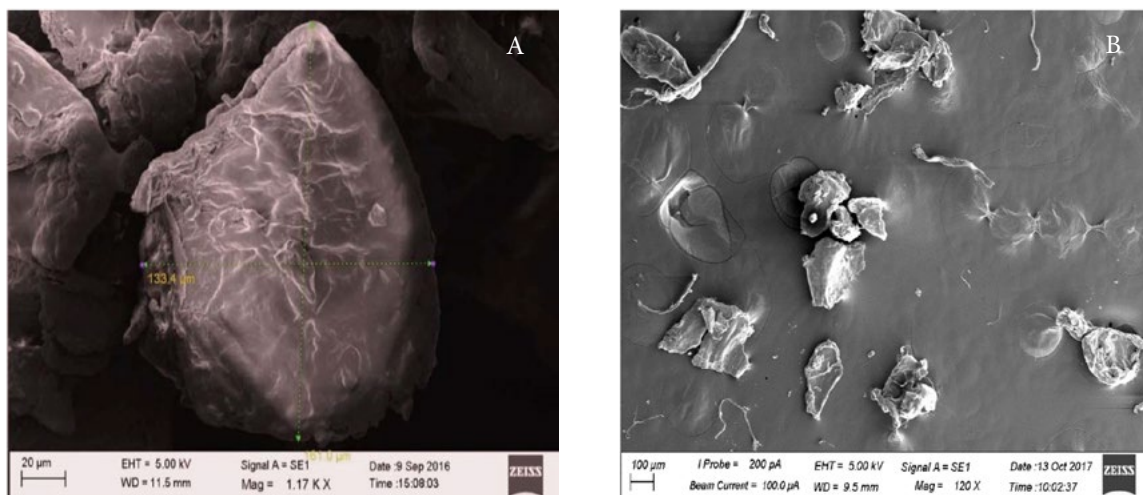


Figure 6. A – The scanning electron microscopic image of lime oil microcapsule ($\times 1.17$ K magnification) B –The scanning electron microscopic image of lime oil microcapsules ($\times 120$ magnification)

3. 3. Determination of the Loading and Loading Efficiency of Lime Oil Microcapsules

The loading efficiency signifies the fraction of lime oil incorporated into microcapsules compared to the total volume of lime used to synthesize the microcapsules. The loading of the lime oil microcapsules was found to be $2940 \pm 138 \mu\text{L/g}$ and the loading efficiency was found to be $82 \pm 4\%$.

3. 4 Folin Ciocalteu Assay

Folin Ciocalteu reagent has the ability to react with a wide range of anti-oxidants present in the test sample.

The results of the Folin Ciocalteu assay are shown below in Table 2.

According to the results in Table 2, it can be concluded that the AOC of lime oil was retained after the encapsulation process. However, the AOC of crushed microcapsules was higher than that resulted from a similar amount

Table 2. Antioxidant capacity (AOC) of unencapsulated lime oil and lime oil microcapsules

Test sample	AOC ($\mu\text{g PGE/g}$)
Unencapsulated lime oil*	916 ± 8
Crushed microcapsules	1336 ± 17

* An equivalent amount of lime oil to that in the crushed microcapsules sample

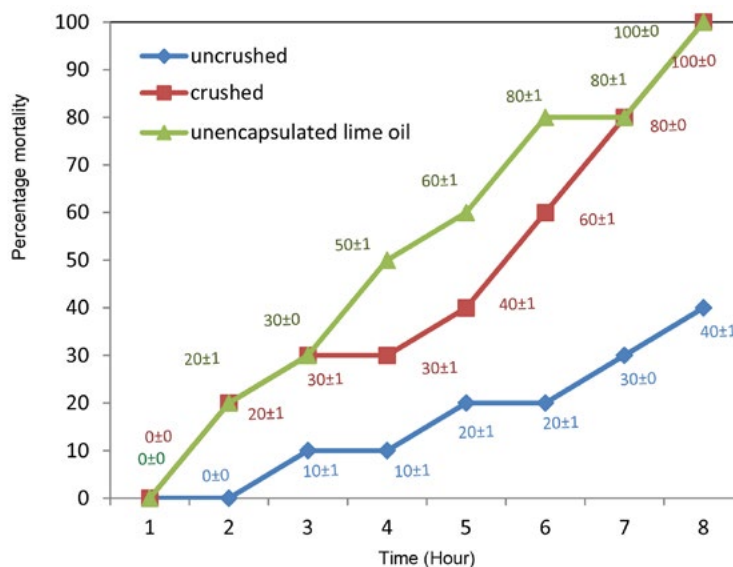


Figure 7. Percentage mortality of shrimp nauplii against time for different lime oil samples

of unencapsulated lime oil. It has been reported that chitosan is an anti-oxidant agent.^{25,26} Therefore, it can be concluded that the extra AOC could be due to the chitosan wall material used to synthesize the lime oil microcapsules.

3. 5. Brine Shrimp Lethality Assay to Test the Cytotoxicity of Lime Oil Microcapsules

The brine shrimp lethality assay carried out with *Artemia salina* naupili can be used to monitor the cytotoxic activity of unencapsulated and encapsulated lime oil.²⁷ The results of the brine shrimp lethality assay are shown in Figure 7.

According to the results, it can be concluded that the brine shrimp lethality was minimized when lime oil was encapsulated compared to the direct use of lime oil.

3. 6. Antibacterial Activity of Lime Oil Microcapsules

The results of the antibacterial studies are shown in Table 3.

Unencapsulated lime oil resulted in inhibition zones for all four tested bacterial strains. Similarly, the crushed microcapsules displayed inhibition zones against all the bacterial strains. However, intact microcapsules did not show inhibition zones against any of the four strains. Therefore, it can be concluded that the encapsulated lime oil was released upon mechanical crushing and displayed similar antibacterial activity as the unencapsulated lime oil.

3. 7. Incorporation of Lime Oil Microcapsules Into Cotton Fabric

Lime oil microcapsules were incorporated into a cotton fabric using succinic acid as the binder. Cotton is composed of cellulose which is the most commonly used natural polymer and it can be chemically modified at the hydroxyl groups that enable the esterification with succinic acid which helps in the attachment of microcapsules to the cotton fabric upon ironing. This is possible as cellulose esters are formed upon heating.¹⁹ A saturated solution of succinic acid was used to dip the microcapsules. These microcapsules were then filtered and used to prepare an

Table 3. Diameter of the inhibition zones for bacterial species with different lime oil samples

Sample	Diameter of the inhibition zone (mm)			
	<i>E.coli</i>	<i>B.cereus</i>	<i>S.typhimurium</i>	<i>S.aureus</i>
Positive control (25 μ L/mL Gentamicin)	24 \pm 0	23 \pm 1	24 \pm 0	24 \pm 1
Negative control (70% ethanol)	NI	NI	NI	NI
Unencapsulated lime oil*	8 \pm 0	8 \pm 1	7 \pm 0	8 \pm 1
Crushed lime oil microcapsules	8 \pm 0	8 \pm 1	7 \pm 0	7 \pm 1
Intact lime oil microcapsules	NI	NI	NI	NI

* An equivalent amount of lime oil to that encapsulated in the crushed microcapsules. NI = No inhibition

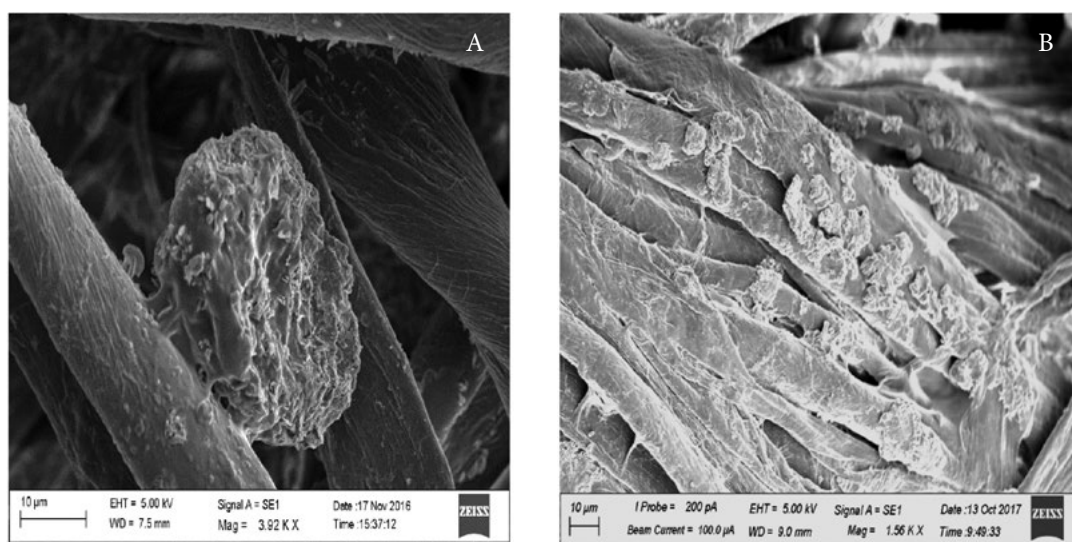


Figure 8. A – SEM images of lime oil microcapsule incorporated textile before washing (\times 3.92 K magnification) B– SEM images of lime oil microcapsules incorporated textile before washing (\times 1.56 K magnification)

aqueous solution of 0.3% microcapsules which was used to dip the cotton fabric.

3. 8. Investigation of Microcapsule Incorporated Cotton Fabric by SEM

The morphological characterization of the resultant lime oil microcapsule incorporated cotton fabric was carried out using scanning electron microscopy. According to the SEM images, adhesion of lime oil microcapsules to the cotton fiber surface can be confirmed (Figure 8).

Furthermore, it was also observed that the lime oil microcapsules retained on the cotton fabric even after being subjected mechanical washing under a rotational speed of 500 rpm (Figure 9).

3. 9. Investigation of Antibacterial Activity of Microcapsule Incorporated Cotton Fabric

The fabric incorporated with lime oil microcapsules was subjected to antibacterial studies. The results of these studies are shown in Table 4.

Cotton fabric containing lime oil microcapsules showed clear inhibition zones against all four bacterial strains compared to the cotton fabric disks without the lime oil microcapsules (negative control). The antibacterial activity of cotton fabric significantly increased when the microcapsules on the fabric were subjected to crushing. Therefore, it can be concluded that the lime oil microcapsule incorporated cotton fabric displays significant antibacterial activity against *E. coli*, *B. cereus*, *S. typhimurium* and *S. aureus* bacterial species upon breakage of the wall of the microcapsules. Furthermore, the lime oil microcapsule incorporated cotton fabric was subjected to washing under 500 rpm rotational speed for 30 min to confer the tolerable washing conditions of the microcapsule treated cotton fabric.

According to the results shown in Table 5, inhibition zones were recorded for all four bacterial strains when the microcapsule containing fabric was washed and then subjected to crushing. However, it can be concluded that the lime oil microcapsules that were attached to the fabric were washed out up to a certain extent under the specified wash conditions with a rotational speed of 500 rpm.

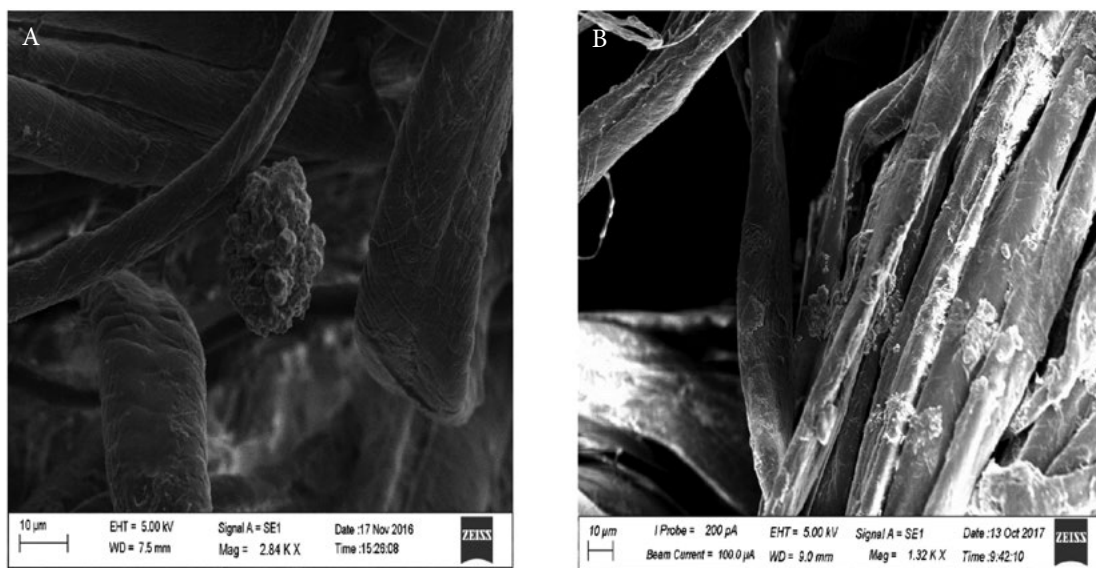


Figure 9. A – SEM images of lime oil microcapsule incorporated textile after washing at 500 rpm ($\times 2.84$ K magnification) B – SEM images of lime oil microcapsules incorporated textile after washing at 500 rpm ($\times 1.32$ K magnification)

Table 4. Antibacterial assay results for the lime oil microcapsule incorporated cotton fabric

Bacterial species	Diameter of the inhibition zone (mm)			
	Positive control (Gentamicin) 25 $\mu\text{L}/\text{mL}$	Negative control [#]	LO incorporated cotton fabric Fabric with intact microcapsules	Fabric subjected to mechanical crushing
<i>E. coli</i>	16 \pm 0	NI	7 \pm 0	10 \pm 0
<i>B. cereus</i>	20 \pm 0	NI	8 \pm 0	14 \pm 1
<i>S. typhimurium</i>	16 \pm 0	NI	7 \pm 0	10 \pm 0
<i>S. aureus</i>	21 \pm 0	NI	7 \pm 0	11 \pm 0

[#] Cotton fabric without lime oil microcapsules NI = No inhibition

Table 5. Antibacterial activity of the microcapsule incorporated cotton fabric after subjecting to washing conditions

Bacterial species	Diameter of the inhibition zones (mm) 500 rpm rotational speed	
	Before crushing	After crushing
<i>E. coli</i>	NI	8 ± 0
<i>B. cereus</i>	NI	8 ± 1
<i>S. typhimurium</i>	NI	7 ± 0
<i>S. aureus</i>	NI	7 ± 1

NI = No inhibition

Three main features of the microcapsule incorporated cotton fabric could be illustrated according to the overall results of this study. However, to improve the retention of microcapsules on the cotton fabric upon washing, a stronger fabric binder can be used during the incorporation of lime oil microcapsules to the fabric.

4. Conclusion

Lime oil microcapsules were successfully prepared via the complex coacervation method using gum arabic and chitosan wall materials. The antioxidant activity and the antibacterial activity of lime oil were preserved upon microencapsulation. The synthesized lime oil microcapsules displayed antibacterial activity against all the four tested bacterial species. Additionally, the cytotoxic activity of unencapsulated lime oil was masked upon microencapsulation. The synthesized lime oil microcapsules were successfully incorporated in to the cotton fabric using succinic acid as the binder. The lime oil incorporated cotton fabric displayed significant antibacterial activity upon mechanical crushing of its microcapsules. The lime oil microcapsules incorporated fabric retained its microcapsules and antibacterial activity even after a mild washing step.

5. References

- S. Y. Cheng, M. C. W. Yuen, C. W. Kan, K. L. Cheuk, C. H. Chui, K. H. Lam, *Int J Mol med.* **2009**, *24*, 411–419.
- M. Leskovšek, G. Jedrinović, U. S. Elesini, *Acta Chim. Slov.* **2004**, *51*, 699–715.
- F. M. Bezerra, O. G. Carmona, C. G. Carmona, M. J. Lis, F. F. Moraes, *Cellulose.* **2016**, *23*(2), 1459–1470.
DOI:10.1007/s10570-016-0882-5
- M. Stoppa, A. Chiolerio, *Sensors* **2014**, *14*, 11957–11992.
DOI:10.3390/s140711957
- S. Y. Cheng, C. W. M. Yuen, C. W. Kan, K. K. L. Cheuk, *RJTA.* **2008**, *12*(4), 41–51.
- A. Jamekhorshid, S. M. Sadrameli, M. Farid, *Renew. Sustain. Energy Rev.* **2014**, *31*, 531–542.
DOI:10.1016/j.rser.2013.12.033
- F. Ozyıldız, S. Karagonlu, G. Basal, A. Uzel, O. Bayraktar, *Lett Appl Microbiol.* **2012**, *56*, 168–179.
DOI:10.1111/lam.12028
- N. V. N. Jyothi, P. M. Prasanna, S. N. Sakarkar, K. S. Prabha, P. S. Ramaiah, G. Y. Srawan. *J. Microencapsul.* **2010**, *27*(3), 187–197. DOI:10.3109/02652040903131301
- S. Khushboo, M. D. Ela, *IOSR-JPTE*, **2015**, *2*(2), 1–4.
- Y. L. X. Zhang, S. Abbas, E. Karangwa, *J Food Eng.* **2012**, *111*, 225–233
- M. A. Teixeira, O. Rodriguez, S. Rodrigues, I. Martins, A. E. Rodrigues. *AIChE J.* **2012**, *58*, 1939–1950.
DOI:10.1002/aic.12715
- G. Nelson, *Int. J. Pharm.* **2002**, *242*, 55 – 62.
DOI:10.1016/S0378-5173(02)00141-2
- B. Golja, B. Sumiga, P. F. Tavcer. *J Color. Technol.* **2013**, *129*, 338–346. DOI:10.1111/cote.12044
- L. J. Reddy, R. D. Jalli, B. Jose, S. Gopu. *AJBPR*, **2012**, *2*, 346–354
- R. Gobato, A. Gobato, D. F. G. Fedrigo. *Parana J Sci Educ.* **2015**, *1*, 1–10.
- S. Mahmud, M. Saleem, S. Siddique, R. Ahmed, R. Khanum, Z. Perveen. *J. Saudi Chem. Soc.* **2009**, *13*, 195–198
DOI:10.1016/j.jscs.2009.03.001
- M. C. Colecio-Juárez, R. E. Rubio-Núñez, J. E. Botello-Álvarez, G. M. Martínez-González1, J. L. Navarrete-Bolaños, H. Jiménez-Islas. *Chil J Agr.* **2012**, *72*(2), 275–280.
- D. Hamdan, M. Z. E-Readi, E. Nibret, F. Sporer, N. Farrag, A. E-Shazly, M. Wink. *Pharmazie*, **2010**, *65*, 141–147.
- T.A.Lazalle, Method and composition to infuse an active ingredient into clothes and use of binder agent for microcapsules of said composition, EP Patent Number 2682454A1, date of patent January 8, **2014**.
- Amid, M. Manap, Y. Zohdi, N. K. *Molecules*, **2014**, *19*, 3731–3743. DOI:10.3390/molecules19033731
- Soliman, E. A. El-moghazy, A. Y. El-din, M. S. M.; Massoud, M. A. *Journal of encasulation and adsorption studies* **2013**, 48–55.
- Patrick, K. E. Abbas, S. Ntsama, I. S. B. Zhang, X. *Pak. J. Food Sci.* **2013**, *23* (1), 17–25.
- Teklani, P.; Perera, B. G. K. *Int j Res Pharm Sci.* **2016**, *6* (1), 30–35.
- Agbor, G. A. Vinson, J. A. Donnelly, P. E. *Int J Food Sci Nutr Diet.* **2014**, *3*(8), 147–156.

25. H. Espinosa-Andrews, J. G. Baez-Gonzalez, F. Cruz-Sosa, E. J. Vernon-Carter. *Biomacromolecules*, **2007**, 8, 1313–1318
DOI:10.1021/bm0611634
26. Dutta, P. K. Dutta, J. Tripathi, V. S. *J Sci Ind Res*, **2004**, 63, pp 20–31
27. Hamid, K. Sultana, S. Urmi, K. F. Ullahc, M. O. Zulfiker, A. H. Hossain, Jordan, A. *Int. J. Biol. Sci*, **2011**, 4 (1), 51–54.

Povzetek

V pričujoči študiji smo se osredotočili na uporabo tehnike mikrokapsulacije za pripravo antioksidantne in antibakterijske aktivne "pametne" bombažne tkanine, ki vsebuje enkapsulirano olje limete (LO). Mikrokapsule z oljem limete so bile pripravljene s kompleksno koacervacijsko metodo z uporabo hitozana in gumi arabike kot materialov za stene kapsul. Z metodama UV-VIS in FTIR spektroskopije smo preverili uspešno enkapsulacijo olja limete. Sintetizirane mikrokapsule z oljem limete so nepravilnih oblik in se glede na optične in SEM slike razlikujejo po velikosti (15–160 μm). Ugotovljeno je bilo, da je nalaganje mikrokapsul znašalo $2943 \pm 128 \mu\text{L/g}$ z učinkovitostjo nalaganja $82 \pm 4\%$. Antioksidativna aktivnost mikrokapsul z oljem limete je bila $1336 \pm 17 \mu\text{g PGE/g}$ (test Folin-Ciocalteu). Analiza smrtnosti solinskih rakcev kaže, da je bila citotoksičnost olja limete minimalizirana z mikrokapsulacijo. Sukcinsko kislino smo uporabili kot vezivo za pritrnitev mikrokapsul z oljem limete na bombažno tkanino. Slike SEM so potrdile stabilno pritrnitev mikrokapsul na bombažna vlakna. Bombažna tkanina, ki vsebuje mikrokapsule z oljem limete, je pokazala pomembno protibakterijsko aktivnost napram štirim vrstam bakterij tako pred kot tudi po pranju.

Scientific paper

Effect of Chemical Pre-treatments on Bioethanol Production from *Chlorella minutissima*

Burcu Şerbetçioğlu Sert, Benan İnan and Didem Özçimen*

Faculty of Chemical and Metallurgical Engineering, Department of Bioengineering, Yildiz Technical University, Davutpasa Campus, 34220 Esenler-Istanbul, Turkey

* Corresponding author: E-mail: ozcimen@yildiz.edu.tr

Received: 01-08-2017

Abstract

In recent years, algal bioethanol production comes into prominence as a trend towards sustainable development. Due to being sustainable energy source and environmental friendly, bioethanol production from algae is becoming increasingly popular all over the world. However, yield of bioethanol production from algae is lower than first generation feedstock's currently, and needs to be improved. In order to increase bioethanol yield, pre-treatments should be performed as cell disruption process on algal biomass. For this reason, researchers investigate the most appropriate pre-treatment method and its parameters for high yield bioethanol production from algae. In this study, cultivated *Chlorella minutissima* was utilized for bioethanol production. Effects of pre-treatment method (dilute acid and alkaline), chemical concentration, pre-treatment temperature and pre-treatment time on bioethanol yield were investigated. It was found that, the highest bioethanol yield was obtained as 18.52% with acid pre-treatment at pre-treatment temperature of 100 °C and pre-treatment time of 60 minutes.

Keywords: Bioethanol, biofuel, biomass, *Chlorella minutissima*, microalgae

1. Introduction

Increase in the world population and emerging industry cause an increase in energy demand which are met by fossil fuels. However, fossil fuel resources are exhausting from day to day, and this decline in the reserves increases the price of petroleum fuels because of political impacts. Negative effects of petroleum fuels on environment, increased greenhouse gas emissions and global warming cause countries to take action on this matter. In order to reduce the environmental problems, increase socio-economic development and provide sustainable energy, utilizing renewable energy technologies such as solar, wind, hydro, and biomass, has been considered.¹ As a renewable energy source, biofuel is one of the promising alternatives to the fossil fuels. Today, bioethanol has been identified as the most widely used biofuel for transportation worldwide.² Bioethanol is produced from sugars and starch-rich raw materials such as corn, wheat and sugarcane. It can be blended with gasoline in different ratios, and there are specially designed engines which can use 100% bioethanol.² Bioethanol has excellent fuel properties for spark ignition internal combustion engines because of its high octane and heat of vaporization. In comparison with gasoline, these properties make ethanol more

efficient as a pure fuel.³ Currently, bioethanol production is mostly carried out with sugarcane and corn as first generation bioethanol feedstock. Still, it is merely meet the current demand, and there are many conflicts and debates about their sustainability due to the depletion of water sources and the use of arable land to produce biomass for bioethanol production.^{4,5} Although lignocellulosic biomass is an alternative source for first generation bioethanol feedstocks, it requires intensive labor and a high capital cost for processing.⁵ Algae are considered as third generation biofuel feedstock and capable of generating more organic carbon per hectare than terrestrial plants. Except Asia, algae avoid the food versus fuel argument since they are not a major food source.⁶ Biomass production of algae is 5–10-times greater than that of land-based plants due to their more photosynthetic efficiency.⁵ Algae grow rapidly and can be easily grown in various aquatic environments such as fresh water, saline water or municipal waste water. Microalgae don't need structural biopolymers such as hemicellulose and lignin which are necessary for terrestrial plants. This simplifies the process of bioethanol production from microalgae.⁷ Microalgae which have high amount of starch such as *Chlorella*, *Dunaliella*, *Chlamydomonas*, *Scenedesmus* are very useful for bioethanol production. Like as other bioethanol feed-

stocks, algae are pre-treated with various methods before fermentation process. Although there are different pre-treatment methods for different biomass sources such as physical, chemical, physio-chemical and biological pre-treatments, chemical pre-treatments are the most used techniques for pre-treatment of algal biomass.⁸ Chemical pre-treatments are easy to perform, and good conversion yields can be achieved with these pre-treatments in a short time.⁹ According to the BP statistical review of world energy-2016 report, ethanol production of the world is higher than biodiesel production.¹⁰ In the last decade, the increase of the production of ethanol is quite remarkable, and due to the global warming and high oil prices, it is considered that the ethanol production will continue to increase. Although there are a lot of studies on biodiesel production from different type of microalgae species in the literature, researches on bioethanol production from microalgae are less. In this study, cultivation of *C. minutissima* was carried out in lab-scale reactor, and the growth of microalgae was monitored with optical density analysis. Obtained algal biomass was analyzed with various analytical methods. During the bioethanol production from *C. minutissima*, in order to compare the effect of pre-treatment methods on bioethanol yield, acid and alkaline pre-treatments were performed. Effects of concentration, pre-treatment temperature and pre-treatment time on bioethanol yield were also investigated. There is not any study which is on the bioethanol production from *C. minutissima* and the comparison of chemical pre-treatment methods in the literature. The results of this study will contribute to the further studies and industrial applications by determining the efficient pre-treatment conditions for bioethanol production from microalgae.

2. Experimental Section

2. 1. Materials

C. minutissima microalgae was cultivated in Bioengineering Department of Yıldız Technical University. In the cultivation step, BBM culture media was prepared with 0.075 g K_2HPO_4 , 0.014 g KH_2PO_4 , 0.075 g $MgSO_4 \cdot 7H_2O$, 0.09 g $NaNO_3$, 0.025 g $CaCl_2 \cdot 2H_2O$, 0.025 g $NaCl$, 0.05 g $EDTA-Na_4$, 0.00498 g $FeSO_4 \cdot 7H_2O$, 0.01142 g H_3BO_3 , 0.232 mg $MnCl_2 \cdot 4H_2O$, 1.41 mg $ZnSO_4 \cdot 7H_2O$, 0.252 mg $CuSO_4 \cdot 5H_2O$, 0.192 mg $NaMoO_4 \cdot 5H_2O$. All of these chemicals were supplied from Merck. As for the pre-treatments and analytical measurements, KOH (Merck) and H_2SO_4 (98% concentrated, Merck), and 96% purity ethanol (Merck), phenol (Sigma-Aldrich) and D-Glucose (Sigma-Aldrich) were used, respectively. LB Broth (Merck) was supplied to use in fermentation step.

2. 2. Biomass Cultivation

Cultures of the *C. minutissima* were firstly cultivated in 500 mL Erlenmeyer flasks in BBM medium at pH 7.8 in

a shaking incubator set to 150 rpm at 25 ± 3 °C under continuous illumination. In logarithmic phase of the cultures, 10% (v/v) inoculum was transferred to the 20 L photobioreactor, and cultivation was carried out with working volume of 15 L at 27 °C and pH 8.3. A pump was used for aeration of the culture medium. Bioreactor was exposed to six pink-fluorescent lamps continuously (4500 lux). Growth of the culture was monitored by optical density measurement. Samples were taken from the photobioreactor and analysed daily. The conductivity of the medium and pH were measured as 256 mS/cm and 8.2, respectively. Harvested algae were centrifuged and dried in an oven for 24 h at 70 °C.

2. 3. Pre-treatment of Microalgal Biomass

Dried microalgal biomass was pre-treated to degrade cellulosic cell wall for accessing fermentable carbohydrate components. Acid pre-treatments were performed with 0.5 N, 1 N, 2 N, 3 N and 5 N H_2SO_4 solutions at different temperatures (100 °C, 120 °C and 140 °C) and pre-treatment times (15, 30 and 60 minutes). Pre-treatment conditions were chosen according to the previous studies in the literature. In order to compare the effect of pre-treatment type on bioethanol yield, alkaline pre-treatments were also carried out. Alkaline pre-treatments were conducted with various concentrations of KOH solutions (0.5%, 0.75%, 1%, 1.5% and 2% (w/v)) at the different pre-treatment temperatures (80 °C, 100 °C and 120 °C) and pre-treatment times (15, 30 and 60 minutes). After pre-treatments, samples in flasks were cooled down to the room temperature. The liquid from pre-treatment was neutralized before the fermentation. pH was maintained at 4.8 by alkaline/acid solutions.

2. 4. Bioethanol Production

The day before the fermentation, *S. cerevisia* yeast was cultured in flask with LB medium at the temperature of 40 °C and 150 rpm shaking speed. 3% (v/v) of yeast was inoculated to the pre-treated samples and fermentation was carried out in an incubator set to 150 rpm and 40 °C for 48 h. 5 ml were taken from the samples to determine the concentration of bioethanol by gas chromatography (GC) analysis.

2. 5. Analytical Methods

During the microalgae cultivation, optical density measurement of the culture was used to monitor the algal growth. Optical density was measured by using UV-visible spectrophotometer at 680 nm. Productivity of *C. minutissima* was expressed as the specific growth rate (μ) and doubling time (t_d) by using the Equation 1–2 from the cell density change during specific time period of exponential phase.¹¹

$$\mu = \frac{\ln \frac{N(t)}{N(0)}}{t} \quad (1)$$

$$td = \frac{\ln 2}{\mu} \quad (2)$$

Carbohydrate analysis, lipid analysis and protein analysis were carried out with Phenol-sulfuric acid method, Soxhlet Ethanol Extraction and Lowry method, respectively.

Characterization of *C. minutissima* was also performed with Fourier Transform Infrared spectroscopy (FTIR spectroscopy) and proximate analysis. Proximate analysis was performed with TA instrument (Q600 SDT) according to ASTM-E 1755-01 and ASTM-D E872-82 standards. FTIR spectroscopy was carried out with the instrument of Thermoscientific (Nicolet 6700) and functional groups were determined in the wavenumber range of an IR spectrum of 600–4000 cm^{-1} .

YL 6100 GC gas chromatography was used to evaluate bioethanol concentration. Samples from fermentation process (at 24 h and 48 h) were taken and prepared for GC instrument for further analysis. Firstly, samples were filtered using 0.45 μm filters to avoid blocking in column. The GC gas chromatograph contains flame ionization detector (FID) and 30 m \times 0.32 mm \times 0.25 μm ZB-FFAP column. The temperature of injector, detector and oven were maintained at 150 $^{\circ}\text{C}$, 250 $^{\circ}\text{C}$ and 100 $^{\circ}\text{C}$, respectively. Hydrogen was used as carrier gas. Bioethanol concentration was calculated using calibration curve that was prepared by the different concentration of bioethanol standards (0.1%–10% (v/v)). The mean and standard deviations of the data were calculated, and data were presented as the mean of three.

3. Results and Discussion

3.1. Growth of *C. minutissima* Microalgae

Growth of *C. minutissima* was monitored by optical density measurement. Specific growth rate was calculated as 0.0879 day^{-1} and the doubling time of the microalgal cells was calculated as 7.8 days in photobioreactor environment. Although there are studies in which microalgae have less doubling time than 7 days, it is a remarkable growth because the aeration may overwhelm stress in photobioreactor environment and microalgae may need more time to multiply according to Kawaroe et al.¹² Lim et al. also reported that doubling time of microalgae can be up to 6–7 days in 100 ml of flask.¹³ Results of chemical composition and proximate analysis of *C. minutissima* were given in the Table 1, and FTIR analysis results were given in the Table 2 and Fig 1. As can be seen from the FTIR results given in Table 2, aliphatic CH stretching at 2922 cm^{-1} is caused by cycloparaffin structure.¹⁴ C=C ring stretching in bands between 1400 and 1600 cm^{-1} indicate presence of alkenes.¹⁵ Bands show that symmetrical and asymmetrical C–H stretching linked to $-\text{CH}_2$ group, derived from ali-

phatic hydrocarbons and saturated aliphatic cyclic hydrocarbon.¹⁶ 1743 cm^{-1} band (C = O) indicates the presence of lipids, fatty acids and ester groups. The region from 1200 to 900 cm^{-1} signifies a sequence of bands due to C–O, C–C and C–O–C stretching vibrations of polysaccharides.

Table 1. Chemical composition and proximate analysis of *C. minutissima*

Biochemical Analysis	Content (%)	Proximate Analysis	Content (%)
Carbohydrate	33.05	Ash	9.39
Protein	24.69	Moisture	4.71
Lipid	42.26	Volatile substance	75.63
		Fixed carbon	10.04

Table 2. FTIR analysis of *C. minutissima*

Wave number (cm^{-1})	Functional Groups
3275	–OH stretching
2922	Aliphatic CH stretching
1743	C=O stretching
1643	Aromatic C=C ring stretching
1537	Aromatic C=C ring stretching
1462	CH stretching in methyl lipids
1398	Aliphatic CH_3 deformation
1274	Aromatic CO– stretching
1257	Aliphatic C–N stretching
1037	Aliphatic ether C–O and alcohol C–O stretching
765	4 adjacent H deformation

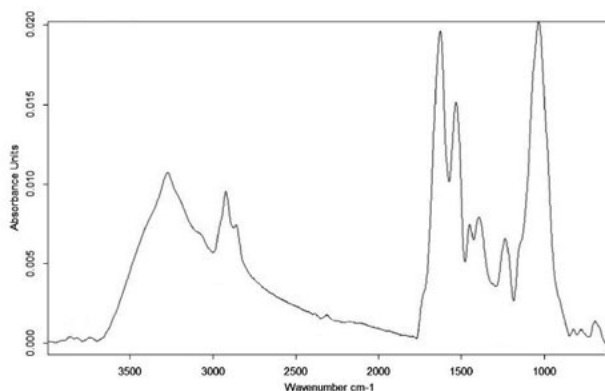


Fig 1. FTIR spectrum of *C. minutissima*

3.2. Effect of Acid and Alkaline Concentrations on Bioethanol Production

In order to investigate the effect of acid concentration on bioethanol yield, acid pre-treatments were performed with 0.5 N, 1 N, 2 N, 3 N and 5N H_2SO_4 solutions

under the temperature of 100 °C and pre-treatment time of 60 min. As can be seen in the Fig 2, bioethanol yields were obtained between 2.92–4.78% for 24 h and 5.26–18.52% for 48 h fermentation time. It was found that bioethanol yield increases up to a certain acid concentration. The highest bioethanol yield was obtained under 1 N H₂SO₄ acid concentration. Above 1 N H₂SO₄, bioethanol yields decreased with 2 N, 3 N and 5 N acid pre-treatments. It is considered that toxic components such as furfuraldehyde, acetate and hydroxymethylfurfuraldehyde may occur due to the effect of acid pre-treatment, and they inhibit the fermentation.¹⁷ Decrease in bioethanol yield in high acid concentrations of pre-treatment was observed. In the study of pre-treatment of *Sargassum* spp. with 1.0–5.0% (m/v) H₂SO₄, it was found that the best result was obtained with 3.4–4.6% acid pre-treatment, and bioethanol yield decreased with increasing acid concentrations.¹⁸ In another study, *Gracilaria* sp. was pretreated with 0.05, 0.1, 0.3 and 0.5 N H₂SO₄, and the highest bioethanol yield was achieved with 1 N acid pre-treatment.¹⁹

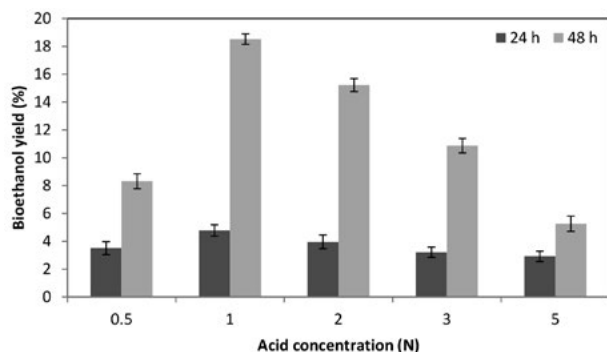


Fig 2. Bioethanol yields obtained from acid pre-treated (at 100 °C, 60 min) microalgae

Experimental data obtained under the conditions of 0.5%, 0.75%, 1%, 1.5%, and 2% (w/v) KOH solutions at 100 °C and 60 min were given in the Fig 3. It was determined that bioethanol yield was changed between 1.01–1.92 % for 24 h, and %1.43–6.11% for 48 h fermentation time. The highest bioethanol yield was obtained with 0.75% (w/v) KOH solution pre-treatment. Like as acid pre-treatment, a decrease was also observed with increasing alkaline concentrations above this concentration. In the literature, the highest bioethanol yield was achieved by pretreating *Chlorococcum infusionum* microalgae under the conditions of 0.75% (w/v) NaOH pre-treatment.²⁰ Also, this can be seen in alkaline pre-treatment of *Ulva lactuca* macroalgae collected from Marmara Sea. It was reported that, bioethanol productivity increased up to a certain concentration, and then it was started to decrease.²¹ The results obtained from this study are in agreement with these studies for bioethanol production. According to the results, it can be said that, acid pre-treatment is more efficient method than alkaline pre-treatment for algal biomass.

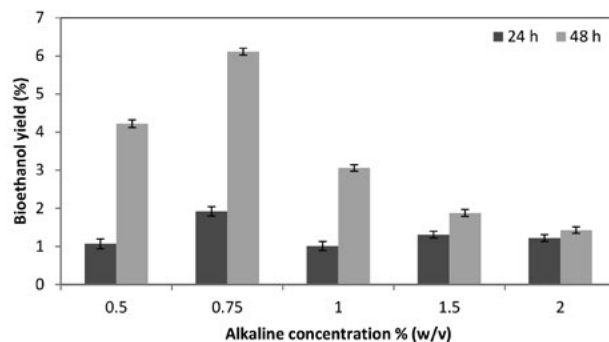


Fig 3. Bioethanol yield obtained after from alkaline pre-treated (at 100 °C, 60 min) microalgae

3. 3. Effect of Pre-treatment Temperature on Bioethanol Production

Results obtained from the experiments performed at 100 °C, 120 °C and 140 °C with 1 N and 5 N H₂SO₄ solutions for 60 min, were given in Fig 4. As it was shown in the figure, bioethanol yield increased up to 120 °C with both 1 N and 5 N pre-treatments. On the other hand, pre-treatments conducted at 140 °C resulted with a decrease in bioethanol yield. Bioethanol yield determined after pre-treatments carried out at high temperatures, increases up to a certain temperature and then, it decreases. This is due to the pre-treatments which change direct solubility of sugars and disrupt the structure of sugar based components.²² Generally, it is reported that, raw materials which contain lignin and hemicellulose, were pretreated at the temperatures above 160 °C with 0.5–1.5% (v/v) acid solutions.²³ In another study, corn fibers were pretreated with sulfuric acid at the temperatures of 120 °C and 140 °C and 60 min pre-treatment time. It was observed that, yield of monomeric carbohydrates decreases with increasing pre-treatment temperatures.²⁴ It is indicated in the literature, experiments should be performed under low pre-treatment temperature and acid concentrations when lignin content of raw materials are not high. Since structure of microalgae is simpler than other materials, it is assumed that monomeric carbohydrates are decomposed to toxic compounds at high temperatures.

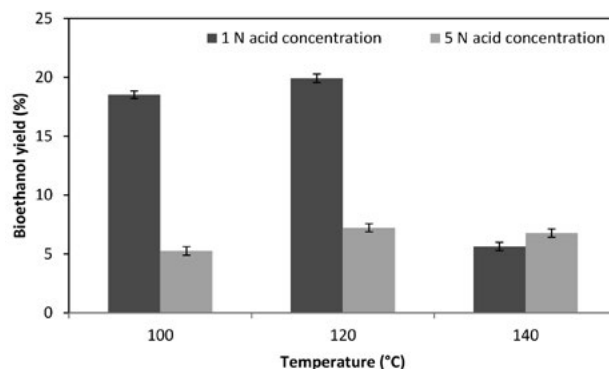


Fig 4. Effect of different acid pre-treatment temperatures on bioethanol yield

Unlike acid pre-treatments, bioethanol yield increased up to 100 °C, then decreased at 120 °C with 0.75% (w/v) KOH alkaline pre-treatment, however, it increased up to 120 °C with 1.5% (w/v) KOH alkaline pre-treatment (Fig 5). It is in agreement with the study carried out with *Chlorococcum infusioinum* microalgae which were pretreated with 0.75% (w/v) NaOH solution for 60 min at 80 °C and 120 °C. In that study, bioethanol yields were obtained as 21.26% and 23.37%, respectively. In higher concentrations of NaOH, yield was determined as 23.75% at 80 °C, and it decreased to 18.74% at 120 °C.²⁰ Therefore, effect of different values of different parameters in the same time is variable and it can be said that it is difficult to assess a parameter alone independently.

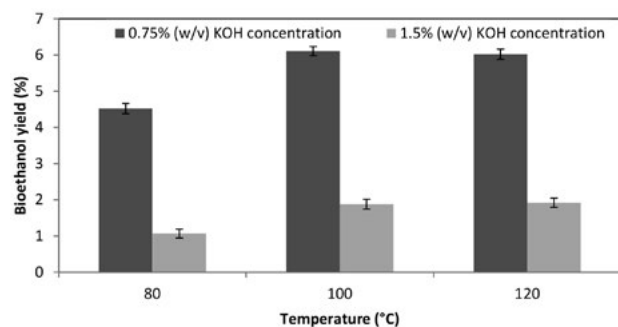


Fig 5. Effect of different alkaline pre-treatment temperatures on bioethanol yield

3. 4. Effect of Pre-treatment Time on Bioethanol Production

In order to investigate the effect of different pre-treatment times on bioethanol production yield, 1 N and 5 N H_2SO_4 acid pre-treatments were carried out at the temperature of 120 °C in the pre-treatment times of 15, 30 and 60 minutes. According to Fig 6, increasing pre-treatment time increases bioethanol yield in both 1 N and 5 N acid pre-treatments. In the literature, the highest bioethanol yield was obtained for *Scenedesmus obliquus* microalgae under 2% H_2SO_4 pre-treatment at 121 °C for 20 min.²⁵ In

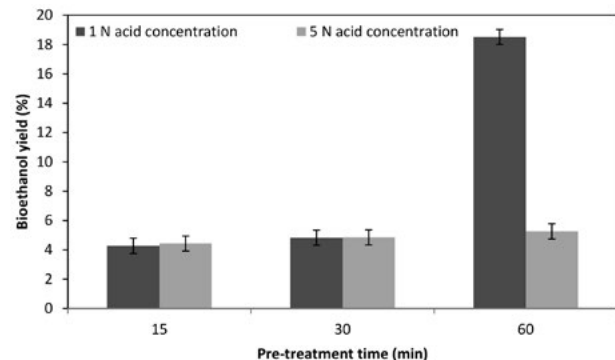


Fig 6. Effect of different acid pre-treatment times on bioethanol yield

another study, corn cob was pretreated with 1% HCl solution for 20–40 min at 100–130 °C, and it was observed that bioethanol yield increased with increasing pre-treatment time.²⁶ This effect was also seen in the study of pretreating *Kappaphycus alvarezii* macroalgae with 1–1.5–2% H_2SO_4 at 121 °C for 20, 40 and 60 min. It was found that the highest productivity was achieved with 1% H_2SO_4 solution and 60 min pre-treatment time.²³

Results of the experiments conducted at 100 °C for 15, 30 and 60 min with 0.75 and 1.5% (w/v) KOH solution were given in Fig 7. As can be seen in Fig 7, the highest yield was obtained under the conditions of 0.75% (w/v) KOH solution for 60 min. On the other hand, the highest yield was obtained with 15 min using 1.5% (w/v) KOH solution. Results of bioethanol yields were similar for 15–30 min pre-treatments under the condition of 0.75% (w/v) KOH pre-treatment, however, it was observed that an increase was occurred after 60 min. On the other hand, bioethanol yield decreased after 15 min pre-treatment time with 1.5% (w/v) KOH pre-treatment. In the study which performs alkaline pre-treatment on *Chlorococcum infusioinum* microalgae, bioethanol yield increased from 12.88% to 21.26% at 80 °C with the pre-treatment time of 30 and 60 min after the treatment of 0.75% (w/v) NaOH solution. However a slight decrease was seen at 120 °C under the same pre-treatment time. After the treatment of 2% (w/v) NaOH solutions, small increases and decreases were observed at the temperatures of 80 °C and 120 °C for 30 and 60 min.²⁰

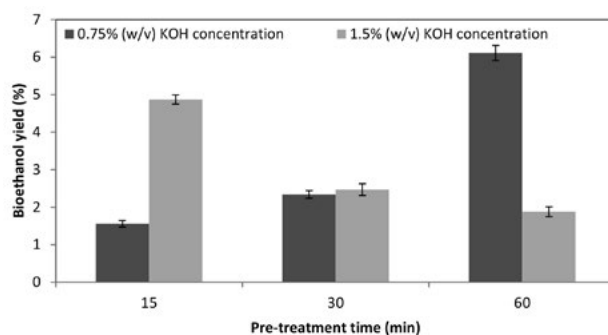


Fig 7. Effect of different alkaline pre-treatment times on bioethanol yield

4. Conclusion

In this study, *C. minutissima* was cultivated for bioethanol production, and applications of acid and alkaline pre-treatments were conducted before the fermentation, and effects of solution concentration, pre-treatment time and pre-treatment temperature on bioethanol yield were investigated. When acid pre-treatment was performed at 100 °C with 1 N H_2SO_4 for 60 minutes, the highest bioethanol concentration was obtained as 18.52% which was almost three times higher than alkaline

pre-treatment. Nowadays, algae are mostly utilized for biodiesel production due to their high lipid content. However, high operational costs lead the investigators to find new production methods or utilize algal biomass completely with biorefinery aspects. Algae have considerable carbohydrate content that cannot be ignored. Bioethanol production from algae is a technology ongoing in the last decade and open to development. Nevertheless, innovative and efficient fermentation processes and pre-treatment techniques are still needed to make ethanol production preferable.

5. Acknowledgement

The authors acknowledge financial support from the Yıldız Technical University Scientific Research project (2015-07-04-YL03) provided for this work.

6. References

1. D. Özçimen, A. Ersoy-Meriçboyu, *Fuel Process. Technol.* **2008**, *89(11)*, 1041–1046. DOI:10.1016/j.fuproc.2008.04.006
2. A. Cesaro, V. Belgiorno, *Energ.* **2015**, *8(8)*, 8121–8144. DOI:10.3390/en8088121
3. J. Yu, T. Tan, *Fuel Process. Technol.* **2008**, *89(11)*, 1056–1059. DOI:10.1016/j.fuproc.2008.04.008
4. M. Vohra, J. Manwar, R. Manmode, S. Padgilwar, S. Patil, *J. Environ. Chem. Eng.* **2014**, *2(1)*, 573–584. DOI:10.1016/j.jece.2013.10.013
5. R. Bibi, Z. Ahmad, M. Imran, S. Hussain, A. Ditta, S. Mahmood, A. Khalid, *Renewable Sustainable Energy Rev.* **2017**, *71*, 976–985. DOI:10.1016/j.rser.2016.12.126
6. J. M. M. Adams, G. Bleathman, D. Thomas, J.A. Gallagher, *J. Appl. Phycol.* **2017**, 1–7.
7. R. P. John, G. S. Anisha, K. M. Nampoothiri, A. Pandey, *Biore-sour. Technol.* **2011**, *102(1)*: 186–193. DOI:10.1016/j.biortech.2010.06.139
8. J. Zhao, L. Xia, *Fuel Process. Technol.* **2010**, *91(12)*, 1807–1811. DOI:10.1016/j.fuproc.2010.08.002
9. J. Hill, E. Nelson, D. Tilman, S. Polasky, D. Tiffany, *Proc. Natl. Acad. Sci.* **2006**, *103(30)*: 11206–11210. DOI:10.1073/pnas.0604600103
10. BP Statistical Review of World Energy June 2016, <https://www.bp.com/content/dam/bp/pdf/energy-economics/statistical-review-2016/bp-statistical-review-of-world-energy-2016-full-report.pdf>, (assessed: February 01, 2017)
11. F. Widdel, Theory and measurement of bacterial growth. Di Dalam Grundpraktikum Mikrobiologie, **2007**, 1–11. Retrieved from <https://www.mpi-bremen.de/Binaries/Binary13037/Wachstumsversuch.pdf>, (assessed: February 15, 2017)
12. M. Kawaroe, J. Hwangbo, D. Augustine, H. A. Putra, *Aquaculture, Aquarium, Conservation & Legislation-International Journal of the Bioflux Society (AACL Bioflux)*, **2015**, *8(5)*.
13. D. K. Lim, S. Garg, M. Timmins, E.S. Zhang, S.R. Thomas-Hall, H. Schuhmann, P.M. Schenk, *PLoS One*, **2012**, *7(7)*, 1–13 DOI:10.1371/journal.pone.0040751
14. J. A. Vieira Costa, M. G. de Morais, in A. Pandey, D. Lee, Y. Chisti, and C. Rsocol (Ed.): *Biofuels From Algae*, Elsevier, USA. **2014**, pp.1–22.
15. T. Aysu, M. M. Küçük, *Energ.* **2014**, *64*, 1002–1025. DOI:10.1016/j.energy.2013.11.053
16. G. Y. Elbeyli, PhD Thesis, Yıldız Technical University, **2005**, Istanbul, Turkey.
17. J. W. Lee, J. Y. Kim, H. M. Jang, M. W. Lee, J. M. Park, *Biore-sour. Technol.* **2015**, *182*: 296–301 DOI:10.1016/j.biortech.2015.01.116
18. M. G. Borines, R. L. de Leon, J. L. Cuello, *Biore-sour. Technol.* **2013**, *138*: 22–29. DOI:10.1016/j.biortech.2013.03.108
19. F. C. Wu, J. Y. Wu, Y. J. Liao, M. Y. Wang, L. Shih, *Biore-sour. Technol.* **2014**, *156*: 126–131 DOI:10.1016/j.biortech.2014.01.024
20. R. Harun, W. S. Y. Jason, T. Cherrington, M. K. Danquah, *Appl Energy.* **2011**, *88*, 3464–3467. DOI:10.1016/j.apenergy.2010.10.048
21. Inan, B, Master's Thesis. Yıldız Technical University, **2014**, Istanbul, Turkey.
22. R. Harun, M. K. Danquah, *Process Biochem.*, **2011**, *46(1)*: 304–309. DOI:10.1016/j.procbio.2010.08.027
23. P. L. Hargreaves, C. A. Barcelos, A. C. Augusto da Costa, N. Pereira Jr., *Biore-sour. Technol.* **2013**, *134*: 257–263. DOI:10.1016/j.biortech.2013.02.002
24. H. Noureddini, J. Byun, *Biore-sour. Technol.* **2010**, *101(3)*: 1060–1067. DOI:10.1016/j.biortech.2009.08.094
25. J. Lee, P. Li, J. Lee, H. J. Ryu, K. K. Oha, *Biore-sour. Technol.* **2013**, *127*:119–125. DOI:10.1016/j.biortech.2012.09.122
26. S. Zu, W. Li, M. Zhang, Z. Li, Z. Wang, H. Jameel, H. Chang, *Biore-sour. Technol.* **2014**, *152*: 364–370. DOI:10.1016/j.biortech.2013.11.034

Povzetek

Zaradi okolju prijazne tehnologije postaja v zadnjih letih po vsem svetu vse bolj popularna proizvodnja bioetanola iz algne biomase. Žal so izkoristki v primerjavi z drugimi tradicionalnimi surovinami slabi, zato jih je potrebno izboljšati. Podobno kot pri prvi in drugi generaciji surovin za proizvodnjo bioetanola se izvajajo različne vrste predpriprav algne biomase. Na tem področju raziskovalci proučujejo primerno metodo in ustrezne parametre za visoke izkoristke. V predstavljeni raziskavi je bila za optimiranje predpriprave uporabljena biomasa alge *Chlorella minutissima* v kislem in bazičnem mediju. Proučevani so bili vplivi koncentracije kemikalij, temperature in časa na izkoristek proizvodnje etanola. Rezultati so pokazali, da je bil najvišji izkoristek dosežen s predpripravo v kislem mediju.

Scientific paper

A Comparative Study on a Cationic Dye Removal through Homogeneous and Heterogeneous Fenton Oxidation Systems

Shima Rahim Pouran,^{1,*} Abolfazl Bayrami,² Mohammad Saleh Shafeeyan,^{3,*} Abdul Aziz Abdul Raman⁴ and Wan Mohd Ashri Wan Daud⁴

¹ Research Laboratory of Advanced Water and Wastewater Treatment Processes, Department of Applied Chemistry, Faculty of Chemistry, University of Tabriz, 51666-16471 Tabriz, Iran.

² Department of Biology, Faculty of Science, University of Mohaghegh Ardabili, Ardabil, Iran.

³ Department of Chemical and Materials Engineering, Buein Zahra Technical University, Qazvin, Iran.

⁴ Chemical Engineering Department, Faculty of Engineering, University of Malaya, 50603 Kuala Lumpur, Malaysia.

* Corresponding author: E-mail: rahimpooran@yahoo.com (S. Rahim Pouran), ms.shafeeyan@gmail.com (M.S. Shafeeyan)

Received: 03-08-2017

Abstract

Oxidative treatment of a cationic dye solution, methylene blue, was investigated using magnetite nanoparticles and goethite in heterogeneous Fenton-like reaction, and ferrous ions in homogeneous Fenton-reaction. The aim was to compare the degradation efficiencies of the studied catalysts for decolorization of methylene blue solution as the model organic pollutant. Response surface methodology (RSM) was applied to determine the optimal operational conditions for magnetite/H₂O₂ and goethite/H₂O₂ systems. The [H₂O₂] of 0.2 M, catalyst dosage of 1 g/L, pH 9.0 and reaction time of 5h were chosen by RSM. The pH value of 3.0 was used in the case of Fe²⁺/H₂O₂ system. The experimental results showed that homogeneous Fenton oxidation system was the most effective system under both acidic and neutral conditions but decreased at pH value of 9.0 due to the decrease in available Fe²⁺ ions in the solution and generation of ferric hydroxide sludge. Fe₃O₄/H₂O₂ system represented better removal efficiency than FeO(OH)/H₂O₂ system that could be attributed to the presence of Fe^{II} cations in magnetite structure and its larger surface area.

Keywords: Heterogeneous Fenton, Response surface methodology, Magnetite nano-particles, Goethite

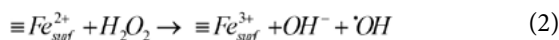
1. Introduction

Tones of synthetic dyes are produced universally due to their wide applications in many industries, especially textiles. Since dyes are considered as one of the severe environmental pollutants, a large number of studies were opened to minimize their impact on human health and the environment.^{1–6} Advanced oxidation processes (AOPs) are among the most accepted treatment methods for removal of dyes and pigments. The generation of highly reactive species is the key factor for effective decomposition of organic pollutants through AOPs. Fenton reaction has attracted considerable attention due to its simple equipment, ease of operation and higher efficiency.^{7–10} In this reaction, the catalytic activity of iron species leads to H₂O₂ breakdown into highly reactive hydroxyl radicals (Eq. 1):



There are large numbers of studies on Fenton treatment of various industrial wastewaters and synthetic solutions at laboratory or pilot plant scales.¹¹ Fenton treatment of synthetic dye solutions such as Alizarin red S dye (C.I. 58005),¹² Acid Blue 193 and Reactive Black 39,¹³ C.I. Basic Red 46 (BR46),¹⁴ and C.I. Acid Red 14 azo dye,¹⁵ are number of the examples reported in literature. In conventional Fenton reaction, using iron salts (Fe²⁺ and Fe³⁺ ions), due to the availability of the reactants in the reaction solution, the degradation rate is high and under the optimal condition, and decolorization occurs within a short reaction time. However, this reaction is effective only at acidic condition of pH 3.0, while the soluble iron is precipitated as ferric hydroxide at higher pH conditions, resulting in the

catalyst withdrawal from the reaction medium. Accordingly, the catalyst recovery is also impracticable. In light of this, a number of solutions have been proposed to overcome the shortcomings of homogeneous Fenton reaction. Application of chelating agents,¹¹ and heterogeneous catalysts,^{11,16} are examples to stabilize the iron in the solution and expand the applicable pH range of the reaction. Large numbers of heterogeneous iron compounds such as zero-valent iron (ZVI),¹⁷ clays, silica, zeolites,¹⁸ and iron minerals,¹⁶ have been studied for dye wastewater treatment through Fenton reaction. In heterogeneous catalysts, iron is fixed in the structure and activates the reaction over broad range of pH (Eq. 2). In addition, it can be simply separated from the solution by magnet or filtering.



In the present study, magnetite and goethite were chosen for heterogeneous Fenton treatment of synthetic MB wastewater. Methylene blue (MB) was selected as the model dye pollutant because of its extensive application in textile industry and recalcitrant nature. Central composite design (CCD) was used to optimize the Fenton-like reactions. The main objective of this study was to assess the efficiency of Fenton reaction catalyzed by magnetite nanoparticles and goethite as heterogeneous catalysts. In addition, the decolorization efficiencies of the studied heterogeneous catalysts were compared with homogeneous Fenton under various pH conditions.

2. Experimental

2.1. Chemicals

All the chemicals were of reagent grade and used without further purification. Catalase (10,000–40,000 units/mg protein), magnetite (Fe₃O₄) and goethite (HFeO₂) were purchased from Sigma Aldrich. Methylene blue (MB), Hydrogen peroxide (H₂O₂, 30% w/w), Ferrous sulfate (FeSO₄·7H₂O), Sodium hydroxide (NaOH) and Sulfuric acid (H₂SO₄) were purchased from Merck. The ferrous (Fe²⁺) catalyst was prepared by dissolving FeSO₄ in distilled water and was used immediately to avoid the rapid oxidation of Fe²⁺.

2.2. Homogeneous Fenton Experiments

Fenton experiments were carried out in batch using a 250 mL borosilicate glass beaker with 100 mL of MB solution at initial pH of 3.0 ± 0.1 (known as the optimum pH),¹⁹ and temperature of 25 °C. The MB solution was acidified using sulfuric acid that was monitored using a Cyber Scan pH meter (Eutech, Thermo Fisher Scientific). Subsequently, a fixed amount of Fe²⁺ was added and Fenton reaction was initiated by addition of predetermined amount of H₂O₂ solution under constant magnetic stirring

to homogenize the mixture.¹¹ At the end of the stipulated time period, the pH was readjusted to 10.0 ± 0.5, leading to reaction termination. The residual H₂O₂ was removed from the solution using a few drops of catalase enzyme (10 V/V).²⁰ A 0.22 μm Millipore filter was used to remove the ferric hydroxide precipitate before the remnants of the MB concentration was monitored. Prior to the measurement, a calibration curve was obtained using standard MB solutions with known concentrations. The following equation (Eq.3) was used to calculate the percentages of color removal:

$$\text{Color removal (\%)} = \frac{(X_0 - X_t)}{X_0} \times 100 \quad (3)$$

where, X₀ is the initial value of color (mg/L) and X_t is the measured value of color (mg/L) after defined reaction time. The reaction was repeated at pH 7.0 ± 0.1 to assess the effectivity at neutral condition and at pH 9.0 ± 0.1. The measurements were done at least in duplicate and the results were expressed as mean values of the measurements with an experimental error below 5%.

2.3. Heterogeneous Fenton Experiments

The MB degradation studies by nano-magnetite and goethite samples were carried out in a batch system at 25 °C. The initial pH of the dye solution was adjusted to 9.0 using NaOH solution. A predetermined amount of each sample was added to dye solution (50 mg/L) and constantly stirred mechanically at 170 rpm for 60 min, to achieve sorption equilibrium. Then, depending on the experimental design, 0.1–0.3 mol/L H₂O₂ was added to solutions to initiate Fenton reaction. After 300 min, the catalyst particles were separated from the solution by centrifugation at 3500 rpm for 5 min and the equilibrium concentration of MB was determined by a UV-Vis spectrophotometer (Spectroquant® Pharo 300) at λ_{max} 664 nm using Eq. (3). The experiments were repeated at pH 7.0 ± 0.1 using 1 g/L of each sample and 0.2 mol/L H₂O₂ (optimum values) to assess the efficiency at neutral condition.

2.4. Design of Experiments (DOE)

Design Expert Software (version 9.0.3) was used for the statistical design of experiments, development of regression models, data analysis and optimization of Fenton-like reactions. Response surface methodology (RSM) was employed to assess the individual and interactive effects of two independent variables: (A) H₂O₂ and (B) catalyst concentrations on color removal efficiencies (%) of both hetero-catalysts. For both catalysts, a face centered CCD that consists of 4 factorial points, 4 axial points and 3 replicates at the center points were applied. The center points were used to estimate the experimental error and the duplicability of the data. The ranges between 0.1–0.3

mol/L for [H₂O₂], 0.5–1.5 g/L for catalysts concentration and oxidation reaction time of 300 min were chosen based on the preliminary studies and the literatures.^{21–23}

A total of 11 experiments were performed for each hetero-catalyst in which three of them were at the center point: (A) = 0.2, (B) = 1. The following second order polynomial equation (Eq. 4) was used to predict the studied variable factors as a function of independent variables and the interaction among them:

$$Y = b_0 + \sum_{i=1}^k b_i X_i + \sum_{i=1}^k b_{ii} X_i^2 + \sum_{i=1}^k \sum_{j=1}^k b_{ij} X_i X_j + \varepsilon \quad (4)$$

where, Y is the predicted dependent variable, b₀ is constant coefficient, b_i, b_{ii} and b_{ij} are regression coefficients, i and j are index numbers, k is number of patterns, X_i and X_j are independent variables and ε is the random error.²⁴ The analysis of variance (ANOVA) was used to assess the significance and adequacy of the model. The fitness of the polynomial models was expressed by the coefficients of determination, R², R²_{adj} and R²_{pred}. The main indicators that were used to show the significance of the model were Fisher variation ratio (F-value), probability value (Prob > F) with 95% confidence level and adequate precision. The final model for each response was obtained after elimination of insignificant terms (p > 0.05) based on F-test and the 3-D plots were presented. Furthermore, the optimum values for independent variables were identified and further experiments were performed to verify the regression models.^{25–26}

3. Results and Discussion

3.1. Experimental Design and ANOVA Analysis

Table 1 presents the results obtained from the heterogeneous Fenton experiments for the magnetite and goethite catalyzed reactions.

Two quadratic models were proposed to describe the color removal efficiencies through Fenton catalyzed by magnetite and goethite (Eqs. 5 and 6):

Magnetite:

$$\begin{aligned} \text{Color removal (\%)} = & +50.00000 + 4.64912 \times \text{catalyst} + \\ & 79.91228 \times H_2O_2 + 35.00000 \times \text{catalyst} \times H_2O_2 - \\ & 3.15789 \times \text{catalyst}^2 \end{aligned} \quad (5)$$

Goethite:

$$\begin{aligned} \text{Color removal (\%)} = & +50.73333 + 7.93333 \times \text{catalyst} + \\ & 13.33333 \times H_2O_2 + 30.00000 \times \text{catalyst} \times H_2O_2 - \\ & 4.10000 \times \text{catalyst}^2 \end{aligned} \quad (6)$$

In these equations, the positive and negative symbols signify the synergistic or antagonistic effects respectively. Analysis of variance (ANOVA) was performed to evaluate the “goodness of Fit” of the proposed models. The results of ANOVA for both catalysts are given in Table 2. From the results, the p-values of both catalysts for the studied response were less than 0.05 (< 0.0001 and 0.0002) that shows the models were significant and could be used for prediction of the studied response. Furthermore, in order to assess the quality of the equations, regression coefficients of R², adjusted R² and predicted R² were used. The closeness of R² values to 1.00 showed that the models were highly reliable regarding experiments repetition. The values obtained for magnetite and goethite were respectively R²: 0.98 and 0.99, Adj R²: 0.97 and 0.98 and Pred R²: 0.87 and 0.95 that showed the significance of the models to predict the studied response. The difference less than 0.2 between pred-R² and adj-R² indicates a good agreement in the results for both catalysts.

Moreover, the results for adequate precision (the ratio of signal to noise) were 25.162 and 37.337 that were much greater than the required value of 4.0. This shows

Table 1. Experimental Design Matrix and Response for Magnetite and Goethite

Run No.	A: catalyst (g/L)	B: H ₂ O ₂ (mol/L)	Color removal (%)	
			Magnetite	Goethite
1	1	0.2	68	63
2	1	0.2	67	64
3	0.5	0.1	59	56
4	1.5	0.3	74	71
5	1.5	0.1	61	59
6	1	0.2	67	63
7	0.5	0.2	64	60
8	1	0.1	62	59
9	1.5	0.2	69	65
10	0.5	0.3	65	62
11	1	0.3	69	67

Table 2. Analysis of variance (ANOVA) results for magnetite and goethite

Source	Sum of squares	Degrees of freedom	Mean square	F-value	p-value (Prob > F)
Magnetite					
Model	180.07	5	36.01	63.46.....	0.0002
Residual	2.84	5	0.57
Lack of Fit	2.17	3	0.72	2.717.....	0.3308
Pure Error	0.67	2	0.33
Cor Total	182.91	16	
Goethite					
Model	173.19	5	34.64	128.21.....	<0.0001
Residual	1.35	5	0.27
Lack of Fit	0.68	3	0.23	0.68.....	0.6395
Pure Error	0.67	2	0.33
Cor Total	174.55	10	

an acceptable signal and demonstrates that the models could navigate the design space. On the other hand, the lack of fit values for both hetero-catalysts were not significant that is the satisfactory result for the proposed models because it implies the models were fit to predict the amount of decolorization within the studied range of variables.²⁷

3. 2. Optimized Condition

The optimal conditions for heterogeneous Fenton reactions were obtained by design expert software. The condition proposed for both catalysts were [Catalyst] 1 g/L, [H₂O₂] 0.2 mol/L, at pH 9 and reaction time of 300 minutes. This condition was chosen based on the “maximum” color removal while using “in range” values of Fenton reagents. The color removal (%) of 67.32 and 63.37 were predicted by software at optimum values for magnetite and goethite catalyzed Fenton reactions respectively. The predicted values were in very close agreement with experimental values by deviation errors less than 0.1% that indicates the developed models can correlate the amount of catalyst and hydrogen peroxide to decolorization (%) with high accuracy.

3. 3. Effects of the Fenton Reagents on Decolorization Efficiency

The effects of the initial concentrations of H₂O₂ and the hetero-catalysts on decolorization efficacy are shown in Fig. 1a and 1b.

As can be seen in the graphs, the increase in H₂O₂ concentration was favored for decolorization in both catalysts. This is due to the generation of sufficient amount of •OH radicals. However, when the amount of H₂O₂ exceeded up to 0.3 mol/L, the efficiency decreased due to the •OH scavenging effects of H₂O₂ (Eq. 7) that leads to the genera-

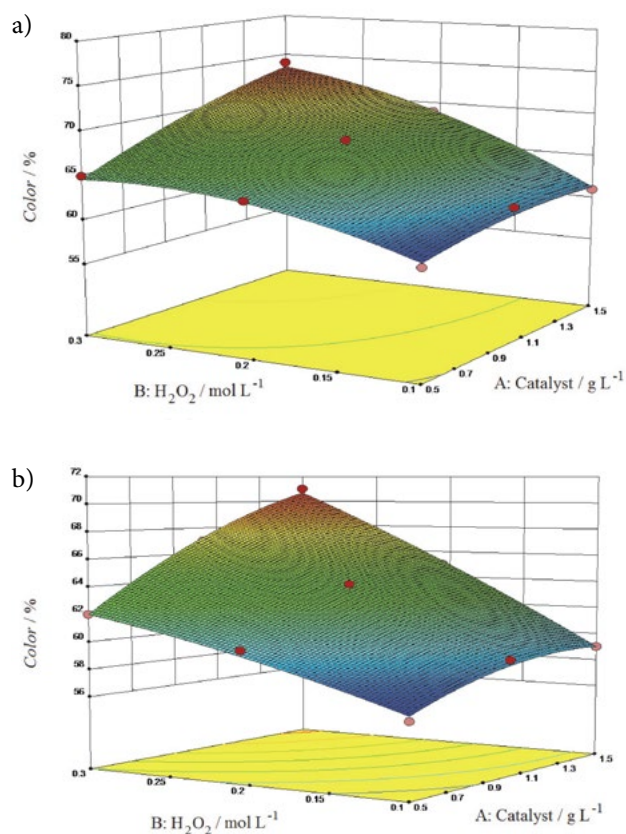
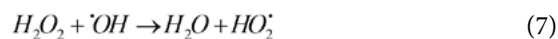


Fig 1. The 3-D response surface of the effect of catalyst and [H₂O₂] on color removal (%) using (a) nano-magnetite and (b) goethite in Fenton-like reaction

tion of hydroperoxyl radical (HO₂•). HO₂• radicals are relatively less active than •OH radicals and also lead to a further decline in •OH availability in reaction solution as shown in Eq. (8):





Similarly, higher concentrations of both catalysts resulted in higher removal efficiencies when appropriate amount of H_2O_2 was available in the reaction medium. It is worth noting that in heterogeneous catalysis, adsorption of the probe molecule on the surface of the catalyst plays a critical role in degradation reaction where the degradation occurs on the surface of the catalyst. To achieve this, there should be an interaction between the catalyst surface and the pollutant molecules. For this, one of the main surface characteristics that should be considered is the point of zero charge (pH_{pzc}) of the employed catalysts. The pH_{pzc} is a pH value that the surface of the catalyst is neutral. The surface is acidic at pH values below pH_{pzc} and is basic at pH values above pH_{pzc} . Since, methylene blue is a cationic dye, it is attracted toward the surface at $pH > pH_{pzc}$. The pH_{pzc} of magnetite and goethite are 6.0–6.8 and 7.4–8.2, respectively.²²

Therefore, the pH value of 9 was chosen in present study as optimum value to increase the adsorption of MB on the surface of the both hetero-catalysts.

On the other hand, the experiments were carried out at pH 7 to assess the decolorization effectiveness of the employed catalysts at neutral condition and under the optimum concentrations of Fenton reagents. As explained earlier, the pH_{pzc} of the magnetite is less than 7, thus MB adsorbed on its surface and resulted in accelerated color removal. However, the removal efficiency at pH 7 was less than pH 9. On the contrary, there was no adsorption of MB on the surface of goethite at $pH < pH_{pzc}$ due to electrostatic repulsions between the cationic dye molecules and positively charged surface of goethite. Accordingly, the decolorization rate decreased below 10%.

3. 4. Comparison Between Homogeneous and Heterogeneous Processes

In order to compare the effectiveness of the heterogeneous Fenton process with homogeneous reaction, a set of experiments were conducted with soluble iron under the same optimized Fenton reagents, with varying pH conditions of 3 (optimal value for homogeneous reaction), 7 and 9. The color of MB solution immediately disappeared under the studied condition with pH 3. Under neutral condition, although, much of the soluble iron was precipitated as ferric hydroxide, still the decolorization rate was much higher than heterogeneous process in which MB degradation was accomplished within a minute. This was because the amount of used soluble iron for degradation of 50 ppm MB was higher than the required amount. Similar trend was observed at pH 9 but degradation process took longer time of about 25 min.

Since, there is no mass transfer limitation in homogeneous reaction; the amount of utilized Fenton reagents in heterogeneous reaction was much higher than that of

required for homogeneous reaction. On this basis, the Fenton reagents concentrations decreased 10 times and additional experiments were carried out using $[Fe^{2+}]$ 0.1 g/L and $[H_2O_2]$ 0.02 mol/L at pH 3, 7 and 9. Comparatively, very fast decolorization was observed at pH 3. At neutral condition, despite of ferric hydroxide generation, MB removal was completed within a few minutes. In contrast, it took about 15 h to remove 85% of color at pH 9.

Although, homogeneous Fenton represented significantly higher removal efficiencies over a short reaction time, the generated sludge is an important issue that should be addressed; especially for treatments at large scales. In addition, to attain complete mineralization of pollutant, acidification of the neutral or basic wastewaters is required. Moreover, the catalyst is not recoverable.³⁰ In contrast, in heterogeneous reaction, the iron oxides could be simply separated from the solution by magnet and re-used for several runs with inconsiderable decrease in their efficiency.³¹ In light of this, future studies should focus on production of new heterogeneous catalysts that not only overcome homogeneous Fenton shortcomings but activate Fenton reaction effectively.

4. Conclusion

In this study, two iron oxides, nano-magnetite and goethite, were used in Fenton-like degradation of a cationic dye in aqueous solution. The heterogeneous reactions were designed by CCD and the optimized values of [catalyst] 1 g/L and $[H_2O_2]$ 0.2 mol/L were established by software. The color removal efficiencies of 67% and 63% were obtained at pH 9 and over 300 minutes by magnetite and goethite catalyzed Fenton reactions, respectively. The comparative studies between heterogeneous and homogeneous Fenton reactions revealed the effectiveness of homogeneous Fenton with significantly lower Fenton reagents (up to 10 times) and higher reaction rate at acidic and neutral condition. However, at basic condition, the degradation efficiency decreased and ferric hydroxide precipitated. Acceptable degradation efficiency at neutral condition along with easier catalyst recovery and reuse make magnetite as a potential solution to prevail the inconveniences accompanied homogeneous Fenton reaction. However, future work in this field should put emphasis on modification in magnetite structure to increase its activity in Fenton reaction and the rate of pollutant degradation.

5. References

1. A. Török, E. Buta, C. Indolean, S. Tonk, L. Silaghi-Dumitrescu, C. Majdik, *Acta Chim. Slov.* **2015**, *62*, 452–461. DOI:0.17344/acsi.2014.1109
2. S. T. Ong, H. Y. Gan, L. E. Leow, *Acta Chim. Slov.* **2017**, *64*, 144–158. DOI:10.17344/acsi.2016.2983

3. W. Anku, S. O. B. Oppong, S. K. Shukla, P. P. Govender, *Acta Chim. Slov.* **2016**, *63*, 380–391. DOI:10.17344/acsi.2016.2385
4. T. Jerič, R. J. M. Bisselink, W. van Tongeren, A. M. Le Marechal, *Acta Chim. Slov.* **2013**, *60*, 666–672.
5. S. Rahim Pouran, A. Bayrami, A. R. Abdul Aziz, W. M. A. Wan Daud, M. S. Shafeeyan, Comprehensive study on the influence of molybdenum substitution on characteristics and catalytic performance of magnetite nanoparticles, *Res. Chem. Intermed.* **2018**, In press.
6. M. R. D. Khaki, M. S. Shafeeyan, A. A. A. Raman, W. M. A. W. Daud, *J. Environ. Manage.* **2017**, *198*, 78–94.
7. M. Strlič, J. Kolar, V. S. Šelih, D. Kočar, B. Pihlara, *Acta Chim. Slov.* **2003**, *50*, 619–632.
8. A. Žgajnar Gotvajn, J. Zagorc-Končan, *Acta Chim. Slov.* **2005**, *52*, 131–137.
9. J. Malešič, J. Kolar, M. Strlič, S. Polanc, *Acta Chim. Slov.* **2006**, *53*, 450–456.
10. S. Rahim Pouran, A. Bayrami, A. R. Abdul Aziz, W. M. A. Wan Daud, M. S. Shafeeyan, *J. Mol. Liq.* **2016**, *222*, 1076–1084.
11. S. Rahim Pouran, A. R. Abdul Aziz, W. M. A. Wan Daud, *J. Indust. Eng. Chem.* **2015**, *21*, 53–69. DOI:10.1016/j.jiec.2014.05.005
12. C. V. dos Santos Allan, C. Masini Jorge, *Talanta* **2009**, *77*, 1081–1086. DOI:10.1016/j.talanta.2008.08.006
13. I. Arslan-Alaton, G. Tureli, T. Olmez-Hanci, *J. Photochem. Photobiol.* **2009**, *202*, 142–153. DOI:10.1016/j.jphotochem.2008.11.019
14. A. R. Khataee, M. Zarei, L. Moradkhannejhad, *Desalination* **2010**, *258*, 112–119. DOI:10.1016/j.desal.2010.03.028
15. A. Aleboeyh, N. Daneshvar, M. B. Kasiri, *Chem. Eng. Process. Process Intensif.* **2008**, *47*, 827–832. DOI:10.1016/j.ccep.2007.01.033
16. S. Rahim Pouran, A. A. Abdul Raman, W. M. A. Wan Daud, *J. Clean. Product.* **2014**, *64*, 24–35. DOI:10.1016/j.jclepro.2013.09.013
17. I. Grčić, S. Papić, K. Žižek, N. Koprivanac, *Chem. Eng. J.* **2012**, *195-196*, 77–90. DOI:10.1016/j.cej.2012.04.093
18. S. Navalon, M. Alvaro, H. Garcia, *Appl. Catal. B.* **2010**, *99*, 1–26. DOI:10.1016/j.apcatb.2010.07.006
19. F. J. Rivas, F. J. Beltrán, O. Gimeno, J. Frades, *J. Agricult. Food chem.* **2001**, *49*, 1873–1880. DOI:10.1021/jf001223b
20. W. Liu, S. A. Andrews, M. I. Stefan, J. R. Bolton, *Water Res.* **2003**, *37*, 3697–703. DOI:10.1016/S0043-1354(03)00264-1
21. J. Rodriguez-Chueca, A. Mediano, M. P. Ormad, R. Mosteo, J. L. Ovelleiro, *Water Res.* **2014**, *60*, 250–258. DOI:10.1016/j.watres.2014.04.040
22. D. B. Hasan, S. R. Pouran, A. A. A. Aziz, S. M. Nashwan, W. M. A. W. Daud, M. G. Shaaban, *J. Indust. Eng. Chem.* **2015**, *25*, 186–191. DOI:10.1016/j.jiec.2014.10.033
23. A. Houshmand, W. M. A. Wan Daud, M. S. Shafeeyan, *Bull. Chem. Soc. Jpn.* **2011**, *84*, 1251–1260.
24. M. S. Shafeeyan, A. Houshmand, A. Arami-Niya, H. Razaghizadeh, W. M. A. Wan Daud, *Bull. Korean Chem. Soc.* **2015**, *36*, 533–538.
25. A. Shamiri, M. S. Shafeeyan, H. C. Tee, C. Y. Leo, M. K. Aroua, N. Aghamohammadi, *J. Nat. Gas Sci. Eng.* **2016**, *35*, 605–613.
26. A. Houshmand, W. M. A. W. Daud, M. S. Shafeeyan, *Bull. Chem. Soc. Jpn.* **2011**, *84*, 1251–1260. DOI:10.1246/bcsj.20110145
27. A. Arami-Niya, W. M. A. W. Daud, F. S. Mjalli, F. Abnisa, M. S. Shafeeyan, *Chem. Eng. Res. Design* **2012**, *90*, 776–784. DOI:10.1016/j.cherd.2011.10.001
28. C. Appel, L. Q. Ma, R. D. Rhue, E. Kennelle, *Geoderma* **2003**, *90*, 77–93. DOI:10.1016/S0016-7061(02)00316-6
29. B. H. Diy'uddeen, S. Rahim Pouran, A. R. Abdul Aziz, W. M. A. W. Daud, *RSC Adv.* **2015**, *5*, 68159–68168.
30. S. Rahim Pouran, A. R. Abdul Aziz, W. M. A. Wan Daud, M. S. Shafeeyan, *RSC Adv.* **2015**, *5*, 87535–87549.

Povzetek

Narejena je bila primerjava učinkovitosti dveh postopkov razbarvanja raztopine barvila metilen modro s Fentonovo oksidacijo: heterogena reakcija z nanodelci magnetita in goetita ter homogena reakcija z železovimi ioni. Za določitev optimalnih pogojev v sistemu magnetit/H₂O₂ in goetit/H₂O₂ je bila uporabljena RSM metoda, ki je dala reakcijske pogoje: 0,2 M [H₂O₂], koncentracija katalizatorja 1 g L⁻¹, pH 9,0 in reakcijski čas 5h. V sistemu Fe⁺² / H₂O₂ je razbarvanje potekalo pri pH 3,0. Eksperimentalni rezultati kažejo, da je homogena Fentonova reakcija najbolj učinkovita v kisljih in nevtralnih pogojih, pri pH 9,0 pa učinkovitost pade zaradi zmanjšanja koncentracije Fe⁺² ionov v raztopini in nastanka gošče železovega hidroksida. Sistem Fe₃O₄ / H₂O₂ je bolj učinkovit od sistema FeO (OH) / H₂O₂, kar lahko pripišemo prisotnosti FeII kationov v strukturi magnetita in njegovi večji površini.

Scientific paper

Antioxidative Activity of Methanolic and Water Extracts from the Hyperthermophilic Archaeon *Aeropyrum pernix* K1

Mihaela Skrt,¹ Polona Jamnik¹ and Nataša Poklar Ulrih^{1,2,*}¹ Department of Food Science and Technology, Biotechnical Faculty, University of Ljubljana, Jamnikarjeva 101, 1000 Ljubljana, Slovenia² Centre of Excellence for Integrated Approaches in Chemistry and Biology of Proteins (CipKeBiP), Jamova 39, 1000 Ljubljana, Slovenia* Corresponding author: E-mail: poklar.natasa@bf.uni-lj.si
Tel: +386-1-3203780; Fax: +386-1-2566296

Received: 18-08-2017

Abstract

The hyperthermophilic archaeon *Aeropyrum pernix* has adapted to optimal growth under high temperatures in saline environments and under oxidizing conditions. In the present study, we focused on the antioxidative activity of proteins from *A. pernix* K1. Following high temperature methanol and water extractions of the protein from the biomass of *A. pernix* K1, the total sulphhydryl groups and radical scavenging activities were investigated. The total protein in the methanolic extract was 36% lower and showed 10% fewer sulphhydryl groups than that from the water extract. However, the radical scavenging activity of the water extract was four-fold greater than for the methanolic extract. The proteins of both of these extracts were separated by two-dimensional electrophoresis, and selected proteins were identified using mass spectrometry. The majority of these identified proteins were intracellular proteins, such as those involved in oxidative stress responses and osmotic stress responses, and proteins with hydrolase and dehydrogenase activities. These proteins are also common to most organisms, and included putative uncharacterized proteins.

Keywords: *Aeropyrum pernix* K1, methanol/ water extraction, antioxidant activity, proteins

1. Introduction

Hyperthermophilic microorganisms have developed various mechanisms of molecular adaptation to survive at extreme temperatures of up to 105 °C, and also under oxidizing conditions. Adaptations to proteins to maintain their activities under these conditions are therefore crucial for the survival of hyperthermophiles.¹ However, in comparison to bacteria and eukaryotes, relatively little is known about the molecular mechanisms of the responses to extreme conditions of hyperthermophilic archaea.

Most aerobes have multiple pathways for the detoxification of reactive oxygen species, and most of these include synthesis of superoxide dismutase (SOD), which catalyzes the conversion of superoxide radicals to oxygen and hydrogen peroxide. The mechanisms responsible for oxidative stress responses have been only

partially defined in some archaea. Among the aerobic hyperthermophilic archaea, SODs have been reported for *Pyrobaculum aerophilum* and *Aeropyrum pernix*.^{2,3} From genomic sequence data, it has been suggested that the majority of aerobic hyperthermophilic archaea use a SOD-peroxyredoxine (Prx) system.⁴ The Prxs are thiol-dependent peroxidases that catalyze the detoxification of various peroxide substrates, such as H₂O₂, peroxinitrite, and hydroperoxides, and that control some signal transduction pathways in eukaryotic cells.⁵ Prxs are present in all cellular organisms, and they represent a ubiquitous family of antioxidant enzymes.

In 2005, the structure of an archaeal Prx from the aerobic hyperthermophilic crenarchaeon *A. pernix* K1 was reported, and a new oxidation mechanism of active oxygen removal by an antioxidant protein was defined. This oxidation reaction occurs through a novel

mechanism, in which cysteine and neighboring histidine residues form a sulfurane derivative that acts as a reaction intermediate.⁵ An archaeal antioxidant Dps-like protein that can oxidize Fe(II) to Fe(III) using H₂O₂ as an oxidant was characterized from the hyperthermophilic acidophile *Sulfolobus solfataricus*.⁶ In a recent study of hyperthermophilic microorganisms, the *Thermococcus kodakarensis* KOD1 proteome response to unstable environment conditions was analyzed, and 42 proteins were up-regulated in response to oxidative stress.⁷ For superoxide dismutase from *A. pernix* K1, this enzyme was shown to be tolerant to organic media.⁸ Such discoveries make hyperthermophilic organisms a very interesting source for various industrial applications.^{9–12}

Aeropyrum pernix K1 is a strictly aerobic hyperthermophilic archaeon that grows optimally from 90 °C to 95 °C, and although the proteome of *A. pernix* K1 was analyzed in 2006, little is known about its enzymatic and nonenzymatic antioxidant systems.^{11,12–14} Such hyperthermophilic organisms might be good sources for various compounds that have great potential for biotechnological applications.

The aim of the present study was to compare the antioxidative activities of extracts obtained from *A. pernix* using two different solvents, as methanol and water, and to identify the compounds responsible for the antioxidative activities of these extracts. The extracts were analyzed for total sulfhydryl groups using Ellman's reagent, and antioxidant activity was measured using 1,1-diphenyl-2-picryl-hydrazil (DPPH). The proteins from both of these extracts were analyzed by two-dimensional (2-D) gel electrophoresis, and some of them were identified by mass spectrometry.

2. Experimental

2.1. Growth Media and Preparation of the Crude Extracts

The archaeon *A. pernix* K1 was cultivated at 92 °C according to Milek et al.¹⁵ The biomass was harvested at the late exponential growth phase, and washed with 20 mM HEPES, pH 7.0, 3% NaCl. The biomass was then resuspended in 50% aqueous methanol or in water (using Milli-Q water). After shaking for 2 h at 75 °C, the methanol/ water phase was recovered by centrifugation at 10,000× *g* for 10 min. The extract was evaporated to dryness under reduced pressure at 45 °C. The residue obtained was dissolved in Milli-Q water and analyzed as described below.

2.2. Total Protein of Archaeal Biomass

The total protein of the archaeal biomass was determined according to the Stickland method¹⁶, with a

few modifications. Briefly, 0.5 mL 3 M NaOH was added to 1.0 mL of the appropriate resuspended biomass. The samples were kept at 100 °C for 5 min, and following cooling, 0.5 mL 2.5% CuSO₄ × 5H₂O was added. The samples were mixed and incubated at room temperature for 5 min and then centrifuged in a benchtop centrifuge at 1,300× *g* for 10 min. The absorbance of the supernatant was measured at 555 nm, against a blank sample prepared with Milli-Q water instead of the resuspended biomass. Bovine serum albumin (Sigma-Aldrich) was used as the protein standard.

2.3. Determination of Protein Concentrations in Extracts

The protein concentrations of the crude methanolic and water extracts were determined by the method of Bradford, using a commercial dye reagent with bovine serum albumin (Sigma-Aldrich) as the standard for the protein calibration curves.¹⁷

2.4. Radical Scavenging Activity Using the DPPH Assay

Prior to the DPPH assay, the residues from the methanolic and water extractions were diluted with Milli-Q water to the same concentration of residue (mg) per milliliter water. The radical scavenging activity was determined according to a slightly modified method of Brand-Williams et al.¹⁸ Briefly, the DPPH radical was prepared in methanol to a final concentration of 0.1 mM. Then 50 µL samples were added to 1.45 mL 0.1 mM DPPH radical solution, and kept in the dark for 30 min. The control sample was prepared in the same way, using 50 µL Milli-Q water instead of the sample solution. The absorbance at 517 nm, A_{517} , was recorded with a spectrophotometer (UV-VIS, model 8453; Hewlett-Packard). The absorbance of the samples and the control were measured against a methanol blank, and the scavenging activity was calculated according to following equation, and expressed as antioxidant potential (AOP):

$$AOP (\%) = \frac{(A_{517control} - A_{517sample})}{A_{517control}} \times 100 \quad (1)$$

where $A_{517control}$ and $A_{517sample}$ are the measured absorbances of the control and the sample, respectively.

2.5. Quantitative Determination of Total Sulfhydryl Groups

The total sulfhydryl groups were determined in the crude methanol and water extracts according to the Ellman method¹⁹, with slight modifications. Briefly, mixtures of 200 µL extract, 800 µL 100 mM phosphate buffer (pH 8.0) and 16.7 µL 10.0 mM Ellman's reagent (5,5'-dithiobis-2-nitrobenzoic acid; DTNB; Sigma-Aldrich), were mixed

and left at room temperature for 5 min in the dark. The absorbance at 412 nm was then measured against a blank sample, using a spectrophotometer (HP 8453; Hewlett Packard). The concentrations of sulfhydryl groups were calculated according to the following formula:

$$C_{SH} = \frac{A_{412}}{\epsilon \times l} \times D \quad (2)$$

where C_{SH} is the molar concentration of the total thiol groups (mol/L), A_{412} is the measured absorbance at 412 nm, ϵ is the molar absorption coefficient of TNB (13,600 M⁻¹cm⁻¹), l is the optical path length (cm), and D is the dilution factor. The total thiol group (SH) content was expressed in μ mol SH/g dry extract.

2. 6. Two-dimensional Electrophoresis

Prior to 2-D gel electrophoresis, 50- μ L aliquots of the methanolic and water extracts were appropriately diluted with Milli-Q water and treated using 2-D Clean-Up kits (GE Healthcare), according to the manufacturer instructions.

The 2-D electrophoresis was performed according to G6rg²⁰, with minor modifications. Briefly, the samples (100 μ g protein) were mixed with rehydration solution (7 M urea, 2 M thiourea, 2% CHAPS, 2% immobilized pH gradient [IPG] buffer [pH 4–7], 18 mM dithiothreitol, and a trace of bromphenol blue), and applied to 13-cm IPG pH 4 to 7 strips (GE Healthcare). After rehydration, a first dimension of isoelectric focusing was carried out at 20 °C (Multiphore II apparatus; GE Healthcare), according to the following voltage program: 300 V (gradient over 1 min), 300 V (fixed for 1 h), 3,500 V (gradient over 1.5 h) and 3,500 V (fixed for 5 h). Prior to the second dimension of the 2-D electrophoresis, the IPG strips were equilibrated for 15 min in sodium dodecyl sulfate (SDS) equilibration buffer (75 mM Tris/HCl, pH 8.8, 6 M urea, 30% glycerol, 2% SDS, and a trace of bromphenol blue) containing 1% dithiothreitol, and then containing 4.8% iodoacetamide for an additional 15 min. The second dimension (SDS polyacrylamide gel electrophoresis) was carried out with 12% running gels on a vertical discontinuous electrophoretic system (SE 600; Hoefer Scientific Instruments), at a constant 20 mA/gel for 15 min, and then at a constant 40 mA/gel until the bromphenol blue reached the bottom of the gel. The 2-D gels were stained with SYPRO Ruby (Invitrogen), and then documented using a CAM-GX-CHEMI HR system (Syngene). The gels were run as triplicates. To align the gels, the 2-D Dymension software (Syngene) was used.

2. 7. Protein Identification

Randomly chosen protein spots were excised from the gels and analyzed by liquid chromatography–tandem mass spectrometry (LC-MS/MS) using an ESI-TRAP

instrument at the University of Aberdeen (Aberdeen Proteomics). The Mascot software was used to search the NCBI nr 20091002 database. The taxonomy search parameter was Archaea (Archaeobacteria), and the tryptic digest was applied with a maximum number of one missed cleavage. The peptide mass tolerance was set to ± 1.5 Da, and the fragment mass tolerance to ± 0.5 Da. Additionally, carbamidomethylation of Cys and oxidation of Met were considered as possible fixed and variable modifications, respectively.

2. 8. Bioinformatic Analyses

Similarity searching was carried out with Uniprot using BLAST (UniProt: <http://www.uniprot.org>). Orthology was investigated using the Kyoto Encyclopedia of Genes and Genomes (KEGG) database (Uniprot; <http://www.uniprot.org>). Multiple sequence alignments were performed using the CLUSTAL Omega program (<http://www.ebi.ac.uk/Tools/msa/clustalo/>). ProtParam was used to analyze the amino-acid compositions (<http://www.expasy.org/cgi-bin/protparam>). NetPhos 2.0 was used to predict Ser, Thr, and Tyr phosphorylation sites (<http://www.cbs.dtu.dk/services/NetPhos/>). Conserved domains within protein sequences were defined using the NCBI CD server (<http://www.ncbi.nlm.nih.gov/Structure/cdd/wrpsb.cgi>). The domain organization of protein sequences was searched using the Pfam database (<http://pfam.sanger.ac.uk/>).

3. Results and Discussion

3. 1. Antioxidant Activity, and Total Protein and Sulfhydryl Groups

To determine the antioxidative activity of the hyperthermophilic archaeon *A. pernix* K1, the extracts were prepared using two different solvents: 50% aqueous methanol, and water at high temperature (75 °C). The antioxidant activities of these methanolic and water extracts were determined according to the free radical DPPH method, and are expressed as antioxidant potential (AOP). The AOP of the methanolic and water extracts were 4.9% and 20.3%, respectively (Table 1).

The total protein content in the *A. pernix* K1 biomass was 473 (± 5) mg/g dry biomass. This biomass was used for the preparation of the methanolic and water extracts, with the total protein of the methanolic and water extracts of 0.115 mg/mg dry extract and 0.318 mg/mg dry extract, respectively (Table 1).

The total free sulfhydryl groups in the methanolic extracts was 0.092 μ mol SH/g dry extract, and in water extracts, 1.10 μ mol SH/g dry extract (Table 1).

Organisms have complex systems of enzymatic (e.g., superoxide dismutase, peroxidase) and nonenzymatic (e.g., ascorbic acid, flavonoids, glutathione) antioxidant defense systems against harmful effects of free radicals

and other oxidants.²¹ Antioxidant properties of natural sources have been reported mostly from higher plants²², with few reports carried out for hyperthermophilic organisms.^{2,3,6,23,24}

To determine the antioxidant activities of the present biological samples, extraction is the first step, where the choice of the solvent for the extraction is of particular importance. Here, the AOP of the water extract was four-fold greater than that of the methanolic extract (Table 1). As no classical biosynthetic pathways of polyphenols have been annotated for the hyperthermophilic *A. pernix*, and some antioxidant enzymes, such as SOD³ and Prx⁵ are already known for hyperthermophilic archaea, we assumed that the higher AOP of the water extract would correlate to protein content. Therefore, we focused on the protein (Table 1).

Furthermore, the total free sulfhydryl groups were determined for both extracts, and this was higher for the water extract (Table 1). This might be explained in terms of the greater water solubility of sulfhydryl compounds, and also their contribution to AOP, although further studies are needed to confirm this.

Table 1. Protein, sulfhydryl groups, and radical scavenging activity of the crude methanolic and water extracts.

Crude extract	Total protein (mg/mg dry extract)	Total sulfhydryl group ($\mu\text{mol/g}$ dry extract)	Antioxidative potential (%)
Methanolic	0.115 ± 0.003	0.092 ± 0.001	4.9 ± 0.5
Water	0.318 ± 0.003	1.10 ± 0.03	20.3 ± 0.1

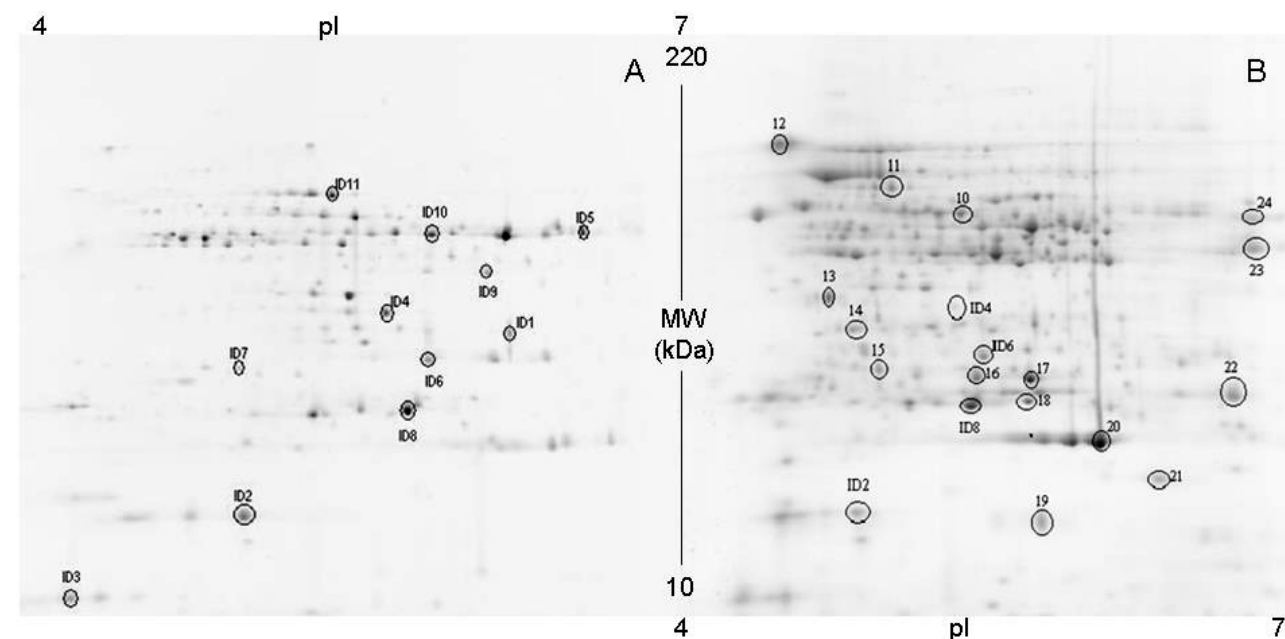


Figure 1. Representative two-dimensional protein profiles from the crude methanol extract (A) and the crude water extract (B) from *A. pernix* K1 grown at pH 7 and 92 °C. The proteins in the circled spots were identified by LC/MS-MS. Circled spots marked with ID 4 to 8 indicate the same proteins identified that were in both extracts.

3. 2. Two-dimensional and LC-MS/MS

Analysis of the Protein of the Extracts

The protein of the crude methanolic and water extracts was analyzed using 2-D electrophoresis (Figure 1). Eleven randomly chosen proteins from the methanolic extract and 19 from the water extract were identified using LC-MS/MS (Tables 2, 3). The molecular masses (theoretical) of the proteins were in the range of 15,360 Da (Q9Y9S7) to 60,392 Da (Q9Y9J7), and the isoelectric points (pIs) (theoretical) for all of the proteins identified were <7.0, with the exception of the elongation factor Q9YAV0, and the putative dehydrogenase Q9YDK1, with pIs of *ca.* 9.

A scheme of the gene locations in the genome of *A. pernix* was constructed using the BioNumerics software (version 7.6.1; Applied Maths), from which it can be seen that the genes listed in Table 2 and Table 3 are scattered around the genome (Supplementary Figure 1).

The majority of the proteins identified from these extracts of *A. pernix* K1 were intracellular proteins, and for better clarity they were classified into six different subgroups: proteins involved in oxidative stress responses; proteins involved in osmotic stress responses; proteins with hydrolase activities; dehydrogenases; proteins common to most organisms; and putative uncharacterized proteins.

3. 2. 1. Proteins Involved in Oxidative Stress responses

Thiol peroxidase and superoxide dismutase were identified in the methanolic and water extracts, which are known to have roles in responses to oxidative stress. Protein spot ID2 from the methanol and water extracts

Table 2. Protein from the spots from the crude methanol extract identified by LC-MS/MS and through searches with the NCBI database. ^aData from NCBI, ^bAccession number in the UniProtKB database.

Protein spot ID	Protein	Accession number ^a	ORF ^a	Transcript ID ^a	Accession number ^a	Theoretical M _r (Da)	pI	Mascot score	Sequence coverage (%)
1	Malate dehydrogenase	gi 116062469	APE_0672.1	BAA79645.2	Q9YEA1	33469	6.06	996	69
2	Thiol peroxidase	gi 116063062	APE_2125.1	BAA81136.2	Q9YA14	18532	5.33	305	77
3	Hypothetical protein	gi 116063103	APE_2211.1	BAA81223.2	Q9Y9S7	15358	5.10	794	82
4	Polyamine aminopropyltransferase	gi 116062511	APE_0767.1	BAA79745.2	Q9YE02	35595	5.66	722	47
5	NADP-dependent glutamate dehydrogenase	gi 116062758	APE_1386.1	BAA80383.2	Q9YC65	46142	6.42	593	51
6	Succinyl-CoA ligase [ADP-forming] subunit alpha	gi 116062642	APE_1072.1	BAA80057.2	Q9YD40	30934	5.77	680	71
7	Hypothetical protein	gi 116062760	APE_1388.1	BAA80385.2	Q9YC63	31969	5.20	388	23
8	UPF0173 metal-dependent hydrolase	gi 5104787	APE_1117	BAA80102.1	Q9Y CZ5	25927	5.70	733	42
9	Succinyl-CoA synthetase beta chain	gi 116062641	APE_1065.1	BAA80050.2	Q9YD47	41519	6.00	539	24
10	NADP-dependent glutamate dehydrogenase	gi 116062758	APE_1386.1	BAA80383.2	Q9YC65	46142	6.50	578	19
11	Carboxypeptidase	gi 116062910	APE_1775.1	BAA80778.2	Q9YB20	57988	5.50	613	19

Table 3. Protein spots from the crude water extract identified by LC-MS/MS and through searches with the NCBI database. ^aData from NCBI, ^bAccession number in the UniProtKB database.

Protein spot ID	Protein	Accession number ^a	ORF ^a	Transcript ID ^a	Accession number ^a	Theoretical M _r (Da)	pI	Mascot score	Sequence coverage (%)
2	Thiol peroxidase	gi 116063062	APE_2125.1	BAA81136.2	Q9YA14	18770	5.33	248	71
4	Polyamine aminopropyltransferase	gi 116062511	APE_0767.1	BAA79745.2	Q9YE02	35595	5.66	622	43
6	Succinyl-CoA ligase [ADP-forming] subunit alpha	gi 116062642	APE_1072.1	BAA80057.2	Q9YD40	30934	5.77	897	73
8	UPF0173 metal-dependent hydrolase	gi 5104787	APE_1117	BAA80102.1	Q9Y CZ5	25927	5.72	556	56
10	Glutamine synthetase	gi 116063069	APE_2142.1	BAA81153.2	Q9Y9Z7	50743	5.61	667	49
11	NADP-dependent glyceraldehyde-3-phosphate dehydrogenase	gi 116062915	APE_1786.1	BAA80789.2	Q9YB09	56162	5.58	1314	63
12	NADP-dependent glyceraldehyde-3-phosphate dehydrogenase	gi 116062915	APE_1786.1	BAA80789.2	Q9YB09	56162	5.58	794	33
13	Putative methylcobalamin: homocysteine methyltransferase	gi 116063025	APE_2050.1	BAA81060.2	Q9YA89	36553	5.13	928	68
14	Thermosome beta subunit	gi 116063040	APE_2072.1	BAA81083.2	Q9YA66	60392	5.34	499	16
15	Putative sugar-phosphate nucleotidyl transferase	gi 5105992	APE_2291	BAA81303.1	Q9Y9J7	26747	5.41	531	48
16	ABC transporter	gi 116062880	APE_1688.1	BAA80689.2	Q9YBA9	30466	6.04	470	39
17	ABC transporter	gi 116062880	APE_1688.1	BAA80689.2	Q9YBA9	30466	6.04	669	51
18	Deoxyribose phosphate aldolase	gi 116063194	APE_2437.1	BAA81452.2	Q9Y948	24497	6.00	592	57
19	Putative uncharacterized protein	gi 116062872	APE_1660.1	BAA80661.2	Q9YBD7	16607	6.63	376	56
20	Superoxide dismutase [Mn/Fe]	gi 5104403	APE_0741	BAA79718.1	Q9Y8H8	24562	6.50	746	74
21	Putative uncharacterized protein	gi 5106093	APE_2389	BAA81404.1	Q9Y996	20683	8.17	376	40
22	Putative dehydrogenase	gi 5104581	APE_0912	BAA79896.1	Q9YDK1	27807	9.04	726	69
23	Elongation factor 1-alpha	gi 5105535	APE_1844	BAA80848.1	Q9YAV0	48632	9.22	835	40
24	Elongation factor 1-alpha	gi 5105535	APE_1844	BAA80848.1	Q9YAV0	48632	9.22	625	39

was identified as thiol peroxidase (Q9YA14), which contains three Cys residues. The NCBI CD database²⁵ search indicated a specific hit for the protein to have a conserved PRX_alkyl-hydroperoxide-reductase-(Ahp)-E-like domain, so the protein appears to belong to the Prx family, with a greater similarity to the 2-Cys class of Prxs. The Prxs are thiol-specific antioxidant proteins with peroxidase activity, whereby hydrogen peroxide, peroxynitrate, and organic hydroperoxides are reduced using equivalents derived from thioredoxin, glutathione, trypanothione, and AhpF. The 2-Cys class of Prxs use cell-specific disulfide oxidoreductases to reduce the disulfide bond formed between the oxidized peroxidatic Cys (C_p-SOH) intermediate and the second redox-active Cys, the resolving Cys (C_r-SH).⁵ The Prxs have been described for all cellular organisms. The sequence similarity search (UniProtKB, Blast) for protein thiol peroxidase (Q9YA14) showed 63% identity with AhpC/ thiol-specific antioxidant (A4WK54) from the Archaea *Pyrobaculum arsenaticum* (strain DSM 13514/ JCM 11321), and 63% identity with bacterioferritin comigratory protein homolog (Q8ZUL0) from the Archaea *P. aerophilum*. Both of these proteins belong to the AhpC/ thiol-specific antioxidant protein family. AhpC directly reduces organic hyperoxides into the reduced dithiol form. Thiol-specific antioxidants are physiologically important antioxidants that constitute an enzymatic defense against sulfur-containing radicals.²⁶

Protein spot ID20 from the water extract was identified as SOD (Q9Y8H8) (Table 3). SODs catalyze the disproportion of superoxide into hydrogen peroxide and oxygen. The SOD gene of *A. pernix* was first cloned and expressed in *Escherichia coli* in 1999.³ *A. pernix* SOD was shown to be cambialistic, active with either Mn or Fe, and more thermostable with Mn. The molecular weight of this soluble enzyme was 24.5 kDa, with a pI of 6.5.³ Based on the finding that SOD from hyperthermophilic *A. pernix* K1 is stable also in organic solvents⁸, we hypothesized that the antioxidative activity of methanol extracts would

be higher than for the water extracts, but this was not confirmed in our study.

3. 2. 2. Proteins Involved in Osmotic Stress Responses

Aeropyrum pernix is hyperthermophilic archaeon that grows optimally in a salinity of 3.5%, and therefore it must be able to adjust to alterations in salt concentrations in the environment. In the methanolic extract, we identified a hypothetical protein with accession number Q9Y9S7, that might be involved in responses to osmotic stress. The sequence similarity searches for this putative uncharacterized protein, ID3 (Q9Y9S7), showed that it appeared to be related to the osmotically induced protein C (OsmC) family of proteins. OsmC is a stress-inducible protein that has been identified in *E. coli*, and it is involved in the intracellular defense mechanisms against oxidative stress caused by exposure to elevated osmolarity.²⁷ This protein family also contains an organic hydroperoxide detoxification protein that has a novel pattern of oxidative stress regulation.²⁸ The Pfam²⁹ database searches also indicated that protein Q9Y9S7 from the hyperthermophilic *A. pernix* K1 has a conserved domain that is shared with the OsmC family. Multiple sequence alignments with the Clustal Omega program³⁰ were carried out for Q9Y9S7 and several archaeal OsmC proteins (Figure 2). These findings showed two conserved Cys residues in all of the aligned sequences. The OsmC family from mesophilic and thermophilic organisms has been shown to have two conserved Cys residues.³¹ Q9Y9S7 from the hyperthermophilic *A. pernix* K1 contains these two conserved Cys residues at amino-acid positions 63 and 115, and three Cys residues have been shown for the hyperthermophilic *Thermococcus kokadakaensis* KOD1, and for *Pyrococcus horikoshii* OT3 and *Pyrococcus furiosus* DSM 3638. The OsmC protein from the hyperthermophilic *T. kokadakaensis* KOD1 was identified as a protein

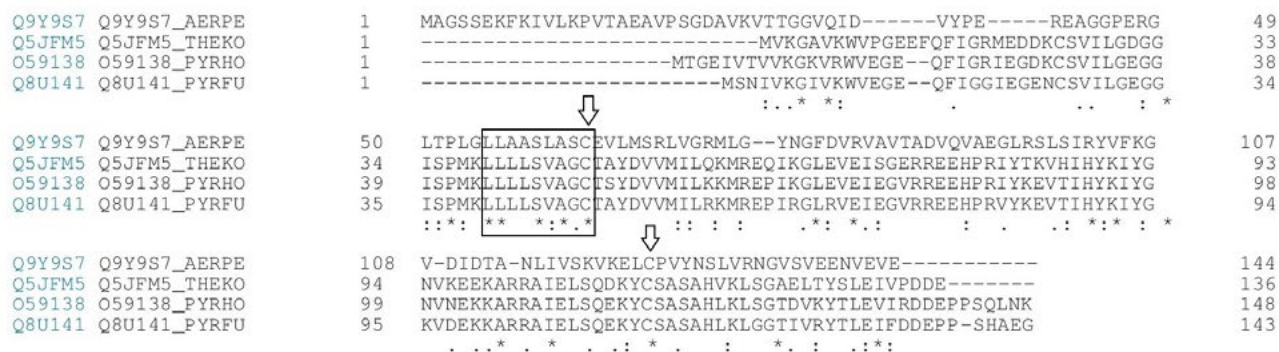


Figure 2. Multiple sequence alignment for Q9Y9S7 and several hyperthermophilic archaeal OsmC homologs. The origins of the sequences were as follows: hyperthermophilic *T. kokadakaensis* KOD1 (Q5JFM5), *P. horikoshii* OT-3 (O59138; NP_143334) and *P. furiosus* DSM 3638 (Q8U141; NP_579117). The alignment was constructed using the Clustal Omega program. Residues are marked according to the following criteria: *, identical residues; colon (:), residues with conserved substitutions; full stop (.), residues with semi-conserved substitutions; ⇓, conserved Cys residues; numbers at the ends of each line (right-hand side), numbers of amino-acid residues.

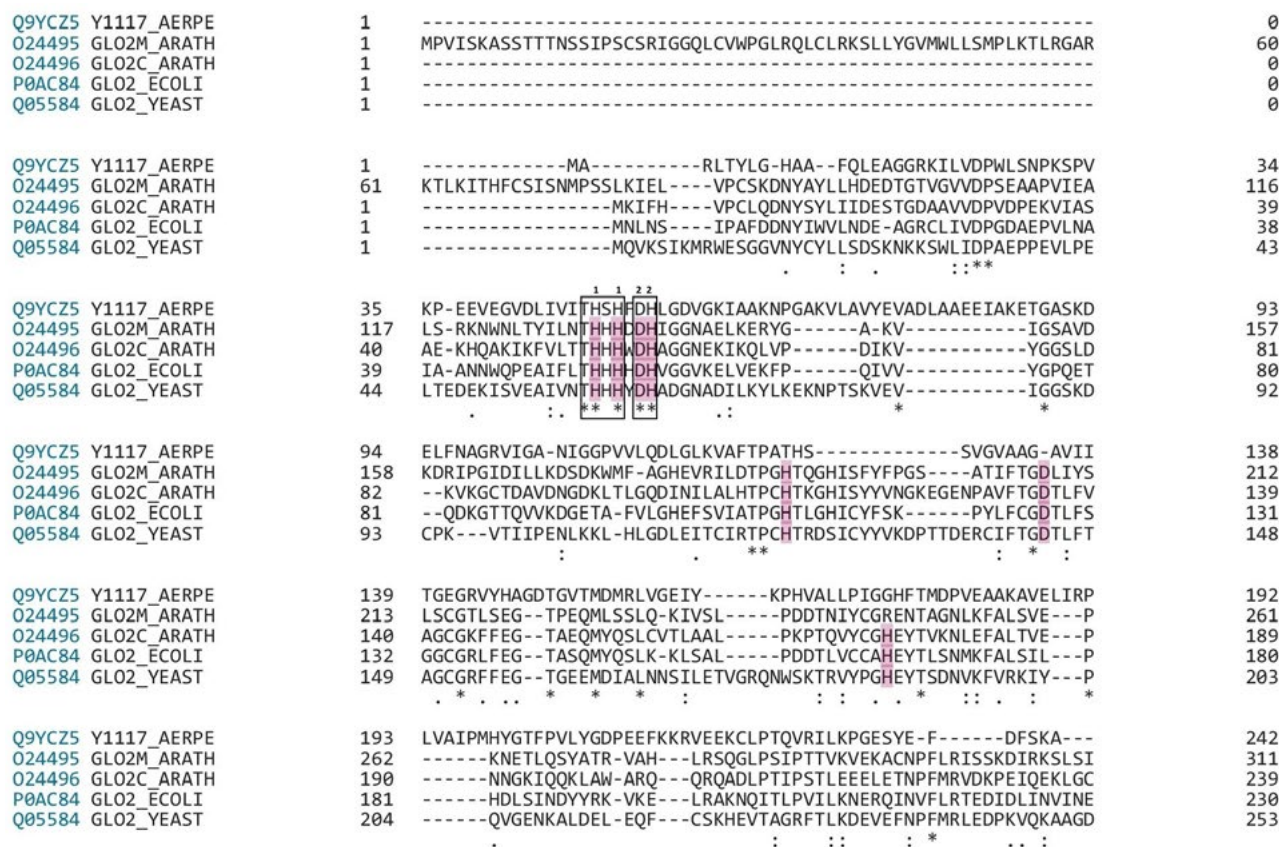


Figure 3. Multiple sequence alignment for Q9YCZ5 from *A. pernix* K1 and several proteins with known functions from zinc metallo-hydrolases group 2 (glyoxalase II), representing the hydroxyacylglutathione hydrolases (EC 3.1.2.6). Sequences: UPF0173 metal-dependent hydrolase from *A. pernix* K1 (Q9YCZ5); GLX2-1 from *Arabidopsis thaliana* (O24495, mitochondrial); GLX-2 from *A. thaliana* (O24496); gloB from *E. coli* (strain K12-POAC84); and GLO2 from *Saccharomyces cerevisiae* (Q05584). The alignment was constructed using the Clustal Omega program. *, identical residues; colon (:), residues with conserved substitutions; full stop (.), residues with semi-conserved substitutions; boxes with marks 1 and 2, residues that coordinate zincs 1, 2, respectively; numbers at the ends of each line (right-hand side), numbers of amino-acid residues.

that is overexpressed in response to osmotic stress, but not under heat and oxidative stress, and it can act as an organic and inorganic hydroperoxide peroxidase at high temperatures.³² All of these database searches indicated that the protein Q9Y9S7 from *A. pernix* K1 should be an OsmC-like protein.

3. 2. 3. Proteins With Hydrolase Activity

Protein spot ID8 (Q9YCZ5) was identified as the UPF0173 metal-dependent hydrolase, a member with an unidentified protein function. The Pfam database searches revealed that protein Q9YCZ5 has a lactamase B domain and it is a member of the metallo-β-lactamase superfamily. The β-lactamases are enzymes that hydrolyse β-lactam antibiotics and are responsible for the resistance of some bacteria to β-lactam antibiotics.³² The metallo-β-lactamases are class B β-lactamases that require Zn²⁺ for their function, with members distributed over three domains of living organisms: Eukarya, Archaea, and Bacteria.^{33,34} Most members of this superfamily share five conserved motifs, the most characteristic of which is a His-X-His-

X-Asp-His signature.²⁸ The family members include class B β-lactamase, thiolesterases, members of the glyoxalase II family, an mRNA 3'-processing protein, a DNA cross-link-repair enzyme, and a DNA-uptake-related protein, and as such, their sequences are highly divergent.³⁴ These proteins belong to the zinc metallo-hydrolase family of the β-lactamase fold. Based on their biological functions, the members of the zinc metallo-hydrolase family have been classified into 16 groups.³⁴ Some of these include one Zn²⁺ per molecule or require a binuclear active site, or they can have two iron ions per molecule.^{35,36–38} Multiple sequence alignments with the Clustal Omega program were carried out for Q9YCZ5 from *A. pernix* K1 and several proteins with known functions from the zinc metallo-hydrolases group 2 (glyoxalases II)³⁴ These revealed four of five highly conserved segments that are found in glyoxalases II (Figure 3). Glyoxalases II catalyze hydrolysis of the thiolester of S-D-lactoglutathione to produce glutathione and D-lactic acid, and they include two Zn²⁺ per molecule for their catalytic activity.³⁹ The UniProt database search for the alignment of the individual proteins (excluding Q9YCZ5) showed that His and Asp are the amino-acid residues that

bind two Zn^{2+} per subunit (Figure 3). Sequence alignments of Q9YCZ5 with glyoxalases II revealed that Q9YCZ5 has four highly conserved amino-acid residues: His49, His51, Asp53, and His54, which are also possible binding sites for Zn^{2+} . The ratio of total negatively charged amino-acids to positively charged amino-acids was in favor of the negatively charged residues in all of the aligned amino-acid sequences. The calculated pIs with the ProtParam program for the aligned proteins were from 5.43 (GLO2_ECOLI) to 6.14 (GLO2M_ARATH), with 5.72 for Q9YCZ5 from *A. pernix* K1. It can thus be concluded that this hypothetical protein, Q9YCZ5, from *A. pernix* K1 is related to the glyoxalases II, although this protein family shows sequence similarity to class B β -lactamase.⁴⁰ As such, protein Q9YCZ5 from *A. pernix* K1 might also have a role in detoxification of glycolysis by-products.

Protein spot ID11 (Q9YB20) from the crude methanol extract was identified as the protein with the highest molecular weight, of 57,988 Da. Q9YB20 is a carboxypeptidase (EC 3.4.24) with metallo-carboxypeptidase activity. These carboxypeptidases catalyze the hydrolysis of C-terminal amino-acids from polypeptide chains by a mechanism in which water acts as the nucleophile, one or two metal ions hold the water molecule in place, and the charged amino-acid side chains are ligands for the metal ions. The known metal ligands are His, Glu, Asp, and/or Lys, and at least one other residue is required for catalysis, which might have an electrophilic role. Of the known metalloproteases, around 50% of them contain an HEXXH motif.⁴¹ According to the MEROPS peptidase database (<http://merops.sanger.ac.uk/about/index.shtml>), Q9YB20 from *A. pernix* K1 belongs to the M32 peptidase family and the carboxypeptidase Taq family, with the MEROPS name for Q9YB20 of carboxypeptidase Pfu. M32 family members contain two Zn^{2+} -binding His residues and a catalytic Glu residue in a HEXXH Zn^{2+} -binding motif, a motif that is most commonly found in zinc endopeptidases and aminopeptidases.⁴² The third Zn^{2+} ligand is a Glu that is in a HES motif, further towards the C-terminus of the carboxypeptidase Taq family. Carboxypeptidase Taq is a Zn^{2+} -containing thermostable metallopeptidase.⁴³ The ScanProsite⁴⁴ (<http://www.expasy.ch/tools/scanprosite/>) sequence searches for Q9YB20 from *A. pernix* K1 revealed an AVIHEFGHAL motif as a Zn^{2+} -binding region between amino-acids 265 and 274. Carboxypeptidase Pfu was originally isolated and purified from the hyperthermophilic archaeon *P. furiosus*, and it was characterized as a cobalt-activated carboxypeptidase.⁴⁵

3. 2. 4. Dehydrogenases

Dehydrogenases acting on CH-OH or CH-NH₂ groups of donors were identified in the methanolic and water extracts. Protein spot ID1 was identified as malate dehydrogenase (MDH; accession number Q9YEA1; MDH_AERPE; EC 1.1.1.37), with 69% sequence coverage.

Sequence similarity searches showed that this protein belongs to the lactate dehydrogenase (LDH)/ MDH superfamily and the MDH type 3 family. The FASTA⁴⁶ sequence for Q9YEA1 revealed no Cys and Trp among the 308 amino acids. MDH_AERPE is an intracellular oxidoreductase, and it has been shown that it has a specificity for NADP⁺ (K_M , 0.019 mM) over the NAD⁺ coenzyme (K_M , 0.12 mM) for (S)-malate oxidation, and unlike MDH from other sources, it can readily catalyze tartrate oxidation. MDH_AERPE is a homotetrameric protein with a molecular mass of about 110 kDa.⁴⁷ Homotetrameric MDH has also been characterized from the hyperthermophilic Archaea *Methanocaldococcus jannaschii*, and from a dimer MDH from the hyperthermophilic Archaea *Arhaeoglobus fulgidus*; the dimer MDH from *A. fulgidus* lacks the sequence that mediates the dimer-dimer interaction.⁴⁸ Structural comparisons of MDHs have revealed that the hyperthermostability of MDH_AERPE appears to be attributable to its smaller cavity volume and larger number of ion pairs and ion-pair networks.⁴⁷

Protein Q9YC65 from the methanolic extract (an NADP-dependent glutamate dehydrogenase) was identified in two spots, spot ID5 and spot ID10, with slightly different pIs, of 6.42 and 6.50, respectively, but the same molecular masses (Figure 1, Table 1). This might have resulted from post-translational modifications, such as glycosylation, phosphorylation or proteolytic cleavage, which have been seen to occur with proteins in Archaea.⁴⁹ We used different tools for posttranslational modification predictions, and the only positive posttranslation modification for Q9YC65 was detected with NetPhos 2.0⁵⁰: Ser, Thr, and Tyr phosphorylation. Altogether, eight Ser, eight Thr, and five Tyr were predicted for posttranslational phosphorylation, with the highest scores for Ser116 (0.994), Ser395 (0.995), Thr43 (0.865), and Tyr147 (0.994).

We also identified an unusual member of the short-chain dehydrogenase/ reductase (SDR) family proteins: putative dehydrogenase, identified from water extracts (protein spot ID22). This dehydrogenase from *A. pernix* is unusual because of a unique catalytic triade of Ser-Ser-Arg, instead of the usually present catalytic triad composed of Ser-Tyr-Lys in the other SDR family proteins.^{51,52}

In the sample obtained from the water extract, some common dehydrogenases of the Calvin cycle were identified in protein spots ID11 and ID22 (Table 3).

3. 2. 5. Proteins Common to Most Organisms

Some proteins that can be found in all known organisms were also identified in these spots: ID4, ID6, ID10, ID13, ID15, ID16, ID17, ID18, ID23, and ID24, and their identification characteristics are summarized in Table 3. They participate in biosynthetic processes, such as amino-acid synthesis (ID13), polyamine synthesis (ID4) and protein synthesis (ID23, ID24), and they are part of the TCA cycle (ID6) or the pentose phosphate pathway

(ID18), or they are involved in substrate uptake and export, like ABC transporters (ID16, ID17). Various substrate-binding proteins from the ABC transporter family have already been identified in archaeon *A. pernix* K1 using a proteomic approach.⁵³

3. 2. 6. Putative Uncharacterized Proteins

Three putative uncharacterized proteins were identified in protein spots ID7, ID19, and ID20 (Tables 2, 3). The Pfam searches for protein ID7 defined two significant matches: one match was shared with the DUF1028 family of bacterial and archaeal proteins of unknown function, where some members are associated with a C-terminal peptidoglycan-binding domain; the other match found a putative peptidoglycan-binding domain shared with the peptidoglycan-binding-2 family. As archaeal cell walls lack peptidoglycan, and as some archaeal species have pseudopeptidoglycan⁵⁴, it is more likely that this protein is involved in maintenance of surface structures.

The Pfam search for protein ID19 found that this protein has a CoA binding domain with a Rossmann fold where the cofactor NAD⁺ binds.

Putative uncharacterized protein Q9Y996 has a DUF35 oligonucleotide/ oligosaccharide-binding (OB)-fold domain, a domain with unknown function that is conserved in hypothetical archaeal and bacterial proteins. The OB fold is at the C-terminal of the approximately 70-amino-acid-long domain.⁵⁵

4. Conclusions

Despite the low number of proteins identified in both of these extracts, those identified included some antioxidant proteins, such as SOD and thiol peroxidase, and a protein with a potential molecular function as a stress response, which might be responsible for the antioxidant activities of these extracts.

The antioxidative activity of the water extract was higher in comparison to that of the methanol extract, which indicates that the right selection of solvent is an important parameter in the preparation of *A. pernix* K1 biomass extracts with antioxidant activity.

5. Acknowledgements

This study was supported by the Ministry of Higher Education, Science and Technology of the Republic of Slovenia (Research program: Biochemical and Biophysical Characterization of Natural Compounds: P4-0121). The Aberdeen Proteome Facility is funded jointly by the Scottish Higher Education Funding Council (SHEFC), the Biotechnology and Biological Sciences Research Council (BBSRC), and the University of Aberdeen.

6. References

1. C. J. Reed, H. Lewis, E. Trejo, V. Winston, C. Evilia, *Archaea* **2013**, Article ID 373275. DOI:10.1155/2013/373275
2. M. M. Whittaker, J. W. Whittaker, *J. Biol. Inorg. Chem.* **2000**, *5*, 402–408. DOI:10.1111/j.1432-1033.1968.tb00383.x
3. S. Yamano, Y. Sako, N. Nomura, T. Maruyama, *J. Biochem.* **1999**, *126*, 218–225. DOI:10.1093/oxfordjournals.jbchem.a022426
4. E. Pedone, S. Bartolucci, G. Fiorentino, *Front. Biosci.* **2004**, *9*, 2909–2926. DOI:10.2741/1447
5. E. Mizohata, H. Sakai, E. Fusatomi, T. Terada, K. Murayama, M. Shirouzu, Y. Shigeyuki, *J. Mol. Biol.* **2005**, *354*, 317–329. DOI: 10.1016/j.jmb.2005.09.006
6. B. Wiedenheft, J. Mosolf, D. Willits, M. Yeager, K. A. Dryden, M. Young, T. Douglas, *Proc. Natl. Acad. Sci. U. S. A.* **2005**, *102*, 10551–10556. DOI: 10.1073/pnas.0501497102
7. B. Jia, J. Liu, L. Van Duyet, Y. Sun, Y. H. Xuan, G.-W. Cheong, *Front. Microbiol.* **2015**, *6*: 605. DOI:10.3389/fmicb.2015.00605
8. T. Nakamura, K. Torikai, K. Uegaki, J. Morita, K. Machida, A. Suzuki, Y. Kawata, *FEBS J.* **2011**, *278*, 598–609. DOI: 10.1111/j.1742-4658.2010.07977.x.
9. J. A. Littlechild, *Archaea*, **2015**, *2015*, 10 pg. Article ID 14767 DOI:10.1155/2015/147671
10. M. Li, L. Zhu, W. Wang, *SpringerPlus* **2016**, *5*, 1–10. DOI: 10.1186/s40064-016-1854-9 DOI:10.1186/s40064-016-1854-9
11. Y. Sako, N. Nomura, A. Uchida, Y. Ishida, H. Morii, Y. Koga, T. Hoaki, T. Maruyama, *Int. J. Syst. Bacteriol.* **1996**, *46*, 1070–1077. DOI: 10.1099/00207713-46-4-1070
12. S. Yamazuki, J. Yamazuki, K. Nishijima, R. Otsuka, M. Mise, H. Ishikawa, K. Sasaki, S. I. Tago, K. Isono, *Mol. Cell.* **2006**, *5*, 811–823. DOI: 10.1074/mcp.M500312-MCP200
13. G. Palmieri, A. Casbarra, I. Fiume, G. Catara, A. Capasso, G. Marino, S. Onesti, M. Rossi, *Extremophiles* **2006**, *10*, 393–402. DOI: 10.1007/s00792-006-0508-1
14. G. Palmieri, R. Cannio, I. Fiume, M. Rossi, G. Pocsfalvi, *Mol. Cell. Proteomics* **2009**, *8*, 2570–2581. DOI: 10.1074/mcp.M900012-MCP200
15. I. Milek, B. Cigić, M. Skrt, G. Kaletunc, N. Poklar Ulrih, *Can. J. Microbiol.* **2005**, *51*, 805–809. DOI: 10.1139/w05-060
16. L. H. Stickland, *J. Gen. Microbiol.* **1951**, *5*, 698–703. DOI: 10.1099/00221287-5-4-698. DOI:10.1099/00221287-5-4-698
17. M. M. Bradford, *Anal. Biochem.* **1976**, *72*, 248–254. DOI:10.1016/0003-2697(76)90527-3
18. W. Brand-Williams, M. E. Cuvelier, C. Berset, *LWT-Food Sci. Technol.* **1995**, *28*–30. DOI:10.1016/S0023-6438(95)80008-5
19. G. L. Ellman, *Arch. Biochem.* **1959**, *82*, 70–77. DOI:10.1016/0003-9861(59)90090-6
20. A. Görg, *Nature* **1991**, *349*, 545–546. DOI:10.1038/349545a0
21. S. Noori, *Sci. Rep.* **2012**, *1*, 1–9. DOI: 10.4172/scientificreports.413
22. M. S. Brewer, *Compr. Rev. Food Sci. Food Saf.* **2011**, *10*, 221–247. DOI: 10.1111/j.1541-4337.2011.00156.x

23. S. J. Jeon, K. Ishikawa, *J. Biol. Chem.* **2003**, 278, 24174–24180. DOI: 10.1074/jbc.M300618200
24. M. V. Weinberg, F. E. Jr. Jenney, X. Cui, M. W. W. Adams, *J. Bacteriol.* **2004**, 186, 7888–7895. DOI: 10.1128/JB.186.23.7888-7895.2004
25. A. Marchler-Bauer, S. Lu, J. B. Anderson, F. Chitsaz, M. K. Derbyshire, C. DeWeese-Scott, J.H. Fong, L. Y. Geer, R. C. Geer, N.R. Gonzales, M. Gwadz, D. I. Hurwitz, J. D. Jackson, Z. Ke, C. J. Lanczycki, F. Lu, G. H. Marchler, M. Mullokandov, M. V. Omelchenko, C. L. Robertson, J. S. Song, N. Thanki, R. A. Yamashita, D. Zhang, N. Zhang, C. Zheng, S. H. Bryant, *Nucleic Acids Res.* **2011**, 39, D225–D229. DOI: 10.1093/nar/gkq1189
26. Z. A. Wood, E. Schroder, J. Robin Harris, L. B. Poole, *Trends Biochem. Sci.* **2003**, 28, 32–40. DOI:10.1016/S0968-0004(02)00003-8
27. S. Gordia, C. Gutierrez, *Mol. Microbiol.* 1996, 19, 729–736. DOI: 10.1046/j.1365-2958.1996.418945.x
28. S. Mongkolsuk, W. Praituan, S. Loprasert, M. Fuangthong, S. Chamnongpol, *J. Bacteriol.* **1998**, 180, 2636–2643.
29. R. D. Finn, J. Mistry, J. Tate, P. Coghill, A. Heger, J. E. Pollington, O. L. Gavin, P. Gunasekaran, G. Ceric, K. Forslund, L. Holm, E. L. L. Sonnhammer, S. R. Eddy, A. Bateman, **2010**, 38, D211–D222. DOI: 10.1093/nar/gkp985
30. F. Sievers, A. Wilm, D. Dineen, T. J. Gibson, K. Karplus, W. Li, R. Lopez, H. McWilliam, M. Remmert, J. Söding, J. D. Thompson, D. G. Higgins, *Mol Syst Biol.* **2011**, 7, 1–6. DOI:10.1038/msb.2011.75
31. S. C. Park, B. P. Pham, L. V. Duyet, B. Jia, S. Lee, R. Yu, S. W. Han, J. K. Yang, K. S. Hahm, G. W. Cheong, *Biochim. Biophys. Acta* **2008**, 1784, 783–788. DOI: 10.1016/j.bbapap.2008.02.002
32. M. I. Page, A. Badarau, *Bioinorg. Chem. Appl.* **2008**, 2008, Article ID 576297. DOI:10.1155/2008/576297
33. C. Bebrone, *Biochem. Pharmacol.* **2007**, 74, 1686–1701. DOI:10.1016/j.bcp.2007.05.021
34. H. Daiyasu, K. Osaka, Y. Ishino, H. Toh, *FEBS Lett.* **2001**, 503, 1–6. DOI: 10.1016/S0014-5793(01)02686-2
35. J. A. Cricco, A. J. Vila, *Curr. Pharm. Des.* **1999**, 5, 915–927.
36. C. Frazão, G. Silva, C. M. Gomes, P. Matias, R. Coelho, L. Sieker, S. Macedo, M. Y. Liu, S. Oliveira, M. Teixeira, A. V. Xavier, C. Rodrigues-Pousada, M. A. Carrondo, J. L. Gall, *Nat. Struct.* **2000**, 7, 1041–1045. DOI:10.1038/80961
37. S. Y. Gu, X. X. Yan, D. C. Liang, *Proteins* **2008**, 72, 531–536. DOI: 10.1002/prot.22069
38. A. Yamamura, J. Ohtsuka, K. Kubota, Y. Agari, A. Ebihara, N. Nakagawa, K. Nagata, M. Tanokura, *Proteins* **2008**, 73, 1053–1057. DOI: 10.1002/prot.22215
39. A. D. Cameron, M. Ridderström, B. Olin, B. Mannervik, *Structure* **1999**, 7, 1067–1078. DOI:10.1016/S0969-2126(99)80174-9
40. A. F. Neuwald, J. S. Liu, D. J. Lipman, C. E. Lawrence, *Nucleic Acids Res.* **1997**, 25, 1665–1677. DOI:10.1093/nar/25.9.1665
41. N. D. Rawlings, A. J. Barret, *Methods Enzymol.* **1995**, 248, 183–228. DOI: 10.1016/0076-6879(95)48015-3
42. S. H. Lee, H. Taguchi, E. Yoshimura, E. Minagawa, S. Kaminogawa, T. Ohta, H. Matsuzawa, *Protein Eng.* **1996**, 9, 467–469. DOI: 10.1093/protein/9.6.467
43. S. H. Lee, H. Taguchi, E. Yoshimura, E. Minagawa, S. Kaminogawa, T. Ohta, H. Matsuzawa, *Biosci., Biotechnol.* **1994**, 58, 1490–1495. DOI: 10.1271/bbb.58.1490
44. E. Castro, C. J. A. Sigrist, A. Gattiker, V. Bulliard, P. S. Langendijk-Genevaux, E. Gasteiger, A. Bairoch, N. Hulo, *Nucleic Acids Res.* **2006**, 34, W362–W365. DOI: 10.1093/nar/gkl124
45. T. C. Cheng, V. Ramakrishnan, S. I. Chan, *Protein Sci.* **1999**, 8, 2474–2486. DOI: 10.1110/ps.8.11.2474
46. W. R. Pearson, D. J. Lipman, *Proc. Natl. Acad. Sci. U. S. A.* **1988**, 85, 2444–2448. DOI:10.1073/pnas.85.8.2444
47. R. Kawakami, H. Sakuraba, S. Goda, H. Tsuge, T. Ohshima, *Biochim. Biophys. Acta* **2009**, 1794, 1496–1504. DOI: 10.1016/j.bbapap.2009.06.014
48. D. Madern, C. Ebel, H. A. Dale, T. Lien, I. H. Steen, N. K. Birkeland, G. Zaccari, *Biochemistry* **2001**, 40, 10310–10316. DOI: 10.1021/bi010168c
49. J. Eichler, M. W. W. Adams, *Microbiol. Mol. Biol. Rev.* **2005**, 69, 393–425. DOI: 10.1021/bi010168c
50. N. Blom, S. Gammeltoft and S. Brunak, *J. Mol. Biol.* **1999**, 294, 1351–1362. DOI: 10.1006/jmbi.1999.3310
51. A. Yamamura, T. Ichimura, F. Mimoto, J. Ohtsuka, K. I. Miyazono, M. Okai, M. Kamo, W. C. Lee, K. Nagata, M. Tanokura, *Proteins*, **2008**, 70, 1640–1645. DOI: 10.1002/prot.21860
52. T. Tanabe, N. Tanaka, K. Uchikawa, T. Kabashima, K. Ito, T. Nonaka, Y. Mitsui, M. Tsuru, T. Yoshimoto, *J. Biochem.* **1998**, 124, 634–641. DOI:10.1093/oxfordjournals.jbchem.a022159
53. P. Jamnik, M. Meglen, P. Raspor, N. Poklar Ulrih, *World J. Microbiol. Biotechnol.* **2010**, 26, 1579–1586. DOI: 10.1007/s11274-010-0333-7
54. O. Kandler, H. König, *Cell. Mol. Life Sci.* **1998**, 54, 305–308. DOI: 10.1007/s000180050156
55. A. G. Murzin, *EMBO J.* **1993**, 12, 861–867.

Povzetek

Hipertermofilna arheja *Aeropyrum pernix* je prilagojena za življenje pri visokih temperaturah, v slanem okolju in pri oksidativnih pogojih. V tej raziskavi smo se osredotočili na antioksidativno aktivnost proteinov iz *A. pernix* K1. Proteine smo iz biomase *A. pernix* ekstrahirali v metanolu in vodi pri visoki temperaturi. V ekstraktih smo določili skupne tiolne skupine in antioksidativno učinkovitost. V metanolnem ekstraktu je bila vsebnost skupnih proteinov za 36 % nižja kot v vodnem ekstraktu, prav tako je bilo za 10 % manj določenih skupnih tiolnih skupin. Antioksidativna učinkovitost vodnega ekstrakta je bila štirikrat višja kot metanolnega. Proteine smo iz obeh ekstraktov ločili z dvodimenzionalno elektroforezo, izbrane proteine pa analizirali z masno spektrometrijo. Večina identificiranih proteinov sodi med intracelularne proteine, ki so vključeni v oksidativni in osmolarni stresni odgovor. Identificirani smo tudi nekaj proteinov s hidrolitično in dehidrogenazno aktivnostjo.

Scientific paper

Understanding the Inhibition of Mild Steel Corrosion by Dianiline Schiff Bases: a DFT Investigation

Salah Eddine Hachani*, Zelikha Necira, Djamel Eddine Mazouzi and Nadia Nebbache

Laboratory of Applied Chemistry LCA, Faculty of Science, University of Biskra, B.P. 145, RP. 07000 Biskra, Algeria

* Corresponding author: E-mail: salaho_hachani@yahoo.fr
Phone number: +213791162887

Received: 28-08-2017

Abstract

Quantum chemical calculations at DFT/B3LYP level of theory with 6-31G, 6-311G, and 6-311G(d,p) basis sets were done to correlate the inhibition of mild steel corrosion in 1 M H₂SO₄ by four dianiline Schiff bases namely N,N'-Bis(benzylidene)-4,4'-dianiline (DAA), N,N'-Bis (benzylidene)-4,4'-methylenedianiline (MDAA), N,N' Bis(benzylidene)-4,4'-sulphonyldianiline (SDAA) and N,N'-Bis(benzylidene)-4,4'-oxydianiline (ODAA) with their electronic and structural properties. Quantum chemical parameters such as the E_{HOMO}, E_{LUMO}, energy gap (ΔE), dipole moment (μ), global softness (σ), and global hardness (η) were calculated and discussed to provide valuable explanations for the reactivity and selectivity of the studied inhibitors. The results obtained showed a certain relationship to the experimental inhibition efficiency results earlier reported.

Keywords: Dianiline Schiff bases, corrosion, inhibition, mild steel, 1 M H₂SO₄, DFT

1. Introduction

The prevention of mild steel against corrosion has attracted great attention from both academia and industry due to the important role of mild steel in several industrial applications such as storage and transportation of various chemical solutions.¹ Mild steel equipments must be regularly cleaned to prevent damage and maintain the application efficiency. Acid solution is extensively used in chemical cleaning of mild steel which leads, after a certain time, to corrode its surfaces.^{2,3}

The protection of mild steel using corrosion inhibitors is one of the most practical processes.⁴ Organic compounds containing heteroatoms with lone pairs of electrons (oxygen, sulfur, nitrogen, and phosphorus), aromatic rings, and π-electrons in triple or conjugated double bonds are considered to be excellent corrosion inhibitors.⁵ The corrosion inhibitory of such organic compounds is closely related to their adherence on metal surfaces via a physical adsorption (physisorption) which arises from electrostatic interactions between the inhibitor and the metallic surface or via chemical adsorption (chemisorption) by coordination bonds.^{6,7}

Schiff bases are organic compounds obtained from the condensation of carbonyls and amines. This type of

compounds has a well-known popularity in the field of materials science due to their potential advantages such as easy synthetic route, high purity, low toxicity, and their eco-friendly nature.⁸⁻¹⁰ The experimental studies on corrosion inhibitors have demonstrated that Schiff base molecules can be used as effective corrosion inhibitors in different aggressive media.¹¹

Experimental techniques such as weight loss measurements, potentiodynamic polarization and electrochemical impedance spectroscopy are useful in understanding the corrosion inhibition mechanisms but they are expensive and time-consuming.^{12,13} Computer hardware and software advances have motivated scientists to use theoretical chemistry in the field of corrosion research. Density functional theory (DFT) method is a very reliable tool effectively used to understand the chemical reactivity and site selectivity of the molecular systems and to describe the structural nature of the inhibitor on the corrosion process.¹⁴

Theoretical investigations using density functional theory (DFT) calculations in both gas and aqueous phases have been carried out in the field of corrosion research to explore the correlations of the experimental inhibition efficiencies with the molecular structures of corrosion inhibitors.¹⁵⁻¹⁷ The calculated results indicated that the inhi-

bition efficiency of each molecule depends on its molecular structure and global reactivity descriptors such as its highest occupied molecular orbital energy (E_{HOMO}), lowest unoccupied molecular orbital energy (E_{LUMO}), energy difference HOMO–LUMO (ΔE), electronegativity (χ), global hardness (η), softness (σ), and the fraction of electrons transferred (ΔN).

In a study,¹⁸ the inhibition of mild steel corrosion in sulfuric acid media by dianiline Schiff bases namely N,N'-Bis(benzylidene)-4,4'-dianiline (DAA), N,N'-Bis(benzylidene)-4,4'-methylenedianiline (MDAA), N,N'-Bis(benzylidene)-4,4'-sulphonyldianiline (SDAA) and N,N'-Bis(benzylidene)-4,4'-oxydianiline (ODAA) (Fig. 1) was investigated. A good inhibition activity has been reported for the four compounds under probe.

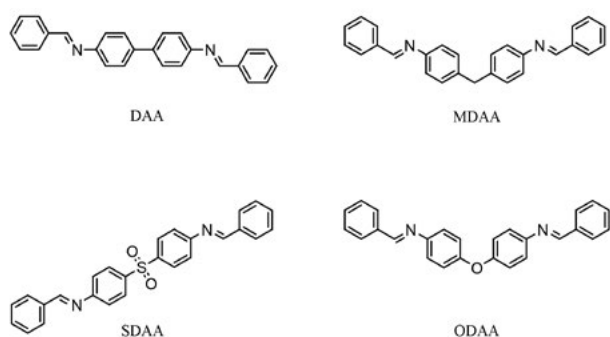


Figure 1: Chemical molecular structures of the studied dianiline Schiff bases.

To the best of our knowledge, there is no theoretical background has been proposed to explain the relationship between the experimental protection efficiencies of the dianiline Schiff bases inhibitors and their molecular and electronic properties.

The present theoretical investigation aims to provide supportive explanations for the observed experimental results of the inhibition effects. Global chemical reactivity parameters including the energies of frontier orbitals (E_{HOMO} and E_{LUMO}), energy gap (ΔE), dipole moment (μ), hardness (η), softness (σ), the fraction of electrons transferred (ΔN), and total energy (TE) were reported and discussed.

2. Computational details

Density functional theory (DFT) method is theoretical approach widely applied to predict the chemical reactivity of molecules due to its ability to give accurate geometries and electronic properties of chemical compounds.¹⁹ DFT with Beck's three parameter exchange functional along with the Lee-Yang-Parr non local correlation functional (B3LYP) has been largely used to study of chemical reactivity and selectivity of the inhibitor molecules.²⁰ In the current contribution, calculations at DFT/B3LYP have

been done in vacuo at the neutral forms of the dianiline Schiff bases molecules. 6-31G, 6-311G and 6-311G(d,p) basis sets were selected to optimize the molecular structures at minimum energy level and considered adequate enough to calculate the global reactivity descriptors for the tested molecules. The input files of the studied dianiline Schiff bases were built using Gauss View 5.0.8.²¹ The calculations were carried out using Gaussian 03W program package.²²

According to the Koopmans' theorem,²³ electronic molecular descriptors such as the ionization potential (I) and electron affinity (A) are related to HOMO and LUMO energies and they are given by the relations 1 and 2:

$$I = -E_{HOMO} \quad (1)$$

$$A = -E_{LUMO} \quad (2)$$

According to Pearson,²⁴ the electronegativity (χ), global hardness (η), and global softness (σ) can be calculated from the ionization potential (I) and electron affinity (A) using the following equations:

$$\chi = (I + A)/2 \quad (3)$$

$$\eta = (I - A)/2 \quad (4)$$

$$\sigma = 1/\eta \quad (5)$$

The fraction of electrons transferred (ΔN) from the chemical species to the metal surface is calculated using Pearson's equation²⁵:

$$\Delta N = (\Phi - \chi_{inh})/2(\eta_{Fe} + \eta_{inh}) \quad (6)$$

Where Φ is the work function of the iron surface with the value of 4.82 eV for Fe (110). χ_{inh} is the absolute electronegativity of the inhibitor molecule, η_{Fe} and η_{inh} are the absolute hardness of iron and the inhibitor molecule respectively. In this study, we consider η_{Fe} 0 eV to compute the fraction of electrons transferred (ΔN) for each inhibitor.^{26,27}

3. Results and Discussions

3. 1. Results of the Calculations for Non-protonated Species

The inhibition effects of four dianiline Schiff bases on the mild steel corrosion in 1.0 M H_2SO_4 solution were experimentally investigated using different techniques such as weight loss test, polarization measurements, and electrochemical impedance spectroscopy.¹⁸ The experimental results showed that the investigated compounds can act as good inhibitors and DDA exhibits the best inhi-

bition efficacy. The experimental inhibition efficiencies of the studied compounds follow the order: MDAA \approx DAA > SDAA > ODAA.¹⁸

In the present contribution, quantum chemical calculations have been performed to find the relationship between the molecular electronic features of the studied inhibitors and their experimental inhibition efficiencies. The optimized molecular structures of the dianiline Schiff bases inhibitors under investigation are shown in Figure 2.

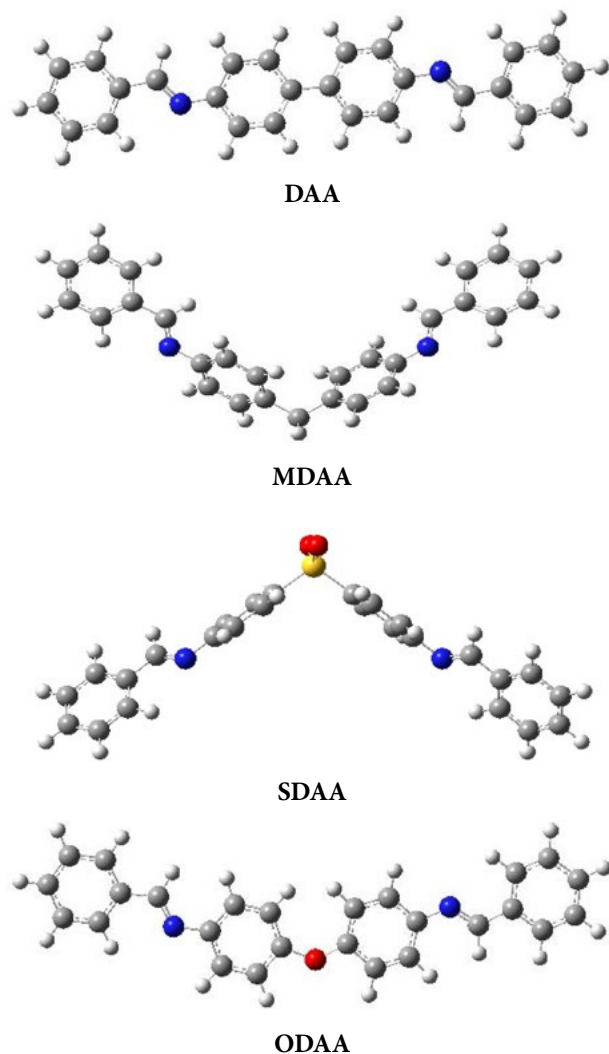


Figure 2: Optimized molecular structures of non-protonated inhibitor molecules using B3LYP/6-31 G calculation level.

The molecular geometry is a critical parameter used to evaluate the adsorption of the inhibitor on metal surface. Molecules having planar molecular structure have a greater tendency to adsorb on metal surface than molecules having less planar geometry.²⁸ The geometries of the molecules under probe given in Figure 3, show that DAA and ODAA are highly planar while MDAA and SDAA are less planar. The adsorbability of the tested molecules on

the mild steel surface would probably be ranked as follows: DAA \approx ODAA > SDAA \approx MDAA, this result indicates that DAA has a greater tendency to adsorb on metal surface compared to the other studied molecules.

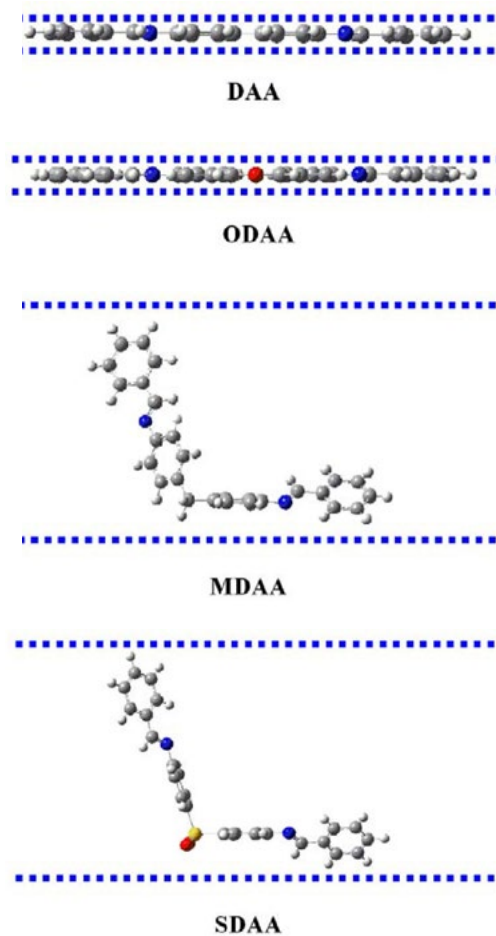


Figure 3: Geometry planarity of the studied dianiline Schiff bases.

Beside the molecular geometries of the studied inhibitors, an analysis of other quantum chemical parameters as E_{HOMO} , E_{LUMO} , ΔE , global softness (σ), global hardness (η), and fraction of electrons transferred (ΔN) are efficient for finding which inhibitor molecule has greater ability to donate electrons, receive electrons from the metal or bind more strongly to the metallic surface to act as suitable corrosion inhibitor.

Table 1 and 2 give the calculated quantum chemical descriptors for the molecules under probe. In the light of total energy data given in Table 1, it can be seen that the best corrosion inhibitor (DAA) has the highest total energy (-30260.1092 eV) among the studied molecules, which confirms that DDA has highest chemical reactivity towards mild steel surface.

It is well known that inhibitor reactivity is closely related to its adsorption on metal surface via donor-acceptor

Table 1: Calculated quantum chemical descriptors for non-protonated molecules in gas phase.

	TE (eV)	μ (D)	E_{HOMO} (eV)	E_{LUMO} (eV)	ΔE (eV)
6-31G					
DAA	-30260.1092	0.0000	-5.4975	-2.0762	-3.4213
MDAA	-31329.6100	2.2011	-5.7291	-1.6443	-4.0848
SDAA	-45182.0792	7.1350	-6.3688	-2.1325	-4.2363
ODAA	-32305.6070	1.0153	-5.4815	-1.8293	-3.6522
6-311G					
DAA	-30266.3755	0.0000	-5.7336	-2.3107	-3.4229
MDAA	-31336.1285	2.2899	-5.9646	-1.8730	-4.0916
SDAA	-45190.3736	7.1574	-6.6143	-2.3471	-4.2672
ODAA	-32312.5246	1.0582	-5.7260	-2.0682	-3.6578
6-311G(d,p)					
DAA	-30274.5902	0.0000	-5.6522	-2.2930	-3.3592
MDAA	-31344.6963	2.4538	-5.9243	-1.8450	-4.0793
SDAA	-45203.7810	5.9356	-6.4268	-2.2685	-4.1583
ODAA	-32321.4565	0.8956	-5.6265	-2.0400	-3.5865

Table 2: Calculated quantum chemical descriptors for non-protonated molecules in gas phase.

	I (eV)	A (eV)	χ (eV)	η (eV)	σ (eV ⁻¹)	ΔN
6-31G						
DAA	5.4975	2.0762	3.7868	1.7106	0.5846	0.3020
MDAA	5.7291	1.6443	3.6867	2.0424	0.4896	0.2774
SDAA	6.3688	2.1325	4.2506	2.1182	0.4721	0.1344
ODAA	5.4815	1.8293	3.6554	1.8261	0.5476	0.3189
6-311G						
DAA	5.7336	2.3107	4.0221	1.7114	0.5843	0.2331
MDAA	5.9646	1.8730	3.9188	2.0458	0.4888	0.2202
SDAA	6.6143	2.3471	4.4807	2.1336	0.4687	0.0795
ODAA	5.7260	2.0682	3.8971	1.8289	0.5468	0.2523
6-311G(d,p)						
DAA	5.6522	2.2930	3.9726	1.6796	0.5954	0.2523
MDAA	5.9243	1.8450	3.8846	2.0396	0.4903	0.2293
SDAA	6.4268	2.2685	4.3476	2.0791	0.4810	0.1136
ODAA	5.6265	2.0400	3.8332	1.7932	0.5577	0.2751

interactions. According to Fukui's frontier molecular orbital theory, HOMO and LUMO energies are very useful in understanding the adsorption reactivity of a molecule.²⁹ E_{HOMO} describes the electron-donating ability of the inhibitor; higher E_{HOMO} facilitates the electron donation from the inhibitor to the vacant d orbitals of metal atoms. E_{LUMO} is related to electron-accepting ability of the inhibitor; lower E_{LUMO} indicates high capacity of the inhibitor to receive electrons from metal surface. HOMO and LUMO distribution in the non-protonated dianiline Schiff bases under probe is shown in Figure 4. The calculated energies corresponding to these frontier orbitals are presented in Table 1. It can be observed that E_{HOMO} values increase in the order: SDAA < MDAA < DAA < ODAA, indicating that the studied inhibitors donate electrons to mild steel surface following the order: ODAA > DAA > MDAA >

SDAA, these results are not in good agreement with the experimental inhibition efficiencies.

The energy gap (ΔE): the energy difference between HOMO and LUMO is also an important parameter used to evaluate the inhibitor reactivity towards the metal surface.²² As ΔE decreases, the chemical reactivity increases leading to an increase in the adsorption of the inhibitor molecules on the metallic surface.³⁰ The calculated ΔE values for non-protonated molecules under investigation are given in Table 1, it can be seen that the trend of ΔE is as follows: DAA > ODAA > MDAA > SDAA, which is not in agreement with the experimental findings.

Electronegativity (χ) is a chemical property that describes the molecule capability to attract electrons. High inhibition efficiency is expected for the molecules having lower electronegativity because they could easily donate

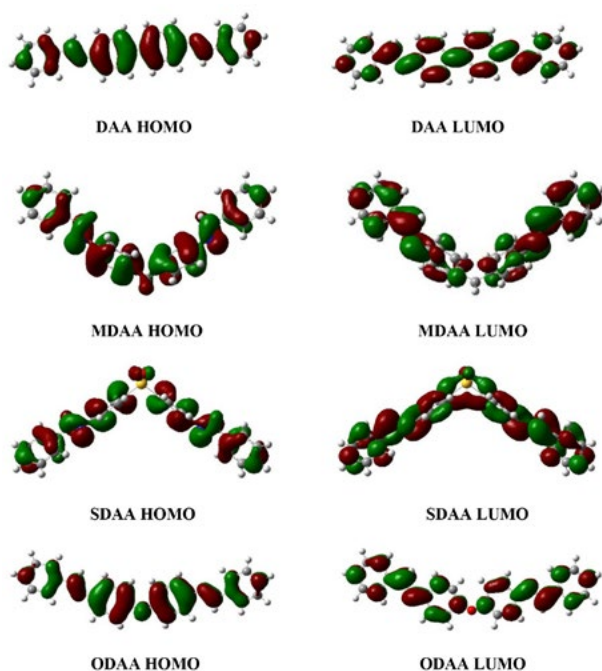


Figure 4: HOMO and LUMO orbitals of non-protonated inhibitor molecules using B3LYP/6-31G calculation level.

their electrons to the metal surface.³¹ Table 2 gives the calculated electronegativity (χ) data of the studied molecules, it is clear that the calculated electronegativity values exhibit the tendency: SDAA > DAA > MDAA > ODAA, which does not correlate with the experimental inhibition efficiency results.

Global hardness (η) is a measure of molecule resistance towards electron cloud polarization or deformation of molecules under small perturbations of the chemical reaction.³² The inhibitor with the least value of global hardness is expected to have the highest inhibition efficiency.³³ The calculated global hardness values displayed in Table 2 show that DAA has the lowest global hardness value, which confirms its highest inhibition efficiency.

Global Softness (σ) is an important quantum parameter used to explain chemical reactivity of the molecule. The adsorption on metal surface occurs at the part of the molecule where softness has higher value.³⁴ It can be seen from Table 2 that the calculated softness values of the studied inhibitors increase as follows: SDAA < MDAA < ODAA < DAA, indicating that DAA has stronger adsorption on metal surface compared to the absorption of MDAA, SDAA, and ODAA, respectively.

The fraction of electrons transferred (ΔN) from the inhibitor to the metallic surface is calculated using Pearson's formula (Eq. 6). According to Lukovits et al.³⁵ the inhibition activity increases with increasing of electron-donating ability of the molecule to the metal surface if $\Delta N < 3.6$. It is apparent from Table 2 that ΔN values are positive and are below 3.6, indicating the tendency of the tested

Schiff bases to give electrons to mild steel surface. The electron donation of the studied inhibitors increases in the order: SDAA < MDAA < DAA < ODAA, this result is in negative correlation with the experimental results of the inhibition efficiency.

The dipole moment (μ) results from non-uniform distribution of charges on the various atoms in the molecule.³⁶ High dipole moment is required to ensure a better molecule adsorption on metal surfaces.³⁷ The dipole moment values presented in Table 1, show that the trend of the μ values is: SDAA > MDAA > ODAA > DAA, which does not correlate well with the experimental data. Similar irregularities in the correlation of dipole moment with the experimental inhibition efficiency results have also been reported.³⁸

3. 2. Results of the Calculations for Protonated Species

In acidic solution, corrosion inhibitor compounds can be easily protonated due to the presence of heteroatoms with a number of lone pairs of electrons in their molecular structures. In such cases, it is important to investigate the properties of the corrosion inhibitor in the protonated form and compare it with those of the non-protonated form to find the preferred form of the inhibitor to interact with the metal surface.

In the case of dianiline Schiff bases under investigation, N atoms in each compound are the possible sites for

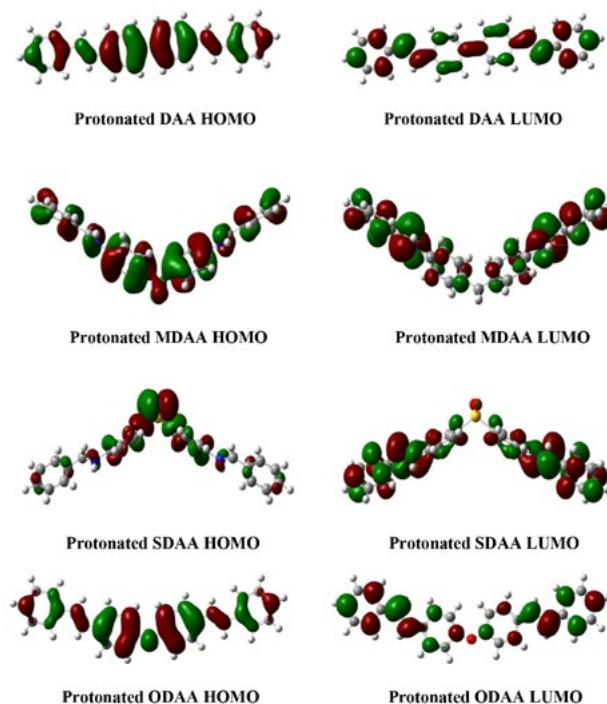


Figure 5: HOMO and LUMO orbitals of the protonated inhibitor molecules at B3LYP/6-31G level.

Table 3: Calculated quantum chemical descriptors for protonated molecules in gas phase.

	TE (eV)	μ (D)	E_{HOMO} (eV)	E_{LUMO} (eV)	ΔE (eV)
6-31G					
DAA	-30280.0092	0.0005	-11.3172	-8.3724	-2.9448
MDAA	-31349.6019	2.9911	-11.5562	-8.0977	-3.4585
SDAA	-45201.3503	12.7733	-11.8510	-8.3963	-3.4547
ODAA	-32325.5683	2.4108	-11.0725	-8.1590	-2.9135
6-311G					
DAA	-30285.9332	0.0005	-11.5032	-8.5425	-2.9607
MDAA	-31355.7800	2.9757	-11.7743	-8.2511	-3.5232
SDAA	-45209.3033	12.8562	-12.0919	-8.5542	-3.5377
ODAA	-32332.1408	2.4482	-11.2662	-8.3324	-2.9338
6-311G(d,p)					
DAA	-30293.9643	0.0006	-11.4840	-8.5295	-2.9545
MDAA	-31364.1282	3.0031	-11.7249	-8.2678	-3.4571
SDAA	-45222.6089	11.8761	-12.1723	-8.5209	-3.6514
ODAA	-32340.9189	2.1829	-11.2466	-8.2979	-2.9487

Table 4: Calculated quantum chemical descriptors for protonated molecules in gas phase.

	I (eV)	A (eV)	χ (eV)	η (eV)	σ (eV ⁻¹)	ΔN
6-31G						
DAA	11.3172	8.3724	9.8448	1.4724	0.6792	-1.7063
MDAA	11.5562	8.0977	9.8269	1.7292	0.5783	-1.4477
SDAA	11.8510	8.3963	10.1236	1.7273	0.5789	-1.5352
ODAA	11.0725	8.1590	9.6157	1.4567	0.6865	-1.6461
6-311G						
DAA	11.5032	8.5425	10.0228	1.4803	0.6755	-1.7573
MDAA	11.7743	8.2511	10.0127	1.7616	0.5677	-1.4738
SDAA	12.0919	8.5542	10.3230	1.7688	0.5653	-1.5556
ODAA	11.2662	8.3324	9.7993	1.4669	0.6817	-1.6972
6-311G(d,p)						
DAA	11.4840	8.5295	10.0067	1.4772	0.6769	-1.7556
MDAA	11.7249	8.2678	9.9963	1.7285	0.5785	-1.4973
SDAA	12.1723	8.5209	10.3466	1.8257	0.5477	-1.5136
ODAA	11.2466	8.2979	9.7722	1.4743	0.6783	-1.6795

protonation. The calculations for the protonated form have been performed using the same basis sets as the case of non-protonated species, the quantum chemical parameters related to the global reactivity of the protonated species are reported in Table 3 and 4.

The electronic distribution of HOMO and LUMO orbitals in the protonated species is presented in Figure 5.

The comparison of E_{HOMO} , E_{LUMO} , and ΔE of the protonated species and those of the non-protonated species revealed that E_{HOMO} for the protonated form is lower than for the non-protonated form, suggesting that the non-protonated form has a greater tendency to donate electrons to the poor metal atoms than the protonated form. E_{LUMO} has lower values in the protonated form than in the non-protonated form, which means that the protonated form has a greater tendency to accept elec-

trons from the metal than the non-protonated species. The energy gap (ΔE) values are greater for the protonated form than for the non-protonated form, indicating that the non-protonated species has a greater tendency to adsorb on the metal surface than the protonated species.

The fraction of electrons transferred (ΔN) values of the protonated species are negative, indicating that the protonated form is more electron deficient than the non-protonated form.

The dipole moment is higher for the protonated species than for the non-protonated species suggesting that dipole-dipole interactions are more predominant in the interaction between the metal surface and the protonated form than in the interaction between the metal surface and the non-protonated form.

4. Conclusion

This study aims to bridge the gap between the corrosion inhibition efficiencies of four dianiline Schiff bases and their electronic and molecular properties. DFT calculations at B3LYP functional with 6-31G, 6-311G, and 6-311G(d,p) basis sets were employed at the non-protonated and protonated forms of the studied molecules. It was concluded from this study that:

- DAA has the highest total energy among the studied dianiline Schiff bases, confirming its highest reactivity towards metal surface.
- Quantum parameters such as global hardness (η) and global softness (σ) support that DAA has the highest inhibition efficiency.
- No direct relationship between the experimental results of the inhibition efficiencies and both gap energy (ΔE), electronegativity (χ), the fraction of electrons transferred (ΔN), and dipole moment (μ).
- The comparison between the results of the non-protonated species and those of the protonated species showed that the non-protonated form of the dianiline Schiff bases is the preferred form to interact with the metal surface.

Acknowledgment: The authors would like to thank Professor Bachir Abdelmalik from the department of computer science, University of Biskra-Algeria for his English skills.

Funding: This research did not receive any specific grant from funding agencies in the public, commercial, or not-for-profit sectors.

5. References

1. Y. Liang, C. Wang, J. S. Li, L. J. Wang, J. J. Fu, *Int. J. Electrochem. Sci.* **2015**, *10*, 8072–8086.
2. S. A. A. El-Maksoud, A. S. Fouda, *Mater. Chem. Phys.* **2005**, *93*, 84–90. DOI:10.1016/j.matchemphys.2005.02.020
3. H. Keles, M. Keles, I. Dehri, O. Serindag, *Mater. Chem. Phys.* **2008**, *12*, 173–179. DOI:10.1016/j.matchemphys.2008.05.027
4. L. Guo, X. Ren, Y. Zhou, S. Xu, Y. Gong, S. Zhang, *Arab. J. Chem.* **2017**, *10*, 121–130. DOI:10.1016/j.arabj.2015.01.005
5. N. O. Eddy, *Port. Electrochim. Acta.* **2009**, *27*, 579–589. DOI:10.4152/pea.200905579
6. R. Solmaz, E. A. Sahin, A. Doner, G. Kardas, *Corros. Sci.* **2011**, *53*, 3231–3240. DOI:10.1016/j.corsci.2011.05.067
7. O. K. Abiola, N. C. Oforka, *Mater. Chem. Phys.* **2004**, *83*, 315–322. DOI:10.1016/j.matchemphys.2003.10.001
8. H. D. Lece, K. C. Emregul, O. Atakol, *Corros. Sci.* **2008**, *50*, 1460–1468. DOI:10.1016/j.corsci.2008.01.014
9. S. Issaadi, T. Douadi, A. Zouaoui, S. Chafaa, M. A. Khan, G. Bouet, *Corros. Sci.* **2011**, *53*, 1484–1488. DOI:10.1016/j.corsci.2011.01.022
10. K. R. Ansari, M. A. Quraishi, A. Singh, *Corros. Sci.* **2014**, *79*, 5–15. DOI:10.1016/j.corsci.2013.10.009
11. M. Behpour, S. M. Ghoreishi, N. Soltani, M. Salavati-Niasari, *Corros. Sci.* **2009**, *51*, 1073–1082. DOI:10.1016/j.corsci.2009.02.011
12. M. G. V. Satyanarayana, V. Himabindu, Y. Kalpana, M. R. Kumar, K. Kumar, *J. Mol. Struct. (THEOCHEM)*. **2009**, *912*, 113–118. DOI:10.1016/j.theochem.2009.01.005
13. T. H. Muster, A. E. Hughes, S. A. Furman, T. Harvey, N. Sherman, S. Hardin, P. Corrigan, D. Lau, F. H. Scholes, P. A. White, M. Glenn, S. J. Garcia, J. M. C. Mol, *Electrochim. Acta.* **2009**, *54*, 3402–3411. DOI:10.1016/j.electacta.2008.12.051
14. S. K. Saha, P. Banerjee, *RSC Adv.* **2015**, *5*, 71120–71130.
15. S. Erdogan, Z. S. Safi, S. Kaya, D. O. Isin, L. Guo, C. Kaya, *J. Mol. Struct.* **2017**, *1134*, 751–761. DOI:10.1016/j.molstruc.2017.01.037
16. Z. El Adnani, M. Mcharfi, M. Sfaira, M. Benzakour, A. T. Benjelloun, M. Ebn Touhami, *Corros. Sci.* **2013**, *68*, 223–230. DOI:10.1016/j.corsci.2012.11.020
17. H. Lgaz, K. Subrahmanya Bhat, R. Salghi, Shubhalaxmi, S. Jodeh, M. Algarra, B. Hammouti, I. H. Ali, A. Essamri, *Journal of Molecular Liquids*, **2017**, *238*, 71–83. DOI:10.1016/j.molliq.2017.04.124
18. S. Chitra, K. S. Parameswari, *Int. J. Electrochem. Sci.* **2010**, *5*, 1675–1697.
19. C. O. Gretir, B. Mihci, G. Bereket, *J. Mol. Struct. (THEOCHEM)*. **1999**, *488*, 223–231. DOI:10.1016/S0166-1280(99)00033-0
20. S. G. Zhang, W. Lei, M. Z. Xia, F. Y. Wang, *J. Mol. Struct. (THEOCHEM)*. **2005**, *732*, 173–182. DOI:10.1016/j.theochem.2005.02.091
21. I. B. Obot, S. Kaya, C. Kaya, B. Tuzun, *Res Chem Intermed.* **2016**, *42*, 4963–4983. DOI:10.1007/s11164-015-2339-0
22. A. Zarrouk, I. El Ouali, M. Bouachrine, B. Hammouti, Y. Ramli, E. M. Essassi, I. Warad, A. Aouniti, R. Salghi, *Res Chem Intermed.* **2013**, *39*, 1125–1133. DOI:10.1007/s11164-012-0671-1
23. T. Koopmans, *Physica E.* **1934**, *1*, 104–113.
24. R. G. Pearson, *Inorg. Chem.* **1988**, *27*, 734–740. DOI:10.1021/ic00277a030
25. S. Martinez, *Mater. Chem. Phys.*, **2003**, *77*, 97–102. DOI:10.1016/S0254-0584(01)00569-7
26. R. G. Pearson, *Coord. Chem. Rev.*, **1990**, *100*, 403–425. DOI:10.1016/0010-8545(90)85016-L
27. A. Kokalj, *Chem. Phys.*, **2012**, *393*, 1–12. DOI:10.1016/j.chemphys.2011.10.021
28. E. E. Ebenso, M. M. Kabanda, T. Arslan, M. Saracoglu, F. Kandemirli, L. C. Murulana, K. A. Singh, K. S. Shukla, B. Hammouti, K. F. Khaled, M. A. Quraishi, I. B. Obot, N. O. Eddy, *Int. J. Electrochem. Sci.* **2012**, *7*, 5643–5676.
29. K. Ramya, K. K. Anupama, K. M. Shainy, *Egypt. J. Petrol.* **2017**, *26*, 421–437. DOI:10.1016/j.ejpe.2016.06.001
30. I. B. Obot, Z. M. Gasem, *Corros. Sci.* **2014**, *83*, 359–366. DOI:10.1016/j.corsci.2014.03.008
31. A. Dutta, S. K. Saha, P. Banerjee, D. Sukul, *Corros. Sci.* **2015**, *98*, 541–550. DOI:10.1016/j.corsci.2015.05.065

32. N.O. Obi-Egbedi, I. B. Obot, M. I. El-Khaiary, S. A. Umoren, E. E. Ebenso, *Int. J. Electrochem. Sci.* **2011**, *6*, 5649–5675.
33. E. E. Ebenso, D. A. Isabirye, N. O. Eddy, *Int. J. Mol. Sci.* **2010**, *11*, 2473–2498. DOI:10.3390/ijms11062473
34. R. Hasanov, M. Sadikoglu, S. Bilgic, *Appl. Surf. Sci.* **2007**, *253*, 3913–3921. DOI:10.1016/j.apsusc.2006.08.025
35. I. Lukovits, E. Kalman, F. Zucchi, *Corrosion.* **2001**, *57*, 3–8. DOI:10.5006/1.3290328
36. O. Kikuchi, *Quant. Struct-Act. Relat.* **1987**, *6*, 179–184. DOI:10.1002/qsar.19870060406
37. X. Li, S. Deng, H. Fu, T. Li, *Electrochim. Acta.* **2009**, *54*, 4089–4098. DOI:10.1016/j.electacta.2009.02.084
38. A. El Assyry, B. Benali, B. Lakhrissi, M. El Faydy, M. Ebn Touhami, R. Touir, M. Touil, *Res Chem Intermed.* **2015**, *41*, 3419–3431. DOI:10.1007/s11164-013-1445-0

Povzetek

S kvantno kemijskimi računi na nivoju DFT/B3LYP teorije s 6-31G, 6-311G in 6-311G (d,p) smo proučevali inhibicijo korozije jekla v 1 M H₂SO₄ s štirimi dianilinskimi Schiffovimi bazami N,N'-Bis (benziliden) -4,4'-dianilin (DAA), N,N'-Bis (benziliden) -4,4'-metilendianilin (MDAA), N, N ,Bis (benziliden) -4,4'-sulfonildianilin (SDAA) in N,N'-Bis (benziliden) -4,4'-oksidianilin (ODAA). Izračunali smo kvantne kemijske parametre: E_{HOMO}, E_{LUMO}, energijsko vrzel (ΔE), dipolni moment (μ), globalno mehkost (σ) in globalno trdnost (η), s katerimi smo razložili reaktivnost in selektivnost preučevanih inhibitorje.

Scientific paper

Diaquabis(2,2'-dipyridylamine)M(II) Terephthalate Dihydrates, M(II) = Ni, Co: Synthesis, Crystal Structures, Thermal and Magnetic Properties

Lidija Radovanović,^{1,*} Jelena Rogan,² Dejan Poleti,² Marko V. Rodić³
and Zvonko Jagličić⁴

¹ Innovation Centre - Faculty of Technology and Metallurgy, University of Belgrade, Karnegijeva 4, 11000 Belgrade, Serbia

² Department of General and Inorganic Chemistry, Faculty of Technology and Metallurgy, University of Belgrade, Karnegijeva 4, 11000 Belgrade, Serbia

³ Faculty of Sciences, University of Novi Sad, Trg Dositeja Obradovića 3, 21000 Novi Sad, Serbia

⁴ Faculty of Civil and Geodetic Engineering & Institute of Mathematics, Physics and Mechanics, University of Ljubljana, Jamova 2, 1000 Ljubljana, Slovenia

* Corresponding author: E-mail: lradovanovic@tmf.bg.ac.rs
phone: +381 11 3303784

Received: 29-08-2017

Abstract

Two new isostructural M(II) (M = Ni, Co) complexes with 2,2'-dipyridylamine (dipya) and dianion of terephthalic acid (H₂tpht), [M(dipya)₂(H₂O)₂](tpht) · 2H₂O, have been synthesized by ligand exchange reaction and characterized by single-crystal X-ray diffraction, FTIR spectroscopy, TG/DSC analysis and magnetic measurements. The crystal structures of [M(dipya)₂(H₂O)₂](tpht) · 2H₂O consist of discrete complex units in which M(II) adopts deformed octahedral geometries. Two dipya ligands and two water molecules are coordinated to M(II) atom, tpht acts as a counter ion, while additional two water molecules remained uncoordinated. By numerous hydrogen bonds, all structural fragments are connected in three different chains which extend along [100], [010] and [001] directions, giving as a result a complex 3D network. The stabilization of 3D structure is accomplished by non-covalent face to face π - π interactions among pyridyl ring of dipya and benzene ring of tpht from adjacent chains. Towards the applied magnetic field, the both complexes exhibited almost perfect paramagnetic behavior.

Keywords: Co(II), Ni(II), 1,4-benzenedicarboxylate, discrete complex, magnetism

1. Introduction

The design and synthesis of mixed-ligand coordination compounds are of great significance in modern inorganic chemistry, which arise from their potential applications as functional materials and fascinating variety of topologies.¹ Concerning such topologies and functional properties, the essential step is to use the appropriate organic building units as well as metal ions. The anion of 1,4-benzenedicarboxylic (terephthalic, H₂tpht) acid, as one out of three positional isomers of benzenedicarboxylic (BDC) acids, is widely used as bridging ligand for designing new metal-organic compounds,^{2,3} especially due to its diversity of the coordination modes, high struc-

tural stability, rigidity and planarity. Earlier studies^{4,5} have vigorously stated that the usage of tpht ligand in combination with aromatic diamines as secondary ligands could afford a wide range of intriguing multi-dimensional structures with transition metal (TM) ions. The interest in tpht complexes is related to the molecular magnetism, and most published articles were focused on Cu(II) complexes and their magnetic properties together with an orbital interpretation of the magnetic exchange mechanism.⁵⁻⁹

2,2'-Dipyridylamine (dipya) as aromatic diamine ligand was not frequently used in combination with tpht. The survey of CSD showed¹⁰ that only seven dipya-tpht complexes with different TM ions as nodes are structurally

characterized: $[\text{Mn}(\text{dipya})_2(\text{tpht})]_n$,¹¹ $[\text{Mn}(\text{dipya})(\text{H}_2\text{O})_4](\text{tpht})$,¹¹ $[\text{M}(\text{dipya})(\text{tpht})(\text{H}_2\text{O})_2] \cdot \text{H}_2\text{O}$ ($\text{M} = \text{Co}, \text{Ni}$),¹² $[\text{Cu}(\text{dipya})(\text{tpht})]_n$,¹³ $\{[\text{Cu}_2(\text{dipya})_2(\text{tpht})_2] \cdot 2\text{H}_2\text{O}\}_n$ ¹⁴ and $\{[\text{Zn}(\text{dipya})(\text{tpht})] \cdot \text{H}_2\text{O}\}_n$.¹⁵ All Cu(II) compounds, $[\text{Mn}(\text{dipya})_2(\text{tpht})]_n$ and $\{[\text{Zn}(\text{dipya})(\text{tpht})] \cdot \text{H}_2\text{O}\}_n$ complexes take the form of zigzag chains, with tpht ligand acting in the range from bis-monodentate to bis-chelate bridge. On the other hand, Co(II) and Ni(II) compounds consist of discrete complex units, with tpht coordinated with only one COO group in a chelate mode, while another COO group remained uncoordinated. Only in $[\text{Mn}(\text{dipya})(\text{H}_2\text{O})_4](\text{tpht})$, tpht was a counter anion. The role of tpht as counter anion as well as the hydrogen bond acceptor is not uncommon and it was described earlier for some TM–tpht complexes.^{16–21} As a continuation of our ongoing studies on ternary TM complexes with tpht ions and some aromatic diamines, we present here the synthesis, crystal structure, thermal and magnetic properties of two new coordination compounds, with general formula $[\text{M}(\text{dipya})_2(\text{H}_2\text{O})_2](\text{tpht}) \cdot 2\text{H}_2\text{O}$, where $\text{M}(\text{II}) = \text{Ni}, \text{Co}$.

2. Experimental

2.1. Materials and Measurements

Beside dipya and 1,10-phenanthroline (phen) which were of purum quality, all reagents were of analytical grade and used without further purification. $\text{Ni}(\text{NO}_3)_2 \cdot 6\text{H}_2\text{O}$, $\text{Co}(\text{NO}_3)_2 \cdot 6\text{H}_2\text{O}$ and phen were purchased from Merck (Germany). $\text{Mn}(\text{NO}_3)_2 \cdot 6\text{H}_2\text{O}$ was supplied by Carlo Erba (Italia), while dipya and EtOH were supplied by Sigma-Aldrich (USA). NaOH and H_2tpht were purchased by Alkaloid (Macedonia) and Ventron (United Kingdom), respectively.

FTIR spectra were recorded on a Bomem MB-100, Hartmann Braun FTIR spectrophotometer (4000–400 cm^{-1} region) using KBr pellets. Thermal properties of the complexes were examined from room temperature up to 1100 °C on an SDT Q600 TGA/DSC instrument (TA Instruments). The heating rate was 10 °C min^{-1} using less than 10 mg sample mass. The furnace atmosphere consisted of dry nitrogen at a flow rate of 100 $\text{cm}^3 \text{min}^{-1}$. X-ray powder diffraction (XRPD) data were collected over the range $5^\circ < 2\theta < 80^\circ$ (step scan: 0.50 s, step width: $0.02^\circ 2\theta$) at room temperature using an Ital Structure APD2000 X-ray diffractometer with $\text{Cu K}\alpha$ radiation ($\lambda = 1.5418 \text{ \AA}$). The phase purity of the products after thermal decomposition of the complexes is confirmed by comparison of the XRPD data to the JCPDS cards. Magnetic properties were studied between 2 and 300 K in a magnetic field of $H = 1000 \text{ Oe}$ and at a constant temperature of 5 K between $H = \pm 50 \text{ kOe}$ with a Quantum Design MPMS-XL-5 SQUID magnetometer. The measured data were corrected for a sample holder contribution and for a temperature independent Larmor diamagnetism of core electrons obtained from Pascal's tables.²²

2.2. Synthesis of $[\text{Ni}(\text{dipya})_2(\text{H}_2\text{O})_2](\text{tpht}) \cdot 2\text{H}_2\text{O}$, (1)

The synthesis of the complex **1** has been an attempt to obtain Ni–tpht complex with two N,N-donor ligands, dipya and 1,10-phenanthroline (phen), in the same structure. Into an aqueous solution of $\text{Ni}(\text{NO}_3)_2 \cdot 6\text{H}_2\text{O}$ (0.291 g, 1.00 mmol) in 100 mL of water a mixed solution of dipya (0.171 g, 1.00 mmol) and phen (0.198 g, 1.00 mmol) in 15 mL of EtOH was added. Then, the 50 mL of an aqueous solution of Na_2tpht (0.208 g, 1.00 mmol) was added drop wise at room temperature under continuous magnetic stirring. The final solution was transferred to a crystallization dish and left under ambient conditions for slow evaporation. The violet single crystals of suitable size, insoluble in water, ethanol and DMSO, were obtained after 15 days. Single-crystal XRD analysis confirmed that dipya is the only N,N-donor ligand in the complex **1**. Yield: 42 %; FTIR (cm^{-1}): 3410 (O–H and N–H), 1639 (C=N), 1564 (COO), 1487 (C–C), 1369 (COO), 770 (C–H).

2.3. Synthesis of $[\text{Co}(\text{dipya})_2(\text{H}_2\text{O})_2](\text{tpht}) \cdot 2\text{H}_2\text{O}$, (2)

The synthesis of the complex **2** has been an attempt to obtain a heterometallic Mn–Co complex with tpht and dipya ligands. The reaction mixture of 1 M $\text{Mn}(\text{NO}_3)_2$ (0.1 cm^3 , 0.1 mmol), 1 M $\text{Co}(\text{NO}_3)_2$ (0.1 cm^3 , 0.1 mmol), dipya (0.0342 g, 0.2 mmol), 0.2 M Na_2tpht (1.0 cm^3 , 0.2 mmol) and H_2O (3 cm^3) was placed in a Teflon-lined steel autoclave, heated for 96 h at 160 °C and cooled for 8 h to room temperature. The orange single crystals, insoluble in water, ethanol and DMSO, were obtained. AAS was confirmed the presence of Co(II) ions only in the obtained crystals. Yield: 38 %; FTIR (cm^{-1}): 3416 (O–H and N–H), 1637 (C=N), 1560 (COO), 1473 (C–C), 1369 (COO), 770 (C–H).

2.4. X-ray Structure Determination of **1** and **2**

Single-crystal X-ray diffraction data for **1** and **2** were collected at room temperature (298 K) on an Oxford Gemini S diffractometer equipped with CCD detector using monochromatized $\text{Mo K}\alpha$ radiation ($\lambda = 0.71073 \text{ \AA}$). Intensities were corrected for absorption using the multi-scan method. Because of the dimensions of the single crystal **1** (Table 1), additional Gaussian correction for absorption was applied. The structures were solved by direct methods using SIR2014²³ and refined on F^2 by full-matrix least-squares using the programs SHELXL-2014/7²⁴ and WinGX.²⁵ All non-hydrogen atoms were refined anisotropically. Positions of the H atoms connected to C and N atoms were calculated on geometric criteria and refined using the riding model with $U_{\text{iso}} = 1.2U_{\text{eq}}$ (C, N). In both structures, one water molecule was disordered with congener atoms, O8A and O8B, having about 60 and 40% site occupancies. Water H atoms for O1 and O2 were found in

ΔF maps. Water H atoms for O8A and O8B were also found in ΔF maps and refined with O–H distances restrained to 0.85 Å. Positions of water H atoms for O7 were calculated using the program HYDROGEN²⁶ and added to the structural model before the final cycle of refinement with fixed coordinates and with $U_{\text{iso}}(\text{H}) = 1.5U_{\text{eq}}(\text{O})$. For water H34 atom in **1** and H33 atom in **2** were not possible to identify suitable hydrogen bond acceptors. Selected crystal data and refinement results for **1** and **2** are listed in Table 1.

3. Results and Discussion

3. 1. Description of the Crystal Structures

According to the single-crystal X-ray diffraction analysis, complexes **1** and **2** crystallize in the monoclinic $P2_1/c$ space group. The solid-state structures consist of individual $[\text{M}(\text{dipya})_2(\text{H}_2\text{O})_2]^{2+}$ entities, two counter tpht²⁻ ions and two lattice water molecules (Figures 1 and S1). Due to the isostructurality of the structures, only the figures related to **1** will be presented in the manuscript. The geometry around the M(II) center is distorted octahedral with three N atoms (N1, N2 and N5) from two chelate dipya ligands and O1 atom from one water molecule in

equatorial plane, while N4 atom from dipya and O2 atom from another water molecule occupy the apical positions. The bond lengths and angles (Table 2) are as expected for dipya–tpht TM complexes with octahedral environment.^{11–14} The deviation of M(II) atom from planarity of the equatorial plane is not substantial, being 0.0024(6) Å for **1** and only 0.0011(6) Å for **2**, while the shortest M(II)⋯M(II) distances are 7.660(2) and 7.664(2) Å in **1** and **2**, respectively. The similar $[\text{M}(\text{dipya})_2(\text{H}_2\text{O})_2]^{2+}$ cation was also found in compound $[\text{Co}(\text{dipya})_2(\text{H}_2\text{O})_2][\text{Hdipya}] [\text{PCoW}_{11}\text{O}_{39}]$,²⁷ but with slightly smaller deviation of Co(II) atom from the basal plane of polyhedron (0.009 Å).

Since the crystallographic inversion centers coincide with the centers of both tpht aromatic rings, only a half of each tpht ion belongs to the asymmetric unit. In the packing, the dihedral angle between two tpht aromatic rings amounts 74.3(1)° in **1** and 75.1(1)° in **2**. The deviation from planarity of tpht ligands is noticeable with the angle between C26–C28 ring and adjacent COO group of 25.6(2)° in **1** and 26.0(2)° in **2**, while the analogous angle for C22–C24 ring is 18.6(1)° in both complexes. As it was mentioned in the introduction, in TM–tpht complexes (containing at least one tpht as a counter anion) with different N,N-donor ligands,^{16–21} these angles were found to be in the range between 17.4 and 29.0°.

Table 1. Crystal data and structure refinements for **1** and **2**.

Complex	1	2
Formula	C ₂₈ H ₃₀ N ₆ O ₈ Ni	C ₂₈ H ₃₀ N ₆ O ₈ Co
Formula weight (g mol ⁻¹)	637.29	637.51
Crystal size (mm ³)	0.62 × 0.44 × 0.40	0.24 × 0.24 × 0.12
Crystal system	Monoclinic	Monoclinic
Space group	$P2_1/c$	$P2_1/c$
<i>a</i> (Å)	9.705(2)	9.746(2)
<i>b</i> (Å)	9.795(2)	9.797(2)
<i>c</i> (Å)	30.303(6)	30.287(6)
α (°)	90	90
β (°)	97.43(3)	97.40(3)
γ (°)	90	90
<i>V</i> (Å ³)	2856.5(10)	2867.9(10)
<i>Z</i>	4	4
<i>F</i> (000)	1328	1324
μ (mm ⁻¹)	0.741	0.659
ρ_c (g cm ⁻³)	1.482	1.477
Reflections collected/unique	17377/5603	29474/5630
R_{int}	0.0268	0.0234
Data/restraints/parameters	4892/4/420	5260/4/420
<i>R</i> indices [$I > 2\sigma(I)$]	$R = 0.0395$, $R_w = 0.0882^\dagger$	$R = 0.0354$, $R_w = 0.0833^\ddagger$
<i>R</i> indices (all data)	$R = 0.0478$, $R_w = 0.0920$	$R = 0.0388$, $R_w = 0.0851$
Goodness-of-fit	1.121	1.152
$\Delta\rho_{\text{max}}$, $\Delta\rho_{\text{min}}$ (e Å ⁻³)	0.529, -0.382	0.318, -0.391

[†] $w = 1 / [s^2 \cdot (F_o^2) + (0.0341 \cdot P)^2 + 1.9123 \cdot P]$ where $P = (F_o^2 + 2 \cdot F_c^2) / 3$ [‡] $w = 1 / [s^2 \cdot (F_o^2) + (0.0337 \cdot P)^2 + 1.6366 \cdot P]$ where $P = (F_o^2 + 2 \cdot F_c^2) / 3$

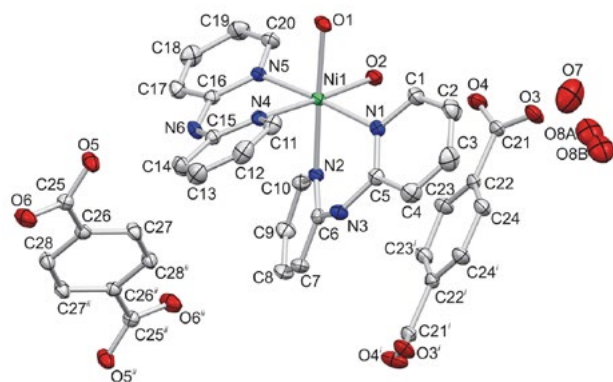


Figure 1. Structural fragment of **1** with atomic numbering scheme (hydrogen atoms are omitted for the sake of clarity). The thermal ellipsoids are plotted at the 30% probability level. Symmetry codes: (i) $-x + 1, y, -z + \frac{1}{2}$, (ii) $-x + 1, -y + 2, -z$.

The stabilization of the crystal lattices of **1** and **2** is achieved by the hydrogen bonds and non-covalent interactions. The hydrogen bond network (Table 3) includes all

Table 2. Selected bond lengths and angles for **1** and **2**.

Bond lengths, Å		Angles, °	
1			
Ni1–N1	2.086(2)	N1–Ni1–N2	84.42(8)
Ni1–N2	2.098(2)	N1–Ni1–N4	93.88(7)
Ni1–N4	2.090(2)	N1–Ni1–N5	176.1(1)
Ni1–N5	2.097(2)	N1–Ni1–O1	94.01(8)
Ni1–O1	2.084(2)	N1–Ni1–O2	89.17(8)
Ni1–O2	2.070(2)	N2–Ni1–N4	90.23(7)
		N2–Ni1–N5	91.66(7)
		N2–Ni1–O1	178.2(1)
		N2–Ni1–O2	90.68(8)
		N4–Ni1–N5	86.19(7)
		N4–Ni1–O1	90.78(8)
		N4–Ni1–O2	176.9(1)
		N5–Ni1–O1	89.90(7)
		N5–Ni1–O2	90.82(8)
		O1–Ni1–O2	88.39(8)
2			
Co1–N1	2.131(2)	N1–Co1–N2	82.47(6)
Co1–N2	2.152(2)	N1–Co1–N4	94.58(6)
Co1–N4	2.142(2)	N1–Co1–N5	174.1(1)
Co1–N5	2.140(2)	N1–Co1–O1	93.48(7)
Co1–O1	2.091(2)	N1–Co1–O2	89.51(6)
Co1–O2	2.097(2)	N2–Co1–N4	88.93(6)
		N2–Co1–N5	91.64(6)
		N2–Co1–O1	176.0(1)
		N2–Co1–O2	91.41(6)
		N4–Co1–N5	84.92(6)
		N4–Co1–O1	91.44(7)
		N4–Co1–O2	175.9(1)
		N5–Co1–O1	92.41(6)
		N5–Co1–O2	90.98(6)
		O1–Co1–O2	88.50(7)

water molecules, all COO⁻ groups and both dipya ligands as it is shown in Figures 2 and S2. The analysis of the crystal packing in **1** and **2** manifested the difference in the position of the O7 water molecule that is in **2** shifted to the symmetry equivalent position relative to its position in **1**. The network of hydrogen bonds permit the formation of three supramolecular chains along [100], [010] and [001] directions and thus forming 3D network. The centroid Cg...Cg distances found between C6–C10/N2 pyridyl ring of dipya and C22–C24 aromatic ring are 3.904(2) and 3.899(1) Å in **1** and **2**, respectively. These distances indicate weak face to face π - π interactions (Figures 3 and S3).²⁸ Furthermore, several C–H...O and one C–H...N interactions, which geometries are presented in Table S1, form short contact clusters allowing additional networking in both structures.

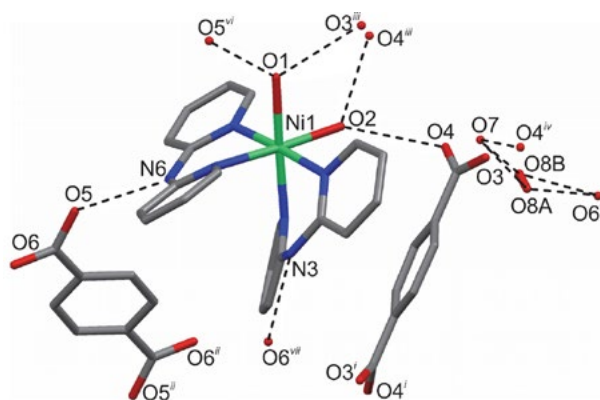


Figure 2. The network of hydrogen bonds (presented by dashed lines) in **1**. Hydrogen atoms are omitted for the sake of clarity.

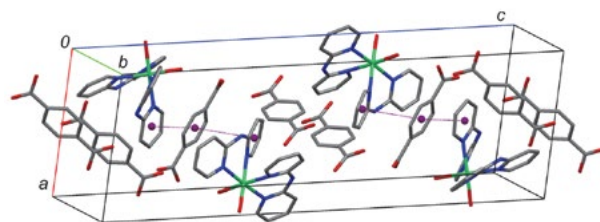


Figure 3. Projection of the crystal packing of **1** in almost *ac*-plane. The π - π interactions between structural fragments are presented by purple lines.

3. 2. Thermal Properties

The dehydration of **1** is an endothermic process occurring in a single step up to 153 °C with a loss of four water molecules (found 11.4%, calc. 11.3%) (Figure 4). The determined enthalpy of dehydration obtained by integration of DSC peak area is 218 kJ mol⁻¹, and it is in a good agreement with values that were already found for several similar ternary BDC complexes.^{11,29,30} It was previously evaluated that average molar enthalpy per one hydrogen

Table 3. The geometry of hydrogen bonds for **1** and **2**.

<i>D</i> -H... <i>A</i>	<i>d</i> (<i>D</i> -H), Å	<i>d</i> (<i>D</i> ... <i>A</i>), Å	<i>d</i> (H... <i>A</i>), Å	<i>D</i> -H... <i>A</i> , °
1				
O1-H30...O3 ⁱⁱⁱ	0.858(5)	2.729(3)	1.874(5)	174(3)
O1-H29...O5 ^{vi}	0.801(3)	2.848(3)	2.054(3)	171(3)
O2-H32...O4	0.739(7)	2.998(3)	2.361(9)	145(4)
O2-H31...O4 ⁱⁱⁱ	0.816(8)	2.617(3)	1.803(8)	176(4)
O7-H33...O4 ^{iv}	0.870(9)	2.830(4)	2.004(1)	158(5)
O8A-H36...O6 ^v	0.830(1)	2.870(1)	2.139(2)	147(3)
O8B-H36...O6 ^v	0.855(8)	2.978(7)	2.139(2)	167(3)
O8A-H35...O7	0.891(6)	2.887(2)	2.025(5)	162(3)
O8B-H35...O7	0.817(1)	2.775(6)	2.025(5)	153(4)
N3-H3A...O6 ^{vii}	0.86	2.887(3)	2.09	154
N6-H6...O5	0.86	2.809(3)	2.04	149
2				
O1-H30...O3 ⁱⁱⁱ	0.812(2)	2.717(3)	1.909(2)	174(3)
O1-H29...O5 ^{vi}	0.806(6)	2.824(2)	2.019(5)	176(3)
O2-H32...O4	0.734(1)	2.968(2)	2.305(2)	151(3)
O2-H31...O4 ⁱⁱⁱ	0.835(4)	2.610(2)	1.776(4)	175(3)
O7-H34...O4	0.828(1)	2.828(3)	2.034(1)	161(4)
O8A-H35...O6 ^v	0.814(6)	2.864(8)	2.137(7)	149(2)
O8B-H35...O6 ^v	0.853(1)	2.966(2)	2.137(7)	164(3)
O8A-H36...O7 ^{iv}	0.901(9)	2.875(9)	2.023(9)	157(3)
O8B-H36...O7 ^{iv}	0.804(2)	2.779(2)	2.023(9)	157(3)
N3-H3A...O6 ^{vii}	0.86	2.884(2)	2.09	153
N6-H6...O5	0.86	2.810(2)	2.02	152

Symmetry codes: **1** (iii) $-x, y, -z + \frac{1}{2}$; (iv) $x, y - 1, z$; (v) $x, -y + 1, z + \frac{1}{2}$; (vi) $-x, -y + 1, -z$; (vii) $-x + 1, -y + 1, -z$;
2 (iii) $-x, y, -z + \frac{1}{2}$; (iv) $x, y - 1, z$; (v) $x, -y + 1, z + \frac{1}{2}$; (vi) $-x, -y + 1, -z$; (vii) $-x + 1, -y + 1, -z$.

bond is about 16 kJ mol⁻¹.³⁰ In **1**, four water molecules participate in the formation of even nine hydrogen bonds, thus it can be concluded that molar enthalpy per one Ni-OH₂ coordinative bond is equal to 37 kJ mol⁻¹. Further

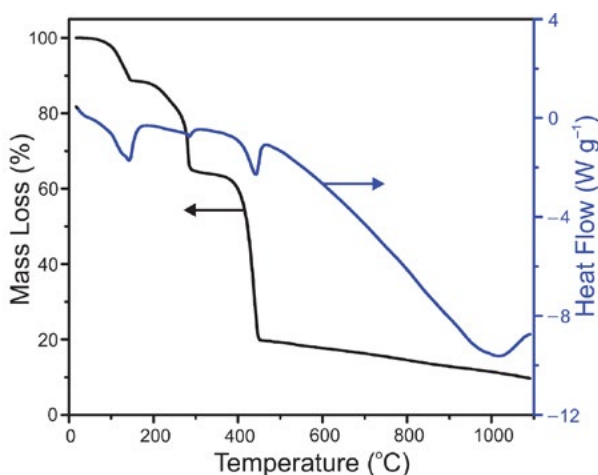


Figure 4. TGA and DSC curves for **1** obtained at heating rate of 10 °C min⁻¹ in flowing N₂ (exo up).

degradation of complex happens in two temperature ranges, 153–336 °C and 336–1100 °C, with a loss of complete tpht anion (found 36.1%, calc. 37.1%) and two dipya molecules (found 90.3%, calc. 90.8%), respectively. The final residual mass 9.68% (calc. 9.21%) is in good agreement with the formation of pure Ni as a decomposition product, whose identity was verified by XRPD (Figure S4). In inert atmosphere, the decomposition of TM complexes to pure metal is not unusual as it was proven in previous studies.^{31,32} The thermal behavior of **2** follows a very similar pattern, giving metallic Co as a final product (found 9.88%, calc. 9.24%, Figure S5). Both products obtained after decomposition of the complexes at 1100 °C were analyzed using XRPD (Figures S4 and S6) and the presence of Ni and Co for **1** and **2**, respectively, was confirmed by comparing the XRPD patterns with standard cards.

3. 3. Magnetic Properties

Temperature dependent susceptibility of **1** measured in a magnetic field of $H = 1000$ Oe is shown in Figure 5a. It follows a Curie-like $1/T$ dependence. Only a small deviation from a perfect paramagnetic behavior can be seen as a

small decrease of the product χT below 10 K in otherwise temperature constant product χT (inset in Figure 5a). The value of χT between 20 and 300 K is 1.2 emu K mol⁻¹, which falls in the expected range for uncoupled Ni(II) ion.³³ The magnetization curve of **1** at 5 K is presented in Figure 5b. The measured data can be excellently described with a Brillouin function (full green line) for spin $S = 1$ as expected for Ni(II).

Taking into account the constant χT for $T > 20$ K and paramagnetic behavior of isothermal magnetization, we ascribe the weak temperature variation of the product χT below 10 K to a zero-field splitting of Ni(II) ion with d^8 configuration in a distorted octahedral environment. The average susceptibility for polycrystalline sample $\chi = (\chi_z + 2\chi_x) / 3$ and $g_z = g_x = g$ can be written as²²

$$\chi = \frac{2N_A g^2 \mu_B^2 (2k_B T / D) [1 - \exp(D/k_B T)] + \exp(D/k_B T)}{3k_B T + 1 + 2\exp(-D/k_B T)} \quad (1)$$

where N_A is Avogadro number, μ_B is Bohr magneton and D is zero-field splitting parameter. The result of fitting procedure (full line in inset in Figure 5a) are parameters $g = 2.19$ and $D = 3.6$ cm⁻¹ with $\bar{R}^2 > 0.96$. The zero-field splitting parameter D is of the same order as determined in our previous work.²⁹

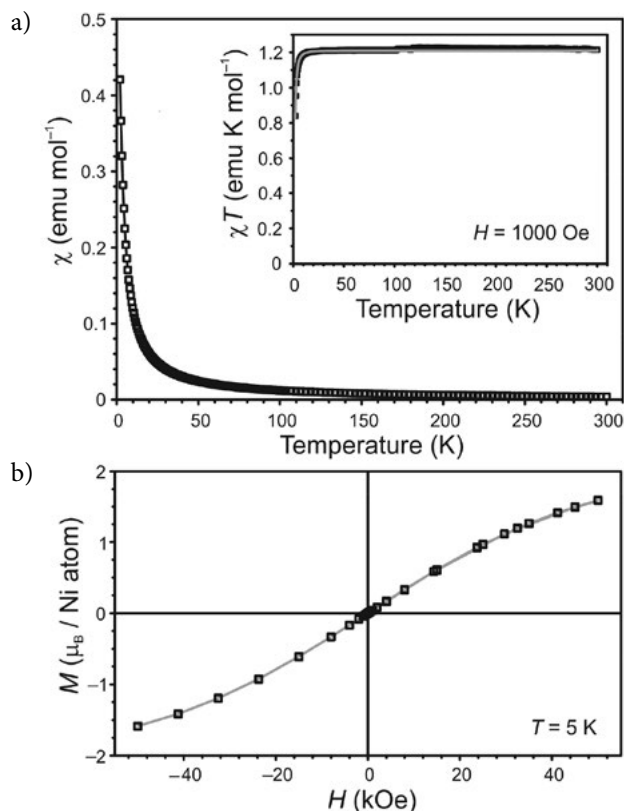


Figure 5. Temperature variation of magnetic susceptibility measured in $H = 1000$ Oe of **1** and the product χT . The green line is a fit with function (1) (a). Isothermal magnetization at 5 K and a Brillouin function (green line) for spin $J = 1$ of **1** (b).

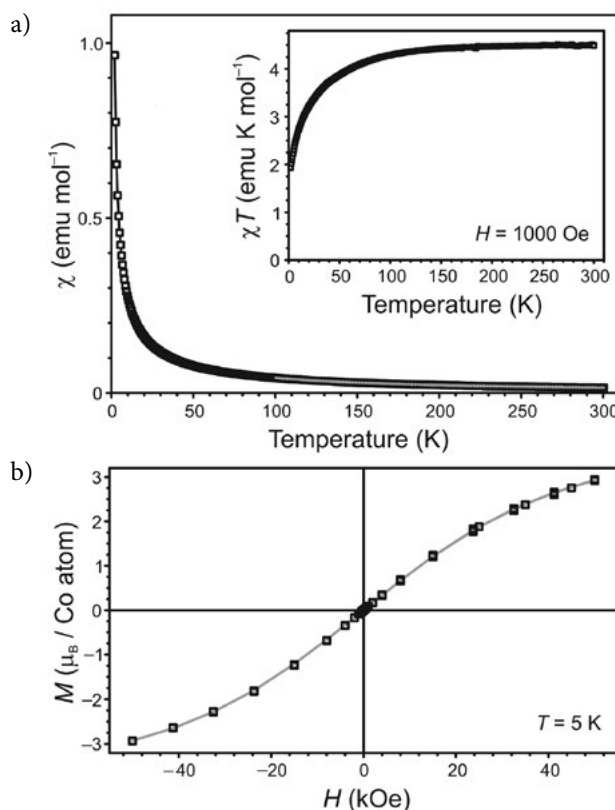


Figure 6. Temperature variation of magnetic susceptibility and the product χT (inset) measured in $H = 1000$ Oe of **2**. The green line is a fit with the Curie-Weiss function (a). Isothermal magnetization at 5 K and a Brillouin function (green line) for spin $J = 3/2$ of **2** (b).

Figure 6a shows the susceptibility for **2** in a temperature range from 2 to 300 K. The Curie-Weiss fit $\chi = C / (T - \theta)$ was performed on the data for $T > 100$ K. The obtained Curie constant, $C = 4.6$ emu K mol⁻¹, is in the range for Co(II) ions with a total electronic spin angular momentum $S = 3/2$ and a non-zero contribution of total orbital angular momentum L .³³ The negative Curie-Weiss temperature $\theta = -7.9$ K is in agreement with the reduction of the product χT (inset in Figure 6a) with decreasing temperature. The negative θ can be an indication of a weak antiferromagnetic interaction between magnetic moments or the result of a single ion effects (L - S coupling of Co(II) ions³⁴ in distorted octahedral environment and zero-field splitting). As the isothermal magnetization (Figure 6b) perfectly follows the Brillouin function for isolated ions with no indication of antiferromagnetic interaction, we contribute the negative θ and reduction of the product χT with decreasing temperature to the combined effect of L - S coupling and zero-field splitting of non-interacting Co(II) ions.

4. Conclusion

Two discrete, isostructural complexes, $[M(\text{dipy})_2(\text{H}_2\text{O})_2](\text{tpht}) \cdot 2\text{H}_2\text{O}$ ($M = \text{Ni}, \text{Co}$), have been synthesized

by ligand exchange reaction. The compounds are structurally characterized and their spectral, thermal and magnetic properties were determined. Single crystal X-ray analysis revealed that the geometry around M(II) ions is deformed octahedral, while the supramolecular packing is achieved by the combination of hydrogen bonds, π - π , C–H...O and C–H...N interactions. Thermal decomposition of both complexes up to 1100 °C yielded pure metals. The temperature dependent magnetic susceptibility data indicated that there were not magnetic interaction between M(II) ions. The contribution of the *L*-*S* coupling is observed with parameters *g* and *D* of 2.19 and 3.6 cm⁻¹, respectively, for **1** and θ of -7.9 K for **2**.

5. Acknowledgements

This work was supported financially by the Ministry of Education, Science and Technological Development of the Republic of Serbia (Grant No. III45007) and from Slovenian Research Agency (Grant No. P2-0348).

6. Appendix A. Supplementary Materials

CCDC 1539377 and 1539378 contain the supplementary crystallographic data for compounds **1** and **2**. These data can be obtained free of charge from the Cambridge Crystallographic Data Centre via www.ccdc.cam.ac.uk/data_request/cif. Supplementary data associated with this article can be found, in the online version.

7. References

1. T. R. Cook, Y. R. Zheng, P. J. Stang, *Chem. Rev.* **2013**, *113*, 734–777. DOI:10.1021/cr3002824
2. Z. H. Li, W. J. Ao, X. X. Wang, X. Z. Fu, *Acta Crystallogr.* **2006**, *E62*, m1048–m1050. DOI:10.1107/S1600536806012748
3. C. B. Ma, M. Q. Hu, C. X. Zhang, F. Chen, C. N. Chen, Q. T. Liu, *Acta Crystallogr.* **2004**, *C60*, m288–m290. DOI:10.1107/S0108270104007565
4. G. H. Wang, Z. G. Li, H. Q. Jia, N. H. Hu, J. W. Xu, *Cryst. Growth Des.* **2008**, *8*, 1932–1939. DOI:10.1021/cg701232n
5. B. P. Yang, H. Y. Zeng, J. G. Mao, G. C. Guo, J. S. Huang, *Transit. Met. Chem.* **2003**, *28*, 600–605. DOI:10.1023/A:1025096207371
6. E. G. Bakalbassis, J. Mrozinski, C. A. Tsipis, *Inorg. Chem.* **1985**, *24*, 3548–3553. DOI:10.1021/ic00216a015
7. C. Janiak, *Dalton Trans.* **2003**, 2781–2804. DOI:10.1039/b305705b
8. C. S. Hong, Y. S. You, *Polyhedron* **2004**, *23*, 3043–3050. DOI:10.1016/j.poly.2004.09.019
9. H. X. Zhang, B. S. Kang, A. W. Xu, Z. N. Chen, Z. Y. Zhou, A. S. C. Chan, K. B. Yu, C. Ren, *J. Chem. Soc., Dalton Trans.* **2001**, 2559–2566. DOI:10.1039/b102570h
10. C. R. Groom, I. J. Bruno, M. P. Lightfoot, S. C. Ward, *Acta Crystallogr.* **2016**, *B72*, 171–179. DOI:10.1107/S2052520616003954
11. L. Radovanović, J. Rogan, D. Poleti, M. V. Rodić, N. Begović, *Inorg. Chim. Acta* **2016**, *445*, 46–56. DOI:10.1016/j.ica.2016.02.026
12. J. Rogan, D. Poleti, Lj. Karanović, G. A. Bogdanović, A. Spasojević-de Biré, D. M. Petrović, *Polyhedron* **2000**, *19*, 1415–1421. DOI:10.1016/S0277-5387(00)00435-6
13. E. Yang, Y. Zheng, G. Y. Chen, *Acta Crystallogr.* **2006**, *E62*, m1079–m1080. DOI:10.1107/S1600536806013717
14. Lj. Karanović, D. Poleti, J. Rogan, G. A. Bogdanović, A. Spasojević-de Biré, *Acta Crystallogr.* **2002**, *C58*, m275–m279. DOI:10.1107/S0108270102004341
15. L. Radovanović, J. Rogan, D. Poleti, M. Milutinović, M. V. Rodić, *Polyhedron* **2016**, *112*, 18–26. DOI:10.1016/j.poly.2016.03.054
16. H. Xu, Y. Liang, Z. Su, Y. Zhao, K. Shao, H. Zhang, S. Yue, *Acta Crystallogr.* **2004**, *E60*, m142–m144. DOI:10.1107/S1600536803029210
17. W. Huang, D. Hu, S. Gou, H. Qian, H. K. Fun, S. S. S. Raj, Q. Meng, *J. Mol. Struct.* **2003**, *649*, 269–278. DOI:10.1016/S0022-2860(03)00080-2
18. H. P. Xiao, Z. Shi, L. G. Zhu, R. R. Xu, W. Q. Pang, *Acta Crystallogr.* **2003**, *C59*, m82–m83. DOI:10.1107/S0108270103002087
19. X. Li, D. Cheng, J. Lin, Z. Li, Y. Zheng, *Cryst. Growth Des.* **2008**, *8*, 2853–2861. DOI:10.1021/cg701150q
20. H. M. Zhang, L. P. Lu, S. S. Feng, S. D. Qin, M. L. Zhu, *Acta Crystallogr.* **2005**, *E61*, m1027–m1029. DOI:10.1107/S160053680501322X
21. R. P. Sharma, A. Singh, P. Venugopalan, W. T. A. Harrison, *J. Mol. Struct.* **2010**, *980*, 72–77. DOI:10.1016/j.molstruc.2010.06.039
22. O. Kahn, in: *Molecular Magnetism*, VCH Publishing, **1993**.
23. M. C. Burla, R. Caliandro, B. Carrozzini, G. L. Cascarano, C. Giacovazzo, M. Mallamo, A. Mazzzone, G. Polidori, *J. Appl. Crystallogr.* **2015**, *48*, 306–309. DOI:10.1107/S1600576715001132
24. G. M. Sheldrick, *Acta Crystallogr.* **2015**, *C71*, 3–8. DOI:10.1107/S2053229614024218
25. L. J. Farrugia, *J. Appl. Crystallogr.* **2012**, *45*, 849–854. DOI:10.1107/S0021889812029111
26. M. Nardelli, *J. Appl. Crystallogr.* **1999**, *32*, 563–571. DOI:10.1107/S0021889899002666
27. B. Yan, Y. Xu, X. Bu, N. K. Goh, L. S. Chia, G. D. Stucky, *J. Chem. Soc., Dalton Trans.* **2001**, 2009–2014. DOI:10.1039/b103024h
28. C. Janiak, *J. Chem. Soc., Dalton Trans.* **2000**, 3885–3896. DOI:10.1039/b003010o
29. J. Rogan, D. Poleti, Lj. Karanović, Z. Jagličić, *J. Mol. Struct.* **2011**, *985*, 371–379. DOI:10.1016/j.molstruc.2010.11.024
30. J. Rogan, D. Poleti, *Thermochim. Acta* **2004**, *413*, 227–234. DOI:10.1016/j.tca.2003.10.015

31. N. Parveen, R. Nazir, M. Mazhar, *J. Therm. Anal. Calorim.* **2013**, *111*, 93–99.
DOI:10.1007/s10973-011-2185-2
32. C. Hopa, R. Kurtaran, M. Alkan, H. Kara, R. Hughes, *Transit. Met. Chem.* **2010**, *35*, 1013–1018.
DOI:10.1007/s11243-010-9424-4
33. N. W. Ashcroft, N. D. Mermin, in: *Solid State Physics*, Saunders College Publishing, USA, **1976**.
34. F. Lloret, M. Julve, J. Cano, R. Ruiz-García, E. Pardo, *Inorg. Chim. Acta* **2008**, *361*, 3432–3445.
DOI:10.1016/j.ica.2008.03.114

Povzetek

Z reakcijo izmenjave ligandov smo sintetizirali dva nova izostrukturna M(II) (M = Ni, Co) kompleksa z 2,2'-dipiridilaminom (dipya) in dianionom tereftaline kisline (H_2tpht), $[M(dipya)_2(H_2O)_2](tpht) \cdot 2H_2O$, in ju okarakterizirali z monokristalno rentgensko difrakcijo, FTIR spektroskopijo, TG/DSC analizo in magnetnimi meritvami. Kristalni strukturi $[M(dipya)_2(H_2O)_2](tpht) \cdot 2H_2O$ sta zgrajeni iz izoliranih kompleksnih enot, v katerih ima M(II) ion popačeno oktaedrično geometrijo. Dva dipya liganda in dve molekuli vode so koordinirani na M(II) ion, tpht je protiion, preostali dve molekuli vode sta v strukturi nekoordinirani. Strukturni fragmenti so povezani preko številnih vodikovih vezi v tri verige vzdolž [100], [010] in [001] smeri, kar vodi do nastanka 3D mreže. Stabilizacija 3D strukture je dosežena z neovalentnimi π - π interakcijami med piridinskimi obroči dipya ligandov in benzenovih obročev tpht anionov iz sosednjih verig. V magnetnem polju izkazujeta oba kompleksa popolno paramagnetno obnašanje.

Scientific paper

Synthesis and Antibacterial Evaluation of Some New 1,4-Dihydropyridines in the Presence of Fe₃O₄@Silica Sulfonic Acid Nanocomposite as Catalyst

Seyed Mostafa Hasan Nasrollahi,¹ Mohammad Ali Ghasemzadeh^{1,*} and Mohammad Reza Zolfaghari²

¹Department of Chemistry, Qom Branch, Islamic Azad University, Qom, I. R. Iran

²Department of Microbiology, Qom Branch, Islamic Azad University, Qom, I. R. Iran.

* Corresponding author: E-mail: ghasemzadeh@qom-iau.ac.ir

Received: 01-09-2017

Abstract

The synthesis of heterocyclic compounds has been a topic of significant interest because of their broad applications. In this research an effective and eco-friendly approach for the synthesis 1,4-dihydropyridines has been developed via the four-component reactions of arylamines, acetylenedicarboxylates, aromatic aldehydes and ethyl acetoacetate in the presence of Fe₃O₄@SiO₂@OSO₃H nanocomposite under solvent-free conditions. The advantages of this method involve the green reaction conditions, simple workup, broad substrates, excellent yields and the reuse of the nanocatalyst. One of the indicators to measure antimicrobial activity is Minimum Inhibitory Concentrations (MIC) that this measure and heterocyclic compounds synthesis inhibition zone diameter was measured on examined bacteria using well diffusion, disc diffusion and determination of antibiotic susceptibility. The results of all three methods suggested the susceptibility of *Staphylococcus aureus* to synthesized heterocyclic compounds. It can be concluded from the results that these compounds have high antibiotic properties and can be useful in other research and biomedical applications.

Keywords: 1,4-dihydropyridine, antibacterial activity, Fe₃O₄@silica sulfonic acid, nanocomposite, multi-component reaction, solvent-free

1. Introduction

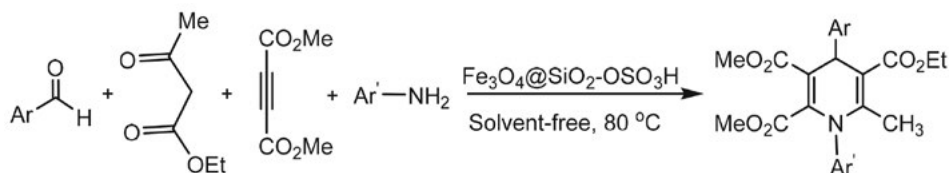
Multi-component reactions (MCR) have appeared as an efficient and powerful approach in modern synthetic organic chemistry due to their valuable features such as: atomic economy, straightforward reaction design, atomic economy, and the opportunity to construct target compounds by introducing diverse elements in a single chemical event. Since all of the employed organic reagents are consumed and incorporated into the target compound, purification of products which results from MCR, is also simple.¹

Many reactions proceed efficiently in the solid state.² Indeed, in many cases, solid-state organic reaction occurs more efficiently and selectively than its solution counterpart does, since molecules in a crystal are arranged tightly and regularly. Furthermore, the solid state reaction (or solvent-free reaction) has many advantages including reduced

pollution, low costs and simplicity in process and handling, these factors are especially important in industry.^{3–7}

1,4-dihydropyridines (1,4-DHPs) represent an important class of compounds which are found in many active biological products, such as vasodilator, bronchodilator and also they have been used as anti-atherosclerotic, antitumor, geroprotective, hepatoprotective and antidiabetic agents.⁸ Numerous synthetic methods have been reported for the preparation of 1,4-dihydropyridine derivatives under classical or modified conditions.^{9–15}

1,4-dihydropyridines are generally synthesized by Hantzsch reaction which involve the condensation of aldehydes, β -ketoester and ammonia or ammonium acetate. In addition various catalysts like as TMSI,¹⁶ Yb(OTf)₃,¹⁷ CAN,¹⁸ silica gel/NaHSO₄¹⁹ and Sc(OTf)₃¹¹ have been utilized for the preparation of 1,4-dihydropyridines. On the other hand, different reagents and conditions have been employed for the oxidation of 1,4-DHPs.^{20–23} In spite of po-



Scheme 1. One-pot synthesis of 1,4-DHPs catalyzed by $\text{Fe}_3\text{O}_4@SiO_2\text{-OSO}_3\text{H}$ nanocomposite

tential utility of these reagents, most of the existing methods for the synthesis of 1,4-DHPs suffer from drawbacks such as low yields, long reaction times, occurrence of several side products, use of stoichiometric amount of reagents and strong oxidants, use of expensive and toxic transition metallic reagents. Therefore, exploring new catalytic system preferably in an environmentally benign method to overcome such drawbacks is a challenging task to the organic chemists.

In recent years, the magnetically sulfonic acids were applied as an effective nanocatalyst in many organic reactions such as: preparation of 3,6-di(pyridin-3-yl)-1*H*-pyrazolo[3,4-*b*]pyridine-5-carbonitriles,²⁴ pyrano coumarins,²⁵ amides,²⁶ quinazoline derivatives,²⁷ and formylation of alcohols and amines.²⁸

In continue of our attempts towards the improvement of the synthetic methods using heterogeneous catalysts,^{29–33} Here we report a new and efficient pathway for the preparation of 1,4-DHPs via multi-component synthesis of arylamine, dimethyl acetylenedicarboxylate, aromatic aldehyde and ethyl acetoacetate by using $\text{Fe}_3\text{O}_4@silica$ sulfuric acid core-shell nanocomposite (Scheme 1).

2. Experimental

2.1. Chemicals and Apparatus

Chemicals were purchased from the Sigma-Aldrich and Merck in high purity. All of the materials were of commercial reagent grade and were used without further purification. All melting points are uncorrected and were determined in capillary tube on Boetius melting point microscope. NMR spectra were obtained on a Bruker DRX-400 MHz spectrometer (^1H NMR at 400 Hz, ^{13}C NMR at 100 Hz) with CDCl_3 as solvent using TMS as an internal standard. Chemical shifts (δ) are given in ppm and coupling constants (*J*) in Hz. FT-IR spectrum was recorded on Magna-IR, spectrometer 550. The elemental analyses (C, H, N) were obtained from a Carlo ERBA Model EA 1108 analyzer. Powder X-ray diffraction (XRD) was carried out on a Philips diffractometer of X'pert Company with mono chromatized Cu K α radiation ($\lambda = 1.5406 \text{ \AA}$). Microscopic morphology of products was visualized by SEM (LEO 1455VP). The mass spectra were recorded on a Joel D-30 instrument at an ionization potential of 70 eV. The compositional analysis was done by energy dispersive analysis of X-ray (EDX, Kevex, Delta Class I).

2.2. Antimicrobial Activity Determination

2.2.1. Well Diffusion

Determining the inhibition zone of diffusion was performed by Well Agar Diffusion according to Douglas & Barki method.³⁴ On MRS broth, half McFarland bacterial suspension was cultured using plate spread method and after 5–10 minutes, wells were prepared (6mm) so that wells distance from plate edge was 1.5 cm and from each other was 2–2.5 cm.

Then a different concentration of oil (6 concentrations) was poured in the well (50 μl). Plates were placed in the refrigerator for 1–2 hours to let antimicrobial agents to distribute in the environment. Then plates were incubated for 24 hours at 37 °C. Then inhibition zone was measured using a caliper.

2.2.2. Determination of Antibiotic Susceptibility

In antimicrobial susceptibility test, Bauer-Kirby disk diffusion method was used on Muller-Hinton Agar and inhibition zone was studied on the basis of recommendations of the National Committee for Clinical Laboratory Standards (NCCLS).³⁵ Antibiotics used in this study include Vancomycin and Oxacillin.

2.2.3. Disk Diffusion Method

To examine antimicrobial activity of samples disk diffusion method was used in Mueller-Hinton agar. In this way, after the preparation of heterocyclic compounds in question, and examining their features, sterile paper discs with a diameter of 6 mm were prepared and stained with 20 ml of heterocyclic compounds then they were incubated for 24 hours at 37 °C. The bacteria were cultured on Mueller Hinton agar and were placed at appropriate intervals and a disk impregnated with solvent used as was witness. After 24 h of incubation the inhibition zone diameter was measured and evaluated.

2.3. Preparation of Fe_3O_4 Nanoparticles

Fe_3O_4 MNPs were prepared according to a previously reported procedure by Zhang et. al using the chemical co-precipitation method.³⁶ Typically, $\text{FeCl}_3 \cdot 6\text{H}_2\text{O}$ (2.7 g) and $\text{FeCl}_2 \cdot 4\text{H}_2\text{O}$ (1 g) were dissolved in 100 ml of 1.2 mmol l⁻¹ aqueous HCl followed by ultrasonic bath for 30 min. Then, 1.25 mol l⁻¹ aqueous NaOH (150 ml) was added un-

der vigorous stirring and a black precipitate was immediately formed. The resulting transparent solution was heated at 80 °C with rapid mechanical stirring under N₂ atmosphere. After vigorous stirring for 2 h, The black products were centrifuged, filtered out and washed with deionized water and alcohol for several times, and finally dried at 60 °C for 12 h.

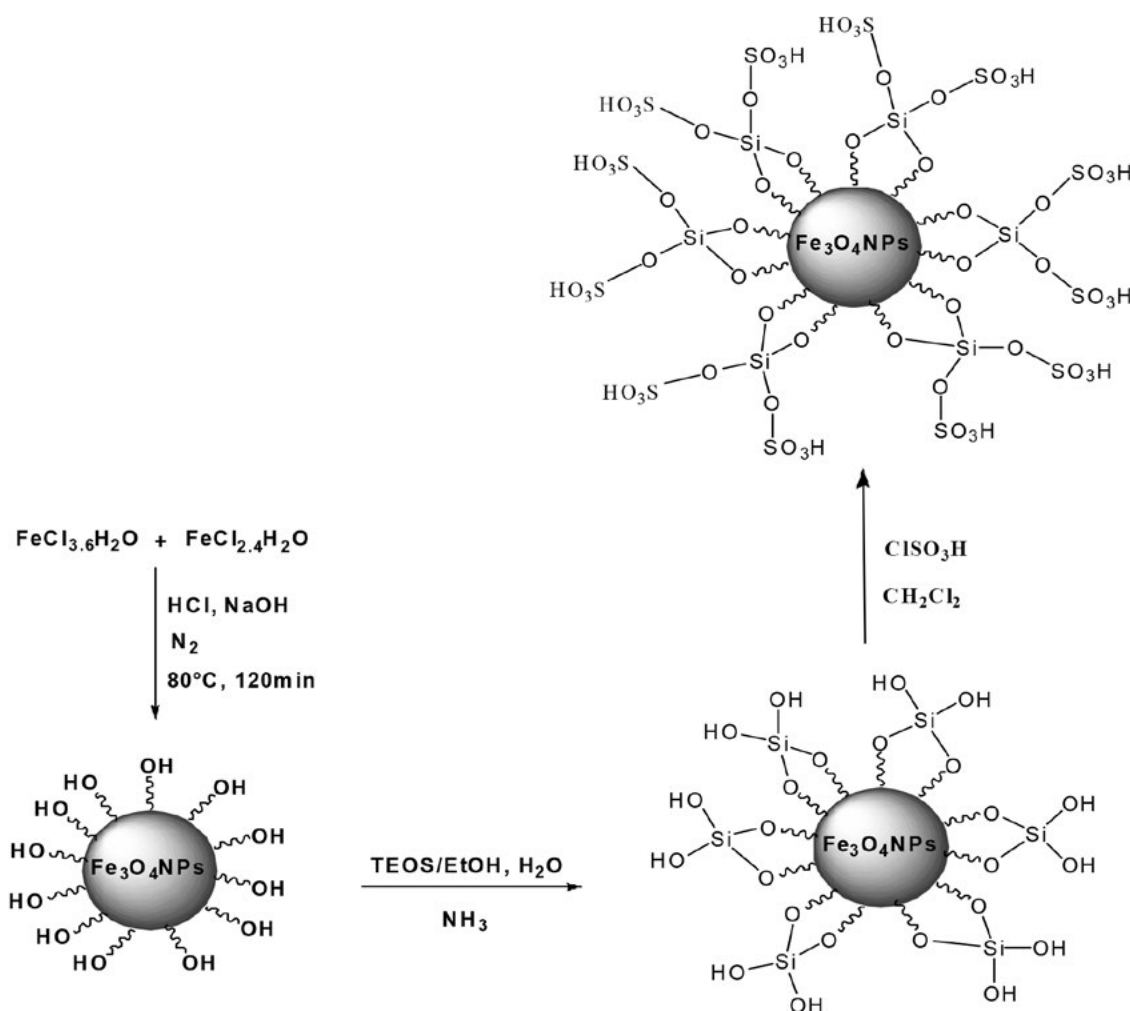
2. 4. Preparation of Fe₃O₄@SiO₂ Nanoparticles

Fe₃O₄@SiO₂ core-shell particles were prepared via modified Stöber sol-gel process.³⁷ 30 mg as-prepared Fe₃O₄ submicrospheres were ultrasonically dispersed in a solution containing 160 mL ethanol, 40 mL water and 10 mL concentrated ammonia (28 wt%). Then, 0.4 mL TEOS was added dropwise to the solution under sonication, followed mechanically stirring for 3 h at room temperature. Subsequently, the resulting particles were separated using a magnet and washed with deionized water and ethanol. The step was repeated several times before drying at 60 °C for 12 h.

2. 5. Preparation of Fe₃O₄@SiO₂-SO₃H Nanocomposite

Fe₃O₄@SiO₂-SO₃H nanocomposites were prepared according to a previously reported procedure.³⁸ A 500-mL suction flask was equipped with a constant pressure dropping funnel. The gas outlet was connected to a vacuum system through an adsorbing solution of alkali trap. Fe₃O₄@Silica (2.5 g) was added to the flask and dispersed by ultrasonics for 10 min in CH₂Cl₂ (75 mL). Chlorosulfonic acid (1.75 g, 1 mL, 15 mmol) in CH₂Cl₂ (20 mL) was added dropwise over a period of 30 min at room temperature. After completion of the addition, the mixture was shaken for 90 min, while the residual HCl was eliminated by suction. Then, the Fe₃O₄@Silica sulfonic acid was separated from the reaction mixture by a magnetic field and washed several times with dried CH₂Cl₂. Finally, Fe₃O₄@Silica sulfonic acid was dried under vacuum at 60 °C (Scheme 2).

The content of sulfonic acid was determined using back titration method. Firstly, the Fe₃O₄@SiO₂-OSO₃H nanocomposite (0.01 g) was added to aqueous solution of



Scheme 2. The reaction pathway for the preparation of Fe₃O₄@SiO₂-OSO₃H nanocomposite

KOH (2 mL, 0.1 mol/L) and the reaction mixture was stirred for 30 min. Then, the nanocatalyst was filtered and the clear solution was kept for further analysis. To obtain the amount of sulfonic acid loading on the $\text{Fe}_3\text{O}_4@ \text{SiO}_2\text{-OSO}_3\text{H}$, the solution was titrated with HCl (0.1 mol/L) until neutralization. The H^+ contain of the magnetic nanocatalyst was 0.28 mmol/g.

2. 6. General Procedure for the Preparation of 1,4-dihydropyridines

A mixture of arylamine (1 mmol) and dimethyl acetylenedicarboxylate (1 mmol) were stirred at room temperature for 10 min. Then aromatic aldehyde (1 mmol), ethyl acetoacetate (1 mmol) and $\text{Fe}_3\text{O}_4@ \text{SiO}_2\text{-SO}_3\text{H}$ nanocomposite (0.2 g) were added to it. The mixture was heated to 80 °C under solvent-free condition for an appropriate time. After completion of the reaction as indicated by TLC, the reaction mixture was allowed to cool to room temperature and solid obtained was dissolved in dichloromethane, the catalyst was insoluble in CH_2Cl_2 and separated by using an external magnet. The solvent was evaporated and the residue was recrystallized from ethanol to afford the pure product.

All of the products were characterized and identified with ^1H NMR, ^{13}C NMR and FT-IR spectroscopy techniques. Spectral data of the new products are given below.

5-ethyl-2,3-dimethyl-1-(4-methoxyphenyl)-6-methyl-4-(4-nitrophenyl)-1,4-dihydropyridine-2,3,5-tricarboxylate (5c):

Yellow solid; m.p. = 170–172 °C; ^1H NMR (400 MHz, CDCl_3) δ : 1.12 (t, 3H, $J=6.8$ Hz, CH_3), 1.42 (s, 3H, CH_3), 3.35 (s, 3H, OCH_3), 3.71 (s, 3H, OCH_3), 4.03 (s, 3H, OCH_3), 4.15 (q, 2H, $J=6.8$ Hz, CH_2), 5.11 (s, 1H, CH), 6.85–7.40 (m, 8H, ArH). ^{13}C NMR (100 MHz, CDCl_3) δ : 14.4, 17.3, 37.2, 52.0, 52.4, 54.1, 60.6, 106.4, 121.4, 128.1, 128.8, 130.1, 130.4, 132.1, 133.0, 142.4, 148.3, 149.3, 151.6, 163.5, 165.3, 168.1. FT-IR (KBr) ν : 2989, 2841, 1750, 1697, 1640, 1584, 1530, 1509, 1435, 1355, 1311, 1290, 1251, 1232, 1207, 1135, 1111, 1081, 1033, 967, 934, 895, 856, 827, 802, 764 cm^{-1} ; MS (EI) (m/z): 510.16 (M^+); Anal. Calcd. For $\text{C}_{26}\text{H}_{26}\text{N}_2\text{O}_9$: C 61.17, H 5.13, N 5.49. Found C 61.01, H 5.18. N 5.53.

5-ethyl-2,3-dimethyl-4-(4-bromophenyl)-1-(4-methoxyphenyl)-6-methyl-1,4-dihydropyridine-2,3,5-tricarboxylate (5e):

Yellow solid; m.p. = 145–147 °C; ^1H NMR (400 MHz, CDCl_3) δ : 1.12 (t, 3H, $J=6.5$ Hz, CH_3), 1.42 (s, 3H, CH_3), 4.14 (s, 3H, OCH_3), 4.20 (s, 3H, OCH_3), 4.25 (s, 3H, OCH_3), 4.50 (q, 2H, $J=6.5$ Hz, CH_2), 5.45 (s, 1H, CH), 6.83–6.87 (d, 2H, $J=7.8$ Hz, ArH), 7.23–7.31 (m, 4H, ArH), 7.48–7.51 (d, 2H, $J=7.8$ Hz, ArH). ^{13}C NMR (100 MHz, CDCl_3) δ : 14.2, 17.8, 37.7, 51.5, 52.4, 55.1, 60.9, 106.4, 121.4, 128.1, 128.8, 130.1, 130.4, 132.1, 132.9, 142.4, 148.0, 148.3, 150.6, 158.2, 164.9, 167.3. FT-IR (KBr) ν : 2954, 2840, 1745, 1704, 1641,

1586, 1511, 1437, 1367, 1326, 1283, 1250, 1205, 1085, 1032, 966, 924, 855, 826, 792, 761 cm^{-1} ; MS (EI) (m/z): 543.09 (M^+); Anal. Calcd. For $\text{C}_{26}\text{H}_{26}\text{BrNO}_7$: C 57.36, H 4.81, N 2.57. Found C 57.25, H 4.89. N 2.61.

5-ethyl-2,3-dimethyl-4-(4-bromophenyl)-1-(4-chlorophenyl)-6-methyl-1,4-dihydropyridine-2,3,5-tricarboxylate (5f):

Yellow solid; m.p. = 127–129 °C; ^1H NMR (400 MHz, CDCl_3) δ : 1.17 (t, 3H, $J=7.1$ Hz, CH_3), 1.45 (s, 3H, CH_3), 3.45 (s, 3H, OCH_3), 3.61 (s, 3H, OCH_3), 4.24 (q, 2H, $J=7.1$ Hz, CH_2), 5.16 (s, 1H, CH), 6.83–7.41 (m, 8H, ArH). ^{13}C NMR (100 MHz, CDCl_3) δ : 14.2, 17.9, 37.5, 51.59, 52.4, 60.8, 105.1, 106.3, 129.1, 130.0, 130.3, 130.9, 131.5, 133.0, 136.6, 142.8, 144.3, 145.9, 158.2, 164.9, 167.0. FT-IR (KBr) ν : 2983, 2948, 1744, 1703, 1640, 1588, 1488, 1432, 1366, 1326, 1279, 1247, 1210, 1122, 1084, 1035, 1007, 965, 923, 826 cm^{-1} ; MS (EI) (m/z): 547.04 (M^+); Anal. Calcd. For $\text{C}_{25}\text{H}_{25}\text{BrClNO}_6$: C 54.71, H 4.22, N 2.55. Found C 54.62, H 4.28. N 2.70.

5-ethyl-2,3-dimethyl-6-methyl-4-(thiophen-2-yl)-1-(p-tolyl)-1,4-dihydropyridine-2,3,5-tricarboxylate (5m):

Yellow solid; m.p. = 112–115 °C; ^1H NMR (400 MHz, CDCl_3) δ : 1.09 (t, 3H, $J=7.5$ Hz, CH_3), 1.56 (s, 3H, CH_3), 2.11 (s, 3H, CH_3), 3.72 (s, 3H, OCH_3), 3.98 (s, 3H, OCH_3), 4.10 (q, 2H, $J=7.5$ Hz, CH_2), 5.21 (s, 1H, CH), 6.93–7.54 (m, 7H, ArH). ^{13}C NMR (100 MHz, CDCl_3) δ : 14.1, 17.1, 21.2, 35.6, 51.8, 52.4, 61.5, 111.3, 122.1, 129.8, 131.3, 132.1, 133.7, 134.5, 138.0, 147.1, 148.9, 150.3, 152.8, 164.1, 167.1, 168.6. FT-IR (KBr) ν : 2971, 2854, 1743, 1691, 1655, 1573, 1522, 1509, 1421, 1311, 1293, 1255, 1144, 1112, 1021, 998, 926, 833, 812, 764 cm^{-1} ; MS (EI) (m/z): 455.53 (M^+); Anal. Calcd. For $\text{C}_{24}\text{H}_{25}\text{NO}_6\text{S}$: C 63.28, H 5.53, N 3.07. Found C 63.12, H 5.62. N 2.12.

5-ethyl-2,3-dimethyl-4-(furan-2-yl)-6-methyl-1-(p-tolyl)-1,4-dihydropyridine-2,3,5-tricarboxylate (5n):

Yellow solid; m.p. = 105–106 °C; ^1H NMR (400 MHz, CDCl_3) δ : 1.11 (t, 3H, $J=7.3$ Hz, CH_3), 1.52 (s, 3H, CH_3), 2.15 (s, 3H, CH_3), 3.81 (s, 3H, OCH_3), 3.95 (s, 3H, OCH_3), 4.06 (q, 2H, $J=7.3$ Hz, CH_2), 5.17 (s, 1H, CH), 6.97–7.68 (m, 7H, ArH). ^{13}C NMR (100 MHz, CDCl_3) δ : 14.4, 16.9, 22.3, 35.3, 50.9, 52.1, 61.5, 111.1, 121.8, 130.6, 132.7, 134.31, 135.1, 135.9, 140.4, 145.3, 149.7, 151.6, 155.84, 163.2, 166.9, 167.4. FT-IR (KBr) ν : 2953, 2871, 1747, 1688, 1643, 1592, 1526, 1522, 1423, 1308, 1273, 1253, 1226, 1118, 1026, 998, 923, 841, 771 cm^{-1} ; MS (EI) (m/z): 439.46 (M^+); Anal. Calcd. For $\text{C}_{24}\text{H}_{25}\text{NO}_7$: C 65.59, H 5.73, N 3.19. Found C 65.68, H 5.77. N 3.11.

3. Results and Discussion

In the preliminary experiments $\text{Fe}_3\text{O}_4@ \text{SiO}_2\text{-OSO}_3\text{H}$ nanocomposite was prepared and characterized by EDX, FE-SEM and FT-IR analysis.

The morphology and structure of the prepared sample was characterized by scanning electron microscopy (FE-SEM). As shown in Figure 1 the average particle size of the prepared $\text{Fe}_3\text{O}_4@\text{SiO}_2\text{-OSO}_3\text{H}$ nanocomposite has been found to be 8–10 nm.

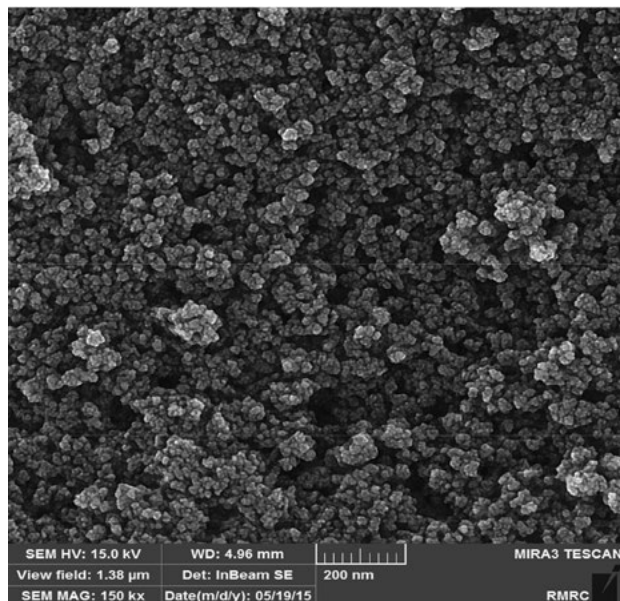


Figure 1. FE-SEM image of $\text{Fe}_3\text{O}_4@\text{SiO}_2\text{-OSO}_3\text{H}$ nanocomposite

Further information about the chemical structure of $\text{Fe}_3\text{O}_4@\text{SiO}_2\text{-OSO}_3\text{H}$ nanocomposite was obtained from FT-IR spectroscopy (Figure 2). The analysis indicated three

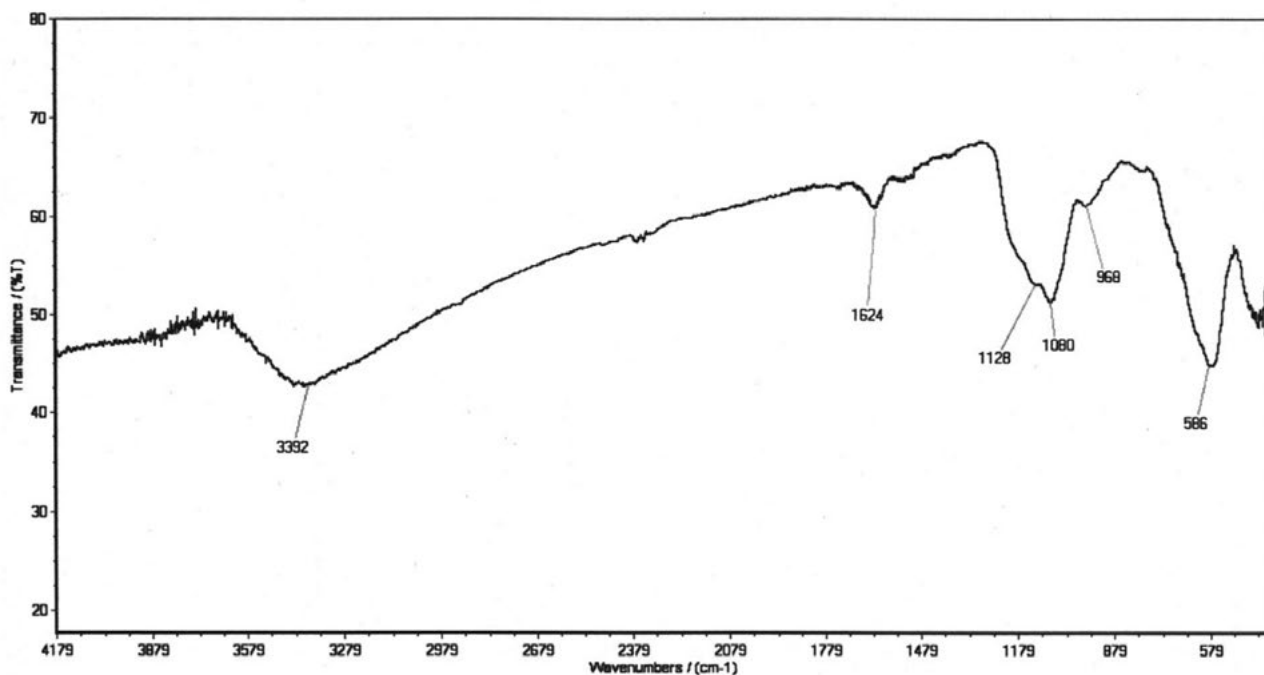


Figure 2. FT-IR spectrum of $\text{Fe}_3\text{O}_4@\text{SiO}_2\text{-OSO}_3\text{H}$ nanocomposite

strong absorption bond at 586 cm^{-1} corresponding to the vibration of Fe-O in Fe_3O_4 . The next strong peak at 1080 cm^{-1} is attributed to the Si-O-Si bond stretching of $\text{Fe}_3\text{O}_4@\text{SiO}_2\text{-SO}_3\text{H}$. The weak intensity band at 968 cm^{-1} can be ascribed to the stretching of non-bridging oxygen atoms in Si-OH bond. Therefore, silica coating on the surface of Fe_3O_4 was confirmed by these absorption bonds. The presence of sulfonyl groups is proved by 1217 cm^{-1} and 1128 cm^{-1} bonds that were covered by a stronger absorption of Si-O bond at 1080 cm^{-1} . The last strong peak appeared at about $2600\text{--}3700\text{ cm}^{-1}$ due to the stretching of OH groups in the SO_3H .

The chemical purity of the samples as well as their stoichiometry was tested by EDX study. The EDX spec-

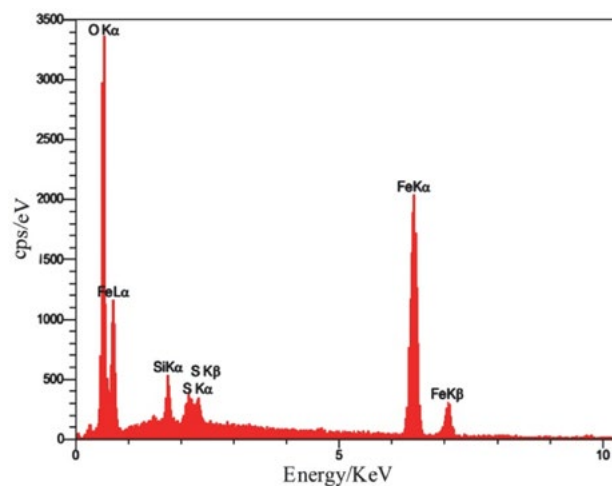


Figure 3. The EDX spectrum of $\text{Fe}_3\text{O}_4@\text{SiO}_2\text{-OSO}_3\text{H}$ nanocomposite

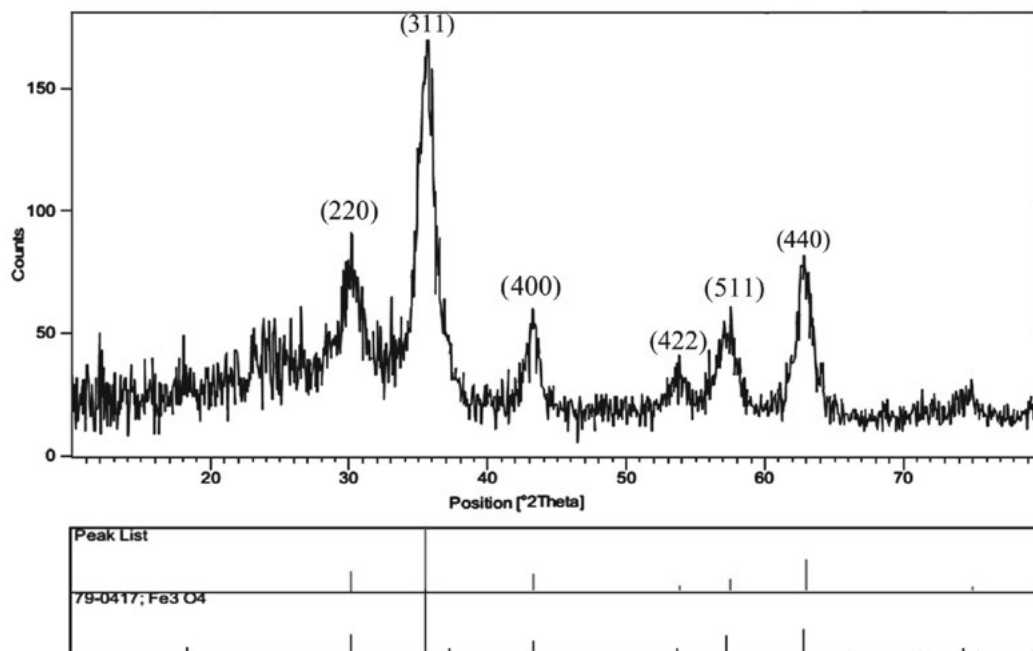


Figure 4. The XRD pattern of $\text{Fe}_3\text{O}_4@SiO_2\text{-OSO}_3\text{H}$ nanocomposite

trum of $\text{Fe}_3\text{O}_4@SiO_2\text{-OSO}_3\text{H}$ nanocomposite shows that the elemental compositions are (Fe, O, S and Si) which have possess nanostructure (Figure 3).

Figure 4 shows the XRD pattern of the prepared $\text{Fe}_3\text{O}_4@SiO_2\text{-OSO}_3\text{H}$. All the XRD patterns show raising background which is attributed to X-ray fluorescence since Cu-K α has been used as the X-ray source during the measurements.

The reflections of XRD pattern of $\text{Fe}_3\text{O}_4@SiO_2\text{-OSO}_3\text{H}$ (2 θ = 30.2°, 36.4°, 43.7°, 53.5°, 56.3°, 62.3°, and 73.8°) in Figure 4 confirm the synthesis of cubic normal spinel Fe_3O_4 (JCPDS file no. 79-0417).³⁹ These results represent the stability of the crystalline phase of Fe_3O_4 nanoparticles during silica coating and surface sulfonic acid functionalization.

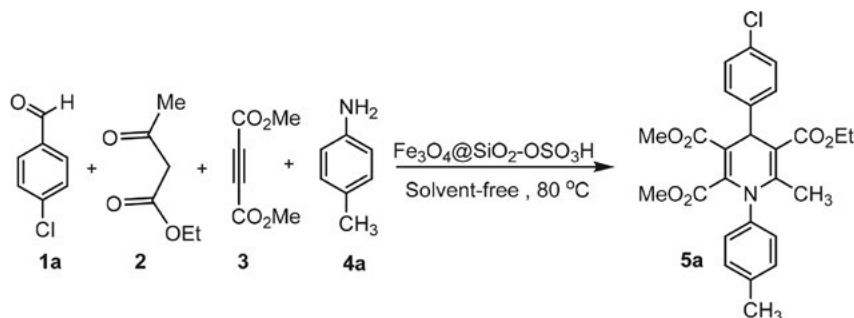
To optimize the reaction conditions the condensation of *p*-toluidine (1 mmol), dimethyl acetylenedicarboxylate (1 mmol), 4-chlorobenzaldehyde (1 mmol) and ethyl acetoacetate (1 mmol), as a model reaction, were studied in the presence of different amounts of $\text{Fe}_3\text{O}_4@SiO_2\text{-OSO}_3\text{H}$

OSO_3H nanocomposite under solvent-free conditions (Scheme 3). The respective results in Table 1 indicate that the best results were attained when the reaction was performed by using 0.02g of the catalyst at 80 °C. To demonstrate that heat cannot thermodynamically promote the reaction in the absence of catalyst; the model reaction was examined at 80 °C under catalyst-free conditions. In these

Table 1. The Effect of the catalyst amount and temperature on the model study

Entry	Catalyst (g)	Temp. (°C)	Time (min)	Yields(%) ^a
1	–	80	120	trace
2	0.03	80	60	91
3	0.02	80	60	91
4	0.01	80	90	82
5	0.02	50	90	71
6	0.02	100	70	91

^a Isolated yield.



Scheme 3. The model reaction for the synthesis of 1,4-dihydropyridine 5a

conditions, desired product was obtained in trace after 120 min. This observation indicated clearly that heat cannot promote the reaction without catalyst. Thus presence of catalyst is essential for this reaction.

After optimization of the reaction conditions, the efficiency and scope of the catalyst were evaluated by the reaction of arylamines, dimethyl acetylenedicarboxylate, aryl aldehydes and ethyl acetoacetate by using 0.02 g of $\text{Fe}_3\text{O}_4@/\text{SiO}_2\text{-OSO}_3\text{H}$ nanocomposite at 80 °C. The corresponding results are summarized in Table 2. As it can be seen from Table 2, all reactions proceeded efficiently to afford the desired 1,4-dihydro-pyridines in high yields and short reaction times. Therefore, $\text{Fe}_3\text{O}_4@/\text{SiO}_2\text{-OSO}_3\text{H}$ nanocomposite was efficient to catalysis the one-pot four-component reactions.

The influence of electron-withdrawing and electron-donating substituents on the aromatic ring of aldehydes upon the reaction yields and times was investigated. The results in Table 2 show that the aromatic aldehydes bearing

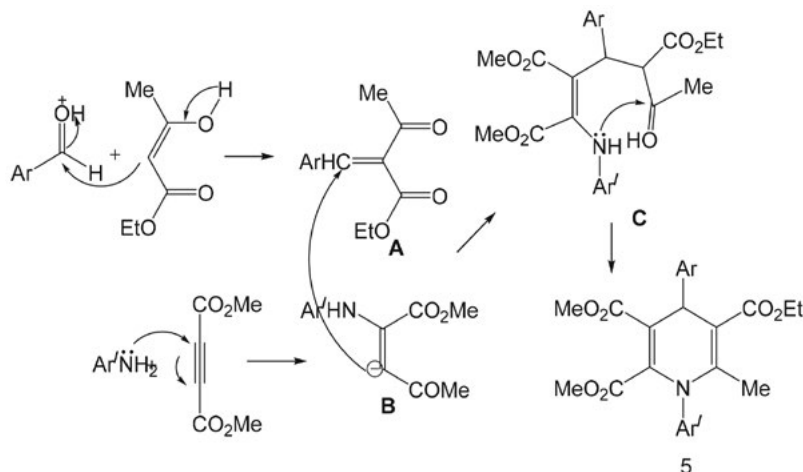
both electron-donating and electron-withdrawing groups presented excellent yield of desired products.

A plausible mechanism for the preparation of highly functionalized dihydropyridines using $\text{Fe}_3\text{O}_4@/\text{SiO}_2\text{-OSO}_3\text{H}$ nanocomposite has on the basis of our experimental results together with some literature⁴⁰ been shown in Scheme 3. It is likely that $\text{Fe}_3\text{O}_4@/\text{SiO}_2\text{-OSO}_3\text{H}$ MNPs acts as a Bronsted acid and increases the electrophilicity of the carbonyl groups of the aldehydes and intermediates. Firstly, the Knoevenagel condensation of aromatic aldehyde with ethyl acetoacetate is suggested to give the intermediate A, Then nucleophilic attack of arylamine to dimethyl acetylenedicarboxylate leads to formation of intermediate B. Secondly, the Michael addition of β -enamino ester intermediate (B) to arylidenecyanoacetate (A) afforded the addition of intermediate (C). At last in intermediate(C), the intramolecular nucleophilic addition of amino group to carbonyl group formed the final 1,4- dihydropyridine(Scheme 4).

Table 2. The synthesis of 1,4-dihydropyridines using $\text{Fe}_3\text{O}_4@/\text{SiO}_2\text{-SO}_3\text{H}$ under solvent-free conditions at 80 °C.

Entry	Ar	Ar'	Product	Time (min)	Yield (%)	Lit. m.p (°C)	M.p (°C)
1	4-Cl-Ph	4-CH ₃ -Ph	5a	60	91	132–133	(133–135) ⁴⁰
2	3-NO ₂ -Ph	4-CH ₃ -Ph	5b	60	89	137–138	(135–137) ⁴⁰
3	4-NO ₂ -Ph	4-OCH ₃ -Ph	5c	45	93	170–172	–
4	3-NO ₂ -Ph	4-OCH ₃ -Ph	5d	70	90	154–156	(155–157) ⁴⁰
5	4-Br-Ph	4-OCH ₃ -Ph	5e	60	92	145–147	–
6	4-Br-Ph	4-Cl-Ph	5f	70	85	127–129	–
7	4-Cl-Ph	4-Cl-Ph	5g	60	85	131–133	(132–134) ⁴⁰
8	3-NO ₂ -Ph	4-Cl-Ph	5h	70	88	143–145	(143–145) ⁴⁰
9	4-Cl-Ph	4-OCH ₃ -Ph	5i	50	87	128–130	(129–131) ⁴⁰
10	4-OCH ₃ -Ph	4-CH ₃ -Ph	5j	80	83	109–112	(110–112) ⁴⁰
11	4-F-Ph	4-CH ₃ -Ph	5k	60	90	105–107	(104–106) ⁴⁰
12	3-NO ₂ -Ph	Ph	5l	70	88	153–155	(151–153) ⁴⁰
13	Thiophen-2-yl	4-CH ₃ -Ph	5m	80	85	112–115	–
14	Furan-2-yl	4-CH ₃ -Ph	5n	75	90	105–106	–

^aIsolated yield.



Scheme 4. Proposed reaction pathway for the synthesis of 1,4-dihydropyridines

3. 1. Results of Antimicrobial Activities:

3. 1. 2. Well Diffusion Method

Among the bacterial strains studied inhibition diameters of *Staphylococcus aureus* in the presence of 5-ethyl 2,3-dimethyl 1-(4-methoxyphenyl)-6-methyl-4-(4-nitrophenyl)-1,4-dihydropyridine-2,3,5-tricarboxylate (5c), 5-ethyl 2,3-dimethyl 4-(4-bromophenyl)-1-(4-methoxyphenyl)-6-methyl-1,4-dihydropyridine-2,3,5-tricarboxylate (5e), 5-ethyl 2,3-dimethyl 4-(4-bromophenyl)-1-(4-chlorophenyl)-6-methyl-1,4-dihydropyridine-2,3,5-tricarboxylate (5f) were 16, 15 and 17 mm respectively. But other bacterial strains showed no inhibition zone.

3. 1. 3. Determination of Antibiotic Susceptibility

The results of the antibiogram for *Staphylococcus aureus* strain showed that this bacterium is sensitive to Vancomycin antibiotic

3. 1. 4. Disc Diffusion Method

In this test, as well as well diffusion method inhibition diameters of *Staphylococcus aureus* in the presence of 5-ethyl 2,3-dimethyl 1-(4-methoxyphenyl)-6-methyl-4-(4-nitrophenyl)-1,4-dihydropyridine-2,3,5-tricarboxylate (5c), 5-ethyl 2,3-dimethyl 4-(4-bromophenyl)-1-(4-methoxyphenyl)-6-methyl-1,4-dihydropyridine-2,3,5-tricarboxylate (5e), 5-ethyl 2,3-dimethyl 4-(4-bromophenyl)-1-(4-chlorophenyl)-6-methyl-1,4-dihydropyridine-2,3,5-tricarboxylate (5f) was 15, 14, 16 mm respectively.

3. 2. Recycling and the Reusability of the Catalyst

Reusability is one of the most significant properties of the prepared catalysts. Upon completion of the reaction, dichloromethane was added to the reaction mixture, the catalyst was insoluble in CH_2Cl_2 and it could therefore be recycled by a simple filtration. The nanocatalyst was then washed three to four times with methanol and dried at 80 °C for 7 h for the next runs. To investigate the reusability of the catalyst, the model study was repeated using recovered Fe_3O_4 @silica sulfonic acid nanocomposite under optimized reaction conditions. The summarized results of Ta-

ble 3 show that the nanocatalyst could be reused for five times with a minimal loss of its activity. In addition, sulfonic acid contain of the Fe_3O_4 @ SiO_2 @ OSO_3H was evaluated by back titration after five runs (0.24 mmol/g) that shows no significant loss in activity.

4. Conclusion

In conclusion, we have developed a simple and efficient approach for the synthesis of 1,4-dihydropyridines by one-pot four-component reaction of arylamine, dimethyl acetylenedicarboxylate, aromatic aldehyde and ethyl acetoacetate in the presence of Fe_3O_4 @ SiO_2 - OSO_3H nanocatalyst under solvent-free conditions. The present methodology offers several advantages, such as good yields, short reaction times, ease of separation, recyclability of the magnetic nanocatalyst, simple purification and environmentally benign. These compounds showed high antibiotic properties and can be useful in other research and biomedical applications.

4. 1. Acknowledgements

The author gratefully acknowledges the financial support of this work by the Research Affairs Office of the Islamic Azad University, Qom Branch, Qom, I. R. Iran [grant number 2014-13929].

5. References

1. A. Nefzi, J. M. Ostresh, R. A. Houghten, *Chem. Rev.* **1997**, *97*, 449–472. DOI:10.1021/cr960010b
2. K. K. Boroujeni, Z. Heidari, R. Khalifeh, *Acta. Chim. Slov.* **2016**, *63*, 602–608. DOI:10.17344/acsi.2016.2291
3. S. M. Roopan, F. R. Nawaz Khan, *Chem. Pap.* **2010**, *64*, 812–817.
4. A. Bharathi, S. M. Roopan, A. Kajbafvala, R. D. Padmaja, M. S. Darsana, G. Nandhini Kumari, *Chin. Chem. Lett.* **2014**, *25*, 324–326. DOI:10.1016/j.ccl.2013.11.040
5. S. M. Roopan, F. R. Nawaz Khan, *Chem. Pap.* **2010**, *64*, 678–682.
6. S. M. Roopan, F. R. Nawaz Khan, J. S. Jin, *Res. Chem. Intermed.* **2012**, *38*, 443–451. DOI:10.1007/s11164-011-0361-4
7. S. M. Roopan, F. R. Nawaz Khan, J. S. Jin, *Chem. Pap.* **2011**, *65*, 345–351.
8. R. Shan, C. Velazquez, *J. Med. Chem.* **2004**, *47*, 254–261. DOI:10.1021/jm030333h
9. L. Ohberg, J. Wesman, *Synlett.* **2001**, *8*, 1296–1298. DOI:10.1055/s-2001-16043
10. A. Dondoni, A. Massi, E. Minghini, V. Bertolasi, *Tetrahedron.* **2004**, *60*, 2311–2326. DOI:10.1016/j.tet.2004.01.011
11. J. L. Donelson, R. A. Gibbs, S. K. De, *J. Mol. Cat. A: Chem.* **2006**, *256*, 309–311. DOI:10.1016/j.molcata.2006.03.079
12. S. J. Ji, Z. Q. Jiang, J. Lu, T. P. Loh, *Synlett.* **2004**, 831–835. DOI:10.1055/s-2004-820035

Table 3. Reusability of the Fe_3O_4 @ SiO_2 - OSO_3H nanocatalyst

Number of cycle	Yield (%) ^a
1	91
2	90
3	90
4	88
5	85

^aYields refer to the isolated pure product

13. S. Ko, M. N. V. Sastry, C. Lin, C. F. Yao, *Tetrahedron Lett.* **2005**, 46, 5771–5774. DOI:10.1016/j.tetlet.2005.05.148
14. I. B. Dzvinchuk, N. A. Tolmacheva, *Chem. Heterocycl. Comp.* **2001**, 37, 506–508. DOI:10.1023/A:1017668408493
15. V. A. Chebanov, V. E. Saraev, K. M. Kobzar, S. M. Desenko, V. D. Orlov, E. A. Gura, *Chem. Heterocycl. Comp.* **2004**, 40, 475–480. DOI:10.1023/B:COHC.0000033541.49115.a0
16. G. Sabitha, G. S. Reddy, C. S. Reddy, J. S. Yadav, *Tetrahedron Lett.* **2003**, 44, 4129–4131. DOI:10.1016/S0040-4039(03)00813-X
17. L. M. Wang, J. Sheng, L. Zhang, J. Han, Z. Y. Fan, H. Tian, C. Y. Qian, *Tetrahedron.* **2005**, 61, 1539. DOI:10.1016/j.tet.2004.11.079
18. S. Ko, C. F. Yao, *Tetrahedron.* **2006**, 62, 7293–7299. DOI:10.1016/j.tet.2006.05.037
19. M. A. Chariand, K. Syamasundar, *Catal. Commun.* **2005**, 6, 624–626. DOI:10.1016/j.catcom.2005.03.010
20. S. H. Mashraqui, M. A. Karnik, *Tetrahedron Lett.* **1998**, 39, 4895–4898. DOI:10.1016/S0040-4039(98)00889-2
21. R. S. Varma, D. Kumar, *Tetrahedron Lett.* **1999**, 40, 21–24. DOI:10.1016/S0040-4039(98)80007-5
22. Y. Z. Mao, M. Z. Jin, Z. L. Liu, L. M. Wu, *Org. Lett.* **2000**, 2, 741–742. DOI:10.1021/ol990367c
23. N. Nakamichi, Y. Kawashita, M. Hayashi, *Org. Lett.* **2002**, 4, 3955–3957. DOI:10.1021/ol0268135
24. M. Zhang, P. Liu, Y. H. Liu, Z. R. Shang, H. C. Hu, Z. H. Zhang, *RSC Adv.* **2016**, 6, 106160–106170.
25. M. Farahi, B. Karami, R. Keshavarz, F. Khosravian, *RSC Adv.* **2017**, 7, 46644–46650.
26. X. N. Zhao, H. C. Hu, F. J. Zhang, Z. H. Zhang, *J. Appl. Catal. A: Gen.* **2014**, 482, 258–265. DOI:10.1016/j.apcata.2014.06.006
27. A. Maleki, T. Kari, M. Aghaei, *J. Porous Mater.* **2017**, 24, 1481–1496. DOI:10.1007/s10934-017-0388-z
28. S. Taheri, H. Veisi, M. Hekmati, *New J. Chem.* **2017**, 41, 5075–5081. DOI:10.1039/C7NJ00417F
29. M. A. Ghasemzadeh, *Acta. Chim. Slov.* **2015**, 62, 977–985. DOI:10.17344/acsi.2015.1501
30. M. A. Ghasemzadeh, M. H. Abdollahi-Basir, M. Babaei, *Green Chem. Lett. Rev.* **2015**, 8, 40–49. DOI:10.1080/17518253.2015.1107139
31. M. A. Ghasemzadeh, B. Mirhosseini-Eshkevari, M. H. Abdollahi-Basir, *Comb. Chem. High. T. Scr.* **2016**, 19, 592–601.
32. M. A. Ghasemzadeh, N. Ghasemi-Seresht, *Res. Chem. Intermed.* **2015**, 41, 8625–8636. DOI:10.1007/s11164-014-1915-z
33. M. A. Ghasemzadeh, B. Molaei, M. H. Abdollahi-Basir, F. Zamani, *Acta. Chim. Slov.* **2017**, 64, 73–82. DOI:10.17344/acsi.2016.2823
34. B. Jean, R. Franklin, A. Patricia, A. Janet, M. George, *Approved standard–Tenth edition.* **2015**, 35, M07-A10.
35. D. M. Livermore, D. F. Brown, *J. Antimicrob. Chemother.* **2001**, 48, 59–64. DOI:10.1093/jac/48.suppl_1.59
36. Y. Hu, Z. Zhang, H. Zhang, L. Luo, S. Yao, *J. Solid State Electrochem.* **2012**, 16, 857–867. DOI:10.1007/s10008-011-1434-4
37. Y. H. Deng, D. W. Qi, C. H. Deng, X. M. Zhang, D. Y. Zhao, *J. Am. Chem. Soc.* **2008**, 130, 28–29. DOI:10.1021/ja0777584
38. A. R. Kiasat, J. Davarpanah, *J. Mol. Catal. A: Chem.* **2013**, 373, 46–54. DOI:10.1016/j.molcata.2013.03.003
39. T. Z. Yang, C. M. Shen, H. J. Gao, *J. Phys. Chem. B.* **2005**, 109, 23233–23236. DOI:10.1021/jp054291f
40. W. Ping, X. Er-Yan, S. Jing, Y. Chao-Guo, *Chem. Res. Chinese U.* **2012**, 28, 652–655.

Povzetek

Sinteza heterocikličnih spojin je zaradi njihove široke uporabe velikega pomena. V tej raziskavi smo s pomočjo reakcij štirih reaktantov arilaminov, acetilendikarboksilatov, aromatskih aldehydov in etil acetoacetata v prisotnosti nanocompozita $\text{Fe}_3\text{O}_4/\text{SiO}_2/\text{OSO}_3\text{H}$ razvili sintezno metodo za pripravo 1,4-dihidropiridinov. Prednosti opisane metode so: okolju prijazni reakcijski pogoji, enostaven način izvedbe, širok nabor substratov, odlični izkoristki in ponovna uporaba nanokatalizatorja. Eden od indikatorjev za merjenje protimikrobne aktivnosti je minimalna inhibitorna koncentracija (MIC), ki je bila na preiskovanih bakterijah izmerjena s premerom območja inhibicije rasti od prisotnosti sintetiziranih heterocikličnih spojin z uporabo delucijske difuzije, difuzije diska in določanja občutljivosti na antibiotike. Rezultati vseh treh metod so pokazali občutljivost *Staphylococcus aureus* na sintetizirane heterociklične spojine. Iz rezultatov lahko sklepamo, da imajo te spojine dobre antibiotične lastnosti in so lahko uporabne tudi pri drugih raziskovalnih in biomedicinskih aplikacijah.

Scientific paper

The Cl Functionalized Aluminum Nitride (AlN) and Aluminum Phosphide (AlP) Nanocone Sheets as Hydrogen Selenide (H₂Se) Sensor: a Density Functional Investigation

Seyyed Milad Abrishamifar,¹ Negar Heidari,² Razieh Razavi,³
Milad Janghorban Lariche^{4,*} and Meysam Najafi^{5,*}

¹ Department of Chemical Engineering, New York International University of Technology and Management, New York, USA

² Department of Chemistry, Faculty of Science, Borujerd Branch, Islamic Azad University, Borujerd, Iran

³ Department of Chemistry, Faculty of Science, University of Jiroft, Jiroft, Iran

⁴ Abadan School of Medical Sciences, Abadan, IRAN

⁵ Medical Biology Research Center, Kermanshah University of Medical Sciences, Kermanshah 67149-67346, Iran

* Corresponding author: E-mail: janghorban@abadanums.ac.ir and meysamnajafi2016@gmail.com

Phone: +98-8337243181 Fax: +98-8337243181

Received: 06-09-2017

Abstract

The adsorption of H₂Se molecule on AlN-NCS and AlP-NCS surfaces were investigated by using of DFT calculations. The potentials of Cl-functionalized AlN-NCS and AlP-NCS for H₂Se adsorption were examined. All processes of H₂Se-adsorption on considered nanocone sheets were exothermic reactions. The calculated $|E_{ad}|$ amount of complex H₂Se with AlP-NCS was higher than AlN-NCS. The functionalization of considered nanocone sheets with Cl atom increase $|E_{ad}|$ amount of H₂Se. Results reveal that, obtained E_{ad} amounts of considered nanocone sheets have linear relationships with corresponding orbital energy amounts. Finally, the novel nanocone sheets with higher efficiency to adsorption of H₂Se can be proposed.

Keywords: DFT, nanocone, H₂Se, function, gas sensor

1. Introduction

Hydrogen selenide (H₂Se) as main toxic gas can be produced via reaction of selenium and hydrogen gas and it can be formed by reaction of acids with selenide. Some paths to H₂Se preparation in large and small scales have been investigated. The presence of H₂Se on exposed fur animals would result in relatively high oral doses resulting from preening and possibly skin permeation.¹⁻³

H₂Se is the most toxic gases with a contact boundary of 0.05 ppm over an 8 hour cycle and H₂Se at really low concentrations is very infuriating smell resembling that of leaking gases.^{1,2} Growth of H₂Se resultant from reticence of the Se methylation metabolism, the detoxification way of selenium, is found resulting frequent oral administration of toxic dose of selenocystine.⁴⁻⁶

Aluminum nitride nanocone sheet (AlN-NCS) have been synthesized and it has wide band gap and so it has various applications in optics, electronics and photoelectronics.⁷ The previous studies shown that AlN-NCS and AlP-NCS were uniform and Al, P and N atoms on surface of AlN-NCS and AlP-NCS have 3-fold coordinate. The creation of unsaturated sites on Al, P and N atoms play main roles in gas adsorption and so AlN-NCS and AlP-NCS can be gas sensors with the highest performance.⁸⁻¹²

The adsorptions of toxic gases with various compounds to identify the suitable sensor are important works to solve the environmental problems. In previous studies, widely in chemical processes the various nanostructures because of their sensitivity and activity have been used and results have been shown that functionalization of na-

nostructure can improvement the capability of nanostructures to detect toxic gases.^{13–17}

In previous papers the adsorption of various gases such as SO₂, H₂S, CO₂ and CO on surfaces of nanostructures have been investigated.^{18–34} Zaboli and et al.³⁵ the adsorptions of the H₂S, H₂Se and SO₂ molecules on the surface of fullerene by the density functional theory investigated. Obtained results shown that, the adsorption energy amounts of gas molecule were short, so, the sensor were possess at short recovery times.³⁵ Also results shown that H₂Se molecule with adsorption energy of about –11.28 kJ/mol has the strongest adsorption on surface of fullerene.³⁵

In previous study theoretical methods have been used to investigation influence of metal oxides on various polymers such as polyvinyl alcohol and polyaniline. Results show that, addition of metal oxides increase the total dipole moments of polymers and decrease the band gap energies of polymers. Results shown that predictable dipole moment of studied compounds reflects their potential to interact with their neighboring molecules and higher dipole moment of assumed structures was joint with the higher activity for various applications.^{35–37}

Ibrahim and et al. used theoretical methods to study the dipole moment and geometrical structures of COOH. Their results show that increase of dipole moments are suitable pointer to ability of considered structures. Also they used DFT to study composite of divalent zinc and results show that obtained dipole moment was 23.4 Debye and band gap energy was 0.49 eV. Results shown that decorated CNT can form stable structures with increased molecular dimensions and decorated CNT can be a suitable sensor to volatile matter.^{38–40}

In present work, the adsorptions of H₂Se molecule on surfaces of AlN-NCS and AlP-NCS were examined theoretically. The Cl-functionalized effects on ability of AlN-NCS and AlP-NCS to adsorption of H₂Se were calculated via theoretical method. The orbital energy amounts of considered nanocone sheets were calculated and relationships between orbital energy and E_{ad} amounts of considered nanocone sheets were examined. The initial points of this work are: (1) to find the ability of AlN-NCS and AlP-NCS to H₂Se-adsorption; (2) to categorize the influences of Cl functionalization of NCS on capability of AlN-NCS and AlP-NCS; (3) to discovery the linear relationships between adsorption and orbital energy NCS; (5) To propose the novel NCSs with the highest capacity to H₂Se-adsorption.

2. Computational Details

The geometry of AlN-NCS, AlP-NCS and their Cl functionalized derivatives were optimized via DFT method, B3LYP functional and 6-311G (d,p) basis set in GAMESS software.^{41,42} The geometry of complexes of H₂Se molecule and considered AlN-NCSs and AlP-NCSs were

optimized (obtained structures of considered complexes were reported in figure 1). In order to remove the border effects, termination atoms of considered AlN-NCSs and AlP-NCSs were sodden via hydrogen atoms. In this work, frequency calculations were done in order to confirm the structures were true minima.^{43–46}

In this work, adsorption energy (E_{ad}) and free energy (G_{ad}) amounts of H₂Se molecule on considered AlN-NCSs and AlP-NCSs were obtained via equations 1 and 2, respectively:

$$E_{ad} = E(\text{nanocone sheet}/\text{H}_2\text{Se}) - E(\text{nanocone sheet}) - E(\text{H}_2\text{Se}) + E_{\text{BSSE}} \quad (1)$$

$$G_{ad} = G(\text{nanocone sheet}/\text{H}_2\text{Se}) - G(\text{nanocone sheet}) - G(\text{H}_2\text{Se}) \quad (2)$$

where E (nanocone sheet/H₂Se) is energy of complexes of H₂Se and considered nanostructures. The E (H₂Se) and E (nanocone sheet) are energies of H₂Se molecule and considered nanostructures, respectively. The negative amounts of E_{ad} and G_{ad} indicated that H₂Se molecule and AlN-NCSs and AlP-NCSs have exothermic interactions. In this work also the Basis set superposition error (BSSE) amounts of interactions of H₂Se-nanostructures were calculated.⁴⁷

3. Results and Discussion

3.1. E_{ad} and G_{ad} Amounts of H₂Se-nanocone Sheet

In this section E_{ad} and G_{ad} amounts of H₂Se adsorption on surface of AlN-NCS, AlP-NCS, Cl-AlN-NCS and Cl-AlP-NCS in table 1 were presented. In table 1 the E_{ad} and G_{ad} amounts of H₂Se-NCS and H₂Se-Cl-NCS were negative and so the interactions of H₂Se and considered nanocone sheets were exothermic reactions. The |E_{ad}| and |G_{ad}| amounts of H₂Se-AlP-NCS were higher than corresponding values of H₂Se-AlN-NCS ca 41.5 and 43.4 kJ/mol, respectively.

The |E_{ad}| and |G_{ad}| amounts of H₂Se-Cl-AlP-NCS were higher than corresponding values of H₂Se-Cl-AlN-NCS ca 18.3 and 18.2 kJ/mol, respectively. Also |E_{ad}| and |G_{ad}| amounts of H₂Se-Cl-AlP-NCS were higher than corresponding values of H₂Se-AlP-NCS ca 21.2 kJ/mol and 20.3 kJ/mol, respectively.

In table 1 the |E_{ad}| and |G_{ad}| amounts of H₂Se-NCS and H₂Se-Cl-NCS were decreased as follow: AlN-NCS < Cl-AlN-NCS < AlP-NCS < Cl-AlP-NCS. Data in table 1 consummated that Cl-AlP-NCS and AlN-NCS have the highest and the lowest performances to H₂Se-adsorption, respectively. Results in table 1 can be expounded that phosphor and chlorine atoms can stable the AlP-NCS, AlP-Cl-NCS and their H₂Se complexes; therefore the |E_{ad}| and |G_{ad}| amounts of AlP-NCS AlP-Cl-NCS were higher than corresponding values of AlN-NCS.⁴⁸

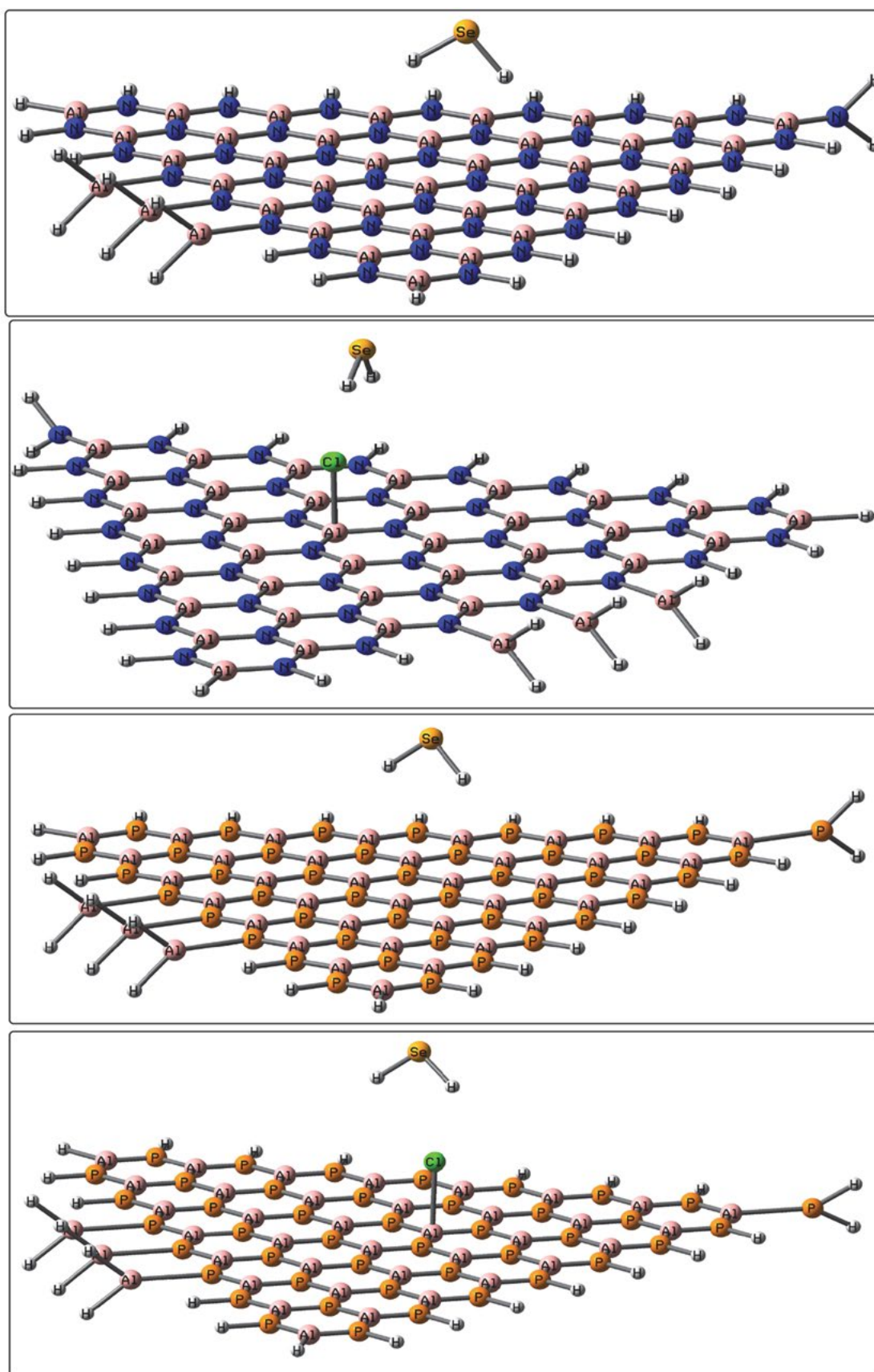


Figure 1. Complexes of H_2Se with AlN-NCS, AlP-NCS, Cl-AlN-NCS and Cl-AlP-NCS.

Table 1. Calculated E_{ad} and G_{ad} of H_2Se on AlN-NCS, AIP-NCS, Cl-AlN-NCS and Cl-AIP-NCS surfaces.

G_{ad} (kJ/mol)	E_{ad} (kJ/mol)	Nanostructure
-368.6	-377.3	AlN-NCS
-412.0	-418.8	AIP-NCS
-386.9	-395.6	Cl-AlN-NCS
-432.3	-440.0	Cl-AIP-NCS

Table 2. Calculated orbital energy amounts of AlN-NCS, AIP-NCS, Cl-AlN-NCS and Cl-AIP-NCS.

E_{HLG} (kJ/mol)	E_{LUMO} (kJ/mol)	E_{HOMO} (kJ/mol)	Nanostructure
222.0	-378.3	-600.2	AlN-NCS
193.0	-384.1	-577.1	AIP-NCS
173.7	-396.6	-570.3	Cl-AlN-NCS
136.1	-410.1	-546.2	Cl-AIP-NCS

3. 2. Orbital Energies of Considered Nanocone Sheets

In this section orbital energy amounts of AlN-NCS, AIP-NCS, AlN-NCS, AIP-NCS were calculated and obtained amounts were represented in table 2 and relationships of orbital energy amounts in table 2 and E_{ad} amounts in table 1 were examined. In table 2, AlN-NCS and Cl-AIP-NCS have the highest and the lowest amounts of $|E_{HOMO}|$, respectively.

Therefore in table 2 the Cl-AIP-NCS and AlN-NCS have the highest and the lowest inclination to lose an electron, respectively. In table 2, the $|E_{LUMO}|$ amounts of studied nanostructures were decrease as follow: AlN-NCS < Cl-AlN-NCS < AIP-NCS < Cl-AIP-NCS. In table 2, Cl-AIP-NCS and AlN-NCS have the highest and the lowest amounts of $|E_{LUMO}|$, respectively. Therefore in table 2 the Cl-AIP-NCS and AlN-NCS have the highest and the lowest capability to receive an electron, respectively.

In table 2, E_{HLG} amounts of considered nanocone sheets were decrease as follow: AlN-NCS > Cl-AlN-NCS > AIP-NCS > Cl-AIP-NCS. In table 2, Cl-AIP-NCS and AlN-NCS have the lowest and the highest amounts of E_{HLG} , respectively. So, in table 2 the Cl-AIP-NCS and AlN-NCS have the highest and the lowest reactivity. In table 2, AIP-NCS has higher $|E_{LUMO}|$ and lower $|E_{HOMO}|$ amounts than AlN-NCS. In table 2, Cl-AlN-NCS and Cl-AIP-NCS have higher $|E_{LUMO}|$ and lower $|E_{LUMO}|$ amounts than AlN-NCS and AIP-NCS. So, Cl functionalization increase the capability of AlN-NCS and AIP-NCS to H_2Se adsorption.

In this section, relationships between E_{ad} and orbital energy amounts of considered nanocone sheets were examined. The E_{ad} amounts of complexes of H_2Se -NCS in table 1 were modified against the orbital energy amounts of complexes of H_2Se -NCS in table 2. The equations 3-5 were calculated from these modifications as follow:

$$E_{ad} = -1.09 \times (E_{HOMO}) - 1032 \quad (3)$$

$$E_{ad} = 1.43 \times (E_{HOMO}) + 152 \quad (4)$$

$$E_{ad} = 0.63 \times (E_{HLG}) - 523 \quad (5)$$

The relationship constants of equations 3-5 were ca 0.994, 0.997 and 0.994, respectively and so there are linear relationship between E_{ad} and orbital energy amounts of complexes H_2Se -NCS.

In tables 1 and 2 the E_{ad} and orbital energy amounts of H_2Se -NCS complexes have similar trends and it can be established that ability of considered nanocone sheets to H_2Se -adsorption were decreased as follow: AlN-NCS < Cl-AlN-NCS < AIP-NCS < Cl-AIP-NCS. Finally, Cl-AIP-NCS and AlN-NCS have the highest and the lowest capacity to H_2Se -adsorption and also E_{ad} and orbital energy amounts were main factors to predicate of ability of NCS to H_2Se -adsorption.

4. Conclusion

The potentials of AlN-NCS, AIP-NCS, Cl-AlN-NCS and Cl-AIP-NCS to adsorption of H_2Se molecule via DFT method and B3LYP functional were examined. The interactions of H_2Se with considered nanocone sheets were exothermic processes and these interactions were possible theoretically. The $|E_{ad}|$ amount of H_2Se -AIP-NCS were higher than those of H_2Se -AlN-NCS. The considered Cl-AIP-NCS and Cl-AlN-NCS have higher $|E_{ad}|$ amounts than AIP-NCS and AlN-NCS, respectively. There were linear relationships between of E_{ad} and orbital energy amounts of considered NCSs. The E_{ad} and orbital energy amounts can be considers as main scale to predicate the ability of nanocone sheets to H_2Se -adsorption.

5. References

1. A. Afshar, M. Salami Hosseini, E. Behzadfar, *Sci. Iran. Trans. C* **2014**, *21*, 2107–2115.
DOI:10.1016/j.snb.2011.04.070
2. T. Hübert, L. Boon-Brett, G. Black, U. Banach, *Sens. Actu. B: Chem.* **2011**, *157*, 329–352.
3. M. Ibrahim, E. Koglin, *Acta Chim. Slov.* **2005**, *52*, 159–163.
4. K. Nakamuro, T. Okuno, T. Hasegawa, *J. Heal. Sci.* **2000**, *46*, 418–421. DOI:10.1248/jhs.46.418
5. A. Kiani, P. Haratipour, M. Ahmadi, R. Zare-Dorabei, A. Mahmoodi, *J. Water Supply. Res. T.* **2017**, *66*, 239–248.
6. K. Ho, W. Hung, *Sens. Actu. B: Chem.* **2001**, *79*, 11–16.
DOI:10.1016/S0925-4005(01)00782-1
7. M. Ari, M. L. Cohen, *Phys. Review B* **1997**, *56*, 6737–6741.
DOI:10.1103/PhysRevB.56.6737
8. A. Aquila, *Opt. Express.* **2012**, *20*, 2706–2716.
DOI:10.1364/OE.20.002706
9. J. C. Yang and P. K. Dutta, *Sens. Actu. B: Chem.* **2010**, *143*,

- 459–463. DOI:10.1016/j.snb.2009.09.023
10. Z. Parsaee, P. Haratipour, M. Janghorban Lariche, A. Vojood, *Ultrason. Sonochem.* **2018**, *41*, 337–349. DOI:10.1016/j.ultsonch.2017.09.054
11. A. Khodadadi, A. M. Miri, *Sen. Acta. B: Chem.* **2001**, *80*, 267–271. DOI:10.1016/S0925-4005(01)00915-7
12. G. Korotcenkov, *Sen. Acta. B: Chem.* **2007**, *121*, 664–678. DOI:10.1016/j.snb.2006.04.092
13. M. Najafi, M. Najafi, H. Najafi, *J. Theor. Comput. Chem.* **2013**, *12*, 1250–116. DOI:10.1142/S0219633612501167
14. J. B. Halpern, A. Bello, J. Gilcrease, G. L. Harris, *Microelectron. J.* **2009**, *40*, 316–318. DOI:10.1016/j.mejo.2008.07.022
15. P. Haratipour, A. Baghban, A. H. Mohammadi, S. H. Hosseini Nazhad, A. Bahadori, *J. Mol. Liq.* **2017**, *242*, 146–159. DOI:10.1016/j.molliq.2017.06.123
16. A. Ahmadi, J. Beheshtian, M. Kamfiroozi, *J. Mol. Model.* **2012**, *18*, 1729–1734. DOI:10.1007/s00894-011-1202-5
17. J. Beheshtian, M. Kamfiroozi, Z. Bagheri, A. Ahmadi, *Comp. Mater. Sci.* **2012**, *54*, 115–118. DOI:10.1016/j.commatsci.2011.09.039
18. M. Zaboli, H. Raissi and F. Farzad, *Intern. J. Adv. Biotech. Rese.* **2016**, *7*, 1227–1232.
19. W. G. Liu, G. H. Chen, X. C. Huang, *J. Phys. Chem. C* **2012**, *116*, 4957–4964. DOI:10.1021/jp2124857
20. K. Rezouali, M. A. Belkhir, A. Houari, J. Bai, *Comput. Mater. Sci.* **2009**, *45*, 305–309. DOI:10.1016/j.commatsci.2008.10.004
21. D. Zhang, R. Q. Zhang, *Chem. Phys. Letters* **2003**, *371*, 426–432. DOI:10.1016/S0009-2614(03)00289-6
22. Y. F. Zhukovskii, N. Pugno, A. I. Popov, *J. Phys. Cond. Matter* **2007**, *19*, 395021–395038. DOI:10.1088/0953-8984/19/39/395021
23. M. Zhao, Y. Xia, Z. Tan, X. Liu, F. Li, *Chem. Phys. Letters* **2004**, *389*, 160–164. DOI:10.1016/j.cplett.2004.03.082
24. R. Thapa, B. Saha, N. S. Das, U. N. Maiti, *Appl. Sur. Sci.* **2010**, *256*, 3988–3992. DOI:10.1016/j.apsusc.2010.01.062
25. F. Li, C. Zhang, P. Wang, P. Li, *Appl. Sur. Sci.* **2012**, *258*, 6621–6626. DOI:10.1016/j.apsusc.2012.03.090
26. D. Tasis, N. Tagmatarchis, A. Bianco, M. Parto, *Chem. Rev.* **2006**, *106*, 1105–1136. DOI:10.1021/cr050569o
27. S. Y. Xie, W. Wang, K. A. S. Fernando, *Chem. Commun.* **2005**, *29*, 3670–3672. DOI:10.1039/b505330g
28. C. Y. Zhi, Y. Bando, C. C. Tang, *Angew. Chem. Int. Edit.* **2005**, *44*, 7929–7932. DOI:10.1002/anie.200502591
29. M. T. Baei, A. A. Peyghan, Z. Bagheri, *Superlattice Microst.* **2012**, *53*, 9–15. DOI:10.1016/j.spmi.2012.09.010
30. J. Andzelm, C. Kolmel, *J. Chem. Phys.* **1995**, *103*, 9312–9320. DOI:10.1063/1.469990
31. A. Warshel, *Israel J. Chem.* **1973**, *11*, 709–717. DOI:10.1002/ijch.197300067
32. A. Rahimi, M. Sepehr, M. J. Lariche, M. Mesbah, A. Kasa-eipoor, E. H. Malekshah, *Physica E: Low Dimens. Syst. Nanostruct.* **2018**, *97*, 347–362. DOI:10.1016/j.physe.2017.12.003
33. A. Ahmadi, J. Beheshtian, N. L. Hadipour, *Physica E* **2011**, *43*, 1717–1719. DOI:10.1016/j.physe.2011.05.029
34. A. Ahmadi, M. Kamfiroozi, J. Beheshtian, N. Hadipour, *Struct. Chem.* **2011**, *22*, 1261–1265. DOI:10.1007/s11224-011-9820-1
35. Y. Jiao, A. Du, Z. Zhu, V. Rudolph, S. C. Smith, *J. Mater. Chem.* **2010**, *20*, 10426–10430. DOI:10.1039/c0jm01416h
36. N. S. Alghunaim, A. Omar, H. Elhaes, M. Ibrahim, *J. Comput. Theor. Nanosci.* **2017**, *14*, 2838–2843. DOI:10.1166/jctn.2017.6583
37. A. M. F. Galal, E. M. Shalaby, A. Abouelsayed, M. A. Ibrahim, E. Al-Ashkar, A. G. Hanna *Spectrochim. Acta A Mol. Biomol. Spectrosc.* **2018**, *188*, 213–221. DOI:10.1016/j.saa.2017.06.068
38. A. Okasha, D. Atta, W. M. Badawy, M. V. Frontasyeva, H. Elhaes, M. Ibrahim, *J. Comput. Theor. Nanosci.* **2017**, *14*, 1357–1361. DOI:10.1166/jctn.2017.6457
39. M. Ibrahim, K. T. Kholmurodov, I. N. Fadeikina, S. V. Morzhuhina, E. S. Popova, H. Elhaes, A. A. Mahmoud, *J. Comput. Theor. Nanosci.* **2017**, *14*, 4133–4136. DOI:10.1166/jctn.2017.6797
40. H. Elhaes, A. Fakhry, M. Ibrahim, *Sensor Lett.* **2017**, *15*, 604–607. DOI:10.1166/sl.2017.3853
41. M. Schmidt, T. Windus, M. Dupuis, *J. Comput. Chem.* **1993**, *14*, 1347–1363. DOI:10.1002/jcc.540141112
42. S. Grimme, *J. Comput. Chem.* **2004**, *25*, 1463–1471. DOI:10.1002/jcc.20078
43. J. Andzelm, C. Kolmel, *J. Chem. Phys.* **1995**, *103*, 9312–9320. DOI:10.1063/1.469990
44. Z. Parsaee, P. Haratipour, M. J. Lariche, A. Vojood, *Ultrason. Sonochem.* **2018**, *41*, 337–349. DOI:10.1016/j.ultsonch.2017.09.054
45. M. H. Doranehgard, H. Samadyar, M. Mesbah, P. Haratipour, S. Samiezade, *Fuel*, **2017**, *202*, 29–35. DOI:10.1016/j.fuel.2017.04.014
46. T. C. Dinadayalane, J. S. Murray, *J. Chem. Theory Comp.* **2010**, *6*, 1351–1357. DOI:10.1021/ct900669t
47. S. F. Boys, F. Bernardi, *Mol. Phys.* **1970**, *19*, 553–566. DOI:10.1080/00268977000101561
48. A. Baghban, J. Sasanipour, P. Haratipour, M. Alizad, M. Vafae Ayouri, *Chem. Eng. Res. Des.* **2017**, *126*, 67–75. DOI:10.1016/j.cherd.2017.08.007

Povzetek

Z uporabo teorije gostotnega funkcionala (DFT) smo raziskovali adsorpcijo molekule H₂Se na površinah AlN-NCS in AlP-NCS nanostožcev. Preučili smo potencialne Cl-funkcionaliziranih AlN-NCS in AlP-NCS za adsorpcijo H₂Se in ugotovili, da so vsi procesi adsorpcije H₂Se na obravnavanih površinah nanostožcev eksotermne reakcije. Izračunana energija adsorpcije, |E_{ad}| tvorbe kompleksa H₂Se z AlP-NCS je bila višja od |E_{ad}| za nastanek kompleksa z AlN-NCS. Rezultati kažejo, da so dobljene vrednosti |E_{ad}| linearno odvisne od orbitalnih energij. Proučevane površine nanostožcev bi bile primerne kot substrat z večjo učinkovitostjo adsorpcije H₂Se.

Scientific paper

Study on the Chelate Formation and the Ion-association of Anionic Chelate of Molybdenum(VI) with 3,5-Dinitrocatechol and Monotetrazolium Cation

Kirila Stojnova,¹ Vidka Divarova,² Petya Racheva,² Kristina Bozhinova³
and Vanya Lekova^{1*}

¹ Department of General and Inorganic Chemistry, Faculty of Chemistry, Plovdiv University "Paisii Hilendarski",
24 Tsar Assen Street, Plovdiv 4000, Bulgaria

² Department of Chemical Sciences, Faculty of Pharmacy, Medical University-Plovdiv,
15A Vasil Aprilov Boulevard, Plovdiv 4002, Bulgaria

³ Institute of General and Inorganic Chemistry, Bulgarian Academy of Science,
1113 Acad. G. Bonchev St, Sofia, Bulgaria

* Corresponding author: E-mail: vanlek@uni-plovdiv.bg;
tel.: +35932261420

Received: 21-09-2017

Abstract

The equilibria of the chelate formation and ion-association in the liquid-liquid extraction system Mo(VI)-3,5-DNC-INT-H₂O-CHCl₃ were studied by spectrophotometry. The optimum conditions for the chelate formation and extraction of the ion-associated complex formed between the anionic chelate of Mo(VI)-3,5-dinitrocatechol (3,5-DNC) and the cation of 2-(4-iodophenyl)-3-(4-nitrophenyl)-5-phenyl-2H-tetrazolium chloride (INT) were established. The validity of Beer's law was checked and some analytical characteristics were calculated. The effect of various co-existing ions and reagents on the process of complex formation was investigated. The molar ratio of the components in the ternary ion-associated complex Mo(VI)-3,5-DNC-INT was determined by independent methods. The association process in aqueous phase and the extraction equilibria were investigated and quantitatively characterized. The following key constants of the processes were calculated: association constant, distribution constant, extraction constant and recovery factor. Based on this, a reaction scheme, a general formula and a structure of the complex were suggested.

Keywords: molybdenum(VI); chelate formation, ion-associate; extraction equilibria

1. Introduction

The molybdenum and its compounds are widely used in various important areas of technology, science, and medicine. Molybdenum is present in all living plant and animal matter in micro-trace quantities and it is essential from a biochemical point of view. It stimulates the synthesis of nucleic acids and proteins. In the biological systems, the molybdenum forms complexes with the carboxylic or hydroxide groups of tyrosine and serine. The most important utilization of the molybdenum atom in the living organisms is as a metal hetero-atom at the active site in certain enzymes, e.g. xanthine oxidase, aldehyde oxidase, sulfite oxidase, nitrate reductase and dimethyl sulfoxide reductase.¹⁻⁴

The molybdenum has a rich chemistry, it occurs in various oxidation states, coordination numbers and geometries.^{1,5,6} Molybdenum(VI) forms complexes with various natural organic ligands, such as polyphenols and their functional derivatives, polyhydroxycarboxylic acids, aminopolycarboxylic acids, hydroxamic acids, amines (primary, secondary and tertiary), 8-hydroxyquinoline and its derivatives, aldehyde hydrazones, oximes, β -diketones, fluorones, hydroxyazodyes, biomolecules (chitosan, chitin, D-glucosamine, L-alanine, L-phenylalanine).⁷⁻²⁰ Molybdenum(VI) gives colored chelates with aromatic compounds, containing two or more hydroxyl groups in *ortho* position relative to each other. The colored anionic chelates of molybdenum(VI) form ion-associated complexes

with bulky organic cations, like methyltriocylammonium, cetylpyridinium, cetyltrimethylammonium, tetraphenylammonium tetraphenylphosphonium.^{7,21–23}

The preparation and application of ion-associated complexes of anionic chelates of metals with various natural organic and inorganic ligands with N- and O-containing donor atoms and with the participation of mono and ditetrazolium cations is a special scientific research field of the chemistry of the coordination compounds. It is up-to-date topic, not only as a theoretical background for the preparation of novel ion-associated complexes, but mainly due to the possibility for their application in the analytical chemistry for determination of various metals in natural, industrial, pharmaceutical and biological samples, addressing in such a way a number of ecological issues. The structure and properties of tetrazolium salts determine their ability to form ion-associated complexes. The bulky hydrophobic organic substituents in the molecules of the tetrazolium salts increase the extractability of the ion associated complexes. The presence of a quaternary nitrogen atom in the molecules of the tetrazolium salts determines the ability to form ionic associates in the aqueous phase without protonation, as opposed to the amines.^{24–26} Tetrazolium salts are used as reagents for the preparation of various ion-associated complexes of metals, e.g. W(VI), Ge(IV), Tl(III), Nb(V), V(V), Ga(III), Co(II).^{26–31}

The extraction spectrophotometry is a relatively simple, convenient, rapid to perform and inexpensive method for preparation and characterization of new complex compounds as well as for their application in the chemical analysis.^{32–38} The liquid-liquid extraction is a part of the chemistry of the solutions and the coordination compounds. It is applied to study the processes of complex formation and the extraction equilibria.

The aim of this research was to study spectrophotometrically the extraction equilibria of the complex formation between the anionic chelate of Mo(VI)-3,5-dinitrocatechol (3,5-DNC) and the cation of 2-(4-iodophenyl)-3-(4-nitrophenyl)-5-phenyl-2H-tetrazolium chloride (INT) in the liquid-liquid system Mo(VI)-3,5-DNC-INT-H₂O-CHCl₃ as well as to evaluate the possible applications of the system for determination of traces of molybdenum(VI) in alloys, biological, medical and pharmaceutical samples.

2. Experimental

2. 1. Reagents and Apparatus

Na₂MoO₄·2H₂O (Fluka AG, p.a.): an aqueous 1.04 × 10⁻² M solution was prepared. 3,5-Dinitrocatechol (3,5-DNC) (Sigma-Aldrich, p.a.): 3,5-DNC was dissolved in CHCl₃ to give a 1.0 × 10⁻³ M solution. 2-(4-Iodophenyl)-3-(4-nitrophenyl)-5-phenyl-2H-tetrazolium chloride (INT) (Sigma-Aldrich, p.a.): an aqueous 2.0 × 10⁻³ M solution was prepared. H₂SO₄ (95–97 % for analysis, Merck): a 2 M solution was prepared. The concentration of H₂SO₄ was

determined titrimetrically. A Camspec M508 spectrophotometer (UK), equipped with 10 mm path length cells, was employed for measurement of the absorbance. The organic solvent CHCl₃ was additionally distilled.

2. 2. Procedure for Establishment of the Optimum Conditions for Complex Formation

The required aliquots of the solutions of Mo(VI), INT and H₂SO₄ were introduced into 250 mL separatory funnels. The resulting solutions were diluted with distilled water to a total volume of 10 mL. A required aliquot of a chloroform solution of 3,5-DNC was added and then the organic phase was adjusted to a volume of 10 mL with chloroform. The funnels were shaken for a fixed time (up to 240 s). A portion of the organic extract was filtered through a filter paper into a 1 cm cell and the absorbance was measured against a blank. The blank extraction was performed in the same manner in the absence of molybdenum.

2. 3. Procedure for Determination of the Distribution Constant

The distribution constant (K_D) was determined by Eq. (1), where A_1 and A_3 are the absorbance (measured against blanks) obtained after a single and triple extraction, respectively.

$$K_D = A_1 / (A_3 - A_1) \quad (1)$$

The single extraction and the first stage of the triple extraction were performed under the optimum conditions for complex formation (Table 1, column 1). The organic layers were transferred into 25 mL calibrated flasks and the flask from the single extraction was brought to volume with chloroform. The second stage of the triple extraction was performed by adding 7 mL of chloroform to the aqueous phase that remained after the first stage. After extraction, the obtained extract was added to this first stage of the triple extraction. The third stage of the triple extraction was performed in the same manner as for the second stage and the extract was added to those of the first two stages. The volume of the flask was brought to the mark with chloroform. The calibrated flasks were shaken before the spectrophotometric measurements.³⁹

3. Results and Discussion

3. 1. Optimum Extraction-Spectrophotometric Conditions

The absorption spectrum of the extract of the ion-associated complex formed between the anionic chelate of Mo(VI)-3,5-DNC and the cation of monotetrazolium salt

INT in CHCl_3 was characterized by an absorption maximum in the visible range ($\lambda_{\text{max}} = 395 \text{ nm}$) (Figure 1.). The acidity of the aqueous phase influences on the extraction of the anionic chelate Mo(VI)-3,5-DNC into the organic phase in the form of ion-associate with the monotetrazolium cation of INT. The maximum and constant extraction of the ion-associated complex is achieved in strongly acidic solution of $(1.6\text{--}6.0) \times 10^{-1} \text{ M H}_2\text{SO}_4$. The results from the experiments showed that the extraction equilibrium cannot be achieved within less than 30 s. The prolonged shaking does not have an impact on the absorbance. The next experiments were performed for 1 min. The chelate formation of Mo(VI)-3,5-DNC requires 3.6-fold excess of 3,5-DNC ($\geq 1.0 \times 10^{-4} \text{ M}$) and 7.1-fold excess of INT ($\geq 2.0 \times 10^{-4} \text{ M}$) for maximum association and extraction.

The optimum experimental conditions for the extraction of the ion-associated complex are summarized in Table 1, column 1.

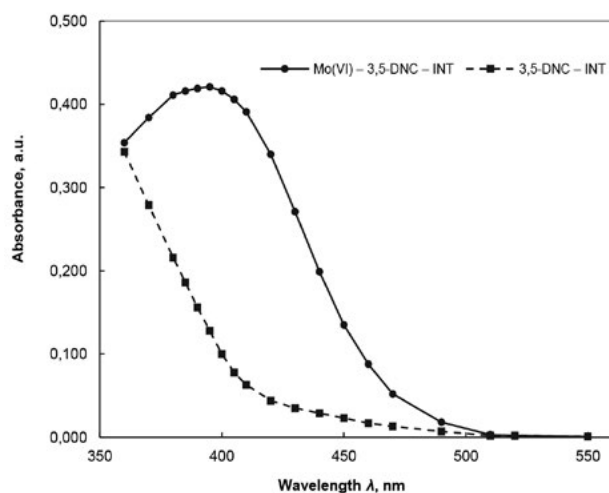


Figure 1. Absorption spectra of the complex Mo(VI)-3,5-DNC-INT and of the blank sample 3,5-DNC-INT in CHCl_3
 $C_{\text{Mo(VI)}} = 2.08 \times 10^{-5} \text{ M}$; $C_{3,5\text{-DNC}} = 2.0 \times 10^{-4} \text{ M}$, $C_{\text{INT}} = 2.0 \times 10^{-4} \text{ M}$;
 $C_{\text{H}_2\text{SO}_4} = 4.0 \times 10^{-1} \text{ M}$; $\lambda = 395 \text{ nm}$; $\tau = 1 \text{ min}$

3. 2. Beer's Law, Apparent Molar Absorptivity and Other Analytical Characteristics

The range of obedience to Beer's law, i.e. the linear relationship between the molybdenum concentration in the aqueous phase ($C_{\text{Mo(VI)}}$, $\mu\text{g mL}^{-1}$) and the absorbance of the ion-association complex in the organic phase after extraction regression analysis under the optimum conditions for complex formation was used. The equation of a straight line was found to be $Y = 0.2081X + 0.0098$ with a correlation coefficient squared 0.9968. Under the optimum conditions for complex formation, the linearity is observed for concentrations up to $4.99 \mu\text{g mL}^{-1} \text{ Mo(VI)}$. Further analytical characteristics, e.g. apparent molar absorptivity ϵ' , Sandell's sensitivity, limit of detection and limit of quantification, are shown in Table 1, column 2.

3. 3. Effect of Co-existing Ions and Reagents on the Complex Formation

The effect of various co-existing ions and reagents on the process of complex formation between the anionic chelate Mo(VI)-3,5-DNC and monotetrazolium cation was studied under optimum extraction conditions (Table 1, column 1). The concentration of Mo(VI) in the presence of the co-existing ions and reagents was determined from the sequence of Beer's law. A deviation of $\pm 3\%$ from the absorbance of the complex in the absence of co-existing ions was accepted as an interfering effect. The results are presented in Table 2. From them, it can be concluded that most of the ions studied do not interfere, but some of them, like Al(III), Fe(II) and Cr(VI) in concentrations higher than the indicated ones, hinder the extraction of Mo(VI) as an associated complex with 3,5-DNC and INT. The extraction equilibrium is hindered by Fe(III), V(V) and W(VI). The extraction equilibrium is severely interfered by Fe(III), V(V) and W(VI) ions at very low concentrations. The interfering ions can be masked or removed from the extraction system to avoid this. Our investiga-

Table 1. Optimum extraction-spectrophotometric conditions and analytical characteristics of the system Mo(VI)-3,5-DNC-INT- H_2O - CHCl_3

Optimum conditions	Analytical characteristic
Absorption maximum (λ_{max}) 395 nm	Apparent molar absorptivity (ϵ') $(2.05 \pm 0.06) \times 10^4 \text{ L mol}^{-1} \text{ cm}^{-1}$
Volume of the aqueous phase 10 mL	True molar absorptivity (ϵ) $(1.92 \pm 0.07) \times 10^4 \text{ L mol}^{-1} \text{ cm}^{-1}$
Volume of the organic phase 10 mL	Sandell's sensitivity (SS) 4.68 ng cm^{-2}
Concentration of H_2SO_4 in the aqueous phase $(1.6\text{--}6.0) \times 10^{-1} \text{ M}$	Adherence to Beer's law up to $4.99 \mu\text{g cm}^{-3}$
Shaking time (τ) 1 min	Relative standard deviation (RSD) 1.92%
Concentration of 3,5-DNC $C_{3,5\text{-DNC}} \geq 1.0 \times 10^{-4} \text{ M}$	Limit of detection (LOD) $0.31 \mu\text{g cm}^{-3}$
Concentration of INT $C_{\text{INT}} \geq 2.0 \times 10^{-4} \text{ M}$	Limit of quantification (LOQ) $1.03 \mu\text{g cm}^{-3}$

tions as well as the studies published in the literature show that the same co-existing ions, like Al(III), Fe(II) and Fe(III) can be removed by their pre-precipitation with OH⁻ at pH = 11.⁴⁰ The co-existing ions, like Fe(II), Fe(III) and Al(III) can be masked with added Complexone III, Complexone IV or L-ascorbic acid in concentrations lower than the indicated. Vanadium(V) can be co-precipitated with Fe(III) in alkali medium.⁴¹

Table 2. Effect of co-existing ions and reagents on the complex formation of the ion-associate Mo(VI)-3,5-DNC-INT for extraction in the presence of 20 µg Mo(VI)

Co-existing ion and reagent	Co-existing ion and reagent, µg/10 cm ³ aqueous phase	Mo(VI) found, µg	R, %
Na ⁺	10000	20.45	102.25
K ⁺	10000	20.21	101.05
Mg ²⁺	10000	20.55	102.75
Ca ²⁺	10000	20.07	100.35
Cu ²⁺	10000	19.54	97.68
Zn ²⁺	10000	19.98	99.92
Cd ²⁺	10000	20.39	101.95
Ni ²⁺	10000	19.77	98.86
Co ²⁺	10000	20.39	101.95
Al ³⁺	2000	20.09	100.45
Cr ³⁺	10000	19.94	99.68
Fe ²⁺	750	19.61	98.05
Fe ³⁺	100	16.21	81.03
V(V)	100	21.83	109.14
Cr(VI)	100	20.39	101.96
W(VI)	50	25.95	129.75
F ⁻	10000	20.53	102.65
Br ⁻	10000	20.55	102.77
PO ₄ ³⁻	10000	20.19	100.97
P ₂ O ₇ ⁴⁻	10000	19.84	99.18
C ₂ O ₄ ²⁻	10000	13.98	69.89
CH ₃ COO ⁻	10000	20.55	102.74
C ₄ H ₄ O ₆ ²⁻	10000	20.22	101.11
C ₆ H ₅ O ₇ ³⁻	10000	20.24	100.21
Complexone III	10000	20.07	100.35
Complexone IV	10000	20.41	102.03
L- Ascorbic acid	1000	20.04	100.18

3. 4. Molar Ratios of the Complex, Reaction Scheme and Suggested General Formula

The molar ratios of the complex were determined by three independent methods: the mobile equilibrium method, the straight-line method of Asmus and the method of continuous variations.⁴² Results from the application of these independent methods are shown in Figures 2–5, respectively. On the basis of the results it can be concluded that Mo(VI), 3,5-DNC and INT interact in molar ratio 1:2:2.

The carried out experiments showed that the complex formation and the extraction of the ion-associated

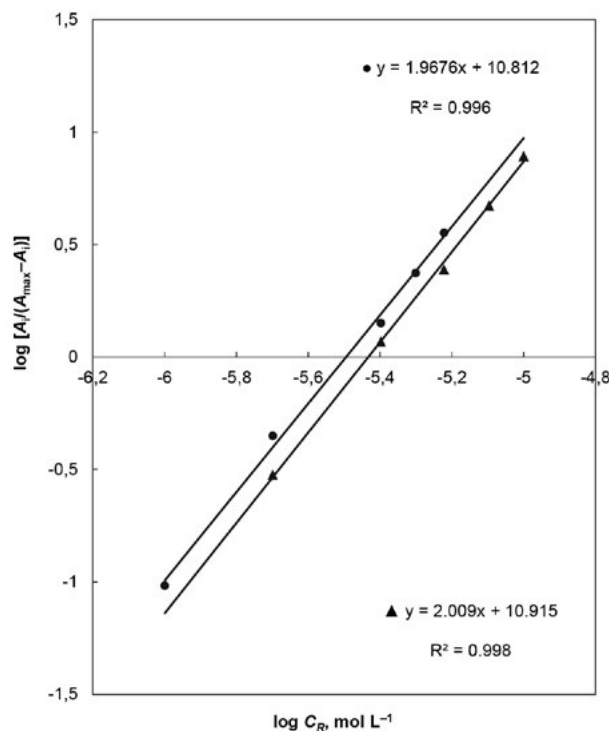


Figure 2. Straight lines by the mobile equilibrium method for determination of the molar ratios Mo(VI):3,5-DNC and Mo(VI):INT $C_{\text{Mo(VI)}} = 2.08 \times 10^{-5} \text{ M}$; $C_{\text{H}_2\text{SO}_4} = 4.0 \times 10^{-1} \text{ M}$; $\lambda = 395 \text{ nm}$; $\tau = 1 \text{ min}$
 ● Mo(VI) : 3,5-DNC, $C_{\text{INT}} = 2.0 \times 10^{-4} \text{ M}$;
 ▲ Mo(VI) : INT, $C_{\text{3,5-DNC}} = 2.0 \times 10^{-4} \text{ M}$

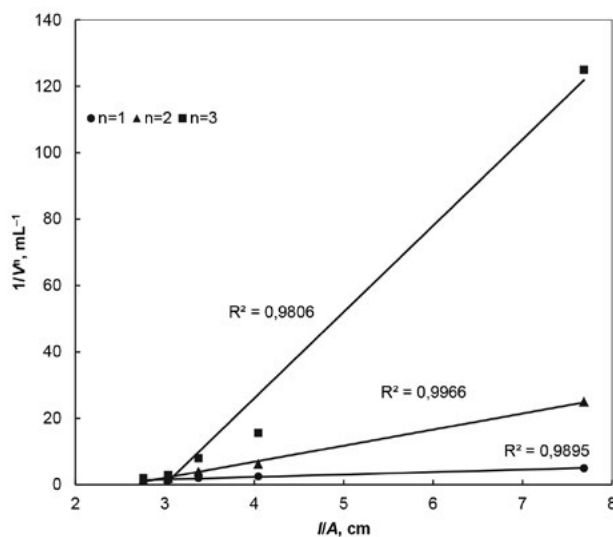


Figure 3. Determination of molar ratio (n) Mo(VI):3,5-DNC by the method of Asmus $C_{\text{Mo(VI)}} = 2.08 \times 10^{-5} \text{ M}$; $C_{\text{INT}} = 2.0 \times 10^{-4} \text{ M}$; $C_{\text{H}_2\text{SO}_4} = 4.0 \times 10^{-1} \text{ M}$; $\lambda = 395 \text{ nm}$; $\tau = 1 \text{ min}$

complex occurred in strongly acidic solution. Under these conditions, the complex formation of anionic chelate Mo(VI)-3,5-DNC is given by the equation (2):

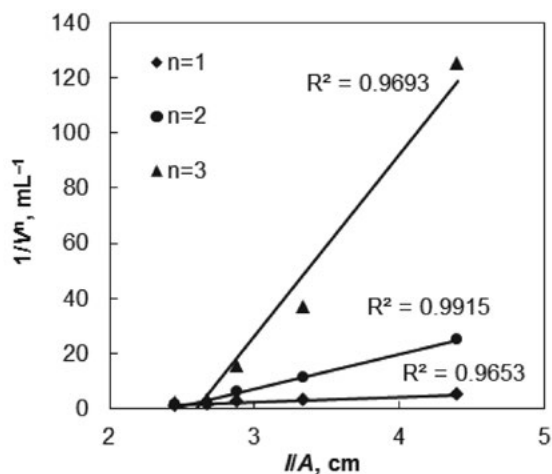


Figure 4. Determination of the molar ratio (n) Mo(VI):INT by the method of Asmus

$C_{\text{Mo(VI)}} = 2.08 \times 10^{-5} \text{ M}$; $C_{\text{3,5-DNC}} = 2.0 \times 10^{-4} \text{ M}$;
 $C_{\text{H}_2\text{SO}_4} = 4.0 \times 10^{-1} \text{ M}$; $\lambda = 395 \text{ nm}$; $\tau = 1 \text{ min}$

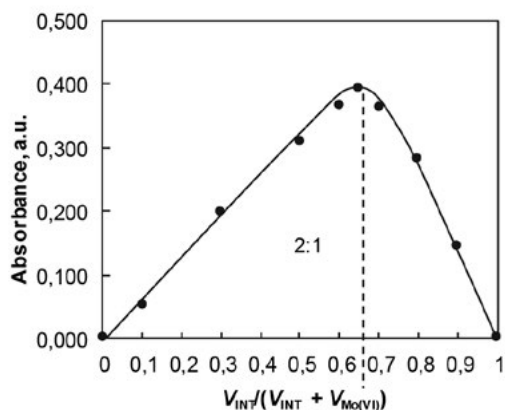
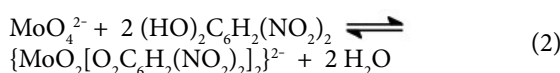
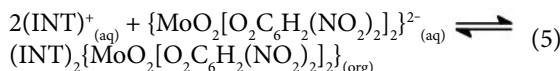
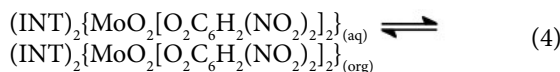
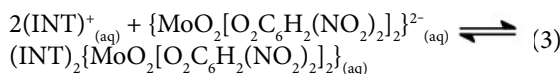


Figure 5. Determination of the molar ratio (n) Mo(VI):INT by the method of continuous variations

$C_{\text{Mo(VI)}} + C_{\text{INT}} = 8.0 \times 10^{-5} \text{ M}$; $C_{\text{3,5-DNC}} = 2.0 \times 10^{-4} \text{ M}$;
 $C_{\text{H}_2\text{SO}_4} = 4.0 \times 10^{-1} \text{ M}$; $\lambda = 395 \text{ nm}$; $\tau = 1 \text{ min}$



Having in mind the reaction of chelate formation of Mo(VI)-3,5-DNC and the molar ratio indicated above, it can be suggested that the formation of the ion-associate in the aqueous phase, its distribution between the aqueous and the organic phases and its extraction in chloroform can be given by the following equations (3–5).



Therefore, the ion-associated chelate of Mo(VI)-3,5-DNC with INT can be represented by the general formula $(\text{INT})_2\{\text{MoO}_2[\text{O}_2\text{C}_6\text{H}_2(\text{NO}_2)_2]_2\}$.

3. 5. Extraction Equilibria, True Molar Absorptivity

Recovery Factor and Structure of the Complex

The association process in aqueous phase and the extraction equilibria were investigated and quantitatively characterized with respect to the following key constants: association constant, distribution constant, extraction constant and recovery factor.

The association constant β and the true molar absorptivity ε were determined by the method of Komar-Tolmachev from equation (6):⁴²

$$\beta = (l/n)^n / [\varepsilon (\text{tg } \alpha)^{n+1}] \quad (6)$$

where l is the cuvette thickness ($l = 1 \text{ cm}$); n is the molar ratio between the components independently determined (e.g. by the mobile equilibrium method, the straight-line method of Asmus or the method of continuous variations) ($n = 2$), ε is the true molar absorptivity.

The true molar absorptivity ε was determined by the method of Komar-Tolmachev from the equation of a straight line (Figure 6) and its value is given in Table 1, column 2.

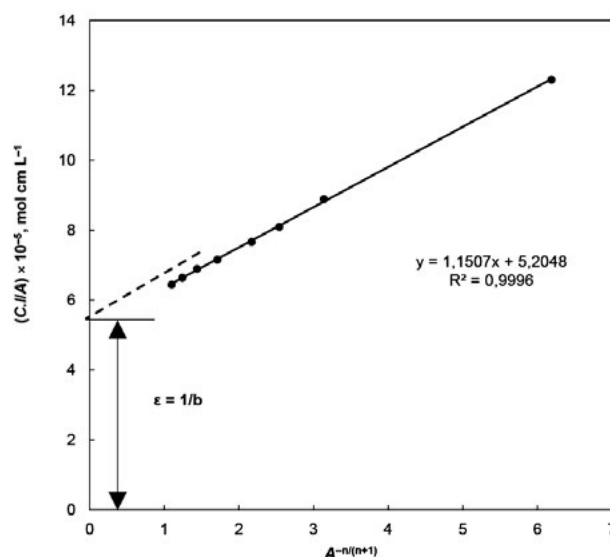


Figure 6. Dependency of (C/l) on $A^{-n/(n+1)}$ (method of Komar-Tolmachev)

$C = C_{\text{Mo(VI)}}$; $C_{\text{INT}} = 2 C_{\text{Mo(VI)}}$; $C_{\text{3,5-DNC}} = 2.0 \times 10^{-4} \text{ M}$;
 A – absorbance; l – cell thickness, $l = 1 \text{ cm}$; $n = 2$

The distribution constant (K_D) was determined by the equation (7), where A_1 and A_3 are the absorbance (measured against blanks) obtained after a single and triple extraction, respectively.

$$K_D = \frac{\{(INT)_2\{MoO_2[O_2C_6H_2(NO_2)_2]\}_2\} (org) / \{(INT)_2\{MoO_2[O_2C_6H_2(NO_2)_2]\}_2\} (aq)}{= A_1 / (A_3 - A_1)} \quad (7)$$

The recovery factor was determined from the equation (8):

$$R\% = 100 K_D / (K_D + 1) \quad (8)$$

The extraction constant K_{ex} was calculated by two independent methods:

$$(i) \log K_{ex} = \log K_D + \log \beta \quad (9)$$

where β was determined by the method of Komar-Tolmachev.

(ii) the method of Likussar-Boltz:⁴³

The method uses the data from the method of continuous variations (Figure 5.). The extraction constant K_{ex} was calculated by the equation of Likussar-Boltz for molar ratio 1:2 (equation 10):

$$\log K_{ex} = 0,3522 - 2 \log K + \log Y_{max} - 3 \log (1 - Y_{max}) \quad (10)$$

where K is the total concentration of reagents ($K = C_{Mo(VI)} + C_{INT} = 8.0 \times 10^{-5} M$); Y_{max} and $(1 - Y_{max})$ are determined by additionally plotted normalized absorption curve ($Y_{max} = 0.849$; $(1 - Y_{max}) = 0.151$) (Figure 5).

The values of the equilibrium constants and the recovery factor are presented in Table 3.

The results obtained by independent methods are statistically similar and confirm the proposed scheme of the process of complex formation of the ion-pair in the aqueous phase, its distribution between the aqueous and the organic phases and its extraction in chloroform. Based on this, the proposed structure of the ion-associated complex is represented in Figure 7.

4. Conclusion

The equilibria of the chelate formation and extraction of the ion-associated complex formed between the anionic chelate of Mo(IV)-3,5-dinitro catechol (3,5-DNC) and the cation of 2-(4-iodophenyl)-3-(4-nitrophenyl)-5-phenyl-2H-tetrazolium chloride (INT) was studied by spectrophotometry. The optimum conditions for the association in aqueous phase and extraction of the ion-associated complex into chloroform were established. The validity of Beer's law was checked and the effect of co-existing ions and reagents on the process of complex formation was studied. The equilibrium constants and analytical characteristics needed for the quantitative assessment of the extraction equilibrium were calculated, i.e. the association constant (β), the distribution constant (K_D), the extraction constant (K_{ex}), the recovery factor (R), the apparent molar absorptivity (ϵ'), the true molar absorptivity (ϵ), the limit of detection (LOD), the limit of quantification (LOQ) and the Sandell's sensitivity (SS). From the analytical characteristics of the extraction system Mo(VI)-3,5-DNC-INT- H_2O - $CHCl_3$, it can be concluded that the ion-associate formed between

Table 3. Values of the equilibrium constants and the recovery factor

Equilibrium constant and recovery factor	Value
Equilibrium (equation 3) – Association constant β $\beta = (INT)_2\{MoO_2[O_2C_6H_2(NO_2)_2]\}_2(aq) / \{[(INT)^+]^2(aq) \beta \{MoO_2[O_2C_6H_2(NO_2)_2]\}_2(aq)\}$	$\log \beta = (9.93 \pm 1.38)^a$
Equilibrium (equation 4) – Distribution constant K_D $K_D = \{(INT)_2\{MoO_2[O_2C_6H_2(NO_2)_2]\}_2\} (org) / \{(INT)_2\{MoO_2[O_2C_6H_2(NO_2)_2]\}_2\} (aq)$	$\log K_D = (1.23 \pm 0.01)^b$ $\log K_{ex} = (11.16 \pm 1.39)^c$
Equilibrium (equation 5) – Extraction constant K_{ex} $K_{ex} = \{(INT)_2\{MoO_2[O_2C_6H_2(NO_2)_2]\}_2\} (org) / \{[(INT)^+]^2(aq) \beta \{MoO_2[O_2C_6H_2(NO_2)_2]\}_2(aq)\}$	$\log K_{ex} = (10.95 \pm 0.15)^d$
Recovery factor $R\%$	$R = (94.39 \pm 0.05)\%^e$

^a Calculated by Komar-Tolmachev method (equation 6); ^b Calculated by equation (7); ^c Calculated by equation (9), where β is determined by the Komar-Tolmachev method; ^d Calculated by Likussar-Boltz method (equation (10)); ^e Calculated by equation (8).

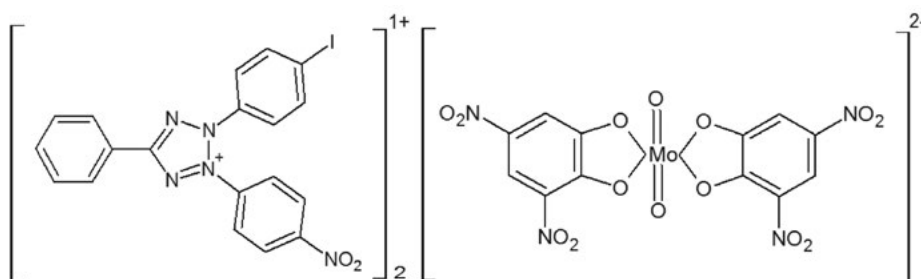


Figure 7. Structure of the ion-associated complex Mo(VI)-3,5-DNC-INT

the anionic chelate of Mo(VI)-3,5-DNC and the monotetrazolium cation allows determinations of Mo(VI) with a high sensitivity. The presence of hydrophobic substituents, phenyl groups in the molecule of the monotetrazolium cation, increased the solubility of the ion-associated complex in the organic solvent. The molar ratio of the components, determined by independent methods, shows that the ion-associated complex could be represented with the general formula $(INT)_2\{MoO_2[O_2C_6H_2(NO_2)_2]_2\}$. A corresponding reaction scheme and a structure of the complex were also suggested.

5. Acknowledgements

The authors would like to thank the Research Fund of the University of Plovdiv for the financial support of the current research.

6. References

1. Y. D. Tretyakov, L. I. Martinenko, A. N. Grigorev: Inorganic Chemistry, Moscow University, Moscow, Russia, **2007**, pp. 309–369
2. M. Huyz: Inorganic Chemistry of Biological Processes, Mir, Moscow, Russia, **1983**, pp. 220–226.
3. T. Ardan, J. Kovaceva, J. Ceikova, *Acta Histochem.* **2004**, *106*, 69–75. DOI:10.1016/j.achtis.2003.08.001
4. P. Tavares, A. S. Pereira, J. J. G. Moura, I. Moura, *J. Inorg. Biochem.* **2006**, *100*, 2087–2100. DOI:10.1016/j.jinorgbio.2006.09.03
5. F. A. Cotton, G. Wilkinson, C. A. Murillo, M. Bochmann: Advanced Inorganic Chemistry, sixth ed., Wiley Publishers, New Jersey, **1999**, pp. 844–883.
6. V. V. Skopenko, A. Y. Tsvadze, L. I. Sabranskiy, A. D. Garnovskiy: Coordination Chemistry, Akademkniga, Moscow, Russia, **2007**, pp. 76–81.
7. A. P. Vinogradov: Analytical Chemistry of Elements - Molybdenum, Nauka, Moscow, Russia, **1962**, pp. 25–97.
8. V. M. Ivanov, G. A. Kochelaeva, *J. Anal. Chem.* **2003**, *58*, 31–37. DOI:10.1023/A:1021830013973
9. M. L. Harikumaran Nair, Anju. S. Appukuttan, *J. Korean Chem. Soc.* **2012**, *56*, 217–227. DOI:10.5012/jkcs.2012.56.2.217
10. T. Nakamura, S. Nishihama, K. Yoshizuka, *Solvent Extr. Res. Dev.* **2009**, *16*, 47–56.
11. L. Xue, D. Deng, Y. Xu, Q. Wang, *Russ. J. Coord. Chem.* **2016**, *42*, 137–142. DOI: 10.1134/S1070328416020093
12. V. M. Ivanov, G. A. Kochelaeva, G. V. Prokhorova, *J. Anal. Chem.* **2002**, *57*, 758–772. DOI:10.1023/A:1020015521584
13. P. A. Petrov, M. Y. Afonin, D. Y. Naumov, S. N. Konchenko, A. V. Piskunov, *Russ. J. Coord. Chem.* **2015**, *41*, 31–36. DOI:10.1134/S1070328415010078
14. W. X. Xu, W. H. Li, *Russ. J. Coord. Chem.* **2012**, *38*, 92–98. DOI:10.1134/S107032841202011X
15. F. L. Fan, F. A. Lei, L. N. Zhang, J. Bai, M. S. Lin, H. J. Ding, X. L. Wu, D. Nayak, Z. Qin, *Solvent Extr. Ion Exch.* **2009**, *27*, 395–407. DOI:10.1080/07366290902821305
16. S. Tascioglu, E. Kaki, S. Tascioglu, *J. Appl. Spectrosc.* **2012**, *79*, 540–546. DOI:10.1007/s10812-012-9637-8
17. S. J. Kokake, A. A. Gavande, V. K. Vikhe, H. R. Aher, S. R. Kuchekar, *Indian J. Chem. Techn.* **2010**, *17*, 154–157.
18. J. Y. Lee, J. R. Kumar, H. S. Jeon, J. S. Kim, *Chem. Eng.* **2010**, *54*, 27–31. DOI:10.3311/pp.ch.2010-1.04
19. P. K. Parhi, K.-H. Park, H. Kim, J. Park, *Hydrometallurgy* **2011**, *105*, 195–200. DOI:10.1016/j.hydromet.2010.09.004
20. J. Kim, S. Park, S. Kim, *Fluid Phase Equilib.* **2010**, *295*, 172–176. DOI:10.1016/j.fluid.2010.04.016
21. A. T. Pilipenko, M. M. Tananayko: Mixed Ligands and Mixed Metal Complexes and their Application in Analytical Chemistry, Khimiya, Moscow, Russia, **1983**, pp. 101–125.
22. J. L. Martinez-Vidal, A. R. Fernandez-Alba, F. Salinas, *Analyst* **1990**, *3*, 329–331. DOI:10.1039/an9901500329
23. M. L. C. Passos, M. Lucia M. F. S. Saraiva, J. F. C. Lima, *Anal. Sci.* **2005**, *12*, 1509–1515. DOI:10.2116/analsci.211509
24. A. W. Nineham, *Chem. Rev.* **1955**, *55*, 355–483. DOI:10.1021/cr50002a004
25. H. Şenöz, *Hacettepe J. Biol. & Chem.* **2012**, *40*, 293–301.
26. K. Gavazov, A. Dimitrov, V. Lekova, *Russ. Chem. Rev.* **2007**, *76*, 169–179. DOI:10.1070/RC2007v076n02ABEH003655
27. K. B. Gavazov, V. D. Lekova, G. I. Patrovov, *Acta Chim. Slov.* **2006**, *53*, 506–511.
28. V. Divarova, V. Lekova, P. Racheva, K. Stojnova, A. Dimitrov, *Acta Chim. Slov.* **2014**, *61*, 813–818.
29. V. V. Divarova, K. T. Stojnova P. V. Racheva, V. D. Lekova, *J. Appl. Spectrosc.* **2017**, *84*, 231–236. DOI:10.1007/s10812-017-0456-9
30. V. Divarova, K. Stojnova, P. Racheva, V. Lekova, *Acta Chim. Slov.* **2016**, *63*, 97–103. DOI:10.17344/acsi.2015.1987
31. P. Racheva, K. Stojnova, V. Divarova, V. Lekova, *Acta Chim. Slov.* **2017**, *64*, 365–372. DOI:10.17344/acsi.2017.3214
32. A. K. Babko, A. T. Pilipenko: Photometric Analysis, Khimiya, Moscow, Russia, **1968**, pp. 159–164.
33. J. Inczédy: Analytical Applications of Complex Equilibria, Mir, Moscow, Russia, **1979**, pp. 225–242.
34. T. P. Rao, M. L. P. Reddy, A. R. Pillai, *Talanta* **1998**, *46*, 765–813. DOI:10.1016/S0039-9140(97)00262-2
35. A. N. Turanov, V. K. Karandashev, V. E. Baulin, E. V. Kirillov, S. V. Kirillov, V. N. Rychkov, A. Y. Tsvadze, *Russ. J. Inorg. Chem.* **2016**, *61*, 1335–1338. DOI:10.1134/S0036023616100211
36. A. N. Turanov, V. K. Karandashev, O. I. Artyushin, E. V. Sharova, *Solvent Extr. Ion Exch.* **2015**, *33*, 540–553. DOI:10.1080/07366299.2015.1067052
37. V. A. Mikhaylov: Extraction Chemistry, Nauka, Novosibirsk, Russia, **1984**, pp. 194–249.
38. G. Kristian: Analytical Chemistry, BINOM, Moscow, Russia, **2009**, pp. 414–426.
39. K. Stojnova, V. Divarova, P. Racheva, K. Bozhinova, V. Lekova, *Acta Chim. Slov.* **2016**, *63*, 654–660. DOI:10.17344/acsi.2016.2513

40. Z. Marczenko, M. Baltcerzak: UV-Vis Spectrophotometric Methods Applied to the Inorganic Analysis, BINOM, Moscow, Russia, 2009, pp. 169-174.
41. B. F. Quin, R. R. Brooks, *Anal. Chim. Acta* 1975, 74, 75-84. DOI:10.1016/S0003-2670(01)82781-1
42. M. I. Bulatov, I. P. Kalinkin: Practical Handbook on Photometric Methods of Analysis, Khimiya, Leningrad, Russia, 1986, pp. 174-264.
43. W. Likussar, D. F. Boltz, *Anal. Chem* 1971, 43, 1265-1272. DOI:10.1021/ac60304a006

Povzetek

S spektrofotometričnimi metodami smo proučili ravnotežja tvorbe kelata in ionskega asociata v tekočina-tekočina ekstrakcijskem sistemu $\text{Mo(VI)-3,5-DNC-INT-H}_2\text{O-CHCl}_3$. Določili smo optimalne pogoje za tvorbo kelata in ekstrakcijo ionskega asociata nastalega med anionskim kelatom $\text{Mo(VI)-3,5-dinitrokatehol (3,5-DNC)}$ in kationom iz spojine 2-(4-jodofenil)-3-(4-nitrofenil)-5-fenil-2*H*-tetrazolijevega klorida (INT). Preverili smo veljavnost Beerovega zakona in izračunali nekatere analize karakteristike. Preverili smo vpliv različnih ionov in reagentov na proces tvorbe kompleksa. Molsko razmerje komponent v ternarnem kompleksu ionskega asociata $\text{Mo(VI)-3,5-DNC-INT}$ smo določili z neodvisnimi metodami. Proučili smo asociacijski proces v vodni fazi in ekstrakcijsko ravnotežje, ki smo ga tudi kvantitativno okarakterizirali. Izračunali smo sledeče najpomembnejše konstante procesov: asociacijska konstanta, distribucijska konstanta, ekstrakcijska konstanta in izkoristek ekstrakcije. Na podlagi dobljenih podatkov je predlagana reakcijska shema, splošna formula in struktura kompleksa.

Scientific paper

Biosorption of 2,4,6-trichlorophenol from Aqueous Medium Using Agro-waste: Pine (*Pinus densiflora* Sieb) Bark Powder

Nadavala Siva Kumar,* Mohammad Asif, Mansour I Al-Hazzaa and Ahmed A. Ibrahim

Department of Chemical Engineering, College of Engineering, King Saud University, P.O. Box 800, Riyadh 11421, Saudi Arabia

* Corresponding author: E-mail: shivanadavala@gmail.com, snadavala@ksu.edu.sa

Received: 01-10-2017

Abstract

Most industrial waste discharges are often contaminated with phenolic compounds, which constitute a major source of water pollution owing to their toxicity and low biodegradability. Development of cost-effective treatment of such industrial wastewater is therefore of paramount importance. Towards this end, we explore the efficacy of Pine bark powder (PBP), which is an agricultural solid waste material, as a low-cost biosorbent without any pre-treatment, for the adsorptive removal of 2,4,6-trichlorophenol (2,4,6-TCP) from aqueous media. The PBP was thoroughly characterized and the effect of important adsorption parameters were examined in the present investigation. The batch equilibrium data were analyzed using well-known isotherm models. Freundlich isotherm model provided the best description of the equilibrium biosorption behavior. At 25 ± 1 °C, the maximum biosorption capacity (q_{max}) was 289.09 mg/g, which is higher than most biosorbents reported in the literature while the removal as high as 97% was obtained. Moreover, the biosorption process was fast, attaining equilibrium in less than 120 min of contact. The Elovich model accurately described the kinetics data. In view of high biosorption capacity and fast removal rates, PBP can be used for an efficient and cost-effective treatment of 2,4,6-TCP contaminated wastewater.

Keywords: Biosorption, Pine bark powder, 2,4,6-trichlorophenol, Kinetics and Isotherm models

1. Introduction

Water pollution is a major global environmental concern that requires immediate attention and sustainable solutions. Its main sources are untreated industrial effluents that release wastewater contaminated with VOCs, metal ions, and phenolic compounds into the environment.¹ Among these pollutants, phenolic derivative 2,4,6-Trichlorophenol (TCP), is a known toxin owing to its positioning of the chlorine atoms (at position 2, 4 and 6) in the phenol ring.² Often, industrial waste-water from paints, pharmaceuticals, pesticides, wood, pulp and paper industries are heavily contaminated with chlorophenols,^{3,4} which require pre-treatment before discharging into the environment. However, the structural stability and persistence of 2,4,6-TCP makes its removal quite challenging.⁵ The position of chlorine atoms relative to the hydroxyl group and the stable carbon-chlorine bond and are responsible for its toxicity. Exposure of humans to 2,4,6-TCP via inhalation leads to

respiratory problems, altered pulmonary function and pulmonary lesions. Besides, even low concentrations (0.1 mg/L) of chlorophenols give undesirable palatability to the potable water.⁶ Both IARC (International Agency for Research on Cancer) and United States Environmental Protection Agency (USEPA, 1999) classify 2,4,6-TCP as a probable carcinogen to humans under group B2.⁷

For the removal of 2,4,6-TCP from the waste-water, several techniques, e.g. chemical-biological oxidation, microbial degradation, photocatalytic, ion exchange resins, catalytic oxidation processes have been suggested in the literature.^{8–11} However, most separation techniques are often expensive, necessitating the development of alternative treatment technology that is both efficient and affordable. Biosorption is a cost-effective, efficient, and environmentally friendly technique that is fast emerging as an alternative to conventional separation techniques.¹² This led to the investigation of sorption capacities of lignocellulosic

residues and agricultural wastes, which are abundantly available and do not require regeneration due to their low cost.^{13–26} Owing to abundance and ease of availability, Pine bark can prove to be a cost-effective alternative to other adsorbents used for wastewater treatment. In fact, the Pine bark was found to be effective in the removal of phenolic compounds (Phenol, 2-Chlorophenol and 4-Chlorophenol).²⁷ Pine (*Pinus densiflora*) belongs to the family pinaceae, and is commonly found around the world.

In the current study, we have investigated the efficacy of the low-cost PBP adsorbent for the treatment of wastewater contaminated with 2,4,6-TCP. In the following, we first describe the synthesis of the PBP, followed by its rigorous characterization using BET surface area, FTIR spectroscopy, XRD, SEM, and elemental analysis to determine the carbon, hydrogen, and nitrogen (CHN) and the presence of various functional groups. The effect important adsorption parameters, such as the solution pH, biosorbent dosage, initial adsorbate concentrations and the contact time are examined on the uptake efficiency of the PBP. Both experimental kinetic and equilibrium data were processed with the help of well-known theoretical models. Finally, the removal efficacy of the present biosorbent is compared with other adsorbents reported in the literature.

2. Materials and Methods

2.1. Materials

Chemicals and other materials were obtained from Aldrich (St. Louis, USA). These chemicals were not purified prior to use. The chemical formula of 2,4,6-TCP is $C_6H_3Cl_3O$. Its molecular weight is 197.46 g/mol. 1.0 g of 2,4,6-TCP was dissolved in 1 litre of double distilled water to prepare the stock solution, which was used to prepare different solutions in the concentration range of 100–400 mg/L. We adjusted the solution pH by adding 0.1 M NaOH and 0.1 M HCl solutions.

2.2. Preparation of Pine Bark Powder Biosorbent

The first step consisted of removing the dust and dirt particles from the pine tree bark by washing with distilled water. It was then dried at 60 °C for 48 h. Next, it was ground using a laboratory mill and sieved to obtain powder with narrow particle size distribution, which varied from 55 to 75 μm . In order to remove the lignin content of the powdered sample, it was soaked in 0.1 M NaOH followed by 0.1 M H_2SO_4 . It was again washed using distilled water then oven dried at 70 °C ~ 80 °C for 6 ~ 9 h followed by cooling at ambient conditions. This final product was named 'PBP' (Pine bark powder).

2.3. Batch Adsorption Studies

Biosorption experiments were conducted using 125 mL conical flasks containing 0.1 g of the biosorbent and

100 mL 2,4,6-TCP solutions with initial concentrations varying from 100 to 400 mg/L. The samples were stirred on a shaking water bath temperature controller (25 ± 1 °C at 220 rpm) till equilibrium was attained. The pH was varied from 2.0–10.0 in the present study. The slurry was filtered using ashless Whatman No.50 filter paper (2.7 μm size particle retention) to obtain the supernatant solution. UV-Vis spectrophotometer (Shimadzu UV-1601 Spectrophotometer, Japan) was used to determine the concentrations of 2,4,6-TCP in the supernatant solutions at the wavelength of 296 nm. The amount of 2,4,6-TCP sorbed onto the PBP, q_e (mg/g), was computed using the following material balance relationship,

$$q_e = \frac{(C_0 - C_e)V}{W} \quad (1)$$

where, C_e and C_0 are equilibrium and initial concentrations of 2,4,6-TCP in the solution (mg/L), respectively. W is the PBP mass in mg and V is the solution volume in L. During the batch kinetics studies, the 2,4,6-TCP uptake at a given time t , q_t (mg/g), was computed using,

$$q_t = V(C_0 - C_t)/W \quad (2)$$

where C_t (mg/L) is the concentration of the adsorbate at time, t (min). The 2,4,6-TCP removal was computed by,

$$\text{Removal}(\%) = \frac{(C_0 - C_e)}{C_0} \times 100 \quad (3)$$

3. Results and Discussion

3.1. Characterization of PBP

The adsorbent was characterized to determine ash content, CHN, moisture content, surface properties, and bulk density. These results are shown in Table 1.

Table 1. Elemental analysis, physical and surface characterization of PBP

Parameter	Value
Odor	None
Color	Light Brownish
Moisture content (%)	5
Apparent (bulk) density (g/cm^3)	0.318
Weight loss (%)	42.6
Ash content (%)	5.62
Multi point BET surface area (m^2/g)	1.410
BET surface area (m^2/g)	0.104
Pore radius (A°)	22.35
Carbon (%)	76.41
Hydrogen (%)	5.35
Nitrogen (%)	6.78

3. 1. 1. FTIR Spectral Analysis

The presence of various functional groups involved in 2,4,6-TCP biosorption were determined using FTIR. Fig. 1(a) and 1(b) shows the FTIR spectral data of the virgin PBP and 2,4,6-TCP loaded PBP in the range of 4000–400 cm^{-1} . The main broad band peaks observed at 3377 & 3420 cm^{-1} was assigned to the overlap of -OH stretching vibrations arising from hydroxyl groups and -NH stretching vibration mode of the amine functional groups. The strong absorption band observed at around 2918 cm^{-1} can be attributed to the C-H stretching vibrations of -CH₃ and -CH₂ functional groups. The peak at 1618 cm^{-1} indicate the functional group region of C=O, O-H, and C-O groups. The peak at 1518 cm^{-1} is assigned to a conjugated hydrogen bonded carbonyl group. The presence of car-

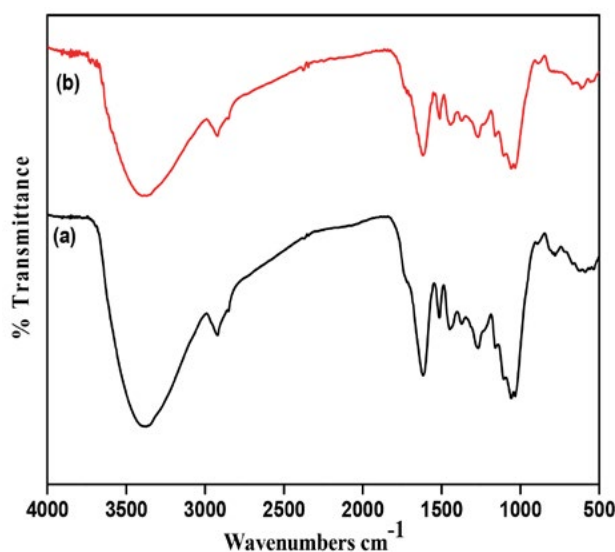


Figure 1. FTIR spectrum of (a) virgin PBP and (b) 2,4,6-trichlorophenol loaded PBP.

boxyl groups (-COOH) is evident from the peak at 1440 cm^{-1} . The peaks at 1059 and 617 cm^{-1} indicate the presence of alkyl halide (C-N and C-Cl stretch). Fig. 1(a) and (b) show some peaks slightly shifted and/or broadened, in wavenumbers from 2913 to 2918 cm^{-1} , 1618 to 1621 cm^{-1} , 1518 to 1510 cm^{-1} , 1440 to 1432 cm^{-1} , 1059 to 1063 cm^{-1} , 878 to 882 cm^{-1} , 767 to 784 cm^{-1} , 612 to 617 cm^{-1} were noticed in the spectra of virgin PBP and 2,4,6-TCP loaded PBP. The functional group(s) involvement is quite prominent as confirmed by the changes observed in FTIR spectrum. The FTIR spectral results further confirmed the fact that PBP is mainly made up of cellulose and lignin, containing functional groups such as hydroxyl, amino and carboxylic groups.

3. 1. 2. Scanning Electron Microscope (SEM) & XRD Analysis

SEM pictures (at different magnifications) revealed dense flaky independent plate like structures with typical agglomeration followed by consistent irregular surface morphology (Fig. 2a, b). The surface of PBP exhibits irregular structure typical of highly porous materials, confirming the possibility of 2,4,6-TCP getting adsorbed on the various parts of the biosorbent (Fig. 2b). X-Ray diffractogram of virgin PBP exhibited broad crested peaks (at $2\theta = 29.8^\circ$ indicating amorphous nature of PBP (figure not shown).

3. 2. Effect of pH

It is a critical parameter that affects the process of the adsorption by influencing the interaction between the adsorbate and the adsorbent. The determination of the optimum pH is therefore vital for the efficient implementation of the adsorption based separation technology.²⁸ The pH was varied from 2.0 to 10.0 in order to examine its effect

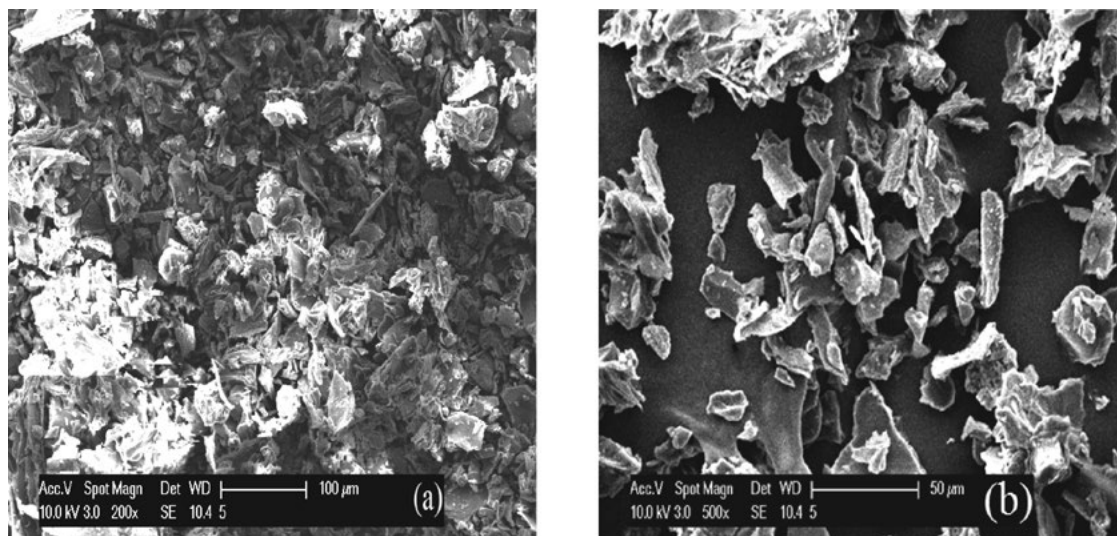


Figure 2. SEM micrographs of PBP at (a) 200x and (b) 500x magnification.

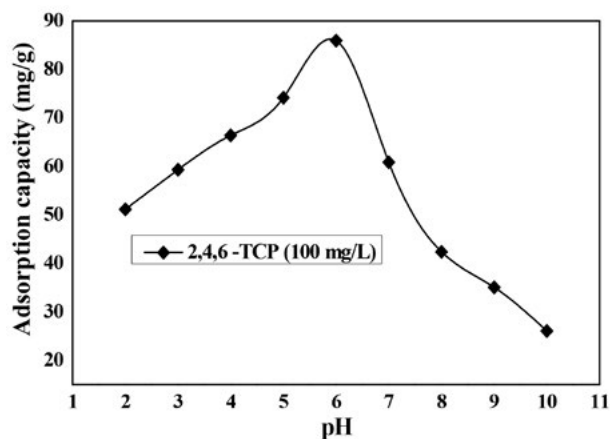


Figure 3. Influence of pH on the 2,4,6-trichlorophenol biosorption onto PBP. Experimental conditions: Temp = 25 ± 1 °C, adsorbent mass = 0.1g, initial concentrations = 100 mg/L, agitation rate = 220 rpm, contact time = 2h.

on the uptake capacity of the PBP. There is a strong correlation between the solution pH and the uptake of the chlorophenol as seen in Fig. 3. The profile shows a global maximum at pH 6. The 2,4,6-TCP is in fact a weak acid having pK_a value of 6.23. Thus, the acidic pH below the pK_a value favours 2,4,6-TCP to remain un-dissociated, and the dispersion interaction predominate.⁶ When the pH value is greater than 6, the biosorption capacity decreases as a result of electrostatic repulsion between the surface site and the negatively charged chlorophenolate anion or due to the chlorophenolate-chlorophenolate anions interaction in the solution.²⁹ At low pH, the protonated chlorophenols were more amenable to adsorption as compared to their ionized forms. A similar analogy was attributed to the 2,4,6-TCP adsorption on other adsorbents, such as PU@PDA@MSNs sponge,³⁰ Acacia leucocephala bark,¹⁹ urea-formaldehyde macroporous foams (UFMF),³¹ coconut shell-based activated carbons,³² oil palm empty fruit bunch-based activated carbons and coconut husk-based activated carbon.^{33,34} Therefore, the optimal pH of 6 was fixed in in the present study.

3. 3. Influence of Biosorbent Dosage

This is a key parameter that affects the cost-effectiveness of the adsorption technology. The amount of PBP was varied from 0.05 to 0.8 g in the test solution ($C_0 = 100$ mg/L) to examine its effect on the removal efficacy the 2,4,6-TCP. Since the equilibrium was attained in 2h, the total contact time was kept 3h in all experiments. It is clear from Fig. 4 that the % removal of chlorophenol increases with the increase in the amount of the biosorbent, reaching as high as 97%, when 0.4 g of the biosorbent was used. This can be attributed to greater availability of the solute molecules per unit mass of the sorbent (i.e., higher solute/adsorbent ratio) resulting in greater removal till saturation conditions are reached. Further increase in the

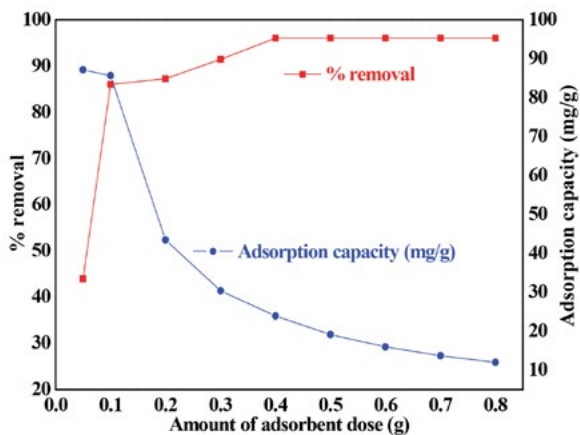


Figure 4. Influence of adsorbent dosage on the 2,4,6-trichlorophenol biosorption onto PBP [Removal (%) and biosorption capacity (mg/g)]. Experimental conditions: Temp = 25 ± 1 °C biosorbent dosage = 0.05–0.8g, initial concentrations = 100 mg/L, pH 6.0, contact time 2h.

amount of PBP however failed to improve the removal efficiency, because increasing the amount of PBP resulted in reduced equilibrium loading capacities, q_e (mg/g), which is in fact the amount of the adsorbate removed per unit mass of biosorbent.

3. 4. Effect of the Initial Concentration and the Contact Time

An important aspect of the efficient and cost-effective implementation of the wastewater treatment process is the equilibrium contact time. Shorter equilibrium contact time enhances the efficiency of the separation process. Fig. 5 shows the progress of the biosorption with time for different strength of 2,4,6-TCP solution. The uptake of 2,4,6-TCP (mg/g) increases with the increase in contact time. The uptake rate is initially faster, but tend to gradually decrease with time as the vacant sites available on the biosorbent surface is gradually occupied by the adsorbate. It took 120 min for the equilibrium to be established. Therefore, the 120 min of contact was fixed for the rest of the batch experiments.

For the adsorptive removal of 2,4,6-TCP, a wide range of adsorption rates has been reported in the literature. Using ash derived from wheat (*Triticum aestivum* L.) straw, Chen et al. reported equilibrium contact time of 7 days, which consisted of initial 3 days of rapid adsorption.³⁵ Using calcined Mg/Al- CO_3 layered double hydroxide (CLDH) obtained equilibrium adsorption time of 180 min for $C_0 = 25$ –400 mg/L.³⁶ Denizli et al. also reported 240 min of equilibrium contact time for $C_0 = 500$ mg/L.³⁷ In another study, 400 min was required for the removal of 2,4,6-TCP using PU@PDA@MSNs sponge for small initial concentrations (50–100 mg/L).³⁰ Radhika et al. found that the equilibrium time was 60–210 min using coconut shell-based commercial grade activated carbon for the initial concentration of 10–100 mg/L.³² Siva Kumar et al. found that the

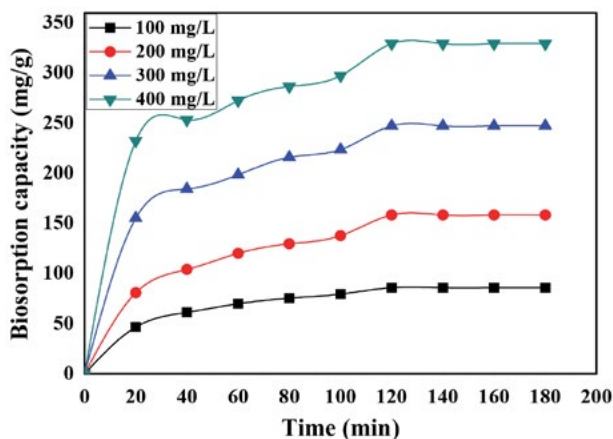


Figure 5. Influence of contact time on the biosorption of the 2,4,6-trichlorophenol for different initial concentrations. (■) $C_0 = 100$ mg/L, (●) $C_0 = 200$ mg/L, (▲) $C_0 = 300$ mg/L, (▼) $C_0 = 400$ mg/L. [Experimental conditions: Temp = 25 ± 1 °C, biosorbent dosage = 0.1g, pH = 6.0, contact time 3h, agitation rate: 220 rpm].

equilibrium time for the 2,4,6-TCP biosorption on *Acacia leucocephala* bark was 180 min for $C_0 = 50$ –200 mg/L.²⁰

3. 5. Biosorption Kinetics

Adsorption kinetics critically affects the performance of an adsorbent. This aspect was therefore investigated for different initial 2,4,6-TCP concentrations in the present study. The experimental data were analyzed using Pseudo-first-order, pseudo-second-order, Elovich model and intra-particle diffusion kinetic models, which are listed in the following. The pseudo-first-order kinetic model is usually represented as:³⁸

$$\log(q_e - q_t) = \log q_e - \frac{k_1 t}{2.303} \quad (4)$$

where k_1 (min^{-1}) is the first order rate constant, which can be evaluated from the slope of the $\log(q_e - q_t)$ versus t (figure not shown). Table 2 lists k_1 values for $C_0 = 100$ –400 mg/L along with correlation coefficients (R^2), which is a statistical measure of the goodness of fit. The actual experimental q_e values are also presented in the table. There is a substantial difference between predicted and experimental values of q_e , which tends to increase with the increase in the solution concentration. For low initial concentrations, the difference is almost 30%, which increase several folds at higher solution concentrations. Clearly, the first order kinetics fails to provide an adequate description of the biosorption of 2,4,6-TCP onto PBP.

The pseudo-second-order kinetic model is generally represented as:³⁹

$$\frac{t}{q_t} = \frac{1}{k_2 q_e^2} + \left(\frac{1}{q_e}\right) t \quad (5)$$

The plot of t/q_t versus t (figure not shown) in the above equation yields the q_e as the slope and k_2 as the intercept. These values are listed in Table 2 along with corresponding values of R^2 . The agreement between predicted and experimental values of q_e is excellent. The difference between the two is low for $C_0 = 100$ mg/L, which unlike the first order kinetic fit, tends to decrease as C_0 increases. For the highest solution concentration considered here, the difference is hardly 2.5%. This confirms the superiority of the pseudo-second-order kinetics as compare to the first-order kinetics.

The biosorption kinetics of 2,4,6-TCP onto PBP was also examined using Elovich equation:⁴⁰

$$q_t = \left(\frac{1}{b}\right) \ln(ab) + \frac{1}{b} \ln t \quad (6)$$

where a (mg/g/min) is the initial biosorption rate and b (g/mg) is the desorption constant related to the chemisorption activation energy and the extent of the surface coverage of the adsorbent. The plot of $\ln t$ versus q_t yields parameters $(1/b)$ and $(1/b)\ln(ab)$ as its slope and the intercept, respectively. From the Table 2, it can be seen that the computed q_e values from Elovich model show good agreement with experimental data.

3. 6. Intraparticle Diffusion Model

The transport of the solute molecules from the bulk liquid to the interiors of the porous structures of the adsorbent involves two mass transport resistances. One is due to the film or the boundary layer surrounding the adsorbent. The greater the thickness of this layer, the higher will be the resistance to the mass transport. Another resistance to the mass transport is due to the movement of the external species inside the pores of the adsorbent, which is also often termed as the intraparticle diffusion. In the literature, the dependence of the concentration of the adsorbate on the time is mathematically expressed as:⁴¹

$$q_t = k_{id} t^{1/2} + C \quad (7)$$

where k_{id} ($\text{mg/g}\cdot\text{min}^{1/2}$) is the slope of the square root of time versus q_t plot while C is the intercept, which is a measure of the boundary layer thickness (figure not shown). The computed k_{id} values are shown in Table 2. If equation (7) yields a linear trend passing through the origin, then the intraparticle diffusion is the lone rate limiting step. From the table, it is clear that the intercept C is not zero. Therefore, the presence of other mass transport mechanism, besides the intraparticle diffusion, cannot be ruled out in the biosorption of 2,4,6-TCP.

Figure 6a-d shows the comparison of the experimental data and model predictions for the 2,4,6-TCP concentrations ranging from 100–400 mg/L. The pseudo-first order, pseudo-second order, intraparticle diffusion and Elovich

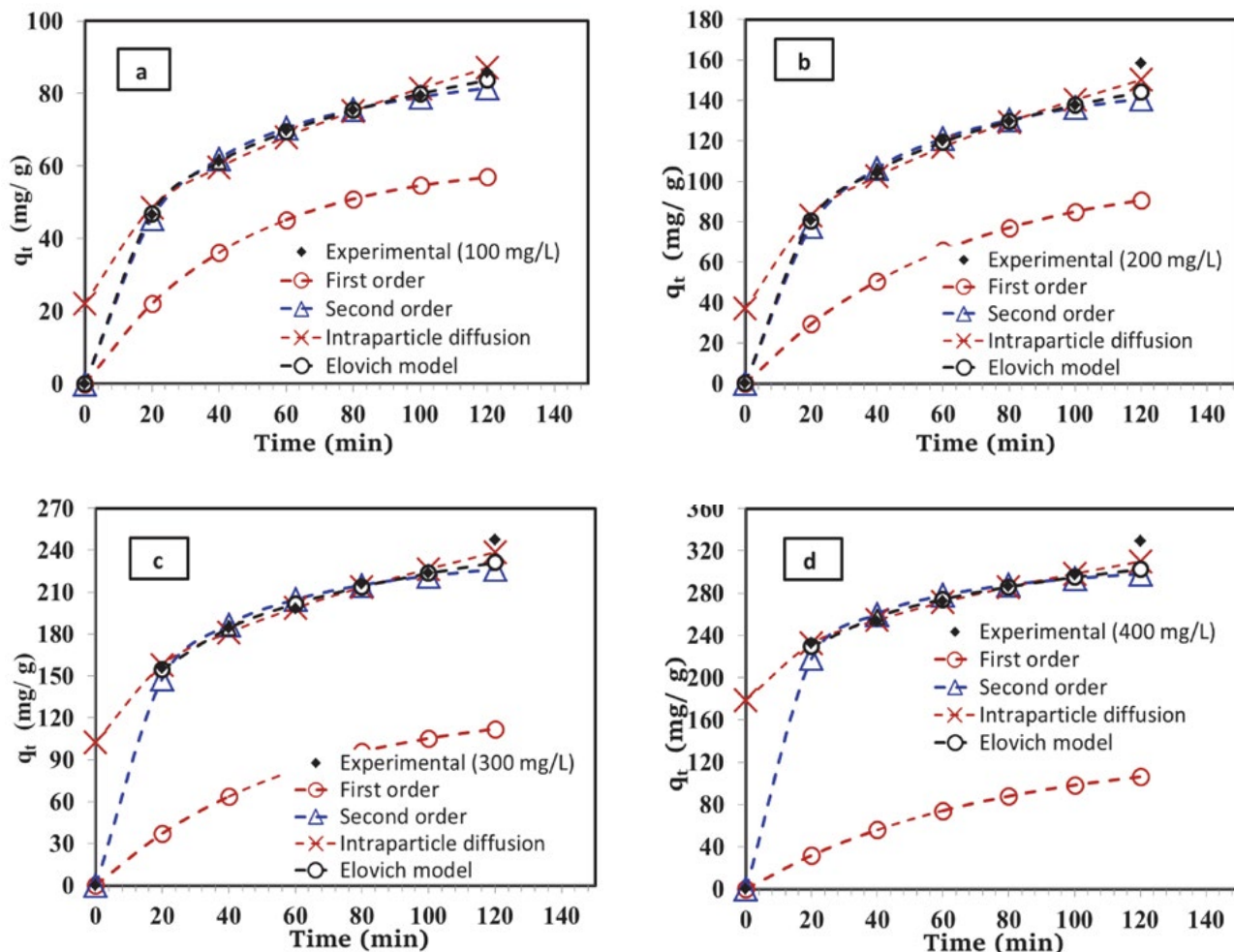


Figure 6. Comparison of experimental and calculated values obtained from the pseudo-first order, pseudo-second order, intraparticle diffusion and Elovich kinetic models (a–d).

vich kinetic equations are considered in the comparison. It is clear from the figures that the predictions of the Elovich kinetic model show an excellent agreement with the experimental data.

3. 7. Validity of Kinetic Models

The validity of three kinetic models in accurately describing the biosorption process was carried out by computing the normalized standard deviation Δq_t (%). It is defined as:

$$\Delta q_t (\%) = 100 \times \sqrt{\frac{\sum_{i=1}^N \left[\frac{(q_{t,exp} - q_{t,cal})}{q_{t,exp}} \right]^2}{(N-1)}} \quad (8)$$

where 'exp', 'cal' and 'N' denote experimental, calculated values and the number of data points, respectively. Lower values of normalized standard deviation Δq_t (%) indicate better data fit. The computed parameters of the models, their corresponding correlation coefficients (R^2), and Δq_t

(%) values are listed in Table 2. The pseudo-first-order kinetic model gives Δq_t (%) as high as 83% while the pseudo-second order and Elovich models give Δq_t (%) values ranging from 1.4–3.5% and 0.50–1.2%, respectively. Based on the correlation coefficients (R^2) and normalized standard deviation Δq_t (%) values, the 2,4,6-TCP adsorption on PBP is best described by the Elovich model model.

3. 8. Biosorption Isotherm Models

In order to mathematically describe the equilibrium distribution of the adsorbate in the liquid solution and the adsorbent, adsorption isotherm models are used. These models accounts for the type of coverage, the nature of the interaction between the adsorbate and the adsorbent surface, and its homogeneity/heterogeneity. In the present study, we focus our attention on three different isotherms models, i.e. Langmuir, Freundlich and Dubinin–Radushkevich to analyze the equilibrium experimental data.

The generalized form of Langmuir isotherm is represented by:⁴²

Table 2. Kinetic parameters biosorption of 2,4,6-TCP on PBP

Parameter	Initial concentration of 2,4,6-trichlorophenol (mg/L)			
	100	200	300	400
$q_{(e, \text{exp})}$ (mg/g)	85.90	158.47	247.20	329.21
Pseudo-first-order-kinetic model				
$q_{(e, \text{cal})}$ (mg/g)	61.14	105.59	128.54	130.49
k_1 (min^{-1})	0.022	0.016	0.017	0.014
R^2	0.979	0.974	0.994	0.999
Δq_t (%)	44	54.31	69.59	83.80
Pseudo-second-order-kinetic model				
$q_{(e, \text{cal})}$ (mg/g)	96.74	168.06	253.08	321.73
k_2 (g/mg/min)	4.6×10^{-4}	2.6×10^{-4}	2.8×10^{-4}	3.3×10^{-4}
R^2	0.999	0.998	0.997	0.997
Δq_t (%)	1.37	2.24	2.95	3.49
Elovich model				
$q_{(e, \text{cal})}$ (mg/g)	83.67	144.15	231.13	302.41
$1/b$ (mg/g)	20.49	35.57	42.64	40.72
R^2	0.999	0.999	0.995	0.986
Δq_t (%)	0.50	0.63	0.95	1.18
Weber-Morris				
k_{id}	5.92	10.32	12.41	11.96
C	22.12	37.06	102.4	178.7
R^2	0.979	0.987	0.989	0.998
Δq_t (%)	3.06	2.36	1.51	0.38

$$\frac{1}{q_e} = \frac{1}{q_m K_L C_e} + \frac{1}{q_m} \quad (9)$$

where q_e (mg/g) is the amount of the solute adsorbed per unit mass of adsorbent, C_e (mg/L) is its equilibrium concentration in solution, q_m is the monolayer biosorption capacity of the adsorbent (mg/g) and K_L (mg/L) is the Langmuir equilibrium constant, respectively. The graph of $1/q_e$ versus $1/C_e$ has been plotted to determine both q_m and K_L . The suitability of Langmuir type adsorption can be analysed using the following dimensionless parameter (R_L):⁴³

$$R_L = \frac{1}{1 + K_L C_0} \quad (10)$$

where C_0 is the initial adsorbate concentration in solution (mg/L). For values of R_L less than unity, the biosorption is favored. R_L values greater than unity indicate that the biosorption process is unfavorable. In the current study, R_L values were found varying from 0 to 1, indicating that Langmuir adsorption is favorable.

Another widely used relationship, Freundlich isotherm model is given as:⁴⁴

$$q_e = K_F C_e^{1/n} \quad (11)$$

where K_F is a constant related to the adsorption capacity

and $(1/n)$ is related to the adsorption intensity. For a favourable sorption, $n > 1$. Taking the log of both sides, the above equation can be linearized as follows:

$$\ln q_e = \ln K_F + \left(\frac{1}{n}\right) \ln C_e \quad (12)$$

In order to gain a greater insight into the biosorption process, one can also use the Dubinin-Radushkevich isotherm model to fit the experimental data. The linearized form of this isotherm model can be mathematically expressed as:⁴⁵

$$\ln q_e = \ln q_m - B \varepsilon^2 \quad (13)$$

where q_m (mg/g) is the maximum adsorption capacity, B is the activity coefficient related to mean adsorption energy, and ε is the Polanyi potential defined as :

$$\varepsilon = R T \ln \left[\frac{1}{C_e} + 1 \right] \quad (14)$$

where R is the gas constant (8.314 J/mol K) and T is the absolute temperature. The mean free energy 'E' of adsorption per molecule of the adsorbate is determined using the constant 'B' using the following relationship:

$$E=(2B)^{-0.5} \tag{15}$$

A plot of ϵ^2 versus $\ln(q_e)$ enables determination of constants E and q_m . The nature of the biosorption process is characterized by the parameter E . Smaller values of E (< 8 kJ/mol) indicate that biosorption is purely physical. On the other hand, higher E values ($8 < E < 16$ kJ/mol) indicate that the sorption process is chemical ion-exchange. We present the model parameters for all the three isotherms, i.e. Freundlich, Langmuir and Dubinin-Radushkevich in Table 3 for comparison along with values of the correlation coefficient (R^2). The predictions of all the isotherm models along with the experimental data are presented in Figure 7. Clearly, the Freundlich isotherm fits the experimental sorption data better than both Langmuir and Dubinin-Radushkevich models.

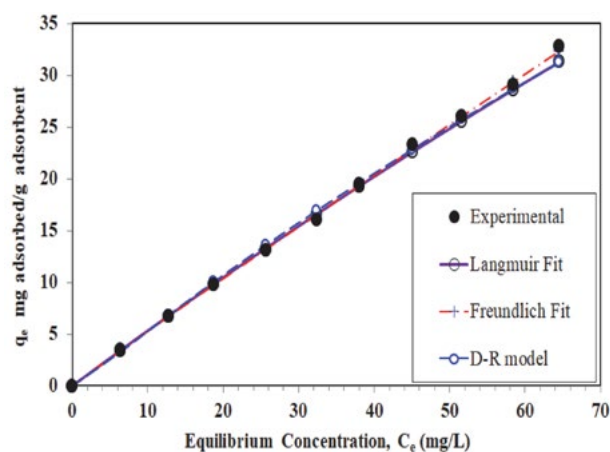


Figure 7. Comparison of experimental data with predictions of isotherm models.

3. 8. 1. Validity of Isotherm Models

The capability of the present isotherm models in accurately describing the biosorption process was evaluated by computing the normalized standard deviation Δq_e (%) as follows:

$$\Delta q_e (\%) = 100 \times \sqrt{\frac{1}{(N-1)} \sum_{i=1}^N \left[\frac{(q_{e,i} - q_{mod,i})}{q_{e,i}} \right]^2} \tag{16}$$

where ' $q_{e,i}$ ', ' $q_{mod,i}$ ' and ' N ' denote experimental, model values and the number of data points, respectively. In all

cases, R^2 values exceeded 0.997 and low Δq_e (%) were obtained in the present study (Table 3). It is however clear from the table that the Freundlich isotherm described the experimental data better than the other two models. This suggests that surface or pore heterogeneity plays a role in 2,4,6-TCP adsorption. The present results also agree with earlier works, which reported that the Freundlich model provided better representation of the 2,4,6-TCP adsorption using oil palm empty fruit bunch and activated clay.^{4,33}

3. 8. 2. Comparison of PBP with Other Adsorbents

Fig. 8 compares the adsorption capacities of various adsorbents reported in the literature. Clearly, PBP is a better adsorbent for the removal of 2,4,6-Trichlorophenol as compared to other reported adsorbents.^{6, 20, 30–32, 36, 46–48.} Its uptake capacity is found to be 289.09 mg/g, which is higher than most other agro-waste based adsorbents. This clearly establishes the efficacy of the PBP for the cost-effective removal of 2,4,6-Trichlorophenol from an aqueous media.

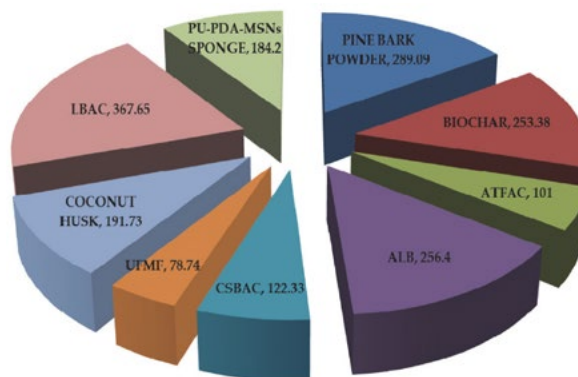


Figure 8. Comparison of maximum monolayer adsorption capacities of various Adsorbents for 2,4,6-TCP. [Acid treated coconut fiber activated carbon (ATFAC); Acacia leucocephala bark (ALB); Coconut shell-based activated carbon (CSBAC); Urea-formaldehyde macroporous foams (UFMF); Loosestrife-based activated carbon (LBAC).

4. Conclusion

In this study, the potential of PBP (agro-waste material) for the 2,4,6-TCP removal from wastewater over a

Table 3. Isotherm parameters for the biosorption of 2,4,6-TCP on PBP

Isotherms	Constants		R ²	Δq_e (%)
Langmuir	q_m (mg/g) 289.09	b (L/mg) 0.002	0.999	2.43
Freundlich	K_F ((mg/g)(L/mg) ^{1/n}) 0.565	n 1.030	0.999	1.48
Dubinin-Radushkevich	q_s (mmol/g) 4.84	E (kJ/mol) 7.60	0.997	3.51

wide range of concentrations has been examined. The FTIR study confirms the presence of hydroxyl, amine and carboxyl functional groups on the surface of the adsorbent, while SEM study reveals irregular porous surface morphology. The biosorbent performed better under acidic conditions (optimal pH of 6). The biosorption process was fast since equilibrium was achieved within 120 minutes of contact. The sorption behaviour was accurately represented by the pseudo-second order kinetics as compared to other kinetic models. With an increase in the PBP dosage, the equilibrium adsorption capacity (mg/g) gradually decreased. On the other hand, the removal capacity as high as 97% was obtained for 0.4 g/L of adsorbent. However, further increase in its dosage failed to improve the removal efficiency. Three different isotherm models (Langmuir, Freundlich and Dubinin–Radushkevich) were used to represent the experimental equilibrium data. The Langmuir isotherm model predicted the maximum biosorption capacity of 289.09 mg/g at 25 ± 1 °C. These findings conclude that PBP, owing to its ease of availability and environment friendly nature, can potentially replace existing sorbents for the removal of 2,4,6-TCP from aqueous media.

5. Acknowledgments

Authors appreciate the support of the Deanship of Scientific Research at the King Saud University for the Research Group RGP-1437-003.

6. References

1. S. K. Nadavala, K. Swayampakula, V. M. Boddu, K. Abburi, *J. Hazard. Mater.* **2009**, *162*, 482–489. DOI:10.1016/j.jhazmat.2008.05.070
2. P. Podkoscielny, A. Dbrowski, O. V. Marijuk, *Appl. Surf. Sci.* **2003**, *205*, 297–303. DOI:10.1016/S0169-4332(02)01154-6
3. R. Gao, J. Wang, *J. Hazard. Mater.* **2007**, *145*, 398–403. DOI:10.1016/j.jhazmat.2006.11.036
4. B. H. Hameed, *Colloid. Surface A.* **2007**, *307*, 45–52. DOI:10.1016/j.colsurfa.2007.05.002
5. R. D. Vidic, M. T. Suidan, R. C. Brenner, *Environ. Sci. Technol.* **1993**, *27*, 2079–2085. DOI:10.1021/es00047a013
6. S. Mubarik, A. Saeed, M. M. Athar, M. Iqbal, *J. Ind. Eng. Chem.* **2016**, *33*, 115–121. DOI:10.1016/j.jiec.2015.09.029
7. Integrated Risk Information System (IRIS) on 2,4,6-Trichlorophenol. National Center for Environmental Assessment, Office of Research and Development, Washington, D. C.: USEPA, **1999**.
8. M. Kurian, R. Babu, *J. Environ. Chem. Eng.* **2013**, *1*, 86–91. DOI:10.1016/j.jece.2013.04.005
9. K. A. McAllister, H. Lee, J. T. Trevors, *Biodegradation.* **1996**, *7*, 1–40. DOI:10.1007/BF00056556
10. C. G. Oh, J. H. Ahn, S. K. Ihm, *Reac. Funct. Poly.* **2003**, *57*, 103–111. DOI:10.1016/j.reactfunctpolym.2003.08.003
11. N. S. Kumar, M. V. Subbaiah, A. S. Reddy, A. Krishnaiah, *J. Chem. Tech. Biotechnol.* **2009**, *84*, 972–981. DOI:10.1002/jctb.2120
12. J. Febrianto, A. N. Kosasih, J. Sunarso, Y. H. Ju, N. Indraswati, S. Ismadji, *J. Hazard. Mater.* **2009**, *162*, 616–645. DOI:10.1016/j.jhazmat.2008.06.042
13. H. Allaboun, F. Abu Al-Rub, *Materials.* **2016**, *9*, 251–265. DOI:10.3390/ma9040251
14. I. P. Bras, L. Santos, A. Alves, *Env. Sci. Technol.* **1999**, *33*, 631–634. DOI:10.1021/es980402v
15. L. Dupont, J. Bouanda, J. Dumonceau, M. Aplincourt, *J. Colloid Interf. Sci.* **2003**, *263*, 35–41. DOI:10.1016/S0021-9797(03)00241-8
16. V. K. Garg, R. Gupta, A. B. Yadav, R. Kumar, *Bioresour. Technol.* **2003**, *89*, 121–124. DOI:10.1016/S0960-8524(03)00058-0
17. J. R. Rao, T. Viraraghavan, *Bioresour. Technol.* **2002**, *85*, 165–171. DOI:10.1016/S0960-8524(02)00079-2
18. N. Ratola, C. Botelho, A. Alves, *J. Chem. Tech. Biotechnol.* **2003**, *78*, 347–351. DOI:10.1002/jctb.784
19. N. Siva Kumar, K. Min, *J. Chil. Chem. Soc.* **2011**, *56*, 539–545. DOI:10.4067/S0717-97072011000100004
20. N. Siva Kumar, H. S. Woo, K. Min, *Colloid. Surface B.* **2012**, *94*, 125–132. DOI:10.1016/j.colsurfb.2012.01.048
21. R. R. Karri, J. N. Sahu, N. S. Jayakumar, *J. Taiwan. Inst. Chem. Eng.* **2017**, *80*, 472–487. DOI:10.1016/j.jtice.2017.08.004
22. R. R. Karri, N. S. Jayakumar, J. N. Sahu, *J. Mol. Liq.* **2017**, *231*, 249–262. DOI:10.1016/j.molliq.2017.02.003
23. L. P. Lingamdinne, J. R. Koduru, R. K. Jyothi, Y. Y. Chang, J. K. Yang, *Desalin. Water. Treat.* **2016**, *57*, 13066–13080. DOI:10.1080/19443994.2015.1055813
24. H. Roh, M. R. Yu, K. Yakkala, J. R. Koduru, J. K. Yang, Y. Y. Chang, *J. Ind. Eng. Chem.* **2015**, *26*, 226–233. DOI:10.1016/j.jiec.2014.11.034
25. G. Vazquez, J. Gonzalez-Alvarez, S. Freire, M. Lopez-Lorenzo, G. Antorrena, *Bioresour. Technol.* **2002**, *82*, 247–251. DOI:10.1016/S0960-8524(01)00186-9
26. G. Vazquez, J. Gonzalez-Alvarez, A. I. Garcia, M. S. Freire, G. Antorrena, *Bioresour. Technol.* **2007**, *98*, 1535–1540. DOI:10.1016/j.biortech.2006.06.024
27. S. K. Nadavala, H. Che Man, H. S. Woo, *BioResources.* **2014**, *9*, 5155–5174. DOI:10.15376/biores.9.3.5155-5174
28. Z. Aksu, J. Yener, *Waste Management.* **2001**, *21*, 695–702. DOI:10.1016/S0956-053X(01)00006-X
29. O. Hamdaoui, E. Naffrechoux, *J. Hazard. Mater.* **2007**, *147*, 381–394. DOI:10.1016/j.jhazmat.2007.01.021
30. S. Liu, J. Pan, J. Cao, X. Dai, M. Meng, R. Wu, J. Yao, Y. Yan, *Chem. Eng. J.* **2016**, *284*, 10–20. DOI:10.1016/j.cej.2015.08.133
31. J. Pan, J. Luo, J. Cao, J. Liu, W. Huang, W. Zhang, L. Yang, *RSC Advances.* **2016**, *6*, 93894–93904. DOI:10.1039/C6RA20919J
32. M. Radhika, K. Palanivelu, *J. Hazard. Mater.* **2006**, *138*, 116–124. DOI:10.1016/j.jhazmat.2006.05.045
33. I. A. W. Tan, A. L. Ahmad, B. H. Hameed, *J. Hazard. Mater.* **2009**, *164*, 473–482. DOI:10.1016/j.jhazmat.2008.08.025

34. B. H. Hameed, I. A. W. Tan, A. L. Ahmad, *Chem. Eng. J.* **2008**, *144*, 235–244. DOI:10.1016/j.cej.2008.01.028
35. G. Chen, Y. Wang, Z. Pei, *Environ. Sci. Pollut. Res.* **2014**, *21*, 2002–2008. DOI:10.1007/s11356-013-2122-y
36. D. Zhang, G. Zhao, J. Yu, T. Yan, M. Zhu, F. Jiao, J. *Wuhan Univ. Technol. Mater. Sci. Ed.* **2016**, *31*, 1211–1218.
37. A. Denizli, N. Cihangir, N. Tuzmen, G. Alsancak, *Bioresour. Technol.* **2005**, *96*, 59–62. DOI:10.1016/j.biortech.2003.11.029
38. S. Y. Lagergren, *Zur Theorie der sogenannten Adsorption geloster Stoffe.* 1898.
39. Y. S. Ho, G. McKay, *Process Biochemistry.* **1999**, *34*, 451–465. DOI:10.1016/S0032-9592(98)00112-5
40. M. Suguna, N. S. Kumar, V. Sreenivasulu, A. Krishnaiah, *Sep. Sci. Technol.* **2014**, *49*, 1613–1622. DOI:10.1080/01496395.2014.901361
41. W. J. Weber, J. C. Morris, *J. Sanitary Eng. Div.* **1963**, *89*, 31–60.
42. I. Langmuir, *J. American Chem. Soc.* **1916**, *38*, 2221–2295. DOI:10.1021/ja02268a002
43. N. Siva Kumar, A. Subba Reddy, V. M. Boddu, A. Krishnaiah, *Toxicol. Environ. Chem.* **2009**, *91*, 1035–1054. DOI:10.1080/02772240802541338
44. A. Moghal, K. Reddy, S. Abu Sayeed Mohammed, M. Ali Al-Shamrani, W. Zahid, *J. Testing Evaluation.* **2017**, *45*, 1–15. DOI:10.1520/JTE20160066
45. M. Dubinin, L. Radushkevich, *Proceedings Academy of Sciences Physics Chemistry Section. USSR.* **1947**, *55*, 331–333, 875–890.
46. J. Fan, J. Zhang, C. Zhang, L. Ren, Q. Shi, *Desalination*, **2011**, *267*, 139–146. DOI:10.1016/j.desal.2010.09.016
47. P. Ojha, S. Rathilal, K. Singh, *South African J. Chem. Eng.* **2014**, *19*, 1–21.
48. I. A. W. Tan, A. L. Ahmad, B. H. Hameed, *J. Hazard. Mater.* **2008**, *153*, 709–717. DOI:10.1016/j.jhazmat.2007.09.014

Povzetek

Večina industrijskih odpadkov je onesnaženih s strupenimi in težko razgradljivimi fenolnimi spojinami. Te predstavljajo glavni vir vodnega onesnaženja, zato je pri čiščenju takšnih industrijskih odpadnih voda poglavitnega pomena razvoj cenovno učinkovitih postopkov. V tem delu je raziskana učinkovitost predhodno neobdelanega prahu borovega lubja (PBP) kot poceni bioadsorbenta za odstranjevanje 2,4,6-triklorofenola (2,4,6-TCP) iz vodnega medija. Rezultati šaržnih raziskav so bili obdelani z znanimi ravnotežnimi modeli, od katerih je Freundlihova izoterma najbolje opisala raziskovano biosorpcijo. Pri $25 \pm 1^\circ\text{C}$ je znašala maksimalna biosorpcijska kapaciteta (q_{max}) 289,09 mg/g, kar je višje od vrednosti za večino bioadsorbentov podanih v literaturi. Odstranjenega je bilo kar 97% 2,4,6-TCP, biosorpcija pa je bila hitra, saj je bilo ravnotežje doseženo v 120 minutah. Elovičev model dobro opiše kinetične podatke. Na osnovi visoke biosorpcijske kapacitete in hitrega odstranjevanja se PBP lahko uporabi za učinkovit in poceni postopek čiščenja odpadne vode, kontaminirane z 2,4,6-TCP.

Scientific paper

Binding Sites of Deprotonated Citric Acid and Ethylenediaminetetraacetic Acid in the Chelation with Ba²⁺, Y³⁺, and Zr⁴⁺ and Their Electronic Properties: a Density Functional Theory Study

Nor Ain Fathihah Abdullah and Lee Sin Ang*

Faculty of Applied Sciences (Physics), Universiti Teknologi MARA Cawangan Perlis, 02600 Arau, Malaysia

* Corresponding author: E-mail: anglee631@perlis.uitm.edu.my

Tel: +604 98 82 573

Received: 02-10-2017

Abstract

Density functional calculations were performed on the metal complexes formed during the synthesis of barium zirconate (BZY). This compound has been synthesized previously, but the molecular interactions present during the formation of the ligand–metal complexes are unknown. In this study, calculations were carried out to determine the preferred coordination sites for the metal complexes. The cations Ba²⁺, Y³⁺, and Zr⁴⁺ were modeled to interact with two deprotonated chelating agents (citric acid [CA] and ethylenediaminetetraacetic acid [EDTA]) at strategic positions. Density functional theory (DFT) at the B3LYP level of theory with basis set 6-31G* and Universal Gaussian Basis Set (UGBS) was used. The relevant geometries, binding energies, and charge distributions of the complexes are reported. It was found that both CA and EDTA can bind the metal cations investigated in this study. Metal cations prefer to form bonds at the electron-rich sites of the chelating agents. Of the three metal cations considered, Zr⁴⁺ was found to possess the strongest bonds to deprotonated CA and EDTA, followed by Y³⁺ and then Ba²⁺.

Keywords: Density functional theory, cations, chelating agents, binding energies, charges

1. Introduction

Currently, perovskite is one of the most studied compounds in the field of materials science.^{1–3} Ceramic perovskite-type oxides, with a general formula ABO₃ where A and B are two metal cations of different sizes, have been studied due to their high conductivity and low activation energy.^{4,5} Cerate zirconate attracts much attention among perovskite-type oxides because it is important for the future development of electrochemical devices such as fuel cells, magnetic refrigeration, and solar cells.^{6–8} Perovskite can be synthesized at low cost as it can be made from common metals and industrial chemicals⁹ and is convenient to prepare.⁷

Many researchers have investigated the role of the chelating agents in the formation of perovskite.^{10–12} As the formation of perovskite involves the complexation process, the interaction between the metal and chelating agent is of utmost importance. Liu et al¹² identified that citric acid (CA) is more effective than ethylenediaminetetraacetic

acid (EDTA) in forming perovskite at low temperatures (<1000 °C). When the chelating agents are used together, the combined CA and EDTA increases the chelating strength to the metal ion, as demonstrated in a study by Osman et al¹¹ in which the CA and EDTA were mixed into a metal nitrate solution to form metal–CA–EDTA complexes with a ratio of 2:1:1. A similar effect was also observed by Tao et al¹³ in the synthesis of La_{0.6}Sr_{0.4}CoO_{3-δ}. CA has three carboxyl groups that can bind with metal cations whereas EDTA has four carboxyl and two amine groups, demonstrating that the strength of the chelating agents affects the interactions during the chelation process.^{12,14}

Despite previous research showing that the use of chelating agents provides a good platform for the production of perovskites, the molecular interactions involved are still unclear. The microscopic behaviors and characteristics of the intermediate structures, as well as the ligand–metal complexes, are unknown. Furthermore, research into the microscopic properties of metal cation complexation with chelating agents is scarce.

Several theoretical studies into the favored sites for complexation have been carried out to find the most stable structure in the intermediate state.^{15–17} Primikyri et al.¹⁵ performed DFT studies on the chelation of Zn to quercetin and luteolin in their neutral and deprotonated forms. It was found that the preferred cation bonding sites were in between the carbonyl and deprotonated hydroxyl groups of quercetin and luteolin. This is in line with the work reported by Leopoldini et al.¹⁶ The preference of metal cations to form complexes at these sites is due to the lone pairs of electrons from the O atoms at the carbonyl and deprotonated hydroxyl groups.

In this study, we intended to confirm the important initial step involved in the one-pot synthesis of barium zirconate (BZY). Metal cations Y^{3+} , Ba^{2+} , and Zr^{4+} were modeled to combine with two chelating agents, CA and EDTA. DFT was employed to determine the interactions between the chelating agents and the metal cations at the microscopic level. This included possible metal cation attachment sites and the electronic structure of the complexes formed. This study focusses only on the interaction between metal and chelating agent with a ratio of 1:1, therefore the effects of coordination sphere saturation in the metal ions has not been discussed.

2. Computational Details

In a previous study, $Ba(NO_3)_2$, $Zr(NO_3)_2 \cdot xH_2O$, and $Y(NO_3)_3 \cdot 5H_2O$ were dissolved to produce the metal cations and form the metal–chelating agent complexes.¹¹ In order to portray correctly the charge state of the metal cations, they have been modeled as having the indicated positive charges in the calculations. To further facilitate the calculations, the existence of Zr^{4+} in the one-pot synthesis is approximated.

The structures of chelating agents CA and EDTA were obtained from the Chemspider database.¹⁸ CA and EDTA were deprotonated at the carboxylic acid groups (COOH), making them negatively charged as in the real system these protons would be dissociated. The deprotonated chelating agents were labeled as CA_{3H} and $EDTA_{4H}$. The metal cations were then attached to the chelating agents at five positions labeled P1 to P5. These positions are shown in Fig. 1.

All calculations were carried out using the Gaussian 09 suite of programs.¹⁹ The B3LYP functional with dual basis sets 6-31G* for C, O, N, and H atoms and Universal Gaussian Basis Set (UGBS) for metal cations was used. The D3 version of Grimme's dispersion correction with Becke-Johnson (BJ) damping was adopted in the metal-complex calculations^{20,21} to improve the dispersion energy in the B3LYP method. All the results were visualized using GaussView²² and Chem3D molecular modeling software.

The binding energy (E_b) was used to compute the stability of the complexes. The E_b of the metal complexes was calculated from the expression:²³

$$E_b = E_{M\text{-complex}} - E_M - E_{\text{chelate}} \quad (1)$$

where $E_{M\text{-complex}}$ is the energy of the metal and chelating agent, E_{chelate} represents the energy of the chelating agent, and E_M is the energy of the metal cation.

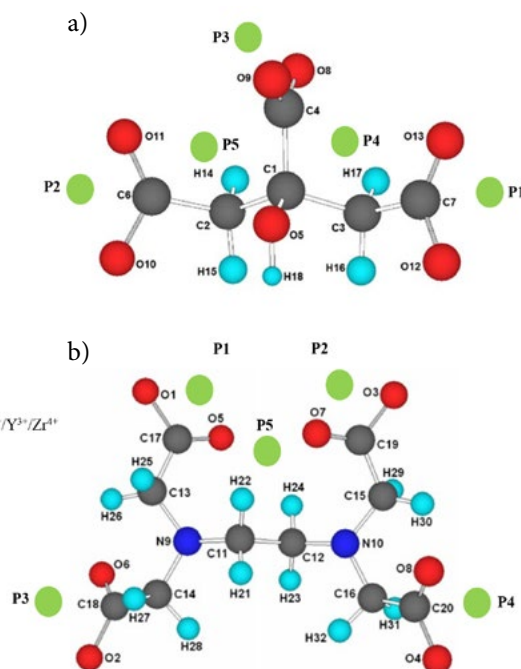


Fig. 1. Molecular structure of (a) CA_{3H} and (b) $EDTA_{4H}$ with metal attachment (Ba^{2+} , Y^{3+} , Zr^{4+}) at different positions (P1 to P5). Metal cations are green and C, O, N, and H are colored grey, red, blue, and turquoise, respectively.

3. Results and Discussion

3.1. Binding Energies

EDTA and CA are chelating agents that can bind to metal cations to form complexes. EDTA is a type of poly-amino carboxylic acid that can bind to a metal via four carboxyl and two amine groups, meaning it has six sites with a lone pair of electrons. CA is a polydentate ligand and can bind to metals via three carboxyl groups with a lone pair of electrons at each. In this study, the binding energies of metal- CA_{3H} and metal- $EDTA_{4H}$ complexes were calculated in order to determine their stability.

At the level of theory B3LYP/6-31G* and UGBS geometry optimization, the following results were obtained: $E(CA_{3H}) = -20626.57$ eV, $E(EDTA_{4H}) = -29911.50$ eV, $E(Ba^{2+}) = -214598.65$ eV, $E(Y^{3+}) = -90707.64$ eV, and $E(Zr^{4+}) = -96342.96$ eV.

The binding energies of CA_{3H} and $EDTA_{4H}$ metal complexes were calculated from equation (1) and are shown in Tables 1 and 2. A higher negative value of E_b indicates higher stability of the complex. Table 1 shows the E_b of metal- CA_{3H} complexes at five different positions of

metal attachment. Ba^{2+} attaches strongly at P2 and has an E_b of -19.39 eV. Interestingly, in $\text{Y-CA}_{3\text{H}}$, the E_b is highest at P4 and P5 and both sites have the same E_b of -21.82 eV. In the $\text{Zr-CA}_{3\text{H}}$ complex, the E_b values at P4 and P5 are similar at -24.89 eV. The highest and most stable E_b was at P3 (-25.69 eV).

The calculated E_b values of metal-EDTA_{4H} complexes are tabulated in Table 2. In $\text{Ba-EDTA}_{4\text{H}}$ complexes, Ba^{2+} prefers to attach at P2 as this E_b (-26.67 eV) is the highest compared to other sites. Table 2 also shows that the E_b for P1 differs from P2 by 0.01 eV. Hence, these two sites in EDTA_{4H} are favorable to Ba^{2+} for attachment. In the $\text{Y-EDTA}_{4\text{H}}$ and $\text{Zr-EDTA}_{4\text{H}}$ complexes, the cations bonded strongly at P5 and exhibited a high E_b values of -33.12 eV and -37.33 eV, respectively.

Table 1. Binding energies (E_b) of $\text{CA}_{3\text{H}}$ complexes. Numbers in bold represent the most stable metal complexes.

Positions	E_b (eV)		
	$\text{Ba-CA}_{3\text{H}}$	$\text{Y-CA}_{3\text{H}}$	$\text{Zr-CA}_{3\text{H}}$
P1	-18.92	-21.65	-24.23
P2	-19.39	-21.65	-24.23
P3	-19.01	-21.72	-25.69
P4	-18.92	-21.82	-24.89
P5	-18.92	-21.82	-24.89

Table 2. Binding energies (E_b) of EDTA_{4H} complexes. Numbers in bold represent the most stable metal complexes.

Positions	E_b (eV)		
	$\text{Ba-EDTA}_{4\text{H}}$	$\text{Y-EDTA}_{4\text{H}}$	$\text{Zr-EDTA}_{4\text{H}}$
P1	-26.66	-29.62	-32.31
P2	-26.67	-29.62	-32.31
P3	-25.71	-27.34	-28.99
P4	-17.08	-27.33	-28.96
P5	-26.56	-33.12	-37.33

The results discussed in the preceding paragraph can be explained using electrostatic potential (ESP) maps for the molecules of CA and EDTA as illustrated in Fig. 2. ESP enables visualization of charge distribution in the molecules using color codes. The red regions indicate more negative potential, while the blue regions indicate less negative potential (or positive potential). As displayed in Fig. 2 (a), the most negative potential is distributed around P4 and P5, in between the central carboxyl group and on the carboxyl groups at either end of the CA molecule. These groups are susceptible to electrophilic attack, hence Ba^{2+} , Y^{3+} , and Zr^{4+} prefer to bind to CA at these two positions. EDTA has four carboxyl and two amine groups susceptible to electrophilic attack, therefore these sites have a high possibility of metal complexation (in Fig. 2 (b), these sites

are shown in orange). As can be seen in Table 2, the binding energies are low at P3 and P4 compared to other positions due to the low negative potential.

At each preferred site, the Ba complexes have the smallest E_b values compared to the other metal complexes. The larger size of Ba^{2+} makes it less stable and prevents the ligand from chelating completely.^{24–26} Zr^{4+} complexes exhibit higher E_b values than Y^{3+} complexes despite being larger in size. The ionic charge for Zr^{4+} is larger than for Y^{3+} and the stability of the metal complex decreases with decreasing ionic charge.^{24,27} These results are supported by Bohm et al.²⁸ in that the interaction energy increases as the size of the metal decreases, $\text{K}^+ > \text{Na}^+ > \text{Li}^+$ with values of -5.65 eV, -8.71 eV, and -12.05 eV, respectively.

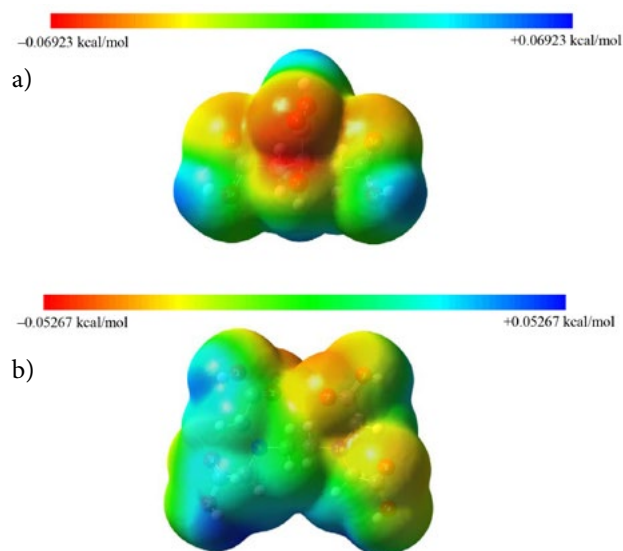


Fig. 2. The electrostatic potential map of (a) CA and (b) EDTA. Isovalue of electron density = 0.0002 au (e/a^3). Refer to figure 1 for the structures without the isosurface.

Based on Tables 1 and 2, similar E_b values are observed at P1/P2 and P4/P5 in $\text{Y-CA}_{3\text{H}}$ and $\text{Zr-CA}_{3\text{H}}$ complexes. This is due to the symmetrical arrangement of the atoms in CA. However, this is not observed in $\text{Ba-CA}_{3\text{H}}$, potentially due to the larger size of Ba^{2+} . Similarly in the $\text{Ba-EDTA}_{4\text{H}}$ complex, it is difficult for Ba^{2+} to reside at any other site on EDTA due to its larger size.

3. 2. Geometry Optimization

Geometry optimizations were performed on the metal complexes using 6-31G* and UGBS basis sets and no imaginary frequencies were observed. The stationary point of each structure where the energy was at a minimum was therefore ascertained.²⁹ The geometrically optimized structures of the most stable metal- $\text{CA}_{3\text{H}}$ and metal- $\text{EDTA}_{4\text{H}}$ complexes formed are shown in Fig. 3 to 8. The

bond lengths between metal and O are discussed since O and N donate electrons and play an important role in the metal interaction.

In general, metal complexation marginally changes the shape of CA_{3H} . Ba^{2+} was found most stable at P2 with bond lengths of $Ba-O5 = 2.704 \text{ \AA}$, $Ba-O9 = 2.602 \text{ \AA}$, and $Ba-O11 = 2.602 \text{ \AA}$ (the optimized structure of $Ba-CA_{3H}$ is shown in Fig. 3). These results concur with findings from a previous study by Makrlík et al.³⁰ where the bond length of Ba^{2+} to oxygen atoms in the beauvericin ligand are 2.5–4.9 \AA .

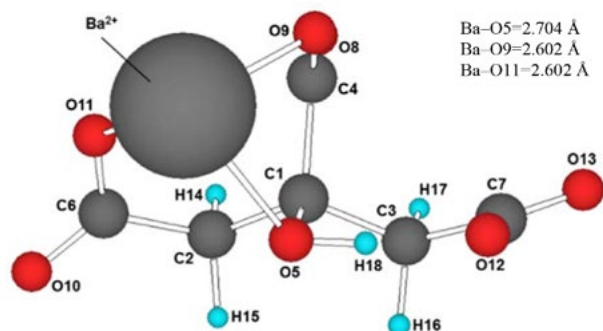


Fig. 3. Optimized structure of the most stable $Ba-CA_{3H}$ complex (P2)

Y^{3+} was found to be the most stable at equivalent sites P4 and P5 (Fig. 4). The cation bonds to three O atoms, two from the carboxyl group and one from the hydroxyl group. The bond lengths obtained for $Y-O9$ at P4 and P5 are 2.160 \AA . $Y-O13$ and $Y-O11$ at P4 and P5, respectively, also had the same bond length at 2.155 \AA . The bond length observed for $Y-O5$ at P4 and P5 differed by 0.001 \AA . This small difference in bond length is negligible. These were in accordance with the Y-O bond lengths observed in a previous study.³¹

As depicted in Fig. 5, Zr^{4+} favored P3 in the $Zr-CA_{3H}$ complex. Zr^{4+} is bonded to three O atoms (O8, O9, and O11) on the carboxyl groups of CA_{3H} . The bond lengths for $Zr-O8$, $Zr-O9$, and $Zr-O11$ are 2.035 \AA , 2.021 \AA , and 2.009 \AA , respectively. Similar bond lengths were recorded by Vlačić et al.³² where bond lengths of Zr-O in $Rh/Ce_{0.5}Zr_{0.5}O_2$ were 1.11–2.34 \AA . The most stable sites in $Ba-CA_{3H}$, $Y-CA_{3H}$, and $Zr-CA_{3H}$ were observed between carboxyl and hydroxyl groups and this is in accordance with results reported by Primikyri et al.¹⁵ and Leopoldini et al.¹⁶

Figs 6 to 8 show the optimized structure of the most stable metal-EDTA_{4H} complexes. There were significant changes to the shape of EDTA_{4H} after metal complexation. EDTA is able to form bonds with any metal and its chela-

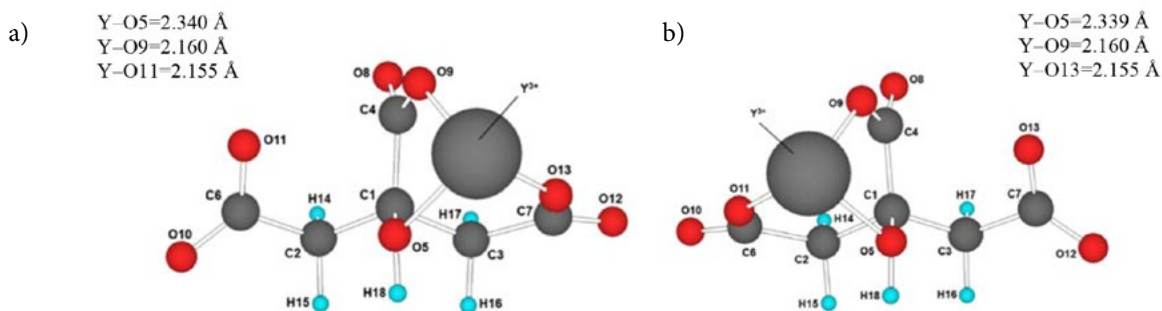


Fig. 4. Optimized structure of the most stable $Y-CA_{3H}$ complex at (a) P4 (b) P5

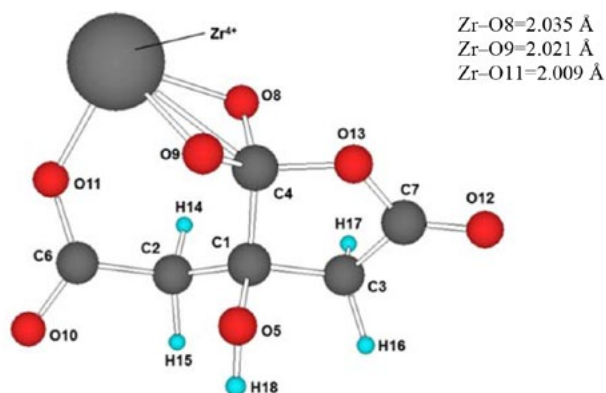


Fig. 5. Optimized structure of the most stable $Zr-CA_{3H}$ complex (P3)

tion depends on the size and ionic charge of the metal cation.³³ The most stable geometrical structure of metal–EDTA_{4H} shows carboxyl O atoms and N atoms moving closer to the metal cation, almost encasing it. Both O and N atoms are able to create bonds with the metal cations as they consist of a lone pair electron.

In the optimized structure of the Ba–EDTA_{4H} complex shown in Fig 6, Ba²⁺ is found to be the most stable at P2. Ba²⁺ bonds to the four nearest O atoms from the carboxyl groups with bond lengths of Ba–O1, Ba–O3, Ba–O5, and Ba–O7 are 2.764 Å, 2.750 Å, 2.710 Å and 2.725 Å, respectively. Furthermore, the geometrical structure of Ba–EDTA_{4H} was similar to the original structure before the addition of Ba²⁺. Several experimental studies encountered problems with BaCO₃ impurities after synthesizing a single layer of perovskites, due to the use of EDTA as the chelating agent.^{11,34} In other reports, triethylenetetraamine (TETA) has been shown to help solve the problem of BaCO₃ impurities at a lower temperature.^{10,35} This may be due to the ability of chelating agents to bind with Ba²⁺. It can be concluded that Ba²⁺ is effectively complexed by the amine group.

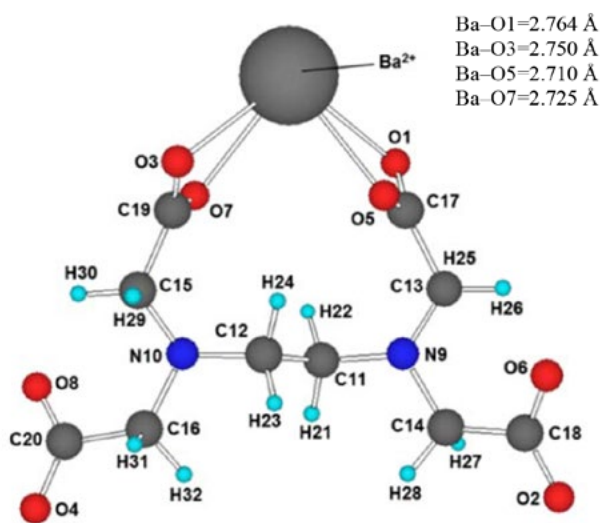


Fig. 6. Optimized structure of the most stable Ba–EDTA_{4H} complex (P2)

From Fig. 7 shows that Y³⁺ is embraced by EDTA_{4H}. A similar geometry was found by Thomas et al³⁶ in an investigation into the molecular structure of aqueous Hg(II)–EDTA. Unlike the Ba–EDTA_{4H} complex, the four carboxyl O atoms and two N atoms in EDTA_{4H} bind strongly to Y³⁺ due to its smaller size, making it easy to be caught by the EDTA ligand. The bond lengths for Y–EDTA_{4H} are as follows: Y–O5 = 2.273 Å, Y–O6 = 2.297 Å, Y–O7 = 2.273 Å, Y–O8 = 2.297 Å, Y–N9 = 2.528 Å, and Y–N10 = 2.527 Å. These bond lengths are consistent with Y–O and Y–N bond lengths observed previously in the formation of guanidinate yttrium complexes.³¹

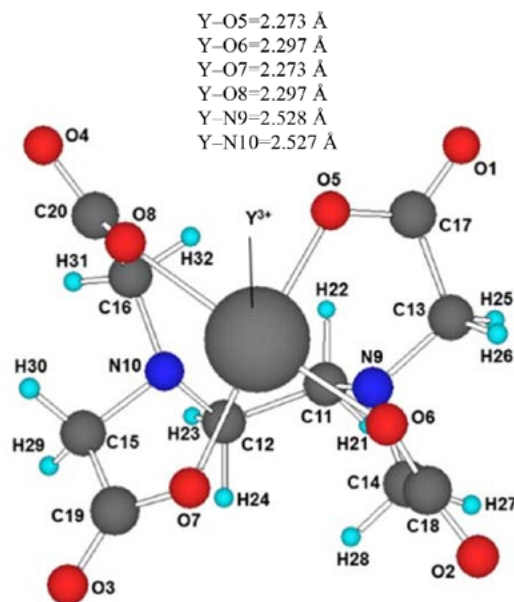


Fig. 7. Optimized structure of the most stable Y–EDTA_{4H} complex (P5)

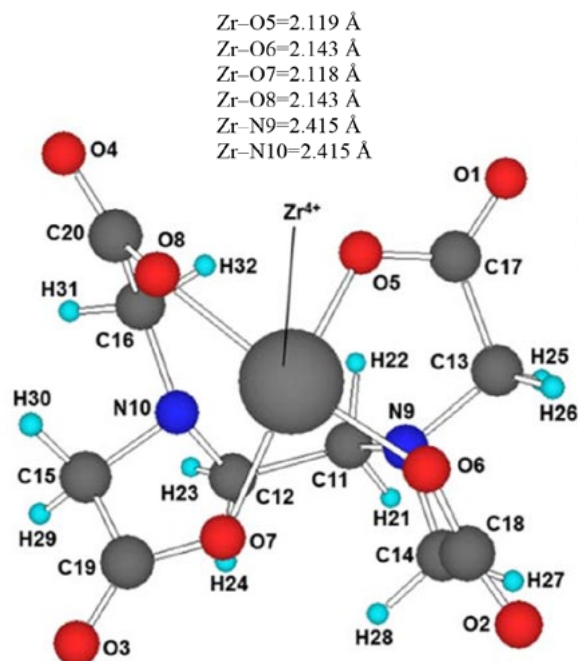


Fig. 8. Optimized structure of the most stable Zr–EDTA_{4H} complex (P5)

Zr⁴⁺ was similarly encased by EDTA_{4H} at P5 in the Zr–EDTA_{4H} complex (Fig. 8). Zr⁴⁺ was bonded to four carboxyl groups and two amine groups from EDTA_{4H}. EDTA_{4H} is able to strongly wrap around metal cations due to lone pairs of electrons from two types of ligand (carboxyl and amine groups). The interaction between Zr⁴⁺ and EDTA_{4H} is the strongest with bond lengths of Zr–O5 = 2.119 Å, Zr–O6 = 2.143 Å, Zr–O7 = 2.118 Å, Zr–O8 =

2.143 Å, Zr–N9 = 2.415 Å, and Zr–N10 = 2.415 Å. The bond lengths measured were in agreement with findings by Suzuki et al,³⁷ where the bond length of Zr–O in [Zr(CO₃)EDTA]²⁺ was determined. Similarly, the bond length is in accordance with findings by Pozhidaev et al³⁸ where the bond length of Zr–O in the crystal structure of Zr–ethylenediaminetetraacetate tetrahydrate was measured to within a range of 2.1–2.3 Å, and Zr–N was 2.43 Å.

3. 3. Mulliken Charges

The Mulliken charges of the most stable metal–CA_{3H} and metal–EDTA_{4H} complexes are shown in Tables 3 and 4. The initial ionic charges of Ba²⁺, Y³⁺, and Zr⁴⁺ decrease after complexation with CA_{3H} and EDTA_{4H}. The decreasing in charge can be attributed to the transfer of electrons from CA and EDTA to the metal.^{39,40} The charge transfer in metal complexes is of utmost important as it influences the

interaction between metal and chelating agent. It can be inferred that the greater the charge reduction in the metal the stronger the interaction in the metal complex.⁴¹

Table 3. Charge of metals after complexation with the chelating agent.

Metals	Mulliken atomic charge of metals in metal complexes		
	Initial	After optimized (CA _{3H})	After optimized (EDTA _{4H})
Ba	+2	+1.544	+1.508
Y	+3	+2.104	+1.449
Zr	+4	+2.672	+1.911

The C atoms, C2 and C3 in CA_{3H} and C11 to C16 in EDTA_{4H} (Table 4), carry negative charges as they are bonded to C and N atoms, respectively. Both atoms attract the bonding pair of electrons to exactly the same extent. That

Table 4. Mulliken charges of the most stable metal–CA_{3H} complexes

Complexes	Atom charges						
	C1	C2	C3	C4	C6	C7	
Ba–CA _{3H}	0.259	-0.367	-0.389	0.511	0.515	0.495	
Y–CA _{3H}	0.215	-0.398	-0.389	0.621	0.587	0.490	
Zr–CA _{3H}	0.181	-0.398	-0.407	0.666	0.627	0.534	
	O5	O8	O9	O10	O11	O12	O13
Ba–CA _{3H}	-0.780	-0.597	-0.675	-0.593	-0.669	-0.632	-0.601
Y–CA _{3H}	-0.739	-0.523	-0.688	-0.511	-0.682	-0.631	-0.598
Zr–CA _{3H}	-0.745	-0.453	-0.723	-0.421	-0.713	-0.590	-0.563
	H14	H15	H16	H17	H18		
Ba–CA _{3H}	0.150	0.123	0.136	0.132	0.438		
Y–CA _{3H}	0.189	0.188	0.135	0.162	0.471		
Zr–CA _{3H}	0.228	0.232	0.177	0.193	0.504		

Table 5. Mulliken charges of the most stable metal–EDTA_{4H} complexes

Complexes	Atom charges								
	O1	O2	O3	O4	O5	O6	O7	O8	N9
Ba–EDTA _{4H}	-0.640	-0.650	-0.643	-0.650	-0.629	-0.619	-0.627	-0.618	-0.359
Y–EDTA _{4H}	-0.535	-0.542	-0.536	-0.542	-0.623	-0.627	-0.623	-0.627	-0.501
Zr–EDTA _{4H}	-0.471	-0.483	-0.471	-0.483	-0.650	-0.653	-0.650	-0.653	-0.532
	C11	C12	C13	C14	C15	C16	C17	C18	C19
Ba–EDTA _{4H}	-0.138	-0.137	-0.208	-0.224	-0.206	-0.224	0.532	0.449	0.526
Y–EDTA _{4H}	-0.145	-0.145	-0.246	-0.239	-0.246	-0.239	0.561	0.572	0.561
Zr–EDTA _{4H}	-0.156	-0.156	-0.266	-0.246	-0.266	-0.246	0.593	0.603	0.593
	H21	H22	H23	H24	H25	H26	H27	H28	
Ba–EDTA _{4H}	0.113	0.143	0.106	0.151	0.095	0.159	0.092	0.129	
Y–EDTA _{4H}	0.173	0.183	0.173	0.183	0.171	0.205	0.170	0.199	
Zr–EDTA _{4H}	0.210	0.205	0.210	0.205	0.214	0.239	0.209	0.229	
	H29	H30	H31	H32	H29	H30	H31		
Ba–EDTA _{4H}	0.095	0.160	0.093	0.130	0.095	0.160	0.093		
Y–EDTA _{4H}	0.171	0.205	0.170	0.199	0.171	0.205	0.170		
Zr–EDTA _{4H}	0.214	0.239	0.209	0.229	0.214	0.239	0.209		

means, on average, the electron pair is found halfway between the two atoms and possesses similar negative charges. These results are consistent with results from Arivazhagan et al⁴² that show higher electronegativity attracts more electrons and vice versa.

C1, C4, C6, and C7 in CA_{3H} and C17 to C20 in EDTA_{4H} (shown in Tables 4 and 5) carry positive charges as they are bonded to O. O atoms have a higher electronegativity than C atoms, meaning an O bond more strongly attracts the bonding pair of electrons compared to a C atom. Consequently, the electron pair is pulled towards the O atom, making the carbon atom positively charged. The same is observed in H atoms. All H atoms have a positive charge. H18 in CA_{3H} has a higher positive charge than other H atoms as it is bonded to an O atom. This is confirmed in a recent study by Gangadhara and Krishnan.⁴³

4. Conclusion

The density functional B3LYP method was used to investigate interactions between chelating agents and metal cations in forming a specific barium zirconate (BZY) compound. The aim of the study was to determine the preferred coordination sites for Ba²⁺, Y³⁺, and Zr⁴⁺ in CA_{3H} and EDTA_{4H}. The results show that CA_{3H} and EDTA_{4H} can bind to the metal cations considered. The metal cations were observed to bind to the electron-rich sites of the chelating agents. Not all sites had the same binding energy, however. Moreover, different cations showed different bonding strengths. Based on the results, Zr⁴⁺ complexation was found to be the most stable compared to the other complexes. Ba²⁺ did not fully chelate to EDTA_{4H}, rendering Ba-EDTA_{4H} the least stable complex. The greater binding energies of EDTA, alongside its ability to bind metals through four carboxyl and two amine groups, confirm its stronger chelating power with respect to CA.

5. References

1. J. Li, J.-L. Luo, K. T. Chuang, A. R. Sanger, *Electrochim. Acta.* **2008**, *53*, 37013707. DOI:10.1016/j.electacta.2007.12.020
2. D. Medvedev, A. Murashkina, E. Pikalova, A. Demin, A. Podias, P. Tsiakaras, *Prog. Mater. Sci.* **2013**, *60*, 72–129. DOI:10.1016/j.pmatsci.2013.08.001
3. N. A. Ibarahim, M. A. M. Ishak, A. Ramli, N. Osman, *Int. J. Ind. Chem.* **2014**, *5*, 1–6. DOI:10.1007/s40090-014-0018-4
4. W. G. Coors, In: C. Sikalidis (Ed.) *Advances in Ceramics - Synthesis and Characterization, Processing and Specific Applications*, CoorsTek, Inc., USA, **2011**, pp 479–498.
5. J. Tong, D. Clark, L. Bernau, A. Subramaniyan, R. O'Hayre, *Solid State Ionics.* **2010**, *181*, 1486–1498. DOI:10.1016/j.ssi.2010.08.022
6. A. B. Stambouli, E. Traversa, *Renew. Sustain. Energy Rev.* **2002**, *6*, 433–455. DOI:10.1016/S1364-0321(02)00014-X
7. Z. Wei, A. Chak-Tong, D. You-Wei, *Chin. Phys. B.* **2013**, *22*, 1–11. <https://iopscience.iop.org/article/10.1088/1674-1056/22/5/057501/meta>
8. N. G. Park, *Mater. Today.* **2015**, *18*, 65–72. DOI:10.1016/j.mattod.2014.07.007
9. U. Wang, 2014, <https://www.wsj.com/articles/perovskite-of-fers-shot-at-cheaper-solar-energy-1411937799> (accessed: February, 2014)
10. N. A. Abdullah, N. Osman, S. Hasan, O. H. Hassan, *Int. J. Electrochem. Sci.* **2012**, *7*, 9401–9409. DOI:10.4028/www.scientific.net/AMR.896.112
11. N. A. Abdullah, S. Hasan, N. Osman, *J. Chem.* **2013**, *2013*, 1–7. DOI:10.1155/2013/908340
12. S. Liu, X. Tan, K. Li, R. Hughes, *Ceram. Int.* **2002**, *28*, 327–335. DOI:10.1016/S0272-8842(01)00098-0
13. Y. Tao, J. Shao, J. Wang, W. G. Wang, *J. Power Sources.* **2008**, *185*, 609–614. DOI:10.1016/j.jpowsour.2008.09.021
14. M. Motta, C. V. Deimling, M. J. Saeki, P. N. Lisboa-Filho, *J. Sol-Gel Sci. Technol.* **2008**, *46*, 201–207. DOI:10.1007/s10971-007-1673-0
15. A. Primikyri, G. Mazzone, C. Lekka, A. G. Tzakos, N. Russo, I. P. Gerathanassis, *J. Phys. Chem.* **2014**, *119*, 83–95. DOI:10.1021/jp509752s
16. M. Leopoldini, N. Russo, S. Chiodo, M. Toscano, *J. Agr. Food Chem.* **2006**, *54*, 6343–6351. DOI:10.1021/jf060986h
17. A. Galano, G. Mazzone, R. Alvarez-Diduk, T. Marino, J. R. Alvarez-Idaboy, N. Russo, *Annu. Rev. Food Sci. Technol.* **2016**, *7*, 335–352. DOI:10.1146/annurev-food-041715-033206
18. Chemspider Search and Share Chemistry, 2014, <https://www.chemspider.com/> (accessed: March, 2014)
19. M. J. Frisch, G. W. Trucks, H. B. Schlegel, G. E. Scuseria, M. A. Robb, J. R. Cheeseman, G. Scalmani, V. Barone, B. Mennucci, G. A. Petersson, H. Nakatsuji, M. Caricato, X. Li, H. P. Hratchian, A. F. Izmaylov, J. Bloino, G. Zheng, J. L. Sonnenberg, M. Hada, M. Ehara, K. Toyota, R. Fukuda, J. Hasegawa, M. Ishida, T. Nakajima, Y. Honda, O. Kitao, H. Nakai, T. Vreven, J. A. Montgomery, Jr., J. E. Peralta, F. Ogliaro, M. Bearpark, J. J. Heyd, E. Brothers, K. N. Kudin, V. N. Staroverov, R. Kobayashi, J. Normand, K. Raghavachari, A. Rendell, J. C. Burant, S. S. Iyengar, J. Tomasi, M. Cossi, N. Rega, M. J. Millam, M. Klene, J. E. Knox, J. B. Cross, V. Bakken, C. Adamo, J. Jaramillo, R. Gomperts, R. E. Stratmann, O. Yazyev, A. J. Austin, R. Cammi, C. Pomelli, J. W. Ochterski, R. L. Martin, K. Morokuma, V. G. Zakrzewski, G. A. Voth, P. Salvador, J. J. Dannenberg, S. Dapprich, A. D. Daniels, Ö. Farkas, J. B. Foresman, J. V. Ortiz, J. Cioslowski, D. J. Fox, Gaussian, Inc., Wallingford CT USA, 2009.
20. S. Grimme, J. Antony, S. Ehrlich, H. Krieg, *J. Chem. Phys.* **2010**, *132*, 1456–1465. DOI:10.1063/1.3382344
21. S. Grimme, S. Ehrlich, L. Goerigk, *J. Comput. Chem.* **2011**, *32*, 1456–1465. DOI:10.1002/jcc.21759
22. R. D. Dennington II, T. A. Keith, J. Millam, Semichem, Inc., USA, 2007.
23. T. Sakajiri, H. Yajima, T. Yamamura, *ISRN Biophys.* **2012**, *2012*, 1–5. DOI:10.5402/2012/124803
24. C. E. Housecroft, A. G. Sharpe, *Inorganic Chemistry*, Ashford

- Colour Press Ltd., Gosport, London, UK, **2005**.
25. M. Satterfield, J. S. Brodbelt, *Inorg. Chem.* **2001**, *40*, 5393–5400. DOI:10.1021/ic010356r
 26. N. F. Dalleska, K. Honma, L. S. Sunderlin, P. B. Armentrout, *J. Am. Chem. Soc.* **1994**, *116*, 3519–3528. DOI:10.1021/ja00087a044
 27. T. Dudev, C. Lim, *J. Am. Chem. Soc.* **2013**, *114*, 538–556. DOI:10.1021/cr4004665
 28. S. Bohm, E. Makrlik, P. Vanura, *Monatsh. Chem.* **2015**, *146*, 1229–1231. DOI:10.1007/s00706-014-1393-4
 29. B. G. Johnson, C. A. Gonzales, P. M. W. Gill, J. A. Pople, *Chem. Phys. Lett.* **1994**, *221*, 100–108. DOI:10.1016/0009-2614(94)87024-1
 30. E. Makrlik, P. Toman, P. Vanura, *J. Radioanal. Nucl. Chem.* **2013**, *295*, 1887–1891. DOI:10.1007/s10967-012-2107-1
 31. M. P. Coles, P. B. Hitchcock, *Inorg. Chim. Acta.* **2004**, *357*, 4330–4334. DOI:10.1016/j.ica.2004.06.015
 32. G. Vlais, P. Fornasiero, S. Geremia, J. Kaspar, M. Graziani, *J. Catal.* **1997**, *168*, 386–392.
 33. A. Kovacs, D. S. Nemcsok, T. Kocsis, *J. Mol. Struct.* **2010**, *950*, 93–97. DOI:10.1016/j.theochem.2010.03.036
 34. N. Osman, N. A. Abdullah, S. Hasan, in: K. Junichi (Ed.), *Thermal Decomposition and Phase Formation of Cerate-Zirconate Ceramics Prepared with Different Chelating Agents: Solid State Ionics: Ionics for Sustainable World - Proceedings of the 13th Asian Conference*, **2013**, pp. 317–323.
 35. N. Osman, N. A. Abdullah, S. Hasan, *Adv. Mater. Res. (Durnten-Zurich, Switz.)* **2014**, *896*, 112–115. DOI:10.4028/www.scientific.net/AMR.896.112
 36. S. A. Thomas, J. F. Gaillard, *J. Phys. Chem.* **2015**, *119*, 2878–2884. DOI:10.1021/acs.jpca.5b00343
 37. T. M. Suzuki, D. A. P. Tanaka, M. A. L. Tanco, M. Kanesato, T. Yokoyama, *J. Environ. Monit.* **2000**, *2*, 550–555. DOI:10.1039/B006738P
 38. A. I. Pozhidaev, M. A. Porai-Koshits, T. N. Polynova, *J. Struct. Chem.* **1974**, *15*, 548–553. DOI:10.1007/BF00747194
 39. F. Y. Adeowo, B. Honarparvar, A. A. Skelton, *RSC Adv.* **2016**, *6*, 79485–79496. DOI:10.1039/C6RA20203A
 40. A. A. Skelton, N. Agrawal, J. R. Fried, *RSC Adv.* **2015**, *5*, 55033–55047. DOI:10.1039/C4RA14000A
 41. F. Y. Adeowo, B. Honarparvar, A. A. Skelton, *J. Phys. Chem. A.* **2017**, *121*, 6054–6062. DOI:10.1021/acs.jpca.7b01017
 42. M. Arivazhagan, S. Manivel, S. Jeyavijayan, R. Meenakshi, *Spectrochim. Acta. A. Mol. Biomol. Spectrosc.* **2015**, *134*, 493–501. DOI:10.1016/j.saa.2014.06.108
 43. R. P. Gangadharan, S. Krishnan, *Acta Phys. Pol. A.* **2014**, *125*, 18–22. DOI:10.12693/APhysPolA.125.18

Povzetek

Z izračuni gostotnega funkcionala smo proučevali kovinske komplekse, ki nastanejo med sintezo barijevega cirkonata (BZY). Molekularne interakcije med tvorbo kompleksov ligand-kovin tekom te sinteze namreč niso znane. V tej študiji so bili izvedeni izračuni za določitev prednostnih koordinacijskih mest za kovinske komplekse. Katione Ba²⁺, Y³⁺ in Zr⁴⁺ smo modelirali tako, da bi na strateških položajih interagirali z dvema deprotoniranimi kelatnima reagentoma (citronska kislina [CA] in etilendiaminetetraoacetna kislina [EDTA]). Uporabili smo teorijo gostotnega funkcionala (DFT) na B3LYP nivoju z osnovnim 6-31G* in univerzalnim Gaussovim (UGBS) baznim setom. Iz dobljenih geometrijskih podatkov, veznih energij in porazdelitev naboja smo ugotovili, da lahko CA in EDTA vežeta proučevane kovinske katione, ki pa težijo k tvorbi vezi na mestih z večjo elektronsko gostoto. Od treh kovinskih kationov je bilo ugotovljeno, da najmočnejše vezi z deprotoniranim CA in EDTA tvori Zr⁴⁺, sledi Y³⁺ in nato Ba²⁺.

Short communication

Investigation of Mechanistic Pathway for Trimethyl Borate Mediated Amidation of (*R*)-Mandelic Acid for the Synthesis of Mirabegron, an Antimuscarinic Agent[#]

Dattatray G. Deshmukh,^{1,2} Mukund N. Bangal,¹ Mukunda R. Patekar,¹
Vijay J. Medhane² and Vijayavithal Thippannachar Mathad^{1,*}

¹Department of Process Research and Development, Megafine Pharma (P) Ltd., 201, Lakhmapur, Dindori, Nashik-422 202, Maharashtra, India.

²Organic Chemistry Research Center, Department of Chemistry, K. T. H. M. College, Nashik-422 002, Maharashtra, India.

* Corresponding author: E-mail: vt.mathad@megafine.in, drvtmathad@yahoo.co.in

Received: 12-16-2017

[#]Megafine Publication Number: MF/027/2017

Abstract

The present work describes investigation of mechanistic pathway for trimethyl borate mediated amidation of (*R*)-mandelic acid (**3**) with 4-nitrophenylethylamine (**2**) to provide (*R*)-2-hydroxy-*N*-[2-(4-nitrophenyl)ethyl]-2-phenylacetamide (**4**) during mirabegron synthesis. Plausible reaction mechanism is proposed by isolating and elucidating the active α -hydroxy ester intermediate **16** from the reaction mass. Trimethyl borate mediated approach proved to be selective in providing **4** without disturbing α -hydroxyl group and stereochemistry of the chiral center, and is also a greener, more economic and production friendly over the reported methods. The developed approach is rapid and efficient for the preparation of **4** with an overall yield of 85–87% and around 99.0% purity by HPLC at scale.

Keywords: Trimethyl borate, amidation, α -hydroxy ester, antimuscarinic drug, mirabegron

1. Introduction

Mirabegron (**1**), chemically known as 2-(2-amino-1,3-thiazol-4-yl)-*N*-[4-(2-((2*R*)-2-hydroxy-2-phenylethyl)amino)ethyl]phenyl]acetamide, is a selective agonist for the human beta 3-adrenoceptor,¹ approved for the treatment of overactive bladder (OAB) syndrome.² It exhibits novel mechanism of action compared to other antimuscarinics by improving the storage capacity of the bladder without inhibiting bladder voiding.³ The drug developed by Astellas Pharma was approved by the United States Food and Drug Administrative (US-FDA) in June 2012 and by European Medicines Agency in December 2012.⁴

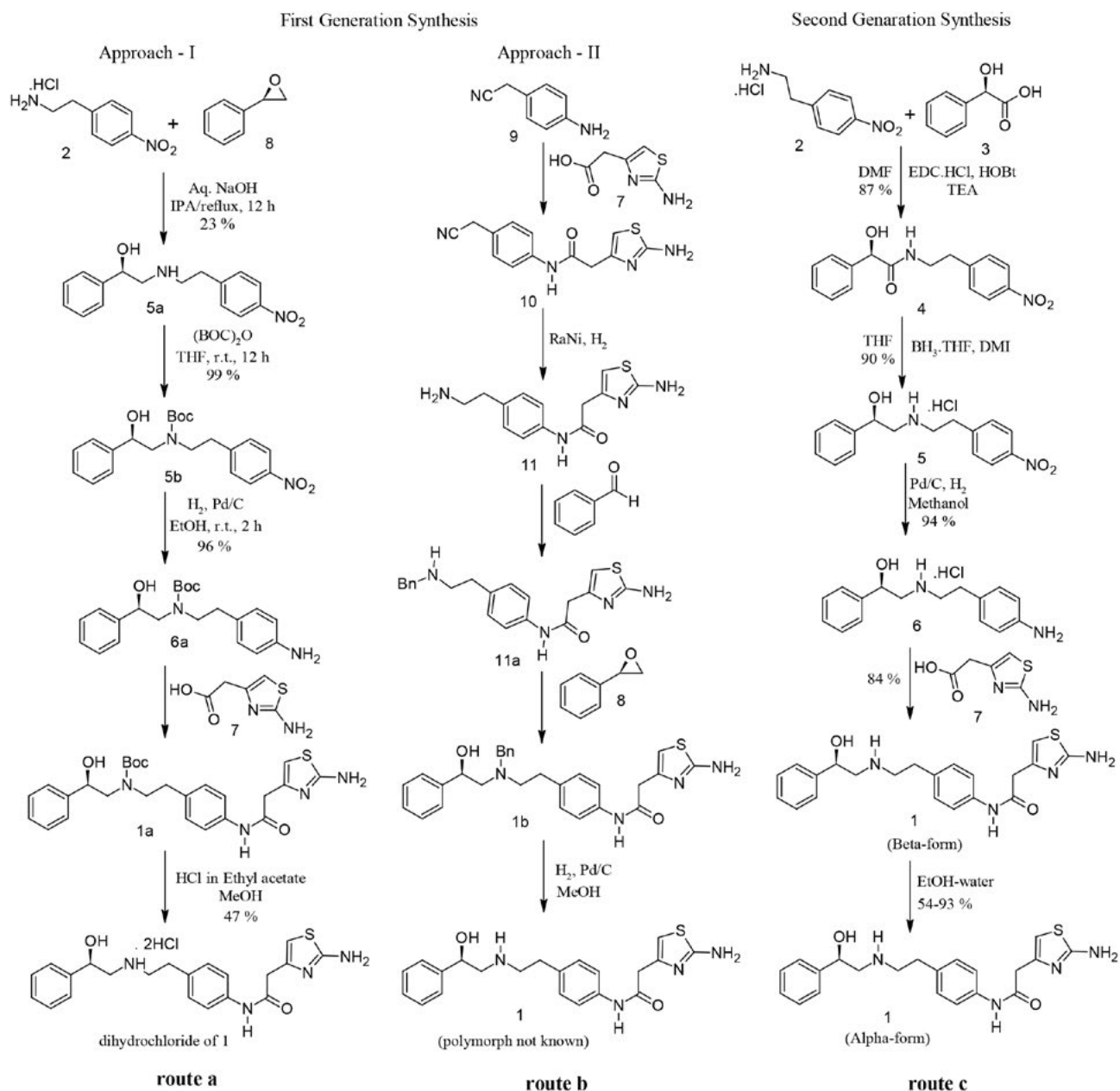
The first generation syntheses,⁵ reported two synthetic approaches for **1** (Scheme 1, route a and b) wherein both the approaches follow opening of epoxide ring of the (*R*)-styrene oxide (**8**). The first approach (Scheme 1, route a) involves nucleophilic addition of **2** on **8** to obtain nitro

amine **5a**. The amino group of **5a** is protected with di-*tert*-butyl-dicarbonate (Boc₂O) to give **5b** which is then reduced using Pd/C to yield aniline derivative **6a**. Aniline **6a** is further condensed with thiazole acid **7** to obtain amide intermediate **1a**. Removal of Boc protection group of **1a** using HCl furnished di-hydrochloride salt of **1** with an overall yield of around 8%. In the second approach (Scheme 1, route b), condensation of (4-aminophenyl)acetonitrile (**9**) and thiazole acid **7** is carried out in the first step, whereas advanced intermediate **11a** is reacted with epoxide **8** in penultimate step to provide **1**. However, detailed synthetic procedure for the route b is not provided in the report. Both of these approaches have several disadvantages such as extensive use of protecting and de-protecting sequences, expensive (*R*)-styrene oxide (**8**) as the starting material, and poor yields for epoxide ring opening reactions.

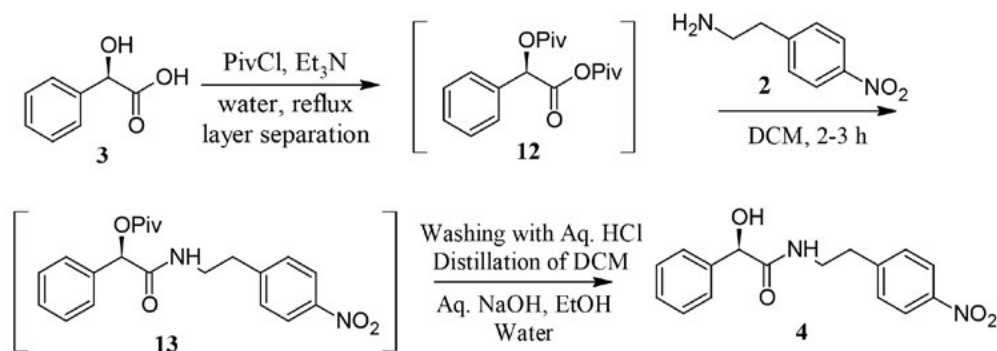
The second generation synthesis,⁶ (Scheme 1, route c) reported for **1** exploited commercially available (*R*)

-mandelic acid (**3**) as the starting material instead of the epoxide **8**. Synthesis commenced with coupling of **2** and **3** in the presence of 1-ethyl-3-(3-(dimethylamino)propyl) carbodiimide hydrochloride (EDCI) as the coupling agent, 1-hydroxybenzotriazole (HOBt) as the catalyst, triethylamine as the base in *N,N*-dimethylformamide (DMF) solvent to provide amide **4**. Amide **4** was reduced using borane-tetrahydrofuran (BH_3 -THF) complex and 1,3-dimethyl-2-imidazolidinone (DMI) to provide amino alcohol **5** which was hydrogenated under Pd-C catalyst to provide di-amine **6**. Coupling of di-amine **6** with thiazole acid **7** in the presence of EDCI furnished **1** in its β -c-

crystalline form. Finally, the β -crystalline form was crystallized in aqueous ethanol to obtain α -crystalline form of **1**. Though the second generation synthesis represents an improvement over the first generation, it still has disadvantages, like the use of expensive EDCI in two steps which also poses increased burden of impurities due to side product formation from EDCI and HOBt. Other methods reported for **1** either involve use of expensive (*R*)-styrene oxide (**8**) as the starting material resulting in low yields (around 11% to 27%) or involve protection and de-protection steps that make the synthesis lengthy and less economic.⁷



Schemes 1. Reported syntheses of mirabegron (**1**).⁵⁻⁶



Scheme 2. Mixed anhydride approach⁸ for the synthesis of the key intermediate 4.

Recent reported approach for the synthesis of 4 replaced EDCI and HOBT with pivaloyl chloride (PivCl) for the condensation of amine 2 with acid 3 via mixed anhydride approach in a biphasic medium comprising dichloromethane (DCM) and water in the presence of triethylamine at reflux temperature (Scheme 2).⁸

The organic layer containing mixed anhydride 12 (having both carboxylic acid groups and hydroxyl group of compound 3 protected with the pivaloyl group), is separated and reacted with amine 2 to obtain pivaloyl ether 13, which is hydrolyzed under basic conditions to provide the desired key intermediate 4. However, usage of PivCl at industrial scale with extended operations like separations, washings, de-protections and distillation makes the process cumbersome and less efficient.

Recently, we have reported⁹ an efficient and first process for the direct isolation of stable α -form crystals of mirabegron (1) from our laboratory. In continuation of our research on mirabegron (1), herein, we report an easy, straightforward, industrially scalable, selective and economic synthesis of the key intermediate (*R*)-2-hydroxy-*N*-[2-(4-nitrophenyl)ethyl]-2-phenylacetamide (4) using trimethylborate as the coupling agent.

2. Results and Discussion

(*R*)-Mandelic acid (3) was found to be an appropriate starting point for mirabegron in view of the cost and commercial availability and was thus selected for the process research and development work (Scheme 1, route c). Use of EDCI and HOBT was not considered for the present work owing to the large quantity requirements and resulting in direct impact on the cost of production of 1. Thus, we began exploring alternatives to develop cost effective approach by employing simple, easily available and user friendly acid activating agents to manufacture large quantities of amide 4. The commonly known methods for activation of carboxylic acid is to make its derivatives, such as acid halides, mixed anhydrides or to use activating agents, such as DCC, EDCI, HATU, HBTU, and BOP-Cl. How-

ever, these methods have some disadvantages, for example, use of halogenating agents to prepare acid halides may affect chiral purity of 3, employing mixed anhydride method is not straightforward and requires additional efforts to overcome side product formation,¹⁰ and use of activating agents such as DCC, EDCI, HATU, HBTU, BOP-Cl and others does not only increases manufacturing cost but also increases burden of control of corresponding by-products in active pharmaceutical ingredient (API).¹⁰

Boric acid [B(OH)₃] and their derivatives are green, inexpensive and readily available catalysts for direct formation of amide bond, thus attracting our attention.^{11–14} We first attempted to carry out amidation between amine 2 and acid 3 using boric acid, including efforts of trapping water (*i.e.* side product) by means of molecular sieves and Dean–Stark apparatus but none of these attempts gave satisfactory results. As per literature reports, catalytic activity of boric acid was enhanced by converting it to borate esters by introducing mono-hydroxyl or di-hydroxyl functional groups, such as cresol or tetrachlorocatechol.^{15–16} However, to minimize the burden of atom economy, we attempted the use of a simple and commercially available trimethylborate [B(OMe)₃] as the coupling agent.

Feasibility of B(OMe)₃ was explored during the screening experiments using various solvents [DMF, THF, 2Me-THF, acetonitrile (ACN), DMSO] in the presence of different bases (TEA, K₂CO₃, NaHCO₃, DIPEA). The outcome of the screening experiments is shown in Table 1. Accordingly, the coupling reaction was proved to be successful when Hünig's base [*N,N*-diisopropylethylamine (DIPEA)] was employed in acetonitrile as the solvent (Table 1, entry 7).

Further, to increase the yield and quality a set of optimization experiments were designed and executed. During the optimization it was observed that, when 2, 3, B(OMe)₃ and DIPEA were added together in ACN and heated to reflux, 40–45% of amine 2 was found unreacted in the reaction mass even after 15 hours. On the contrary, when acid 3 and B(OMe)₃ are allowed to react first in

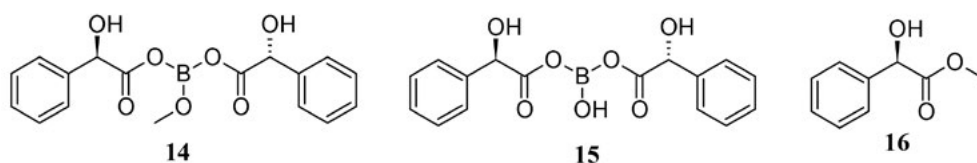
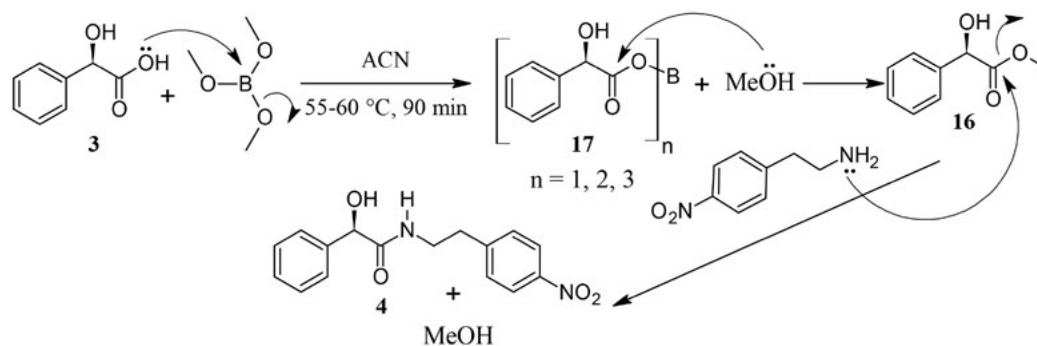
Table 1. Screening of coupling agent, solvent and base for amidation of **2** and **3**.

Entry	B(OMe) ₃ (equiv.)	Solvent (vol.)	Base (equiv.)	Temp. (°C)	Time (h)	Unreacted 2 (%) in reaction mass	Amide (4) Yield ¹ (%)	Purity ² (%)
1	2.0	ACN (15)	TEA (2.0)	reflux	22	30.4	64.8	97.6
2	2.0	ACN (15)	K ₂ CO ₃ (2.0)	reflux	22	32.9	60.1	97.7
3	2.0	ACN (15)	NaHCO ₃ (2.0)	reflux	22	54.9	54.0	n.a.
4	2.0	THF (20)	DIPEA (2.0)	reflux	16	29.6	13.2	n.a.
5	2.0	2-Me-THF (20)	DIPEA (2.0)	reflux	21	21.4	n.a.	60.2
6	2.0	DCM (20)	DIPEA (2.0)	reflux	23	61.9	n.a.	n.a.
7	2.0	ACN (15)	DIPEA (2.0)	reflux	21	25.9	74.3	98.6

¹ Isolated yield; ² Percent purity of isolated **4** by HPLC; n.a: product not isolated.

ACN at elevated temperature followed by the addition of amine **2** and DIPEA, a drastic increase in product formation was observed leaving behind only 10–15% of unreacted amine **2**. To understand the reason behind higher conversion ratio, we conducted an investigation by trapping the reaction intermediate after reacting acid **3** and B(OMe)₃ in ACN. The solvent was distilled out completely, obtained oily residue was triturated in isopropyl ether and resultant gummy solid was analyzed by mass and NMR spectroscopy. The spectral data indicated the presence of **16** as the major constituent along with minor amounts of compounds **14** and **15** as per our primary investigation (Figure 1).

In order to confirm the structure of intermittent intermediate, the oily residue was further purified by column chromatography using ethyl acetate and *n*-heptane as the eluent over silica gel. The white crystalline solid obtained was analyzed by mass and NMR spectroscopy. The obtained spectral data confirmed the structure as methyl ester of (*R*)-mandelic acid (**16**), which was further confirmed by comparing it with methyl ester synthesized by reacting acid **3** and methanol in catalytic amounts of HCl. Further, synthesized and isolated intermediates along with reaction mixture of acid **3** and B(OMe)₃ were analyzed with HPLC using validated HPLC method and it was found that all the three components were eluted at the same

**Figure 1.** Plausible structures of intermediate during the coupling reaction.**Figure 2.** Proposed reaction mechanism for B(OMe)₃ mediated synthesis of amide **4**.

retention times confirming the proposed structure **16**. Accordingly, we propose a plausible reaction mechanism (Figure 2) wherein acid **3** reacts with $B(OMe)_3$ to form the activated borate ester intermediate **17** along with the by-product methanol. Intermediate **17** undergoes nucleophilic reaction with methanol to form **16** which couples with **2** at reflux temperature to provide amide **4** selectively and efficiently.

Based on the above findings, the progress of the reaction was monitored by HPLC for formation of **16** and its subsequent conversion to amide **4**. Further, appropriate reaction parameters were designed to achieve optimized reaction conditions (mole ratio of acid **3**, $B(OMe)_3$ and DIPEA with respect to amine **2**, volume of ACN, time and temperature) for the efficient synthesis of **4** from **2** and **3** via ester intermediate **16**.

Reacting 1.5 mol of acid **3** with 1.5 mol of $B(OMe)_3$ at 55–60 °C for 90 minutes provided quantitative conversion to **16** as monitored by HPLC. However, temperature of more than 60 °C led to the loss of $B(OMe)_3$ due to evaporation. Amine **2** (1.0 mol) and DIPEA (1.5 mol) were then added to the above resulting mixture and heated to reflux temperature for 8–10 hours. Reaction mixture was monitored for the unreacted amine **2** that was consistently found <5% after 8 to 10 hours. Once the desired conversion was achieved, solvent ACN was distilled to half of its initial volume followed by the addition of ethyl acetate and water to the resultant reaction mass. The organic layer from the above reaction mass was separated and washed with 10% HCl solution to remove unreacted amine **2** and 5% NaOH solution to remove unreacted acid **3** from the organic layer containing product **4**. By-product boric acid gets washed out easily with aqueous phase. Organic layer was distilled out completely to provide crude **4** which was recrystallized from toluene to furnish pure amide **4** with 85–87% yield and >98% purity by HPLC (Scheme 3). The experiments conducted to check the

consistency of the established optimized reaction parameters are provided in Table 2.

3. Conclusions

In conclusion, we report an efficient, scalable and economic synthesis of amide **4**, a key intermediate of mirabegron (**1**) prepared via an active ester intermediate **16**. Based on the isolation and identification of the ester intermediate **16**, a plausible mechanism for $B(OMe)_3$ mediated synthesis of amide **4** is proposed. $B(OMe)_3$ used for amide coupling in the present work is simple, cost efficient and easy to handle, therefore preferable over the other reported reagents. The developed process provided amide **4** in 85–87% yield and 98.0–99.6% purity by HPLC on kilogram scale batches, which was further used in production of mirabegron API having high purity.

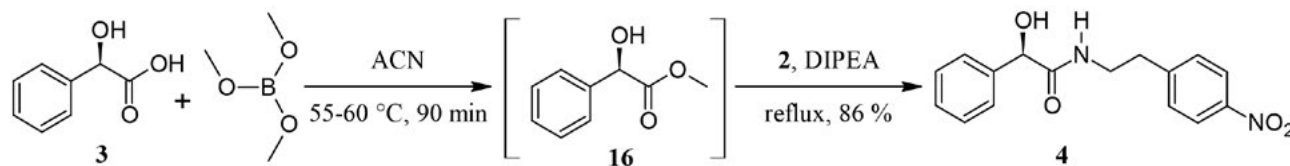
4. Experimental Section

4. 1. Materials

All chemical reagents and solvents were purchased from Megafine Pharma (P) Ltd. Vapi, R. L. Chemical Industries Pvt. Ltd., Alkali metals Ltd., OC Specialties Pvt. Ltd. & Pacific Organics Pvt. Ltd. and Imperial Chemical Corporation and used as received.

4. 2. Instrumental Analysis

The NMR spectra were recorded on Bruker Avance 300 MHz instrument in $DMSO-d_6$; the chemical shifts are reported in δ ppm relative to TMS. Related substance purity and reaction monitoring were monitored by high performance liquid chromatography (HPLC) on Agilent Technologies 1200 series.



Scheme 3. $B(OMe)_3$ mediated synthesis of amide **4**.

Table 2. Details of yield and purity after optimization for the synthesis of **4**.

Entry	$B(OMe)_3$ (equiv.)	Solvent vol. (mL)	Base (equiv.)	Temp. (°C)	Time (h)	Amide (4)	
						Yield (%)	Purity (%)
1	1.5	ACN (12)	DIPEA (1.5)	Reflux	10	85.6	99.44
2	1.5	ACN (12)	DIPEA (1.5)	Reflux	10	85.3	98.54
3	1.5	ACN (12)	DIPEA (1.5)	Reflux	10	86.4	98.90
4	1.5	ACN (12)	DIPEA (1.5)	Reflux	10	85.02	99.60

4. 3. HPLC Method for Calculating the Chemical and Assay Purity

Related substances, assay and chiral purity of mirabegron (**1**) were estimated by a gradient HPLC analysis method developed at Megafine.

a) Related substances of amide **4** was estimated by using Zorbax SB-C8, (150 × 4.6 mm ID), 3.5 μ column; buffer comprising of phosphate buffer contains 3.4 g potassium dihydrogenorthophosphate in 1000 mL of HPLC grade water sonicated to dissolve, adjusted the pH to 6.5 with triethylamine and filtered through 0.45 μm nylon filter and degased. Mobile phase-A comprising a mixture of buffer/methanol in the ratio 80:20 (v/v). Mobile phase-B comprising a mixture of acetonitrile/methanol in the ratio 80:20 (v/v); gradient elution: time (min)/A (v/v):B (v/v), T_{0'}/80:20, T_{8.0}/80:20, T_{25.0}/65:35, T_{40.0}/65:35, T_{43.0}/80:20, T_{50.0}/80:20; flow rate 1.0 mL/min, column temperature 35 °C wavelength 215 nm. The observed retention time of amide **4** under these chromatographic conditions was about 15.0 min.

b) Assay of amide **4** was estimated by using Zorbax SB-C8, (150 × 4.6 mm ID), 3.5 μ column; buffer was phosphate buffer containing 3.4 g potassium dihydrogenorthophosphate in 1000 mL of HPLC grade water, sonicated to dissolve, pH of 6.5 was adjusted with triethylamine and filtered through 0.45 μm nylon filter and degased. Mobile phase comprising of buffer/acetonitrile in the ratio 60:40 (v/v); flow rate 1.0 mL/min; column temperature 35 °C; wavelength 215 nm. The observed retention time of amide **4** under these chromatographic conditions was about 4.7 min.

4. 4. Preparation of Intermediate of (*R*)-mandelic Acid and Trimethyl Borate

A solution of (*R*)-mandelic acid (**3**, 15 g, 98.6 mmol) and trimethyl borate (10.26 g, 98.6 mmol) in acetonitrile (150 mL) was stirred at 55–60 °C. After 4.5 h TLC showed formation of a major spot, reaction mixture was adsorbed on silica gel and product was purified by column chromatography (silica gel: 60–120 mesh, eluent: 10% ethyl acetate in *n*-heptane) providing 10.1 g pure crystalline solid. ¹H NMR (300 MHz, DMSO-*d*₆): δ 7.41–7.29 (m, 5H), 6.09–6.07 (d, *J* = 5.1 Hz, 1H), 5.15–5.13 (d, *J* = 5.1 Hz, 1H), 3.6 (s, 3H). ¹H NMR (300 MHz, DMSO-*d*₆ - D₂O Exchange): δ 7.41–7.29 (m, 5H), 5.14 (s, 1H), 3.6 (s, 3H).

4. 5. Synthesis of Hydroxy-phenyl-acetic Acid Methyl Ester **16**

To a stirred solution of (*R*)-mandelic acid (**3**, 10 g, 65.7 mmol) in methanol (50 mL) was added con. HCl (4 mL) and heated to 65 °C. After maintaining at that temperature for 5 h TLC showed complete conversion of **3**, thereafter methanol was distilled out and water (100 mL) was added to the residue. To the resultant mixture was added

aq. NaHCO₃ solution and the pH was adjusted between 7 and 8. DCM (50 mL) was added and the mixture stirred for 5 min. The layers were separated, and the organic layer was washed with 10% NaHCO₃ solution (25 mL) and 5% brine (25 mL). Organic layer was concentrated to yield hydroxy-phenyl-acetic acid methyl ester **16** as a white solid (7.5 g). ¹H NMR (300 MHz, DMSO-*d*₆): δ 7.43–7.28 (m, 5H), 6.10–6.08 (d, *J* = 5.1 Hz, 1H), 5.17–5.15 (d, *J* = 5.1 Hz, 1H), 3.61 (s, 3H). ¹H NMR (300 MHz, DMSO-*d*₆ - D₂O Exchange): δ 7.41–7.29 (m, 5H), 5.14 (s, 1H), 3.6 (s, 3H).

4. 6. Preparation of (*R*)-2-hydroxy-*N*-[2-(4-nitrophenyl)ethyl]-2-phenylacetamide (**4**)

Acetonitrile (2.0 L), (*R*)-mandelic acid (**3**, 225.3 g, 1.48 mol) and trimethyl borate (153.8 g, 1.48 mol) was added into a RBF at 25–30 °C and stirred to obtain clear solution. The obtained clear solution was heated to 60 °C for 90 min. Amine (**2**, 200 g, 0.987 mol) and DIPEA (191 g, 1.48 mol) was added to the obtained solution at 60 °C and the reaction mixture was heated to reflux and stirred for 11 h. Completion of the reaction was monitored by HPLC. Acetonitrile (1.2 L) was distilled at atmospheric pressure. The concentrated reaction mixture was cooled to 25–30 °C and was diluted with ethyl acetate (1.4 L). Reaction mixture was then twice washed with 1N HCl (1.2 L and 0.8 L) followed by washing with 5% sodium hydroxide solution (1.2 L and 0.8 L). Organic layer was further washed with 10% brine solution (1.2 L) and then concentrated under vacuum below 65 °C to obtain residue. To the obtained residue toluene (1.2 L) was added, heated to 95 °C for 30 min, cooled to 20 °C and stirred for 1–2 h. Precipitated solid was filtered, washed with toluene (100 mL) and dried in a vacuum oven at 50±5 °C for 2–3 h. The dry weight of the amide **4** was 256 g (86.4% yield). Purity by HPLC: 98.9%; *m/z* [M + H]⁺ calcd. for C₁₆H₁₆N₂O₄: 300.30; found: 301. ¹H NMR (300 MHz, DMSO-*d*₆): δ 2.85–2.88 (t, 2H), 3.29–3.43 (m, 2H), 4.83–4.84 (d, 1H), 6.12–6.13 (d, 1H), 7.23–7.31 (m, 5H), 7.38–7.40 (d, 2H), 8.05–8.10 (m, 3H). ¹³C NMR (75.5 MHz, DMSO-*d*₆): δ 172.20, 147.89, 145.97, 141.33, 130.04, 127.86, 127.34, 126.59, 123.24, 73.56, 39.00, 34.77.

5. Acknowledgment

Authors thank the Management of Megafine Pharma (P) Ltd. for permission to publish this work. Authors also thank colleagues of the Analytical Research and Development team for their valuable inputs and support for this work.

6. References

1. J. Gras, *Drugs Today* **2012**, *48*, 25–32.
DOI:10.1358/dot.2012.48.1.1738056

2. T. Yamanishi, C. R. Chapple, K. Yasuda, K. Yoshida, R. Chess-Williams, *Neurourology and Urodynamics* **2003**, *22*, 338–342. DOI:10.1002/nau.10130
3. P. Tyagi, V. Tyagi, M. Chancellor, *Expert Opin. Drug Saf.* **2011**, *10.2*, 287–294. DOI:10.1517/14740338.2011.542146
4. New Class of Treatment for Overactive Bladder Approved in Europe, Astellas Pharma Europe Ltd., Chertsey, UK, 11th January 2013. https://www.astellas.com/en/corporate/news/pdf/131111_eg.pdf
5. T. Maruyama, T. Suzuki, K. Onda, M. Hayakawa, H. Morimoto, T. Kimizuka, T. Matsui, US Patent Number 6,346,532, date of patent Feb 12, **2002**.
6. S. Kawazoe, K. Sakamoto, Y. Awamura, T. Maruyama, T. Suzuki, K. Onda, T. Takasu, US Patent Number 7,342,117, date of patent Mar 11, **2008**.
7. R. Vedantham, B. Kandagatla, S. Vyala, V. V. N. K. V. Prasad Raju, P. Cherukupalli, J. Iqbal, V. H. Dahanukar, M. Kagga, R. Bandichhor, S. Oruganti, *J. Chem. Pharm. Res.* **2015**, *7*, 1473–1478.
8. L. Z. Qi, Y. Z. Zhi, D. L. Qing, M. Z. Zhan, X. Z. Fu, X. Z. Geng, *Org. Process Res. Dev.* **2016**, *20*, 1993–1996. DOI:10.1021/acs.oprd.6b00231
9. D. G. Deshmukh, M. N. Bangal, A. C. Mali, V. J. Medhane, V. T. Mathad, *Acta. Chim. Slov.* **2017**, *64*, 461–466. DOI:10.17344/acsi.2017.329
10. P. W. Tang, *Org. Synth.* **2005**, *81*, 262–272. DOI:10.15227/orgsyn.081.0262
11. K. Arnold, B. Davies, R. L. Giles, C. Grosjean, G. E. Smith, A. Witting, *Adv. Synth. Catal.* **2006**, *348*, 813–820. DOI:10.1002/adsc.200606018
12. H. Charville, D. Jackson, G. Hodges, A. Whiting, *Chem. Commun.* **2010**, *46*, 1813–1823. DOI:10.1039/b923093a
13. P. W. Tang, S. M. Dinh, P. Liu, *Org. Synth.* **2012**, *89*, 432–437. DOI:10.15227/orgsyn.089.0432
14. R. K. Mylavarapu, G. C. M. Kondaiah, N. Kolla, R. Veeramalla, P. Koikonda, A. Bhattacharya, R. Bandichhor, *Org. Process Res. Dev.* **2007**, *11*, 1065–1068. DOI:10.1021/op700098w
15. P. Starkov, T. D. Sheppard, *Org. Biomol. Chem.* **2011**, *9*, 1320–1323. DOI:10.1039/c0ob01069c
16. T. Maki, K. Ishihara, H. Yamamoto, *Org. Lett.* **2006**, *8*, 1431–1434. DOI:10.1021/ol060216r

Povzetek

V članku opisujemo raziskavo mehanistične poti amidiranja (*R*)-mandljeve kisline (**3**) s 4-nitrofeniletilaminom (**2**) pod vplivom trimetil borata, ki vodi do nastanka (*R*)-2-hidroksi-*N*-[2-(4-nitrofenil)etil]-2-fenilacetamida (**4**), intermedija v sintezi mirabegrona. Na osnovi izolacije in karakterizacije aktivnega α -hidroksiestrskega intermedija **16** iz reakcijske zmesi smo predlagali smiselen reakcijski mehanizem. Pristop z uporabo trimetil borata se je izkazal kot selektivna pot do spojine **4**, saj stranska α -hidroksi skupina reakcije ni motila, prav tako pa med reakcijo ni prišlo do racemizacije kiralnega centra. V primerjavi z doslej znanimi pristopi je opisana metoda okolju prijaznejša, bolj ekonomična in primernejša za industrijsko proizvodnjo. Metoda je hitra in učinkovita pot za pripravo **4** s celokupnim izkoristkom 85–87 % in približno 99.0 % čistočo (ugotovljeno s HPLC).

Short communication

Ultrasound Assisted 1,4-diazabicyclo[2.2.2] Octaniumdiacetate Multicomponent Synthesis of Benzodiazepines: A Novel, Highly Efficient and Green Protocol

Shahriar Sarhandi, Leila Zare Fekri* and Esmail Vessally

Department of Chemistry, Payame Noor University, PO Box 19395-3697 Tehran, Iran

* Corresponding author: E-mail: zare@pnu.ac.ir, chem_zare@yahoo.com

Received: 30-07-2017

Abstract

A simple and efficient method is presented for the synthesis of benzodiazepines through the multicomponent reaction of *o*-phenylenediamine, various aldehydes and 5,5-dimethylcyclohexane-1,3-dione (dimedone) in the presence of the acidic bis ionic liquid 1,4-diazabicyclo[2.2.2]octanium diacetate under ultrasound irradiation. The ionic liquid used is recoverable and reusable. This procedure is simple and environmentally friendly, and offers easy work-up, mild conditions and excellent yield in a short reaction time. All of the synthesized compounds were characterized by IR, ¹H NMR, mass spectrometry and elemental analysis.

Keywords: Dimedone, benzodiazepines, ionic liquid, green chemistry

1. Introduction

Benzodiazepine rings are important building blocks of heterocyclic and pharmaceutical compounds because they are anti-inflammatory, antidepressive, anticonvulsant, antiviral, antimicrobial, anti-HIV, antianxiety, anti-ulcerative, antitumor, analgesic, antihistaminic, anti-allergic, hypnotic and antipyretic.^{1–7} Some benzodiazepines are used in industry as dyes.⁸ Others are useful precursors for the synthesis of fused-ring compounds such as oxazino-, triazolo-, tetrazolo-, oxadiazolo- and furanobenzodiazepines.^{9–12}

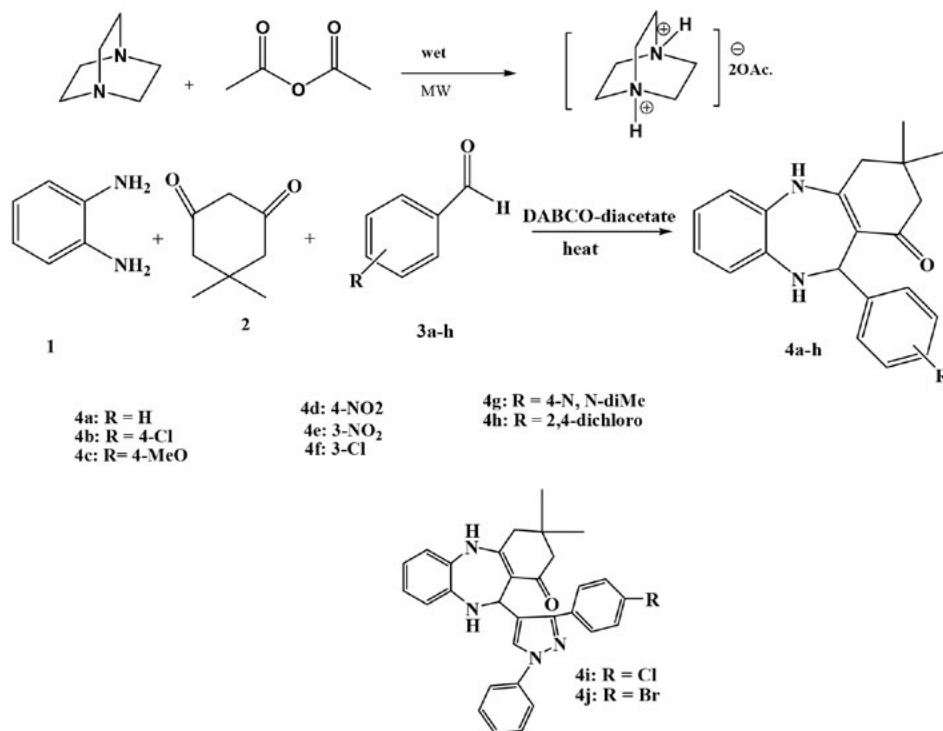
Benzodiazepines are generally synthesized by the reaction of β -haloketones with *o*-phenylenediamine,¹³ condensation of α,β -unsaturated compounds with *o*-phenylenediamines¹⁴ and condensation of ketones with *o*-phenylenediamine in the presence of ytterbium trichloride.¹⁵ The disadvantages of previously reported procedures for the synthesis of benzodiazepines are their multi-step reactions, anhydrous conditions, tedious work-up, long reaction times and generation of undesirable by-products.^{16–18}

Multicomponent reactions (MCRs) are efficient tools in modern synthetic organic chemistry because they are fast, simple, offer high-atomic efficiency, are environ-

mentally friendly and save time and energy.^{19–23} On the other hand, ionic liquids are suitable compounds because they are non-flammable, non-volatile, soluble, exhibit polarity and are highly thermal and chemically stable.²⁴ MCRs combined with ionic liquid can assist in the synthesis of the benzodiazepines to reduce the cost of starting materials and decrease the generation of undesirable by-products. In continuation of our studies on the green synthesis of organic materials,^{25–29} some derivatives of benzodiazepine were synthesized using the ionic liquid 1,4-diazabicyclo[2.2.2]octaniumdiacetate (DABCO-diacetate) under ultrasound irradiation in an MCR.

2. Results and Discussion

The MCR of benzaldehyde, 5,5-dimethylcyclohexane-1,3-dione (dimedone) and *o*-phenylenediamine is essentially a condensation reaction. The reaction rate can be increased either by activating the carbonyl group of aldehydes using acidic reagents or using a strong nucleophilic dimedone derivative in basic media. In the current study, we used the acidic bis ionic liquid DABCO-diacetate as green media for the synthesis of benzodiazepines in a condensation reaction of *o*-phenylenediamine, aldehydes and/or dimedone (Scheme 1).



Scheme 1. Multicomponent synthesis of benzodiazepines in the presence of DABCO-diacetate.

Initially, a sample reaction was carried out using 4-nitrobenzaldehyde (1mmol) **3d**, *o*-phenylenediamine **1** (1 mmol) and dimedone **2** (1 mmol) in DABCO-diacetate as an efficient catalyst for the synthesis of benzodiazepines **4a**. This protocol proceeded smoothly at room temperature to afford product **4a** in a fairly high yield. The reactions were also carried out using the neutral ionic liquids [BMIM]Br and [BMIM]BF₄ or in the absence of ionic liquids for purpose of comparison with our target reaction. It was interesting to note that the sample reaction did not proceed in the presence or absence of imidazolium ionic liquids, confirming the important role of DABCO-diacetate in the synthesis of benzodiazepines.

To optimize the amount of ionic liquid media required for this reaction, a sample reaction was carried out

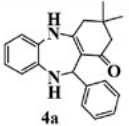
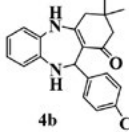
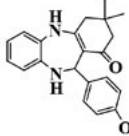
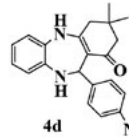
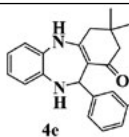
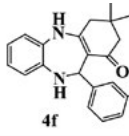
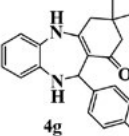
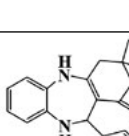
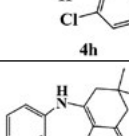
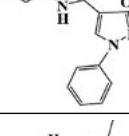
using different quantities of ionic liquid. The best results were obtained with 0.5 mmol of DABCO-diacetate per 1 mmol of substrate. For further investigation, the reaction between 4-nitrobenzaldehyde, *o*-phenylenediamine and dimedone was done in the presence of a catalytic amount of DABCO-diacetate at different temperatures. When the reaction was performed at room temperature, product **4a** formed smoothly at a low yield. To achieve better results, the temperature was increased to 90 °C and benzodiazepine **4a** was obtained at a yield of 82%. The results are summarized in Table 1.

Recently, ultrasound irradiation has been introduced as a useful, clean and mild protocol for organic synthesis. The well-known features of ultrasound-assisted reactions are formation of purer products at high yields, increased

Table 1. Optimization of reaction conditions.

entry	catalyst	Catalyst amount (mmol)	Reaction conditions	Time (min)	Yield (%)
1	–	–	Reflux in EtOH	720	–
2	[BMIM]Br	0.5	Stir, rt	720	11
3	[BMIM]BF ₄	0.5	Stir,rt	720	7
4	DABCO-diacetate	0.5	Stir, rt	240	86
5	DABCO-diacetate	0.3	Stir, rt	90	81
6	DABCO-diacetate	0.7	Stir, rt	90	87
7	DABCO-diacetate	0.5	Heat, 90°C	60	89
8	DABCO-diacetate	0.5	Ultrasound, rt	8	98
9	DABCO-diacetate	0.5	Ultrasound, 40 °C	8	96
10	DABCO-diacetate	0.5	Ultrasound, 60 °C	6	97

Table 2. Synthesis scope of benzodiazepines 4a–j.

entry	product	Heat, 90 °C		Ultrasound, rt		Mp (°C)	
		Time (min)	Yield (%) ^{a,b}	Time (min)	Yield (%) ^{a,b}	found	reported
1		75	82	10	95	248–250	251–252 ¹⁸
2		60	84	8	97	238–240	239–240 ¹⁸
3		60	85	8	96	198–200	203–205 ¹⁸
4		60	89	8	98	271–273	274–275 ¹⁸
5		75	88	10	95	262–264	–
6		75	89	10	96	248–250	–
7		90	85	12	93	231–232	232–233 ³⁰
8		90	83	15	94	198–200	203–205 ¹⁸
9		90	81	17	94	209–210	–
10		60	82	6	95	245–247	–

^a Isolated yield. ^b Products characterized by comparison of spectroscopic and physical data with those of samples synthesized using proposed procedures.

selectivity, enhanced reaction rates, easier experimental procedures and cleaner reactions. For these reasons, we were interested in the synthesis of benzodiazepines under ultrasound irradiation at various temperatures. The results are summarized in Table 1. Ultrasonic irradiation at room temperature was the best choice to shorten the reaction times and enhance productivity. The reaction scope was checked using various aromatic aldehydes for reaction with **1** and **2** under optimized conditions. The results are summarized in Table 2.

As shown in Table 2, the reaction under ultrasound irradiation at room temperature afforded products in shorter reaction times at higher yields. The structures of products **4a–j** were characterized by IR, ^1H NMR, mass spectroscopy, elemental analysis and by comparison of their melting points with those of available authentic samples.

A reasonable mechanism for the formation of benzodiazepines is shown in Scheme 2. Initially, DABCO-diacetate can increase the electrophilic character of the carbonyl species through its inherent Brønsted acidity under ultrasound irradiation. Because the ionic liquid can polarize the carbonyl group of aldehyde, the nucleophilic addition of dimedone **2** and subsequent dehydration led to intermediate **6**. The Michael addition reaction between **1** and **6** afforded intermediate **7**, followed by simple condensation of the amino group with carbonyl and dehydration, leading to product **4**.

3. Experimental

Melting points were measured on an Electrothermal 9100 apparatus. The IR spectra were determined using a Shimadzu IR-470 spectrometer. The ^1H NMR spectra were recorded on a 400 MHz Bruker DRX-400 using CDCl_3 as

the solvent and TMS as the internal standard. The chemicals were purchased from Merck and Fluka. Elemental analysis was done on a Carlo-Erba EA1110CNNO-S analyzer and the results agreed with the calculated values. All solvents used were dried and distilled according to standard procedures. For the ultrasound reactions, an Astra 3D ultrasound apparatus (9.5 dm³, 45 kHz frequency, input power with heating at 305 W, 2 transducers) from Techno-Gaz was used.

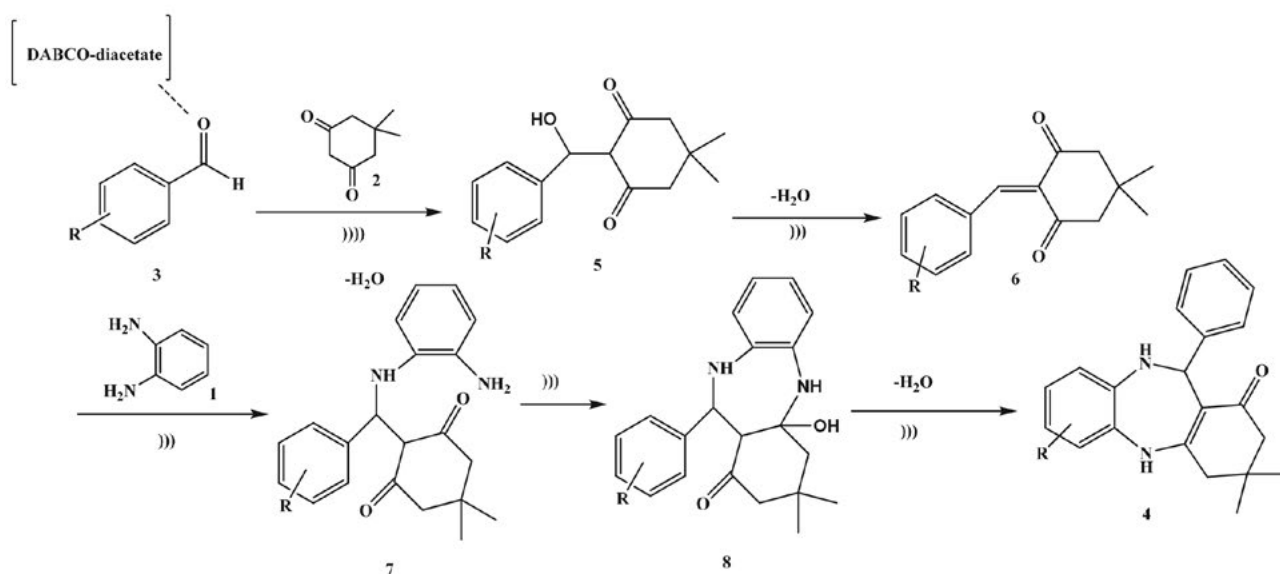
3. 1. Synthesis of DABCO-diacetate

This ionic liquid was synthesized as already described by Fekri et al.^{27–29}

A mixture of 1,4-diaza-bicyclo[2.2.2]octane (10 mmol) and acetic acid (20 mmol) was irradiated using microwave (180 W) for 2 min at 100 °C three times. After completion of the reaction, the mixture was washed with diethyl ether (3×10 mL). The organic product was extracted from the liquid phase and evaporated under vacuum to produce the desired ionic liquid. The analytical data for DABCO-diAc is as follows: yellow oil; ^1H NMR (400 MHz, CDCl_3) δ 2.16 (s, 2H); 3.01 (s, 12H); 14.11 (s, 2H) ppm; ^{13}C NMR (100 MHz, CDCl_3) δ 21.95; 44.54, 175.87 ppm.

3. 2. General Procedure for Synthesis of Benzodiazepines

A mixture of appropriate *o*-phenyldiamine (1 mmol), the corresponding aldehydes (1 mmol), dimedone and DABCO-diacetate (0.5 mmol) was placed into a Pyrex open vessel and irradiated in a water bath under silent conditions by ultrasound (45 kHz) at room temperature for the required reaction times as indicated in Table 2. Af-



Scheme 2. Plausible mechanistic method for synthesis of benzodiazepines.

ter completion of the reaction, as indicated by TLC, the reaction mixture was dissolved in 20 mL of H₂O. The product was separated by filtration, recrystallized from EtOH and dried to afford the crystalline compounds **4a–j**. The ionic liquid was recovered for subsequent use. All synthesized compounds were characterized by their physical constant, IR, ¹H NMR, mass spectroscopy and elemental analysis.

3,3-dimethyl-11-phenyl-2,3,4,5,10,11-hexahydro-1H-dibenzo [b,e][1,4]diazepin-1-one (4a): Off white solid; mp: 248–250 °C (reported 251–252 °C),¹⁸ IR (KBr): ν 3473 (N-H stretch), 2987, 1727 (C=O stretch), 1606 (C=C aromatic), 1537, 1346, 1206 cm⁻¹; ¹H NMR (400 MHz, CDCl₃): δ 1.09 (s, 6H, CH₃), 2.2 (s, 2H, CH₂), 2.4 (s, 2H, CH₂), 5.05 (s, 1H, C-H), 6.73–6.87 (m, 5H, Ar), 7.09 (d, *J* = 8.2 Hz, 2H, Ar), 7.37 (t, *J* = 7.8 Hz, 2H, Ar) ppm. HR-MS (*m/z* 334). Anal. calcd. for C₂₂H₂₆N₂O: C, 79.00; H, 7.84; N, 8.38. Found: C, 79.04; H, 7.86; N, 8.36.

11-(4-chlorophenyl)-3,3-dimethyl-2,3,4,5,10,11-hexahydro-1H-dibenzo [b,e][1,4]diazepin-1-one (4b): Off white solid; mp: 238–240 °C (reported 239–240 °C),¹⁸ IR (KBr): ν 3314 (N-H stretch), 3098, 2956, 1732 (C=O stretch), 1612 (C=C aromatic), 1476, 1343, 1098 (C-Cl stretch) cm⁻¹; ¹H NMR (400 MHz, CDCl₃): δ 1.09 (s, 6H, CH₃), 2.3 (s, 4H, CH₂), 5.05 (s, 1H, C-H), 6.68 (d, *J* = 8.4 Hz, 2H, Ar), 6.87–6.93 (m, 2H, Ar), 7.15 (d, *J* = 8.0 Hz, 2H, Ar), 7.86 (d, *J* = 8.4 Hz, 2H, Ar) ppm. HR-MS (*m/z* 352). Anal. calcd. for C₂₁H₂₁ClN₂O: C, 71.48; H, 6.00; N, 7.94. Found: C, 71.50; H, 6.06; N, 7.96.

11-(4-methoxyphenyl)-3,3-dimethyl-2,3,4,5,10,11-hexahydro-1H-dibenzo [b,e][1,4]diazepin-1-one (4c): Off white solid; mp: 198–200 °C (reported 203–205 °C),¹⁸ IR (KBr): ν 3232 (N-H stretch), 3018, 2983, 1743 (C=O stretch), 1609 (C=C stretch), 1465, 1328, 1248 (C-O stretch), 1011 cm⁻¹; ¹H NMR (400 MHz, CDCl₃): δ 1.03 (s, 6H, CH₃), 1.92 (s, 4H, CH₂), 3.82 (s, 3H, OCH₃), 5.12 (s, 1H, N-H), 7.29–7.34 (m, 2H, Ar), 7.66–7.70 (m, 3H, Ar), 8.27 (d, *J* = 8.4 Hz, 1H, Ar), 8.53 (d, *J* = 8.0 Hz, 1H, Ar), 8.87 (t, *J* = 1.6 Hz, 1H, Ar) ppm. HR-MS (*m/z* 348). Anal. calcd. for C₂₂H₂₄N₂O₂: C, 75.83; H, 6.94; N, 8.04. Found: C, 75.80; H, 6.98; N, 8.06.

3,3-dimethyl-11-(4-nitrophenyl)-2,3,4,5,10,11-hexahydro-1H-dibenzo [b,e][1,4]diazepin-1-one (4d): White solid; mp: 271–273 °C (reported 274–275 °C),¹⁸ IR (KBr): ν 3214 (N-H stretch), 3098, 2956, 1731 (C=O stretch), 1609 (C=C aromatic), 1567 (NO₂ stretch), 1445, 1324 (NO₂ stretch), 1129 cm⁻¹; ¹H NMR (400 MHz, CDCl₃): δ 1.13 (s, 6H, CH₃), 1.89 (s, 4H, CH₂), 5.08 (s, 1H, N-H), 6.87 (d, *J* = 8.2 Hz, 2H, Ar), 7.11 (t, *J* = 7.5 Hz, 1H, Ar), 7.23–7.32 (m, 3H, Ar), 7.67 (d, *J* = 8.2 Hz, 2H, Ar) ppm. HR-MS (*m/z* 379). Anal. calcd. for C₂₁H₂₁N₃O₃: C, 69.41; H, 5.82; N, 11.56. Found: C, 69.40; H, 5.88; N, 11.56.

3,3-dimethyl-11-(3-nitrophenyl)-2,3,4,5,10,11-hexahydro-1H-dibenzo [b,e][1,4]diazepin-1-one (4e): Off white solid; mp: 262–264 °C, IR (KBr): ν 3314 (N-H stretch), 2987, 1742 (C=O stretch), 1600 (C=C aromatic), 1543 (NO₂ stretch), 1456, 1387 (NO₂ stretch), 1243 cm⁻¹; ¹H NMR (400 MHz, CDCl₃): δ 0.91 (s, 6H, CH₃), 2.17 (s, 4H, CH₂), 5.09 (s, 1H, N-H), 7.16 (s, 1H, Ar), 7.32 (d, *J* = 8.6 Hz, 2H, Ar), 7.73 (d, *J* = 8.1 Hz, 1H, Ar), 8.05–8.17 (m, 3H, Ar), 8.43 (d, *J* = 7.8 Hz, 1H, N-H) ppm. HR-MS (*m/z* 379). Anal. calcd. for C₂₁H₂₁N₃O₃: C, 69.41; H, 5.82; N, 11.56. Found: C, 69.45; H, 5.85; N, 11.59.

3,3-dimethyl-11-(3-chlorophenyl)-2,3,4,5,10,11-hexahydro-1H-dibenzo [b,e][1,4]diazepin-1-one (4f): White solid; mp: 248–250 °C, IR (KBr): ν 3231 (N-H), 3089, 2987, 1738 (C=O stretch), 1604 (C=C stretch), 1565, 1450, 1242, 1123 (C-Cl stretch) cm⁻¹; ¹H NMR (400 MHz, CDCl₃): δ 0.97 (s, 6H, CH₃), 2.1 (s, 4H, CH₂), 5.10 (s, 1H, C-H), 7.53 (t, *J* = 7.6 Hz, 2H, Ar), 7.66 (d, *J* = 7.6 Hz, 2H, Ar), 8.08–8.12 (m, 1H, Ar), 8.15–8.17 (m, 2H, Ar), 8.20–8.23 (m, 1H) ppm. HR-MS (*m/z* 352). Anal. calcd. for C₂₁H₂₁ClN₂O: C, 71.48; H, 6.00; N, 7.94. Found: C, 71.51; H, 6.03; N, 7.96.

11-(4-(dimethylamino)phenyl)-3,3-dimethyl-2,3,4,5,10,11-hexahydro-1H-dibenzo [b,e][1,4]diazepin-1-one (4g): White solid; mp: 231–232 °C (reported 232–233 °C),³⁰ IR (KBr): ν 3423 (N-H stretch), 2956, 1735 (C=O stretch), 1601 (C=C stretch), 1463, 1360, 1228, 1145 cm⁻¹; ¹H NMR (400 MHz, CDCl₃): δ 0.96 (s, 6H, CH₃), 2.07 (s, 2H, CH₂), 2.32 (s, 2H, CH₂), 2.56 (s, 6H, N(CH₃)₂), 5.04 (s, 1H, C-H), 7.01–7.03 (m, 2H, Ar), 7.55–7.57 (m, 2H, Ar), 7.73 (dd, *J* = 3.2 Hz, *J* = 5.6 Hz, 1H, Ar), 7.85 (d, *J* = 8.4 Hz, 2H, Ar) ppm. HR-MS (*m/z* 361). Anal. calcd. for C₂₃H₂₇N₃O: C, 76.42; H, 7.53; N, 11.62. Found: C, 76.46; H, 7.53; N, 11.66.

11-(2,4-dichlorophenyl)-3,3-dimethyl-2,3,4,5,10,11-hexahydro-1H-dibenzo [b,e][1,4]diazepin-1-one (4h): Off white solid; mp: 198–200 °C (reported 203–205 °C),¹⁸ IR (KBr): ν 3312 (N-H stretch), 3109, 2987, 1743 (C=O stretch), 1457, 1358, 1192 (C-Cl stretch) cm⁻¹; ¹H NMR (400 MHz, CDCl₃): δ 0.98 (br s, 6H, CH₃), 1.85 (d, *J* = 7.2 Hz, 2H, CH₂), 2.47 (d, *J* = 28.7 Hz, 2H, CH₂), 5.30 (s, 1H, C-H), 7.09–7.14 (m, 1H, Ar), 7.17–7.19 (m, 1H, Ar), 7.20–7.22 (m, 1H, Ar), 7.23–7.29 (m, 2H, Ar), 7.53–7.55 (m, 1H, Ar), 7.75–7.79 (m, 1H, Ar) ppm. HR-MS (*m/z* 386). Anal. calcd. for C₂₁H₂₀Cl₂N₂O: C, 65.12; H, 5.20; N, 7.23. Found: C, 65.10; H, 5.23; N, 7.23.

11-(3-(4-chlorophenyl)-1-phenyl-1H-pyrazol-4-yl)-3,3-dimethyl-2,3,4,5,10,11-hexahydro-1H-dibenzo [b,e][1,4]diazepin-1-one (4i): White solid; mp: 209–210 °C, IR (KBr): ν 3652 (N-H stretch), 2956, 1733 (C=O stretch), 1608 (C=C stretch), 1460, 1375, 1259, 1097 (C-Cl stretch) cm⁻¹; ¹H NMR (400 MHz, CDCl₃): δ 1.05 (s, 6H, CH₃),

2.20 (s, 2H, CH₂), 2.30 (s, 2H, CH₂), 5.05 (s, 1H, C-H), 6.71–6.82 (m, 3H, Ar), 7.01 (s, 3H, Ar), 7.35–7.41 (m, 1H, Ar), 7.44 (s, 1H, Ar), 7.54–7.56 (m, 2H, Ar), 7.71–7.78 (m, 2H, Ar), 7.87 (d, *J* = 8.8 Hz, 2H, Ar) ppm. HR-MS (*m/z* 494). Anal. calcd. for C₃₀H₂₇ClN₄O: C, 72.79; H, 5.50; N, 11.32. Found: C, 72.75; H, 5.536; N, 11.33.

11-(3-(4-bromophenyl)-1-phenyl-1H-pyrazol-4-yl)-3,3-dimethyl-2,3,4,5,10,11-hexahydro-1H-dibenzo[b,e][1,4]diazepin-1-one (4j) White solid; mp: 245–247 °C, IR (KBr): ν 3431 (N-H stretch), 2956, 1733 (C=O stretch), 1593 (C=C stretch), 1460, 1375, 1093 (C-Br stretch) cm⁻¹; ¹H NMR (400 MHz, CDCl₃): δ 0.97 (s, 6H, CH₃), 2.30 (s, 4H, CH₂), 5.05 (s, 1H, C-H), 7.01 (s, 2H, Ar), 7.39 (t, *J* = 7.2 Hz, 2H, Ar), 7.50–7.51 (m, 2H, Ar), 7.52–7.53 (m, 2H, Ar), 7.55–7.57 (m, 1H, Ar), 7.70–7.72 (m, 2H, Ar), 7.83 (d, *J* = 8.0 Hz, 3H, Ar) ppm. HR-MS (*m/z* 538). Anal. calcd. for C₃₀H₂₇BrN₄O: C, 66.79; H, 5.04; N, 10.39. Found: C, 66.76; H, 5.00; N, 10.38.

4. Conclusion

In conclusion, DABCO-diacetate was used under ultrasound irradiation as a mild and efficient protocol for synthesis of diazepines. This method can be very useful for synthesis because it offers a high yield and decreased reaction time. DABCO-diacetate is inexpensive, non-toxic and easy to handle, and can act as green media. Its simple work-up procedure, short reaction time and high yield of the product are additional advantages of this protocol.

5. Acknowledgement

Financial support from the Research Council of Payame Noor University of Rasht and Zanjan is gratefully acknowledged.

6. References

- G. Roma, G. C. Grossi, M. Di Braccio, M. Ghia, F. Mattioli, *Eur. J. Med. Chem.* **1991**, 26, 489–496. DOI:10.1016/0223-5234(91)90144-C
- B. Narayana, K. K. Vijaya Raj, B. V. Ashalatha, N. Suchetha Kumari, *Eur. J. Med. Chem.* **2006**, 41, 417–422. DOI:10.1016/j.ejmech.2005.12.003
- J. R. Kavali, B. V. Badami, *Farmaco* **2000**, 55, 406–409. DOI:10.1016/S0014-827X(00)00061-6
- R. Kumar, Y. C. Joshi, *Arkivoc* **2007**, 142–149.
- M. Di Braccio, G. C. Grossi, G. Roma, L. Vargiu, M. Mura, M. E. Marongiu, *Eur. J. Med. Chem.* **2001**, 36, 935–949. DOI:10.1016/S0223-5234(01)01283-1
- A. Kamal, N. Shankaraiah, S. Prabhakar, C. R. Reddy, N. Markandeya, K. Laxma, X. Devaiah, *Bioorg. Med. Chem. Lett.* **2008**, 18, 2434–2439. DOI:10.1016/j.bmcl.2008.02.047
- (a) H. Al Muhaimed, *J. Int. Med. Res.* **1997**, 25, 175–181; DOI:10.1177/030006059702500401
(b) L. J. Scott, C. J. Dunn, G. Mallarkey, M. Sharpe, *Drugs* **2002**, 62, 1503–1538; DOI:10.2165/00003495-200262100-00006
(c) H. Nakano, T. Inoue, N. Kawasaki, H. Miyataka, H. Matsumoto, T. Taguchi, N. Inagaki, H. Nagai, T. Satoh, *Bioorg. Med. Chem.* **2000**, 8, 373–380; DOI:10.1016/S0968-0896(99)00291-6
(d) G. Cohn, *Ber.* **1899**, 32, 2242–2254. DOI:10.1002/cber.189903202152
- R. C. Haris, J. M. Straley, 1968, US Patent 1,537,757. Chem. Abstr.1970, 73, 100054w.
- A. M. El-Sayed, H. Abdel-Ghany, A. M. M. El-Saghier, *Synth. Commun.* **1999**, 29, 3561–3572. DOI:10.1080/00397919908085990
- Ch.- W. Kuo, Ch.- Ch. Wang, V. Kavala, Ch.- F. Yao, *Molecules* **2008**, 13, 2313–2325.
- S. Gunawan, M. Ayaz, F. De Moliner, B. Frett, Ch. Kaiser, N. Patrick, Zh. Xu, Ch. Hulme, *Tetrahedron.* **2012**, 68, 5606–5611. DOI:10.1016/j.tet.2012.04.068
- S. Sharma, D. N. Prasad, R. K. Singh, *J. Chem. Pharm. Res.* **2011**, 3, 382–389.
- W. Ried, E. Torinus, *Chem. Ber.* **1959**, 92, 2902–2916. DOI:10.1002/cber.19590921138
- P. Stahlhofen, W. Ried, *Chem. Ber.* **1957**, 90, 815–824. DOI:10.1002/cber.19570900528
- J. Wu, F. Xu, Zh. Zhou, Q. Shen, *Synth. Commun.* **2006**, 36, 457–464. DOI:10.1080/00397910500383527
- (a) J. Fu, S. J. Shuttleworth, R. V. Connors, A. Chai, Coward, *P. Bioorg. Med. Chem. Lett.* **2009**, 19, 4264–4267. DOI:10.1016/j.bmcl.2009.05.124
(b) D. McGowan, O. Nyanguile, M. D. Cummings, S. Vendeveille, K. Vandyck, W. Van den Broeck, C. W. Boutton, H. De Bondt, L. Quirynen, K. Amssoms, J. Fr. Bonfanti, S. Last, K. Rombauts, A. Tahri, L. Hu, F. Delouvroy, K. Vermeiren, G. Vandercruyssen, L. Van der Helm, E. Cleiren, W. Mostmans, P. Lory, G. Pille, K. Van Emelen, G. Fanning, F. Pauwels, T.-I. Lin, K. Simmen, P. Raboisson, *Bioorg. Med. Chem. Lett.* **2009**, 19, 2492–2496. DOI:10.1016/j.bmcl.2009.03.035
- (a) L. Yu. Ukhin, K. Yu. Suponitskii, E. N. Shepelenko, L. V. Belousova, Zh. I. Orlova, G. S. Borodkin, *Russ. Chem. Bullet.* **2011**, 60, 1729–1733. DOI:10.1007/s11172-011-0258-9
(b) E. C. Cortés, M. A. Baños, O. G.-M. De Cortés, *J. Heterocycl. Chem.* **2004**, 41, 277–280. DOI:10.1002/jhet.5570410221
(c) E. C. Cortes, O. E. A. Meneses, O. Garcia-Mellado, O. C. Zuniga, E. B. Naranjo-Rodriguez, *J. Heterocycl. Chem.* **2009**, 46, 1113–1118. DOI:10.1002/jhet.159
(d) E. Cortes Cortes, A. M. Hernandez Sanabria, O. Garcia-Mellado, *J. Heterocycl. Chem.* **2002**, 39, 55–59. DOI:10.1002/jhet.5570390107
(e) E. C. Cortes, A. L. V. Cornejo, G.-M. O. de Cortes, *J. Heterocycl. Chem.* **2007**, 44, 183–187. DOI:10.1002/jhet.5570440128

18. N. N. Kolos, E. N. Yurchenko, V. D. Orlov, S. V. Shishkina, O. V. Shishkin, *Chem. Heterocycl. Compd.* **2004**, *40*, 1550–1559. DOI:10.1007/s10593-005-0098-3
19. L. Moradi, M. Aghamohammad Sadegh, *Acta. Chim. Slov.* **2017**, *64*, 506–512. DOI:10.17344/acsi.2017.3417
20. A. Z. Halimehjani, I. N. Namboothiri, S. E. Hooshmand, *RSC Adv.* **2014**, *4*, 48022–48084.
21. A. Z. Halimehjani, I. N. Namboothiri, S. E. Hooshmand, *RSC Adv.* **2014**, *4*, 51794–51829.
22. V. Estévez, M. Villacampa, J. C. Menéndez, *Chem. Soc. Rev.* **2014**, *43*, 4633–4637. DOI:10.1039/C3CS60015G
23. M. A. Ghasemzadeh, M. H. Abdollahi-Basir, *Acta. Chim. Slov.* **2016**, *63*, 627–637. DOI:10.17344/acsi.2016.2386
24. T. Welton, *Chem. Rev.* **1999**, *99*, 2071–2084. DOI:10.1021/cr980032t
25. L. Z. Fekri, M. Nikpassand, R. Maleki, *J. Mol. Liq.* **2016**, *222*, 77–81. DOI:10.1016/j.molliq.2016.07.009
26. L. Z. Fekri, H. S. Fard, *Acta. Chim. Slov.* **2016**, *63*, 263–270. DOI:10.17344/acsi.2015.2096
27. L. Z. Fekri, M. Movaghari, *Lett. Org. Chem.* **2016**, *13*, 406–413. DOI:10.2174/1570178613666160524160125
28. L. Zare, N. O. Mahmoodi, A. Yahyazadeh, M. Nikpassand, *Ultrason. Sonochem.* **2012**, *19*, 740–744. DOI:10.1016/j.ultsonch.2011.11.008
29. L. Zare Fekri, M. Nikpassand, *Lett. Org. Chem.* **2017**, *14*, 494–502.
30. X.-T. Zhu, J. -Y. Liu, B. Jiang, Sh. -J. Tu. *J. Hetero. Chem.* **2015**, *52*, 92–96. DOI:10.1002/jhet.1988

Povzetek

V prispevku je predstavljena enostavna in učinkovita metoda priprave benzodiazepinov v večkomponentni reakciji *o*-fenilendiamina, različnih aldehydov in 5,5-dimetilcikloheksan-1,3-diona (dimedona) v prisotnosti kisle bis ionske tekočine 1,4-diazabicyclo[2.2.2]oktanijevega diacetata, z uporabo ultrazvoka. Uporabljeno ionsko tekočino lahko regeneriramo in ponovno uporabimo. Metoda je enostavna in okolju prijazna, omogoča enostavno izolacijo, mile reakcijske pogoje in odličen izkoristek v kratkem reakcijskem času. Vse pripravljene spojine so bile okarakterizirane z IR, ¹H NMR in masno spektrometrijo ter elementno analizo.

DRUŠTVENE VESTI IN DRUGE AKTIVNOSTI SOCIETY NEWS, ANNOUNCEMENTS, ACTIVITIES

Vsebina

Doktorska in magistrska dela, diplome v letu 2017	S3
Koledar važnejših znanstvenih srečanj s področja kemije, kemijske tehnologije in kemijskega inženirstva	S31
Navodila za avtorje	S38

Contents

Doctoral theses, master degree theses, and diplomas in 2017	S3
Scientific meetings – chemistry, chemical technology and chemical engineering	S31
Instructions for authors	S38

UNIVERZA V LJUBLJANI
FAKULTETA ZA KEMIJO IN KEMIJSKO TEHNOLOGIJO

1. januar – 31. december 2017

DOKTORATI

DOKTORSKI ŠTUDIJSKI PROGRAM KEMIJSKE ZNANOSTI

KEMIJA

Miha KASTELIC

VPLIV DODANE SOLI NA STABILNOST RAZTOPIN
GLOBULARNIH PROTEINOV V VODI
Mentor: prof. dr. Vojeslav Vlachy
Datum zagovora: 29. 3. 2017

Vojč KOČMAN

STRUKTURNE ŠTUDIJE Z GVANINI BOGATIH
OLIGONUKLEOTIDOV POVEZANIH Z AVTIZMOM
Mentor: prof. dr. Janez Plavec
Datum zagovora: 9. 6. 2017

Andreja PONDELAK

UTRJEVANJE MINERALNIH POVRŠIN S TOPNIMI
ZEMELJSKOALKALIJSKIMI SPOJINAMI
Mentorica: doc. dr. Andrijana Sever Škapin
Somentorica: izr. prof. dr. Romana Cerc Korošec
Datum zagovora: 22. 6. 2017

Eva PUŠAVEC KIRAR

CIKLOADICIJE (S)-A-AMINOALKIL INONOV IN ENONOV
Mentor: prof. dr. Jurij Svete
Datum zagovora: 23. 6. 2017

Darja MAUČEC

RAZVOJ POROZNIH KATALIZATORJEV ZA RAZGRADNJO
BARVIL V ODPADNIH VODAH Z NAPREDNIMI
OKSIDACIJSKIMI PROCESI
Mentorica: prof. dr. Nataša Novak Tušar
Somentor: prof. dr. Anton Meden
Datum zagovora: 11. 7. 2017

BIOKEMIJA

Valerija KOVAČ

STRUKTURNE IN FIZIKALNOKEMIJSKE LASTNOSTI
SKRAJŠANE OBLIKE ČLOVEŠKEGA PRIONSKEGA
PROTEINA PrP226*
Mentorica: prof. dr. Vladka Čurin Šerbec
Somentor: prof. dr. Janez Plavec
Datum zagovora: 10. 5. 2017

Vid PUŽ

STRUKTURNI VPOGLED V INTERAKCIJE PROTEINOV
Z-DISKA
Mentorica: prof. dr. Kristina Djinović Carugo
Datum zagovora: 3. 10. 2017

KEMIJSKO INŽENIRSTVO

Natalija RAVBER

EMULZIJSKA KOPOLIMERIZACIJA BUTIL
POLIGLUKOZIDNEGA ESTRA MALEINSKE KISLINE
Mentor: prof. dr. Matjaž Krajnc
Datum zagovora: 10. 4. 2017

Gregor KRIŽAN

SINTEZA LITIJEVIH INSERCIJSKIH MATERIALOV V
REAKTORJU S TERMOAKUSTIČNIM GORILNIKOM
Mentor: prof. dr. Miran Gaberšček
Datum zagovora: 17. 11. 2017

Simona GOLOB

METODOLOGIJA DOLOČITVE KRITERIJEV
SPREJEMLJIVOSTI TVEGANJA ZA OBRATE SEVESO
Mentor: doc. dr. Mitja Robert Kožuh
Somentor: prof. dr. Peter Bukovec
Datum zagovora: 28. 6. 2017

MAGISTRSKI ŠTUDIJI

MAGISTRSKI ŠTUDIJSKI PROGRAM 2. STOPNJE - KEMIJA

Gašper ŽAKELJ

TEORETIČNE RAZISKAVE SOLVATACIJE NEPOLARNEGA
TOPLJENCA V METANOLU
Mentor: izr. prof. dr. Tomaž Urbič
Datum zagovora: 6. 1. 2017

Mojca VENE

METODE ZA DOLOČANJE KONCENTRACIJE
ANTIKOAGULANTA
Mentorica: izr. prof. dr. Nataša Gros
Datum zagovora: 30. 1. 2017

Tanja LIPEC

SINTEZA IN KARAKTERIZACIJA PROTIRAKAVIH
ORGANORUTENIJEVIH SPOJIN Z B-DIKETONATI
Mentor: prof. dr. Iztok Turel
Datum zagovora: 10. 2. 2017

Mateja KOŽAR

SINTEZA IN KARAKTERIZACIJA KOORDINACIJSKIH
SPOJIN NEKATERIH KOVIN 3D BLOKA Z N- IN/ALI
O-DONORSKIMI LIGANDI
Mentor: izr. prof. dr. Boris Čeh
Datum zagovora: 24. 2. 2017

Luka HRIBERNIK

AEROBNO OKSIDATIVNO HALOGENIRANJE TIOLOV S
HCl/HBr V PRISOTNOSTI NH₄NO₃
Mentor: izr. prof. dr. Marjan Jereb
Datum zagovora: 7. 3. 2017

Rebeka CIGALE

OPTIMIZACIJA PRIPRAVE VZORCA IN METODE ZA
DOLOČANJE STEROIDNIH HORMONOV
Mentorica: prof. dr. Helena Prosen
Somentorica: prof. dr. Ksenija Šinigoj Gačnik
Datum zagovora: 24. 5. 2017

Sara RAŽMAN

SPEKTROSKOPSKA IN KROMATOGRFSKA ANALIZA
STABILNOSTI AZO PIGMENTA
Mentorica: izr. prof. dr. Irena Kralj Cigić
Datum zagovora: 22. 6. 2017

Patricija HRIBAR

KOORDINACIJSKE SPOJINE NEKATERIH KOVINSKIH
IONOV Z N-ETOKSİKARBONILMETIL-N'-(2-PIRIDIL)
TIOSEČNINO
Mentor: doc. dr. Andrej Pevec
Datum zagovora: 23. 6. 2017

Blaž GRJOL

FOTOKEMIJSKE PRETVORBE ARIL SUBSTITUIRANIH
KETONOV Z N-BROMOSUKCINIMIDOM POD
REAKCIJSKIMI POGOJI BREZ TOPILA
Mentor: izr. prof. dr. Marjan Jereb
Datum zagovora: 28. 6. 2017

Jernej JEREBIC

SINTEZA IN KARAKTERIZACIJA OKSIDOVANADIJEVIH
KOMPLEKSOV S FLUORIDNIM LIGANDOM
Mentor: prof. dr. Alojz Demšar
Datum zagovora: 3. 7. 2017

Kristina GAVRANIĆ

ŠTUDIJA PROCESA GALVANSKE IZMENJAVE V
SINTEZI PtCu₃/C KATALIZATORJA S PRETOČNO
ELEKTROKEMIJSKO CELICO
Mentor: prof. dr. Miran Gaberšček
Datum zagovora: 6. 7. 2017

Bor Lucijan TUREK

SINTEZE RAZLIČNIH N-SUBSTITUIRANIH MALEIMIDOV
IN NJIHOVA UPORABA PRI [4+2] CIKLOADICIJAH Z
ANTRACENOM IN IZBRANIMI 2H-PIRAN-2-ONI
Mentor: prof. dr. Marijan Kočevar
Somentor: doc. dr. Krištof Kranjc
Datum zagovora: 24. 7. 2017

Jure CERAR

STRUKTURNE RAZISKAVE PREPROSTIH GLIKOLOV NA
OSNOVI RENTGENSKEGA SIPANJA
Mentor: izr. prof. dr. Matija Tomšič
Datum zagovora: 24. 8. 2017

Nejc PETEK

SINTEZA IN BIOLOŠKA AKTIVNOST NOVIH 7 (1
AMINOALKIL)PIRAZOLO[1,5 A]PIRIMIDINOV
Mentor: prof. dr. Jurij Svete
Datum zagovora: 28. 8. 2017

Lovel KUKULJAN

SINTEZA IN MOLEKULSKO MODELIRANJE IZBRANIH
ENERGETSKIH MOLEKUL TEMELJEČIH NA
1,2,4-TRIAZOLU
Mentor: doc. dr. Krištof Kranjc
Datum zagovora: 29. 8. 2017

Urška MOHORIC

SKLOPITEV MIKROEMULZIJSKE ELEKTROKINETIČNE
KROMATOGRAFIJE BREZ SURFAKTANTOV (SF-MEEKC) Z
ESI-MS IN UV DETEKCIJO ZA DOLOČITEV HIDROFILNIH
IN HIDROFOBNIH VITAMINOV
Mentor: izr. prof. dr. Mitja Kolar
Datum zagovora: 31. 8. 2017

Žiga TKALEC

TRANSFORMACIJE FENIL ALENIL ETROV Z
N-(TRIFLUOROMETILTIO)ANILINOM
Mentor: izr. prof. dr. Marjan Jereb
Datum zagovora: 31. 8. 2017

Damir HAMULIČ

HIBRIDNE PREVLEKE NA OSNOVI SILANA IN AKRILATA
ZA ZAŠČITO ALUMINIJA IN NJEGOVH ZLITIN

Mentor: izr. prof. dr. Marjan Jereb
Somentorica: znan. svet. dr. Ingrid Milošev
Datum zagovora: 1. 9. 2017

Urška ZUPANČIČ

VPLIV IZBRANIH PIGMENTOV NA OKSIDACIJO
LANENEGA OLJA

Mentorica: izr. prof. dr. Irena Kralj Cigić
Datum zagovora: 7. 9. 2017

Valentina METLIČAR

DOLOČANJE TEŽKIH KOVIN V PRSTI Z ICP-OES

Mentor: izr. prof. dr. Mitja Kolar
Datum zagovora: 7. 9. 2017

Martin ROZMAN

IZDELAVA IN KARAKTERIZACIJA ELEKTROKEMIJSKIH
SISTEMOV ZA ELEKTROKROMNE IN FOTOVOLTAIČNE
APLIKACIJE

Mentor: doc. dr. Miha Lukšič
Somentor: prof. dr. Miran Gaberšček
Datum zagovora: 8. 9. 2017

Matic URLEP

SINTEZA 6-SUBSTITUIRANIH 2-PIRONOV IN NJIHOVA
REAKTIVNOST V DIELS-ALDERJEVI CIKLOADICIJI

Mentor: izr. prof. dr. Franc Požgan
Datum zagovora: 11. 9. 2017

Mateja ŠKRATEK

KOORDINACIJSKE SPOJINE ELEMENTOV PRVE
VRSTE PREHODNIH KOVIN S TIOCIANATOM TER
NIKOTINAMIDOM ALI 1,2,4-TRIAZOLOM

Mentor: doc. dr. Bojan Kozlevčar
Datum zagovora: 11. 9. 2017

Leja ROVAN

PORAZDELITEV ²¹⁰Po V ORGANIH RIB IZ TRŽAŠKEGA
ZALIVA (SEVERNI JADRAN)

Mentorica: prof. dr. Helena Prosen
Datum zagovora: 11. 9. 2017

Gorazd KODERMAN PODBORŠEK

VPLIV DOPIRANJA TITANOVEGA DIOKSIDA S SILICIJEM
ALI ŽELEZOM NA FOTOKATALITSKO AKTIVNOST
TANKIH PLASTI

Mentorica: doc. dr. Irena Kozjek Škofic
Datum zagovora: 12. 9. 2017

Evelin GRUDEN

VPLIV DODATKA BIOGLJA RAZLIČNEGA IZVORA NA
MOBILNOST KOVIN V JALOVINSKEM MATERIALU

Mentorica: doc. dr. Marija Zupančič
Datum zagovora: 12. 9. 2017

Simon BABNIK

KOORDINACIJSKE SPOJINE Z IZONIKOTINAMIDOM IN
DIMETILFORMAMIDOM

Mentor: doc. dr. Bojan Kozlevčar
Datum zagovora: 14. 9. 2017

Martina ŠTEFKO

PRIPRAVA Ba1-XSRXTIO3 S TOPOKEMIJSKO PRETVORBO
IZ Bi4Ti3O12 TER DOLOČITEV STRUKTURNIH IN
FEROELEKTRIČNIH LASTNOSTI PRODUKTA

Mentorica: dr. Marjeta Maček Kržmanc
Somentor: prof. dr. Anton Meden
Datum zagovora: 14. 9. 2017

Daša PAVC

NMR STRUKTURNA ŠTUDIJA Z GVANINI BOGATIH DNA
OLIGONUKLEOTIDOV Z GC KONCI

Mentor: prof. dr. Janez Plavec
Datum zagovora: 14. 9. 2017

Gregor KODRIČ

TRANSFORMACIJE TRIFLUOROMETILTOLIRANIH
ORGANSKIH SPOJIN

Mentor: izr. prof. dr. Marjan Jereb
Somentor: izr. prof. dr. Jernej Iskra
Datum zagovora: 15. 9. 2017

Tina KAPITLER

RAZVOJ NIKLJEVEGA KATALIZATORJA NA ZEOLITNEM
NOSILCU S HIERARHIČNO PORAZDELITVIJO POR ZA
PRETVORBO LIGNINA

Mentorica: izr. prof. dr. Amalija Golobič
Somentorica: prof. dr. Nataša Novak Tušar
Datum zagovora: 20. 9. 2017

Monika MANFREDA

VISOKOTEMPERATURNNA OKSIDACIJA Fe-Cr-AI ZLITINE

Mentorica: prof. dr. Romana Cerc Korošec
Somentorica: dr. Polona Umek
Datum zagovora: 20. 9. 2017

Tilen VOLČANŠEK

SINTEZA MODELNIH SPOJIN POMALIDOMIDA

Mentor: prof. dr. Marijan Kočevar
Datum zagovora: 20. 9. 2017

Mateja MIHELAC

FUNKCIONALIZACIJA KSANTATOV S
TRIFLUOROMETANSULFENAMIDOM

Mentor: izr. prof. dr. Marjan Jereb
Datum zagovora: 21. 9. 2017

Paulina PRŠLJA

MONTE CARLO SIMULACIJE MEŠANIC VODE IN
PREPOSTIH ALKOHOLOV

Mentor: izr. prof. dr. Tomaž Urbič
Datum zagovora: 25. 9. 2017

Monika ŽNIDARŠIČ

VPLIV VODIKOVEGA PEROKSIDA IN SERUMSKEGA
ALBUMINA NA KOROZIJSKE LASTNOSTI TITANOVE
ZLITINE V SIMULIRANI FIZIOLOŠKI RAZTOPINI

Mentor: doc. dr. Črtomir Podlipnik
Somentorica: znan. svet. dr. Ingrid Milošev
Datum zagovora: 26. 9. 2017

Urška VIDEMŠEK

REAKCIJE KOMPLEKSNIH ORGANOKOVINSKIH
HIDRIDOV Z REAKTIVNIMI KISIKOVIMI ZVRSTMI

Mentor: izr. prof. dr. Janez Cerkovnik
Datum zagovora: 28. 9. 2017

Ana SKVARČA

SINTEZA ANALOGOEV FDDNP S HETARILACETILENSKO SKUPINO

Mentor: prof. dr. Andrej Petrič

Datum zagovora: 6. 10. 2017

Žiga BABNIK

PRETVORBE O-DERIVATIZIRANIH ESTROV

ROSUVASTATINA

Mentor:izr. prof. dr. Franc Požgan

Datum zagovora: 17. 10. 2017

Miha MRZLIKAR

DOLOČITEV NEONIKOTINOIDNIH PESTICIDOV V MEDU

Mentorica: prof. dr. Helena Prosen

Somentorica: prof. dr. Ester Heath

Datum zagovora: 22. 11. 2017

MAGISTRSKI ŠTUDIJSKI PROGRAM 2. STOPNJE – KEMIJSKO INŽENIRSTVO**Nives AHLIN**

VPLIV IZBRANIH ANORGANSKIH ONESNAŽEVAL NA AKTIVNOST LIGNINOLITIČNIH ENCIMOV GLIVE DICHOMITUS SQUALENS

Mentor: prof. dr. Aleksander Pavko

Datum zagovora: 25. 1. 2017

Miha DELALUT

ZAGON IN OPTIMIZACIJA DELOVANJA LABORATORIJSKE ULTRAFILTRACIJSKE NAPRAVE

Mentor: prof. dr. Aleksander Pavko

Datum zagovora: 15. 2. 2017

Valentina REBEC

PREUČEVANJE STABILNOSTI STRUKTURE POLISAHARIDOV Z REOLOŠKIMI METODAMI

Mentor: prof. dr. Igor Plazl

Somentor: doc. dr. Anatolij Nikonov

Datum zagovora: 15. 2. 2017

Tara KUKOVEC

SINTEZA IN KARAKTERIZACIJA BENZOKSAZINSKIH SMOL Z DODATKOM DVOFUNKCIONALNIH MONOMEROV

Mentorica: prof. dr. Urška Šebenik

Datum zagovora: 24. 3. 2017

Marko SKVARČA

KARAKTERIZACIJA ADSORPCIJSKIH LASTNOSTI LESNEGA BIOOGLJA

Mentorica:izr. prof. dr. Andreja Žgajnar Gotvajn

Datum zagovora: 11. 4. 2017

Naja VRANKAR

VPLIV MIKROPLASTIKE NA VODNE RASTLINE

Mentorica:izr. prof. dr. Andreja Žgajnar Gotvajn

Somentorica: doc. dr. Anita Jemec

Datum zagovora: 11. 4. 2017

Nuška PEREC

EMULZIJSKA POLIMERIZACIJA LEPIL, OBČUTLJIVIH NA PRITISK, Z LASTNOSTMI NABREKANJA

Mentor: prof. dr. Matjaž Krajnc

Datum zagovora: 17. 5. 2017

Ivan PRIBEC

UPORABA MREŽNE BOLTZMANNOVE METODE PRI OPISU KEMIJSKIH REAKCIJ

Mentor: prof. dr. Igor Plazl

Somentor:izr. prof. dr. Tomaž Urbič

Datum zagovora: 29. 5. 2017

Veronika KALAR

BIOKATALITSKI PROCES Z MIKROREAKTORJI V MAGNETNEM POLJU

Mentorica: prof. dr. Polona Žnidaršič Plazl

Datum zagovora: 7. 7. 2017

Eva CIZEL

SINTEZA IN KARAKTERIZACIJA ZLITIN V SISTEMU Li – B

Mentor: doc. dr. Boštjan Genorio

Datum zagovora: 7. 7. 2017

Amra HUSEJNOVIĆ

MODIFIKACIJA STEKLENIH POVRŠIN S POLIMERNIM SLOJEM

Mentor: prof. dr. Matjaž Krajnc

Datum zagovora: 11. 7. 2017

Sabina KOLŠEK

VPLIV BAKROVIH NANODELCEV NA PROCES KOMPOSTIRANJA

Mentorica:izr. prof. dr. Andreja Žgajnar Gotvajn

Somentorica: doc. dr. Anita Jemec

Datum zagovora: 24. 8. 2017

Aneja TULJAK

KROMATOGRAFSKO ČIŠČENJE BAKTERIOFAGOV

Mentor:izr. prof. Aleš Podgornik

Datum zagovora: 31. 8. 2017

Matic KORENT

SINTEZA IN KARAKTERIZACIJA BUTIL POLIGLUKOZIDA

Mentor: prof. dr. Matjaž Krajnc

Datum zagovora: 4. 9. 2017

Klavdija TOMŠE

PEROVSKITNI MATERIALI ZA ANODE VISOKOTEMPERATURNIH GORIVNIH CELIC

Mentorica: doc. dr. Klementina Zupan

Datum zagovora: 8. 9. 2017

Alen OBLAK

SINTEZA AKRILATNIH LEPIL, OBČUTLJIVIH NA PRITISK, V MASI Z UV-POLIMERIZACIJO

Mentor: doc. dr. Jernej Kajtna

Somentor: doc. dr. Aleš Ručigaj

Datum zagovora: 11. 9. 2017

Anže BELOVIČ

OPTIMIZACIJA MIKROREAKTORJA S STRNJENIM SLOJEM IMOBILIZIRANE B-GALAKTOZIDAZE

Mentorica: prof. dr. Polona Žnidaršič Plazl

Datum zagovora: 11. 9. 2017

Anja SLAVIČ

BIORAZGRADNJA UMETNEGA SLADILA SAHARIN V POVRŠINSKIH IN PODZEMNIH VODAH

Mentorica: izr. prof. dr. Andreja Žgajnar Gotvajn

Datum zagovora: 11. 9. 2017

Lea UDOVČ

ANALIZA ANTIMIKROBNIH LASTNOSTI NANOKOMPOZITOV NA OSNOVI FERITA IN FUNKCIONALIZIRANEGA ZLATA

Mentor: prof. dr. Danilo Suvorov

Datum zagovora: 15. 9. 2017

Matej LESAR

VPLIV SESTAVE IN SINTEZNIH PARAMETROV NA STRUKTURO IN LASTNOSTI SUPERABSORBENTA NA OSNOVI AKRILAMIDA

Mentorica: prof. dr. Urška Šebenik

Datum zagovora: 19. 9. 2017

Jaka OREHEK

MODELIRANJE KRISTALIZACIJE AKTIVNE FARMACEVTSKE UČINKOVINE V PRETOČNEM CEVNEM SESTAVU

Mentor: izr. prof. Aleš Podgornik

Somentor: dr. Petar Djinović

Datum zagovora: 19. 9. 2017

Luka GRM

VPLIV SNOVNEGA PRENOSA KISIKA V SUBMERZNI KULTIVACIJI GLIVE CORYCEPS SINENSIS

Mentor: izr. prof. Aleš Podgornik

Datum zagovora: 22. 9. 2017

Antonija KIRAC

SINTEZA IN KARAKTERIZACIJA RAZLIČNIH STRUKTUR GRAFEN OKSIDA

Mentor: doc. dr. Boštjan Genorio

Datum zagovora: 25. 9. 2017

Urban GARTNER

PREUČEVANJE MOŽNOSTI UPORABE GLIVE TRAMETES VERSICOLOR ZA SINTEZO NANODELCEV IN BIOREMEDIACIJO

Mentorica: izr. prof. dr. Andreja Žgajnar Gotvajn

Datum zagovora: 26. 9. 2017

Dani ŠAVLI

DOLOČITEV VPLIVA TEMPERATURE SINTRANJA NA PREVODNOST LSCM-KERAMIKE S POMOČJO MERJENJA ELEKTROKEMIJSKE IMPEDANČNE SPEKTROSKOPIJE

Mentor: izr. prof. dr. Marjan Marinšek

Datum zagovora: 26. 9. 2017

Belkisa VELAGIĆ

BIOREMEDIACIJA ORGANSKEGA POLUTANTA LINDANA S POMOČJO GLIVNIH ENCIMOV

Mentor: prof. dr. Aleksander Pavko

Datum zagovora: 28. 9. 2017

Maja RAMIČ

ČIŠČENJE PLAZMIDNE DNA Z IONSKO-IZMENJEVALNO KROMATOGRAFIJO

Mentor: izr. prof. Aleš Podgornik

Datum zagovora: 29. 9. 2017

Janja FORTIN

PRIPRAVA IN KARAKTERIZACIJA poliHIPE POLIMEROV

Mentor: izr. prof. Aleš Podgornik

Datum zagovora: 29. 9. 2017

Sanja POPOVIČ

VREDNOTENJE UČINKOVITOSTI EKSTRACELULARNIH LIGNINOLITIČNIH ENCIMOV GLIVE DICHOMITUS SQUALENS ZA RAZGRADNJO ANTIBIOTIKA TIAMULIN FUMARAT

Mentorica: izr. prof. dr. Andreja Žgajnar Gotvajn

Datum zagovora: 3. 10. 2017

Karin ČESNIK

PRIPRAVA DOPIRANIH PEROVSKITNIH MATERIALOV Z ZGOREVALNO SINTEZO

Mentor: izr. prof. dr. Marjan Marinšek

Datum zagovora: 6. 10. 2017

Saša BALAŽIČ

ŠTUDIJA RAZGRADNJE ANTIBIOTIKA Z OZONACIJO V MIKROREAKTORJU

Mentor: prof. dr. Igor Plazl

Somentor: izr. prof. dr. Janez Cerkovnik

Datum zagovora: 25. 10. 2017

Maja PETERKOVIČ

ANALIZA OBČUTLJIVOSTI SINTETIZIRANEGA ORGANSKEGA-ANORGANSKEGA PEROVSKITA CH₃NH₄PbI₃

Mentor: izr. prof. dr. Marjan Marinšek

Datum zagovora: 8. 11. 2017

Rok GRM

SINTRANJE IN KARAKTERIZACIJA TiO₂ Z DODATKI

Mentor: izr. prof. dr. Marjan Marinšek

Datum zagovora: 21. 11. 2017

MAGISTRSKI ŠTUDIJSKI PROGRAM 2. STOPNJE – BIOKEMIJA**Tjaša BLATNIK**

KVANTITATIVNA PROTEOMSKA ANALIZA S
SEKRETORNO FOSFOLIPAZO A2 INDUCIRANIH
LIPIDNIH KAPLJIC V CELICAH RAKA DOJKE

Mentor: prof. dr. Igor Križaj
Datum zagovora: 16. 2. 2017

Jernej PUŠNIK

ANALIZA TRANSKRIPTOMA MODRASOVH STRUPNIH
ŽLEZ

Mentor: prof. dr. Igor Križaj
Somentor: prof. dr. Jože Pungertar
Datum zagovora: 23. 2. 2017

Veronika JARC

POGOSTOST OKUŽBE S POKSVIRUSI PRI
PROSTOŽIVEČIH SESALCIH V SLOVENIJI

Mentorica: prof. dr. Tatjana Avšič Županc
Datum zagovora: 28. 3. 2017

Daša JANEŠ

MORFOLOŠKA IN MOLEKULARNOGENETSKA
PRIMERJAVA OKOLJSKIH IN KLINIČNIH SEVOV
KVASOVKE CANDIDA PARAPSILOSIS

Mentorica: prof. dr. Nina Gunde Cimerman
Datum zagovora: 30. 3. 2017

Elmina HANDANOVIĆ

PRIPRAVA FUZIJSKEGA PROTEINA ANTIMLKL-EGFP/
MCHERRY ZA DETEKCIJO N-KONČNE DOMENE
PROTEINA MLKL

Mentor: doc. dr. Gregor Gunčar
Datum zagovora: 7. 4. 2017

Ana KAPRALJEVIĆ

UČINEK IBOGAINA NA PREŽIVETJE DOPAMINSKIH
NEVRONOV V TKIVNI KO-KULTURI NIGRE IN
STRIATUMA

Mentor: prof. dr. Marko Živin
Datum zagovora: 9. 5. 2017

Nives NARAGLAV

RAZVOJ NANOLIPOSOMSKEGA CEPIVA PROTI LYMSKI
BORELIOZI

Mentor: doc. dr. Gregor Gunčar
Datum zagovora: 16. 5. 2017

Nikolina NOVAK

DOLOČANJE NEVROTROFIČNEGA RASTNEGA
DEJAVNIKA GLIALNEGA IZVORA V PLAZMI ZDRAVIH
OSEB IN BOLNIKOV S KRONIČNO LEDVIČNO
BOLEZNIJO S TESTOM ELISA

Mentorica: prof. dr. Vladka Čurin Šerbec
Datum zagovora: 28. 6. 2017

Jernej MUSTAR

RAZVOJ REPORTERSKEGA SISTEMA NA OSNOVI
B-GALAKTOZIDAZE ZA DOLOČANJE MOČI
PROMOTORJEV V CIANOBAKTERIJI SYNECHOCYSTIS SP.
PCC 6803

Mentor: izr. prof. dr. Marko Dolinar
Datum zagovora: 13. 7. 2017

Iza OGRIS

BIOKEMIJSKA OPREDELITEV NARAVNIH MUTANT
LANOSTEROL 14A-DEMETILAZE V ČLOVEŠKI
POPULACIJI

Mentorica: prof. dr. Damjana Rozman
Somentorica: dr. Simona Golič Grdadolnik
Datum zagovora: 17. 8. 2017

Urška KOTNIK

VLOGA ERITROPOETINSKEGA RECEPTORJA PRI
REZISTENCI NA TAMOKSIFEN

Mentorica: izr. prof. dr. Nataša Debeljak
Datum zagovora: 22. 8. 2017

Andrej VRANKAR

HOLESTEROL IN CIRKADIANA URA: IZSLEDKI NA
CELICAH Z IZBITIM GENOM CYP51

Mentorica: prof. dr. Damjana Rozman
Datum zagovora: 24. 8. 2017

Rok RAZPOTNIK

IZRAŽANJE ENOVERIŽNEGA VARIABILNEGA
FRAGMENTA V5B2 V SESALSKIH CELICAH

Mentorica: prof. dr. Vladka Čurin Šerbec
Somentor: dr. Uroš Rajčević
Datum zagovora: 30. 8. 2017

Eva VIDAK

PRIPRAVA REKOMBINANTNE ČLOVEŠKE KASPAZE-1 IN
IDENTIFIKACIJA NJENIH ZUNAJCELIČNIH SUBSTRATOV

Mentor: prof. ddr. Boris Turk
Datum zagovora: 6. 9. 2017

Ester MERLJAK

ORTOGONALNOST IN UČINKOVITOST
HETERODIMERIZACIJE MODULOV OBVITIH VIJAČNIC V
SESALSKI CELIČNI LINIJI HEK293T

Mentorica: dr. Helena Gradišar
Somentor: izr. prof. dr. Marko Dolinar
Datum zagovora: 7. 9. 2017

Nejc PETRIŠIČ

BIOKEMIJSKA IN BIOFIZIKALNA KARAKTERIZACIJA
FOSFOLIPAZ PI-PLC IN PC-PLC IZ PATOGENE BAKTERIJE
LISTERIA MONOCYTOGENES

Mentor: izr. prof. Aleš Podgornik
Somentor: prof. dr. Janez Plavec
Datum zagovora: 11. 9. 2017

Urban JAVORŠEK

VPLIV SELEKTIVNE INHIBICIJE KATEPSINA B Z DARPINI
PRI CELIČNI SMRTI

Mentor: prof. ddr. Boris Turk
Datum zagovora: 11. 9. 2017

Erik MRŠNIK

ANALIZA POTENCIALNIH ALOSTERIČNIH MEST
KATEPSINOV V IN S NA PODLAGI HOMOLOGIJE S
KATEPSINOM K

Mentor: doc. dr. Marko Novinec
Datum zagovora: 11. 9. 2017

Urša ŠUŠTAR

VPLIV PALMITATA IN GENA TST NA VNETHJE IN INZULINSKO REZISTENCO PRI ADIPOCITIH
Mentor: prof. dr. Simon Horvat
Datum zagovora: 12. 9. 2017

Špela POHLEVEN

OPREDELITEV NOVIH ALELOV ZA HIPERHOLESTEROLEMIJO Z ASOCIACIJSKO ANALIZO NA CELOTNEM GENOMU IN UPORABO ZDRUŽENIH VZORCEV DNA
Mentor: prof. dr. Simon Horvat
Somentorica: doc. dr. Katarina Trebušak Podkrajšek
Datum zagovora: 12. 9. 2017

Anka HOTKO

IZRAŽANJE IN METILACIJA GENA ZA RELN PRI ŽRTVAH SAMOMORA
Mentorica: doc. dr. Alja Videtič Paska
Datum zagovora: 12. 9. 2017

Tina SNOJ

IZRAŽANJE REKOMBINANTNEGA ČLOVEŠKEGA KATEPSINA C V BAKTERIJI ESCHERICHIA COLI IN NJEGOVA KARAKTERIZACIJA
Mentor: doc. dr. Marko Novinec
Datum zagovora: 13. 9. 2017

Maruša PROLIČ KALINŠEK

KONFORMACIJSKA STABILNOST PROTEINA MLKL UDELEŽENEGA V NEKROPTOZI
Mentor: prof. dr. Jurij Lah
Datum zagovora: 14. 9. 2017

Benjamin BAJŽELJ

VPLIV 2,2,2-TRIFLUOROETANOLA (TFE) IN TEMPERATURE NA ZVITJE INTRINZIČNO NEUREJENIH PEPTIDOV IZ BAKTERIJSKIH SISTEMOV TOKSIN-ANTITOKSIN
Mentor: prof. dr. Jurij Lah
Datum zagovora: 14. 9. 2017

Špela TOMAŽ

PRIDOBIVANJE PROTEINOV IMUNSKE SIGNALIZACIJE KROMPIRJA IN PROTEINOV KROMPIRJEVEGA VIRUSA Y V BAKTERIJI ESCHERICHIA COLI TER KRISTALIZACIJA KROMPIRJEVEGA PROTEINA TGA2.1
Mentorica: prof. dr. Kristina Gruden
Somentor: prof. dr. Dušan Turk
Datum zagovora: 15. 9. 2017

Luka SMOLE

IZVEDBA LOGIČNE OPERACIJE NOR Z UPORABO SISTEMA CRISPR V SESALSKIH CELICAH
Mentor: prof. dr. Roman Jerala
Datum zagovora: 19. 9. 2017

Ana GROM

OPTIMIZACIJA ALOSTERIČNIH EFEKTORJEV KATEPSINA K NA OSNOVI ZNANE STRUKTURE EFEKTORJA
Mentor: doc. dr. Marko Novinec
Datum zagovora: 27. 9. 2017

Luka KAVČIČ

ANALIZA STRUKTURNIH LASTNOSTI A-HIDRAZINOPEPTIDOV Z UPORABO NMR SPEKTROSKOPIJE
Mentor: prof. dr. Janez Plavec
Datum zagovora: 27. 9. 2017

Nastja ŠTEMBERGER

ORGANOTIPIČNE MOŽGANSKE KULTURE MLADIH PODGAN KOT MODEL ZA RAZVOJ DOPAMINERGIČNE HIPERSENZITIVNOSTI PRI PARKINSONOVI BOLEZNI
Mentor: prof. dr. Marko Živin
Datum zagovora: 29. 9. 2017

Urška RAUTER

IDENTIFIKACIJA IN KARAKTERIZACIJA GLIV OSAMLJENIH IZ ATMOSFERE IN SNEŽNIH POVRŠIN
Mentorica: prof. dr. Nina Gunde Cimerman
Datum zagovora: 29. 9. 2017

Marko RADOJKOVIČ

IDENTIFIKACIJA OPTIMALNEGA OGRODJA NANOTELES IN PRIPRAVA NANOTELESA PROTI PSA S TEM OGRODJEJEM
Mentor: doc. dr. Gregor Gunčar
Datum zagovora: 29. 9. 2017

Jure ZABRET

IZRAŽANJE IN KARAKTERIZACIJA ORTOKASPAZ CIANOBAKTERIJE MICROCYSTIS AERUGINOSA NIES 843
Mentor:izr. prof. dr. Marko Dolinar
Datum zagovora: 5. 10. 2017

Eva KOROŠEC

UPORABNOST pH-SENZORJEV ZA BIOMEDICINSKE APLIKACIJE
Mentor:izr. prof. dr. Mitja Kolar
Datum zagovora: 24. 10. 2017

Maja KOSTANJEVEC

OPTIMIZACIJA PRIPRAVE KOLAGENSKIH PEPTIDOV
Mentor: doc. dr. Miha Pavšič
Datum zagovora: 10. 11. 2017

Ana UNKOVIČ

SPREMLJANJE PORAZDELJEVANJA NANODELCEV V NORMALNIH IN RAKAVIH UROTELIJSKIH CELICAH IN PO TUNELSKIH MEMBRANSKIH NANOCEVKAH
Mentorica:izr. prof. dr. Mateja Erdani Kreft
Datum zagovora: 15. 11. 2017

Angelika VIŽINTIN

PRIPRAVA VEKTORSKIH KONSTRUKTOV ZA UGOTAVLJANJE KOMPATIBILNOSTI TOKSINOV IN ANTITOKSINOV V CIANOBAKTERIJI SYNECHOCYSTIS SP. PCC6803 IN NJIHOVO TESTIRANJE
Mentor:izr. prof. dr. Marko Dolinar
Datum zagovora: 30. 11. 2017

Tim BOŽIČ

NMR ŠTUDIJE STRUKTURNE RAZNOLIKOSTI Z GVANINI IN CITOZINI BOGATIH RNA OLIGONUKLEOTIDOV VPLETENIH V NEVRODEGENERATIVNE BOLEZNI
Mentor: prof. dr. Janez Plavec
Somentor:izr. prof. dr. Boris Rogelj
Datum zagovora: 15. 12. 2017

Jan ROZMAN

VPLIV NUKLEOTIDNIH MODIFIKACIJ NA ZVIJANJE Z
GVANINI BOGATEGA ZAPOREDJA IZ GENA RANKL

Mentor: prof. dr. Janez Plavec

Datum zagovora: 18. 12. 2017

Živa REJC

ANALIZA ODZIVA NARAVNE IMUNOSTI PRI
PEDIATRIČNIH BOLNIKI S HIPERHOLESTEROLEMIJO
IN VPLIV TERAPIJE

Mentor: prof. dr. Simon Horvat

Datum zagovora: 22. 12. 2017

MAGISTRSKI ŠTUDIJSKI PROGRAM 2. STOPNJE – KEMIJSKO IZOBRAŽEVANJE**Eva KRAJNC**

POMEN MODRIH INDOLNIH PIGMENTOV, BAKROVEGA
FTALOCIANINA, INDIGA IN INDIGO KARMINA V
PROCESU POUČEVANJA

Mentor: doc. dr. Krištof Kranjc

Datum zagovora: 6. 7. 2017

Gašper PERNEK

FOTOKATALITSKA OKSIDACIJA KARBOKSAMIDOV S
SISTEMOM Fe³⁺/O₂

Mentorica: izr. prof. dr. Irena Kralj Cigić

Datum zagovora: 28. 9. 2017

Gašper MURN

POSTOPKI PRIPRAVE IN KARAKTERIZACIJE
UTEKOČINJENEGA LESA PRIMERNI ZA
DEMONSTRACIJO V SREDNJIH ŠOLAH

Mentor: doc. dr. Miha Lukšič

Datum zagovora: 13. 7. 2017

MAGISTRSKI ŠTUDIJSKI PROGRAM 2. STOPNJE – TEHNIŠKA VARNOST**Uroš APOTEKAR**

VPLIVI NA OKOLJE IZ ASFALTNE BAZE IN NJHOVO
OBVLADOVANJE

Mentor: izr. prof. dr. Matevž Pompe

Datum zagovora: 4. 7. 2017

Petra BROVČ

PREUČEVANJE POLIURETANSKIH PEN Z METODAMI
TERMIČNE ANALIZE

Mentorica: prof. dr. Romana Cerc Korošec

Datum zagovora: 28. 9. 2017

Ciril ŠTERN

POŽARNA ODPORNOST SKELETNIH LESENIH
KONSTRUKCIJ

Mentor: prof. dr. Simon Schnabl

Somentor: doc. dr. Tomaž Hozjan

Datum zagovora: 22. 8. 2017

Tina BREGAR

PRIPRAVA NAČRTA ZA GOSPODARJENJA Z ODPADKI ZA
FAKULTETO ZE KEMIJO IN KEMIJSKO TEHNOLOGIJO
UNIVERZE V LJUBLJANI

Mentorica: izr. prof. dr. Andreja Žgajnar Gotvajn

Datum zagovora: 28. 9. 2017

Klemen PUTAR

PREPREČEVANJE POŠKODB Z OSTRIMI PREDMETI V
ZDRAVSTVENI NEGI

Mentor: prof. dr. Marjan Bilban

Datum zagovora: 29. 8. 2017

Nataša KUČIŠ

DELOVNE NEZGODE V ZASEBNIH GOZDOVIH

Mentor: doc. dr. Jože Šrekl

Datum zagovora: 4. 10. 2017

Franc Branko MOČNIK

OCENA TVEGANJA KROŽNE ŽAGE ATIKA TK 250

Mentor: doc. dr. Boris Jerman

Datum zagovora: 28. 9. 2017

Denis MLAKAR

UPRAVLJANJE S TVEGANJI V FARMACEVTSKEM
RAZVOJU

Mentor: doc. dr. Mitja Robert Kožuh

Datum zagovora: 30. 11. 2017

Maja JUNC

OBRAVNAVA SKLADIŠČA VODIKOVEGA KLORIDA Z
VIDIKA VARNOSTI

Mentorica: doc. dr. Barbara Novosel

Datum zagovora: 28. 9. 2017

Tina POŽENEL

RAZISKAVE UČINKOVITOSTI PROTIPOŽARNEGA
PREMAZA

Mentor: prof. dr. Simon Schnabl

Somentorica: doc. dr. Barbara Novosel

Datum zagovora: 22. 12. 2017

Snežana PAVLOVIČ

TERMIČNE LASTNOSTI KAMENIH IN STEKLENIH VOLN
RAZLIČNIH PROIZVAJALCEV

Mentorica: prof. dr. Romana Cerc Korošec

Datum zagovora: 28. 9. 2017

DIPLOME – UNIVERZITETNI ŠTUDIJI**KEMIJA – 1. STOPNJA**

Domen SMODIŠACILIRANJE 1,3-DIARILTRIAZENOV Z ANHIDRIDOM
JANTARNE KISLINE

Mentor: prof. dr. Janez Košmrlj

Datum zagovora: 2. 2. 2017

Martina ANDREJAŠIČ

SINTEZA PCP KLEŠČASTIH KOMPLEKSOV

Mentor:izr. prof. dr. Janez Cerkovnik

Datum zagovora: 10. 3. 2017

Leja ERZINSINTEZA IN KARAKTERIZACIJA BAKROVIH
METANOATOV VEZANIH S PIRIDINOM

Mentorica:izr. prof. dr. Amalija Golobič

Datum zagovora: 26. 6. 2017

Rok TOMŠIČDOLOČANJE TRIAZINSKIH PESTICIDOV V VODI S SPE-
HPLC

Mentorica: prof. dr. Helena Prosen

Datum zagovora: 29. 6. 2017

Tjaša KLAVŽARPRIPRAVA KOMPLEKSOV S KOVINAMI POZNEGA
PREHODA

Mentor:izr. prof. dr. Janez Cerkovnik

Datum zagovora: 4. 7. 2017

Jure DRAGAN

SVETLOBA KOT ORODJE PRI KEMIJSKIH RAZISKAVAH

Mentor:izr. prof. dr. Matija Tomšič

Datum zagovora: 5. 7. 2017

Urša ROZMANPd-KATALIZIRANO NEPOSREDNO ARILIRANJE
HETEROCKILOV Z BROMOKINOLINI

Mentor:izr. prof. dr. Bogdan Štefane

Datum zagovora: 28. 8. 2017

Tisa ŽEVART

IZBRANE REAKCIJE ARIL HALOGENIDOV S PALADIJEM

Mentor: doc. dr. Martin Gazvoda

Datum zagovora: 28. 8. 2017

Tjaša PAVČNIK

SINTEZA IZBRANIH DIARILJODONIJEVIH SOLI

Mentor: prof. dr. Janez Košmrlj

Datum zagovora: 28. 8. 2017

Aljaž ŠKRJANC

SINTEZA IZBRANIH DIAZENOV NA OSNOVI PIPERIDINA

Mentor: prof. dr. Janez Košmrlj

Datum zagovora: 28. 8. 2017

Maša KASTNER

SINTEZA 2-ARIL SUBSTITUIRANIH PIRIMIDINOV

Mentor:izr. prof. dr. Bogdan Štefane

Datum zagovora: 28. 8. 2017

Tjaša PODLOGARSINTEZA IZBRANIH DIAZENOV NA OSNOVI
DIMETILAMINA

Mentor: prof. dr. Janez Košmrlj

Datum zagovora: 29. 8. 2017

Tjaša KRISTANCKOORDINACIJSKE SPOJINE BAKRA(II) S KINALDINATOM
IN PIRIDINSKIMI LIGANDI

Mentorica: doc. dr. Barbara Modec

Datum zagovora: 29. 8. 2017

Urša ZUPANCBAKROVE IN ŽELEZOVE SPOJINE Z
ACETILACETONATOM

Mentor: doc. dr. Bojan Kozlevčar

Datum zagovora: 30. 8. 2017

Teja GABRŠČEKOPTIMIZACIJA SINTEZE 6-(4-METILPIPERAZIN-
1-KARBONIL)PIKOLINSKE KISLINE ZA PRIPRAVO
CINKOVIH KOORDINACIJSKIH SPOJIN

Mentor:izr. prof. dr. Franc Perdih

Datum zagovora: 30. 8. 2017

Lia ŠIBAVRENTGENSKA STRUKTURNA ANALIZA NEKATERIH
NIKLJEVIH KOMPLEKSOV S TRIDENTATNIMI LIGANDI

Mentor: doc. dr. Andrej Pevec

Datum zagovora: 30. 8. 2017

Domen JERONČIČVALIDACIJA KIVETNEGA TESTA ZA DOLOČANJE
ADSORBLJIVIH ORGANSKIH HALOGENOV V ODPADNI
VODI

Mentorica: doc. dr. Barbara Modec

Datum zagovora: 31. 8. 2017

Tjaša LISAC

RENTGENSKA PRAŠKOVNA ANALIZA SOLI

Mentorica:izr. prof. dr. Amalija Golobič

Datum zagovora: 4. 9. 2017

Simon MADŽARACPRIMERJAVA REAKTIVNOSTI ORGANSKIH MOLEKUL
POD KLASIČNIMI IN ZELENIMI POGOJI

Mentor:izr. prof. dr. Marjan Jereb

Datum zagovora: 4. 9. 2017

Deja ŠELIHVALIDACIJA POSTOPKA DOLOČITVE V VZORCIH
ŽVEPLOVE (VI) KISLINE IN OVREDNOTENJE MERILNE
NEGOTOVOSTI REZULTATA DOLOČITVE ŽELEZA

Mentor: doc. dr. Andrej Pevec

Datum zagovora: 4. 9. 2017

Tjaša RIJAVEC

SINTEZA IN KARAKTERIZACIJA ORGANOKOVINSKIH KOMPLEKSOV Z NEKATERIMI 2-MERKAPTOPIRIDIN-N-OKSIDI

Mentor: prof. dr. Iztok Turel

Datum zagovora: 5. 9. 2017

Kaja PANCAR

VPLIV ČASA TERMIČNE OBDELAVE NA HITROST RAZGRADNJE BARVILA PLASMOCORINTH B S FOTOKATALITSKO AKTIVNIMI TANKIMI PLASTMI TiO₂

Mentorica: prof. dr. Romana Cerc Korošec

Datum zagovora: 6. 9. 2017

Andraž OŠTREK

SINTEZA BICIKLO[2.2.2]OKTENOV Z DIELS-ALDERJEVO REAKCIJO, NADALJNJE N-KLORIRANJE IN POSKUS TVORBE KOKRISTALOV

Mentor: doc. dr. Krištof Kranjc

Datum zagovora: 7. 9. 2017

Anja Marija PILAR

DOLOČITEV SLEDOV URANA IN TORIJA V ELEKTROLITSKEM BAKRU Z NEVTRONSKO AKTIVACIJSKO ANALIZO

Mentorica: prof. dr. Helena Prosen

Datum zagovora: 7. 9. 2017

Tjaša BLATNIK

DOLOČANJE ORGANSKIH KISLIN V ZRAKU Z IONSKO KROMATOGRAFIJO

Mentorica: izr. prof. dr. Irena Kralj Cigič

Datum zagovora: 7. 9. 2017

Luka REPAR

SINTEZA NEKATERIH AMIDINOV IN NADALJNJA PRETVORBA DO 2-ARILPIRIMIDINOV

Mentor: izr. prof. dr. Franc Požgan

Datum zagovora: 11. 9. 2017

Tomaž KOTNIK

PRIPRAVA HIDRIDOV S KOVINAMI POZNEGA PREHODA

Mentor: izr. prof. dr. Janez Cerkovnik

Datum zagovora: 11. 9. 2017

Samo KREVS

SINTEZA 3-ACILAMINSKIH DERIVATOV 2H-PIRAN-2-ONOV IN NJIHOVE NADALJNJE PRETVORBE Z RAZLIČNIMI DIENOFILI S POMOČJO DIELS-ALDERJEVIH REAKCIJ

Mentor: doc. dr. Krištof Kranjc

Datum zagovora: 12. 9. 2017

Blaž KOZJAN

SOČASNA UPORABA VEČIH SEPARACIJSKIH MEHANIZMOV PRI DOLOČEVANJU FARMACEVTSKIH UČINKOVIN

Mentor: izr. prof. dr. Drago Kočar

Datum zagovora: 12. 9. 2017

Aljaž ŠINKOVEC

SINTEZE 5,6-DISUBSTITUIRANIH 3-BENZOILAMINO-2H-PIRAN-2-ONOV KOT DIENOV ZA NADALJNJE CIKLOADICIJE

Mentor: doc. dr. Krištof Kranjc

Datum zagovora: 12. 9. 2017

Anja AJDOVEC

PRIPRAVA SUKINIMIDNIH DERIVATOV BICIKLO[2.2.2]OKTENA, NJIHOVIH N-KLORO ANALOGOVI TER DOLOČITEV KRISTALNE STRUKTURE KOKRISTALA S 4,4'-BIPIRIDILOM

Mentor: doc. dr. Krištof Kranjc

Datum zagovora: 12. 9. 2017

Nejc POVIRK

DOLOČANJE MINERALNE SESTAVE TAL NA PODROČJU IHANA Z RENTGENSKO PRAŠKOVNO DIFRAKCIJO

Mentor: prof. dr. Anton Meden

Datum zagovora: 12. 9. 2017

Teja PODRŽAJ

VPLIV UPORABE RAZLIČNIH TOPIL NA POJAV SISTEMSKIH VRHOV PRI HPLC

Mentor: izr. prof. dr. Drago Kočar

Datum zagovora: 12. 9. 2017

Grega KOS

PRETVORBE BICIKLO[2.2.2]OKTENOV Z ETANDIAMINOM IN Z N1-(2-AMINOETIL)ETAN-1,2-DIAMINOM KOT MOŽNE POTI DO FUNKCIONALNIH POLIMEROV

Mentor: doc. dr. Krištof Kranjc

Datum zagovora: 12. 9. 2017

Vita HUDI

MODELNI OPIS EPIDEMIJE EBOLE 2014-2016

Mentor: doc. dr. Miha Lukšič

Datum zagovora: 13. 9. 2017

Tjaša PAVLOVČIČ

LASTNOSTI, UPORABA IN PROTIKOROZIJSKA ZAŠČITA MAGNEZIJEVIH ZLITIN

Mentor: izr. prof. dr. Matija Tomšič

Datum zagovora: 13. 9. 2017

Luka CIBER

ORGANOKATALIZIRANE 1,2-ADICIJE 5-BENZILPIROLONA Z DERIVATI ISATINIMINA

Mentor: doc. dr. Uroš Grošelj

Datum zagovora: 13. 9. 2017

Maja MAJCEN

KARAKTERIZACIJA VZORCEV KALIJ-NATRIJEVEGA NIOBATA Z RENTGENSKO PRAŠKOVNO DIFRAKCIJO

Mentor: prof. dr. Anton Meden

Datum zagovora: 13. 9. 2017

Jan GNIDOVEC

ORGANOKATALIZIRANE REAKCIJE ISATIN IMINOV S PIROLONOM NA OSNOVI ORNITINA

Mentor: doc. dr. Uroš Grošelj

Datum zagovora: 13. 9. 2017

Andrej GRUDEN

RAZISKOVANJE REAKTIVNOSTI RUTENIJEVIH KOMPLEKSOV S TIOSEMIKARBAZONI

Mentor: prof. dr. Iztok Turel

Datum zagovora: 13. 9. 2017

Matej KOLARIČ

SINTEZA RUTENIJEVIH FOTOSENZIBILIZATORJEV S TREMI RAZLIČNIMI BIDENTATNIMI LIGANDI
Mentor: izr. prof. dr. Franc Požgan
Datum zagovora: 13. 9. 2017

Meta VRABEC

PRETVORBE ORGANSKIH SNOVI NA KLASIČEN IN ZELEN NAČIN
Mentor: izr. prof. dr. Marjan Jereb
Datum zagovora: 13. 9. 2017

Miha RAVBAR

UPORABA NA POLIMER IMOBILIZIRANEGA BAKROVEGA KATALIZATORJA ZA »KLIK« REAKCIJE
Mentor: izr. prof. dr. Jernej Iskra
Datum zagovora: 14. 9. 2017

Erik TROBEC

SINTEZA METIL N-BOC-5,5-DIMETIL-4-OKSO-4,5-DIHIDRO-1H-PIROL-3-KARBOKSILATA
Mentor: prof. dr. Jurij Svete
Datum zagovora: 14. 9. 2017

Dejan SLAPŠAK

ELEKTROKEMIJSKE METODE PRI ŠTUDIJU INTERAKCIJ FITATOV S Cu^+ in Cu^{2+} IONI
Mentor: izr. prof. dr. Mitja Kolar
Datum zagovora: 14. 9. 2017

Domen OBREZ

UPORABNOST FITINSKE KISLINE PRI ŠTUDIJU KOROZIJE BAKRA
Mentor: izr. prof. dr. Mitja Kolar
Datum zagovora: 14. 9. 2017

Petra STARE

VPLIV PUFRA NA POJAV SISTEMSKIH VRHOV PRI HPLC
Mentor: izr. prof. dr. Drago Kočar
Datum zagovora: 14. 9. 2017

Martina MOŽE

VOLTAMETRIČNA KARAKTERITACIJA INTERAKCIJ ŽELEZOVEGA IN FITATNEGA IONA NA HMDE
Mentor: izr. prof. dr. Mitja Kolar
Datum zagovora: 14. 9. 2017

Jan PETROVČIČ

UPORABA REAGENTOV NA OSNOVI IMIDAZOLIJEVEGA FLUORIDA ZA NUKLEOFILNO FLUORIRANJE
Mentor: izr. prof. dr. Jernej Iskra
Datum zagovora: 14. 9. 2017

Lea KASTELEC

DOLOČANJE KALCIJA Z IONOSELEKTIVNO ELEKTRODO
Mentor: izr. prof. dr. Mitja Kolar
Datum zagovora: 14. 9. 2017

Neža LUPŠINA

KATALITSKE REAKCIJE V SINTEZI SUBSTITUIRANIH FENILPIRIMIDINOV
Mentor: izr. prof. dr. Franc Požgan
Datum zagovora: 14. 9. 2017

Deja ZUPANČIČ

SINTEZA IZBRANIH ALKIL INDOLIZIN-KARBOKSILATOV
Mentor: prof. dr. Janez Košmrlj
Datum zagovora: 14. 9. 2017

Urška JELENOVEC

ŽELEZO, VEZANO NA HIPERZAMREŽEN POLIPIRIDIN KOT KATALIZATOR ZA OKSIDACIJO BENZIL ALKOHOLA
Mentor: izr. prof. dr. Jernej Iskra
Datum zagovora: 14. 9. 2017

Vesna ZUPANČIČ

SPEKTROSKOPSKE METODE ZA DOLOČANJE KALCIJA V PREHRANSKIH DODATKIH
Mentor: izr. prof. dr. Mitja Kolar
Datum zagovora: 14. 9. 2017

Nataša ERJAVŠEK

PRETVORBE ORGANSKIH SPOJIN NA TRADICIONALEN IN ALTERNATIVEN NAČIN
Mentor: izr. prof. dr. Marjan Jereb
Datum zagovora: 15. 9. 2017

Nina CESAR

IZLUŽEVANJE POTENCIALNO STRUPENIH ELEMENTOV IZ JALOVINSKEGA MATERIALA PO STABILIZACIJI
Mentorica: doc. dr. Marija Zupančič
Datum zagovora: 15. 9. 2017

Matic POKORN

ORGANOKATALIZIRANE REAKCIJE 5-IZOBUTILPIROLONA Z DERIVATI ISATINIMINA
Mentor: doc. dr. Uroš Grošelj
Datum zagovora: 15. 9. 2017

Urška PETRAČ

TEKOČINSKOSCINTILACIJSKA SPEKTROMetriJA: SKUPNA AKTIVNOST SEVALCEV ALFA IN BETA V VODI
Mentorica: izr. prof. dr. Nataša Gros
Datum zagovora: 15. 9. 2017

Irena HAFNER

POTENCIOMETRIČNE TITRACIJE PUFRSKIH SNOVI IN ZMESI
Mentorica: izr. prof. dr. Nataša Gros
Datum zagovora: 28. 9. 2017

Urška ŽONTA

OVREDNOTENJE TOPLOTNIH LASTNOSTI POLIMERNE ELEKTROIZOLACIJSKE PREVLEKE AKTIVNIH KOMPONENT ELEKTROMOTORJEV
Mentor: izr. prof. dr. Matija Tomšič
Datum zagovora: 29. 9. 2017

Rok KAUFMAN

RAZUMEVANJE KONCEPTA ENTROPIJE IN DRUGEGA ZAKONA TERMODINAMIKE
Mentor: prof. dr. Andrej Jamnik
Datum zagovora: 19. 10. 2017

KEMIJSKO INŽENIRSTVO – 1. STOPNJA**Rok NOVAK**

KOMPOZITNI MATERIALI ZA ZAJEMANJE SONČNE ENERGIJE

Mentor: prof. dr. Miran Gaberšček

Datum zagovora: 2. 2. 2017

Katarina KADIVNIK

SINTEZA KOPOLIMERNIH MIKROSFERNIH AKRILATNIH LEPIL Z UPORABO RAZLIČNIH KOMONOMEROV TER NJIHOV VPLIV NA ADHEZIJO NA NIZKO ENERGETSKE SUBSTRATE

Mentor: doc. dr. Jernej Kajtna

Datum zagovora: 25. 4. 2017

Miha HORVAT

FIZIKALNE IN KEMIJSKE METODE ZA IZBOLJŠANJE ADHEZIJE NA NIZKOENERGIJSKE POVRŠINE

Mentor: doc. dr. Jernej Kajtna

Datum zagovora: 10. 5. 2017

Andreja PETROVIČ

BIOSENSOR BASED ON CARBON NANOTUBE TRANSDUCER

Mentorica: prof. dr. Polona Žnidaršič Plazl

Datum zagovora: 15. 5. 2017

Blaž OBLAK

POVEČANJE POVRŠINE V MIKROSISTEMIH Z NANOSTRUKTURIRANIMI MATERIALI

Mentor: prof. dr. Igor Plazl

Datum zagovora: 17. 5. 2017

Tine PLAVČAK

LOČEVANJE KAPLJEVINA-KAPLJEVINA Z MIKROFLUIDNIMI NAPRAVAMI

Mentorica: prof. dr. Polona Žnidaršič Plazl

Datum zagovora: 7. 7. 2017

Jernej ROZMANSINTEZA IN DIELEKTRIČNE LASTNOSTI SILENITNE KERAMIKE Z Co²⁺, Ga³⁺ IN V⁵⁺ KATIONI

Mentor: prof. dr. Danilo Suvorov

Datum zagovora: 13. 7. 2017

Blaž REGINA

INTEGRIRANI PROCESI V KONTINUIRNO DELUJOČIH NAPRAVAH

Mentorica: prof. dr. Polona Žnidaršič Plazl

Datum zagovora: 17. 7. 2017

Barbara VREČER

HIDROTERMALNA SINTEZA KREMENA V REAKTORJU

Mentor: izr. prof. Aleš Podgornik

Datum zagovora: 30. 8. 2017

Elena SPASEVSKA

GRAFENSKI MATERIALI ZA PROTIKOROZIJSKO ZASCITO

Mentor: doc. dr. Boštjan Genorio

Datum zagovora: 31. 8. 2017

Sandra ZAPLOTNIK

ŠTUDIJA IZDELAVE EMULZIJ S POMOČJO ULTRAZVOKA – 2. STOPNJA

Mentor: izr. prof. dr. Matevž Dular

Datum zagovora: 1. 9. 2017

Petra MARKOVIČ

SINTEZA IN KARAKTERIZACIJA POLIMERNIH MATERIALOV S SPOSOBNOSTJO SPOMINSKEGA EFEKTA

Mentor: doc. dr. Aleš Ručigaj

Datum zagovora: 4. 9. 2017

Mitja ROBIČ

IZOLACIJA PRODUKTA NANODELCEV ŽELEZOVEGA OKSIDA

Mentorica: prof. dr. Urška Šebenik

Datum zagovora: 4. 9. 2017

Mark SELAN

NITRIRANJE 8-HIDROKSIKINOLINA IN NEKATERIH NJEGOVIH DERIVATOV S PRETOČNO KEMIJO

Mentor: prof. dr. Igor Plazl

Datum zagovora: 5. 9. 2017

Barbara DEBEVEC

UPORABA OZONACIJE ZA ODSTRANJEVANJE UMETNIH SLADIL IZ VODNE RAZTOPINE

Mentorica: izr. prof. dr. Andreja Žgajnar Gotvajn

Datum zagovora: 7. 9. 2017

Matic ZIBELNIK

ANODNI MATERIALI ZA GORIVNE CELICE S TRDNIM ELEKTROLITOM NA OSNOVI PEROVSKITNE STRUKTURE

Mentor: izr. prof. dr. Marjan Marinšek

Datum zagovora: 8. 9. 2017

Luka PAVKO

TOPNOST FARMACEVTSKIH UČINKOVIN IN NJIHOVA ODSTRANITEV IZ PROIZVODNE LINIJE

Mentor: izr. prof. Aleš Podgornik

Datum zagovora: 8. 9. 2017

Domen OŠTIR

SINTEZA IN KARAKTERIZACIJA GRAFENA DOPIRANEGA Z DUŠIKOM

Mentor: doc. dr. Boštjan Genorio

Datum zagovora: 8. 9. 2017

Ana LISAC

MATEMATIČNO MODELIRANJE RAZMNOŽEVANJA BAKTERIOFAGOV V PRETOČNEM MEŠALNEM REAKTORJU

Mentor: izr. prof. Aleš Podgornik

Datum zagovora: 13. 9. 2017

Žiga KOBAL

KOMUNALNE ČISTILNE NAPRAVE NA OBČUTLJIVIH OBMOČJIH REPUBLIKE SLOVENIJE

Mentorica: izr. prof. dr. Andreja Žgajnar Gotvajn

Datum zagovora: 13. 9. 2017

Silvo KOMATARNANODELCI V ODPADNIH VODAH IN NJIHOV VPLIV NA
BIOLOŠKO ČISTILNO NAPRAVO

Mentorica: izr. prof. dr. Andreja Žgajnar Gotvajn

Datum zagovora: 13. 9. 2017

Neva IHANEC

KRIOGELI

Mentor: izr. prof. Aleš Podgornik

Datum zagovora: 13. 9. 2017

Matej SAŠEKPREGLED IN UPORABA ODPADNIH ŽELEZOVIH
MATERIALOV ZA FENTONOVO OKSIDACIJO

Mentorica: doc. dr. Gabriela Kalčikova

Datum zagovora: 13. 9. 2017

Matej KRNC

pH ODZIVNI POLIMERI

Mentor: izr. prof. Aleš Podgornik

Datum zagovora: 13. 9. 2017

Tilen TURK

MIKROPLASTIKA V OKOLJU

Mentorica: doc. dr. Gabriela Kalčikova

Datum zagovora: 13. 9. 2017

Klemen PLAHUTAPRIMERJAVA ŠARŽNE IN KONTINUIRNE PROIZVODNJE
V FARMACEVTSKI INDUSTRIJI

Mentor: prof. dr. Igor Plazl

Datum zagovora: 13. 9. 2017

Andraž VERLIČ

ADSORPCIJA POLUTANTOV NA MIKROPLASTIKO

Mentorica: doc. dr. Gabriela Kalčikova

Datum zagovora: 13. 9. 2017

Ula ROZMANVPLIV ANTIBIOTIKA TIAMULINA NA VODNE
ORGANIZME

Mentorica: doc. dr. Gabriela Kalčikova

Datum zagovora: 13. 9. 2017

Žiga FIDLER

DISIPATIVNA DINAMIKA DELCEV

Mentor: prof. dr. Igor Plazl

Datum zagovora: 14. 9. 2017

Tomaž RAKUŠSINTEZA IN KARAKTERIZACIJA MoS₂

Mentor: doc. dr. Boštjan Genorio

Datum zagovora: 14. 9. 2017

Nikola STOJANOVIĆ

MIKROSTRUKTURA ZAVORNIH PLOŠČIC

Mentor: izr. prof. dr. Marjan Marinšek

Datum zagovora: 15. 9. 2017

Luka GOLOBENCIMSKO KATALIZIRANE KASKADNE REAKCIJE V
MIKROKANALIH

Mentorica: prof. dr. Polona Žnidaršič Plazl

Datum zagovora: 15. 9. 2017

Ajda KUNAVARČRNILO NA OSNOVI GRAFENSKIH MATERIALOV ZA
TISKANJE TANKIH FILMOV

Mentor: doc. dr. Boštjan Genorio

Datum zagovora: 15. 9. 2017

Jan ZUPANČIČINTEGRACIJA BOKATALITSKIH PROCESOV V
MIKROFLUIDNIH NAPRAVAH

Mentorica: prof. dr. Polona Žnidaršič Plazl

Datum zagovora: 15. 9. 2017

Matej ŠVERKOPOMEN VISKOZNOSTI PRI OBVLADOVANJU
STABILNOSTI BIKOMPONENTNEGA PREDENJA

Mentor: prof. dr. Igor Plazl

Datum zagovora: 15. 9. 2017

Julija SIMAKOVIČŠTUDIJA IZDELAVE EMULZIJE S POMOČJO
ULTRAZVOKA – 1. STOPNJA

Mentor: izr. prof. dr. Matevž Dular

Datum zagovora: 15. 9. 2017

Žan KOVAČIČSINTEZA POLIMERA NA OSNOVI REVERZIBILNE DIELS-
ALDER REAKCIJE

Mentor: doc. dr. Aleš Ručigaj

Datum zagovora: 15. 9. 2017

Uroš KARLIČKARAKTERIZACIJA MEHANSKIH LASTNOSTI POROZNIH
POLIMEROV

Mentor: izr. prof. Aleš Podgornik

Datum zagovora: 19. 9. 2017

Darja PUKLAVECSINTEZA IN KARAKTERIZACIJA POLIMERNIH
MATERIALOV S SPOSOBNOSTJO SAMOCELJENJA NA
OSNOVI DIELS-ALDER REAKCIJE

Mentor: doc. dr. Aleš Ručigaj

Datum zagovora: 20. 11. 2017

BIOKEMIJA – 1. STOPNJA**Gašper MARINŠEK**

KARAKTERIZACIJA NEKATERIH MUTANT ČLOVEŠKEGA KATEPSINA B

Mentor: doc. dr. Marko Novinec

Datum zagovora: 20. 2. 2017

Uroš ZAVRTANIK

KORELACIJA MED VEZAVNIMI POVRŠINAMI IN TERMODINAMIKO VEZANJA FRAGMENTOV KAMELOIDNIH PROTITELES Z ANTIGENI

Mentor: prof. dr. Jurij Lah

Datum zagovora: 3. 7. 2017

Tilen TRŠELIČ

IZRAŽANJE SKRAJŠANIH OBLIK ČLOVEŠKEGA TESTIKANA-1 IN ISKANJE NJUNIH INTERAKCIJSKIH PARTNERJEV V ZUNAJCELIČNEM MATRIKSU

Mentor: doc. dr. Miha Pavšič

Datum zagovora: 5. 7. 2017

Klara LENART

PRIPRAVA TREH REKOMBINANTNIH ORTOKASPAZ IZ CIANOBAKTERIJ MICROCYSTIS AERUGINOSA PCC 7806 IN SYNECHOCYSTIS SP. PCC 6803 V BAKTERIJI ESCHERICHIA COLI

Mentor: izr. prof. dr. Marko Dolinar

Datum zagovora: 5. 7. 2017

Živa MORAVEC

PRIPRAVA KIMERNIH DIMERIZACIJSKIH OBLIK PROTEINA EpCAM

Mentorica: prof. dr. Brigita Lenarčič

Datum zagovora: 13. 7. 2017

Lara JERMAN

ANALIZA POGOSTOSTI NAPOVEDANIH CEPITVENIH MEST KASPAZ NA EKSONSKIH STIKIH PROTEINOV PRI ČLOVEKU

Mentor: doc. dr. Gregor Gunčar

Datum zagovora: 23. 8. 2017

Neža KORITNIK

IZOLACIJA PROTEINA CRISP IZ STRUPA MODRASA (VIPERA AMMODYTES AMMODYTES) IN STRUKTURNA KARAKTERIZACIJA NJEGOVIH IZOBLIK

Mentor: prof. dr. Igor Križaj

Datum zagovora: 23. 8. 2017

Luka DEJANOVIČ

NAČRTOVANJE IN PRIPRAVA RAZLIČNIH OBLIK ZNOTRAJCELIČNEGA DELA PROTEINA EpCAM

Mentorica: prof. dr. Brigita Lenarčič

Datum zagovora: 28. 8. 2017

Klara KURET

PRIPRAVA REKOMBINANTNEGA B-KATENINA IN FHL2 TER OPTIMIZACIJA PROIZVODNEGA PROCESA

Mentorica: prof. dr. Brigita Lenarčič

Datum zagovora: 28. 8. 2017

Urša ČERČEK

POVEZAVA MED NASTANKOM STRESNIH GRANUL IN AGREGACIJO TDP-43 V SESALSKIH CELICAH

Mentor: izr. prof. dr. Boris Rogelj

Datum zagovora: 6. 9. 2017

Fran KRSTANOVIČ

FILOGENOMSKA ANALIZA PROTEINSKIH TVORCEV POR PRI EVKARIONTIH

Mentor: izr. prof. dr. Dušan Kordiš

Datum zagovora: 8. 9. 2017

Peter PEČAN

FILOGENOMSKA ANALIZA PROTEAZNIH INHIBITORJEV PRI PROKARIONTIH

Mentor: izr. prof. dr. Dušan Kordiš

Datum zagovora: 8. 9. 2017

Urška KAŠNIK

VPLIV AKTIVACIJE Z G-PROTEINI SKLOPLJENIH RECEPTORJEV NA NASTANEK LIPIDNIH KAPLJIC V PODGANJIH ASTROCITIH V KULTURI

Mentorica: doc. dr. Nina Vardjan

Datum zagovora: 11. 9. 2017

Miha KOPRIVNIKAR KRAJNC

RAZNOLIKOST IZRAŽANJA KATEPSINOV K IN X NA TKIVNIH REZINAH GLIOBLASTOMA

Mentorica: prof. dr. Tamara Lah Turnšek

Datum zagovora: 11. 9. 2017

Blaž LEBAR

OPREDELITEV IZRAŽANJA RECEPTORJA ZA ERITROPOETIN Z METODO PO FAR-WESTERNU IN DVOJNIM PRENOSOM

Mentorica: izr. prof. dr. Nataša Debeljak

Datum zagovora: 12. 9. 2017

Špela MALENŠEK

RAZVOJ IN KARAKTERIZACIJA REGULATORJEV GENOV LEF1, GATA1, GATA3 IN IRF4

Mentor: prof. dr. Simon Horvat

Datum zagovora: 13. 9. 2017

Valentina LEVAK

PREVERJANJE INSEKTICIDNE UČINKOVITOSTI dsRNA PROTI KOLORADSKEMU HROŠČU

Mentorica: prof. dr. Kristina Gruden

Datum zagovora: 13. 9. 2017

Katja ČOP

IZBOR NORMALIZACIJSKE METODE ZA KVANTITATIVNO DOLOČITEV PROTEINOV V CELIČNIH LINIJAH RAKA DOJKE

Mentorica: izr. prof. dr. Nataša Debeljak

Datum zagovora: 13. 9. 2017

Ernest ŠPRAGER

PRIPRAVA FUZIJSKEGA PROTEINA NANOTELESA M33 Z APEX2 ZA IMUNODETEKCIJO MLKL

Mentor: doc. dr. Gregor Gunčar

Datum zagovora: 13. 9. 2017

Tadej SATLER

VPLIV ZAMENJAVE NEKATERIH OHRANJENIH
GLICINSKIH OSTANKOV NA AKTIVNOST KATEPSINA K
Mentor: doc. dr. Marko Novinec
Datum zagovora: 13. 9. 2017

Gašper VIRANT

KALORIMETRIČNO DOLOČANJE KONFORMACIJSKEGA
PREHODA POLIKARBOKSILNIH KISLIN
Mentorica: prof. dr. Ksenija Kogej
Datum zagovora: 13. 9. 2017

Rok MIKLAVČIČ

PRIPRAVA PROTEINOV rPE6 IN VP8 V E. COLI ZA
AFINITETNO LOČEVANJE GLIKOPROTEINOV
Mentor: doc. dr. Gregor Gunčar
Datum zagovora: 13. 9. 2017

Jerneja OVČAR

PRIMERJAVA SIGNALNIH POTI, KI JIH SPROŽI
CITOKIN TNF ALFA NA CELIČNI LINIJI ČLOVEŠKEGA
ADENOKARCINOMA DEBELEGA ČREVEESA HT-29
Mentor: prof. ddr. Boris Turk
Datum zagovora: 14. 9. 2017

Gašper ŽUN

ANALIZA GENA PIG1 KOT POTENCIALNEGA
VZROČNEGA GENA ZA FENOTIPSKO VARIACIJO V
AKUMULACIJI NEVTRALNIH LIPIDOV PRI KVASOVKI
SACCHAROMYCES CEREVISIAE
Mentor: izr. prof. dr. Uroš Petrovič
Datum zagovora: 14. 9. 2017

Tjaša SORČAN

VPLIV METABOLIČNEGA STRESA PRI ZAŠČITI
KARDIOMIOCIT PRED STRESOM ENDOPLAZEMSKEGA
RETIKULUMA
Mentorica: doc. dr. Tadeja Režen
Datum zagovora: 15. 9. 2017

Nina MAVEC

VPLIV OKSIDACIJE GVANINA NA STRUKTURO
G-KVADRUPLEKSOV V PROMOTORSKIH REGIJAH
Mentor: prof. dr. Janez Plavec
Datum zagovora: 15. 9. 2017

Ana POTOČNIK

VPLIV NATRIJEVEGA HIPOKLORITA NA RAST IZBRANIH
GLIV
Mentorica: prof. dr. Nina Gunde Cimerman
Datum zagovora: 27. 9. 2017

Katja BREZOVAR

VPLIV NEKATERIH ALOSTERIČNIH EFEKTORJEV
KATEPSINA K NA KATEPSIN S
Mentor: doc. dr. Marko Novinec
Datum zagovora: 5. 10. 2017

Peter PEKLAR

DOLOČEVANJE VSEBNOSTI KLORIDNIH IONOV V
POLIMERNIH MATERIALIH
Mentor: izr. prof. dr. Mitja Kolar
Datum zagovora: 16. 10. 2017

TEHNIŠKA VARNOST – 1- STOPNJA**Jure SELAN**

VARNOSTNA KULTURA PRI VIŠJE IN NIŽJE
KVALIFICIRANIH DELAVCIH
Mentor: doc. dr. Mitja Robert Kožuh
Datum zagovora: 13. 9. 2017

Blaž ZUPANČIČ

VARNOSTNA KULTURA V CIVILNEM LETALSTVU
Mentor: doc. dr. Mitja Robert Kožuh
Datum zagovora: 14. 9. 2017

Luka MAROLT

PREPREČEVANJE ZASTRUPITEV Z OGLJIKOVIM OKSIDOM
Mentorica: doc. dr. Barbara Novosel
Datum zagovora: 14. 9. 2017

Klemen BORIN

POZARNA VARNOST SONČNIH ELEKTRARN
Mentor: prof. dr. Simon Schnabl
Datum zagovora: 14. 9. 2017

Sara KOTNIK

UPORABA NANOTEHNOLOGIJE PRI OBDELAVI PITNE
VODE
Mentorica: izr. prof. dr. Andreja Žgajnar Gotvajn
Datum zagovora: 14. 9. 2017

Barbara JESENKO

STATISTIČNA ANALIZA VARNOSTI V LETALSKEM
PROMETU
Mentor: izr. prof. dr. Tomaž Urbič
Datum zagovora: 14. 9. 2017

Sebastjan TUHTAR

POŽARNA VARNOST V DELAVNICAH
IN LAKIRNICAH
Mentor: doc. dr. Domen Kušar
Datum zagovora: 15. 9. 2017

Lara BOŽIČ

NASILJE TRETJIH OSEB - ŠTUDIJA PRIMERA
ZDRAVSTVENE ORGANIZACIJE
Mentorica: doc. dr. Marija Molan
Datum zagovora: 15. 9. 2017

Manca ZMRZLIKAR

VPLIV PENILA NA LASTNOSTI PENE KOT GASILNEGA
SREDSTVA
Mentor: prof. dr. Simon Schnabl
Datum zagovora: 15. 9. 2017

Peter VIRŠEK

VARNO OBRATOVANJE PLINOVODNEGA OMREŽJA

Mentorica: doc. dr. Barbara Novosel

Datum zagovora: 15. 9. 2017

Anja ŽEROVNIKZAHTEVE VARSTVA PRED POŽAROM ZA GARAŽNE HIŠE
ZA PARKIRANJE ELEKTRIČNIH AVTOMOBILOV

Mentor: doc. dr. Domen Kušar

Datum zagovora: 30. 11. 2017

Kristina SCHWEDZAŠČITNA OPREMA DELOVNIH SREDSTEV S
POUDARKOM NA VARNOSTNIH NAPRAVAH

Mentor: doc. dr. Boris Jerman

Datum zagovora: 1. 12. 2017

DIPLOME – VISOKOŠOLSKI STROKOVNI ŠTUDIJI**KEMIJSKA TEHNOLOGIJA – 1. STOPNJA****Vesna RIFELJ**RAZVOJ MIKROSTRUKTURE KERAMIKE NA OSNOVI
LANTAN STRONCIJ MANGAN KROM OKSIDA

Mentor:izr. prof. dr. Marjan Marinšek

Datum zagovora: 11. 1. 2017

Neža ŽIBERTTERMODINAMIKA MICELIZACIJE NATRIJEVEGA
DODECILBENZEN SULFONATA TER MOŽNOSTI
NJEGOVEGA ODSTRANJEVANJA IZ VODNIH RAZTOPIN

Mentor: dr. Bojan Šarac

Datum zagovora: 10. 2. 2017

Zala DOLŽANSINTEZA 2H-PIRAN-2-ONSKIH DERIVATOV IN
NJIHOVE NADALJNJE [4+2] CIKLOADICIJE Z
MALEINANHIDRIDOM

Mentor: doc. dr. Krištof Kranjc

Datum zagovora: 13. 2. 2017

Anja PAPEŽ

PRETVORBE VANILINA Z IZBRANIMI REAKCIJAMI

Mentor:izr. prof. dr. Franci Kovač

Datum zagovora: 15. 2. 2017

Janja FINKSINTEZA KURKUMINA MODIFICIRANEGA S
HEKSANOJSKO KISLINO

Mentor: prof. dr. Darko Dolenc

Datum zagovora: 20. 2. 2017

Nina BUKOVACDOLOČEVANJE STOPNJE SUBSTITUCIJE
KARBOKSIMETIL ŠKROBA V INDUSTRIJSKIH IZDELKIH

Mentor: doc. dr. Janez Cerar

Datum zagovora: 21. 2. 2017

Tjaša SLAKNEUTRALIZACIJSKE TITRACIJE S POTENCIOMETRIČNO
IN SPEKTROFOTOMETRIČNO DOLOČITVIJO KONČNE
TOČK

Mentor:izr. prof. dr. Mitja Kolar

Datum zagovora: 3. 3. 2017

Kaja KOŠMRLJOVREDNOTENJE KAKOVOSTI REKE SAVINJE IN
REČNEGA PRITOKA VOGLAJNA

Mentorica: dr. Tatjana Zupančič

Datum zagovora: 22. 3. 2017

Maja STAGLIČIČTVORBA KOKRISTALOV DIATRIZOIČNE KISLINE S
PIRIDINSKIMI DERIVATI

Mentor:izr. prof. dr. Franc Perdih

Datum zagovora: 10. 5. 2017

Monika SIMČIČANALIZA KOMERCIALNO DOSTOPNIH ZDRAVIL Z
RENTGENSKO PRAŠKOVNO DIFRAKCIJO

Mentor: prof. dr. Anton Meden

Datum zagovora: 30. 5. 2017

Eva KORUNIČ

KROMOVE SPOJINE S PIPERAZINOM

Mentorica: doc. dr. Saša Petriček

Datum zagovora: 30. 5. 2017

Maša OCEPEKPROUČEVANJE ČASOVNE ODVISNOSTI UČINKOVITOSTI
STABILIZACIJE POTENCIALNO STRUPENIH ELEMENTOV
V jalovini z uporabo hidroksiapatita in biooglja

Mentor: doc. dr. Marija Zupančič

Datum zagovora: 1. 6. 2017

Aleksandra ZAMANSINTEZA SPOJIN Cu(nia)₂X IN NJIHOVA KARAKTERIZACIJA

Mentorica: doc. dr. Nives Kitanovski

Datum zagovora: 14. 6. 2017

Tilen TRČEK

LASTNOSTI GALENSKIH PRIPRAVKOV PREVODNOST IN pH

Mentorica: prof. dr. Ksenija Kogej

Datum zagovora: 21. 6. 2017

Nina BREMECPRIPRAVA SILIL SUBSTITUIRANIH BENZOJSKIH KISLIN Z
GRIGNARDOVIMI REAGENTI

Mentor:izr. prof. dr. Janez Cerkovnik

Datum zagovora: 4. 7. 2017

Timo RADOVIĆ

RENTGENSKA PRAŠKOVNA ANALIZA SREBROVIH
KOMPLEKSOV Z DERIVATI PIRIDIN-2-KARBOKSILNE
KISLINE

Mentor: izr. prof. dr. Franc Perdih

Datum zagovora: 4. 7. 2017

Valentina DUŠAK

BAKROVE KOORDINACIJSKE SPOJINE Z ANIONOM
GLUTARNE KISLINE

Mentorica: prof. dr. Ksenija Kogej

Datum zagovora: 4. 7. 2017

Leon BAUMKIRHER

OPTIMIZACIJA SINTEZE VODOTOPNE SOLI FULERENA
Th-C66(COONa)₁₂

Mentor: doc. dr. Janez Cerar

Datum zagovora: 11. 7. 2017

Anamarija POVŠIČ

SINTEZA ARIL-SUBSTITUIRANIH PIRAZINOV IN
KINOKSALINOV

Mentor: izr. prof. dr. Franc Požarnik

Datum zagovora: 13. 7. 2017

Dominik ROR

GOSTOTNA ANOMALIJA V RAZTOPINAH
IZOPROPANOLA IN LITIJEVEGA KLORIDA

Mentor: izr. prof. dr. Tomaž Urbič

Datum zagovora: 21. 7. 2017

Primož HORVAT

KOEFICIENTI AKTIVNOSTI MOČNIH KISLIN IN BAZ

Mentorica: prof. dr. Barbara Hribar Lee

Datum zagovora: 24. 8. 2017

Urban Anton PENKO NATLAČEN

POMEN VAKUUMSKE TEHNOLOGIJE V KEMIJI:
MATERIALI IN ČRPALKE

Mentor: dr. Andrej Godec

Datum zagovora: 28. 8. 2017

Ivo URH

DINAMIKA PROTONA IN HIDROKSIDNEGA IONA V
TEKOČI VODI

Mentor: doc. dr. Miha Lukšič

Datum zagovora: 30. 8. 2017

Eva TADIĆ

VALIDACIJA ANALIZNEGA POSTOPKA ZA DOLOČANJE
VSEBNOSTI IN ENAKOMERNOSTI AKTIVNE
UČINKOVINE V TABLETAH

Mentor: izr. prof. dr. Mitja Kolar

Datum zagovora: 4. 9. 2017

Klara ŽVAB

REOLOŠKE LASTNOSTI RAZTOPINE POLI(AKRILAMID-
AKRILNA KISLINA)

Mentor: dr. Branko Alič

Datum zagovora: 4. 9. 2017

Katarina JAMŠEK

OPTIMIZACIJA SINTEZ RUTENIJEVIH
KOORDINACIJSKIH SPOJIN Z NEKATERIMI N,N-
KELATNIMI LIGANDI

Mentor: prof. dr. Iztok Turel

Datum zagovora: 5. 9. 2017

Mateja BUKOVEC

KARAKTERIZACIJA IN SINTEZA BAKROVEGA(II)
OKTANOATA

Mentorica: doc. dr. Nives Kitanovski

Datum zagovora: 6. 9. 2017

Tea PODRŽAJ

6-METIL-3-BENZOILAMINO-2H-PIRAN-2-ONI IN
NJIHOVI DERIVATI KOT DIENI ZA IZBRANE [4+2]
CIKLOADICIJE

Mentor: doc. dr. Krištof Kranjc

Datum zagovora: 7. 9. 2017

Natalija GORENC

VPLIV SESTAVE MOBILNE FAZE NA OBLIKO
KROMATOGRAFSKIH VRHOV

Mentor: izr. prof. dr. Matevž Pompe

Datum zagovora: 7. 9. 2017

Eva KOŽUH

FORMACIJA ELEKTROAKTIVNEGA LIPIDNEGA
DVOSLOJA NA SENZORSKIH POVRŠINAH ZA RAZVOJ
IONSKEH SENZORJEV

Mentorica: dr. Tatjana Zupančič

Datum zagovora: 7. 9. 2017

Sarah GJEREK

FAZNA ANALIZA RAZLIČNIH ANORGANSKIH VZORCEV
S PRAŠKOVNO DIFRAKCIJO

Mentorica: izr. prof. dr. Amalija Golobič

Datum zagovora: 8. 9. 2017

Suzana KOREVEC

SINTEZA SUPERABSORBENTA NA OSNOVI AKRILAMIDA
IN AKRILNE KISLINE Z DODATKOM AMONIJEVEGA
CIRKONIJEVEGA KARBONATA KOT ZAMREŽEVALA

Mentor: dr. Branko Alič

Datum zagovora: 11. 9. 2017

Sandra DESPOTOVIČ

SINTEZE 5-METOKSIFENIL- IN 6-TERC-BUTIL-
SUBSTITUIRANIH 2H-PIRAN-2-ONOV IN NADALJNJE
[4+2] CIKLOADICIJE Z MALEINANHIDRIDOM

Mentor: doc. dr. Krištof Kranjc

Datum zagovora: 12. 9. 2017

Laura HRKA

SAMOČISTILNE TANKE PLASTI TiO₂ IZ TiCl₄ NA STEKLU
IN KOVINI

Mentorica: prof. dr. Urška Lavrenčič Štangar

Datum zagovora: 12. 9. 2017

Domen BOMBEK

ORGANOKATALIZIRANE REAKCIJE
5-(4-METOKSIBENZIL)PIROLONA S TRANS-B-
NITROSTIRENI

Mentor: doc. dr. Uroš Grošelj

Datum zagovora: 13. 9. 2017

Simon BUKOVEC

MINERALNA SESTAVA KAMNIN VZDOLŽ POTOKA
SUŠICA NA OBROBJU KOČEVSKÉ PLANOTE

Mentor: prof. dr. Anton Meden

Datum zagovora: 13. 9. 2017

Tina BROJAN

FLAVONOIDI, KOT LIGANDI ZA RAZLIČNE PROTEINSKE
TARČE VIRUSA EBOLE

Mentor: doc. dr. Črtomir Podlipnik

Datum zagovora: 14. 9. 2017

Miha IVANETIČ

DOLOČEVANJE MAKROMOLEKUL Z VELIKOSTNO
IZKLUČITVENO KROMATOGRAFIJO

Mentor: izr. prof. dr. Drago Kočar

Datum zagovora: 14. 9. 2017

Aleksandra MEDVED

ANALIZA SPEKTROPOLARIMETRIČNIH PODATKOV IN
STRUKTURNE LASTNOSTI PROTEINOV

Mentor: prof. dr. Jurij Lah

Datum zagovora: 14. 9. 2017

Kim PLUT

PRIPRAVA IZBRANIH HALO ACETILIDOV

Mentor: Martin Gazvoda

Datum zagovora: 14. 9. 2017

Katja METELKO

ANALIZA SPEKTROPOLARIMETRIČNIH PODATKOV IN
STRUKTURNE LASTNOSTI MOLEKULE DNA

Mentor: prof. dr. Jurij Lah

Datum zagovora: 14. 9. 2017

Sabina DERLINK

DOLOČANJE VSEBNOSTI FOLNE KISLINE V TABLETIH IN
PREHRANSKIH DOPOLNILIH

Mentorica: dr. Tatjana Zupančič

Datum zagovora: 14. 9. 2017

Sara ARTAČ

PREIZKUŠANJE EKSTRAKCIJE ONESNAŽEVAL PCB IZ TAL
IN SEDIMENTOV

Mentorica: prof. dr. Helena Prosen

Datum zagovora: 15. 9. 2017

Žiga DRKUŠIČ

RAZLIČNI PIRIDINKARBOKSAMIDI KOT KATIONI V
HEKSAFLUORIDOSILIKATNIH SOLEH

Mentor: doc. dr. Andrej Pevec

Datum zagovora: 18. 9. 2017

Majk FIDERŠEK

ORGANOKATALIZIRANE REAKCIJE 5-(4-NITROBENZIL)
PIROLONA Z NITROALKENI

Mentor: doc. dr. Uroš Grošelj

Datum zagovora: 22. 9. 2017

Klavdija ANŽELJ

VOLUMSKE SPREMEMBE PRI MEŠANJU VODNIH
RAZTOPIN 1 : 1 SOLI IN ALKOHOLOV

Mentor: doc. dr. Janez Cerar

Datum zagovora: 22. 9. 2017

Anja OREL

KARAKTERIZACIJA IN SINTEZA SPOJINE
[Cu(C₇H₅O₃)₂(C₆H₆N₂O)₂(H₂O)₂]

Mentorica: doc. dr. Nives Kitanovski

Datum zagovora: 27. 9. 2017

Tamara ĐORĐEVIĆ

POSTAVITEV IN TESTIRANJE KOMPAKTNEGA
REAKTORJA ZA FOTOKATALITSKO RAZGRADNJO
ONESNAŽIL V VODI

Mentorica: prof. dr. Urška Lavrenčič Štangar

Datum zagovora: 27. 9. 2017

Tjaša GROS

UPORABA FARMAKOFORNIH MODELOV PRI
MODELIRANJU INHIBITORJEV KINAZE B-RAF

Mentor: doc. dr. Črtomir Podlipnik

Datum zagovora: 27. 9. 2017

Katja HRLEC

ISKANJE INHIBITORJEV PROTEINA EBOLAVIRUSA VP35
Z UPORABO VIRTUALNEGA REŠETANJA

Mentor: doc. dr. Črtomir Podlipnik

Datum zagovora: 27. 9. 2017

Grega LONGHINO

IZBRANE REAKCIJE BENZALDEHIDOV Z WITTIGOVIM
REAGENTOM

Mentor: izr. prof. dr. Janez Cerkovnik

Datum zagovora: 27. 9. 2017

Sanja VASIČ

VOLUMSKE SPREMEMBE PRI MEŠANJU RAZTOPIN
1,1-ELEKTROLITOV

Mentor: doc. dr. Janez Cerar

Datum zagovora: 29. 9. 2017

Katarina DUŠAK

BAKROVE KOORDINACIJSKE SPOJINE Z ANIONOM
GLUTARNE KISLINE

Mentor: doc. dr. Bojan Kozlevčar

Datum zagovora: 29. 9. 2017

Tina PAVLIČ

PARAMETRI ODPADNIH VODA: MOTNOST IN
VALIDACIJA MERILNIKOV MOTNOSTI

Mentor: dr. Andrej Godec

Datum zagovora: 29. 9. 2017

Zala ŠUMAN

SAMOPOPRAVLJIVI BETON

Mentor: izr. prof. dr. Marjan Marinšek

Datum zagovora: 29. 9. 2017

Sabina SELIMANOVIĆ

FIZIKALNI PARAMETRI VULKANSKEGA SISTEMA

Mentor: dr. Andrej Godec

Datum zagovora: 29. 9. 2017

Urša SINUR

VPLIV ZAMREŽEVALCEV NA LASTNOSTI HIDROGELOV

Mentor: dr. Branko Alič

Datum zagovora: 3. 10. 2017

Tanja ŠTEFANČIČ

FAZNA ANALIZA VZORCEV TAL IZ ZAGORICE S
PRAŠKOVNO DIFRAKCIJO
Mentorica:izr. prof. dr. Amalija Golobič
Datum zagovora: 3. 10. 2017

Tjaša TOMAŽIN

RAZLIČNI PIRIDINKARBOKSAMIDI KOT KATIONI V
HEKSAFLUORIDOTITANATNIH SOLEH
Mentor: doc. dr. Andrej Pevec
Datum zagovora: 3. 10. 2017

Kristina VERHOVEC

REGULACIJA TLAKA V LABORATORIJIH V NOVI STAVBI
FAKULTETE ZA KEMIJO IN KEMIJSKO TEHNOLOGIJO
Mentor: doc. dr. Janez Cerar
Datum zagovora: 10. 10. 2017

Zoran MARKOVIČ

UPORABA POVRŠINSKO AKTIVNIH SNOVI PRI
RAZTAPLJANJU TRDNIH FARMACEVTSKIH OBLIK
Mentor: dr. Bojan Šarac
Datum zagovora: 20. 10. 2017

Sanja GAVRIČ

STRUKTURNE ZNAČILNOSTI KOVINSKIH
 β -DIKETONATOV Z BIPRIDILAMINOM
Mentor:izr. prof. dr. Franc Perdih
Datum zagovora: 7. 11. 2017

Andreja LUŠIN

DOLOČANJE DUŠIKA PO KJELDAHLOVI METODI V
VZORCIH PAPIRJA, SMOLE IN V SITOVNI VODI
Mentorica: dr. Tatjana Zupančič
Datum zagovora: 27. 11. 2017

Tajda JEREB

VPLIV RAZLIČNIH MOBILNIH FAZ NA OBLIKO
KROMATOGRFSKEGA VRHA PRI TEKOČINSKI
KROMATOGRAFIJI VISOKE LOČLJIVOSTI
Mentor:izr. prof. dr. Drago Kočar
Datum zagovora: 27. 11. 2017

Almir ALIJA

KALORIČNE VREDNOSTI ŽIVIL
Mentorica: prof. dr. Barbara Hribar Lee
Datum zagovora: 8. 12. 2017

Anton VAMPEL

OPTIMIZACIJA SINTEZE DIMETIL ESTRA PIRIDIN-2,6-
DIKARBOKSILNE KISLINE
Mentor:izr. prof. dr. Franc Perdih
Datum zagovora: 12. 12. 2017

Neva KLANČAR

VPILV OKOLJSKIH FAKTORJEV NA STRUPENOST
NANODELCEV
Mentorica:izr. prof. dr. Andreja Žgajnar Gotvajn
Datum zagovora: 14. 12. 2017

Karin JURČEK

DOLOČANJE ANIONOV V PRAHU S SLIKE
Mentorica:izr. prof. dr. Irena Kralj Cigić
Datum zagovora: 15. 12. 2017

Anja ŠUŠTAR

FAZNA ANALIZA TAL IZ SUHE KRAJINE Z RENTGENSKO
PRAŠKOVNO DIFRAKCIJO
Mentorica:izr. prof. dr. Amalija Golobič
Datum zagovora: 20. 12. 2017

Ana ŠKRLJ

DOLOČANJE ASKORBINSKE KISLINE V PREHRANSKIH
DOPOLNILIH IN FARMACEVTSKIH PRIPRAVKIH
Z UPORABO MOLEKULSKE ABSORPCIJSKE
SPEKTROFOTOMETRIJE, TEKOČINSKE
KROMATOGRAFIJE VISOKE LOČLJIVOSTI IN REDOKS
TITRACIJE
Mentorica: dr. Tatjana Zupančič
Datum zagovora: 22. 12. 2017

Petra ČOŽ

KOMPLEKSI KOBALTOVEGA(II) KLORIDA IN
3-HIDROKSIPIRIDIN-2-ONA
Mentorica: doc. dr. Saša Petriček
Datum zagovora: 22. 12. 2017

UNIVERZA V MARIBORU
FAKULTETA ZA KEMIJO IN KEMIJSKO TEHNOLOGIJO
1. januar – 31. december 2017

DOKTORATI

DOKTORSKI ŠTUDIJ – 3. STOPNJA

Alejandro BARTOLOME ORTEGA

EKSTRAKCIJA IN SEPARACIJA AKTIVNIH SPOJIN Z
NADKRITIČNO EKSTRAKCIJO IN PREPARATIVNO
NADKRITIČNO KROMATOGRAFIJO

Mentor: red. prof. dr. Željko Knez

Somentorica: red. prof. dr. Mojca Škerget

Datum zagovora: 4. 7. 2017

Lidija KORAT

PRISTOP ZA CELOVIT NADZOR IZPOSTAVLJENOSTI
NEVARNIM SNOVEM NA DELOVNIH MESTIH

Mentor: red. prof. dr. Željko Knez

Somentorica: red. prof. dr. Zorka Novak Pintarič

Datum zagovora: 18. 10. 2017

Milica PANTIČ

VISOKOTLAČNA IMPREGNACIJA MAŠČOBOTOPNIH
VITAMINOV V POLISAHARIDNE AEROGELE

Mentor: red. prof. dr. Zoran Novak

Somentor: red. prof. dr. Željko Knez

Datum zagovora: 18. 4. 2017

Annamaria VUJANOVIĆ

VEČNAMENSKA SINTEZA OSKRBOVALNIH MREŽ
PODJETIJ NA OSNOVI INTEGRACIJE OBNOVLJIVIH
VIROV

Mentor: red. prof. dr. Zdravko Kravanja

Somentorica: red. prof. dr. Zorka Novak Pintarič

Datum zagovora: 23. 6. 2017

Peter BERCE

OPTIMIZACIJA TVORBE FILMA PREMAZOV NA VODNI
OSNOVI Z UPORABO ELEKTROKEMIJSKE IMPEDANČNE
SPEKTROSKOPIJE

Mentorica: doc. dr. Mojca Slemnik

Datum zagovora: 18. 10. 2017

Alen MIUC

DOLOČANJE IN KEMOMETRIJSKA ANALIZA
ORGANSKIH SPOJINADSORBIRANIH NA PRAŠNE DELCE
PM10

Mentor: Doc. dr. Ernest Vončina

Somentor: Izr. prof. dr. Mitja Kolar

Datum zagovora: 20. 10. 2017

MAGISTERIJI

MAGISTRSKI ŠTUDIJ – 2. STOPNJA

Natalija BORINC

AEROBNI METABOLIZEM SLADKORJEV V SIROTKI

Mentorica: red. prof. dr. Andreja Goršek

Somentorica: doc. dr. Darja Pečar

Datum zagovora: 27. 9. 2017

Urška JANČIČ

IMOBILIZACIJA TRANSGLUTAMINAZE NA MAGNETNE
NANODELCE, MODIFICIRANE Z DEKSTRANOM

Mentorica: red. prof. dr. Maja Leitgeb

Datum zagovora: 1. 9. 2017

Jernej ROTAR

VPLIV SESTAVE GOJIŠČA NA PRODUKCIJSKO
SPOSOBNOST SEVA STREPTOMYCES CLAVULIGERUS

Mentor: red. prof. dr. Željko Knez

Somentorica: red. prof. dr. Maja Leitgeb

Datum zagovora: 6. 9. 2017

Tjan SMREČNIK

HIDROLIZA TANINOV S SUBKRITIČNO VODO -
DOLOČITEV OPTIMALNIH POGOJEV

Mentorica: red. prof. dr. Mojca Škerget

Somentor: red. prof. dr. Željko Knez

Datum zagovora: 21. 6. 2017

Katja ČUŠ

TOPNOST ORGANSKIH SPOJIN V PLINIH VISOKE
GOSTOTE TER MATEMATIČNO MODELIRANJE
PODATKOV

Mentorica: red. prof. dr. Mojca Škerget

Somentorica: doc. dr. Maša Knez Hrnčič

Datum zagovora: 18. 1. 2017

Gregor FAKIN

RAZVOJ METODE ZA MERJENJE DIFUZIJSKIH KOEFICIENTOV IN POVRŠINSKIH NAPETOSTI IZ GEOMETRIJE VISEČE KAPLJE S SUPERKRITIČNIMI FLUIDI

Mentor: red. prof. dr. Željko Knez

Somentorica: red. prof. dr. Mojca Škerget

Datum zagovora: 1. 9. 2017

Rok GOMILŠEK

ZAJEMANJE OGLJIKOVEGA DIOKSIDA IZ PROCESA PROIZVODNJE ALUMINIJA

Mentorica: doc. dr. Lidija Čuček

Somentorica: red. prof. dr. Zorka Novak Pintarič

Datum zagovora: 27. 9. 2017

Nuša KUGLER

OPTIMIRANJE PARAMETROV EKSTRAKCIJE LUBJA IGLAVCEV IN KARAKTERIZACIJA EKSTRAKTA

Mentorica: red. prof. dr. Mojca Škerget

Somentor: red. prof. dr. Željko Knez

Datum zagovora: 22. 3. 2017

Alen MOHARIČ

OPTIMIZACIJA PROIZVODNJE SINTEZNEGA PLINA IZ TRDNIH KOMUNALNIH ODPADKOV

Mentorica: doc. dr. Anita Kovač Kralj

Somentorica: doc. dr. Majda Krajnc

Datum zagovora: 22. 3. 2017

Emilijan STRGAR

PROCESNI POGOJI REGENERACIJE ZEOLITNIH ADSORBENTOV

Mentor: red. prof. dr. Željko Knez

Somentor: red. prof. dr. Zoran Novak

Datum zagovora: 15. 2. 2017

Mitja ŠTUMPF

SIMULACIJA OBRATOVANJA VISOKOTEMPERATURNE TOPLOTNE ČRPALKE S SUPERKRITIČNIM OGLJIKOVIM DIOKSIDOM

Mentor: izr. prof. dr. Darko Goričanec

Somentor: asist. dr. Peter Trop

Datum zagovora: 21. 6. 2017

Gašper ZAJC

TOPLOTNE LASTNOSTI FLUIDOV PRI VISOKIH TLAKIH

Mentor: red. prof. dr. Željko Knez

Somentorica: red. prof. dr. Mojca Škerget

Datum zagovora: 27. 9. 2017

Ana BRATUŠA

RAZVOJ NOVIH BIOAKTIVNIH PREVLEK Z VGRAJENIMI ZDRAVILNIMI UČINKOVINAMI NA NiCu NANODELCIH

Mentorica: dr. Irena Ban

Somentor: doc. dr. Uroš Maver

Datum zagovora: 1. 9. 2017

Urška BUKOVŠEK

SINTEZA MAGNETNO-IZLOČLJIVIH KATALIZATORJEV NA OSNOVI Ru NA OGLJIKU

Mentor: doc. dr. Sašo Gyergyek

Somentor: doc. dr. Blaž Likozar

Datum zagovora: 29. 9. 2017

Veronika FURLAN

[6]-GINGEROL KOT NARAVNI LOVILEC KEMIJSKIH KARCINOGENOV - RAČUNALNIŠKI PRISTOP

Mentor: izr. prof. dr. Urban Bren

Somentorica: asist. Eva Španinger

Datum zagovora: 6. 9. 2017

Barbara KAKER

RAZVOJ NiCu NANODELCEV Z RAZLIČNIMI FUNKCIONALNIMI OBLOGAMI

Mentor: doc. dr. Matjaž Kristl

Somentor: doc. dr. Uroš Maver

Datum zagovora: 19. 4. 2017

Bernarda KUSTER

ZNIŽEVANJE KPK V ODPADNI VODI S FENTONOVIM REAGENTOM

Mentorica: izr. prof. dr. Marjana Simonič

Somentorica: red. prof. dr. Zorka Novak Pintarič

Datum zagovora: 27. 9. 2017

Urška MENIČANIN

ZNIŽEVANJE VSEBNOSTI SNOVI V MLEKARSKI ODPADNI VODI

Mentorica: izr. prof. dr. Marjana Simonič

Somentorica: doc. dr. Sandra Janežič

Datum zagovora: 6. 9. 2017

Anja PALKO

VPLIV TEMPERATURE NA HIDROTERMIČNO DEGRADACIJO IN KINETIKO HIDROLIZE RUTINA V MODELNIH IN REALNIH VZORCIH

Mentorica: red. prof. dr. Mojca Škerget

Somentorica: red. prof. dr. Andreja Goršek

Datum zagovora: 19. 4. 2017

Saša REŠETA

PREUČEVANJE KOLOIDNIH LASTNOSTI MAGNETNIH NANODELCEV PREVLEČENIH S POLIPEPTIDOM

Mentor: doc. dr. Sašo Gyergyek

Somentor: dr. David Pahovnik

Datum zagovora: 27. 9. 2017

Petra UTROŠA

NANOPOROZNI POLIMERI IZ PREPLETENIH POLIMERNIH MREŽ

Mentor: doc. dr. Sebastijan Kovačič

Somentor: dr. David Pahovnik

Datum zagovora: 31. 8. 2017

Uroš VESELIČ

VPLIV MIKROVALOV NA STABILNOST DVOJNE VIJAČNICE DNK: RAČUNALNIŠKI PRISTOP

Mentor: izr. prof. dr. Urban Bren

Somentor: Martin Gladović

Datum zagovora: 1. 9. 2017

Dolores ZIMERL

PRIPRAVA ANALOGA FLUORIRANEGA ALKOHOLA V POLIMERNI OBLIKI

Mentor: izr. prof. dr. Jernej Iskra

Somentor: red. prof. dr. Peter Krajnc

Datum zagovora: 18. 5. 2017

DIPLOME – UNIVERZITETNI ŠTUDIJI**UNIVERZITETNI ŠTUDIJI – 1. STOPNJA****Sašo BJELIĆ**

RAČUNALNIŠKE SIMULACIJE INTERAKCIJE SUB- IN SUPERKRITIČNIH FLUIDOV Z RESVERATROLOM

Mentor: izr. prof. dr. Urban Bren

Somentorica: doc. dr. Maša Knez Hrnčič

Datum zagovora: 1. 9. 2017

Klara JEZERNIK

INHIBICIJSKA UČINKOVITOST MEŠANIC NEIONSKE- IONSKE POVRŠINSKO AKTIVNE SNOVI V AGRESIVNEM MEDIJU

Mentorica: izr. prof. dr. Regina Fuchs Godec

Somentor: doc. dr. Matjaž Finšgar

Datum zagovora: 6. 9. 2017

Tadeja KATAN

VEZAVA PALADIJA NA POROZEN ZAMREŽEN POLI(4-VINILPIRIDIN)

Mentor: red. prof. dr. Peter Krajnc

Somentor: izr. prof. dr. Jernej Iskra

Datum zagovora: 31. 8. 2017

Anja KOBALÉ

ZAMREŽEN POLI(4-VINILPIRIDIN) KOT KATALIZATOR NA TRDNEM NOSILCU

Mentor: izr. prof. dr. Jernej Iskra

Somentor: red. prof. dr. Peter Krajnc

Datum zagovora: 31. 8. 2017

Amadeja KOKOL

IN SITU POLIMERIZACIJA GLICIDIL METAKRILATA V POLI(METIL METAKRILATU)

Mentor: red. prof. dr. Peter Krajnc

Somentorica: asist. dr. Muzafera Paljevčac

Datum zagovora: 31. 8. 2017

Marina KOREN

ANALIZA BIOLOŠKIH POTI Z UPORABO ORODIJ GENSKE ONTOLOGIJE ZA GENE POVEZANE Z ASTMO

Mentor: red. prof. dr. Uroš Potočnik

Somentorica: doc. dr. Katja Repnik

Datum zagovora: 12. 7. 2017

Stanko KRAMER

POROZNI ORGANOGELI: SINTEZA IN ABSORPCIJA

Mentor: doc. dr. Sebastijan Kovačič

Datum zagovora: 31. 8. 2017

Davor KRESNIK

POLIMORFIZMI V GENIH FAAH IN ABHD4, VKLJUČENIH V BIOLOŠKO POT ENDOKANABINOIDOV ANANDAMINOV, PRI BOLNIKI Z OTROŠKO ASTMO

Mentor: red. prof. dr. Uroš Potočnik

Datum zagovora: 12. 7. 2017

Nika KUČUK

VPLIV RAZLIČNIH ADITIVOV V IZBRANIH POLIMERNIH MATERIALIH NA RAST GRAM POZITIVNIH IN GRAM NEGATIVNIH MIKROORGANIZMOV

Mentorica: doc. dr. Mateja Primožič

Somentorica: red. prof. dr. Maja Leitgeb

Datum zagovora: 1. 9. 2017

Špela LESIČAR

SINTEZA ZAMREŽENIH ENCIMSKIH SKUPKOV IZ ENCIMA TRANSGLUTAMINAZE

Mentorica: red. prof. dr. Maja Leitgeb

Somentorica: asist. Katja Vasić

Datum zagovora: 1. 9. 2017

Jernej LIPOVEC

MODELIRANJE REAKCIJ NEVTRALIZACIJE V MEŠALNEM REAKTORJU

Mentor: doc. dr. Miloš Bogataj

Somentorica: doc. dr. Lidija Čuček

Datum zagovora: 6. 9. 2017

Medea BREČKO

PRIMERJAVA POSTOPKOV PREDČIŠČENJA ODPADNE VODE PRED VSTOPOM V REVERZNO OSMOZO

Mentorica: izr. prof. dr. Marjana Simonič

Somentorica: dr. Irena Ban

Datum zagovora: 6. 9. 2017

Dominika LOVRENČEC

REŠEVANJE PROBLEMOV S PAMETNIM PISALOM V KEMIJI IN KEMIJSKI TEHNIKI

Mentorica: doc. dr. Majda Krajnc

Somentorica: doc. dr. Anita Kovač Kralj

Datum zagovora: 21. 6. 2017

Mihela MIHELIČ

NOVE POLIMERNE OBLOGE NA OSNOVI DERIVATOV POLIMETAKRILATA NA MEDICINSKEM JEKLU ZA POTENCIALNE BIOMEDICINSKE APLIKACIJE

Mentor: doc. dr. Matjaž Finšgar

Somentor: doc. dr. Uroš Maver

Datum zagovora: 6. 9. 2017

Jaka MIKLAVC

TEHNOLOŠKE REŠITVE PROBLEMATIKE ZATIRANJA NITASTIH ALG V HLADILNIH STOLPIH

Mentorica: red. prof. dr. Andreja Goršek

Somentorica: doc. dr. Darja Pečar

Datum zagovora: 6. 9. 2017

Mihaela PETEK

IMOBILIZACIJA LAKAZE V ZAMREŽENE ENCIMSKE SKUPKE (CLEAs)

Mentorica: red. prof. dr. Maja Leitgeb

Somentorica: asist. Katja Vasić

Datum zagovora: 27. 9. 2017

Katja PUCKO

PREUČEVANJE UČINKOVITOSTI DENITRIFIKACIJE NA ČISTILNI NAPRAVI ODRANCI

Mentorica: izr. prof. dr. Marjana Simonič

Somentor: dr. Janez Petek

Datum zagovora: 22. 3. 2017

Anja RANER

VPLIV AKRILATOV NA STRUKTURO KOPOLIMERNIH MREŽ AKRILAT/TIOL

Mentor: red. prof. dr. Peter Krajnc

Somentorica: asist. dr. Muzafera Paljevac

Datum zagovora: 31. 8. 2017

Ksenija RUTNIK

OPTIMIZACIJA IN VALIDACIJA METODE ZA DOLOČANJE SESTAVE ETERIČNIH OLJ HMELJA S PLINSKO KROMATOGRAFIJO

Mentor: doc. dr. Iztok Jože Košir

Somentor: doc. dr. Matjaž Finšgar

Datum zagovora: 1. 9. 2017

Nina ŠENEKAR

IMOBILIZACIJA LAKAZE V MAGNETNE ZAMREŽENE ENCIMSKE SKUPKE (mCLEAs)

Mentorica: red. prof. dr. Maja Leitgeb

Somentorica: asist. Katja Vasič

Datum zagovora: 6. 9. 2017

Nastja ŠIMENKOIMOBILIZACIJA α -GALAKTOZIDAZE NA MAGNETNE MAGHEMITNE NANODELCE IN ZAMREŽENJE LE-TEH V ENCIMSKE SKUPKE

Mentorica: red. prof. dr. Maja Leitgeb

Somentorica: asist. Katja Vasič

Datum zagovora: 22. 3. 2017

Marko ŠKET

MERILA ZA IZBIRO SCENARIJEV NESREČ ZA DRŽAVNO OCENO TVEGANJA

Mentorica: red. prof. dr. Zorka Novak Pintarič

Somentorica: Jasmina Karba, univ. dipl. inž. grad.

Datum zagovora: 19. 9. 2017

Marko BREZNIK

RACIONALNO NAČRTOVANJE POTENCIALNIH ANTIDEPRESIVOV IZ SKUPINE REVERZIBILNIH INHIBITORJEV MONOAMIN-OKSIDAZE A

Mentor: izr. prof. dr. Urban Bren

Somentor: dr. Janez Konc

Datum zagovora: 19. 6. 2017

Timotej VIDOVIČ

UPORABA LIGNOCELULOZNIH MATERIALOV PRI PROIZVODNJI BIOLINA

Mentor: red. prof. dr. Zdravko Kravanja

Somentorica: doc. dr. Lidija Čuček

Datum zagovora: 27. 9. 2017

Barbara ZAKELŠEK

VPLIV ZEOLITA NA MEHANSKE LASTNOSTI POLIOLEFINOV

Mentor: red. prof. dr. Peter Krajnc

Somentor: dr. Andrej Horvat

Datum zagovora: 19. 9. 2017

Nina ŽUNKO

HIDROTERMIČNA DEGRADACIJA EKSTRAKTA ČEBULE - VPLIV KONCENTRACIJE

Mentorica: red. prof. dr. Mojca Škerget

Somentor: red. prof. dr. Željko Knez

Datum zagovora: 22. 3. 2017

Matic BROZ

POVEZAVA MED POLIMORFIZMI IN GENI OKSIDATIVNEGA STRESA PRI BOLNIKI S POGOSTIMI KOMPLEKSNIMI BOLEZNIMI

Mentor: red. prof. dr. Uroš Potočnik

Somentorica: doc. dr. Katja Repnik

Datum zagovora: 1. 9. 2017

Jan DROFENIK

PCM AKUMULACIJA TOPLOTE V GRADBENIH MATERIALIH

Mentor: izr. prof. dr. Darko Goričanec

Somentorica: doc. dr. Danijela Urbanc

Datum zagovora: 12. 7. 2017

Sanela GERMAN

POROZNE poliHIPE MEMBRANE S TIOL-EN POLIMERIZACIJO

Mentor: red. prof. dr. Peter Krajnc

Somentorica: asist. dr. Muzafera Paljevac

Datum zagovora: 18. 5. 2017

Petra GJURA

ETERIČNA OLJA IN NJIHOVA ANTIOKSIDATIVNOST

Mentorica: red. prof. dr. Mojca Škerget

Somentorica: asist. dr. Petra Kotnik

Datum zagovora: 15. 2. 2017

Patricia GRUŠOVNIK

FUNKCIONALIZACIJA POLI(GLICIDIL) METAKRILATOV Z MULTIFUNKCIONALNIMI AMINI

Mentor: red. prof. dr. Peter Krajnc

Somentorica: asist. dr. Muzafera Paljevac

Datum zagovora: 31. 8. 2017

Domen HORVAT

SUŠENJE LESNIH SEKANCEV V EKSTENZIVNEM NIZKOTEMPERATURNEM SUŠILNEM PROCESU

Mentor: doc. dr. Dušan Klinar

Somentor: doc. dr. Miloš Bogataj

Datum zagovora: 6. 9. 2017

DIPLOME – VISOKOŠOLSKI STROKOVNI ŠTUDIJ

VISOKOŠOLSKI STROKOVNI ŠTUDIJ – 1. STOPNJA

Dragana BJELIĆ

ANALIZA LIGNOCELULOZNIH MATERIALOV Z
RAZLIČNIMI MODIFIKACIJAMI KLASONOVE METODE
Mentorica: doc. dr. Lidija Čuček
Somentorica: doc. dr. Maša Islamčević Razboršek
Datum zagovora: 6. 9. 2017

Nežka BRUNEC

MODELIRANJE IN DINAMIČNA SIMULACIJA
TOPLOTNEGA PRENOSNIKA
Mentor: doc. dr. Miloš Bogataj
Somentorica: red. prof. dr. Zorka Novak Pintarič
Datum zagovora: 1. 9. 2017

Natalija BÜDEFELD

PRIPRAVA MAGNETNIH ZAMREŽENIH ENCIMSKIH
SKUPKOV (CLEAs) IZ TRANSGLUTAMINAZE
Mentorica: red. prof. dr. Maja Leitgeb
Somentorica: asist. Katja Vasić
Datum zagovora: 27. 9. 2017

Tina DVORŠAK

HIDROTERMICNA RAZGRADNJA ODPADKOV IZ
PROIZVODNJE PAPIRJA
Mentorica: red. prof. dr. Mojca Škerget
Somentor: red. prof. dr. Željko Knez
Datum zagovora: 27. 9. 2017

Uroš FILIPIČ

FORMULIRANJE FARMACEVTSKIH UČINKOVIN S PGSS
PROCESOM
Mentorica: doc. dr. Maša Knez Hrnčič
Somentor: asist. Gregor Kravanja
Datum zagovora: 4. 9. 2017

Lara FORSTNER

VPLIV SKUPNIH IONOV NA PREVODNOST
ELEKTROLITSKIH MEŠANIC
Mentorica: doc. dr. Mojca Slemnik
Somentorica: izr. prof. dr. Marjana Simonič
Datum zagovora: 25. 10. 2017

Patricia GOVEDIĆ

INHIBICIJA MODIFICIRANEGA POLIETILENA NA RAST
MIKROBNIH CELIC
Mentorica: doc. dr. Mateja Primožič
Somentorica: red. prof. dr. Maja Leitgeb
Datum zagovora: 1. 9. 2017

Karin HERCOG

KONVERZIJA SLADKORJEV V SUBKRITIČNI VODI
Mentorica: red. prof. dr. Mojca Škerget
Somentor: red. prof. dr. Željko Knez
Datum zagovora: 27. 9. 2017

Laura KALŠEK

STROŠKOVNA PRIMERJAVA RAZLIČNIH IZOLACIJSKIH
MATERIALOV OVOJA ZGRADBE
Mentor: izr. prof. dr. Darko Goričanec
Somentor: asist. dr. Peter Trop
Datum zagovora: 20. 9. 2017

Tadeja KLAJDERIČ

UPORABA CELOVITEGA PROIZVODNEGA
VZDRŽEVANJA ZA ZNIŽANJE PORABE PRALNE VODE
NA POLNILNI LINIJI ČISTILNIH IZDELKOV
Mentorica: red. prof. dr. Zorka Novak Pintarič
Somentorica: izr. prof. dr. Marjana Simonič
Datum zagovora: 25. 10. 2017

Eva KRAJNČAN

VPLIV EKSTRAKCIJSKEGA MEDIJA NA KVALITETO
EKSTRAKTA IZ GOBE *Hericium erinaceus*
Mentorica: doc. dr. Maša Knez Hrnčič
Somentorica: asist. dr. Darija Cör
Datum zagovora: 1. 9. 2017

Anita MALINIČ

ANALIZA SEŽIGA ODPADNIH PLINOV V REFORMERJU
Mentorica: doc. dr. Anita Kovač Kralj
Somentorica: dr. Irena Ban
Datum zagovora: 22. 3. 2017

Andreja PODNAR

UKREPI ZA ZMANJŠANJE NEVARNOSTI VERIŽNIH
UČINKOV
Mentorica: red. prof. dr. Zorka Novak Pintarič
Somentorica: Jasmina Karba, univ. dipl. inž. grad.
Datum zagovora: 6. 9. 2017

Mateja PULKO

UPORABA BIOMIMETIČNIH MEMBRAN PRI
KONCENTRIRANJU NARAVNIH SOKOV
Mentorica: doc. dr. Irena Petrinič
Somentorica: izr. prof. dr. Marjana Simonič
Datum zagovora: 24. 5. 2017

Aljaž RAMOT

VALIDACIJA ELEKTROANALIZNE METODE Z
ANTIMONOVO ELEKTRODO ZA ANALIZO TEŽKIH
KOVIN V SLEDOVIH
Mentor: doc. dr. Matjaž Finšgar
Somentorica: asist. Barbara Petovar
Datum zagovora: 6. 9. 2017

Andreja SEVER

ADSORPCIJA TEŽKIH KOVIN NA BIOOGLJE
Mentorica: red. prof. dr. Mojca Škerget
Somentor: doc. dr. Matjaž Finšgar
Datum zagovora: 27. 9. 2017

Nermin SINANOVIĆSINTEZA IN KARAKTERIZACIJA Bi₂MoO₆ NANODELCEV

Mentor: doc. dr. Matjaž Kristl

Somentorica: dr. Irena Ban

Datum zagovora: 12. 7. 2017

Janez SMERKOLJ

ANAEROBNA DIGESTIJA Z GLIVAMI PREDOBDELANEGA SUBSTRATA

Mentorica: doc. dr. Darja Pečar

Somentorica: red. prof. dr. Andreja Goršek

Datum zagovora: 6. 9. 2017

Barbara SMONKAR

VPLIV DEJAVNIKOV NA SPREMINJANJE pH VREDNOSTI V PROCESU ANAEROBNE DIGESTIJE

Mentorica: doc. dr. Lidija Čuček

Somentorica: doc. dr. Darja Pečar

Datum zagovora: 6. 9. 2017

Urša STRADOVNIK

IZOLACIJA NANOCELULOZE IZ BIOLOŠKEGA MATERIALA

Mentorica: red. prof. dr. Maja Leitgeb

Somentorica: asist. Katja Vasić

Datum zagovora: 26. 6. 2017

Ajda SUŠNIK

ZAŠČITNO DELOVANJE KSANTOHUMOLA (XN) PROTI GENOTOKSIČNIM UČINKOM AFLATOKSINA B1

Mentor: izr. prof. dr. Urban Bren

Somentorica: doc. dr. Bojana Žegura

Datum zagovora: 20. 9. 2017

Aljaž ŠPORIN

UPORABA BIOMASE ZA POVEČANJE IZKORISTKA GEOTERMICNIH ELEKTRARN

Mentor: izr. prof. dr. Darko Goričanec

Somentorica: doc. dr. Danijela Urbanc

Datum zagovora: 4. 9. 2017

Ana TURNŠEK

ODZIV MEHANSKIH LASTNOSTI NA MIKROSTRUKTURNE SPREMEMBE JEKLA 16MnCr5

Mentorica: red. prof. dr. Andreja Goršek

Somentorica: doc. dr. Darja Pečar

Datum zagovora: 22. 3. 2017

Urška VIČARMEHANOKEMIJSKE SINTEZE SELENIDOV PREHODNIH KOVIN 4. PERIODE (M_xSe_y; M=Zn, Ni, Co)

Mentor: doc. dr. Matjaž Kristl

Somentorica: dr. Irena Ban

Datum zagovora: 27. 9. 2017

Aljoša VOUKVPLIV TLAKA NA KRISTALNO STRUKTURU IZLOČENEGA CaCO₃ IZ VODNE RAZTOPINE

Mentorica: izr. prof. dr. Marjana Simonič

Somentorica: dr. Irena Ban

Datum zagovora: 1. 9. 2017

Katja ZEČEVIĆ

ŠTUDIJA UČINKOVITOSTI IMOBILIZACIJE BETA GALAKTOZIDAZE NA ZVITKE STEKLENE TKANINE

Mentorica: doc. dr. Darja Pečar

Somentorica: red. prof. dr. Andreja Goršek

Datum zagovora: 1. 9. 2017

UNIVERZA V NOVI GORICI
FAKULTETA ZA PODIPLOMSKI ŠTUDIJ
1. januar – 31. december 2017

DOKTORATI

PODIPLOMSKI ŠTUDIJSKI PROGRAM ZNANOSTI O OKOLJU – 3. STOPNJA

Tatjana RADOVANOVIĆ VUKAJLOVIĆ
NOVEL METHODS FOR DETECTION OF BIOACTIVE
SUBSTANCES AND THEIR EFFECTS IN ORGANISMS AND
IN THE ENVIRONMENT
Mentor: prof. dr. Mladen Franko
Datum zagovora: 18. 1. 2017

Franja PROSENC
NOVEL METHODS FOR DETECTION AND REMOVAL OF
POLLUTANTS FROM WATERS
Mentor: prof. dr. Mladen Franko
Datum zagovora: 14. 4. 2017

Tina MAVRIČ
SYNTHESIS AND CHARACTERIZATION OF METAL/
SEMICONDUCTOR NANOCOMPOSITES FOR
PHOTOCATALYSIS
Mentor: prof. dr. Matjaž Valant
Somentor: doc. dr. Saim Mustafa Emin
Datum zagovora: 31. 5. 2017

Aleksandar ŠOBOT
THE IMPACT OF EUROPEANISATION ON THE NATURE
PROTECTION SYSTEM OF SELECTED COUNTRIES
OF SOUTHEAST EUROPE ON THE EXAMPLE OF THE
ESTABLISHMENT OF MULTI-LEVEL GOVERNANCE
SYSTEM OF NATURA 2000
Mentor: prof. dr. Andrej A. Lukšič
Datum zagovora: 4. 12. 2017

FAKULTETA ZA ZNANOSTI O OKOLJU
1. januar – 31. december 2017

MAGISTERIJI

ŠTUDIJSKI PROGRAM OKOLJE – 2. STOPNJA

Ana VETERNIK
HETEROGENEOUS PHOTOCATALYTIC OXIDATION
FOR THE REMOVAL OF BISPHENOL A FROM AQUEOUS
SOLUTION OVER TiO₂/GRAPHENE OXIDE (GO) BASED
NANOCOMPOSITES
Mentor: prof. dr. Albin Pintar
Somentor: prof. dr. Marco Bortoluzzi
Datum zagovora: 15. 2. 2017

Ana BRODAR
VSEBNOST IZBRANIH ELEMENTOV V VODI,
SEDIMENTNIH IN BIOLOŠKIH VZORCIH REKE SAVE
Mentorica: doc. dr. Tea Zuliani
Somentor: prof. dr. Janez Ščančar
Datum zagovora: 6. 6. 2017

Miha SKOČIR
POVEČANJE BIORAZGRADLJIVOSTI PRIMARNEGA MULJA
IZ PROIZVODNJE RECIKLIRANEGA PAPIRJA S POMOČJO
UTEKOČINJANJA BIOMASE
Mentor: prof. dr. Gregor Drago Zupančič
Datum zagovora: 21. 6. 2017

Petra MAKORIČ
ANALYSIS OF POLYCHLORINATED BIPHENYLS ADSORBED
ON PLASTIC PELLETS: COMPARISON OF EXTRACTION
TECHNIQUES
Mentorica: dr. Marilyn Pflieger
Datum zagovora: 21. 6. 2017

Janez BALANTIČ

ANALIZA EKSPLOZIVNOSTI IN DOLOČITEV VARNOSTNIH UKREPOV PRI PROIZVODNJI ALUMINIJEVEGA PRAHU

Mentorica: doc. dr. Barbara Novosel

Datum zagovora: 1. 9. 2017

Nana Ivana HRASTNIK

HEAVY METAL ANALYSIS WITH IN SITU PREPARED COPPER FILM ELECTRODE AS A TOOL FOR ENVIRONMENTAL MONITORING

Mentor: prof. dr. Marco Bortoluzzi

Somentor: dr. Vasko Jovanovski

Datum zagovora: 7. 9. 2017

Tina ČUJEC

VPLIV ATMOSFERSKIH AEROSOLOV NA FIZIOLOŠKI IN VNETNI ODZIV MAKROFAGOV

Mentorica: doc. dr. Martina Bergant Marušič

Datum zagovora: 13. 10. 2017

Neža OREL

ODZIV MIKROBNE ZDRUŽBE NA MEŠANICO NEVARNIH SPOJIN

Mentorica: prof. dr. Valentina Turk

Datum zagovora: 5. 12. 2017

DIPLOME

ŠTUDIJSKI PROGRAM OKOLJE – 1. STOPNJA

Ketevan NEPARIDZE

PHOTOLYSIS AND ECOTOXICITY OF THE ANTIBIOTIC CIPROFLOXACIN

Mentorica: dr. Marilyne Pflieger

Datum zagovora: 18. 1. 2017

Sara KLEMENČIČ

VPLIV METFORMINA IN SORODNIH KSENOBIOTIKOV NA VARIABILNOST CELIC RAKA DOJKE

Mentor: doc. dr. Toni Petan

Datum zagovora: 23. 1. 2017

Tjaša GRIVEC

VPLIV KMETIJSKE PRAKSE NA ŠTEVILČNOST TRAVNIŠKIH PTIC

Mentor: prof. dr. Davorin Tome

Datum zagovora: 14. 4. 2017

Samo ŠKRLEC

ZNAČILNOSTI DINAMIKE VSEBNOSTI VODNE PARE V OZRAČJU NAD VIPAVSKO DOLINO Z UPORABO DALJINSKEGA ZAZNAVANJA S SISTEMOM GPS

Mentorica: dr. Asta Gregorič

Somentor: prof. dr. Klemen Bergant

Datum zagovora: 29. 5. 2017

Špela HUDOBIVNIK

MINERALIZACIJA ODVEČNEGA BLATA IZ ČISTILNIH NAPRAV ZA KOMUNALNE ODPADNE VODE S POMOČJO OZONACIJE

Mentor: prof. dr. Gregor Drago Zupančič

Datum zagovora: 30. 6. 2017

Jana SITAR

VPLIV NOTRANJNH IN ZUNANJNH OKOLJSKIH DEJAVNIKOV NA NASTANEK VIRUSOV HPV

Mentorica: doc. dr. Martina Bergant Marušič

Datum zagovora: 16. 11. 2017

Teja CANKAR

OKOLJU PRIJAZNA SINTEZA METANOLA S HIDROGENIRANJEM OGLJIKOVEGA DIOKSIDA PREKO TRIKOMPONENTNIH KATALIZATORJEV

Mentor: doc. dr. Blaž Likozar

Datum zagovora: 16. 11. 2017

KOLENDAR VAŽNEJŠIH ZNANSTVENIH SREČANJ S PODROČJA KEMIJE IN KEMIJSKE TEHNOLOGIJE

SCIENTIFIC MEETINGS – CHEMISTRY AND CHEMICAL ENGINEERING

2018

April 2018

- 15 – 18 PETROMASS 2018 – XI. INTERNATIONAL MASS SPECTROMETRY CONFERENCE ON
PETROCHEMISTRY, ENVIRONMENTAL AND FOOD CHEMISTRY
Bled, Slovenia
Information: <http://www.petromass2018.com/>
- 22 – 26 AICHE SPRING MEETING 2018 AND 14TH GLOBAL CONGRESS ON PROCESS SAFETY
Orlando, FL, USA
Information: <https://www.aiche.org/conferences/aiche-spring-meeting-and-global-congress-on-process-safety/2018>

May 2018

- 7 – 9 6TH INTERNATIONAL CONFERENCE ON POPULATION BALANCE MODELLING
Ghent, Belgium
Information: <http://www.pbm2018.ugent.be/>
- 10 – 12 117TH GENERAL ASSEMBLY OF THE BUNSEN SOCIETY FOR PHYSICAL CHEMISTRY
2018 – KINETICS IN THE REAL WORLD
Hannover, Germany
Information: <http://www.bunsen.de/en/veranstaltungen/veranstaltungskalender/bunsentagung-2018/>
- 13 – 17 SETAC 2018: SESSION ON SUBSTITUTION OF HAZARDOUS CHEMICALS
Rome, Italy
Information: <https://rome.setac.org/>
- 14 – 15 EPNOE JUNIOR SCIENTISTS MEETING
Maribor, Slovenia
Information: <https://3rd-epnoe-jun.sciencesconf.org/>
- 15 – 17 HAZARDS 28
Edinburgh, Scotland
Information: <http://www.icheme.org/hazards28>
- 20 – 23 ISCRE 25 – 25TH INTERNATIONAL SYMPOSIUM ON CHEMICAL REACTION
ENGINEERING
Florence, Italy
Information: <http://www.aidic.it/iscre25/>
- 20 – 23 5TH INTERNATIONAL SCHOOL-CONFERENCE ON CATALYSIS FOR YOUNG
SCIENTISTS “CATALYST DESIGN: FROM MOLECULAR TO INDUSTRIAL LEVEL”
Moscow, Russia
Information: <http://conf.nsc.ru/catdesign2018/en/>
- 20 – 24 EUPOC 2018
Como, Italy
Information: <https://www.eupoc2018.it/>

- 30 – Jun 1 ENVIROCHEM 2018
Kruševac, Serbia
Information: <http://www.envirochem.rs/index-en.html>
-
- June 2018**
- 3 – 6 6TH INTERNATIONAL CONGRESS ON GREEN PROCESS ENGINEERING
Toulouse, France
Information: <http://www.gpe2018.org/>
- 3 – 7 POLYMERS AND ORGANIC CHEMISTRY 2018 (POC 2018)
Palavas Les Flots Palavas, France
Information: <http://poc2018.enscm.fr>
- 4 – 6 IIS PRAGUE 2018 – 13TH INTERNATIONAL SYMPOSIUM ON THE SYNTHESIS AND APPLICATIONS OF ISOTOPES AND ISOTOPICALLY LABELLED COMPOUNDS
Prague, Czech Republic
Information: <http://www.iis-prague2018.cz/>
- 4 – 7 POLYMERS AND ORGANIC CHEMISTRY 2018 (POC 2018)
Montpellier, France
Information: <https://iupac.org/event/polymers-organic-chemistry-2018-poc-2018/>
- 10 – 13 30TH EUROPEAN SYMPOSIUM ON APPLIED THERMODYNAMICS
Prague, Czech Republic
Information: <http://esat2018.cz/>
- 10 – 13 28TH EUROPEAN SYMPOSIUM ON COMPUTER-AIDED PROCESS ENGINEERING
Graz, Austria
Information: <https://www.tugraz.at/events/escape28/home/>
- 11 – 15ACHEMA – WORLD FORUM AND LEADING SHOW FOR THE PROCESS INDUSTRIES
Frankfurt am Main, Germany
Information: <https://www.achema.de/en/home.html>
- 13 – 15 8TH EUROPEAN MEETING ON CHEMICAL INDUSTRY AND ENVIRONMENT
Nantes, France
Information: <http://conferences.imt-atlantique.fr/emchie2018/>
- 13 – 16 CHEMISTRY FOR BEAUTY AND HEALTH
Toruń, Poland
Information: <https://beauty-torun.umk.pl>
- 17 – 21 THE INTERNATIONAL SYMPOSIUM ON INORGANIC AND ENVIRONMENTAL MATERIALS 2018 (ISIEM2018)
Ghent, Belgium
Information: <http://www.isiem2018.org/>
- 17 – 21 82ND PRAGUE MEETING ON MACROMOLECULES – POLYMER NETWORKS AND GELS
Prague, Czech Republic
Information: http://www.imc.cas.cz/sympo/82pmm_png2018/
- 24 – 28 10TH INTERNATIONAL CONFERENCE ON MOLECULAR IMPRINTING, MIP 2018
Jerusalem, Israel
Information: <http://www.ortra.com/events/mip2018>
- 25 – 27 WORLD RENEWABLE ENERGY CONFERENCE
Stockholm, Sweden
Information: <https://renewableenergy.conferencesnest.com/>
- 25 – 27 GLOBAL CHALLENGES IN NEGLECTED TROPICAL DISEASES
San Juan, Puerto Rico
Information: <http://www.cafec.org.pr/ntd2018/>
- 27 – 29 2018 INTERNATIONAL CONFERENCE ON RESOURCE SUSTAINABILITY (icRS 2018)
Beijing, China
Information: <http://www.icrsconf.com>

- 30 – Jul 3 3RD SOUTH EAST EUROPEAN CONFERENCE ON SUSTAINABLE DEVELOPMENT OF ENERGY, WATER AND ENVIRONMENTAL SYSTEMS
Novi Sad, Serbia
Information: <http://www.novisad2018.sdewes.org/>
- July 2018**
-
- 1 – 5 WORLD POLYMER CONGRESS MACRO18
Cairns Queensland, Australia
Information: <http://www.macro18.org>
- 1 – 6 24TH IUPAC INTERNATIONAL CONFERENCE ON PHYSICAL ORGANIC CHEMISTRY (ICPOC 24)
Faro, Portugal
Information: <http://icpoc24.ualg.pt/>
- 2 – 6 XVI INTERNATIONAL IUPAC CONFERENCE ON HIGH TEMPERATURE MATERIALS CHEMISTRY (HTMC-XVI)
Ekaterinburg, Russian Federation
Information: <http://htmc16.ru/>
- 8 – 12 PREPA12 - SYMPOSIUM »SCIENTIFIC BASES FOR THE PREPARATION OF HETEROGENEOUS CATALYSTS«
Louvain-la-Neuve, Belgium
Information: https://www.ldorganisation.com/v2/produits.php?langue=english&cle_menus=1238916539
- 8 – 13 27TH IUPAC INTERNATIONAL SYMPOSIUM ON PHOTOCHEMISTRY
Dublin, Ireland
Information: <https://iupac.org/event/27th-iupac-international-symposium-photochemistry/>
- 8 – 13 22ND INTERNATIONAL CONFERENCE ON PHOSPHORUS CHEMISTRY
Budapest, Hungary
Information: <http://www.icpc22.mke.org.hu/>
- 9 – 13 EUROMEMBRANE 2018
Valencia, Spain
Information: <http://euromembrane2018.org/>
- 10 – 14 25TH INTERNATIONAL CONFERENCE ON CHEMISTRY EDUCATION ICCE 2018)
Sydney, Australia
Information: <http://www.icce2018.org/>
- 15 – 20 THE 18TH INTERNATIONAL SYMPOSIUM ON SOLUBILITY PHENOMENA AND RELATED EQUILIBRIUM PROCESSES (ISSP)
Tours, France
Information: <http://issp18.org/>
- 15 – 20 28TH INTERNATIONAL CONFERENCE ON ORGANOMETALLIC CHEMISTRY
Florence Italy
Information: <http://www.icomc2018.com/>
- 30 – Aug 4 43RD INTERNATIONAL CONFERENCE ON COORDINATION CHEMISTRY
Sendai, Japan
Information: <http://iccc2018.jp>
- August 2018**
-
- 12 – 17 18TH INTERNATIONAL BIOTECHNOLOGY SYMPOSIUM
Montréal, Canada
Information: <http://ibs2018montreal.org/>
- 25 – 29 23RD INTERNATIONAL CONGRESS OF CHEMICAL AND PROCESS ENGINEERING CHISA 2018
Prague, Czech Republic
Information: <http://2018.chisa.cz/>

- 25 – 29 21ST CONFERENCE ON PROCESS INTEGRATION, MODELLING AND OPTIMISATION FOR ENERGY SAVING AND POLLUTION REDUCTION PRES 2018
Prague, Czech Republic
Information: <http://2018.chisa.cz/>
- 26 – 30 ECC7 – 7TH EuCheMS CHEMISTRY CONGRESS
Liverpool, UK
Information: <https://www.euchems2018.org/>
- 26 – 30 35TH INTERNATIONAL CONFERENCE ON SOLUTION CHEMISTRY (ICSC)
Szeged, Hungary
Information: <http://www.mke.org.hu/ICSC2018>
- 26 – 31 22ND INTERNATIONAL MASS SPECTROMETRY CONFERENCE (IMSC) 2018
Florence, Italy
Information: <http://www.imsc2018.it/>
- 30 – 31 ICOSSE 2018 : 20TH INTERNATIONAL CONFERENCE ON OPERATING SYSTEMS AND SOFTWARE ENGINEERING
Bangkok, Thailand
Information: <https://www.waset.org/conference/2018/08/bangkok/ICOSSE>
- 30 – Sep 3 INTERNATIONAL SUMMER SCHOOL “SUPRAMOLECULAR CHEMISTRY IN MEDICINE AND IN TECHNOLOGY: ADVANCES AND CHALLENGES”
Varna, Bulgaria
Information: <http://supramedchem.orgchm.bas.bg>

September 2018

- 2 – 6 SMARTER 6 meeting
Ljubljana, Slovenia
Information: <https://smarter6.ki.si/>
- 2 – 7 69TH ANNUAL MEETING OF THE INTERNATIONAL SOCIETY OF ELECTROCHEMISTRY
Bologna, Italy
Information: <http://annual69.ise-online.org/>
- 2 – 7 32ND CONFERENCE OF EUROPEAN COLLOID AND INTERFACE SOCIETY (ECIS)
Ljubljana, Slovenia
Information: <http://ecis2018.fkkt.uni-lj.si/index.html>
- 3 – 7 25TH INTERNATIONAL CONFERENCE ON HIGH RESOLUTION MOLECULAR SPECTROSCOPY - BILBAO 2018
Bilbao, Spain
Information: <http://www.chem.uni-wuppertal.de/conference/>
- 4 – 7 12TH CONFERENCE ON POLYMER-SOLVENT COMPLEXES AND INTERCALATES (POLYSOLVAT-12)
Grenoble, France
Information: <https://iupac.org/event/12th-conference-polymer-solvent-complexes-intercalates-polysolvat-12/>
- 4 – 7 N-LIGANDS2018 – 7TH EuCheMS CONFERENCE ON NITROGEN-LIGANDS
Lisbon, Portugal
Information: <http://www.n-ligands2018.com/>
- 5 – 7 ADVANCED INORGANIC MATERIALS GREEN AND UNCONVENTIONAL SYNTHESIS APPROACHES AND FUNCTIONAL ASSESSMENT (AIM 2018)
Padova, Italy
Information: <http://www.chimica.unipd.it/silvia.gross/workshop/home.html>
- 9 – 12 24TH CONFERENCE ON ISOPRENOIDS
Bialystok, Poland
Information: <https://isoprenoids-24.uwb.edu.pl/>

- 9 – 12 12TH EUROPEAN SYMPOSIUM ON BIOCHEMICAL ENGINEERING SCIENCES
Lisbon, Portugal
Information: <http://esbes2018.org/>
- 9 – 12 16TH EUROPEAN CONFERENCE ON MIXING
Toulouse, France
Information: <http://inpaint.inp-toulouse.fr/MIXING16/>
- 9 – 13 EUROPEAN CORROSION CONGRESS
Prague, Czech Republic
Information: <http://www.eurocorr2018.org/>
- 9 – 14 8TH IUPAC INTERNATIONAL CONFERENCE ON GREEN CHEMISTRY
Bangkok, Thailand
Information: <http://www.greeniupac2018.com>
- 10 – 14 9TH INTERNATIONAL CONFERENCE FOR CONVEYING AND HANDLING OF
PARTICULATE SOLIDS
London, UK
Information: <http://www.constableandsmith.com/events/chops-2018/>
- 13 – 15 2ND EDITION OF GLOBAL CONFERENCE ON CATALYSIS, CHEMICAL ENGINEERING
& TECHNOLOGY (CAT-2018)
Rome, Italy
Information: <https://catalysis-conferences.magnusgroup.org/>
- 16 – 19 DISTILLATION & ABSORPTION CONFERENCE 2018
Firenze, Italy
Information: <http://www.aidic.it/da2018/>
- 16 – 21 22ND INTERNATIONAL CONFERENCE ON ORGANIC SYNTHESIS (22-ICOS)
Florence, Italy
Information: <http://www.22-icos-florence.it>
- 16 – 21 13TH INTERNATIONAL CONFERENCE ON SOLID STATE CHEMISTRY
Pardubice, Czech Republic
Information: <http://www.ssc-conference.com/2018/>
- 17 – 18 4TH INTERNATIONAL CONFERENCE ON CHEMICAL ENGINEERING
Vancouver, Canada
Information: <https://chemicalengineering.conferenceseries.com/>
- 18 – 21 11TH INTERNATIONAL DRYING SYMPOSIUM
Valencia, Spain
Information: <http://www.ids2018.webs.upv.es/>
- 19 – 21 SLOVENIAN CHEMICAL SOCIETY ANNUAL MEETING 2018
Portorož, Slovenia
Information: <http://chem-soc.si/scs-annual-meeting-2018>
- 19 – 21 17TH RUŽIČKA DAYS »TODAY SCIENCE - TOMORROW INDUSTRY«
Vukovar, Croatia
Information: <http://www.ptfos.unios.hr/ruzicka/2014/>
- 19 – 22 25TH CONGRESS OF THE SOCIETY OF CHEMISTS AND TECHNOLOGISTS OF
MACEDONIA
Ohrid, Macedonia
Information: <http://www.sctm.mk/congress/index.php/SCTM/25Congress>
- 24 – 27 XII ITALIAN FOOD CHEMISTRY CONGRESS (CHIMALI 2018)
Camerino, Italy
Information: <http://chimali2018.unicam.it/>

October 2018

- 10 – 12 EAST-WEST CHEMISTRY CONFERENCE 2018 (EWCC2018)
Lviv, Ukraine
Information: <http://ewcc2018.org/>
- 14 – 17 4TH INTERNATIONAL CONFERENCE ON BIOINSPIRED AND BIOBASED CHEMISTRY
& MATERIALS
Nice, France
Information: <http://www.unice.fr/nice-conference/>
- 14 – 18 14TH IUPAC INTERNATIONAL CONGRESS OF PESTICIDE CHEMISTRY
Rio de Janeiro, Brazil
Information: <https://iupac.org/event/14th-iupac-international-congress-of-pesticide-chemistry/>
- 19 – 21 3RD INTERNATIONAL CONGRESS OF CHEMISTS AND CHEMICAL ENGINEERS OF
BOSNIA AND HERZEGOVINA
Sarajevo, Bosnia and Herzegovina
Information: <http://www.pmf.unsa.ba/hemija/kongres/index.php/en>
- 21 – 24 15TH INTERNATIONAL CONFERENCE ON MICROREACTION TECHNOLOGY
Karlsruhe, Germany
Information: <http://dechema.de/en/IMRET2018.html>
- 24 – 25 IES2018- 25TH SEMINAR AND SYMPOSIUM ON INFORMATION AND EXPERT SYSTEMS
IN THE PROCESS INDUSTRIES
Belgrade, Serbia
Information: <http://bg.ac.rs/en/members/faculties/FTM.php>
- 28 – 31 XXIX INTERAMERICAN CONGRESS OF CHEMICAL ENGINEERING
INCORPORATING THE 68TH CANADIAN CHEMICAL ENGINEERING CONFERENCE
Toronto, Canada
Information: <http://www.csche2018.ca/>

November 2018

- 4 – 7 2018 - SUSTAINABLE INDUSTRIAL PROCESSING SUMMIT
Rio de Janeiro, Brazil
Information: <https://www.flogen.org/sips2018/>
- 5 – 9 XXIII INTERNATIONAL CONFERENCE ON CHEMICAL REACTORS
Ghent, Belgium
Information: http://conf.nsc.ru/CR_23/en/

2019**March 2019**

- 31 – Apr. 4 AIChE SPRING MEETING 2019 AND 15TH GLOBAL CONGRESS ON PROCESS SAFETY
New Orleans, USA
Information: <https://www.aiche.org/conferences/aiche-spring-meeting-and-global-congress-on-process-safety/2019>

May 2019

- 19 – 24 14TH IUPAC INTERNATIONAL CONGRESS OF CROP PROTECTION CHEMISTRY
Ghent, Belgium
Information: <https://www.iupac2019.be>

June 2019

- 2 – 6 14TH INTERNATIONAL SYMPOSIUM ON MACROCYCLIC AND SUPRAMOLECULAR CHEMISTRY
Lecce, Italy
Information: <https://ismsc2019.eu/>
- 16 – 19 LOSS PREVENTION 2019
Delft, The Netherlands
Information: <http://lossprevention2019.org/>
- 16 – 20 17TH INTERNATIONAL CONFERENCE ON CHEMISTRY AND THE ENVIRONMENT – ICCE2019
Thessaloniki, Greece
Information: <http://www.euchems.eu/events/17th-international-conference-chemistry-environment-icce2019/>
- 16 – 20 12TH IWA INTERNATIONAL CONFERENCE ON WATER RECLAMATION AND REUSE
Berlin, Germany
Information: <http://efce.info/IWA+Conference+2019.html>
- 26 – 28 THERMODYNAMICS 2019
Huelva, Spain
Information: <http://efce.info/Thermodynamics+2019.html>
- 26 – 30 6TH EUROPEAN CONFERENCE ON ENVIRONMENTAL APPLICATIONS OF ADVANCED OXIDATION PROCESSES (EAAOP-6)
Portorož, Slovenia
Information: <http://eaaop6.ki.si/>

July 2019

- 1 – 3 CONGRESS ON NUMERICAL METHODS IN ENGINEERING
Guimarães, Portugal
Information: www.cmn2019.pt
- 5 – 12 IUPAC 2019 PARIS FRANCE
Paris, France
Information: <https://www.iupac2019.org/>
- 21 – 26 THE 18TH INTERNATIONAL SYMPOSIUM ON NOVEL AROMATIC COMPOUNDS (ISNA-18)
Sapporo City, Japan
Information: <https://iupac.org/event/18th-international-symposium-novel-aromatic-compounds-isna-18/>

September 2019

- 15 – 19 11TH EUROPEAN CONGRESS OF CHEMICAL ENGINEERING – ECCE11 & 4TH EUROPEAN CONGRESS OF APPLIED BIOTECHNOLOGY – ECAB5
Florence, Italy
Information: http://efce.info/ECCE12_ECAB5-p-112545.html
- 25 – 27 SLOVENIAN CHEMICAL SOCIETY ANNUAL MEETING 2019
Maribor, Slovenia
Information: <http://chem-soc.si/slovenski-kemijski-dnevi-2019>

Acta Chimica Slovenica

Author Guidelines

Submissions

Submission to ACSi is made with the implicit understanding that neither the manuscript nor the essence of its content has been published in whole or in part and that it is not being considered for publication elsewhere. All the listed authors should have agreed on the content and the corresponding (submitting) author is responsible for having ensured that this agreement has been reached. The acceptance of an article is based entirely on its scientific merit, as judged by peer review. There are no page charges for publishing articles in ACSi. The authors are asked to read the Author Guidelines carefully to gain an overview and assess if their manuscript is suitable for ACSi.

Additional information

- Citing spectral and analytical data
- Depositing X-ray data

Submission material

Typical submission consists of:

- full manuscript (PDF file, with title, authors, abstract, keywords, figures and tables embedded, and references)
- supplementary files
 - **Full manuscript** (original Word file)
 - **Statement of novelty** (Word file)
 - **List of suggested reviewers** (Word file)
 - **ZIP file containing graphics** (figures, illustrations, images, photographs)
 - **Graphical abstract** (single graphics file)
 - **Proposed cover picture** (optional, single graphics file)
 - **Appendices** (optional, Word files, graphics files)

Incomplete or not properly prepared submissions will be rejected.

Submission process

Before submission, authors should go through the checklist at the bottom of the page and prepare for submission.

Submission process consists of 5 steps.

Step 1: Starting the submission

- Choose one of the journal sections.
- Confirm all the requirements of the **checklist**.
- Additional plain text comments for the editor can be provided in the relevant text field.

Step 2: Upload submission

- Upload full manuscript in the form of a Word file (with title, authors, abstract, keywords, figures and tables embedded, and references).

Step 3: Enter metadata

- First name, last name, contact email and affiliation for all authors, in relevant order, must be provided. Corresponding author has to be selected. Full postal address and phone number of the corresponding author has to be provided.

- **Title and abstract** must be provided in plain text.
- Keywords must be provided (max. 6, separated by semicolons).
- Data about contributors and supporting agencies may be entered.
- **References** in plain text must be provided in the relevant text field.

Step 4: Upload supplementary files

- Original Word file (original of the PDF uploaded in the step 2)
- **Statement of novelty** in a Word file must be uploaded
- All **graphics** have to be uploaded in a single ZIP file. Graphics should be named Figure 1.jpg, Figure 2.eps, etc.
- **Graphical abstract image** must be uploaded separately
- **Proposed cover picture** (optional) should be uploaded separately.
- Any additional **appendices** (optional) to the paper may be uploaded. Appendices may be published as a supplementary material to the paper, if accepted.
- For each uploaded file the author is asked for additional metadata which may be provided. Depending of the type of the file please provide the relevant title (Statement of novelty, List of suggested reviewers, Figures, Graphical abstract, Proposed cover picture, Appendix).

Step 5: Confirmation

- Final confirmation is required.

Article Types

Feature Articles are contributions that are written on editor's invitation. They should be clear and concise summaries of the most recent activity of the author and his/her research group written with the broad scope of ACSi in mind. They are intended to be general overviews of the authors' subfield of research but should be written in a way that engages and informs scientists in other areas. They should contain the following (see also general directions for article structure in ACSi below): (1) an introduction that acquaints readers with the authors' research field and outlines the important questions to which answers are being sought; (2) interesting, new, and recent contributions of the author(s) to the field; and (3) a summary that presents possible future directions. Manuscripts normally should not exceed 40 pages of one column format (letter size 12, 33 lines per page). Generally, experts in a field who have made important contribution to a specific topic in recent years will be invited by an editor to contribute such an **Invited Feature Article**. Individuals may, however, send a proposal (one-page maximum) for an Invited Feature Article to the Editor-in-Chief for consideration.

Scientific articles should report significant and innovative achievements in chemistry and related sciences and should exhibit a high level of originality. They

should have the following structure:

1. Title (max. 150 characters),
2. Authors and affiliations,
3. Abstract (max. 1000 characters),
4. Keywords (max. 6),
5. Introduction,
6. Experimental,
7. Results and Discussion,
8. Conclusions,
9. Acknowledgements,
10. References.

The sections should be arranged in the sequence generally accepted for publications in the respective fields and should be successively numbered.

Short communications generally follow the same order of sections as Scientific articles, but should be short (max. 2500 words) and report a significant aspect of research work meriting separate publication. Editors may decide that a Scientific paper is categorized as a Short Communication if its length is short.

Technical articles report applications of an already described innovation. Typically, technical articles are not based on new experiments.

Preparation of Submissions

Text of the submitted articles must be prepared with Microsoft Word. Normal style set to single column, 1.5 line spacing, and 12 pt Times New Roman font is recommended. Line numbering (continuous, for the whole document) must be enabled to simplify the reviewing process. For any other format, please consult the editor. Articles should be written in English. Correct spelling and grammar are the sole responsibility of the author(s). Papers should be written in a concise and succinct manner. The authors shall respect the ISO 80000 standard [1], and IUPAC Green Book [2] rules on the names and symbols of quantities and units. The Système International d'Unités (SI) must be used for all dimensional quantities.

Graphics (figures, graphs, illustrations, digital images, photographs) should be inserted in the text where appropriate. The captions should be self-explanatory. Lettering should be readable (suggested 8 point Arial font) with equal size in all figures. Use common programs such as MS Excel or similar to prepare figures (graphs) and ChemDraw to prepare structures in their final size. Width of graphs in the manuscript should be 8 cm. Only in special cases (in case of numerous data, visibility issues) graphs can be 17 cm wide. All graphs in the manuscript should be inserted in relevant places and **aligned left**. The same graphs should be provided separately as images of appropriate resolution (see below) and submitted together in a ZIP file (Graphics ZIP). Please do not submit figures as a Word file. In **graphs**, only the graph area determined by both axes should be in the frame, while a frame around the whole graph should be omitted. The graph area should be white. The legend should be inside the graph area. The style of all graphs should be the same. **Figures and illustrations** should be of sufficient quality for the printed version, i.e. 300 dpi minimum. **Digital images and photographs** should be of high quality (minimum 250 dpi resolution). On submission, figures should be of good enough resolution to be assessed by the referees, ideally as JPEGs. High-resolution figures (in JPEG,

TIFF, or EPS format) might be required if the paper is accepted for publication.

Tables should be prepared in the Word file of the paper as usual Word tables. The captions should appear above the table and should be self-explanatory.

References should be numbered and ordered sequentially as they appear in the text, likewise methods, tables, figure captions. When cited in the text, reference numbers should be superscripted, following punctuation marks. It is the sole responsibility of authors to cite articles that have been submitted to a journal or were in print at the time of submission to ACSi. Formatting of references to published work should follow the journal style; please also consult a recent issue:

1. J. W. Smith, A. G. White, *Acta Chim. Slov.* **2008**, *55*, 1055–1059.
2. M. F. Kemmere, T. F. Keurentjes, in: S. P. Nunes, K. V. Peinemann (Ed.): *Membrane Technology in the Chemical Industry*, Wiley-VCH, Weinheim, Germany, **2008**, pp. 229–255.
3. J. Levec, Arrangement and process for oxidizing an aqueous medium, US Patent Number 5,928,521, date of patent July 27, **1999**.
4. L. A. Bursill, J. M. Thomas, in: R. Sersale, C. Collela, R. Aiello (Eds.), *Recent Progress Report and Discussions: 5th International Zeolite Conference*, Naples, Italy, 1980, Gianini, Naples, **1981**, pp. 25–30.
5. J. Szegezdi, F. Csizmadia, Prediction of dissociation using microconstants, http://www.chemaxon.com/conf/Prediction_of_dissociation_constant_using_microconstants.pdf, (assessed: March 31, 2008)

Titles of journals should be abbreviated according to Chemical Abstracts Service Source Index (CASSI).

Special Notes

- Complete characterization, **including crystal structure**, should be given when the synthesis of new compounds in crystal form is reported.
- Numerical **data should be reported with the number of significant digits corresponding to the magnitude** of experimental uncertainty.
- **The SI system of units and IUPAC recommendations** for nomenclature, symbols and abbreviations should be followed closely. Additionally, the authors should follow the general guidelines when citing spectral and analytical data, and depositing crystallographic data.
- **Characters** should be correctly represented throughout the manuscript: for example, 1 (one) and l (ell), 0 (zero) and O (oh), x (ex), D7 (times sign), B0 (degree sign). Use Symbol font for all Greek letters and mathematical symbols.
- The rules and recommendations of the **IUBMB** and the **International Union of Pure and Applied Chemistry (IUPAC)** should be used for abbreviation of chemical names, nomenclature of chemical compounds, enzyme nomenclature, isotopic compounds, optically active isomers, and spectroscopic data.
- **A conflict of interest** occurs when an individual (author, reviewer, editor) or its organization is involved in multiple interests, one of which could possibly corrupt the motivation for an act in the

other. Financial relationships are the most easily identifiable conflicts of interest, while conflicts can occur also as personal relationships, academic competition, etc. **The Editors** will make effort to ensure that conflicts of interest will not compromise the evaluation process; potential editors and reviewers will be asked to exempt themselves from review process when such conflict of interest exists. When the manuscript is submitted for publication, **the authors** are expected to disclose any relationships that might pose potential conflict of interest with respect to results reported in that manuscript. In the Acknowledgement section the source of funding support should be mentioned. The statement of disclosure must be provided as Comments to Editor during the submission process.

- **Published statement of Informed Consent.** Research described in papers submitted to ACSi must adhere to the principles of the Declaration of Helsinki (<http://www.wma.net/e/policy/b3.htm>). These studies must be approved by an appropriate institutional review board or committee, and informed consent must be obtained from subjects. The Methods section of the paper must include: 1) a statement of protocol approval from an institutional review board or committee and 2), a statement that informed consent was obtained from the human subjects or their representatives.
- **Published Statement of Human and Animal Rights.** When reporting experiments on human subjects, authors should indicate whether the procedures followed were in accordance with the ethical standards of the responsible committee on human experimentation (institutional and national) and with the Helsinki Declaration of 1975, as revised in 2008. If doubt exists whether the research was conducted in accordance with the Helsinki Declaration, the authors must explain the rationale for their approach and demonstrate that the institutional review body explicitly approved the doubtful aspects of the study. When reporting experiments on animals, authors should indicate whether the institutional and national guide for the care and use of laboratory animals was followed.
- To avoid conflict of interest between authors and referees we expect that not more than one referee is from the same country as the corresponding author(s), however, not from the same institution.
- Contributions authored by **Slovenian scientists** are evaluated by non-Slovenian referees.
- Papers describing **microwave-assisted reactions** performed in domestic microwave ovens are not considered for publication in *Acta Chimica Slovenica*.
- *Manuscripts that are **not prepared and submitted** in accord with the instructions for authors are not considered for publication.*

Appendices

Authors are encouraged to make use of supporting information for publication, which is supplementary material (appendices) that is submitted at the same time as the manuscript. It is made available on the Journal's web site and is linked to the article in the

Journal's Web edition. The use of supporting information is particularly appropriate for presenting additional graphs, spectra, tables and discussion and is more likely to be of interest to specialists than to general readers. When preparing supporting information, authors should keep in mind that the supporting information files will not be edited by the editorial staff. In addition, the files should be not too large (upper limit 10 MB) and should be provided in common widely known file formats to be accessible to readers without difficulty. All files of supplementary materials are loaded separately during the submission process as supplementary files.

Proposed Cover Picture and Graphical Abstract Image

Graphical content: an ideally full-colour illustration of resolution 300 dpi from the manuscript must be proposed with the submission. Graphical abstract pictures are printed in size 6.5 x 4 cm (hence minimal resolution of 770 x 470 pixels). Cover picture is printed in size 11 x 9.5 cm (hence minimal resolution of 1300 x 1130 pixels)

Authors are encouraged to submit illustrations as candidates for the journal Cover Picture*. The illustration must be related to the subject matter of the paper. Usually both proposed cover picture and graphical abstract are the same, but authors may provide different pictures as well.

* The authors will be asked to contribute to the costs of the cover picture production.

Statement of novelty

Statement of novelty is provided in a Word file and submitted as a supplementary file in step 4 of submission process. Authors should in no more than 100 words emphasize the scientific novelty of the presented research. Do not repeat for this purpose the content of your abstract.

List of suggested reviewers

List of suggested reviewers is a Word file submitted as a supplementary file in step 4 of submission process. Authors should propose the names, full affiliation (department, institution, city and country) and e-mail addresses of three potential referees. Field of expertise and at least two references relevant to the scientific field of the submitted manuscript must be provided for each of the suggested reviewers. The referees should be knowledgeable about the subject but have no close connection with any of the authors. In addition, referees should be from institutions other than (and preferably countries other than) those of any of the authors.

How to Submit

Users registered in the role of author can start submission by choosing USER HOME link on the top of the page, then choosing the role of the Author and follow the relevant link for starting the submission process. Prior to submission we strongly recommend that you familiarize yourself with the ACSi style by browsing the journal, particularly if you have not submitted to the ACSi before or recently.

Correspondence

All correspondence with the ACSi editor regarding the paper goes through this web site and emails. Emails are sent and recorded in the web site database. In the correspondence with the editorial office please provide ID number of your manuscript. All emails you receive from the system contain relevant links. **Please do not answer the emails directly but use the embedded links in the emails for carrying out relevant actions.** Alternatively, you can carry out all the actions and correspondence through the online system by logging in and selecting relevant options.

Proofs

Proofs will be dispatched via e-mail and corrections should be returned to the editor by e-mail as quickly as possible, normally within 48 hours of receipt. Typing errors should be corrected; other changes of contents will be treated as new submissions.

Submission Preparation Checklist

As part of the submission process, authors are required to check off their submission's compliance with all of the following items, and submissions may be returned to authors that do not adhere to these guidelines.

1. The submission has not been previously published, nor is it under consideration for publication in any other journal (or an explanation has been provided in Comments to the Editor).
2. All the listed authors have agreed on the content and the corresponding (submitting) author is responsible for having ensured that this agreement has been reached.
3. The submission files are in the correct format: manuscript is created in MS Word but will be **submitted in PDF** (for reviewers) as well as in original MS Word format (as a supplementary file for technical editing); diagrams and graphs are created in Excel and saved in one of the file formats: TIFF, EPS or JPG; illustrations are also saved in one of these formats. The preferred position of graphic files in a document is to embed them close to the place where they are mentioned in the text (See **Author guidelines** for details).
4. The manuscript has been examined for spelling and grammar (spell checked).
5. The **title** (maximum 150 characters) briefly explains the contents of the manuscript.
6. Full names (first and last) of all authors together with the affiliation address are provided. Name of author(s) denoted as the corresponding author(s), together with their e-mail address, full postal address and telephone/fax numbers are given.
7. The **abstract** states the objective and conclusions of the research concisely in no more than 150 words.
8. Keywords (minimum three, maximum six) are provided.
9. **Statement of novelty** (maximum 100 words) clearly explaining new findings reported in the manuscript should be prepared as a separate Word file.
10. The text adheres to the stylistic and bibliographic requirements outlined in the **Author guidelines**.
11. Text in normal style is set to single column, 1.5 line spacing, and 12 pt. Times New Roman font is

recommended. All tables, figures and illustrations have appropriate captions and are placed within the text at the appropriate points.

12. Mathematical and chemical equations are provided in separate lines and numbered (Arabic numbers) consecutively in parenthesis at the end of the line. All equation numbers are (if necessary) appropriately included in the text. Corresponding numbers are checked.
13. Tables, Figures, illustrations, are prepared in correct format and resolution (see **Author guidelines**).
14. The lettering used in the figures and graphs do not vary greatly in size. The recommended lettering size is 8 point Arial.
15. Separate files for each figure and illustration are prepared. The names (numbers) of the separate files are the same as they appear in the text. All the figure files are packed for uploading in a single ZIP file.
16. Authors have read **special notes** and have accordingly prepared their manuscript (if necessary).
17. References in the text and in the References are correctly cited. (see **Author guidelines**). All references mentioned in the Reference list are cited in the text, and vice versa.
18. Permission has been obtained for use of copyrighted material from other sources (including the Web).
19. The names, full affiliation (department, institution, city and country), e-mail addresses and references of three potential referees from institutions other than (and preferably countries other than) those of any of the authors are prepared in the word file. At least two relevant references (important papers with high impact factor, head positions of departments, labs, research groups, etc.) for each suggested reviewer must be provided.
20. Full-colour illustration or graph from the manuscript is proposed for graphical abstract.
21. **Appendices** (if appropriate) as supplementary material are prepared and will be submitted at the same time as the manuscript.

Privacy Statement

The names and email addresses entered in this journal site will be used exclusively for the stated purposes of this journal and will not be made available for any other purpose or to any other party.

ISSN: 1580-3155

Koristni naslovi

Slovensko kemijsko društvo
Slovenian Chemical Society



Slovensko kemijsko društvo

www.chem-soc.si

e-mail: chem.soc@ki.si



Wessex Institute of Technology

www.wessex.ac.uk



SETAC

www.setac.org



European Water Association

<http://www.ewa-online.eu/>



European Science Foundation

www.esf.org



European Federation of Chemical Engineering

<https://efce.info/>



IUPAC

INTERNATIONAL UNION OF
PURE AND APPLIED CHEMISTRY

International Union of Pure and Applied Chemistry

<https://iupac.org/>

Novice evropske zveze kemijskih društev (EuCheMS) najdete na:



EuCheMS: Brussels News Updates

<http://www.euchems.eu/newsletters/>



DONAU LAB Ljubljana
Member of LPPgroup

Donau Lab d.o.o., Ljubljana
Tbilisjska 85
SI-1000 Ljubljana
www.donaulab.si
office-si@donaulab.com

Planetarni centrifugalni mikser **ARM-310CE**

Brezkontaktno mešanje in disperzija

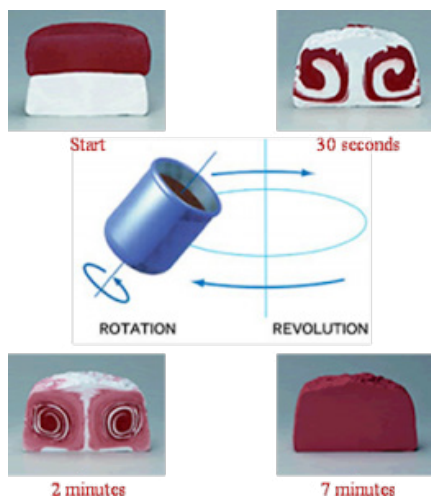
Tudi za zelo viskozne materiale

Širok spekter uporabe

Atraktivna cena



THINKY



Razvoj in inovacije za globalno uspešnost

Znanje, kreativnost zaposlenih in inovacije so ključnega pomena v okolju, kjer nastajajo Heliovi pametni premazi. Z rešitvami, ki zadostijo široki paleti potreb, kontinuiranim razvojem ter s kakovostnimi produkti Helios predstavlja evropski center za inovacije, know-how in poslovni razvoj Skupine Kansai Paint.

www.helios-group.eu



Bilobil®



**Možgane
oskrbi z več
kisika.**

OHRANJAM, KAR SEM.

Bilobil z izvlečkom ginka izboljša oskrbo možganov s kisikom in ohranja miselno vitalnost.

Moj um v vrhunski formi.



www.bilobil.si

Bilobil vsebuje izvleček iz listov Ginkga bilobae.

KRKA

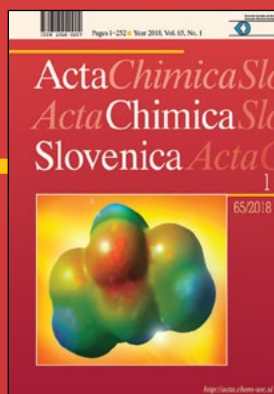
*Naša inovativnost in znanje
za učinkovite in varne
izdelke vrhunske kakovosti.*

Pred uporabo natančno preberite navodilo!
O tveganju in neželenih učinkih se posvetujte z zdravnikom ali s farmacevtom.

ActaChimicaSlovenica

ActaChimicaSlovenica

Cytric acid and EDTA can bind various metal cations, which prefer to form bonds at the electron-rich sites of the chelating agents. Density functional theory was used to obtain geometries, binding energies, and charge distributions of the complexes. Cover picture shows the electrostatic potential map of cytric acid (See page 231).



Year 2018, Vol. 65, No. 1

